

# Thermo-mechanical performance of energy pile groups

THÈSE N° 8138 (2018)

PRÉSENTÉE LE 23 FÉVRIER 2018

À LA FACULTÉ DE L'ENVIRONNEMENT NATUREL, ARCHITECTURAL ET CONSTRUIT  
LABORATOIRE DE MÉCANIQUE DES SOLS - CHAIRE GAZ NATUREL PETROSVIBRI  
PROGRAMME DOCTORAL EN MÉCANIQUE

ÉCOLE POLYTECHNIQUE FÉDÉRALE DE LAUSANNE

POUR L'OBTENTION DU GRADE DE DOCTEUR ÈS SCIENCES

PAR

Alessandro Francesco ROTTA LORIA

acceptée sur proposition du jury:

Prof. F. Gallaire, président du jury  
Prof. L. Laloui, directeur de thèse  
Prof. J. S. McCartney, rapporteur  
Prof. B. M. Chiaia, rapporteur  
Prof. A. Muttoni, rapporteur



ÉCOLE POLYTECHNIQUE  
FÉDÉRALE DE LAUSANNE

Suisse  
2018



*A mia madre, per avermi infuso il piacere dello studio*  
*A mio padre, per avermi trasmesso la passione per le attività*  
*Alle mie sorelle, per essere state esempi di intraprendenza*





# Acknowledgements

The first person I would like to gratefully acknowledge for his crucial role in the development of my Ph.D. is my thesis director, Prof. Lyesse Laloui. Je souhaite le remercier pour les connaissances scientifiques, le professionnalisme et la rigueur qu'il m'a inculqués, ainsi que de m'avoir appris la valeur d'aller aux fondamentaux des problèmes en développant la science. Je souhaite également le remercier pour toutes les opportunités qu'il m'a fournies, ainsi que de m'avoir corrigé quand j'ai fait des erreurs. Tous ces aspects ont fondamentalement contribué à me faire grandir d'un point de vue professionnel et personnel.

I would also like to express my very great appreciation to the other committee members of my final Ph.D. exam, i.e., Prof. François Gallaire, Prof. Bernardino M. Chiaia, Prof. John S. McCartney and Prof. Aurelio Muttoni, for the comments provided as a result of the revision of my work. Je remercie le Prof. Gallaire d'avoir été mon mentor tout au long de mon doctorat. Un grande ringraziamento è dedicato al Prof. Chiaia per avere suscitato in me la passione per la meccanica quando i miei interessi andavano definendosi, così come per la disponibilità e il supporto che mi ha dimostrato in tutti questi anni. I wish to thank Prof. McCartney for inspiring me throughout my Ph.D. via his scientific works as well as for his support and availability in many respects. Un ringraziamento va, inoltre, al Prof. Muttoni per il tempo che mi ha dedicato nel contesto della nostra collaborazione.

I wish to acknowledge the financial support provided by the Swiss National Science Foundation (N. 160117, Division I-III), which practically allowed this work to be carried out.

Ringrazio la Dott.ssa Alice Di Donna per avermi insegnato tanto sulle *energy geostructures* e per aver giocato un ruolo importante nello sviluppo del mio dottorato. A special acknowledgement is devoted to Prof. Charles W.W. Ng for sharing with me milestones that I will always remember when I visited his research group in Hong Kong. I also wish to thank Dr. Anthony Gunawan for contributing to my Hong Kong experience and to the early development of my Ph.D. work. Ringrazio il Prof. Alessio Ferrari per gli insegnamenti che mi ha trasmesso in questi anni e per essere stato un esempio di attenzione per il dettaglio. A great thank also goes to Dr. Fleur Loveridge for her willingness to share her experimental data on energy piles. I would like to thank Prof. William Curtin for instilling in me the importance to be clear and to keep things simple especially when sharing scientific concepts.

Je remercie Etienne Cassini pour nos discussions scientifiques fructueuses et pour le temps remarquable qu'il m'a consacré au cours de mon doctorat. Ringrazio il Dott. Alberto Minardi per essere stato un grande supporto durante la nostra esperienza di dottorato. Ringrazio la Dott.ssa Donatella

Manca per i consigli preziosi che mi ha fornito nel corso degli anni di dottorato. Ringrazio il Dott. Francesco Parisio per essere stato in questi anni una fonte inesauribile di incoraggiamento. Many thanks are dedicated to Dr. Dimitrios Terzis for being a source of inspiration in the professional life. Je remercie le Dr. Chao Li de m'avoir appris beaucoup sur la modélisation numérique. Ringrazio Matteo Bocco e Cristiano Garbellini per i loro contributi preziosi nell'ambito delle nostre collaborazioni. A special thank goes to Barnaby Fryer for his help in many respects related to my research activities. Ringrazio Jacopo Zannin, Gianluca Speranza e il Dott. Aldo Madaschi per gli interessanti confronti. I wish to thank Dr. Melis Sütman for the fruitful discussions we had about energy geostructures. Ringrazio Eleonora Crisci e la Dott.ssa Valentina Favero per essere state un esempio di intraprendenza nella geomeccanica sperimentale. Merci à Dr. Thomas Mimouni pour l'aide apporté avec les expériences *in situ* au début de ma thèse. Je remercie beaucoup Patrick Dubey et ses assistants Bastien, Swann et Mirco de m'avoir aidé avec les expériences *in situ* pendant ma thèse. Je remercie Rosa Ana Turielle et Barbara Tinguely d'avoir suivi les aspects administratifs de mon doctorat. I wish to express my special thanks to all of the other current and past members of the EPFL Geo-related laboratories for further contributing to my doctoral experience: Felipe Orellana, Dott.ssa Marianna Adinolfi, Andrea Salmi, Giovanni Schicchi, Elena Ravera, Jose Bosch, Angelica Tuttolomondo, Erika Cafasso, Samuel Grangier, Mateo Acosta, Corentin Noël, Chiara Cornelio, Prof. Anne-Catherine Dieudonné, Federico Ciardo, Dr. Patrycja Baryla, Gilbert Gruaz, Thibaut Le Gac, Dr. Ali Seiphoori, Dr. Maria Suryatriyastuti, Dr. Fabrice Dupray, Prof. Roman Makhnenko, Dr. Victor Vilarrasa, Laurent Gastaldo, Dr. Federica Sandrone, Dott.ssa Erika Paltrinieri, Dott. Andrea Delisio, Abdusalam Aili, and Prof. Yafei Qiao. A great thank to whom I did not mention, although he/she is aware of having contributed to my doctoral experience as well.

I would like to thank the students I supervised over these years for inspiring me in many ways, allowing me to improve my research and teaching skills, and contributing to my research activities: Niccolò Batini, Aurélien Vadrot, Lea Kaufmann, Pia Hartmann, Hani Taha, Benoît Cousin, Stefano Cingari, Margaux Peltier, Thibaut Duparc, Aymen Achich, Etienne Dominguez, Jose Catala Oltra, Perrine Ratouis and Samuel Kivell.

I also wish to thank the following people for sharing special moments together: Gauthier, Daniel et Blaise; Luca, Giorgio e Cecilia; Shevy and Parag; Charlotte, Grollo, Bernard, Darko, Bastian et Stéphanie; Davide, Elena and Severin. Ringrazio Raffaele per il suo prezioso parere legato ad alcuni aspetti legati alle mie ricerche. Un ringraziamento va a Christian per avermi accolto in der Schweiz.

Ringrazio gli amici Eporediesi e Torinesi per essermi sempre stati vicini, anche da lontano: Ilaria, Isabella, Massimiliano, Andrea, Michele, Edoardo, Mariano, Matteo (Mg), Marco, Ventu, Davide, Francesca, Paola, Alessandro, Carlotta, Matteo e Elena.

Ringrazio di cuore i miei genitori e le mie sorelle per essere stati dei riferimenti costanti nella mia vita e per avermi sempre sostenuto, consigliato e incoraggiato nel cammino intrapreso.

Infine, un profondo ringraziamento è dedicato a Giorgia per avere reso questi anni speciali con il suo sostegno, la sua presenza e il suo costante incoraggiamento, per avermi sempre dimostrato comprensione e fiducia, per avere condiviso progetti e sogni ed essermi stata vicina con il suo sorriso.

# Abstract

Employing geostructures as structural supports and geomaterials as reservoirs for the extraction and storage of heat represent effective means to meet human activity needs since ancient times. This doctoral thesis focuses on the thermo-mechanical behaviour and performance of an innovative, multifunctional technology that couples the aforementioned roles for the structural support and energy supply of any type of built environment, i.e., energy piles. The multifunctional role of energy piles involves mechanical and thermal loads applied to such geostructures. These loads pose unprecedented challenges to engineers because they cause variations in the temperature, stress, deformation and displacement in the subsurface that need to be considered during analysis and design. Prior to this work, a substantial amount of research had been made available to address the thermo-mechanical performance of single energy piles. Design guidance has also been proposed to advise in the geotechnical and structural design of such geostructures. However, energy pile foundations do not consist of a single energy pile but of a group of energy piles. In this framework, (i) limited knowledge, if available, was present to address the thermo-mechanical behaviour and performance of energy pile groups subjected to thermal and mechanical loads; (ii) no simplified models and methods were accessible to perform the analysis and design of energy pile groups against the action of such loads; and (iii) no comprehensive framework for the effect of thermal (and mechanical) loads on the performance and the related design of both single and groups of energy piles was available. To address such challenges, this doctoral research was performed to (i) investigate the thermo-mechanical behaviour and performance of energy pile groups over typical time-scales of practical applications via the first available *in situ* tests and coupled numerical analyses of such geostructures; (ii) provide the only simplified analytical models and methods for predicting the vertical deformation of energy pile groups subjected to thermal and mechanical loads; and (iii) propose a comprehensive framework for the effect of thermal and mechanical loads on the performance and related performance-based design (e.g., geotechnical and structural) of single and groups of energy piles. The results presented in this thesis suggest the conclusion that (a) the thermo-mechanical behaviour and performance of energy pile groups are critically different from those of single energy piles; (b) thermal loads, applied alone or in conjunction to mechanical loads, represent a serviceability and not an ultimate limit state problem; and (c) no energy pile analysis and design can be considered complete without addressing the behaviour of piles as both isolated elements and in a group.

**Keywords:** Energy piles, thermo-mechanical behaviour, performance, group effects, interactions, *in situ* testing, numerical modelling, analytical modelling, interaction factor method, equivalent pier method, performance-based design, design charts, thermo-elasticity, plasticity.



# Résumé

Les ouvrages souterrains et les géomatériaux, utilisés respectivement comme supports structuraux et comme moyen d'échange, de stockage ou d'extraction de chaleur, contribuent à l'activité humaine depuis l'Antiquité. Cette thèse de doctorat étudie le comportement et la performance thermomécanique d'une technologie innovante et multifonction qui associe les rôles structuraux et d'approvisionnement énergétique mentionnés ci-dessus pour tout type d'environnement construit : les pieux énergétiques. Leurs usages multiples soumettent ces géostructures à des charges mécaniques et thermiques. Ces charges posent des défis sans précédent aux ingénieurs car elles incluent des variations de température, de contrainte, de déformation et de déplacement dans le sous-sol qui doivent être prises en compte lors de l'analyse et de la conception des pieux. Avant ce travail, des recherches ont été effectuées pour étudier le comportement et la performance thermomécaniques des pieux énergétiques isolés. Des recommandations ont également été proposées pour leurs conceptions. Cependant, les fondations sur pieux énergétiques sont constituées par des groupes de pieux. Dans ce cadre, (i) les connaissances étaient limitées, sinon absentes, pour expliquer le comportement et la performance thermomécaniques des groupes de pieux énergétiques, soumis à des charges thermiques et mécaniques; (ii) ni modèle ni méthodes simplifiées n'étaient accessibles pour effectuer l'analyse et la conception des groupes de pieux énergétiques sous l'action de ces charges; et (iii) aucun cadre exhaustif sur l'effet des charges thermiques (et mécaniques) sur la performance et la conception de ces éléments n'était défini. Dans le but de relever les défis susmentionnés, cette thèse de doctorat a été réalisée pour (i) étudier le comportement et la performance thermomécaniques des groupes des pieux énergétiques sur des échelles de temps caractéristiques d'applications pratiques, grâce aux premiers tests in situ et analyses numériques disponibles; (ii) fournir les premiers modèles, et méthodes, analytiques simplifiés pour prédire la déformation verticale des groupes de pieux énergétiques; et (iii) proposer un cadre complet décrivant l'effet des charges thermiques et mécaniques sur la performance et la conception (géotechnique et structurelle) des pieux énergétiques. Les résultats présentés dans cette thèse permettent de conclure que (a) le comportement et la performance thermomécanique des groupes de pieux énergétiques diffèrent par rapport à ceux des pieux énergétiques isolés, (b) les charges thermiques, appliquées seules ou en conjonction avec des charges mécaniques, sont un problème à l'état limite de service, mais jamais à l'état limite ultime, et (c) l'analyse et la conception des pieux énergétiques ne peuvent être considérées comme complètes sans aborder le comportement des pieux en tant qu'éléments isolés et dans un groupe.

**Mots-clés :** Pieux énergétiques, comportement thermomécanique, effets de groupe, interactions, tests in situ, modélisation numérique, modélisation analytique, méthode du facteur d'interaction, méthode du pieu équivalent, conception, performance, thermo-élasticité, plasticité.



# Sommario

L'utilizzo di geostrutture per il supporto strutturale e l'impiego di terreni per lo scambio, l'estrazione o lo stoccaggio di energia termica sono tra i metodi più antichi per contribuire all'attività umana. Questa tesi di dottorato indaga il comportamento e la prestazione termo-meccanica di una tecnologia innovativa e multifunzionale che unisce le suddette funzioni di supporto strutturale e di scambiatore di calore per qualsiasi ambiente costruito: i pali energetici. L'operazione dei pali energetici implica che tali elementi strutturali siano soggetti sia a carichi meccanici sia a carichi termici. Questa combinazione di carichi rappresenta una sfida ingegneristica senza precedenti, perché causa nei terreni variazioni di temperatura, sforzo, deformazione e spostamento che devono essere considerate nelle attività di analisi e di progettazione. Prima di questo lavoro, svariate ricerche sono state realizzate per studiare il comportamento e la prestazione termo-meccanica di singoli pali energetici e sono state proposte linee guida per la progettazione di tale tecnologia. Tuttavia, le fondazioni di pali energetici non sono costituite da un solo palo, ma da gruppi di pali energetici. In questo ambito: (i) era disponibile una conoscenza limitata, se non assente, per affrontare il comportamento e la prestazione termo-meccanica di gruppi di pali energetici sottoposti a carichi termici e meccanici; (ii) non erano disponibili modelli e metodi semplificati per l'analisi e la progettazione dei gruppi di pali energetici contro l'azione di tali carichi; e (iii) non esisteva alcun quadro dettagliato relativo alla prestazione e alla relativa progettazione di singoli pali e gruppi di pali energetici. Nel tentativo di affrontare tali sfide, questa tesi di dottorato ha inteso: (i) esaminare il comportamento e la prestazione termo-meccanica dei gruppi di pali energetici attraverso i primi test in sito disponibili al mondo, accoppiati con analisi numeriche; (ii) fornire gli unici modelli e metodi analitici semplificati per la previsione della deformazione verticale dei gruppi di pali energetici sottoposti a carichi termici e meccanici; infine, (iii) proporre un quadro completo circa l'effetto dei carichi termici e meccanici sulla prestazione e la relativa progettazione (geotecnica e strutturale) sia di pali singoli sia di gruppi di pali energetici. I risultati presentati in questa tesi permettono di concludere che: (a) il comportamento termo-meccanico e la prestazione dei gruppi di pali energetici differiscono in modo cruciale rispetto a quelli dei pali energetici singoli, (b) i carichi termici, applicati da soli o in compresenza con i carichi meccanici, rappresentano un problema di stato limite di esercizio e non di stato limite ultimo; (c) nessuna analisi e progettazione di pali energetici può essere considerata completa se non si affronta il comportamento dei pali come elementi isolati e in un gruppo.

**Parole chiave:** Pali energetici, comportamento termo-meccanico, prestazione, effetti di gruppo, interazioni, campagne in sito, modellazione numerica, modellazione analitica, metodo ai fattori d'interazione, metodo del palo equivalente, progettazione prestazionale, termo-elasticità, plasticità.





# Contents

<b>Acknowledgements .....</b>	<b>v</b>
<b>Abstract .....</b>	<b>vii</b>
<b>Résumé.....</b>	<b>ix</b>
<b>Sommario .....</b>	<b>xi</b>
<b>List of Figures .....</b>	<b>xix</b>
<b>List of Tables .....</b>	<b>xxvii</b>
<b>List of Symbols.....</b>	<b>xxix</b>
<b>Introduction .....</b>	<b>1</b>
<b>Chapter 1   Energy geostructures .....</b>	<b>5</b>
<b>1.1   Anthropogenic development and the energy question .....</b>	<b>5</b>
1.1.1   World population .....	5
1.1.2   Energy forms and classification of energy sources .....	6
1.1.3   World energy consumption and supply.....	7
1.1.4   Consequences.....	9
1.1.5   Perspectives .....	11
<b>1.2   Geothermal energy .....</b>	<b>12</b>
1.2.1   Origin .....	12
1.2.2   Geothermal gradient.....	12
1.2.3   Features of geothermal energy .....	13
<b>1.3   Geothermal systems .....</b>	<b>14</b>
1.3.1   Classification of geothermal systems.....	14
1.3.2   Features and uses of geothermal systems.....	14
<b>1.4   The energy geostructure technology .....</b>	<b>17</b>
1.4.1   Roles of energy geostructures .....	17
1.4.2   Materials and technology .....	19
1.4.3   Advantages involved with energy geostructures.....	21

<b>1.5</b>	<b>Energy geostructure operation modes.....</b>	<b>21</b>
1.5.1	Possible operations .....	21
1.5.2	Heat exchange operation.....	22
1.5.3	Heat storage .....	22
<b>1.6</b>	<b>Ground Source Heat Pump Systems .....</b>	<b>23</b>
1.6.1	General.....	23
1.6.2	The primary circuit .....	24
1.6.3	The heat pump or reversed heat pump .....	24
1.6.4	The secondary circuit.....	25
1.6.5	The Coefficient of Performance.....	25
1.6.6	The Seasonal Factor of Performance .....	26
1.6.7	Possible applications of Ground Source Heat Pump Systems .....	26
<b>1.7</b>	<b>Underground Thermal Energy Storage Systems.....</b>	<b>27</b>
<b>1.8</b>	<b>Application and development of energy geostructures .....</b>	<b>27</b>
1.8.1	Historical facts .....	27
1.8.2	Application and development examples based on a literature survey .....	28
<b>1.9</b>	<b>Considerations and challenges from a holistic, integrated perspective .....</b>	<b>29</b>
<b>Chapter 2</b>	<b>The role of thermal loads in the geotechnical and structural performance of energy piles....</b>	<b>35</b>
<b>2.1</b>	<b>Introduction .....</b>	<b>35</b>
<b>2.2</b>	<b>Thermo-mechanical idealisation of energy pile behaviour .....</b>	<b>37</b>
2.2.1	Effect of thermal loads on the mechanical behaviour of energy piles .....	37
2.2.2	Generalised mathematical formulation of vertical energy pile equilibrium.....	41
2.2.3	Thermo-mechanical schemes for energy piles with no base and head restraints .....	43
2.2.4	Thermo-mechanical schemes for energy piles with base or head restraints.....	45
2.2.5	Thermo-mechanical schemes for energy piles with base and head restraints .....	47
2.2.6	Irreversible effects of mechanical and thermal loads on the geotechnical behaviour of energy piles .....	48
2.2.7	Irreversible effects of mechanical and thermal loads on the structural behaviour of energy piles .....	49
<b>2.3</b>	<b>Performance-based design of case studies.....</b>	<b>52</b>
2.3.1	Combination of actions at ultimate limit states .....	52
2.3.2	Partial factors for thermal loads applied to energy piles .....	53
2.3.3	Design situations.....	55
2.3.4	Design approach .....	56
2.3.5	Analysis method .....	58
2.3.6	Design case study and material parameters .....	58
<b>2.4</b>	<b>Unlikelihood of thermal loads exceeding geotechnical ultimate limit states .....</b>	<b>59</b>

2.4.1	Effects of thermal loads based on a strength capacity criterion .....	59
2.4.2	Effects of thermal loads based on a displacement capacity criterion .....	60
2.4.3	Energy pile response for constant applied mechanical load and varying pile length .....	61
2.4.4	Energy pile response for varying applied mechanical load and constant pile length .....	64
<b>2.5</b>	<b>Unlikelihood of thermal loads involving structural ultimate limit states .....</b>	<b>66</b>
2.5.1	Effects of thermal loads from a structural capacity perspective .....	66
2.5.2	Energy pile response for constant applied mechanical load and varying pile length .....	67
2.5.3	Energy pile response for varying applied mechanical load and constant pile length .....	68
2.5.4	Actual response of reinforced concrete members .....	79
<b>2.6</b>	<b>Concluding remarks .....</b>	<b>82</b>
<b>Chapter 3</b>	<b>Thermally induced group effects among energy piles .....</b>	<b>85</b>
<b>3.1</b>	<b>Introduction .....</b>	<b>85</b>
<b>3.2</b>	<b>Experimental testing .....</b>	<b>86</b>
3.2.1	The pile foundation and site .....	86
3.2.2	Features of the experimental tests .....	100
<b>3.3</b>	<b>Numerical modelling .....</b>	<b>100</b>
3.3.1	Finite element model .....	101
3.3.2	Modelling choices .....	101
3.3.3	Boundary and initial conditions .....	103
3.3.4	Classification of the numerical simulations and material properties .....	104
<b>3.4</b>	<b>Comparison between experimental and numerical results – Test 20EP1 .....</b>	<b>106</b>
3.4.1	Temperature variations along the energy piles .....	107
3.4.2	Temperature trends at the energy pile toes .....	110
3.4.3	Temperature variations in the soil .....	110
3.4.4	Vertical strain variations along the energy piles .....	113
3.4.5	Vertical stress variations along the energy piles .....	115
3.4.6	Vertical stress variations at the toe of the operating energy pile .....	118
3.4.7	Variations of radial strain in the operating energy pile .....	118
<b>3.5</b>	<b>Comparison between experimental and numerical results – Test 20EPall .....</b>	<b>120</b>
3.5.1	Impact of number of operating energy piles on vertical deformation .....	120
3.5.2	Impact of number of operating energy piles on vertical stress .....	122
<b>3.6</b>	<b>Discussion .....</b>	<b>125</b>
3.6.1	Comparison between the Class B1 and C1 prediction results – Test 20EP1 .....	125
3.6.2	Key aspects governing the behaviour of energy pile groups .....	127
3.6.3	Design considerations for energy pile groups .....	130
3.6.4	Suitability and limitations of using thermo-elasticity for simulating energy pile groups ..	135

3.6.5	Suitability and limitations of using thermo-mechanical analyses for simulating energy pile groups .....	136
3.7	<b>Concluding remarks.....</b>	138
<b>Chapter 4</b>	<b>The interaction factor method for energy pile groups based on design charts.....</b>	<b>141</b>
4.1	<b>Introduction .....</b>	141
4.2	<b>The interaction factor concept .....</b>	143
4.2.1	The problem: a group of two energy piles .....	143
4.2.2	Idealisation.....	143
4.2.3	Finite element analysis.....	146
4.2.4	The interaction factor.....	149
4.3	<b>Design charts .....</b>	154
4.3.1	Effect of pile spacing, pile slenderness ratio and pile-soil stiffness ratio - piles embedded in uniform soil mass.....	154
4.3.2	Effect of pile spacing, pile slenderness ratio and pile-soil stiffness ratio - piles resting on infinitely rigid soil strata .....	156
4.3.3	Effect of pile slenderness ratio, pile-soil stiffness ratio and base-to-shaft modulus ratio - piles resting on finitely rigid soil strata .....	156
4.3.4	Effect of Poisson's ratio of soil.....	156
4.3.5	Effect of finite layer depth .....	157
4.3.6	Effect of non-uniform soil modulus.....	161
4.3.7	Effect of soil-pile thermal expansion coefficient ratio.....	162
4.4	<b>Application and validation of the interaction factor concept .....</b>	163
4.4.1	Analysis of symmetrical energy pile groups.....	163
4.4.2	Application of the interaction factor concept.....	163
4.4.3	Validation of the interaction factor concept.....	164
4.5	<b>The interaction factor method .....</b>	167
4.5.1	Analysis of general energy pile groups.....	167
4.5.2	Application of the interaction factor method .....	173
4.6	<b>Validation of the interaction factor method.....</b>	178
4.7	<b>Concluding remarks.....</b>	182
<b>Chapter 5</b>	<b>The interaction factor method for energy pile groups based on analytical models.....</b>	<b>185</b>
5.1	<b>Introduction .....</b>	185
5.2	<b>Problem definition and solution approach.....</b>	187
5.2.1	The problem.....	187
5.2.2	Idealisation, hypotheses and considerations .....	187
5.2.3	The solution approach.....	189
5.3	<b>Layer model .....</b>	191

5.3.1	Soil vertical displacement and approximate pile-soil interaction factor .....	191
5.3.2	Receiver pile vertical displacement and corrected pile-soil-pile interaction factor .....	194
<b>5.4</b>	<b>Continuous model.....</b>	<b>197</b>
5.4.1	Soil vertical displacement and approximate pile-soil interaction factor .....	197
5.4.2	Receiver pile vertical displacement and corrected pile-soil-pile interaction factor .....	198
<b>5.5</b>	<b>Application and validation of the performance models .....</b>	<b>200</b>
5.5.1	General information about analyses performed .....	200
5.5.2	Analysis of vertical displacement of a single isolated pile .....	200
5.5.3	Analysis of soil vertical displacement and approximate interaction factor .....	201
5.5.4	Analysis of receiver pile vertical displacement and corrected interaction factor .....	202
5.5.5	Corrected interaction factor for a range of design situations .....	203
5.5.6	Analysis of 5 × 5 square energy pile groups.....	207
<b>5.6</b>	<b>Concluding remarks.....</b>	<b>210</b>
<b>Chapter 6</b>	<b>Non-linear soil deformation and energy pile interaction .....</b>	<b>213</b>
<b>6.1</b>	<b>Introduction .....</b>	<b>213</b>
<b>6.2</b>	<b>Interaction factor analysis of energy pile groups .....</b>	<b>215</b>
6.2.1	Classical interaction factor analysis approach .....	215
6.2.2	Modified interaction factor analysis approach .....	218
<b>6.3</b>	<b>Modelling of pile group tests .....</b>	<b>220</b>
6.3.1	Experimental tests reported by O'Neill et al. (1981).....	220
6.3.2	Models .....	222
<b>6.4</b>	<b>Results .....</b>	<b>225</b>
6.4.1	Validation of the numerical model against experimental results .....	225
6.4.2	Pile group vertical displacement induced by mechanical loading.....	227
6.4.3	Pile group vertical displacement induced by thermal loading .....	228
6.4.4	Interaction factor for energy piles in non-linearly deforming soil .....	230
<b>6.5</b>	<b>Concluding remarks.....</b>	<b>232</b>
<b>Chapter 7</b>	<b>The equivalent pier method for energy pile groups .....</b>	<b>233</b>
<b>7.1</b>	<b>Introduction .....</b>	<b>233</b>
<b>7.2</b>	<b>The equivalent pier method for energy pile groups .....</b>	<b>235</b>
7.2.1	Hypotheses and considerations .....	235
7.2.2	Geometry of the equivalent pier.....	237
7.2.3	Homogenised material properties of the equivalent pier.....	239
7.2.4	Load-displacement description of the equivalent pier .....	244
<b>7.3</b>	<b>Application and validation of the method.....</b>	<b>248</b>
7.3.1	Analysed problems.....	248

7.3.2	Material parameters .....	249
7.3.3	Results.....	251
7.4	Concluding remarks.....	253
<b>Chapter 8</b>	<b>Conclusions and perspectives .....</b>	<b>255</b>
8.1	Summary.....	255
8.2	General conclusions .....	257
8.3	Perspectives.....	259
	<b>Bibliography.....</b>	<b>261</b>
	<b>Appendix A – <i>In situ</i> testing equipment.....</b>	<b>271</b>
	<b>Appendix B - Mathematical formulation employed in the finite element analyses.....</b>	<b>273</b>
	<b><i>Curriculum vitae</i>.....</b>	<b>275</b>

# List of Figures

Figure 1.1: World population trend (data from United Nations (2017)).	6
Figure 1.2: Final energy consumption shares by end users in the European Union in 2015 (data from Eurostat (2017)).	8
Figure 1.3: Final energy consumption in the Swiss building sector in 2012 (data from Kemmler et al. (2013)).	8
Figure 1.4: World final energy consumption from 2000 to 2014 (data from International Energy Agency (2016c)).	9
Figure 1.5: World primary energy supply from 2000 to 2014 (data from International Energy Agency (2016c)).	9
Figure 1.6: World anthropogenic energy-related greenhouse gas emissions by type (data from International Energy Agency (2015)).	10
Figure 1.7: World energy-related CO <sub>2</sub> emissions by sector (data from International Energy Agency (2015)).	11
Figure 1.8: Sketch of typical temperature evolution with depth in the shallow subsurface throughout the year for a temperate climatic zone.	13
Figure 1.9: Sketch of typical temperature evolution with depth in Earth subsurface (redrawn after Boehler (1996)).	13
Figure 1.10: Classification of geothermal systems (redrawn after Geothermie Schweiz).	16
Figure 1.11: Examples of energy piles (image courtesy of Dr. Thomas Mimouni).	18
Figure 1.12: Typical pipes and thermal insulation in an energy pile (image courtesy of Dr. Thomas Mimouni).	20
Figure 1.13: Typical energy geostructure operation modes.	22
Figure 1.14: Typical composition of a ground source heat pump system and associated heating operation mode (modified after Agentur für Erneuerbare Energien, reproduced with permission).	24
Figure 1.15: Number and average length of energy piles by country.	28
Figure 1.16: Installed thermal power by country.	29
Figure 1.17: Cumulative number of energy piles and energy pile projects in the world.	29
Figure 1.18: Typical aspects to consider in the analysis and design of energy geostructures.	30

Figure 2.1: Thermally induced strain caused by (a) heating and (b) cooling of an energy pile under free expansion conditions. ....	39
Figure 2.2: Thermally induced stress caused by (a) heating and (b) cooling of an energy pile under completely blocked conditions. ....	39
Figure 2.3: Impact of system restraint on the thermally induced vertical strain and stress in energy piles.....	41
Figure 2.4: Thermo-mechanical schemes for energy piles characterised by no base and head restraints.....	43
Figure 2.5: Thermo-mechanical schemes for energy piles characterised by base or head restraints. ....	45
Figure 2.6: Thermo-mechanical schemes for energy piles characterised by base and head restraints. ....	49
Figure 2.7: Transition from a composite reinforced concrete cross-section to a section in which only the longitudinal reinforcement contributes to the resistance.....	50
Figure 2.8: Normalised axial loads for energy piles that are free at their head and subjected to heating – constant applied mechanical load and varying pile length.....	70
Figure 2.9: Normalised axial loads for energy piles restrained at their head and subjected to heating – constant applied mechanical load and varying pile length.....	71
Figure 2.10: Normalised axial loads for energy piles that are free at their head and subjected to cooling – constant applied mechanical load and varying pile length.....	72
Figure 2.11: Normalised axial loads for energy piles restrained at their head and subjected to cooling – constant applied mechanical load and varying pile length.....	73
Figure 2.12: Normalised axial loads for energy piles that are free at their head and subjected to heating – varying applied mechanical load and constant pile length. ....	74
Figure 2.13: Normalised axial loads for energy piles of $L/D = 20$ that are restrained at their head and subjected to heating – varying applied mechanical load and constant pile length. ....	75
Figure 2.14: Normalised axial loads for energy piles of $L/D = 50$ that are restrained at their head and subjected to heating – varying applied mechanical load and constant pile length. ....	76
Figure 2.15: Normalised axial loads for energy piles that are free at their head and subjected to cooling – varying applied mechanical load and constant pile length.....	77
Figure 2.16: Normalised axial loads for energy piles of $L/D = 20$ that are restrained at their head and subjected to cooling – varying applied mechanical load and constant pile length. ....	78
Figure 2.17: Normalised axial loads for energy piles of $L/D = 50$ that are restrained at their head and subjected to cooling – varying applied mechanical load and constant pile length. ....	79
Figure 2.18: Relationships between axial cross-sectional load and normalised axial displacement for energy piles made of reinforced concrete. ....	82
Figure 3.1: (a) Plan view of the EPFL Swiss Tech Convention Centre foundation; (b) vertical cross-sections depicting the monitoring instrumentation that was installed in the energy piles and soil; (c) schematic diagram of the soil stratigraphy. Views not to scale. ....	99
Figure 3.2: (a) Geometry, initial and boundary conditions of the finite element model and (b) plan view of the foundation listing the piles and other relevant features. Views not to scale. ...	102
Figure 3.3: Experimentally and numerically imposed inflow temperatures and velocities of the fluid circulating in the pipes of the operating energy pile EP1 with time (Test 20EP1). ....	104



Figure 3.4: Experimentally and numerically imposed average inflow temperatures and velocities of the fluid circulating in the pipes of the operating energy piles EP1, 2, 3 and 4 with time (Test 20EPall). .....	105
Figure 3.5: Comparison between the experimental and numerical temperature variations observed along (a) the operating energy pile EP1 and (b-d) the non-operating energy piles EP2, 3, and 4, after $t = 2, 8, 35$ and $156$ days of testing.....	108
Figure 3.6: Comparison between the experimental and numerical trends of fluid temperature flowing from the pipes of the operating energy pile EP1.....	109
Figure 3.7: Comparison between the experimental and numerical temperature variations observed at the energy pile toes with time. ....	111
Figure 3.8: Comparison between the experimental and numerical temperature variations along profiles (a) P+T1 and (b) P+T2 in the soil at the time steps at which the operating energy pile EP1 was subjected to average temperature variations of $\overline{\Delta T}_{EP1} = 5, 10, 15$ and $20$ °C ( $t = 2, 8, 35$ and $156$ days of testing, respectively). (c) Trends of temperature variations at selected points along the profiles. ....	112
Figure 3.9: Comparison between the experimental and numerical variations in vertical strain observed along (a) the operating energy pile EP1 and (b-d) the non-operating energy piles EP2, 3, and 4, after $t = 2, 8, 35$ and $156$ days of testing. ....	114
Figure 3.10: Comparison between the experimentally observed variations in vertical strain in the non-operating energy pile EP2 after $t = 156$ days of testing and calculated with reference to free thermal expansion conditions. ....	115
Figure 3.11: Comparison between the experimental and numerical vertical stress variations observed along (a) the operating energy pile EP1 and (b-d) the non-operating energy piles EP2, 3, and 4, after $t = 2, 8, 35$ and $156$ days of testing.....	117
Figure 3.12: Comparison between the experimental and numerical vertical stress variations observed at the toe of the operating energy pile EP1 with time. ....	119
Figure 3.13: Comparison between the experimental and numerical radial strain variations observed at a depth of $z = 9$ m in the operating energy pile EP1 with time. ....	119
Figure 3.14: Comparison between the experimentally and numerically observed vertical strain variations. The strain variations, $\Delta \varepsilon_z$ , correspond to the average temperature variations along the uninsulated portion of EP1 of $\overline{\Delta T}_{EP1} = 5, 10, 15$ and $20$ °C (panels (a), (b), (c) and (d), respectively) after $t = 2, 8, 35$ and $156$ days of testing, respectively, during the heating phase of Test 20EP1. The strain variations, $\overline{\Delta \varepsilon_z}$ , correspond to the mean value of the average temperature variations along the uninsulated portions of EP1, 2, 3 and 4 of $\overline{\Delta T}_{EPall} = 5, 10, 15$ and $20$ °C (panels (a), (b), (c) and (d), respectively) after $t = 2, 9, 28$ and $60$ days of testing, respectively, during the heating phase of Test 20EPall.....	121
Figure 3.15: Impact of the energy piles and soil thermal expansion potential on the vertical deformation of the piles during successive stages of the geothermal operation based on experimental results (Test 20EPall).....	122
Figure 3.16: Comparison of the experimentally and numerically observed vertical stress variations. The stress variations, $\Delta \sigma_z$ , correspond to the average temperature variations along the uninsulated portion of EP1 of $\overline{\Delta T}_{EP1} = 5, 10, 15$ and $20$ °C (panels (a), (b), (c) and (d), respectively) after $t = 2, 8, 35$ and $156$ days of testing, respectively, during the heating phase of Test 20EP1. The stress variations, $\overline{\Delta \sigma_z}$ , correspond to the mean value of the average temperature variations along the uninsulated portions of EP1, 2, 3 and 4 of $\overline{\Delta T}_{EPall} = 5, 10, 15$ and $20$ °C (panels (a), (b), (c) and (d),	

respectively) after $t = 2, 9, 28$ and $60$ days of testing, respectively, during the heating phase of Test 20EPall.....	123
Figure 3.17: Impact of the number of operating energy piles on the group vertical stress variation according to the experimental results.....	125
Figure 3.18: Comparison between the variations in vertical strain observed through the Class B1 and C1 numerical predictions and the experimental test along (a) the operating energy pile EP1 and (b) the non-operating energy pile EP2, after $t = 2, 8, 35$ and $156$ days of testing. ....	126
Figure 3.19: Numerical vertical stress variations induced by the superstructure's mechanical loads along energy piles EP1, 2, 3 and 4 (the stress distributions that are associated with the <i>in situ</i> conditions have been subtracted). ....	131
Figure 3.20: Numerical vertical displacement variations induced by the superstructure's mechanical loads and temperature variations along energy piles EP1, 2, 3 and 4 (the displacement distributions that are associated with the <i>in situ</i> conditions have been subtracted). ....	133
Figure 3.21: Impact of the number of operating energy piles on the average vertical pile group displacement. The average vertical displacement $\overline{\Delta w}$ (at the uppermost level of the slab, which corresponds to operating energy pile EP1) is plotted against the average temperature variation $\overline{\Delta T}_{EP1}$ for Test 20EP1, and the average vertical displacement $\overline{\Delta w}$ (at the uppermost level of the slab, which corresponds to operating energy piles EP1, 2, 3 and 4) is plotted against the average temperature variation $\overline{\Delta T}_{EPall}$ for Test 20EPall. The vertical displacement is normalised by the energy pile diameter, $D$ . ....	134
Figure 3.22: Experimentally and numerically observed (a) vertical strain variations along the operating energy pile EP1 for (b) approximately the same average temperature variation that was recorded with depth during the heating and passive cooling phases of the test. ....	136
Figure 3.23: Maximum experimental pore water pressure variations along profiles P+T1 and P+T2 in the soil. ....	137
Figure 3.24: Experimentally observed pore water pressure variations at selected points along profiles P+T1 and P+T2 with time.....	138
Figure 4.1: The modelling approach.....	145
Figure 4.2: The elementary unit.....	145
Figure 4.3: Vertical head displacement characterising a source and receiver pile in the elementary units, as well as corresponding single isolated piles subjected to the same temperature variation applied to the source piles.....	151
Figure 4.4: Displacement interaction between two piles in a deep soil layer. ....	153
Figure 4.5: Interaction factor for predominantly floating and end-bearing energy piles resting on infinitely rigid soil strata and socketed in uniform soil deposits, respectively, under the application of a thermal load. ....	153
Figure 4.6: Interaction factors for predominantly floating energy piles of $L/D = 10$ . ....	154
Figure 4.7: Interaction factors for predominantly floating energy piles of $L/D = 25$ . ....	155
Figure 4.8: Interaction factors for predominantly floating energy piles of $L/D = 50$ . ....	155
Figure 4.9: Interaction factors for predominantly end-bearing energy piles of $L/D = 10$ . ....	157
Figure 4.10: Interaction factors for predominantly end-bearing energy piles of $L/D = 25$ . ....	158
Figure 4.11: Interaction factors for predominantly end-bearing energy piles of $L/D = 50$ . ....	158

Figure 4.12: Correction factor $F_b$ to account for the effect of a finitely rigid bearing stratum for $L/D = 25$ .....	159
Figure 4.13: Correction factor $F_b$ to account for the effect of a finitely rigid bearing stratum for $L/D = 50$ .....	159
Figure 4.14: Correction factor $N_v$ for effect of Poisson's ratio of soil.....	160
Figure 4.15: Correction factor $N_{h_l}$ for effect of finite layer depth.....	160
Figure 4.16: Effect of non-uniform soil modulus on interaction factor.....	161
Figure 4.17: Effect of soil thermal expansion coefficient on interaction factor.....	162
Figure 4.18: Displacement ratio for symmetrical energy pile groups.....	165
Figure 4.19: (a) Effect of interaction on mobilised base resistance, $q_{b,mob}$ . (b) Effect of interaction on distribution of mobilised shaft friction, $q_{s,mob}$ .....	167
Figure 4.20: Key steps for the application of the interaction factor method.....	168
Figure 4.21: Vertical head displacement per unit temperature variation for different $L/D$ – predominantly floating energy pile embedded in uniform mass.....	170
Figure 4.22: Vertical head displacement per unit temperature variation for different $L/D$ – predominantly end-bearing pile resting on finitely rigid soil strata ( $E_{soil,b}/E_{soil,s} = 2$ )... ..	170
Figure 4.23: Vertical head displacement per unit temperature variation for different $L/D$ – predominantly end-bearing pile resting on finitely rigid soil strata ( $E_{soil,b}/E_{soil,s} = 5$ )... ..	171
Figure 4.24: Vertical head displacement per unit temperature variation for different $L/D$ – predominantly end-bearing pile resting on finitely rigid soil strata ( $E_{soil,b}/E_{soil,s} = 10$ )... ..	171
Figure 4.25: Vertical head displacement per unit temperature variation for different $L/D$ – predominantly end-bearing pile resting on finitely rigid soil strata ( $E_{soil,b}/E_{soil,s} = 100$ ).....	172
Figure 4.26: Vertical head displacement per unit temperature variation for different $L/D$ – predominantly end-bearing pile resting on soil strata that can be considered to be infinitely rigid ( $E_{soil,b}/E_{soil,s} \geq 1000$ ).....	172
Figure 4.27: Effect of Poisson's ratio of soil on the displacement ratio.....	173
Figure 4.28: Effect of position on the vertical displacement of the piles.....	174
Figure 4.29: Effect of finite layer depth on the differential displacement of the piles.....	175
Figure 4.30: Configuration of the practical example.....	176
Figure 4.31: Comparison between the results obtained through the proposed analytical approach and those obtained through more rigorous 3-D thermo-mechanical finite element analyses... ..	179
Figure 4.32: Comparison between the results obtained using the proposed analytical approach and those obtained using more rigorous 3-D thermo-mechanical finite element analyses.....	180
Figure 5.1: The solution approach for analysing the vertical displacement of general energy pile groups.....	190
Figure 5.2: The layer model concept: (a) the mode of deformation of a layer of cylindrical elements characterising any pile-soil system and (b) the effect of this mode of deformation.....	192
Figure 5.3: Vertical equilibrium of an element of a receiver pile.....	195

Figure 5.4: The continuous model concept: (a) the reference situation for Mindlin's problem (Mindlin, 1936) and (b) the transposition of this problem to that of a single isolated pile subjected to thermal loading. ....	198
Figure 5.5: Vertical displacement-shear stress relationship estimated through an axisymmetric finite element analysis. ....	202
Figure 5.6: Evolution of the normalised vertical displacement of the soil with the normalised depth for normalised radial distances of (a) $r/D = 2.5$ and (b) $r/D = 4.5$ ; evolution of the associated approximate interaction factor with the normalised depth for normalised radial distances of (c) $r/D = 2.5$ and (d) $r/D = 4.5$ . ....	204
Figure 5.7: Evolution of the corrected interaction factor with the normalised depth for a normalised spacing of (a) $s/D = 3$ and (b) $s/D = 5$ . ....	205
Figure 5.8: Evolution of the corrected and approximate interaction factors with the normalised horizontal distance. ....	205
Figure 5.9: Corrected interaction factors referred to the pile head for $L/D = 25$ in various design conditions. ....	206
Figure 5.10: Corrected interaction factors referred to the pile head for $L/D = 50$ in various design conditions. ....	206
Figure 5.11: Configuration of the practical example. ....	207
Figure 5.12: Analysis of $5 \times 5$ energy pile groups of $L/D = 25$ in various design conditions: (a-b) uniform soil mass and (c-d) non-uniform soil mass. ....	209
Figure 6.1: Vertical equilibrium of a base element of a receiver pile. ....	218
Figure 6.2: Assumed distribution of soil modulus between two piles. $E_{soil}$ = near-pile soil modulus (characteristic of high strain levels); $E_{soil,m} = \mu_E E_{soil}$ (with $\mu_E \geq 1$ ) = soil mass modulus (characteristic of low strain levels); $\bar{E}_{soil}$ = average soil modulus for computing interactions; $s_t$ = transition distance. ....	219
Figure 6.3: The features of the considered site, based on the information reported by O'Neill et al. (1981). ....	221
Figure 6.4: Geometrical configuration of the piles tested by O'Neill et al. (1981) for mechanical loading, further considered in this work for thermal loading. ....	221
Figure 6.5: The finite element model of the single isolated pile. ....	223
Figure 6.6: Evolution of the normalised soil Young's modulus with the normalised pile depth presented by O'Neill et al. (1981) and assumed for this study. ....	225
Figure 6.7: Comparison between the numerically modelled and experimentally observed (a) load-displacement curves for the single isolated pile and (b) evolution of the normalised vertical load with the normalised depth in the pile. ....	226
Figure 6.8: Comparison between the modelled and experimentally observed evolutions of the normalised vertical displacement with the normalised radial distance from the pile axis. ....	226
Figure 6.9: Comparison between the modelled and experimentally observed evolutions of the normalised average vertical head displacement of the piles with the number of directly mechanically loaded piles for the different pile tests considered. ....	228
Figure 6.10: Values of the normalised average soil Young's modulus corresponding to the centre-to-centre spacing between different pairs of piles that are used in the modified interaction factor analysis approach. ....	229

Figure 6.11: The modelled evolutions of the normalised average vertical head displacement of the piles with the number of directly thermally loaded piles for the different pile tests considered. ....	230
Figure 6.12: Evolution of the interaction factor with the centre-to-centre spacing between a pair of piles characterised by linear or non-linear soil deformation. ....	231
Figure 7.1: The modelling approach. ....	239
Figure 7.2: Schematic for the calculation of the Young's modulus of the equivalent pier. ....	240
Figure 7.3: Schematic for the calculation of the linear thermal expansion coefficient of the equivalent pier. ....	241
Figure 7.4: Comparison between the evolutions of the normalised temperature variation with radial distance obtained using the semi-analytical solution and the finite element (FE) method. ....	244
Figure 7.5: Load-displacement relationships for the shaft and base of equivalent piers ((a) and (b)) and single isolated energy piles ((c) and (d)). ....	246
Figure 7.6: Comparison between the results obtained using the proposed equivalent pier method, the interaction factor method and 3-D thermo-mechanical finite element analyses. ....	252



# List of Tables

Table 1.1: Some energy-related unit measures. ....	7
Table 1.2: Examples of aspects involved in the architectural and structural design of buildings and infrastructures involving energy geostructures. ....	32
Table 1.3: Examples of aspects involved in the architectural and structural design of buildings and infrastructures involving energy geostructures. ....	33
Table 2.1: Material properties used for the analyses presented in this study. ....	59
Table 2.2: Normalised vertical head displacements for energy piles of $D = 0.5$ m that are free at their head and subjected to cooling – constant applied mechanical load and varying pile length. ....	62
Table 2.3: Normalised vertical head displacements for energy piles of $D = 1$ m that are free at their head and subjected to cooling – constant applied mechanical load and varying pile length. ....	63
Table 2.4: Normalised vertical head displacements for energy piles of $D = 0.5$ m that are restrained at their head and subjected to cooling – constant applied mechanical load and varying pile length. ....	63
Table 2.5: Normalised vertical head displacements for energy piles of $D = 1$ m that are restrained at their head and subjected to cooling – constant applied mechanical load and varying pile length. ....	63
Table 2.6: Normalised vertical head displacements for energy piles of $D = 0.5$ m that are free at their head and subjected to cooling – varying applied mechanical load and constant pile length. ....	64
Table 2.7: Normalised vertical head displacements for energy piles of $D = 1$ m that are free at their head and subjected to cooling – varying applied mechanical load and constant pile length. ....	65
Table 2.8: Normalised vertical head displacements for energy piles of $D = 0.5$ m that are restrained at their head and subjected to cooling – varying applied mechanical load and constant pile length. ....	65
Table 2.9: Normalised vertical head displacements for energy piles of $D = 1$ m that are restrained at their head and subjected to cooling – varying applied mechanical load and constant pile length. ....	66
Table 3.1: Available experimental tests on single full-scale energy piles. ....	88
Table 3.2: Available centrifuge tests on single energy piles. ....	93

Table 3.3: Available laboratory tests on single energy piles.....	96
Table 3.4: Material properties used for the Class C1 and B1 (in brackets) numerical predictions. .....	107
Table 4.1: Material properties used for the numerical analysis. ....	147
Table 4.2: Parameters of interest for the analysis of energy pile groups. ....	148
Table 4.3: Dimensionless groups of parameters of interest for analysis of energy pile groups, typical values and values used in this study.....	148
Table 4.4: Values of linear thermal expansion coefficient used for addressing non-uniform soil deposits. ....	149
Table 4.5: Comparison of predicted results for a 2×2 group of energy piles. ....	177
Table 5.1: Material properties used for the numerical analyses (Rotta Loria and Laloui, 2016b). .....	201
Table 6.1: Material parameters reported by O'Neill et al. (1981) characterising the considered problem. ....	224
Table 6.2: Material parameters used to model the considered problem.....	224
Table 7.1: Values of the aspect ratio, $AR$ , for the analysed energy pile groups.....	248
Table 7.2: Material parameters for the energy piles and the soil. ....	249
Table 7.3: Equivalent pier-soil interaction parameters. ....	250
Table 7.4: Parameters for the 2×2 energy pile groups.....	250
Table 7.5: Parameters for the 3×3 energy pile groups.....	250
Table 7.6: Parameters for the 4×4 energy pile groups.....	250
Table 7.7: Parameters for the 5×5 energy pile groups.....	251



# List of Symbols

## Roman symbols

Symbol	Variable name	Unit measure
$A$	Cross-sectional area	$\text{m}^2$
$A_b$	Cross-sectional area of pile base	$\text{m}^2$
$A_c$	Cross-sectional area of concrete	$\text{m}^2$
$A_{eq}$	Equivalent cross-sectional area	$\text{m}^2$
$A_{exc}$	Plan area in which the thermal strain potential of soil is in excess of that of piles	$\text{m}^2$
$A_g$	Plan area of pile group	$\text{m}^2$
$A_p$	Cross-sectional area of pipe	$\text{m}^2$
$A_r$	Cross-sectional area of reinforcement	$\text{m}^2$
$A_s$	Area of pile shaft	$\text{m}^2$
$A_{soil}$	Plan area of soil delimiting the shape of the pile group	$\text{m}^2$
$A_{t,EP}$	Total cross-sectional area of piles	$\text{m}^2$
$A_{EP}$	Cross-sectional area of piles	$\text{m}^2$
$A_{S,bpmin}$	Minimum reinforcement area	$\text{m}^2$
$A^*$	Calibration factor	Pa
$AR$	Aspect ratio of pile group	-
$B_{slab}$	Breadth of slab	m
$B^*$	Calibration factor	Pa
$c$	Cohesion	Pa
$c_p$	Specific heat	$\text{J}/(\text{kg}^\circ\text{C})$
$c_{p,f}$	Specific heat of fluid	$\text{J}/(\text{kg}^\circ\text{C})$
$c_{p,s}$	Specific heat of solid particles	$\text{J}/(\text{kg}^\circ\text{C})$
$c_{p,soil}$	Specific heat of soil	$\text{J}/(\text{kg}^\circ\text{C})$
$c_{p,EP}$	Specific heat of pile	$\text{J}/(\text{kg}^\circ\text{C})$
$c_{E,w}$	World primary energy consumption	toe

$c_{E,w,\%}$	Proportion of world primary energy consumption	%
$cty$	Country	-
$COP$	Coefficient of Performance	-
$C^*$	Calibration factor	Pa/°C
$d_p; d_{p,in}$	Inner diameter of pipe	m
$d_{p,out}$	Outer diameter of pipe	m
$d_q$	Factor that accounts for pile depth	-
$D$	Diameter of pile	m
$D_b$	Bending rigidity per unit area	N/m
$D_{eq}$	Equivalent diameter	m
$D_{exc}$	Excess diameter	m
$D_{ijkl}$	Elastic stiffness tensor	Pa
$D_r$	Displacement ratio	-
$DOF$	Degree of freedom	-
$e_{E,w}$	World energy-related greenhouse gas emissions	-
$e_{E,w,s}$	World energy-related CO <sub>2</sub> emissions by sector and region	kg
$e_{E,w,CO_2}$	Proportion of world energy-related CO <sub>2</sub> emissions	%
$e_{E,w,\%}$	Proportion of world energy-related greenhouse gas emissions	%
$E$	Young's modulus	Pa
$E_{eq}$	Equivalent Young's modulus	Pa
$E_c$	Young's modulus of concrete	Pa
$E_d$	Design value of action or action effect	Various
$E_r$	Young's modulus of reinforcement	Pa
$E_{slab}$	Young's modulus of slab	Pa
$E_{soil}$	Young's modulus of soil	Pa
$E_{soil,b}$	Young's modulus of soil at the level of pile base	Pa
$E_{soil,m}$	Young's modulus of soil mass	Pa
$E_{soil,s}$	Young's modulus of soil around the pile shaft	Pa
$E_{EP}$	Young's modulus of pile	Pa
$E_M$	Menard pressuremeter modulus	Pa
$\bar{E}_{soil}$	Average value of Young's modulus of soil	Pa
$f_{cd}$	Design value of compressive strength of concrete	Pa
$f_{ck}$	Characteristic compressive cylinder strength of concrete	Pa
$f_{ct}$	Axial tensile strength of concrete	Pa
$f_{ctd}$	Design value of axial tensile strength of concrete	Pa
$f_{ctm}$	Mean value of axial tensile strength of concrete	Pa
$f_t$	Tensile strength of steel	Pa
$f_y$	Compressive strength of steel	Pa

$f_{yd}$	Design value of steel compressive strength	Pa
$f_{yk}$	Characteristic value of steel compressive strength	Pa
$f_M$	Friction factor	-
$F$	Resonant frequency of wire at actual time	Hz
$F_b$	Correction factor indicating the effect of bearing stratum	-
$F_0$	Resonant frequency of wire at initial time	Hz
$g_i$	Gravity vector	m/s <sup>2</sup>
$G$	Shear modulus	Pa
$G_k$	Permanent load	N
$G_{soil}$	Shear modulus of soil	Pa
$G_{soil,b}$	Shear modulus of soil at the level of pile base	Pa
$G_{soil,s}$	Shear modulus of soil around pile shaft	Pa
$h_{in}$	Convective heat transfer coefficient	W/(m °C)
$h_l$	Model depth	m
$K_b$	Slope of loading/unloading elastic branch of base load-displacement function	Pa/m
$K_g$	Gauge factor	1/Hz <sup>2</sup>
$K_h$	Head stiffness of superstructure or connected structural element	Pa/m
$K_s$	Slope of loading/unloading elastic branch of shaft load-displacement function	Pa/m
$K_{slab}$	Stiffness of slab	Pa/m
$K_{ss}$	Slab-soil stiffness ratio	-
$\bar{K}$	Average value of the relevant coefficient of lateral pressure	-
$K_0$	Coefficient of Earth pressure at rest	-
$l_{OF}$	Length of optical fibre	m
$L$	Length of pile	m
$L_{seg}$	Length of segment	m
$L_{slab}$	Length of slab	m
$\bar{L}$	Average length of pile	m
$L'$	Length of pile after the application of temperature variation	m
$n$	Porosity	-
$n_{p,EP}$	Number of energy pile projects	-
$n_{rc}$	Steel to concrete stiffness ratio	-
$n_{EP}$	Number of piles	-
$\tilde{n}_{EP}$	Number of piles along a row or a column of the pile group in plan view	-
$n_{LP}$	Number of loaded piles	-
$N$	Sectional axial force	N
$N_c, N_q, N_\gamma$	Bearing capacity factors	-
$N_c$	Proportion of sectional axial force received by concrete	N
$N_{cr}$	Axial force needed to crack the concrete	N

$N_{cr,c}$	Axial force mobilised by the concrete upon cracking	N
$N_{cr,d}$	Design value of axial force mobilised by the concrete upon cracking	N
$N_{cr,r}$	Axial force mobilised by the concrete upon cracking	N
$N_d^{th}$	Design value of thermally induced axial force	N
$N_{hl}$	Correction factor for effect of finite layer depth	-
$N_r$	Proportion of sectional axial force received by reinforcement	N
$N_{E,d}$	Design value of acting axial force	N
$N_{E,d}^*$	Design value of acting axial force	N
$N_R$	Resisting axial force	N
$N_{R,d}$	Design value of resisting axial force	N
$N_{R,d}^*$	Design value of resisting axial force	N
$N_v$	Correction factor for effect of Poisson's ratio	-
$Nu$	Nusselt number	-
$Nu_{turb}$	Nusselt number under turbulent flow conditions	-
$p_w$	Pore water pressure	Pa
$P$	Vertical or axial mechanical load	N
$P_b$	Vertical or axial mechanical load applied at pile base	N
$P_d$	Design value of vertical or axial mechanical load	N
$P_k$	Characteristic value of vertical or axial mechanical load	N
$P_p$	Wetted perimeter of pipe cross-section	m
$P_{ref}$	Reference value of vertical mechanical load	N
$P_{E,w}$	World primary energy supply	toe
$P_{E,w,\%}$	Proportion of world primary energy supply	%
$Pr$	Prandtl number	-
$pop$	World population	-
$q_b$	Ultimate base resistance	Pa
$q_{b,mob}$	Mobilised base resistance	Pa
$q_s$	Ultimate shaft resistance	Pa
$q_{s,mob}$	Mobilised shaft resistance	Pa
$\dot{q}_l$	Heat flux per unit length	W/m
$Q_{b,mob}$	Mobilised base capacity	N
$Q_{b,mob}^m$	Mechanical contribution of mobilised base capacity	N
$Q_{b,mob}^{th}$	Thermal contribution of mobilised base capacity	N
$Q_k$	Variable load	N; °C
$Q_{k,1}$	Dominant variable action or action effect	N; °C
$Q_{b,d}$	Design value of base capacity	N
$Q_{s,d}$	Design value of shaft capacity	N
$Q_{s,mob}$	Mobilised shaft capacity	N

$Q_u$	Ultimate capacity	N
$Q_{u,d}$	Design value of ultimate capacity	N
$Q_{s,mob}^m$	Mechanical contribution of mobilised shaft capacity	N
$Q_{s,mob}^{th}$	Thermal contribution of mobilised shaft capacity	N
$Q_{s,mob,down}^{th}$	Thermal contribution of mobilised shaft capacity below null point of shear stress	N
$Q_{s,mob,up}^{th}$	Thermal contribution of mobilised shaft capacity above null point of shear stress	N
$\dot{Q}_{inst}$	Installed power	W
$r$	Radial coordinate	m
$\tilde{r}$	Specific radial distance	m
$r_m$	Magical radius	m
$r_{p,in}$	Inner radius of pipe	m
$r_{p,out}$	Outer radius of pipe	m
$R$	Radius of pile	m
$R_d$	Design value of resistance	Various
$R_{exc}$	Excess radius	m
$R_s$	Settlement ratio	-
$R_1$	Radial distance in Mindlin's solution	m
$R_2$	Radial distance in Mindlin's solution	m
$Re$	Reynolds number	-
$s$	Centre-to-centre distance between piles (spacing)	m
$s_q$	Shape factor	-
$s_t$	Transition distance	m
$S$	Surface	m <sup>2</sup>
$SFP$	Seasonal Factor of Performance	-
$t$	Time	s
$t_{slab}$	Thickness of slab	m
$t_w$	Thickness of wall	m
$t_0$	Initial value of time/reference time	s
$T$	Actual value of temperature	°C
$T_d$	Design value of temperature	°C
$T_{ext}$	Temperature at outer pipe side	°C
$T_f$	Actual value of fluid temperature	°C
$T_k$	Characteristic value of temperature	°C
$T_{EP}$	Actual value of temperature of pile	°C
$T_{in}$	Inflow fluid temperature	°C
$T_{out}$	Outflow fluid temperature	°C
$T_{soil}$	Actual value of temperature of soil	°C
$\bar{T}$	Average value of temperature	°C

---

$\bar{T}_{in}$	Average value of inflow fluid temperature	°C
$\bar{T}_{soil}$	Average value of soil temperature	°C
$T_R$	Actual temperature at pile radius	°C
$T_0$	Initial temperature	°C
$T_\infty$	Temperature at far field	°C
$u$	Horizontal/radial displacement	m
$v$	Horizontal displacement	m
$v_f$	Fluid velocity in relevant direction of pipe (e.g., axial)	m/s
$v_i$	Fluid velocity vector	m/s
$\bar{v}_f$	Average value of fluid velocity in relevant direction of pipes (e.g., axial)	m/s
$w$	Vertical displacement	m
$w^m$	Vertical displacement caused by a mechanical load	m
$w^{th}$	Vertical displacement caused by a thermal load	m
$w^{m+th}$	Vertical displacement caused by mechanical and thermal loads	m
$w_d^m$	Design value of vertical displacement caused by a mechanical load	m
$w_d^{th}$	Design value of vertical displacement caused by a thermal load	m
$w_d^{m+th}$	Design value of vertical displacement caused by mechanical and thermal loads	m
$\bar{w}$	Average value of vertical displacement	m
$w^*$	Vertical displacement of a single source pile in a group	m
$w^1$	Unitary vertical displacement	m
$w^{1,m}$	Unitary vertical displacement caused by a mechanical load	m
$w^{1,th}$	Unitary vertical displacement caused by a thermal load	m
$w_f^{th}$	Vertical displacement under free thermal expansion conditions	m
$w_{qb/2}$	Vertical base displacement mobilised for $q_b/2$	m
$w_{qs/2}$	Vertical shaft displacement mobilised for $q_s/2$	m
$W$	Weight of pile	N
$x$	Horizontal coordinate	m
$y$	Horizontal coordinate	m
$z$	Vertical coordinate or depth	m
$\bar{z}$	Specific vertical coordinate	m
$z_{NP,w}$	Depth of null point of vertical displacement	m
$z_{NP,\tau}$	Depth of null point of shear stress	m

## Greek symbols

Symbol	Variable name	Unit measure
$\alpha$	Linear thermal expansion coefficient	1/°C; $\mu\epsilon/^\circ\text{C}$
$\alpha_d$	Thermal diffusivity	m <sup>2</sup> /s
$\alpha_{eq}$	Equivalent linear thermal expansion coefficient	1/°C; $\mu\epsilon/^\circ\text{C}$
$\alpha_r$	Rheological coefficient	-
$\alpha_{soil}$	Linear thermal expansion coefficient of soil	1/°C; $\mu\epsilon/^\circ\text{C}$
$\alpha_{soil,b}$	Linear thermal expansion coefficient of soil at the level of pile base	1/°C; $\mu\epsilon/^\circ\text{C}$
$\alpha_{soil,s}$	Linear thermal expansion coefficient of soil around the pile shaft	1/°C; $\mu\epsilon/^\circ\text{C}$
$\alpha_{wire}$	Linear thermal expansion coefficient of wire	1/°C; $\mu\epsilon/^\circ\text{C}$
$\alpha_{EP}$	Linear thermal expansion coefficient of pile	1/°C; $\mu\epsilon/^\circ\text{C}$
$\beta_{kl}$	Thermal expansion coefficient vector	1/°C; $\mu\epsilon/^\circ\text{C}$
$\gamma_G$	Partial factor of permanent action or action effects	-
$\gamma_Q$	Partial factor of variable action or action effect	-
$\gamma_{Q,1}$	Partial factor of the dominant variable action or action effect	-
$\gamma_{Q,i}$	Partial factors of the $i$ -th variable actions or action effects	-
$\delta; \delta'$	Pile-soil interface angle of shear strength	°
$\lambda$	Thermal conductivity	W/(m °C)
$\lambda_{eff}$	Effective thermal conductivity	W/(m °C)
$\lambda_f$	Thermal conductivity of fluid	W/(m °C)
$\lambda_{lt}$	Load-transfer coefficient	-
$\lambda_p$	Thermal conductivity of pipe	W/(m °C)
$\lambda_s$	Thermal conductivity of solid particles	W/(m °C)
$\lambda_{soil}$	Thermal conductivity of soil	W/(m °C)
$\lambda_{EP}$	Thermal conductivity of pile	W/(m °C)
$\Lambda$	Pile-soil stiffness ratio	-
$\mu$	Dynamic viscosity of fluid	Pa s
$\mu_E$	Ratio between Young's moduli	-
$\epsilon_{kl}$	Strain tensor	-; $\mu\epsilon$
$\epsilon_r$	Radial strain	-; $\mu\epsilon$
$\epsilon_z$	Vertical strain	-; $\mu\epsilon$
$\epsilon_b^{th}$	Strain under blocked thermal expansion conditions	-; $\mu\epsilon$
$\epsilon_f^{th}$	Strain under free thermal expansion conditions	-; $\mu\epsilon$
$\epsilon_{f,eq}^{th}$	Strain under free thermal expansion conditions of equivalent pier	-; $\mu\epsilon$
$\epsilon_{f,EP}^{th}$	Strain under free thermal expansion conditions of pile	-; $\mu\epsilon$

$\varepsilon_{f,soil}^{th}$	Strain under free thermal expansion conditions of soil	-; $\mu\varepsilon$
$\varepsilon_o^{th}$	Observed thermally induced strain	-; $\mu\varepsilon$
$\bar{\varepsilon}_f^{th}$	Average strain under free thermal expansion conditions	-; $\mu\varepsilon$
$\bar{\varepsilon}_r$	Average value of radial strain	-; $\mu\varepsilon$
$\bar{\varepsilon}_z$	Average value of vertical strain	-; $\mu\varepsilon$
$\bar{\varepsilon}_o^{th}$	Average observed thermally induced strain	-; $\mu\varepsilon$
$\theta$	Angular coordinate	m
$\rho$	Bulk density	kg/m <sup>3</sup>
$\rho_f$	Density of fluid	kg/m <sup>3</sup>
$\rho_r$	Reinforcement ratio	-
$\rho_{r,eff}$	Effective reinforcement ratio	-
$\rho_{r,min}$	Minimum reinforcement ratio	-
$\rho_s$	Density of solid particles	kg/m <sup>3</sup>
$\rho_{soil}$	Bulk density of soil	kg/m <sup>3</sup>
$\rho_{EP}$	Bulk density of pile	kg/m <sup>3</sup>
$\sigma; \sigma_z; \sigma_{zz}$	Total vertical stress	Pa
$\sigma_{vb}$	Total vertical stress at the level of pile base	Pa
$\sigma_b^{th}$	Value of thermally induced stress under blocked conditions	Pa
$\sigma_{b,d}^{th}$	Design value of thermally induced tensile vertical stress	Pa
$\sigma_{ij}$	Total stress tensor	Pa
$\sigma_o^{th}$	Observed value of thermally induced stress	Pa
$\sigma'_{vb}$	Vertical effective stress at the level of pile base	Pa
$\bar{\sigma}_d$	Average value of population standard deviation	°C; m/s
$\bar{\sigma}'_v$	Average value of <i>in situ</i> vertical effective stress	Pa
$\bar{\sigma}_z$	Average value of total vertical stress	Pa
$\bar{\sigma}_o^{th}$	Average observed thermally induced stress	Pa
$\tau; \tau_z; \tau_{rz}$	Shear stress	Pa
$\zeta$	Stiffness reduction factor	-
$\nu$	Poisson's ratio	-
$\nu_{slab}$	Poisson's ratio of slab	-
$\nu_{soil}$	Poisson's ratio of soil	-
$\nu_{soil,b}$	Poisson's ratio of soil at the level of pile base	-
$\nu_{soil,s}$	Poisson's ratio of soil around pile shaft	-
$\nu_{EP}$	Poisson's ratio of pile	-
$Y$	Coefficient relating the average temperature variation in the soil to that in the pile	-
$X$	Soil-pile thermal expansion coefficient ratio	-
$\psi_0$	Factor for combination value of a variable action	-
$\psi_1$	Factor for frequent value of a variable action	-



$\psi_2$	Factor for quasi-permanent value of a variable action	-
$\Omega$	Displacement interaction factor/pile-soil-pile interaction factor/corrected interaction factor	-
$\Omega^m$	Displacement interaction factor for piles subjected to mechanical loads	-
$\Omega^{th}$	Displacement interaction factor for piles subjected to thermal loads	-
$\tilde{\Omega}$	Pile-soil interaction factor/approximate interaction factor	-
$\Omega_{h_l/L \rightarrow \infty}$	Displacement interaction factor for $h_l/L \rightarrow \infty$	-
$\Omega_{\nu_{soil}=0.3}$	Displacement interaction factor for $\nu_{soil} = 0.3$	-

## Operators, functions and counters

Symbol	Name
$d()$	Increment operator
$erfc()$	Complementary Gaussian error function
$\partial$	Derivative
$\Delta$	Difference operator
$\Sigma$	Sum
$\ln()$	Natural logarithm
$\nabla$	Gradient operator
$\nabla \cdot ()$	Divergence operator
$i, j, k, l, m, n$	Counters



# Introduction

## Scope, motivation and challenges

This doctoral thesis focuses on the thermo-mechanical performance of an innovative, multifunctional technology that can be used for energy transfer applications as well as for providing structural support to any type of built environment, i.e., energy piles. Energy piles couple the structural support role of conventional geostructures to the role of conventional geothermal heat exchangers in an unprecedented technology. The operation of energy piles can provide reinforcement to soils for supporting any type of superstructure and at the same time can supply energy for (i) heating and cooling purposes to reach comfort levels in the built environment, (ii) the production of hot water for anthropogenic uses, and (iii) prevention of the icing of pavements and decks of infrastructures.

The multifunctional operation of energy pile technology, which harvests renewable geothermal energy, provides tremendous potential for following international agreements for the development of a low-carbon built environment. From a broader perspective, energy piles can contribute to so-called “sustainable development”. Despite this potential, relatively limited applications of energy piles are currently observed because of several challenges.

The twofold role of energy piles as structural supports and geothermal heat exchangers involves different types of loads, i.e., mechanical loads and thermal loads, applied to such geostructures. These loads pose unprecedented challenges to engineers because they include variations in the temperature, stress, deformation and displacement fields in the subsurface. These variations govern the thermal and mechanical behaviour and performance of the energy piles, with a strong impact on the energy, geotechnical and structural response of such foundations. The abovementioned requires multidisciplinary and integrated competences to perform the analysis, design and application of energy piles. This doctoral dissertation addresses the first two aspects of the aforementioned problem.

Over the last two decades, a large amount of research has been performed to characterise the thermo-mechanical behaviour and performance of energy piles. Several analysis and design tools have been proposed to address this behaviour and performance. Design guidance has been proposed to enhance the worldwide application of energy piles. Several full-scale *in situ* tests, centrifuge experiments, laboratory tests and numerical analyses have been performed in an attempt to provide both experimental and theoretical knowledge in this context. However, prior to this research, three main challenges have arisen in the scope of energy piles:

1. Almost all of the research performed regarding energy piles has considered these geostructures as if they were single isolated elements. However, energy pile foundations do not consist of a single energy pile but of a group of energy piles that function as structural supports and geothermal heat exchangers. A large body of evidence available for conventional piles subjected to only mechanical loads has proven that when the piles are located sufficiently close to each other, different mechanical behaviour of the piles may be expected compared to when the piles are located sufficiently far from each other. The reason for this phenomenon is that group effects and interactions among the piles occur because of the presence and loading (e.g.,

mechanical) of the neighbouring piles. Prior to this work, there was limited knowledge, if available, on the thermo-mechanical behaviour and performance of energy pile groups subjected to thermal and mechanical loads as well as on the potential presence of group effects caused by the loading (e.g., thermal) of energy piles.

2. All of the available analysis and design tools have addressed the behaviour of single energy piles but not the behaviour of energy pile groups, except for the finite element method in some applications. However, although the latter method provides the most rigorous solutions, the computing time and expertise required to run finite element analyses are often considerable and daunting, especially for engineering purposes. Various simplified (approximate) models and methods available for conventional piles subjected to only mechanical loads have proven to be a remarkable capability in capturing the behaviour of these geotechnical structures in a broad range of situations. For this reason, these tools have become key in conventional pile analysis and design. Prior to this work, no simplified models and methods were available to address the potential influence and related response of energy pile groups to thermal (and mechanical) loads for analysis and design purposes.
3. All of the design guidance for energy piles has been fragmented because it has been proposed by different national societies or institutions. Additionally, the guidance has been limited because some institutions employ no or incorrect performance-based procedures. However, the use of performance-based design procedures is essential in the framework of the modern analysis and design of structures because it yields the best trade-offs between performance and economic savings. The European Standards, often called the Eurocodes, currently address the effects of mechanical and thermal loads on the geotechnical and structural behaviour and performance of structures such as piles but lack recognised rules that can be straightforwardly or suitably applied to energy piles. Prior to this work, no comprehensive summary about the role of thermal and mechanical loads in the geotechnical and structural performance and performance-based design of energy piles was available.

## **Contribution**

To address the three aforementioned challenges, this doctoral research has been devoted to investigating the thermo-mechanical behaviour and performance of energy pile groups with a threefold goal:

1. To provide experimental and theoretical knowledge about the thermo-mechanical response of energy pile groups to thermal and mechanical loads. These investigations focus on (i) the potential presence and impact of group effects caused by thermal loads, (ii) the interplay of these loads with mechanical loads and (iii) the impact of mechanical and thermal loads on the geotechnical and structural behaviour of energy piles.
2. To present consistent theoretical approaches based on the sound principles of mechanics for predicting the vertical deformation of energy pile groups subjected to thermal and mechanical loads in a wide range of design cases. This effort is focussed on (i) the development of parametric solutions summarised in design charts and (ii) the proposition and validation of two semi-analytical models addressing the considered problem.

3. To summarise and demonstrate the effect of thermal and mechanical loads on the geotechnical and structural performance of energy piles. This study is focussed on (i) the role of thermal loads in the geotechnical and structural performance-based design of energy piles at ultimate limit states and (ii) the role of thermal loads in the performance-based design of energy piles at serviceability limit states.

### Solution approach

The results presented in this doctoral thesis are derived from investigations based on the development of (i) full-scale *in situ* tests, (ii) coupled, multidimensional numerical analyses and (iii) analytical models (cf., Figure I).

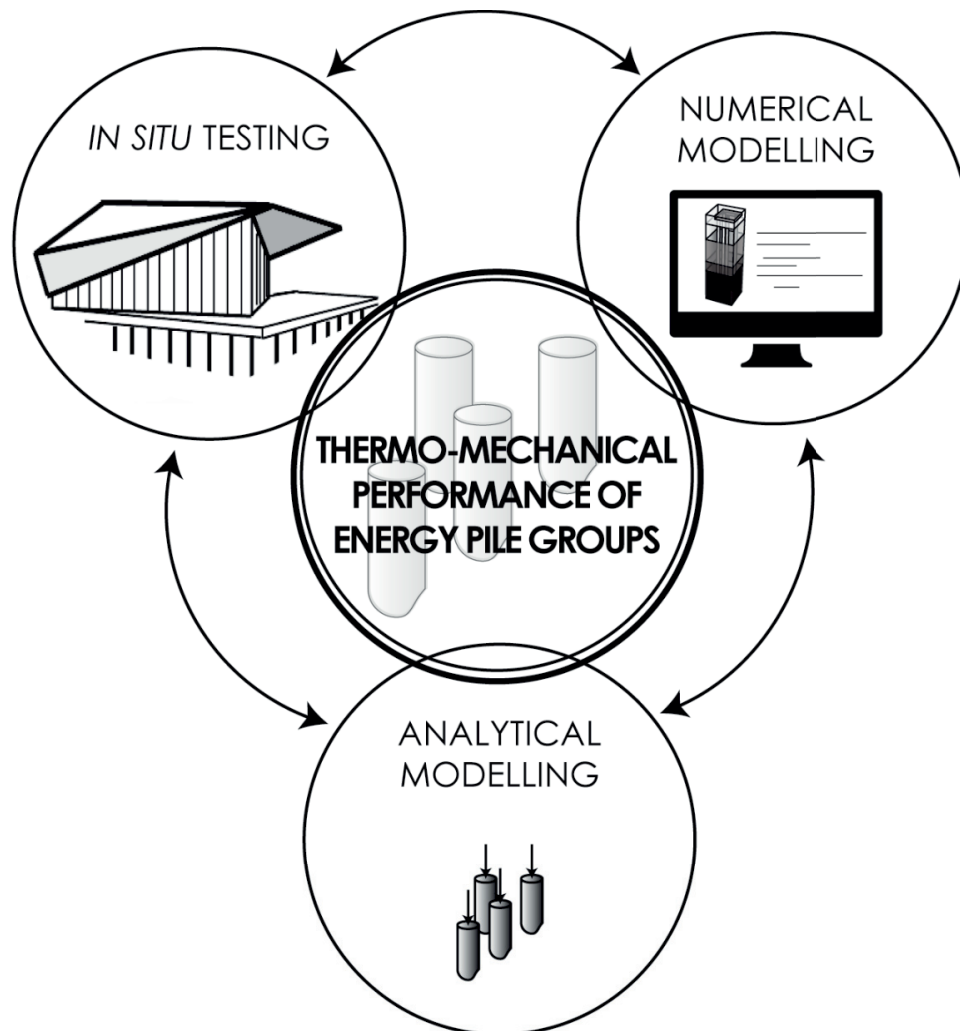


Figure I: Solution approach employed to address the challenges of this doctoral research.

## Structure and features of this doctoral thesis

The structure of this doctoral dissertation is as follows:

- Chapter 1, entitled “Energy geostructures”, presents an introduction to the technology of energy geostructures with a focus on energy piles.
- Chapter 2, entitled “The role of thermal loads in the geotechnical and structural performance of energy piles”, addresses challenge 3. In this chapter, the occurrence of group effects caused by thermal loads is postulated. While an extensive treatment of the considered topic is presented in the following chapters of this thesis, such a chapter is useful prior to the others because it proposes a sound summary of the effect of thermal and mechanical loads on the thermo-mechanical behaviour and performance of energy piles.
- Chapter 3, entitled “Thermally induced group effects among energy piles”, addresses challenge 1.
- Chapters 4, 5, 6 and 7, entitled “The interaction factor method for energy pile groups based on design charts”, “The interaction factor method for energy pile groups based on analytical models”, “Non-linear soil deformation and energy pile interaction” and “The equivalent pier method for energy pile groups”, respectively, address challenge 2.
- Chapter 8, entitled “Conclusions and perspectives”, summarises the contributions provided by this doctoral research and presents future perspectives and developments for the urgent need in the field of energy piles and energy geostructures in general.
- Appendix A, entitled “*In situ* testing equipment”, describes the monitoring instrumentation used for the *in situ* testing activities presented in Chapter 3.
- Appendix B, entitled “Mathematical formulation employed in the finite element analyses”, presents the mathematical formulation employed in the multidimensional, thermo-mechanical finite element analyses employed in Chapters 3-7 as an analysis and validation tool.

Along with the abovementioned research activities about the thermo-mechanical behaviour and performance of energy pile groups, other research activities were performed during this doctoral educational path. These activities investigated the thermo-mechanical behaviour and performance of single energy piles and energy sheet pile walls as well and involved numerical modelling and centrifuge testing. Based on the aforementioned developments, a total of fourteen co-authored research papers and fourteen conference papers and extended abstracts were produced during this doctoral educational path (cf., *Curriculum vitae*) and have been published, or are to be published, in international journals or conference proceedings, respectively.

The adopted sign convention in this manuscript considers compressive stresses, contractive strains and downward displacements (i.e., settlements) to be positive.

## **Chapter 1**

# **Energy geostructures**

In a world increasingly characterised by environmental pollution and depletion of non-renewable energy resources, the conceptual development, analysis, design and application of environmentally friendly technologies to sustain the population needs and progress goals is of crucial importance. Energy geostructures are an innovative, multifunctional technology that can be used to address the aforementioned challenge. Employing geostructures (e.g., piles, walls, tunnels, etc.) for structural support purposes represents an historical means to meet human activity. Employing soils and rocks as reservoirs for the extraction and storage of heat also represents a means to meet human activity since ancient times. Energy geostructures couple the structural support role of ground structures with the role of ground heat exchangers harvesting renewable energy for the heating and cooling of the built environment. This work addresses the technology of energy geostructures, with a particular focus on energy piles, as a breakthrough means for contributing to the sustainability of human activity via the establishment of low-carbon buildings and infrastructures. The following work aims in particular at: (i) introducing the world energy sources and consumption, with a focus on geothermal energy and geothermal systems; (ii) expanding on the technology of energy geostructures with regards to the physical principle, the technical aspects and the typical operations involved with this technology; and (iii) presenting the typical, unprecedented challenges involved in the analysis and design of energy geostructures such as energy piles. The following arguments contribute with the Introduction in justifying the motivation and the need of undertaking this doctoral research.

### **1.1 Anthropogenic development and the energy question**

#### **1.1.1 World population**

The world population continues to markedly grow since the 20<sup>th</sup> century. It currently counts 7.6 billion living human individuals and is expected to continue to grow in the next decades (cf., Figure 1.1). Different scenarios of world population increase can be considered for the future, but the median trend currently predicted approximately accounts for up to 9.8 billion living human individuals by 2050 and 11.2 billion living human individuals by 2100 (United Nations, 2017).

### 1.1.2 Energy forms and classification of energy sources

Energy, which can be appreciated in various forms, represents a key source to meeting human activity needs and development, and can be quantified with different unit measures (cf., Table 1.1). One typical classification of energy sources is based on their availability in nature. This classification includes *primary energy sources* and *secondary energy sources*. Primary energy sources, such as fossil fuels, mineral fuels, solar energy, geothermal energy, wind energy, tidal energy and biomass sources, represent an energy form that has not been subjected to any conversion and is available in nature. Secondary energy sources or energy carriers, such as electrical energy, refined fuels and synthetic fuels, represent an energy form that has been transformed from primary energy sources and is not available in nature.

Depending on whether primary energy sources can renew themselves at a sufficient rate in human time frames or cannot, one further classification can be employed. This classification includes *renewable energy sources* and *non-renewable energy sources*. Renewable energy sources, such as solar energy, geothermal energy, wind energy, tidal energy and biomass sources can renew themselves at a sufficient rate in human time frames. Non-renewable energy sources, such as fossil fuels (e.g., oil, coal and natural gas) and mineral fuels (e.g., natural uranium), cannot renew themselves at a sufficient rate in human time frames.

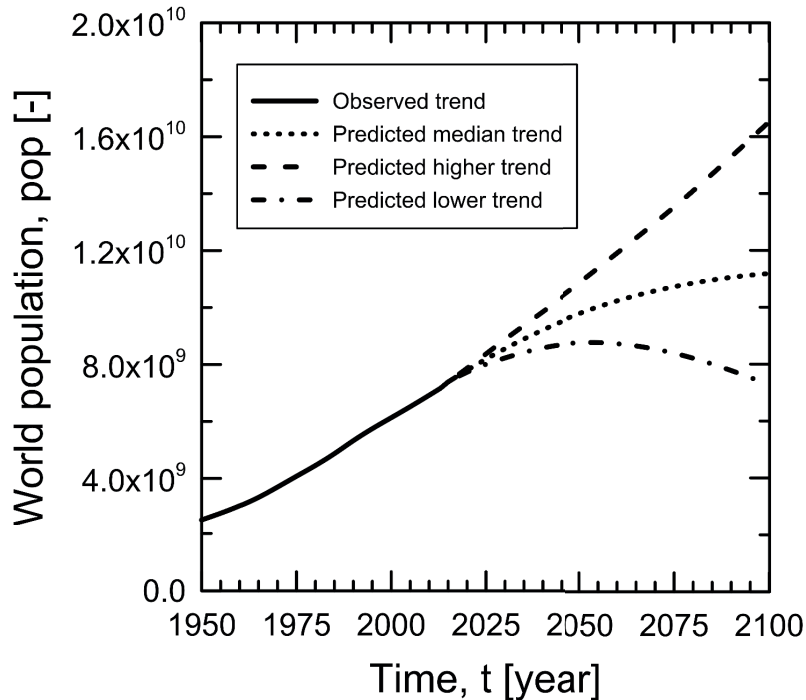


Figure 1.1: World population trend (data from United Nations (2017)).



Table 1.1: Some energy-related unit measures.

Name	Symbol	Description
Joule	[J]	The basic energy unit of the metric system (SI)
Calorie	[cal]	Historically, 1 calorie is the amount of heat required to raise the temperature of 1 gram of water by 1°C, from 14.5 °C to 15.5 °C. More recently, the calorie has been defined in terms of the Joule (thermo-chemical calorie: 1 cal = 4.184 J)
Watt	[W] or [J/s]	A derived unit of power that expresses 1 Joule per second and can be used to quantify the rate of energy transfer
Kilowatt-hour	[kWh]	The standard unit of electricity production and consumption (1 kWh = $3.6 \cdot 10^6$ J)
Gigatonne of oil equivalent	[Gtoe]	An energy equivalence for oil (1 Gtoe = 41.868 EJ)

### 1.1.3 World energy consumption and supply

Various are the uses of energy by human civilisation and associated to these uses there is always an energy supply. Depending on the stage of the utilisation or production of energy, three different definitions are usually employed to characterise the use of energy (as well as the energy itself), that is, *primary energy consumption*, *final energy consumption* and *net energy consumption*, and one definition to characterise the supply of energy, that is, *primary energy supply*. Primary energy consumption refers to the direct use or supply at the source of energy that has not been subjected to any conversion or transformation process. This energy is often termed primary energy or crude energy as well. In most cases, however, energy cannot be used without conversion or transformation processes and for this reason it is refined in the so-called final energy. The final energy consumption represents the total energy consumed by end users (e.g., the building sector, the industry sector, etc.), excluding the energy that is used by the energy sector itself. In the context of constructions, this term is usually associated with the amount of energy supplied that is necessary to run the generator of cold and heat. From the final energy to the net or effective energy that is eventually used, however, there are in many instances various losses associated with the use of devices for further refining, storing or delivering energy. These losses comprise (i) generation losses, (ii) storage losses, (iii) distribution losses and (iv) output losses, and characterise the so-called net energy. The net energy consumption represents the consumption of energy in its final desired form, usually drawn from a consuming device. In the context of constructions, this term is usually associated with the thermal energy to be delivered to, or extracted from, a conditioned space by a heating or cooling system to maintain the set-point temperature during a given period of time for the comfort of the occupants. Often, the consumption of final energy is termed, although inappropriately, energy demand. In reality, energy consumption and demand are two related, yet different, variables. The first one refers to the quantity of energy to add or remove in a space, whereas the last one is the immediate rate of that consumption, i.e., the power at a particular instant in time. For this reason, final energy consumption is measured in kilowatt-hours, whereas the energy demand, i.e., the rate of that consumption, is measured in kilowatts.

In the European Union and in developed countries such as the United States, three dominant end users characterise the final energy consumption since recent decades: the building sector, the industry sector and the transportation sector. In 2015, these three sectors contributed to the total final energy consumption of the European Union by 25.4%, 25.3% and 33.1%, respectively (cf., Figure 1.2) (Eurostat, 2017). In Switzerland, as in many other developed countries, approximately 60 to 85% of the final energy consumption associated with the building sector is for space conditioning and the production of hot water (Kemmler et al., 2013) (cf., Figure 1.3).

Along with the aforementioned statistics, the world final energy consumption and primary energy supply continue to rise to meet the increase in world population and the expansion of economies (cf., Figure 1.4 and Figure 1.5) (International Energy Agency, 2016c). Historically, the global energy market has been, and is still, dominated by the combustion of fossil fuels, i.e., non-renewable primary energy sources. In recent years (since the mid-20<sup>th</sup> century), fossil fuels have met at least 60% of the final energy consumption and at least 80% of the primary energy supply (cf., Figure 1.4 and Figure 1.5).

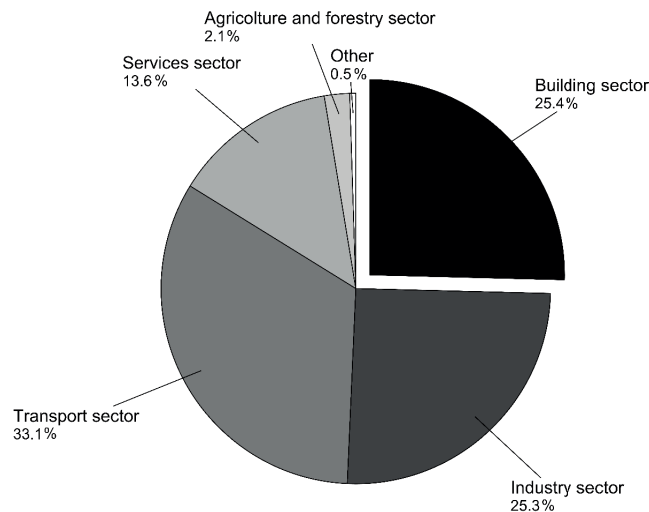


Figure 1.2: Final energy consumption shares by end users in the European Union in 2015 (data from Eurostat (2017)).

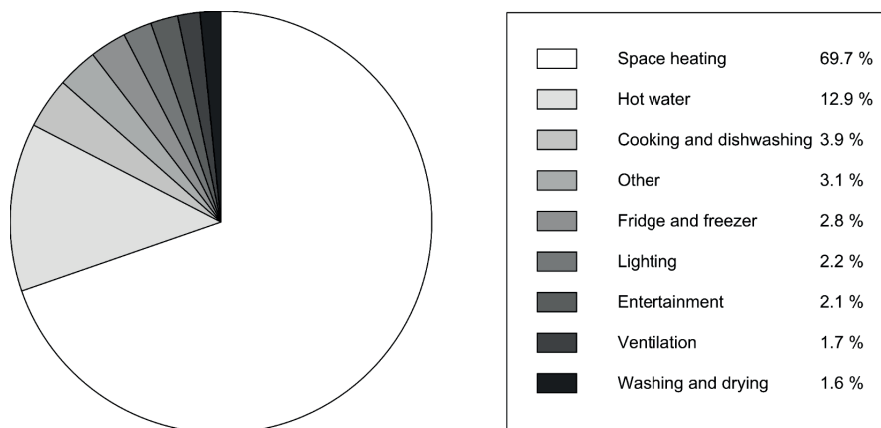


Figure 1.3: Final energy consumption in the Swiss building sector in 2012 (data from Kemmler et al. (2013)).

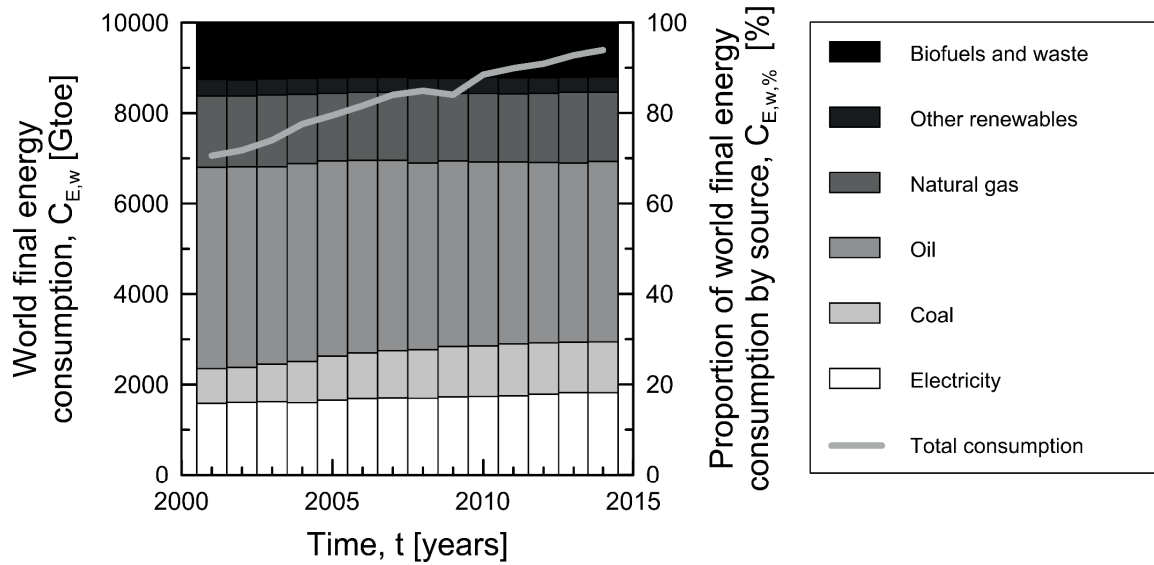


Figure 1.4: World final energy consumption from 2000 to 2014 (data from International Energy Agency (2016c)).

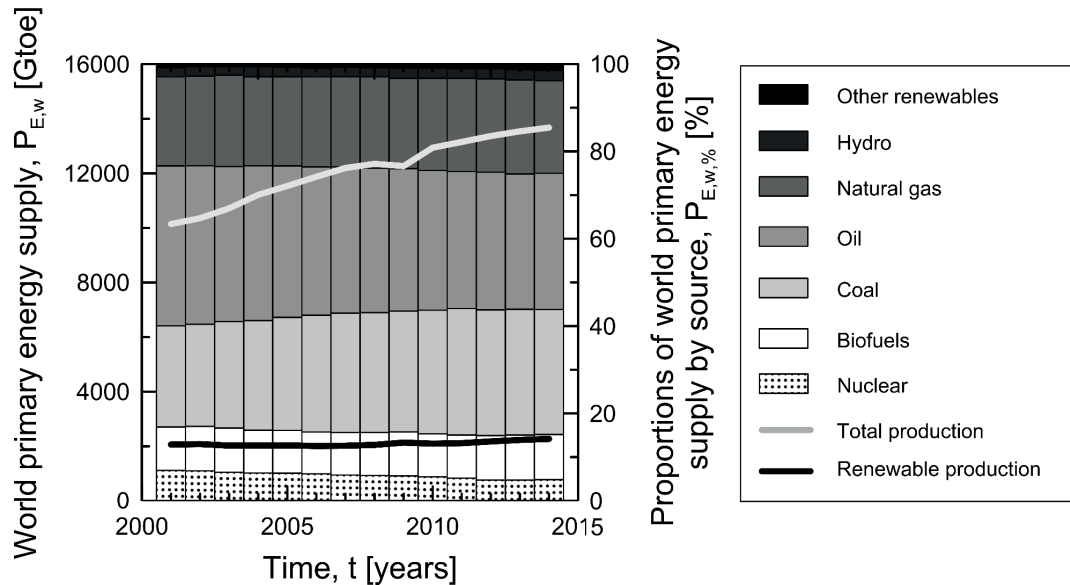


Figure 1.5: World primary energy supply from 2000 to 2014 (data from International Energy Agency (2016c)).

### 1.1.4 Consequences

The historical use of non-renewable energy sources, often unregulated, poorly regulated, inefficient or overly exploited, in contrast to renewable energy sources, has caused, without being limited to, two consequences: (i) the increase in greenhouse gas emissions and (ii) the depletion of non-renewable energy sources.

Greenhouse gas emissions are caused to a substantial amount by fossil fuels combustion. Global dependence on fossil fuels has led to the release of over 1100 Gt of CO<sub>2</sub> in the atmosphere since the

mid-19<sup>th</sup> century to 2007 (Sims et al., 2007), amount that continued to increase up to a first stabilisation in 2014 (International Energy Agency, 2016a). Over 90% of energy-related emissions are carbon dioxide (CO<sub>2</sub>) from fossil fuels combustion (cf., Figure 1.6), the 20% of which can be associated to the building sector, both in developed and developing countries (International Energy Agency, 2015) (cf., Figure 1.7).

Two problems associated with fossil fuels combustion and greenhouse gas emissions are that they represent the most important source of air (and environment) pollutant emissions deriving from anthropogenic development (International Energy Agency, 2016b) and are considered to be the dominant cause of the observed climate change and global warming since the mid-20<sup>th</sup> century (IPCC, 2013), respectively. One problem associated with the depletion of non-renewable energy sources is that, within approximately a century, resorting to these sources will not be technically and economically convenient anymore in many cases (IPCC, 2013).

All of the aforementioned problems have a profound impact on the society, the economy, the politics and the environment. Resorting to renewable energy sources is an essential and effective solution to these problems.

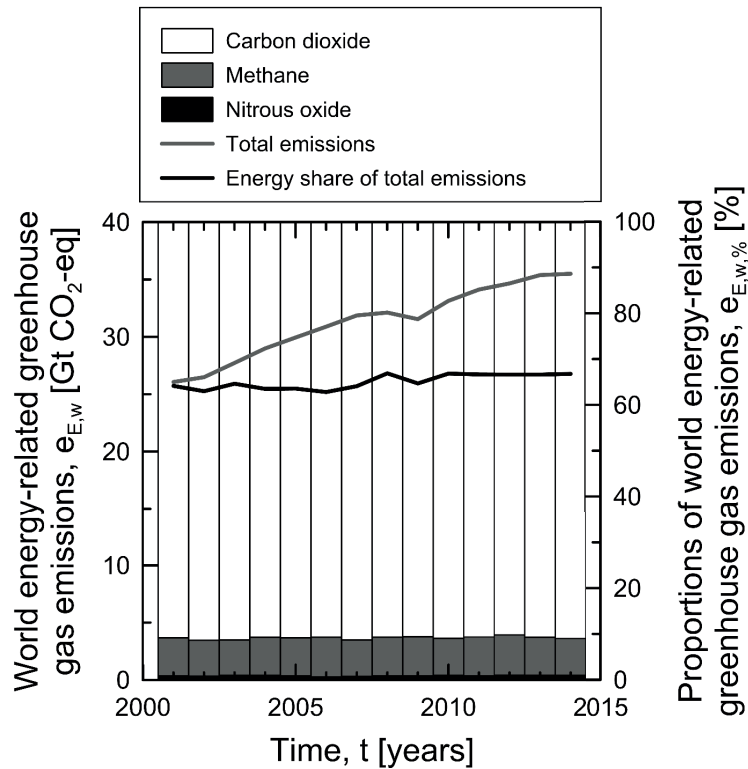


Figure 1.6: World anthropogenic energy-related greenhouse gas emissions by type (data from International Energy Agency (2015)).

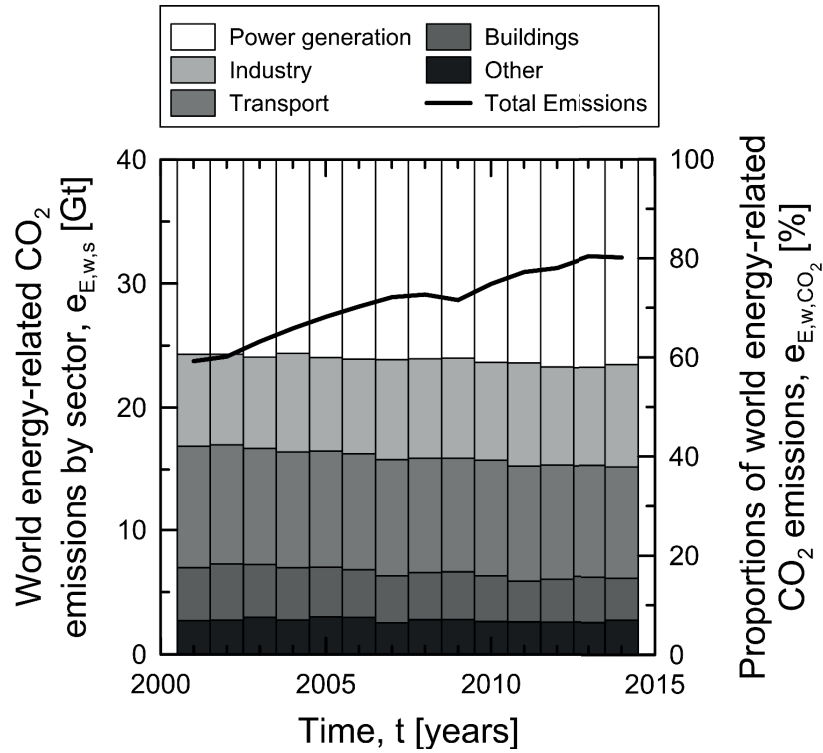


Figure 1.7: World energy-related CO<sub>2</sub> emissions by sector (data from International Energy Agency (2015)).

### 1.1.5 Perspectives

Many are the initiatives, policies, regulations and agreements at the national and international levels that are being promoted and established to target a development that sustains human needs and progress goals with a limited impact on the environment, i.e., a *sustainable development* (see, e.g., Magee et al. (2013)). Undoubtedly, because of the noteworthy influence of the building sector on energy consumption, non-renewable energy exploitation and greenhouse gas emissions, developing buildings and infrastructures characterised by (i) integrated passive design strategies (i.e., approaches and technologies employing ambient energy sources such as daylighting, natural ventilation and solar energy, instead of purchased energy sources like electricity or natural gas to meet people's comfort in the built environment), (ii) high performance building envelopes and energy efficient heating, ventilation and air conditioning (HVAC) systems, as well as lighting and appliances, and (iii) technologies harvesting on-site renewable energy sources can represent a major contribution to a sustainable development. An environment characterised by the aforementioned features (i)-(iii) is usually termed “low-carbon built environment”.

The Energy Performance of Buildings Directives (Energy Performance of Buildings Directive, 2002; Energy Performance of Buildings Directive, 2010), the Carbon Neutral Design Project and the ASHRAE Vision 2020 represent examples of key directives and initiatives for the development of a low-carbon built environment. The goal of the referenced directives and initiatives is to require (or to foster) the design and construction of so-called “nearly zero-energy buildings”, “carbon neutral buildings” and “net zero energy buildings”, respectively, in the years to come. For example, the Energy Performance of Buildings Directives require all new public buildings constructed in the European

Union to be nearly zero-energy from 2018. At the same time, all new buildings should be nearly zero-energy by the end of 2020 following the same EU Directives. The purpose is to develop buildings with significantly reduced energy consumption combined with the increased use of low-carbon energy sources to meet this consumption.

Based on the aforementioned aspects, it appears abundantly clear that the conceptual development, analysis, design and application of environmental friendly technologies harvesting on-site renewable energy sources for targeting the supply of heating and cooling energy to the built environment (i.e., aspect (iii)) represent crucial contributions to a sustainable development.

## **1.2 Geothermal energy**

### **1.2.1 Origin**

Geothermal energy is the natural thermal energy contained in the Earth subsurface. This natural heat results from (i) the formation of the planet, (ii) the radioactive decay of minerals and (iii) the solar energy absorbed at the surface. It is contained in approximately  $1.084 \cdot 10^{21}$  cubic metres of rocks and metallic alloys located in the Earth subsurface (Lee et al., 2007). 99% of this volume is characterised by a temperature higher than 1000 °C, while only 0.1% by a temperature lower than 100 °C (Barbier, 2002).

### **1.2.2 Geothermal gradient**

The temperature field in the subsurface is typically sensitive to atmospheric conditions within the first 10-15 m (cf., Figure 1.8), being usually strongly influenced by daily (day-night) temperature fluctuations and more or less markedly by seasonal temperature fluctuations. Below this region, the temperature remains relatively stable throughout the year, i.e., between 10 °C and 21 °C depending on the latitude, and is approximately equal to the mean annual outside air temperature. Therefore, the ground tends to be warmer than the atmosphere during winter and cooler during summer, a generalisation that applies for most locations around the world regardless of geology (Narsilio et al., 2014). From the aforementioned values, the temperature increases with depth in the Earth crust (Barbier, 2002). An average geothermal gradient of approximately 3 °C per 100 m of depth characterises Earth subsurface down to the upper mantle. This gradient can vary depending on the location from values of 1 °C per 100 m in ancient continental zones of the Earth crust to values of 10 °C per 100 m in areas of active volcanism. At greater depths, this temperature gradient decreases to approximately 0.1 °C per 100 m of depth (cf., Figure 1.9). These temperature levels can be used in geothermal applications to meet human activity needs in the built environment.

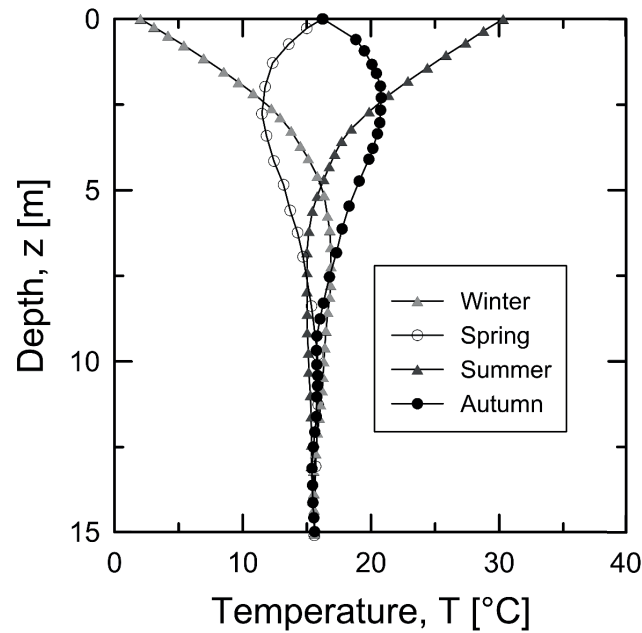


Figure 1.8: Sketch of typical temperature evolution with depth in the shallow subsurface throughout the year for a temperate climatic zone.

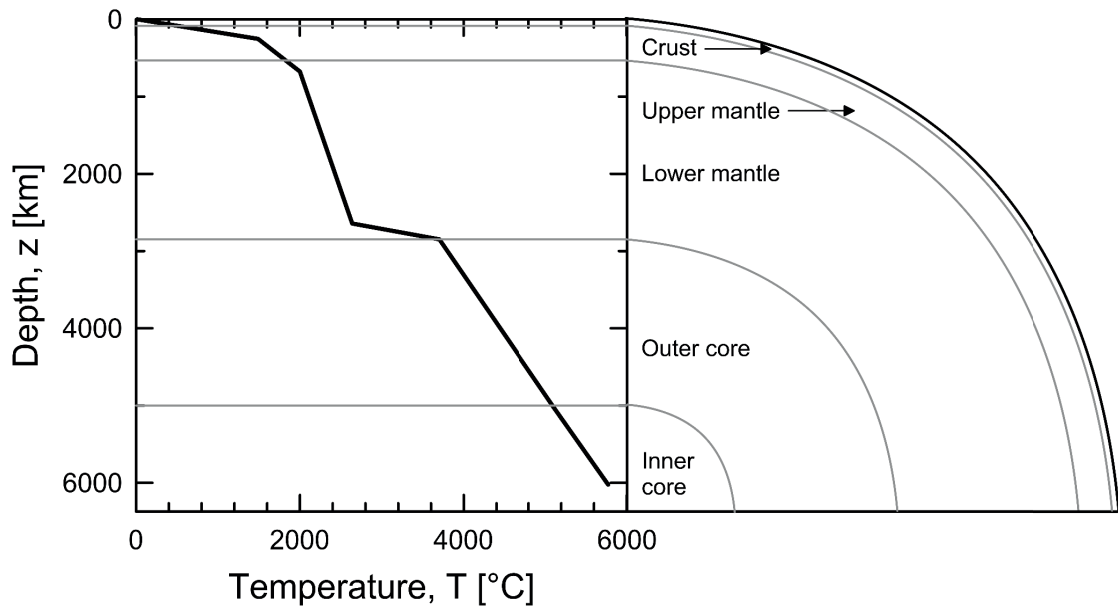


Figure 1.9: Sketch of typical temperature evolution with depth in Earth subsurface (redrawn after Boehler (1996)).

### 1.2.3 Features of geothermal energy

Geothermal energy represents the second most abundant source of primary energy on Earth, after solar energy (Lee et al., 2007). It is classified as both renewable and sustainable (Lund, 2009), and represents one of the energy sources that can be used in the construction sector for the development of low-carbon buildings (in several countries, also resorting to the support of government grants and

incentives). Geothermal energy can be considered as a clean and environmentally friendly energy source as it generates no (or minimal) greenhouse gas emissions because the conversion and utilisation processes do not involve any chemical reactions (e.g., combustion) (Lee et al., 2007). This energy source is also available continuously, regardless of the weather conditions, which makes it attractive in contrast to other renewable energy sources such as solar and wind energy. Among other various positive attributes (Lee et al., 2007), geothermal energy reduces the current dependence on non-renewable energy sources and it can be used for various purposes from a local to a relatively large scale. Because geothermal energy is available almost everywhere, the consequent reduction of energy imports means a reduced dependence on external economic or political situations (Brandl, 2006).

### 1.3 Geothermal systems

#### 1.3.1 Classification of geothermal systems

Geothermal systems are technologies that harvest geothermal energy. Various classifications of geothermal systems can be made, but one classification that is often employed relies on the exploitation depth of the thermal energy present in the subsurface. Depending on whether a lower or greater depth than 400 m (by governmental definition in several countries) is considered, geothermal systems can be classified as *shallow geothermal systems* or *deep geothermal systems*, respectively. Shallow geothermal systems deal with low temperature and enthalpy. Deep geothermal systems deal with medium to high temperature and enthalpy.

#### 1.3.2 Features and uses of geothermal systems

Geothermal systems are made up of three main components: a *heat source*, a *heat sink* and a *heat exchanger*. Typically, the heat source is the ground and the heat sink is a surface environment (in general, a structure), but the opposite can also occur, i.e., the heat source is a surface environment and the heat sink is the ground. The heat exchanger is generally constituted by one or more elements containing a fluid that transfers the heat between the heat source and the heat sink.

Employing the ground as a heat reservoir, i.e., a heat source or sink, is a result of long historical developments that can often be addressed only on the basis of indirect considerations (Cataldi, 1999). Some early development examples of this type are listed hereafter. In early Sumerian and Akkadian times, the ground was employed as a heat sink to store ice (and food) in so-called “ice houses” constructed partly or completely underground (e.g., Dalley, 2002), based on the limited affection of these environments to the surface thermal conditions. In Palaeolithic and ancient Roman times, the ground was used as a heat source for bathing and space heating (e.g., Armstead, 1973), based on the presence of sources of hot water in the subsurface (e.g., thermal springs). In 1904, the ground was used as a heat source for electrical power production via the construction of the first geothermal power plant by Prince Piero Ginori Conti in Italy (e.g., Lungonelli, 2003).

One key feature of geothermal systems is the way the thermal energy that is harvested from the ground is used via such systems. In shallow geothermal systems, an indirect use of geothermal energy is typically made. Machines or devices that modify (enhance or lower) the energy input transferred



between the ground and the target environment, in addition to machines or devices that force a heat carrier fluid to flow (exchanging heat) between them, are employed in such cases. In deep geothermal systems, a direct use of geothermal energy can be made when an indirect use is not targeted. In contrast to the previous case, machines that modify the energy input transferred between the ground and the target environment can be avoided in this condition and only machines that force a heat carrier fluid to flow between the ground and the target environment are required.

Shallow geothermal systems can be used to provide heating, cooling and hot water, using temperatures available underground of less than 25 °C. These systems are suitable for small-scale and domestic use in almost any geographical location. Deep geothermal systems can be used to provide heating and hot water as well as electrical power, using temperatures available underground greater than 25 °C and up to 200 °C (the temperatures required for electrical power generation being generally greater than 175 °C (Narsilio et al., 2014)). These systems are suitable for medium- to large-scale uses, but can be applied in more particular locations than those characterising shallow geothermal systems.

In addition to the previously proposed classification of geothermal systems, one additional criterion is often employed to characterise these systems and is related to the presence of closed- or open-loops in the heat exchanger. Based on this criterion, geothermal systems can be classified in most cases as either *closed-loop* or *open-loop systems*. Closed-loop systems use a water-based mixture circulating through sealed pipes to transfer the heat from the ground to the superstructure or the opposite. Open-loop systems directly use ground water extracted from or injected in aquifers through wells in the considered heat exchange process.

The crucial difference between closed- and open-loop systems is that in the latter systems mass exchange occurs, in contrast to the former, and heat transfer is more favourable. However, although providing the highest energy yield, open-loop systems require the highest financial input and pose the highest technical risks such as underground pollution (Boënnec, 2008). Because there is no mass exchange with the ground, closed-loop systems minimise environmental risks and mineral precipitation issues, and do not require the need to obtain extractive licensing (Narsilio et al., 2014). Shallow geothermal systems can be either open- or closed-loop. Deep geothermal systems are open-loop.

Figure 1.10 presents typical examples of shallow and deep geothermal systems. Typical shallow geothermal systems are horizontal geothermal boreholes, geothermal baskets, groundwater capture systems, vertical geothermal boreholes and *energy geostructures*. Typical deep geothermal systems are thermal springs, hydrothermal systems and petrothermal systems.

*Horizontal geothermal boreholes* are the shallowest type of geothermal systems. These systems typically consist of closed polyethylene pipes ploughed or dug down horizontally in the ground at a few meters of depth (e.g., from a depth of  $z = 2$  to 5 m) next to buildings. In the pipes, a circulating heat carrier fluid allows exchanging the heat present in the ground (predominantly as a consequence of solar radiation) especially for heating purposes in residential, agricultural or aquaculture applications. However, storage purposes can also be achieved in those situations in which the boreholes are placed under buildings.

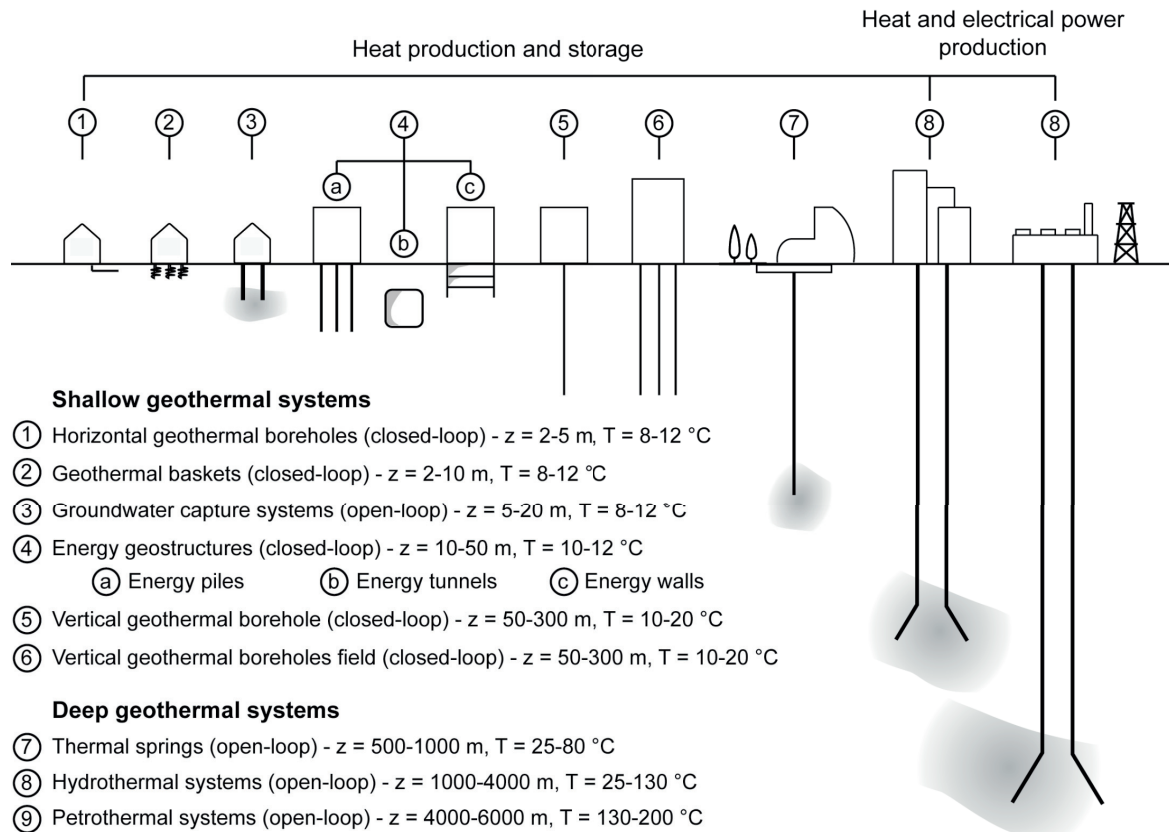


Figure 1.10: Classification of geothermal systems (redrawn after Geothermie Schweiz).

*Geothermal baskets* represent a more compact system than horizontal geothermal boreholes and can be used for similar purposes. These systems are typically buried in the ground at a few meters of depth (e.g., from a depth of  $z = 2$  to  $10$  m) and consist of closed polyethylene pipes fixed in a spiral geometry in which a heat carrier fluid flows. Applications where spiral coils are located in surface water reservoirs next to buildings are also possible, provided that such reservoirs are located deep enough to avoid problematic conditions for the system operation, e.g., freezing of the reservoir water and thus of the circulating heat carrier fluid in the pipes.

*Groundwater capture systems* employ open wells surrounded by groundwater reservoirs located at shallow depths (e.g., from a depth of  $z = 5$  to  $20$  m). These systems can be applied when no hydrological, geological and environmental constraints in general are present. They are typically used for heating purposes by extracting the thermal energy present in the subsurface water. For small constructions, single wells may be used. Larger constructions usually require doublet wells. Extraction and injection wells may be employed to ensure a balanced underground thermal field, which is essential for performance and, in some cases, environmental concerns.

*Vertical geothermal boreholes* consist of closed polyethylene pipes that are embedded vertically in the ground below or next to buildings at deeper depths than in the previous applications (e.g., from a depth of  $z = 50$  to  $300$  m). A filling material (e.g., bentonite) is usually placed in the borehole to enhance the heat exchange between the ground and the pipes. In the pipes, a circulating heat carrier fluid allows exchanging heat for heating, cooling, storage and hot water production purposes in the

most diverse construction types. Single boreholes can supply small residential constructions. Borehole fields are required when aiming to supply with thermal energy bigger constructions. Higher energy input than those transferred through shallower geothermal systems can be achieved through vertical geothermal boreholes because of the higher temperature levels characterising the ground at the considered depths.

*Energy geostructures* are novel geothermal systems detailed later that can be used with comparable and even more favourable outcomes than the previous shallow geothermal systems.

*Thermal springs* may generally be classified as deep geothermal systems, although they can also be found at depths characteristics of shallow geothermal systems. These systems employ open wells surrounded by hot groundwater reservoirs that are located relatively deep in the subsurface (e.g., from a depth of  $z = 500$  to  $1000$  m). They are typically used for bathing and medical purposes by extracting the thermal energy present in the subsurface water.

*Hydrothermal systems* extract groundwater through open wells from depths that allow the temperature and thermal energy present to be sufficiently high for realising large-scale heating applications (e.g., from a depth of  $z = 1000$  to  $4000$  m). Typical uses of these systems are for district heating. Heating of large industrial or agricultural constructions can also be conveniently achieved.

*Petrothermal systems* also extract groundwater through open wells, but from deeper depths than hydrothermal systems (e.g., from a depth of  $z = 4000$  to  $6000$  m). The temperature and thermal energy present in the water at these depths can be used for large-scale electrical power production and supply.

## **1.4 The energy geostructure technology**

### **1.4.1 Roles of energy geostructures**

Energy geostructures, more properly defined in a theoretical sense as thermo-active geostructures, are an innovative technology that couples the structural support role of conventional geostructures to the heat exchanger role of shallow geothermal systems. This technology includes all ground-embedded structures that can be used as structural supports while exchanging heat with the ground. Similar to other shallow geothermal systems, energy geostructures deal with low enthalpy and take advantage of the relatively constant temperature field in the shallow subsurface throughout the year for their heat exchanger role (Batini et al., 2015).

Energy geostructures can involve deep foundations (e.g., piles, piers, barrettes), earth retaining structures (e.g., diaphragm walls and sheet pile walls), shallow foundations (e.g., footings, base slabs), tunnel linings and anchors as well as pavements. The resulting geostructures are so-called energy piles, energy walls, energy slabs, energy tunnels, etc. (cf., Figure 1.11).





Figure 1.11: Examples of energy piles (image courtesy of Dr. Thomas Mimouni).

Various are the purposes of the heat exchange that can be established with energy geostructures. These can consist of (i) heating and cooling superstructures to reach comfort levels in the built environment, (ii) contributing to the production of hot water for anthropogenic, agricultural or tank-farming uses, and (iii) providing heat to prevent the icing of pavements and decks of infrastructures such as roads, bridges, station platforms and airport runways.

The use of energy geostructures for heating and cooling superstructures to reach comfort levels in the built environment can be achieved with the broadest number of energy geostructures, such as energy piles, energy walls, energy slabs and energy tunnels (the latter located close – i.e., within at maximum 400-600 m – to the superstructure they supply with thermal energy).

The use of energy geostructures for contributing to the production of hot water for anthropogenic purposes can nowadays be achieved based on the lower temperature levels needed for this aim (e.g., 45-55 °C) compared to those needed in constructions built since the 20<sup>th</sup> century to few decades ago (e.g., 75-85 °C). Typical energy geostructures that can be employed for this purpose, as well as for contributing to the production of hot water for agricultural or tank-farming purposes, are energy piles and energy walls. The use of energy tunnels in the vicinity of locations where agricultural or tank-farming activities may be developed is also particularly favourable. The reason for this is that significant amounts of heat, which may be wasted otherwise, can be exchanged with the tunnel environment and the surrounding ground. This heat exchange can be particularly favourable especially when tunnels are characterised by a significant length or high traffic, and when they are constructed at significant depths or in mountains where noteworthy geothermal gradients are present.

The use of energy geostructures for providing heat to prevent the icing of pavements and decks of infrastructures such as roads, bridges, station platforms and airport runways can be typically achieved via energy piles supporting bridge piers, energy slabs and energy pavements.

#### **1.4.2 Materials and technology**

Energy geostructures are typically made of reinforced concrete. From a technological perspective, they differ from conventional geostructures only because pipes are fixed along their reinforcing cage or are placed within the filling material (cf., Figure 1.12). The first application is more frequent when dealing with energy walls or tunnels, whereby potential issues due to maintenance of the geostructure or the adjacent environment (e.g., fixing supports to the geostructure that may pierce the pipes embedded within the reinforced concrete) are avoided by placing the pipes along the reinforcing cage on the groundside. Otherwise, embedding the pipes within the concrete is often preferable to ensure adequate concrete cover on the reinforcing cage.

Inside these pipes, a fluid is pumped via electrically driven machines and is used as a thermal energy carrier for the operation of the energy geostructures as in most shallow, closed-loop geothermal systems. Energy geostructures are closed-loop, shallow geothermal systems too.

The pipes mounted along the reinforcement of energy geostructures are usually made of high-density polyethylene and are characterised by a diameter of 20 to 40 mm with a wall thickness of 2 to 4 mm. Two or more pipe loops can be installed in series or in parallel. Typical configurations are the U-shape, double U-shape, W-shape and spiral shape. Thermal insulation of the pipes can be considered for the first meters of the inlet and outlet to limit the influence of the climatic condition on the heat exchange process, aiming at optimising the energy efficiency (Gao et al., 2008; Batini et al., 2015) (cf., Figure 1.12).

Fixing the pipes to the reinforcing cage of energy geostructures can be performed either in a plant or on site. The latter is more common (Brandl, 2006), whereby the piping is delivered to site on reels and a special working area is used. At the inflow and outflow of the pipework of each energy geostructure, a locking valve and a manometer are fixed (Brandl, 2006). These instruments allow the pipe circuit to be pressurised within a range of 5 to 8 bar for integrity check. In most applications, the locking valves and manometers are also used upon concreting to resist the head of the wet concrete without collapsing. Pressure testing for 24 hours after concreting is good practice. The pressure in the pipes is again applied before the working phase involving the construction of the superstructure starts (Brandl, 2006).

The heat carrier fluid (i.e., the heat transfer medium) usually consists of water, water with antifreeze (e.g., glycol), or a saline solution. Glycol–water mixtures containing additives to prevent corrosion are also a well performing and durable solution.





Figure 1.12: Typical pipes and thermal insulation in an energy pile (image courtesy of Dr. Thomas Mimouni).

### **1.4.3 Advantages involved with energy geostructures**

Similar to other technologies harvesting renewable energy, such as conventional geothermal systems, energy geostructures are an environmentally friendly technology that reduces the need of fossil energy sources and hence the greenhouse gas emissions. For this reason, the use of energy geostructures promotes and complies with national and international initiatives, policies, regulations and agreements such as those highlighted above. Furthermore, energy geostructures may be applied with other technologies harvesting renewable energies to form highly efficient systems.

In contrast to conventional shallow geothermal systems, the earth-contact elements that characterise energy geostructures and serve as heat exchangers are already required for structural reasons and need not to be constructed separately (Brandl, 2006). This fact involves savings related to the construction process that should be undertaken in a separate realisation of geostructures and geothermal heat exchangers.

Another key difference between energy geostructures and other conventional closed-loop geothermal systems is that concrete has more favourable thermal properties than the filling materials (e.g., bentonite) of the other geothermal technologies. This feature makes the heat exchange more favourable in the former case compared to the latter. One final difference is that usually the bending radius of the pipes in energy geostructures is greater compared to that characterising the pipes in conventional geothermal heat exchangers. This fact involves a lower flow resistance of the fluid circulating in the pipes, which results in a lower pumping power and, thus, in a lower operation cost.

With reference to the purposes of the heat exchange that can be established with energy geostructures various are the advantages included with energy geostructures compared to other technological systems. The use of energy geostructures for heating and cooling superstructures to reach comfort levels in the built environment reduces the environmental impact of any construction and can be exploited to get incentives for the design project and construction of the superstructure. The use of energy geostructures for contributing to the production of hot water for anthropogenic purposes reduces the costs compared to systems entirely resorting to more conventional technologies and is again characterised by a reduced environmental impact. When energy geostructures are employed for contributing to the production of hot water for agricultural or tank-farming uses, cost savings can be achieved via lower operational costs and environmental impacts. The use of energy geostructures for providing heat to prevent the icing of pavements and decks of infrastructures such as roads, bridges, station platforms and airport runways involves reducing the environmental impacts of these applications because the use of salts or grits is not necessary.

## **1.5 Energy geostructure operation modes**

### **1.5.1 Possible operations**

Two operation modes of energy geostructures involving a markedly different conceptual purpose can be employed: the heat exchange operation and the heat storage operation. Depending on whether energy geostructures are used for heat exchange or storage purposes through the respective operations, so-called “Ground Source Heat Pump Systems” (GSHPs) and “Underground Thermal Energy

Storage Systems” (UTES) are employed, respectively. Figure 1.13 presents a schematic of typical energy geostructures operation modes.

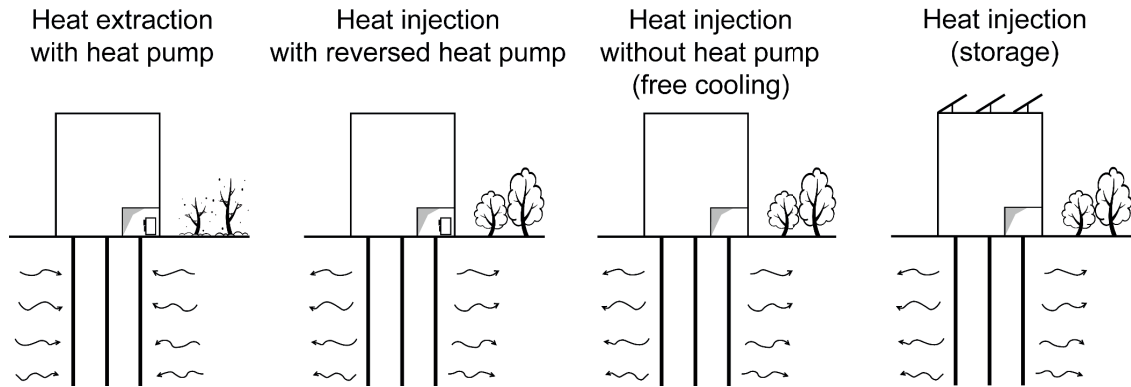


Figure 1.13: Typical energy geostructure operation modes.

### 1.5.2 Heat exchange operation

In this operation, the primary purpose of energy geostructures is to use the ground as a heat reservoir. The heat present in the ground is typically extracted and transferred to the superstructure in cool climates or cold seasons. On the contrary, the heat is typically extracted from the superstructure and injected in the ground in warm climates or during hot seasons.

Two possible uses of the energy geostructures are possible for the heat exchange operation mode:

- a. *Heating and/or cooling only* can be employed when the natural thermal recharge occurring in the ground during non-operating periods of the energy geostructure system is sufficiently high to keep the shallow temperature field in the subsurface undisturbed (except for the influence of climatic conditions) over time. This situation generally characterises energy geostructures in permeable soil with significant groundwater flow.
- b. *Heating and/or cooling combined with heat storage* has to be employed when the natural thermal recharge occurring in the ground during non-operating periods of the energy geostructure system is insufficient to keep the shallow temperature field in the subsurface undisturbed (except for the influence of climatic conditions) over time. This situation generally characterises energy geostructures in low permeable soil with negligible groundwater flow.

### 1.5.3 Heat storage

In this operation, the primary purpose of energy geostructures is to use the ground as a storage medium. Waste heat and solar heat is typically injected in the ground. While solar heat is usually injected in warm climates during hot seasons for a successive heating use in cold seasons, waste heat (involving elevated or low temperatures) can be stored for a successive use in the ground for both heating



and cooling purposes in cool climates or cold seasons and in warm climates or hot seasons, respectively. Heat storage is often required when heating or cooling needs do not match the heating or cooling productions.

## **1.6 Ground Source Heat Pump Systems**

### **1.6.1 General**

Ground Source Heat Pump Systems are constituted by a primary and a secondary circuit that allow the heat to be exchanged between the ground and any considered superstructure via energy geostructures. The primary circuit includes the ground heat exchanger system directly in contact with the ground. The secondary circuit characterises the superstructure to be heated or cooled.

In the primary circuit, heat is exchanged between the ground and the geostructure, and is collected to be transferred to the superstructure. In the secondary circuit, heat is transferred to the superstructure for heating or cooling. In between these two circuits, electrically driven machines such as heat pumps or reversed heat pumps can be employed. These machines are not present in all applications and when heating or cooling functional modes are targeted without them, the resulting energy geostructure operations are called “free heating” or “free cooling” (or geocooling), respectively. The need of using heat pumps or reversed heat pumps depends on the significance of the temperature difference between the primary circuit (i.e., the ground) and the secondary circuit (i.e., the superstructure), such an aspect rendering the heat exchange between the two environments more or less favourable.

The operation of Ground Source Heat Pump Systems can involve sufficiently high temperature levels in the ground or higher temperatures than that of the ground in the secondary circuit when operating for the heating of superstructures. Conversely, the operation of Ground Source Heat Pump Systems can involve sufficiently low temperature levels in the ground or lower temperatures than that of the ground in the secondary circuit when operating for the cooling of superstructures. When the temperature level in the ground is sufficient for the aforementioned purposes, heat pumps or reversed heat pumps are not needed and “free” operations can be achieved. Otherwise, heat pumps or reversed heat pumps are employed to increase and decrease the temperature level (and associated energy input), respectively, in those cases in which the heat originally exchanged with the ground may not be sufficient for heating or cooling purposes. In other words, heat pumps or reversed heat pumps allow overcoming the apparent restriction involved with the use of a cooler ground for heating superstructures or a warmer ground for cooling superstructures, respectively, as a consequence of the fact that these situations defy the second law of thermodynamics, for which heat flows from hot to cold, if left to itself (Narsilio et al., 2014). Typically, heat pumps are employed to rise the temperature level from 10-15 °C to 25-35 °C for the heating of superstructures (Brandl, 2006).

It is worth noting that, even though the term free is used in the related applications, pumping machines using electrical energy are anyhow required to transfer the thermal energy from the soil to the superstructure or the opposite, such an occurrence being ensured by heat pumps when employed. Figure 1.14 presents a schematic of a typical Ground Source Heat Pump System for the heating of a superstructure.

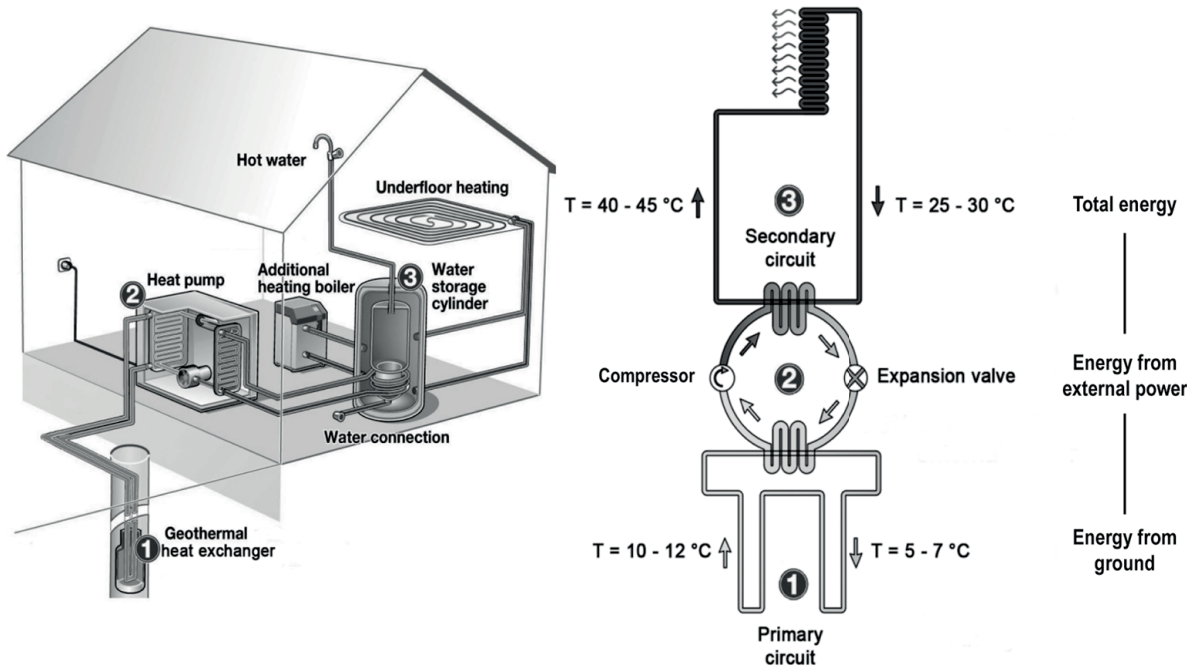


Figure 1.14: Typical composition of a ground source heat pump system and associated heating operation mode (modified after Agentur für Erneuerbare Energien, reproduced with permission).

### 1.6.2 The primary circuit

Heat exchange between the ground and energy geostructures occurs via the heat carrier fluid circulating in the pipes embedded in the energy geostructures (i.e., the ground heat exchangers) and allows exploiting the large thermal storage capabilities of the ground for heating and cooling purposes.

One or more header and manifold blocks are generally present to collect all the pipes arising from the energy geostructure(s). Resilience of these systems is fundamental. Hence, sub-manifolds are generally employed to affect only a minor portion of the energy geostructure system if there are any problems related with the installation or operation of the energy geostructures. These elements, together with the run-out proportion of the pipes that characterise the energy geostructure(s), often lie within the blinding beneath the base slab and constitute the primary circuit together with all of the aforementioned elements.

### 1.6.3 The heat pump or reversed heat pump

Heat pump machines are thermal devices that convert mechanical work into heat. The thermodynamic principle behind heat pumps is that fluids become warmer when they are compressed into a smaller volume. The opposite is true for reversed heat pumps, i.e., fluids become cooler when they are expanded. This fact involves that heat pumps and reversed heat pumps are characterised by the same operating principle (Yunus and Michael, 2006).

Simple heat pumps (e.g., compression heat pumps) comprise four main devices: the evaporator, the compressor, the condenser and the expansion valve. Heat pumps work with a refrigerant, which is a special fluid that (i) circulates in a closed circuit in the heat pump, (ii) undergoes phase transitions from a liquid to a gas and back again, and (iii) evaporates at low temperatures.

In the evaporator, the refrigerant is put in its liquid form in contact with the heat carrier fluid circulating in the pipes of the energy geostructures in the primary circuit and is evaporated in a gas, being its temperature lower than that of the heat carrier fluid and its boiling point (at relatively low pressure) below the entering heat carrier fluid temperature. The phase change from liquid to gas of the refrigerant fluid decreases the temperature of the heat carrier fluid, which is then re-injected in the ground via the pipes of the energy geostructures to warm up again. The refrigerant gas, at low pressure and relatively low temperature, then passes to the compressor.

In the compressor, this gas is compressed by using external energy (e.g., electrical power) to a higher temperature. The refrigerant gas, now at relatively high pressure and temperature, afterward passes to the condenser.

In the condenser, the resulting hot gas supplies the gained heat to a heat carrier fluid circulating in the secondary circuit by condensing (at a much higher temperature than at which it boiled). Eventually, the hot liquid refrigerant at high pressure passes through an expansion valve that returns the pressure and temperature of the liquid to its original conditions prior to the evaporator for starting a new cycle.

The aforementioned process is reversed when reversed heat pumps are used, the refrigerant condensation heating the heat carrier fluid circulating in the primary circuit, which is re-injected in the ground to cool down again.

#### **1.6.4 The secondary circuit**

Heat exchange in the built environment is typically achieved in the secondary circuit through heat exchangers such as underfloor heating ducts, radiators, etc. Temperature values that are adequate to reach comfort levels in living spaces and advantageous for engineering applications (e.g., de-icing of infrastructures) can be achieved through energy geostructures with a highly efficient use of primary energy (Batini et al., 2015).

#### **1.6.5 The Coefficient of Performance**

The amount of external energy input to be supplied to heat pumps has to be kept as low as possible to make the heat pump ecologically and economically desirable, the heat pump efficiency becoming a crucial design parameter. The efficiency of heat pumps can be characterised using the Coefficient of Performance, *COP*, which is a device parameter that defines how much units of heat can be obtained using one unit of electricity. The *COP* is defined as

$$COP = \frac{\text{Energy output after heat pump operation [kW]}}{\text{Energy input for heat pump operation [kW]}} \quad (1.1)$$

The higher the *COP*, the lower the external energy input compared to the energy output (e.g., useful heat). For example, a *COP* of 4 means that from one unit of electrical energy and three units of thermal energy (supplied, e.g., by the ground heat exchanger), four units of usable energy are derived. Usually, geothermal heat pumps have a *COP* in the range of 3.5 to 4. For economic reasons a value of  $COP \geq 4$  may preferably be achieved (Brandl, 2006).

The efficiency of a heat pump is strongly influenced by intrinsic machine features such as efficiency of internal heat exchangers and thermal losses, as well as by the difference between extracted and actually used temperature. A high user temperature (inflow temperature to the heating system of the secondary circuit) and a low extraction temperature (due to a too low return-flow temperature) in the heat exchanger (primary circuit) reduce its efficiency. To have a good efficiency, the usable temperature in the building should not exceed 35-45 °C and the extraction temperature in the pipes should not fall below 0-5 °C (Brandl, 2006). Besides, thermal properties of soils might vary considerably in freezing conditions and it is recommended that excessive heat extraction causing soil freezing should be avoided (SIA-D0190, 2005).

#### 1.6.6 The Seasonal Factor of Performance

The efficiency of ground source heat pump systems along seasons can be characterised through the Seasonal Factor of Performance, *SFP*. This factor includes not only the energy of the heat pump but also that of other energy-consuming elements (e.g., circulation pumps) (Brandl, 2006). The *SFP* is defined as

$$SFP = \frac{\text{Energy output usable from the energy system [kWh]}}{\text{Energy input of the energy system [kWh]}} \quad (1.2)$$

Values of *SFP* of 3.8-4.3 can be achieved with standard electric heat pumps, with an increase of 10-15% when special devices with direct vaporisation are used (Brandl, 2006). The seasonal performance of ground source heat pump systems is generally represented in a Sankey diagram that graphically indicates the energy budget of a system with the internal and external energy fluxes.

#### 1.6.7 Possible applications of Ground Source Heat Pump Systems

Two main types of application of Ground Source Heat Pump Systems can be foreseen depending on the features of the given location and project, and the number of energy geostructures required:

1. *Monovalent systems* relying only on energy geostructures to provide the entire amount of heating and cooling needs. This type of systems is rare but achievable under certain conditions (i.e., significant ground water flow and favourable conditioning loads). In these systems, at least 70% of the extracted energy may be injected when encountering minimum groundwater flow, although injecting more than 90% of the extracted energy may compromise the long-term efficiency of free cooling (SIA-D0190, 2005). An example of such systems is the industrial building Lidwil at Altendorf, Switzerland. The system uses 120 spun energy piles out of 155 spun piles constituting the entire building foundation that are equipped with two U-loops per pile (embedded within a gravel layer characterised by a groundwater velocity between 100 and 150 m/day), and provides 160 kW of heating using three heat pumps of 18 kW each with a *COP* of 2.9-3 (SIA-D0190, 2005).
2. *Bivalent systems* using energy geostructures to provide only a proportion of the heating and cooling needs, the rest being satisfied using conventional heat sources. An example of such systems is the dock Midfield of the Zürich airport, Zürich, Switzerland. The system uses more than 300 energy piles out of 440 piles to provide 65% of the heating needs and 70% of the cooling needs. The remaining proportions come from district heating for heating and from a cooling tower for cooling, respectively (Pahud and Hubbuch, 2007).

## 1.7 Underground Thermal Energy Storage Systems

Underground Thermal Energy Storage Systems allow the heat collected from solar thermal panels or in excess from superstructures use to be exchanged for storage purposes between any considered superstructure and the ground via energy geostructures. In Ground Source Heat Pump Systems, heat exchange between energy geostructures and the surrounding ground should be maximised. In contrast, in Underground Thermal Energy Storage Systems heat exchange between energy geostructures and the surrounding ground should be minimised to preserve heat storage. Underground Thermal Energy Storage Systems are often considered to hold little promise because the heat stored into the ground dissipates rather quickly in most cases (Ingersoll et al., 1954). However, where the site conditions are favourable, they can represent an advantageous solution because large storage volumes can be realised with a low ground occupation at the surface (Pahud, 2002). Underground Thermal Energy Storage Systems are very similar to Ground Source Heat Pump Systems and can be realised with or without heat pumps or reversed heat pumps.

## 1.8 Application and development of energy geostructures

### 1.8.1 Historical facts

Energy geostructures have been increasingly applied worldwide approximately since the 1980's (Brandl, 2006). To date, the highest number of energy geostructure applications involves energy piles, whereas less projects involve energy walls and energy tunnels, for example. Only the advent of the project "Grand Paris express" in France, which may be considered to be the modern urban renovation

of Paris after that introduced by Haussmann during the mid-19<sup>th</sup> century, has caused a major increase in the design for a future application of energy walls and energy tunnel linings.

### 1.8.2 Application and development examples based on a literature survey

Figure 1.15 presents the number and average length of energy piles installed by country, based on available data in the literature and personal communications from companies involved with the construction of energy geostructures worldwide. Leading countries in the application of energy piles currently appear to be United Kingdom, Austria and Switzerland. The average length of the constructed energy piles is of 19 m.

Figure 1.16 presents the installed thermal power by country, based on the same survey. Leading countries in the installed power through energy piles currently appear to be China, Austria and United Kingdom.

Figure 1.17 presents the cumulative number of energy piles and energy pile projects in the world. It is evident that the application of energy piles is remarkably increasing.

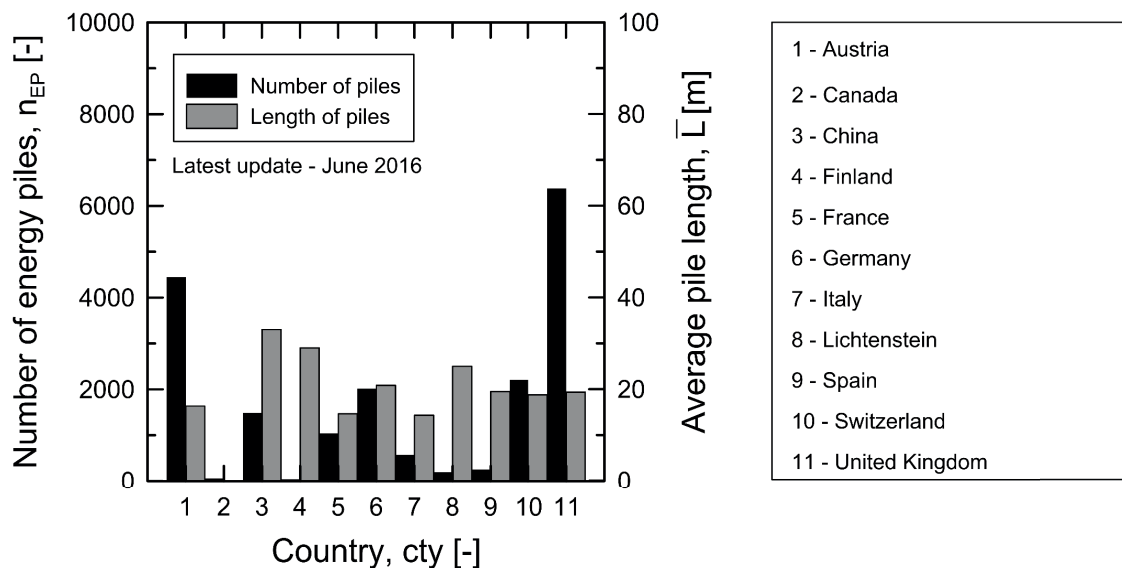


Figure 1.15: Number and average length of energy piles by country.

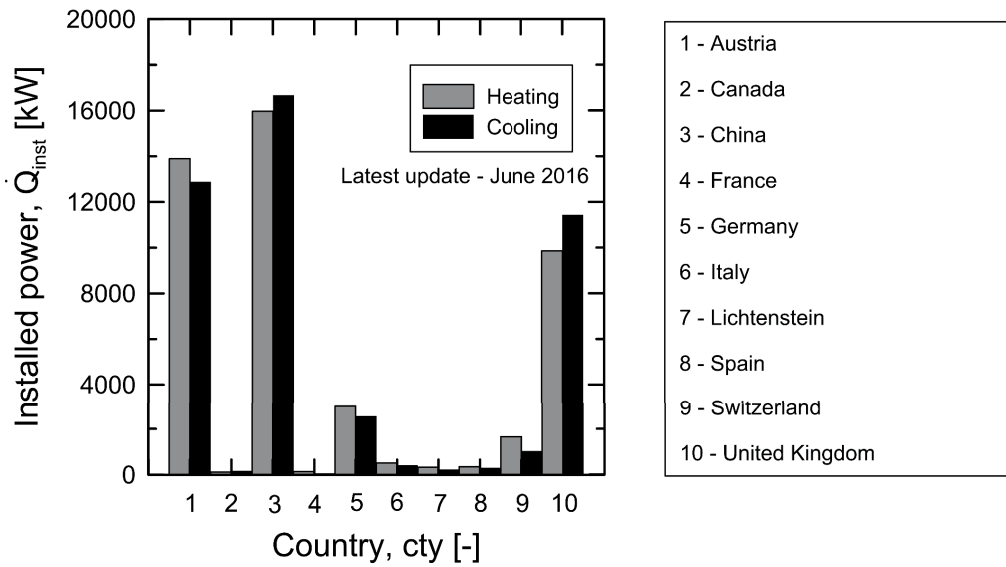


Figure 1.16: Installed thermal power by country.

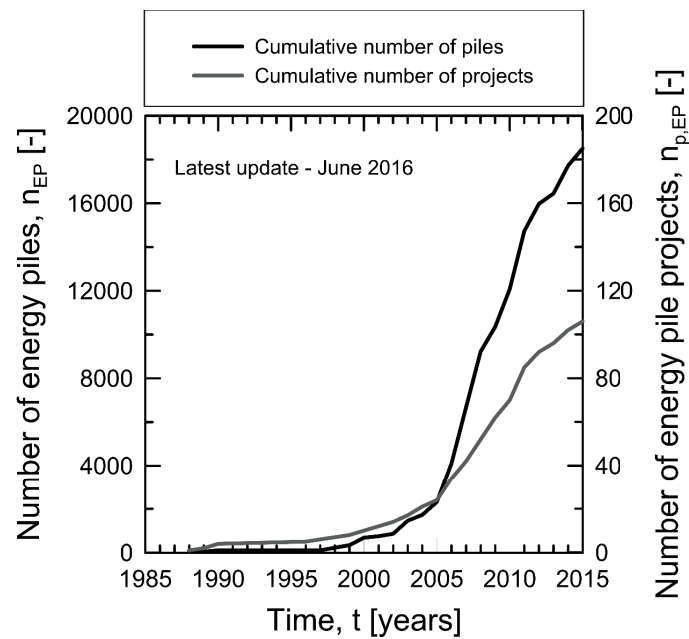


Figure 1.17: Cumulative number of energy piles and energy pile projects in the world.

## 1.9 Considerations and challenges from a holistic, integrated perspective

The multifunctional operation of energy geostructures as structural supports and geothermal heat exchangers involves various challenges. These challenges concern planning, analysis, design (e.g., geotechnical, structural and energy), construction and maintenance aspects in the design project of buildings and infrastructures employing energy geostructures. The focus is given here to the chal-



allenges belonging to the analysis and design of energy geostructures themselves, because these activities crucially contribute to the suitable conceptual development and operation of such technology in the broad picture of the design project of constructions.

The multifunctional role of energy geostructures involves mechanical and thermal loads applied to such elements. These loads cause variations of the temperature, stress, deformation and displacement in the subsurface that need to be considered in analysis and design (cf., Figure 1.18).

The temperature changes caused in the energy geostructures and the subsurface crucially characterise the thermal response, as well as the energy behaviour and performance of such technology. A sound analysis of this problem, specific for any site and energy geostructure, is essential to ensure an adequate energy behaviour and performance, and to justify the use of geostructures as geothermal heat exchangers. This is true for both short- (e.g., hourly, daily) and long-term (e.g., weeks, years) periods.

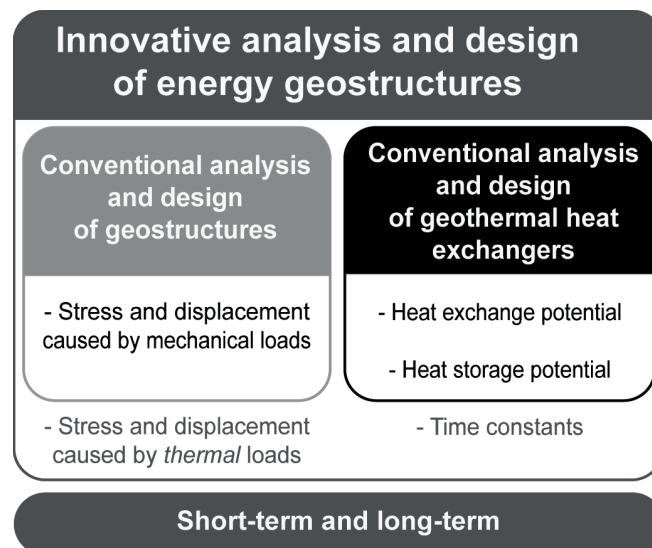


Figure 1.18: Typical aspects to consider in the analysis and design of energy geostructures.

The stress, deformation and displacement fields in the subsurface are not only caused by the conventionally applied mechanical loads to the geostructures, but in the case of energy geostructures by the unprecedented thermal loads applied to such technology as well. Thermal loads are responsible for a dual interplay of stress and strain development in the geostructures and the subsurface. This interplay depends on whether the expansion or contraction caused by the application of the thermal loads to the energy geostructures and the surrounding ground is restrained or allowed. The stress, deformation and displacement caused in the energy geostructures and the subsurface crucially characterise the mechanical response, as well as the geotechnical and structural behaviour and performance of such technology. A comprehensive analysis of this problem, specific for any site and energy geostructure, is essential to ensure an adequate geotechnical and structural behaviour and performance, and to justify the use of geostructures as structural supports. This is true for both short- and long-term periods.



Despite increasing applications of energy geostructures worldwide, in very limited cases an integrated approach to account for the aforementioned aspects and to analyse and design the considered technology is employed. In contrast, the general approach employed to analyse and design energy geostructures is oriented (at least theoretically) to oversizing the considered geostructures (via more substantial or reinforced geostructures) without a sound understanding of the theory and practical consequences involved. This phenomenon is considered to occur in many cases because of the following:

- First, due to the complexity of the problems involved with energy geostructures and the economic pressures that design and constructor companies face in the market to remain competitive in spite of such complexity. The problems involved with the geotechnical, structural and energy analysis and design of energy geostructures are strongly multiphysical and multidisciplinary. They also involve complex conceptual, organisational and management aspects from design project and application perspectives. Aspects involved in the design project of energy geostructures are reported in Table 1.2 and Table 1.3.
- Then, because many are still the gaps between the scientific understanding of energy geostructures and the practical procedures employed to analyse and design the considered technology. The lack of a comprehensive framework allowing for the understanding of the behaviour and performance of energy geostructures, together with the lack of simplified yet suitable tools for the analysis and design of such geostructures, certainly contributed to the aforementioned occurrence up to recent years.
- Finally, because of the lack of comprehensive design methodologies for energy geostructures. The availability of fragmented and limited design guidance (because proposed by different national institutions and not employing at all or correctly a performance-based procedure, respectively) certainly contributed to the last evidence up to recent years.

Analyses and designs of technologies aimed at achieving a trouble-free performance instead of an actual optimal performance have the marked limitation of being uneconomical. Only by understanding the behaviour of any physical problem in a theoretical and empirical sense, and by developing analysis tools and design methodologies can one obtain adequate and economic analyses and designs.

In an attempt to foster the worldwide diffusion of energy geostructures with reference to the aforementioned considerations and the challenges presented in the Introduction, particularly for energy piles, this doctoral research addresses the thermo-mechanical behaviour and performance of energy pile groups. The aim is to cover the essence of the interdisciplinary and integrated competences required in the geotechnical and structural analysis and design of energy piles that civil engineers, architects and urban project managers have to face when addressing such innovative technology.

Table 1.2: Examples of aspects involved in the architectural and structural design of buildings and infrastructures involving energy geostructures.

Architectural design
<ul style="list-style-type: none"> <li>• <b>Establishes the architectural and distributive features of the construction, considering</b> <ul style="list-style-type: none"> <li>• The resources (e.g., economic and financial) available to the project</li> <li>• The location and interaction of the construction with the surrounding systems and environments (e.g., urban, ambient, etc.)</li> <li>• The requirements for occupants use and/or accessibility</li> </ul> </li> <li>• <b>Defines the environmental systems and units characterising the construction</b></li> <li>• <b>Defines the classes of technological systems, technological systems and technological elements (e.g., for building envelope and interior environment, etc.), and the related features, considering</b> <ul style="list-style-type: none"> <li>• The resources (e.g., economic and financial) available to the project</li> <li>• The features of the environmental systems and units characterising the construction</li> <li>• The requirements for occupants use and/or accessibility (e.g., ambient temperature, relative humidity, etc.)</li> <li>• Other complementary requirements targeted by the construction design (e.g., associated with energy performance, environmental impact, etc.)</li> <li>• The capability of the technological solutions to be demounted, maintained, repaired, deconstructed and reconstructed</li> <li>• The life cycle of the technological solutions applied (with regards to the design working life of the structure)</li> </ul> </li> </ul>
Structural design
<ul style="list-style-type: none"> <li>• <b>Defines the features (e.g., dimensional and technological) of the superstructure system upon</b> <ul style="list-style-type: none"> <li>• The choice of the type of superstructure systems based on <ul style="list-style-type: none"> <li>• <i>The architectural and distributive features of the construction</i></li> <li>• <i>The location, use and features of the construction from the perspective of the actions and effects of actions applied to the structure</i></li> <li>• <i>The feasibility of the solution foreseen (e.g., economic, financial and technical)</i></li> </ul> </li> <li>• The establishment of a target structural performance of the superstructure system, based on the verification of the requirements and the consideration of <ul style="list-style-type: none"> <li>• <i>The actions and effects of actions characteristics of the features, location and use of the construction</i></li> <li>• <i>The actions and effects of actions potentially arising from the foundation</i></li> </ul> </li> </ul> </li> <li>• <b>Contributes with the geotechnical design to define the features (e.g., dimensional and technological) of the foundation system upon</b> <ul style="list-style-type: none"> <li>• The verification of the structural performance of the foundation with reference to target requirements and based on the estimate of <ul style="list-style-type: none"> <li>• <i>The actions arising from the superstructure that have to be carried by the foundation</i></li> <li>• <i>The actions characteristics of a specific use or location of the foundation</i></li> </ul> </li> </ul> </li> <li>• <b>Ensures a target structural performance of the superstructure and foundation systems to a certain probable extent in the design working life of the construction</b></li> </ul>

Table 1.3: Examples of aspects involved in the architectural and structural design of buildings and infrastructures involving energy geostructures.

<b>Geotechnical design</b>
<ul style="list-style-type: none"> <li>• <b>Defines the features (e.g., dimensional and technological) of the foundation system upon</b> <ul style="list-style-type: none"> <li>• The choice of the type of foundation systems based on <ul style="list-style-type: none"> <li>• <i>The architectural and distributive features of the construction</i></li> <li>• <i>The features of the superstructure system and the actions involved</i></li> <li>• <i>The geotechnical characterisation of the site</i></li> <li>• <i>The feasibility of the solution foreseen (e.g., economic, financial and technical)</i></li> </ul> </li> <li>• The establishment of a target geotechnical performance of the foundation system, based on the verification of the requirements and the consideration of <ul style="list-style-type: none"> <li>• <i>The actions and effects of actions arising from the superstructure system (e.g., thermal and mechanical actions)</i></li> <li>• <i>The actions and effects of actions potentially arising from the ground</i></li> <li>• <i>The mutual interaction with the solution foreseen by the energy design for the energy foundation</i></li> </ul> </li> </ul> </li> <li>• <b>Ensures a target geotechnical performance of the foundation system to a certain probable extent in the design working life of the construction</b></li> </ul>
<b>Energy design</b>
<ul style="list-style-type: none"> <li>• <b>Defines the features of the systems and plants (e.g., for the production of hot water, the allowance of conditioning, the distribution of electrical power, etc.) foreseen to satisfy the energy needs associated with the features and use of the construction, considering</b> <ul style="list-style-type: none"> <li>• The resources (e.g., economic and financial) available to the project</li> <li>• The location and interaction of the construction with the surrounding environment</li> <li>• The requirements for occupants use in terms of thermo-hygrometric comfort, indoor air quality, etc.</li> <li>• The feasibility and sustainability of the solution</li> <li>• Other complementary requirements targeted by the construction design (e.g., associated with energy performance, environmental impact, etc.)</li> </ul> </li> <li>• <b>Contributes with the geotechnical design to define the features (e.g., dimensional and technological) of the foundation system</b></li> <li>• <b>Ensures a target energy performance of the construction to a certain probable extent in its design working life</b></li> </ul>



## Chapter 2

# The role of thermal loads in the geotechnical and structural performance of energy piles

Over the last decade, increasing efforts have been devoted to proposing recommendations and standards for the geotechnical and structural design of energy piles. The unprecedented action of thermal loads, in conjunction with that of mechanical loads, due to their geothermal and structural support operations, represents a significant challenge. Design guidance is currently available. However, the widespread design approach is prescriptive and not performance-based, and where this latter approach is employed, shortcomings are present. To provide a basis for a novel performance-based design framework, this study investigates, via a theoretical analysis and practical design examples, the role of thermal loads in the geotechnical and structural performance of energy piles. This work shows that *thermal loads involve effects that can be neglected in the performance-based design of energy piles at ultimate limit states*, both from a geotechnical and a structural perspective, *and can be considered relevant only at serviceability limit states*. In the limit state design framework of the Eurocodes, the above holds when (i) a design compressive strength of the reinforced concrete section constituting the pile at least equal to the pile design bearing capacity and (ii) a minimum longitudinal reinforcement for the pile concrete cross-sectional area that can ensure ductility are ensured. The results presented, together with the proposed design approach, reduce the design and verification of energy piles at ultimate limit states as a conventional process against the action of mechanical loads only.

### 2.1 Introduction

Nowadays, it is established that energy piles are a technology with major capabilities to provide energy supply and structural support to the built environment. Over the last three decades, increasing

applications of energy piles characterised by noteworthy thermal performance (i.e., associated with the energy behaviour) have been documented worldwide (Laloui and Di Donna, 2011). In the meantime, no applications of energy piles affected by a lack of required mechanical performance (associated with the geotechnical or structural behaviour) at both ultimate (i.e., failure-related) or serviceability (i.e., deformation-related) limit states have been documented.

However, the absence of applications of energy piles characterised by a lack of required mechanical performance is often not representative of an adequate geotechnical and structural design of such ground structures. In contrast, this evidence is the consequence of a design created (at least theoretically) to overly conservatively tackle (using excessively long or substantial piles) the challenging multiphysical phenomena associated with the mechanical and thermal loads applied to energy piles because of their structural support and geothermal operations.

Designs of structures aimed at achieving a trouble-free performance instead of an actual optimal performance have the marked limitation of being uneconomical. Only by understanding the behaviour of any physical problem in a theoretical and empirical sense and by developing analysis tools and design methodologies can one obtain adequate and economical designs.

Much theoretical (e.g., Laloui et al., 2003; Bourne-Webb et al., 2011; Mimouni and Laloui, 2014; Rotta Loria and Laloui, 2016b; Rotta Loria and Laloui, 2017b) and empirical (e.g., Amatya et al., 2012; Murphy et al., 2015; Rotta Loria and Laloui, 2017d; Di Donna and Laloui, 2015; Di Donna et al., 2015; Yavari et al., 2016) knowledge and many analysis tools (e.g., Knellwolf et al., 2011) are currently available to characterise the mechanical performance of energy piles subjected to mechanical and thermal loads. However, despite some recent research (Xiao et al., 2016), few, limited methodologies for addressing the geotechnical and structural design process – intended as a complex, integrated and iterative process comprising design and verification phases – of energy piles against the action of mechanical and thermal loads have been developed.

In principle, the European Standards, often called the Eurocodes (EN 1990, 2002), are available to address the effects of mechanical and thermal loads on the geotechnical and structural behaviour and performance of structures such as piles. In practice, these standards currently lack recognised rules that can be straightforwardly or suitably applied to consider, in the design process, the effects of thermal loads associated with the geothermal operation of energy piles.

One guide in Switzerland (SIA-D0190, 2005), one standard in the United Kingdom (Ground Source Heat Pump Association, 2012) and one recommendation in France (CFMS-SYNTEC-SOFFONS-FNTP, 2017) currently offer guidance for the geotechnical and structural design of energy piles. However, although they represent groundwork, these contributions are characterised by drawbacks.

The Swiss document (SIA-D0190, 2005) neglects aspects whose relevance for design have been noted in recent years, e.g., the presence and influence of thermally induced group effects on energy pile performance (Rotta Loria and Laloui, 2017d).

The United Kingdom standard (Ground Source Heat Pump Association, 2012), in addition to suffering from the same aforementioned drawback, is applicable to only a limited number of design situations because it is characterised by prescriptive and not performance-based features and involves, in most cases, an excessive oversizing of piles because it is based on worst-case scenario considerations.

The French recommendations (CFMS-SYNTec-SOFFONS-FNTP, 2017), which are based on the groundwork of Burlon et al. (2013) that was more recently enriched by Bourne-Webb et al. (2016b), may in principle be considered the best reference because they adopt a performance-based design approach, being based on the Eurocodes. However, three main limitations exist in practice. First, the recommendations do not include a comprehensive methodological framework for the energy pile design process and focus on only the verification, not the design, of such geostructures. Initial guidance is needed regarding how to design energy piles. Second, the recommendations rely on the arguable proposition of establishing ultimate and serviceability limit state verifications of energy piles by combining the results of analyses while considering the quasi-permanent serviceability limit state load combination. Because the analyses given as example consider non-linear soil behaviour, a misconception regarding the superposition of action effects at serviceability and ultimate limit states exists. Third, the recommendations account for a partial factor for the quasi-permanent value of thermal loads that is not conservative with respect to experimental evidence currently available in the literature.

In addition to the aforementioned design guidance, the most appropriate and effective design approach for energy piles appears as follows: reduce the design process to a conventional pile design process by considering the action of only mechanical loads at ultimate limit states, and verify the performance of energy piles against the combined action of mechanical and thermal loads at serviceability limit states. Such an approach may be considered the most appropriate based on the argument that the effects of thermal loads applied to energy piles are unlikely to involve geotechnical and structural ultimate limit states. The approach may be considered the most effective because it is less time-consuming than a design approach also accounting for the effects of thermal loads at ultimate limit states. Prior to this study, no analyses and evidence supported by performance-based considerations of the effect of thermal loads on the geotechnical and structural performance of energy piles have been made available for validating and proposing the aforementioned design approach.

To address the aforementioned challenge, this study (Rotta Loria et al., 2017a) provides a theoretical analysis and practical design examples – performed in the limit state design framework of the Eurocodes – of the role of thermal loads in the geotechnical and structural performance of energy piles, with a focus on ultimate limit states. Energy piles subjected to axial mechanical loads (e.g., vertical, compressive mechanical loads applied at the pile head) and thermal loads are considered.

First, a thermo-mechanical idealisation of energy pile behaviour is presented. Next, a performance-based design, built within the framework of the Eurocodes at the ultimate limit states of energy piles, with reference to a case study for which material properties were available, is discussed. Then, an analysis of the effects of thermal loads is highlighted. Finally, concluding remarks are summarised.

## **2.2 Thermo-mechanical idealisation of energy pile behaviour**

### **2.2.1 Effect of thermal loads on the mechanical behaviour of energy piles**

The mechanical response that characterises energy piles subjected to thermal loads differs from the response that characterises conventional piles subjected to mechanical loads. This response can be

idealised within a one-dimensional framework (Laloui et al., 2003), in which an energy pile of length  $L$  and linear thermal expansion coefficient  $\alpha_{EP}$  is subjected to a uniform temperature variation  $\Delta T$ .

If an energy pile can deform freely, it is characterised by a thermally induced strain

$$\varepsilon_f^{th} = -\alpha_{EP}\Delta T \quad (2.1)$$

This thermally induced strain leads to a variation in length of the energy pile of

$$\Delta L = L' - L = -L\varepsilon_f^{th} = L\alpha_{EP}\Delta T \quad (2.2)$$

where  $L'$  is the energy pile length after the application of the temperature variation (cf., Figure 2.1).

When the thermally induced deformation is completely blocked

$$\varepsilon_b^{th} = -\varepsilon_f^{th} = \alpha_{EP}\Delta T \quad (2.3)$$

the observed strain is

$$\varepsilon_o^{th} = 0 \quad (2.4)$$

Therefore, a thermally induced stress

$$\sigma_b^{th} = E_{EP}\varepsilon_b^{th} = E_{EP}\alpha_{EP}\Delta T \quad (2.5)$$

arises in an energy pile of Young's modulus  $E_{EP}$  (cf., Figure 2.2).

In reality, energy piles do not deform freely because of the presence of the surrounding soil and superstructure. Therefore, the observed thermally induced strain is generally

$$\varepsilon_o^{th} \leq \varepsilon_f^{th} \quad (2.6)$$

Equation (2.6) implies that only a proportion of the strain is blocked, i.e.,



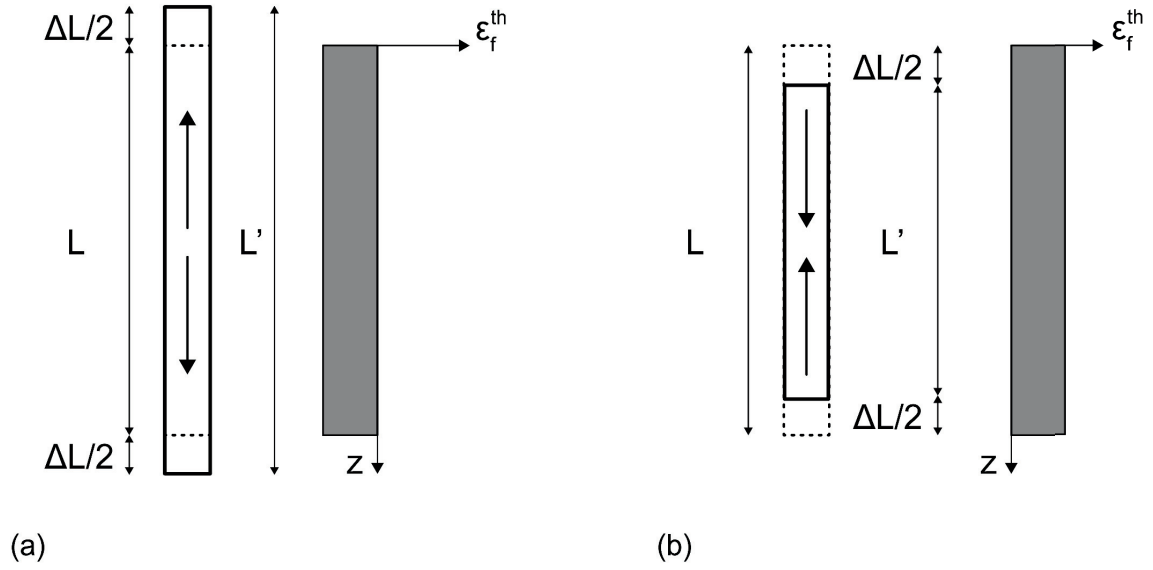


Figure 2.1: Thermally induced strain caused by (a) heating and (b) cooling of an energy pile under free expansion conditions.

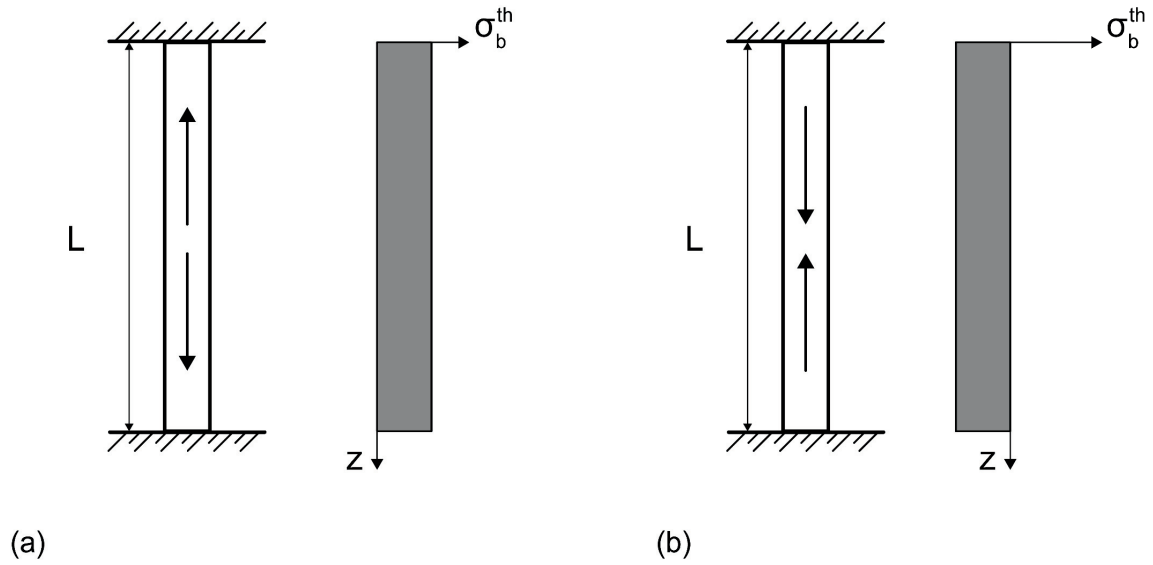


Figure 2.2: Thermally induced stress caused by (a) heating and (b) cooling of an energy pile under completely blocked conditions.

$$\epsilon_b^{th} = \epsilon_o^{th} - \epsilon_f^{th} \quad (2.7)$$

In other words, the response of the energy pile is governed by a certain degree of freedom, defined as (Laloui et al., 2003)

$$DOF = \frac{\varepsilon_o^{th}}{\varepsilon_f^{th}} \quad \text{with} \quad 0 \leq DOF \leq 1 \quad (2.8)$$

The blocked thermally induced strain induces an observed thermally induced stress that can be calculated as

$$\sigma_o^{th} = E_{EP} \varepsilon_b^{th} = E_{EP} (\varepsilon_o^{th} - \varepsilon_f^{th}) = E_{EP} (\varepsilon_o^{th} + \alpha_{EP} \Delta T) = E_{EP} \alpha_{EP} \Delta T (1 - DOF) \quad (2.9)$$

Figure 2.3 shows the impact of the degree of freedom of the energy pile on the development of the average thermally induced deformation,  $\bar{\varepsilon}_o^{th}$ , and stress,  $\bar{\sigma}_o^{th}$ . The higher the restraint provided by the presence of the surrounding soil and the superstructure, the greater the thermally induced stress and the lower the thermally induced strain.

The previously proposed framework implicitly refers to energy piles embedded in typical soil deposits for which the soil-pile thermal expansion coefficient ratio  $X = \alpha_{soil}/\alpha_{EP} \leq 1$ , where  $\alpha_{soil}$  is the linear thermal expansion coefficient of the soil. In rare cases where  $X = \alpha_{soil}/\alpha_{EP} > 1$ , typically at successive stages of geothermal operations, the temperature variation applied to an energy pile and its thermal expansion coefficient do not satisfy inequality (2.6), i.e.,

$$\varepsilon_o^{th} > \varepsilon_f^{th} \quad (2.10)$$

The above occurs because when the linear thermal expansion coefficient of the soil is greater than that of the energy pile, the thermally induced deformation of energy piles is dominated by that of the soil rather than by the deformation of the piles. This phenomenon becomes more pronounced as more soil regions are affected by temperature changes (Rotta Loria and Laloui, 2017d; Bourne-Webb et al., 2016a).

For example, inequality (2.10) indicates that heating thermal loads applied to energy piles can induce tensile stress. This phenomenon, which has been confirmed by full-scale experimental evidence and a numerical analysis (Rotta Loria and Laloui, 2017d), implies that considering situations where  $X = \alpha_{soil}/\alpha_{EP} \leq 1$  enables conservative verifications of the vertical stress within energy piles and non-necessarily suitable verifications of the vertical displacement along energy piles.

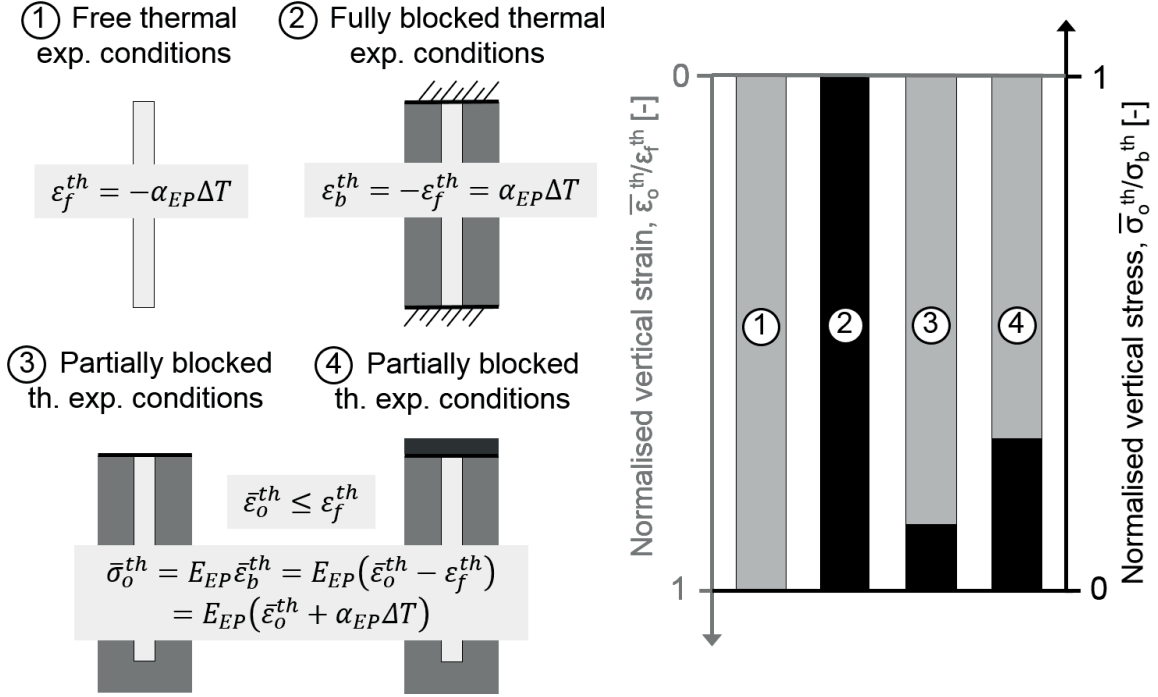


Figure 2.3: Impact of system restraint on the thermally induced vertical strain and stress in energy piles.

### 2.2.2 Generalised mathematical formulation of vertical energy pile equilibrium

The general equation that governs the vertical equilibrium of energy piles is

$$P + \frac{\pi D^2}{4} K_h w(z=0) + W + Q_{s,mob} + Q_{b,mob} = 0 \quad (2.11)$$

where  $P$  is the applied mechanical load,  $K_h$  is the head stiffness of the superstructure or structural element connected to the pile head,  $w(z=0)$  is the pile vertical head displacement (with  $z$  being the vertical coordinate),  $W$  is the pile weight,  $Q_{s,mob}$  is the mobilised shaft capacity and  $Q_{b,mob}$  is the mobilised base capacity. The pile weight is often neglected in practical analyses and designs. Similarly, it is neglected in the following.

When mechanical and thermal loads are applied to energy piles, both  $Q_{s,mob}$  and  $Q_{b,mob}$  can be written in terms of a mechanical and a thermal contribution as

$$Q_{s,mob} = Q_{s,mob}^m + Q_{s,mob}^{th} \quad (2.12)$$

and

$$Q_{b,mob} = Q_{b,mob}^m + Q_{b,mob}^{th} \quad (2.13)$$

Energy piles subjected to a thermal load are generally characterised by two portions that displace in opposite directions from the so-called null point of the vertical displacement (located at a depth,  $z_{NP,w}$ ) (Laloui et al., 2003). Accordingly, shear stress is mobilised in opposite directions at the pile shaft to ensure equilibrium with the surrounding soil from the so-called null point of the shear stress (generally located at a different depth,  $z_{NP,\tau}$ , than that of the null point of the vertical displacement) (Rotta Loria et al., 2017c). Based on the above, the portion of the shaft capacity mobilised by the thermal load,  $Q_{s,mob}^{th}$ , can also be written in terms of two contributions, i.e.,

$$Q_{s,mob}^{th} = Q_{s,mob,up} + Q_{s,mob,down} \quad (2.14)$$

where, for cylindrical energy piles of diameter  $D$ ,

$$Q_{s,mob,up} = \pi D \int_0^{z_{NP,\tau}} \tau \, dz \quad (2.15)$$

and

$$Q_{s,mob,down} = \pi D \int_{z_{NP,\tau}}^L \tau \, dz \quad (2.16)$$

Based on the aforementioned framework, the response of energy piles to mechanical and thermal loads can be represented via thermo-mechanical schemes proposed by Bourne-Webb et al. (2009) and Bourne-Webb et al. (2011). While the original schemes were proposed with reference to experimental data, the revised and novel schemes based on linear thermo-elasticity theory are as follows. Such a choice is considered to be valuable for two reasons: (i) because it shows simple yet realistic evolutions of the influence of mechanical and thermal loads, which can be superimposed via the elastic principle of the superposition of effects and extrapolated to a wide range of design situations characterised by limited loading levels for which reversible conditions are preserved and non-linearity can be neglected; (ii) because it serves as a reference for developing considerations related to more involved situations in which significant loading levels, for which irreversible conditions occur, and non-linearity can no longer be neglected.

Within this context, the energy piles are characterised by a thermo-elastic behaviour, whereas the deep surrounding soil mass exhibits an elastic behaviour.

### 2.2.3 Thermo-mechanical schemes for energy piles with no base and head restraints

The mechanical response of an energy pile with no base and head restraints to an axial mechanical load, a heating or cooling thermal load, and a mechanical and thermal load is depicted in Figure 2.4. The analysed situation may be assumed to characterise energy piles free at their head and embedded in (e.g., soft) soil that provides negligible end-bearing capacity.

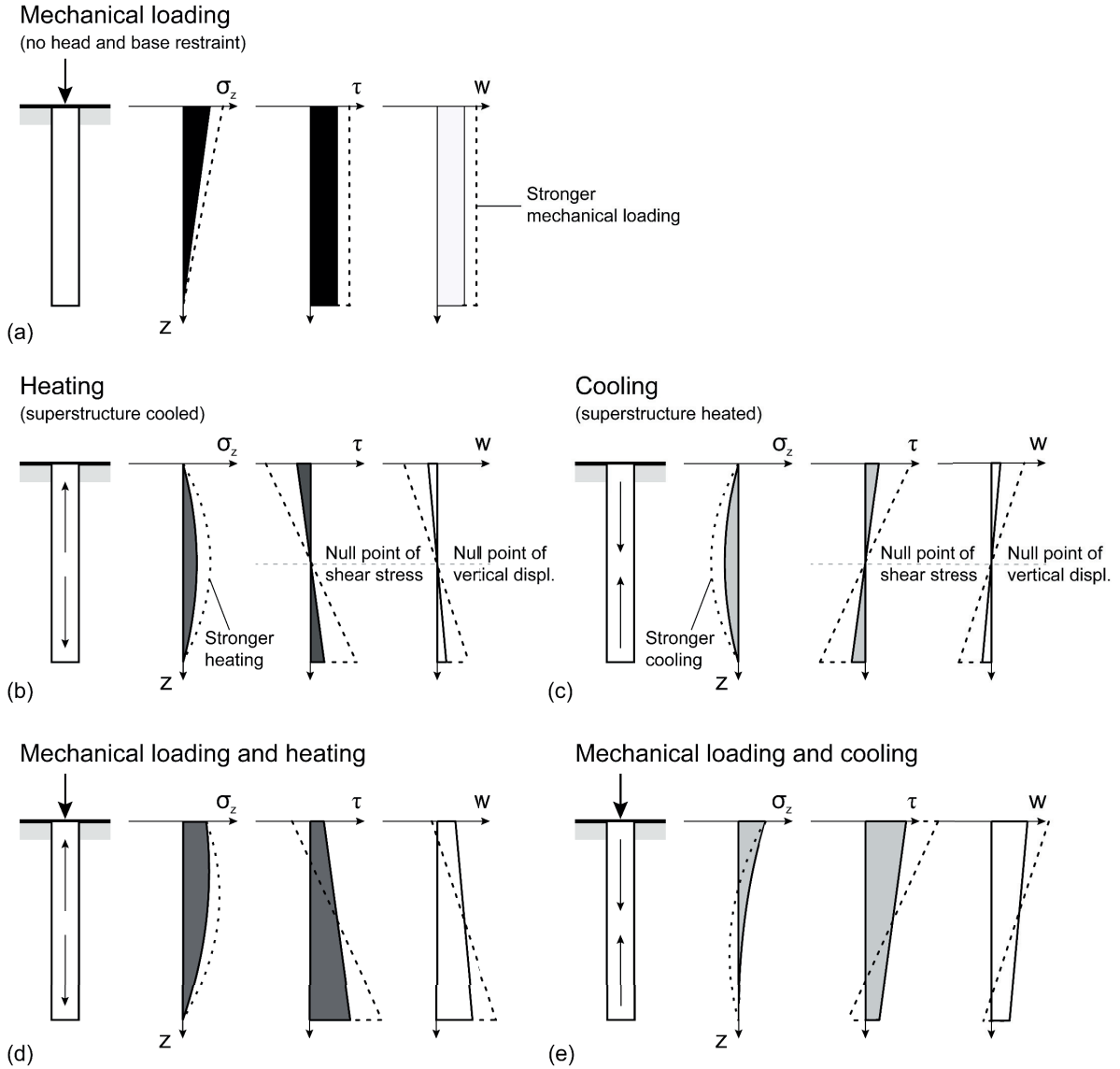


Figure 2.4: Thermo-mechanical schemes for energy piles characterised by no base and head restraints.

For the case of vertical mechanical loading only (cf., Figure 2.4 (a)), equation (2.11) can be written as

$$P + Q_{s,mob}^m = 0 \quad (2.17)$$

The application of an axial mechanical load to the pile head causes an approximately linearly decreasing distribution of compressive vertical stress  $\sigma_z$  along the pile and uniform and approximately constant distributions of positive shear stress  $\tau$  at the pile-soil interface and downward pile displacement  $w$  with depth  $z$ . The higher the pile stiffness, the more uniform and linear the distribution of  $\sigma_z$  with  $z$ , and the more uniform and constant the distributions of  $\tau$  and  $w$  with  $z$ . Soil layering causes a less uniform distribution of all the considered variables. Stronger mechanical loads cause linearly greater stress and displacement variations.

For the case of thermal loading only (cf., Figure 2.4 (b-c)), equation (2.11) can be rewritten as

$$Q_{s,mob}^{th} = Q_{s,mob,up} + Q_{s,mob,down} = 0 \quad (2.18)$$

The application of a heating or cooling thermal load to the pile causes a non-linear distribution of  $\sigma_z$  with  $z$  (symmetrical for heating and cooling), which is characterised by a maximum that coincides with the mid-length of the energy pile, where the null points of the vertical displacement and shear stress are also located. The application of a heating thermal load mobilises negative shear stress and causes heave for the energy pile portion above the null points, while it mobilises positive shear stress and causes settlement for the pile portion below the null points. The shear stress and vertical displacement caused by a heating thermal load develop in the opposite direction compared to those caused by a mechanical load above the null points, whereas these develop in the same direction below the null points. The opposite is true for a cooling thermal load. Shear stress and vertical displacement evolve approximately linearly with depth. The higher the pile stiffness, the more uniform the evolution of  $\sigma_z$  with  $z$ , and the lower the variation of  $\sigma_z$  for the same applied thermal load. Similarly, the higher the pile stiffness, the more uniform the evolutions of  $\tau$  and  $w$  but the higher their variation. Stronger thermal loads cause linearly greater stress and displacement variations.

For the case of mechanical and thermal loading (cf., Figure 2.4 (d-e)), equation (2.11) can be rewritten as

$$P + Q_{s,mob} = P + Q_{s,mob}^m + Q_{s,mob}^{th} = 0 \quad (2.19)$$

The distributions of vertical stress and shear stress with depth as well as of vertical displacement can be obtained via superposition of the previous ones. Tensile stress along the energy piles can arise for low magnitudes of applied mechanical loads and significant cooling.

### 2.2.4 Thermo-mechanical schemes for energy piles with base or head restraints

The mechanical response of an energy pile with base or head restraints to an axial mechanical load, a heating thermal load, and a mechanical and heating thermal load is depicted in Figure 2.5. The former end-restraint condition may be assumed to characterise energy piles free at their head and bearing on (e.g., stiff) soil that provides notable end-bearing capacity. The latter end-restraint condition may be assumed to characterise energy piles, with a slab at their head, embedded in (e.g., soft) soil that provides negligible end-bearing capacity.

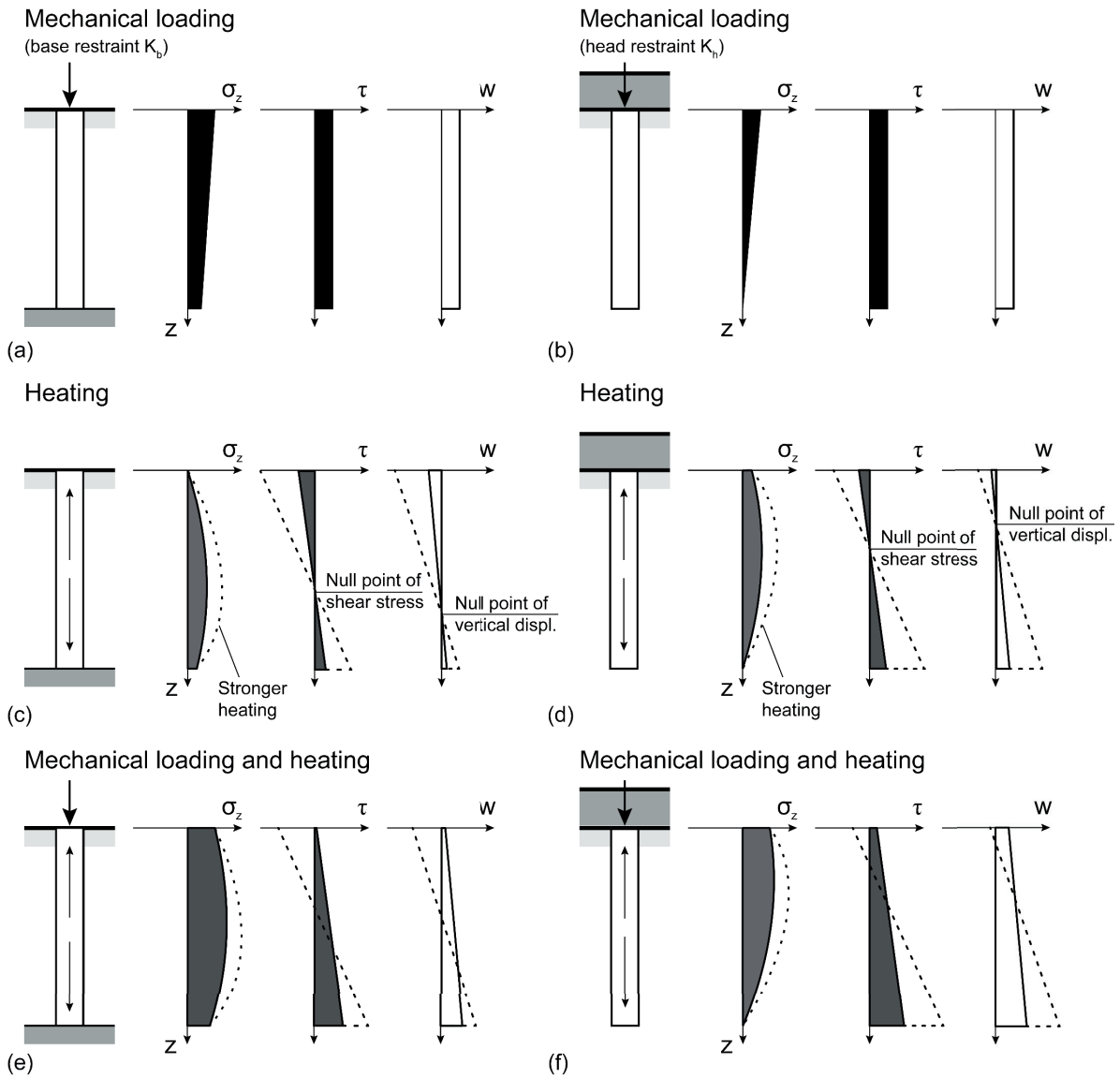


Figure 2.5: Thermo-mechanical schemes for energy piles characterised by base or head restraints.

For the case of vertical mechanical loading only (cf., Figure 2.5 (a-b)), equation (2.11) can be rewritten as

$$P + Q_{s,mob}^m + Q_{b,mob}^m = 0 \quad (2.20)$$

where only the base restraint is present, whereas

$$P + \pi \frac{D^2}{4} K_h w^m(z=0) + Q_{s,mob}^m = 0 \quad (2.21)$$

where only the head restraint is present (with  $w^m(z=0)$  being the pile vertical head displacement caused by the mechanical load).

When a base restraint is present, a greater average vertical stress  $\sigma_z$  (with a value corresponding to  $P$  at the pile head) and lower shear stress  $\tau$  and vertical displacement  $w$  develop along the pile compared to the case of no base and head restraints. This phenomenon arises because of the contribution provided by the base capacity to the vertical pile equilibrium. In these schemes, the base capacity mobilises at the same time as the shaft capacity for any magnitude of applied load, even though this is not necessarily the case in reality.

When a head restraint is present, a smaller average vertical stress  $\sigma_z$  (with a corresponding value lower than that of  $P$  at the pile head) and lower shear stress and vertical displacement variations develop along the pile compared to the case of no base and head restraints. This phenomenon arises because the head restraint reduces the effect of the downward mechanical load. This effect vanishes when the interplay between the mechanical load and the head restraint is not considered because the latter term is neglected. The consequence of such an approach is a pile response to mechanical loading equal to that of the case of no base and head restraints (equations (2.11) and (2.21) coincide).

For the case of heating thermal loading only (cf., Figure 2.5 (c-d)), equation (2.11) can be rewritten as

$$Q_{s,mob}^{th} + Q_{b,mob}^{th} = 0 \quad (2.22)$$

where only the base restraint is present, whereas

$$\pi \frac{D^2}{4} K_h w^{th}(z=0) + Q_{s,mob}^{th} = 0 \quad (2.23)$$

where only the head restraint is present (with  $w^{th}(z=0)$  being the pile vertical head displacement caused by the thermal load).

Different from the situation where no base or head restraints are present, when either a base or head restraint is present, vertical stress  $\sigma_z$  is generated at the restrained pile end by the applied thermal



load. The vertical stress distribution is greater than that in the case with no base and head restraints, in accordance with the discussed effect of the higher restraint of the system (cf., Figure 2.3). The null points of the vertical displacement and shear stress do not coincide but are shifted towards the region of the system characterised by the higher restraint. Lower vertical displacement develops towards the region of the system characterised by higher restraint, while higher displacement develops towards the region characterised by lower restraint compared to the case where the null points are located at the mid-length of the pile. A cooling thermal load yields a symmetrical response of the energy pile. In reality, the reduction of the compressive stress experienced at the pile toe for the case where a base restraint is present can attain at most the sum of any vertical mechanical load applied to the pile and its weight. This phenomenon occurs because soils generally cannot withstand tensile stress.

For the case of mechanical and heating thermal loading (cf., Figure 2.5 (e-f)), equation (2.11) can be rewritten as

$$P + Q_{s,mob} + Q_{b,mob} = 0 \quad (2.24)$$

where the base restraint is present, whereas

$$P + \pi \frac{D^2}{4} K_h w(z=0) + Q_{s,mob} = 0 \quad (2.25)$$

where the head restraint is present (with  $w(z=0) = w^{m+th}(z=0)$ ).

The distributions of vertical stress and shear stress with depth as well as of vertical displacement can be obtained via superposition of the previous ones.

### 2.2.5 Thermo-mechanical schemes for energy piles with base and head restraints

The mechanical response of an energy pile with base and head restraints to an axial mechanical load, a heating thermal load, and a mechanical and heating thermal load is depicted in Figure 2.6. The analysed situation may be assumed to characterise energy piles, with a slab at their head, bearing on (e.g., stiff) soil that provides notable end-bearing capacity. Two different cases involving a base restraint equal to the head restraint and a base restraint equal to one-half of the head restraint are considered.

For the case of vertical mechanical loading only (cf., Figure 2.6 (a-b)), equation (2.11) can be rewritten as

$$P + \pi \frac{D^2}{4} K_h w^m(z=0) + Q_{s,mob}^m + Q_{b,mob}^m = 0 \quad (2.26)$$

In the proposed schemes, the effect of the presence of the slab on the influence of the mechanical load on the pile response is considered. Hence, lower developments of vertical stress and shear stress as well as of vertical displacement are observed for a higher head restraint, compared to the case of a base restraint only. This behaviour may be expected in reality. However, many analyses and designs usually do not account for the interplay between the action of the mechanical load and the head restraint, neglecting the latter term.

For the case of heating thermal loading only (cf., Figure 2.6 (c-d)), equation (2.11) can be rewritten as

$$\pi \frac{D^2}{4} K_h w^{th}(z = 0) + Q_{s,mob}^{th} + Q_{b,mob}^{th} = 0 \quad (2.27)$$

The vertical stress  $\sigma_z$  caused by the thermal load is characterised by a symmetrical distribution with depth  $z$  when the base and head restraints are of the same magnitude, whereas by an asymmetrical distribution when different magnitudes characterise the end restraints. Higher stress develops towards the region of the system characterised by higher restraint. The higher the restraint provided by the end conditions, the higher the vertical stress and the lower the mobilised shear stress and vertical displacement.

For the case of mechanical and heating thermal loading (cf., Figure 2.6 (e-f)), equation (2.11) governs the system, the response of which can be obtained via superposition of the analysed situations.

### 2.2.6 Irreversible effects of mechanical and thermal loads on the geotechnical behaviour of energy piles

Evidence available in the literature shows that significant magnitudes of thermal loads, applied alone or in conjunction with mechanical loads, can cause irreversible, i.e., plastic, phenomena in the soil adjacent to energy piles (see, e.g., (Di Donna and Laloui, 2015; Vega and McCartney, 2014; Di Donna et al., 2015; Yavari et al., 2016)). Irreversible phenomena may limit the use of linear elastic theory and the aforementioned thermo-mechanical schemes to describe the actual geotechnical behaviour of energy piles.

When plastic phenomena develop in soil, stress redistribution around a pile, together with associated redistributions of the vertical stress and displacement along the pile, occurs for further loading. For an energy pile subjected to a given temperature variation in a soil characterised by a linear elasto-plastic behaviour, this redistribution involves, with respect to a linear elastic behaviour, (i) a lower development of shear stress at the pile-soil interface, (ii) a movement of the null points, (iii) a greater vertical displacement at the pile head and (iv) a lower development of vertical stress in the pile as a consequence of the lower restraint characterising the system (Rotta Loria et al., 2015b). The history, magnitude and sequence of the applied loads become crucial aspects of the problem for further loading (or unloading).

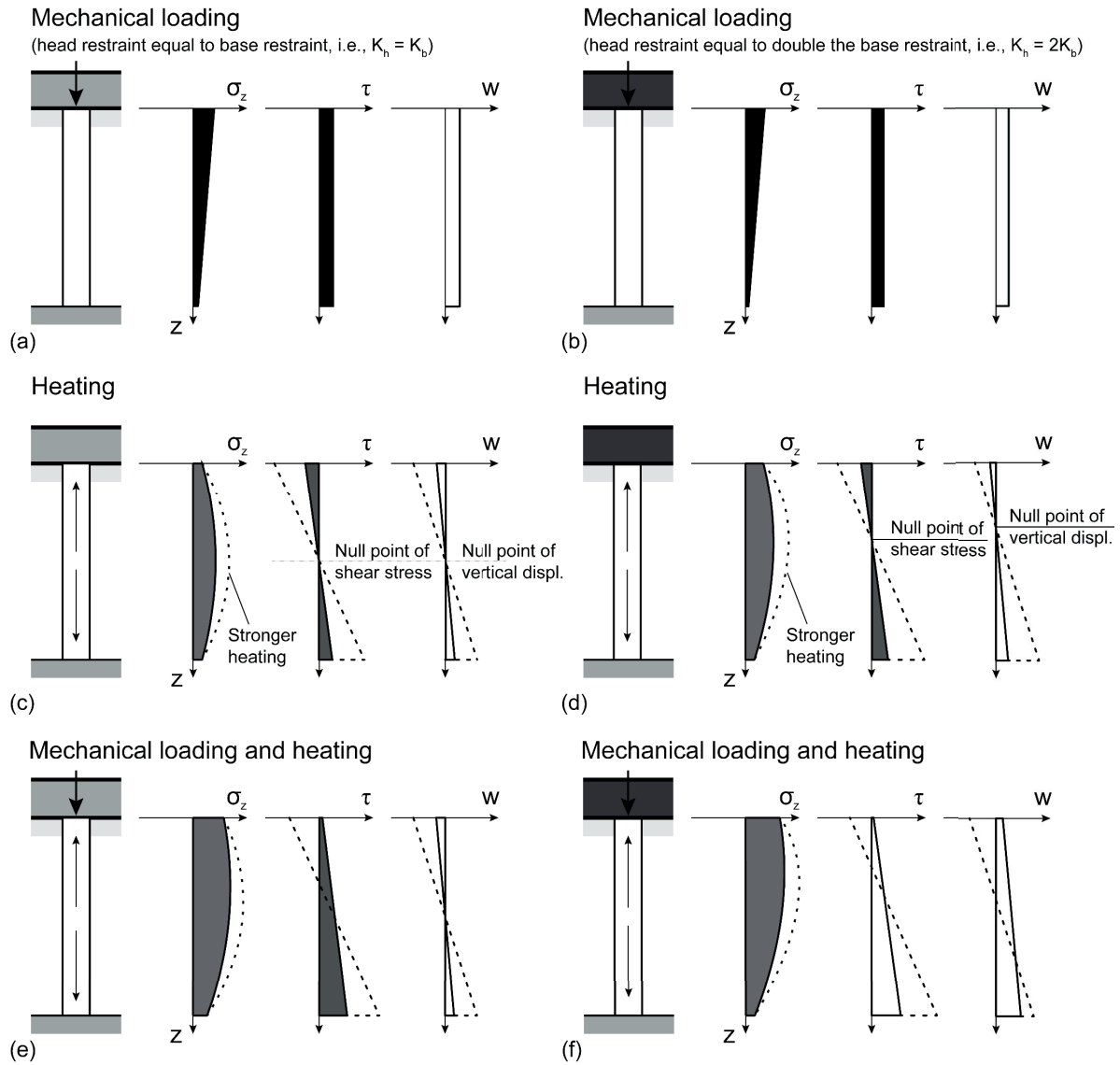


Figure 2.6: Thermo-mechanical schemes for energy piles characterised by base and head restraints.

### 2.2.7 Irreversible effects of mechanical and thermal loads on the structural behaviour of energy piles

In principle, significant magnitudes of thermal loads, applied alone or in conjunction with mechanical loads, may cause irreversible, i.e., plastic, phenomena in the reinforced concrete constituting the energy piles. In practice, no evidence that may effectively corroborate such an occurrence is available in the literature.

As previously stated, irreversible effects caused by mechanical and thermal loads may limit the use of linear elastic theory and the aforementioned thermo-mechanical schemes to describe the actual structural behaviour of energy piles. At the same time, the Eurocodes predict that the design of reinforced concrete structures may be performed assuming (i) uncracked cross-sections, (ii) linear stress-strain relationships and (iii) mean values of the modulus of elasticity (EN 1992, 2004).

Concrete strength is very limited compared to the high resistance of steel, but it plays an important role in the overall behaviour of reinforced concrete sections because the concrete area constitutes the biggest part of the cross-section. Nevertheless, the concrete tensile strength is neglected when constructing (based on the three hypotheses presented above) the so-called “strength domains” or “moment-normal force” diagrams of reinforced concrete sections, where the tensile strength of the section (when no moment is applied) is simply a function of its reinforcement area.

The phenomena that may characterise the irreversible behaviour of reinforced concrete sections subjected to loads of significant magnitudes are the development of cracks and the rupture of the reinforcement steel. For sections subjected to pure tension, the development of cracks corresponds to the transition from a composite cross-section to a section where only the longitudinal reinforcement contributes to the resistance (cf., Figure 2.7).

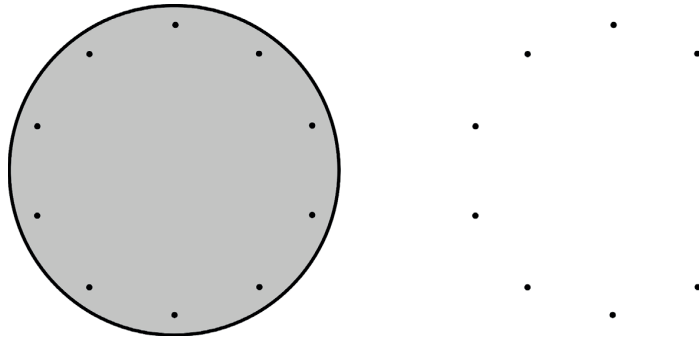


Figure 2.7: Transition from a composite reinforced concrete cross-section to a section in which only the longitudinal reinforcement contributes to the resistance.

The behaviour of single mean reinforced concrete cross-sections, before reaching the tensile strength of concrete, is linear elastic and characteristic of a composite cross-section. In this context, the steel to concrete stiffness ratio is defined as

$$n_{rc} = \frac{E_r}{E_c} \quad (2.28)$$

where  $E_r$  and  $E_c$  are the Young's moduli of the reinforcement steel and concrete, respectively. The reinforcement ratio of the cross-section is

$$\rho_r = \frac{A_r}{A_{EP}} \quad (2.29)$$

where  $A_r$  is the cross-sectional area of the longitudinal reinforcement present in the considered cross-section of energy pile  $A_{EP}$ . In this case, the product of the Young's modulus and cross-section of the energy pile is approximately

$$\begin{aligned}
E_{EP}A_{EP} &= E_cA_c + E_rA_r = E_cA_{EP}(1 - \rho_r) + n_{rc}E_c\rho_rA_{EP} \\
&= E_cA_{EP}[1 + \rho_r(n_{rc} - 1)] \approx E_cA_{EP}
\end{aligned} \tag{2.30}$$

Given a sectional axial force,  $N$ , the proportions of the axial force received by the concrete,  $N_c$ , and by the reinforcement,  $N_r$ , are, respectively,

$$N_c = N \frac{E_cA_c}{E_{EP}A_{EP}} = N \frac{E_cA_{EP}(1 - \rho_r)}{E_cA_{EP}[1 + \rho_r(n_{rc} - 1)]} = N \frac{1 - \rho_r}{1 + \rho_r(n_{rc} - 1)} \tag{2.31}$$

$$N_r = N \frac{E_rA_r}{E_{EP}A_{EP}} = N \frac{n_{rc}E_c\rho_rA_{EP}}{E_cA_{EP}[1 + \rho_r(n_{rc} - 1)]} = N \frac{n_{rc}\rho_r}{1 + \rho_r(n_{rc} - 1)} \tag{2.32}$$

When concrete cracks, a sudden decrease in the stiffness of the section takes place, and stress redistribution occurs from concrete to steel. In this case, the axial strain is

$$\varepsilon_z = \frac{f_{ct}}{E_c} \tag{2.33}$$

where  $f_{ct}$  is the tensile strength of concrete. The axial force needed to crack the reinforced concrete cross-section is

$$\begin{aligned}
N_{cr} &= E_{EP}A_{EP}\varepsilon_z = E_cA_{EP}[1 + \rho_r(n_{rc} - 1)] \frac{f_{ct}}{E_c} = f_{ct}A_{EP}[1 + \rho_r(n_{rc} - 1)] \\
&\approx f_{ct}A_{EP}
\end{aligned} \tag{2.34}$$

The axial force mobilised by concrete and steel upon cracking can be determined, respectively, as

$$N_{cr,c} = A_cf_{ct} = f_{ct}A_{EP}(1 - \rho_r) \approx f_{ct}A_{EP} \tag{2.35}$$

$$N_{cr,r} = N_{cr} \frac{n_{rc}\rho_r}{1 + \rho_r(n_{rc} - 1)} = f_{ct}A_{EP}n_{rc}\rho_r \tag{2.36}$$

After concrete cracks in the reinforced concrete cross-section, only the steel contributes to the resistance against the action effects. In this case,

$$E_{EP}A_{EP} = E_rA_r \quad (2.37)$$

$$N = N_r \quad (2.38)$$

$$N_R = f_y A_r = f_y \rho_r A_{EP} \quad (2.39)$$

where  $N_R$  is the resisting axial force and  $f_y$  is the steel yield strength.

The actual response of *whole reinforced concrete members* differs from that of *single mean cross-sections* described above (the latter actually coinciding with the response of reinforced concrete members characterised by the simultaneous occurrence of cracks). The reason for this is because, in reality, cracking will always occur progressively along reinforced concrete members. Furthermore, the response of any reinforced concrete members differs from that of the reinforcement steel alone because the concrete cannot crack everywhere along the member and the concrete between two cracks contributes to its stiffness (so-called “tension-stiffening” phenomenon).

## 2.3 Performance-based design of case studies

### 2.3.1 Combination of actions at ultimate limit states

A design based on the partial factor method, such as that predicted by the Eurocodes, is considered to be sufficient if no limit state is *exceeded* in all relevant design situations when design values for actions or effects of actions and resistances are introduced in the analysis models (EN 1990, 2002). The prescription (e.g., *inequality*) that must be verified when considering an ultimate limit state is that (EN 1990, 2002)

$$E_d \leq R_d \quad (2.40)$$

where  $E_d$  is the design value of the action or action effects and  $R_d$  is the design value of the resistance.

When persistent and transient design situations at ultimate limit states are considered and the effects of only permanent and variable loads are accounted for, the design effects of actions can be written as (EN 1990, 2002)

$$E_d = \sum_{j \geq 1} \gamma_{G,j} G_{k,j} + \gamma_{Q,1} Q_{k,1} + \sum_{i \geq 1} \gamma_{Q,i} \psi_{0,i} Q_{k,i} \quad (2.41)$$

where  $\gamma_{j,i}$  are the partial factors of the ( $j$ -th and  $i$ -th, respectively) actions or action effects,  $G_{k,j}$  represents the permanent loads,  $Q_{k,1}$  is the dominant variable load,  $\psi_{0,i} Q_{k,i}$  are the values of the

accompanying variable loads, and the coefficients  $\psi_i$  are combination factors. The symbol “+” may be read as “combined with”, and the symbol “ $\Sigma$ ” implies “the combined effect of”.

For simplicity, only transient and design situations with one permanent mechanical load and one variable mechanical load applied to the energy piles, in addition to the thermal load (for the heating season and cooling season), are considered in the following.

### 2.3.2 Partial factors for thermal loads applied to energy piles

Thermal loads involved with energy piles may be considered variable, indirect, free and static actions, as can the thermal actions currently considered in the Eurocodes for different structures, such as buildings and bridges.

Daily and seasonal changes in shade air temperature, solar radiation, and re-radiation are typical examples of thermal actions for buildings and bridges (EN 1991, 2003). Temperature changes associated with the heating or cooling of superstructures are typical examples of thermal actions for energy piles. The magnitude of all the aforementioned thermal actions depends, more or less directly, on local climatic conditions, the orientation of the structure, the structure mass and finishes, and, in the case of building structures, heating, the ventilation regimes and thermal insulation.

The temperature changes applied to energy piles can be defined with reference to the heat inputs involved in the building energy design, the associated thermal powers for heating and cooling, the operation time and the thermal properties of the piles and ground. The resulting characteristic temperature changes are nominal values,  $\Delta T_k$ . Because the temperature changes in energy piles are generally non-uniform within the cross-sectional area of the piles and along their length, best practice methods for selecting the appropriate temperature variation should be considered in the design (Loveridge and Powrie, 2016; Abdelaziz and Ozudogru, 2016b).

Currently, thermal actions (not caused by fire) on buildings are considered in the combinations of actions using factor values for the accompanying variable actions of  $\psi_0 = 0.60$ ,  $\psi_1 = 0.50$  and  $\psi_2 = 0$  (EN 1991, 2003) (where  $\psi_0$  is the factor for combination value of a variable action,  $\psi_1$  is the factor for frequent value of a variable action and  $\psi_2$  is the factor for quasi-permanent value of a variable action). Thermal actions on bridges may be considered differently by employing values of  $\psi_0 = 0.60$ ,  $\psi_1 = 0.60$  and  $\psi_2 = 0.50$  (EN 1991, 2003). The different values of the factors  $\psi_1$  and  $\psi_2$  predicted for bridges compared to those predicted for buildings can be associated with the more burdensome effect of thermal actions on bridges compared to that on buildings. This fact is a consequence of the presence in buildings of envelopes that, in contrast to what occurs on bridges, reduce the effect of thermal actions on the structure.

Thermal actions applied to energy piles have a significant effect on the structure. Therefore, while the combination factors and frequent values of thermal actions applied to buildings appear to also be suitable for thermal actions applied to energy piles, the quasi-permanent value appears to be unsuitable.

Burlon et al. (2013) suggested addressing thermal actions applied to energy piles using the combination factors and frequent values of thermal actions for buildings of  $\psi_0 = 0.60$  and  $\psi_1 = 0.50$  and using the quasi-permanent value of  $\psi_2 = 0.20$  based on temperature data available to the authors.

The value of  $\psi_2$  may be varied as a so-called “nationally determined parameter”. In this study, a different value of the coefficient  $\psi_2$  than those presented above is suggested based on the following arguments.

- i) Seasonal temperature changes applied to energy piles are often characterised by temperature fluctuations throughout the day and progressive variations at the end of each heating-cooling cycle. Daily temperature fluctuations of up to 8 °C and progressive temperature variations of up to 2 °C in the operation of full-scale energy piles subjected to heating and cooling thermal loads over more than three years were noted by Loveridge et al. (2016). Because the average values of variables can represent the accompanying values of variable actions (EN 1990, 2002), the coefficient  $\psi_2$  may be calculated as the ratio between the average temperature variation and the maximum (or minimum) temperature variation observed throughout successive cooling or heating cycles. By considering such an approach, a quasi-permanent value of thermal actions applied to energy piles of  $\psi_2 = 0.50$  is obtained for heating and cooling by referring to the case study proposed by Loveridge et al. (2016).
- ii) Seasonal temperature changes applied to energy piles may be approximately modelled using sinusoidal functions if no temperature fluctuations throughout the day are considered and no temperature variations are assumed to occur cycle after cycle. Half of a sine wave cycle may be considered for one season of heating or cooling. The ratio between the average value of a sine wave over half of a cycle (e.g., a season of heating or cooling) and the maximum (or minimum) value of this function over the same cycle is  $2/\pi = 0.64$ . If such an approach is used to calculate  $\psi_2$ , a value greater than that proposed by Burlon et al. (2013) ( $\psi_2 = 0.20$ ) and that proposed in EN 1991 (2003) for bridges ( $\psi_2 = 0.50$ ) is obtained.

The considerations developed in case (i) are based on the limited full-scale field data available in the literature for energy piles. Those elaborated in case (ii) are indeed simplified. However, they may be considered valuable to account for the effects of thermal loads applied to energy piles in the quasi-permanent load combination. Following an approach in agreement with that of the Eurocodes, accompanying variable action values of  $\psi_0 = 0.60$ ,  $\psi_1 = 0.50$  and  $\psi_2 = 0.50$  are suggested for thermal actions applied to energy piles and are considered herein.

When considering the effects of thermal loads applied to energy piles, equation (2.41) needs to be employed while considering the following:

1. For heating thermal loads, it is not known *a priori* whether the involved effects make them the dominant load. Thus, *different design combinations* must be considered. One combination assumes that the effects of the thermal loads make them the dominant load ( $\Delta T_k = Q_{k,1}$ ), i.e.,



$$E_d = \sum_{j \geq 1} \gamma_{G,j} G_{k,j} + \gamma_{Q,1} \Delta T_k + \gamma_{Q,2} \psi_{0,2} Q_{k,2} + \dots + \gamma_{Q,i} \psi_{0,i} Q_{k,i} \quad (2.42)$$

The other combinations assume that the effects of the thermal loads do not make them the dominant load

$$E_d = \sum_{j \geq 1} \gamma_{G,j} G_{k,j} + \gamma_{Q,1} Q_{k,1} + \gamma_{Q,2} \psi_{0,2} \Delta T_k + \dots + \gamma_{Q,i} \psi_{0,i} Q_{k,i} \quad (2.43)$$

In the context of this study, the considered approach results in two load combinations.

2. For cooling thermal loads, a *unique design combination* must be considered, where  $\Delta T_k = Q_{k,1}$ , i.e.,

$$E_d = \sum_{j \geq 1} G_{k,j} + \gamma_{Q,1} \Delta T_k \quad (2.44)$$

The reason for the above is that the coefficients  $\psi_{0,i}$  and  $\gamma_{G,j}$  are equal to zero and one, respectively, for loads the effects of which are favourable for the performance verification, such as (variable and permanent) compressive loads with respect to cooling thermal loads (which cause a decrease in energy pile compression). In the context of this study, the considered approach results in one load combination.

In the aforementioned design combinations, the value of the characteristic temperature variation  $\Delta T_k$ , rather than the value of the effect of this temperature variation  $Q_k(\Delta T_k)$ , must be used. This approach is generally valid irrespective of whether analyses accounting for a reversible or potentially irreversible mechanical behaviour of the soil are performed, as a hypothesis of superposition between the actions and their effects, which characterises the former type of analyses but not the latter, is not made. The above is considered to be theoretically correct and in contrast with the approach proposed by the French recommendations (CFMS-SYNTEC-SOFFONS-FNTP, 2017).

### 2.3.3 Design situations

Two typical situations may occur when designing piles and are considered in the following:

1. A pile length may be defined for each pile of a foundation to sustain an applied value of the design mechanical load. However, because this process is impractical with regard to project execution, the considered length may be increased and approximated to a more meaningful length. As a result, the actual design bearing capacity of the pile will be increased compared

to the original value. In the following, this design situation is used to characterise energy piles with *constant applied mechanical load and varying pile length*.

2. A design mechanical load may be considered for all piles of a foundation based on the maximum load applied to one or more piles. This approach may be employed to design a single pile for the worst foreseeable condition. However, all the piles of a foundation that may effectively be subjected to a lower design mechanical load will be longer than necessary. In the following, this design situation is used to characterise energy piles with *varying applied mechanical load and constant pile length*.

### 2.3.4 Design approach

The geotechnical bearing capacity of piles is generally achieved for either the design load for which a further increase in settlement does not induce an increase in load or for the design load causing a settlement of 10% of the pile base diameter.

Two failure criteria may be associated with the previous conditions and exploited to develop geotechnical ultimate limit state considerations throughout the design process: a strength failure criterion, considering the available strength at the pile-soil interface, and a displacement failure criterion, considering the allowable settlement of the pile. An ultimate limit state may be reached in the former case due to the loss of vertical equilibrium governed by the design resistance provided by the soil against the design load acting on the pile. An ultimate limit state may be reached in the latter case due to the loss of required behavioural performance of the superstructure (or structural elements) because of inadmissible settlement of the piles.

Full-scale field tests may be performed to address the aforementioned aspects via the analysis of so-called pile load-settlement curves. However, in many cases, analyses based on bearing capacity theory are employed.

In the following, the design bearing capacity of energy piles is estimated via an analytical approach based on bearing capacity theory. An analysis in terms of effective stress is performed, in agreement with extensive evidence suggesting that the considered method is the best to account for actual soil and pile behaviour even when piles in fine-grained soil may be encountered (see, e.g., Burland (1973)). The design ultimate capacity of the piles is estimated as

$$Q_{u,d} = Q_{s,d} + Q_{b,d} = \bar{K} \bar{\sigma}'_v \tan \delta' A_s + \sigma'_{vb} N_q d_q A_b \quad (2.45)$$

where  $Q_{s,d}$  is the design value of the pile shaft capacity, estimated using the classical frictional expression presented by Coulomb (1773);  $Q_{b,d}$  is the design value of the pile base capacity, estimated according to the well-established approach proposed by Hansen (1970) by neglecting the terms involving the bearing capacity factors  $N_c$  and  $N_\gamma$  and assuming a shape factor  $s_q = 1$ ;  $\bar{K}$  is an average value of the relevant coefficient of lateral pressure;  $\bar{\sigma}'_v$  is an average value of the *in-situ* vertical effective stress;  $\delta'$  is the pile-soil interface angle of shear strength;  $A_s$  is the pile shaft area;  $\sigma'_{vb}$  is the

vertical effective stress at the level of the pile base;  $N_q$  is a bearing capacity factor;  $d_q$  is a factor that accounts for the pile depth; and  $A_b$  is the pile base area (for further details, see Bowles (1988)).

The angle of shear strength of the soil is assumed to be under constant volume conditions. Such an approach yields suitable estimates of the bearing capacity (Powrie, 2013). The same angle is considered to realistically characterise the pile-soil interface angle of shear strength in the absence of experimental data (Fleming et al., 2008).

Independent of the failure criterion employed to assess the geotechnical performance of energy piles, two aspects, which must be considered in *any case* to ensure adequate structural performance, are accounted for in this study:

1. A design compressive strength of the reinforced concrete section (e.g., for no moments applied) at least equal to the design bearing capacity of the pile must be ensured. When this approach is not employed, design loads sustained from a geotechnical perspective may induce or exceed an ultimate limit state from a structural perspective. In contrast, the proposed approach is in favour of the development of ultimate limit states from a geotechnical perspective and guarantees a potential ductile collapse mechanism. Increasing the compressive strength of reinforced concrete sections can be achieved, e.g., through an increase of the concrete class or reinforcement. Attention must be given to the technical feasibility of using higher concrete classes with reference to the quality of the concrete, especially when dealing with bored piles.
2. A minimum steel reinforcement area of the reinforced concrete section must be chosen. For example, the Eurocodes currently predict for bored piles the minimum reinforcement area,  $A_{s,bpmin}$ , which must be chosen with respect to the pile cross-sectional area,  $A_{EP}$  (coincident with  $A_b$  for cylindrical piles) (EN 1992, 2004). Although this approach is used in the following developments, it will be eventually remarked that it should be replaced by another discussed more suitable approach.

When the action of thermal loads is considered throughout the geotechnical and structural design process of energy piles, two main approaches, employed in the following, must be accounted for:

1. The vertical stress variations caused by mechanical and thermal loads must be considered with respect to the entire length of energy piles, and the most stressed section must be verified. While the effect of vertical mechanical loads applied to the heads of piles is always the worst at the pile head, the effect of thermal loads varies along the pile length depending on the restraint conditions.
2. The vertical displacement variations caused by mechanical and thermal loads must be considered with respect to the heads of the energy piles during verification. While the displacement caused by vertical mechanical loads may be the same at the head and base of piles, assuming that the piles are infinitely rigid bodies, that caused by thermal loads varies with depth but is relevant only at the pile head from a structural point of view.

While the Eurocodes suggest that the worst-case scenario given by different design approaches may be considered in design (EN 1997, 2004), only the so-called “Design Approach 1 – Combination 1” is considered in the following because it is sufficient for the purpose of this work.

### 2.3.5 Analysis method

Unlike the response of piles subjected to mechanical loads, the response of piles subjected to thermal loads cannot be estimated using closed-form analytical expressions. To overcome this issue, the finite difference method exploiting the load-transfer approach is employed using the Thermo-Pile software.

The considered approach uses tri-linear, elasto-plastic load-transfer curves proposed and validated by Frank and Zhao (1982) and Frank et al. (1991) and extended to energy piles and validated by Knellwolf et al. (2011). It considers a linear thermo-elastic behaviour of the reinforced concrete constituting the energy piles.

### 2.3.6 Design case study and material parameters

In this study, single, isolated, non-displacement energy piles of typical varying slenderness ratio values  $L/D = 20, 30, 40$  and  $50$  and pile diameters of  $D = 0.5, 0.75$  and  $1$  m are analysed. The energy piles are assumed to be embedded in a sand deposit for which detailed material properties are available (Herle and Gudehus, 1999; Maehr and Herle, 2004; Ohde, 1939) (cf., Table 2.1).

Two types of conditions are considered for the energy piles: (i) situations where the piles are free to move at their head and (ii) situations where the piles are restrained at their head because of the presence of a slab. The slab stiffness,  $K_h = K_{slab}$ , is calculated according to Poulos and Davis (1974). Situation (i) is often considered in the design of piles because representative yet conservative analyses of the pile vertical displacement can be carried out. Situation (ii) allows similar estimations of the vertical stress along the piles.

In the analyses, no temperature effects on the shear strength parameters, according to available experimental evidence (Di Donna et al., 2015; Yavari et al., 2016), are considered. The case of no temperature effects also accounts for the elastic properties of the soil, although recent evidence shows that they may be slightly present (Eslami et al., 2017). However, these effects are considered of negligible importance for analyses devoted to assessing the ultimate limit state performance of energy piles.

No cyclic degradation phenomena caused by the actual, long-term, geothermal operation of the energy piles are included in the analyses, being the load combinations used for the nominal values of the heating thermal load and the cooling thermal load. While these effects may be considered in some situations involving serviceability limit states, they should not be considered in situations involving ultimate limit states. This approach is in accordance with that suggested by the French recommendations (CFMS-SYNTEC-SOFFONS-FNTP, 2017).

In all situations, the design mechanical load applied to the energy piles is characterised by a 70% permanent proportion and a 30% variable portion. This approach is often employed in practice for preliminary considerations in the absence of more exhaustive information.

Table 2.1: Material properties used for the analyses presented in this study.

Pile parameters		Soil parameters		Soil-pile interaction parameters	
Young's modulus, $E_{EP}$ : [MPa]	31000*	Shear modulus, $G_{soil}$ : [MPa]	8.46**	Slope of elastic branch of Frank and Zhao's (1982) load-displacement relationship for the pile shaft, $K_s$ : [MPa/m]	19.48*** 15.82****
Poisson's ratio, $\nu_{EP}$ : [-]	0.25	Poisson's ratio, $\nu_{soil}$ : [-]	0.30	Slope of elastic branch of Frank and Zhao's (1982) load-displacement relationship for the pile base, $K_b$ : [MPa/m]	116.87*** 94.92****
Bulk density, $\rho_{EP}$ : [kg/m <sup>3</sup> ]	2450	Bulk density, $\rho_{soil}$ : [kg/m <sup>3</sup> ]	2005	Average shaft resistance for single isolated pile, $q_s$ : [kPa]	9.59*** 19.19****
Linear thermal expansion coefficient, $\alpha_{EP}$ : [1/°C]	$1 \cdot 10^{-5}$	Rheological coefficient, $\alpha_r$ : [-]	1/3	Base resistance for single isolated pile, $q_b$ : [kPa]	3409*** 6818****

\* This *mean* Young's modulus refers to the minimum concrete class C25/30 that is considered for an environmental exposition XC2 as predicted by the Eurocodes. A reinforcement steel B500B is employed in all cases. In the numerical analyses, uncracked cross-sections are considered.

\*\* The shear modulus varies with depth according to the pressure-dependent law proposed by Maehr and Herle (2004)

\*\*\* Referring to a diameter  $D = 0.5$  m and a slenderness ratio  $L/D = 20$

\*\*\*\* Referring to a diameter  $D = 1$  m and a slenderness ratio  $L/D = 20$

## 2.4 Unlikelihood of thermal loads exceeding geotechnical ultimate limit states

### 2.4.1 Effects of thermal loads based on a strength capacity criterion

Considering the geotechnical capacity of energy piles based on a strength failure criterion, local or global full mobilisation of the shaft and base capacities of energy piles may be attained because of the application of significant thermal loads, mechanical loads or a combination of these loads. However, irrespective of whether local or global full mobilisation of the capacity may occur for any magnitude or type of thermal load applied to energy piles, the presence of the null point ensures equilibrium against the forces that are mobilised along the shaft and at the base of the pile because of its thermally induced deformation. In fact, in all situations, the reactions provided by the soil below and above the null point of the shear stress compensate each other and prevent the formation of a collapse mechanism. This fact can be appreciated by considering, e.g., equations (2.18), (2.22) and (2.27). Based on the aforementioned considerations, *thermal loads may not involve a collapse mechanism involving the loss of equilibrium of energy piles from a strength failure criterion perspective, i.e., they cannot involve geotechnical ultimate limit states.*

The analysis of the particular case of an energy pile with fully mobilised shaft and base capacities subjected to a thermal load (which may or may not be the cause of the full capacity mobilisation) is of particular interest in this context. Fully mobilising the shaft and base capacities of an energy pile means that a geotechnical ultimate limit state is attained according to a strength failure criterion and that any further increase in load results in exceeding that ultimate limit state (i.e., formation of a collapse mechanism). Because no soil strength is available in this situation, the energy pile can be considered to be under free expansion conditions. Hence, according to the previously discussed thermo-mechanical framework, the application of a thermal load causes no shear stress around the pile, no variation of vertical stress in the pile, and only vertical displacement along the pile. In this condition, the null point of the vertical displacement is at the pile head for a heating thermal load and at the pile toe for a cooling thermal load. In all other situations in which local full mobilisation of the shaft or base capacities may occur, the null point will be located along the energy pile depending on the restraint conditions. In any of the aforementioned cases, however, vertical equilibrium in terms of a strength failure criterion is always preserved.

#### 2.4.2 Effects of thermal loads based on a displacement capacity criterion

Considering the geotechnical capacity of energy piles based on a displacement failure criterion, the worst condition involves piles with fully mobilised shaft and base capacities subjected to a cooling thermal load (which may or may not be the cause of the full capacity mobilisation) that induces the maximum possible head settlement. Piles with fully mobilised capacities subjected to a heating thermal load are of no concern because such a load causes no head settlement. The application of a heating thermal load in all other cases induces an upward head displacement of the energy piles that may recover or even exceed the head settlement caused by mechanical loads. However, the considered problem represents a serviceability limit state problem, not an ultimate limit state problem, and is not considered in the following.

Typical characteristic values of the variable temperature variation that may be considered in a limit state design framework to represent the action of a cooling thermal load applied to energy piles usually range between  $\Delta T_k = -5$  and  $-10$  °C. At worst, this temperature variation may be  $\Delta T_k = -15$  °C in warm climates. These values may prevent freezing in the subsurface (SIA-D0190, 2005; Ground Source Heat Pump Association, 2012; CFMS-SYNTEC-SOFFONS-FNTP, 2017). Considering the partial factor predicted by the Eurocodes for variable actions (such as thermal actions), i.e.,  $\gamma_Q = 1.5$ , the maximum design temperature variation associated with a cooling thermal load is  $\Delta T_d = \gamma_Q \Delta T_k = 1.5 \cdot -15 = -22.5$  °C. Hence, assuming the occurrence of free expansion conditions for an energy pile characterised by the typical maximum practical length  $L = 50$  m and by a linear thermal expansion coefficient  $\alpha_{EP} = 10$   $\mu\epsilon/^\circ\text{C}$ , a maximum head settlement  $w_d^{th}(z = 0) = w_d^{th} = \alpha_{EP} \Delta T_d L = 11.25$  mm may be expected. For the largest diameters (from  $D = 1$  m to  $D = 1.5$  m) that may be expected for energy piles, the above result corresponds to a design value of thermally induced vertical head settlement ranging from  $w_d^{th} = 1.125\%D$  to  $w_d^{th} = 0.75\%D$ .

Thermally induced group effects caused by the interactions among piles may increase the vertical displacement of energy piles (Rotta Loria and Laloui, 2017d; Rotta Loria and Laloui, 2016b). How-



ever, while these effects are significant at the serviceability limit state because of comparable magnitude to the phenomena involved, they are negligible at ultimate limit states because they are not at all comparable to the relevant phenomena. Based on the aforementioned considerations, *thermal loads may not involve energy pile settlements capable of involving the formation of a collapse mechanism from a displacement failure criterion perspective, i.e., they are unlikely to reach or exceed the geotechnical ultimate limit states*. This fact is considered justifiable irrespective of whether only thermal loads or both mechanical and thermal loads are applied to energy piles because of the following:

1. Energy pile displacements may improbably develop entirely under free expansion conditions, being much lower in magnitude than those mentioned above. Even the fundamental combination of the Eurocodes implies that a lower mechanical load compared to the design bearing capacity may be more likely applied when cooling influences the energy pile. Thus, full mobilisation of the pile capacities and free conditions are not involved.
2. The magnitude of the thermally induced settlements may definitely be considered negligible compared to those for which verifications against mechanical loads are usually performed and considered to be satisfied. The maximum settlements that may be caused by thermal loading are approximately one tenth of the limiting value suggested by the current displacement failure criteria.
3. When a state close to a geotechnical ultimate limit state in terms of a displacement criterion may be achieved because of the action of mechanical loads, it would be senseless to thermally activate energy piles that may be subjected to unacceptable settlements. This consideration allows practically neglecting the considered problem.

The results reported in the following corroborate the aforementioned digression with respect to the considered case studies.

### 2.4.3 Energy pile response for constant applied mechanical load and varying pile length

Table 2.2 and Table 2.3 summarise the vertical head displacement induced by combined mechanical and cooling loads applied to energy piles of slenderness ratios  $L/D = 20$  and  $50$ , which are characterised by diameters of  $D = 0.5$  and  $1$  m, respectively, and free to move at their head. In all cases, the same design mechanical load  $P_d$ , corresponding to the design bearing capacity for  $L/D = 20$ , i.e.,  $Q_{u,d}(L/D = 20)$ , is considered. Two design temperature changes of  $\Delta T_d = \gamma_Q \Delta T_k = 1.5 \cdot -5 = -7.5$  °C and  $\Delta T_d = 1.5 \cdot -15 = -22.5$  °C are considered.

The settlement induced by the combined action of mechanical loading and cooling can be considered negligible in all cases. The thermally induced displacements for  $L/D = 20$  do not develop under free expansion conditions because the actual mechanical load applied to the head of the energy piles is lower than the bearing capacity according to the design combination expressed in equation (2.44), i.e.,  $P_d \equiv G_k$ . Hence, free expansion conditions do not occur.

For the same applied mechanical load and pile diameter, increasing the pile slenderness ratio results in lower head settlement of the energy piles because the bearing load that the piles can sustain is greater. This phenomenon is in accordance with the conventional, justified belief that longer piles ensure greater safety against the action of mechanical loads with respect to geotechnical (and structural) ultimate limit states.

For the same applied thermal load and pile diameter, increasing the pile slenderness ratio results in greater head settlement of the energy piles because even the same thermally induced observed strain causes greater vertical displacements for longer piles. This phenomenon is in contrast with the belief that longer piles may ensure greater safety against the action of thermal loads with respect to geotechnical (and structural) ultimate limit states.

Table 2.2: Normalised vertical head displacements for energy piles of  $D = 0.5$  m that are free at their head and subjected to cooling – constant applied mechanical load and varying pile length.

Pile diameter	Slenderness ratio	Normalised design mechanical load	Design temperature change	Normalised design vertical head displacement induced by load type		
				Mechanical	Thermal	Mechanical and thermal
$D$ [m]	$L/D$ [-]	$P_d/Q_{u,d}$ [-]	$\Delta T_d$ [°C]	$w_d^m/D$ [%]	$w_d^{th}/D$ [%]	$w_d^{m+th}/D$ [%]
0.5	20	1	-7.5	1.28	0.15	1.43
			-22.5	1.28	0.45	1.73
	50	$P_d/Q_{u,d} (L/D = 20)$	-7.5	0.09	0.21	0.30
			-22.5	0.09	0.69	0.78

For the same pile slenderness ratio and a greater pile diameter, greater head settlement of the energy piles is caused by mechanical loads because the bearing load that the piles can sustain and are subjected to is greater. At the same time, for the same pile slenderness ratio and a greater pile diameter, lower head settlement of the energy piles is caused by thermal loads because the bearing load that the piles can sustain is greater.

Based on the above, *if the aim is to limit the vertical displacement of energy piles caused by thermal loads, longer pile lengths should be avoided, while greater pile diameters should be employed.*

Table 2.4 and Table 2.5 show the same variables considered above but refer to energy piles restrained at their head by the presence of a slab of normalised stiffness relative to the soil of  $K_{slab}D/G_{soil}(z = 0) = 10^5$ , where  $G_{soil}(z = 0)$  is the soil shear modulus at the level of the pile head. The same energy pile head settlement values caused by mechanical loads as those of the previous results are observed. This result occurs because the numerical analyses neglect the effect of the head restraint when addressing the action of mechanical loads and consider it only when addressing thermal loads. Near-zero energy pile head settlements are caused by thermal loads because of the marked slab stiffness.



Table 2.3: Normalised vertical head displacements for energy piles of  $D = 1$  m that are free at their head and subjected to cooling – constant applied mechanical load and varying pile length.

Pile diameter	Slenderness ratio	Normalised design mechanical load	Design temperature change	Normalised design vertical head displacement induced by load type		
				Mechanical	Thermal	Mechanical and thermal
$D$	$L/D$	$P_d/Q_{u,d}$	$\Delta T_d$	$w_d^m/D$	$w_d^{th}/D$	$w_d^{m+th}/D$
[m]	[-]	[-]	[°C]	[%]	[%]	[%]
1	20	1	-7.5	1.60	0.15	1.75
			-22.5	1.60	0.45	2.05
	50	$P_d/Q_{u,d}(L/D = 20)$	-7.5	0.15	0.19	0.34
			-22.5	0.15	0.65	0.80

Table 2.4: Normalised vertical head displacements for energy piles of  $D = 0.5$  m that are restrained at their head and subjected to cooling – constant applied mechanical load and varying pile length.

Pile diameter	Slenderness ratio	Normalised design mechanical load	Design temperature change	Normalised design vertical head displacement induced by load type		
				Mechanical	Thermal	Mechanical and thermal
$D$	$L/D$	$P_d/Q_{u,d}$	$\Delta T_d$	$w_d^m/D$	$w_d^{th}/D$	$w_d^{m+th}/D$
[m]	[-]	[-]	[°C]	[%]	[%]	[%]
0.5	20	1	-7.5	1.28	0.00*	1.28
			-22.5	1.28	0.00*	1.28
	50	$P_d/Q_{u,d}(L/D = 20)$	-7.5	0.09	0.00*	0.09
			-22.5	0.09	0.01	0.10

\* Values are nonzero but negligible for the accuracy considered.

Table 2.5: Normalised vertical head displacements for energy piles of  $D = 1$  m that are restrained at their head and subjected to cooling – constant applied mechanical load and varying pile length.

Pile diameter	Slenderness ratio	Normalised design mechanical load	Design temperature change	Normalised design vertical head displacement induced by load type		
				Mechanical	Thermal	Mechanical and thermal
$D$	$L/D$	$P_d/Q_{u,d}$	$\Delta T_d$	$w_d^m/D$	$w_d^{th}/D$	$w_d^{m+th}/D$
[m]	[-]	[-]	[°C]	[%]	[%]	[%]
1	20	1	-7.5	1.60	0.00*	1.60
			-22.5	1.60	0.00*	1.60
	50	$P_d/Q_{u,d}(L/D = 20)$	-7.5	0.15	0.00*	0.15
			-22.5	0.15	0.00*	0.15

\* Values are nonzero but negligible for the accuracy considered.

#### 2.4.4 Energy pile response for varying applied mechanical load and constant pile length

Table 2.6 and Table 2.7 summarise the vertical head displacement induced by combined mechanical loads  $P_d = Q_{u,d}$  and cooling loads  $\Delta T_d = -7.5$  and  $-22.5$  °C applied to energy piles characterised by diameters of  $D = 0.5$  and  $1$  m, respectively, and free to move at their head. The aforementioned design actions are considered for energy piles of slenderness ratios  $L/D = 20$  and  $50$ .

The settlement induced by the combined action of mechanical loading and cooling can again be considered negligible. For the same pile diameter and pile slenderness ratio, decreasing the applied mechanical load results in lower head settlement of the energy piles because the bearing load that the piles can sustain is greater and the irreversible phenomena caused in the soil are less notable. At the same time, decreasing the applied mechanical load involves less marked energy pile head settlement values for the same subsequently applied temperature variation. The lower the applied mechanical load, the larger the load range for which the soil response remains reversible for further thermal loading. Because the response of the pile-soil system is stiffer under reversible conditions compared to that under irreversible conditions, lower vertical displacements are expected in situations where the soil response is predominantly elastic compared to those when the soil response is predominantly plastic.

Table 2.8 and Table 2.9 summarise the same variables considered above but refer to energy piles restrained at their head by the presence of a slab of normalised stiffness relative to the soil of  $K_{slab}D/G_{soil}(z = 0) = 10^5$ .

Table 2.6: Normalised vertical head displacements for energy piles of  $D = 0.5$  m that are free at their head and subjected to cooling – varying applied mechanical load and constant pile length.

Pile diameter	Slenderness ratio	Normalised design mechanical load	Design temperature change	Normalised design vertical head displacement induced by load type		
				Mechanical	Thermal	Mechanical and thermal
$D$ [m]	$L/D$ [-]	$P_d/Q_{u,d}$ [-]	$\Delta T_d$ [°C]	$w_d^m/D$ [%]	$w_d^{th}/D$ [%]	$w_d^{m+th}/D$ [%]
0.5	20	1	-7.5	1.28	0.15	1.43
			-22.5	1.28	0.45	1.73
		0.2	-7.5	0.04	0.10	0.14
			-22.5	0.04	0.30	0.34
	50	1	-7.5	0.09	0.21	0.30
			-22.5	0.09	0.69	0.78
		0.2	-7.5	0.02	0.16	0.18
			-22.5	0.02	0.53	0.55

Table 2.7: Normalised vertical head displacements for energy piles of  $D = 1$  m that are free at their head and subjected to cooling – varying applied mechanical load and constant pile length.

Pile diameter	Slenderness ratio	Normalised design mechanical load	Design temperature change	Normalised design vertical head displacement induced by load type		
				Mechanical	Thermal	Mechanical and thermal
$D$ [m]	$L/D$ [-]	$P_d/Q_{u,d}$ [-]	$\Delta T_d$ [°C]	$w_d^m/D$ [%]	$w_d^{th}/D$ [%]	$w_d^{m+th}/D$ [%]
1	20	1	-7.5	1.60	0.15	1.75
			-22.5	1.60	0.45	2.05
		0.2	-7.5	0.05	0.10	0.15
			-22.5	0.05	0.30	0.35
	50	1	-7.5	0.15	0.19	0.34
			-22.5	0.15	0.65	0.80
		0.2	-7.5	0.03	0.14	0.16
			-22.5	0.03	0.49	0.51

Table 2.8: Normalised vertical head displacements for energy piles of  $D = 0.5$  m that are restrained at their head and subjected to cooling – varying applied mechanical load and constant pile length.

Pile diameter	Slenderness ratio	Normalised design mechanical load	Design temperature change	Normalised design vertical head displacement induced by load type		
				Mechanical	Thermal	Mechanical and thermal
$D$ [m]	$L/D$ [-]	$P_d/Q_{u,d}$ [-]	$\Delta T_d$ [°C]	$w_d^m/D$ [%]	$w_d^{th}/D$ [%]	$w_d^{m+th}/D$ [%]
0.5	20	1	-7.5	1.28	0.00*	1.28
			-22.5	1.28	0.00*	1.28
		0.2	-7.5	0.04	0.00*	0.04
			-22.5	0.04	0.00*	0.04
	50	1	-7.5	0.09	0.09	0.19
			-22.5	0.09	0.09	0.19
		0.2	-7.5	0.02	0.00*	0.02
			-22.5	0.02	0.01	0.03

\* Values are nonzero but negligible for the accuracy considered.

Table 2.9: Normalised vertical head displacements for energy piles of  $D = 1$  m that are restrained at their head and subjected to cooling – varying applied mechanical load and constant pile length.

Pile diameter	Slenderness ratio	Normalised design mechanical load	Design temperature change	Normalised design vertical head displacement induced by load type		
				Mechanical	Thermal	Mechanical and thermal
$D$ [m]	$L/D$ [-]	$P_d/Q_{u,d}$ [-]	$\Delta T_d$ [°C]	$w_d^m/D$ [%]	$w_d^{th}/D$ [%]	$w_d^{m+th}/D$ [%]
1	20	1	-7.5	1.60	0.00*	1.60
			-22.5	1.60	0.00*	1.60
		0.2	-7.5	0.05	0.00*	0.05
			-22.5	0.05	0.00*	0.05
	50	1	-7.5	0.15	0.00*	0.15
			-22.5	0.15	0.00*	0.15
		0.2	-7.5	0.03	0.00*	0.03
			-22.5	0.03	0.00*	0.03

\* Values are nonzero but negligible for the accuracy considered.

## 2.5 Unlikelihood of thermal loads involving structural ultimate limit states

### 2.5.1 Effects of thermal loads from a structural capacity perspective

As previously discussed, in all situations where full mobilisation of the shaft and base capacities does not characterise energy piles, effects caused by thermal loads are present. The most burdensome effect of thermal loads on the structural capacity of reinforced concrete sections may be caused by a cooling thermal load rather than a heating thermal load. The reason for this is that the tensile strength of reinforced concrete that may resist the effects of cooling thermal loads is much less notable than the compressive strength that may resist the effects of heating thermal loads.

Assuming the occurrence of completely blocked conditions for an energy pile characterised by the same properties presented above, in addition to a Young's modulus of  $E_{EP} = 30$  GPa, and subjected to a design cooling load of  $\Delta T_d = -22.5$  °C, a design value of thermally induced tensile vertical stress  $\sigma_{b,d}^{th} = E_{EP} \alpha_{EP} \Delta T = 30 \cdot 10^9 \cdot 10 \cdot 10^{-6} \cdot -22.5 = -6750$  kPa will arise. For diameters from  $D = 1$  m to  $D = 1.5$  m, this result corresponds to a design value of thermally induced variation of the axial force ranging from  $N_d^{th} = \sigma_{b,d}^{th} A_{EP} = -6750 \cdot \pi \cdot 1^2/4 = -5300$  kN to  $N_d^{th} = -6750 \cdot \pi \cdot 1.5^2/4 = -11928$  kN. These values, although referring to unrealistic completely blocked conditions, are markedly high.

The presence of permanent loads may relieve energy piles subjected to cooling thermal loads, while it may further encumber energy piles subjected to heating thermal loads. Thermally induced group effects may significantly reduce (e.g., up to 40%) the effects of thermal loads (Di Donna et al., 2016). However, the effect of both heating and cooling thermal loads may, at first glance, involve structural ultimate limit states.

The results reported in the following expand on the aforementioned digression with respect to the considered case studies.

## 2.5.2 Energy pile response for constant applied mechanical load and varying pile length

### 2.6.2.1 Energy pile heating

Figure 2.8 presents the normalised axial load,  $N_{E,d}/N_{R,d}$ , experienced in the most stressed section along the length of energy piles of varying slenderness ratio,  $L/D$ , and for different pile diameters  $D = 0.5, 0.75$  and  $1$  m. In all situations, the same design mechanical load  $P_d$ , corresponding to the design bearing capacity for  $L/D = 20$ , i.e.,  $Q_{u,d}(L/D = 20)$ , is considered.

The two load combinations expressed in equation (2.42) and equation (2.43) are accounted for. In these two combinations, considering characteristic temperature variation values  $\Delta T_k = 10, 20$  and  $30$  °C, the maximum foreseeable design temperature variation values  $\Delta T_d = \gamma_Q \Delta T_k = 15, 30$  and  $45$  °C, and  $\Delta T_d = \gamma_Q \psi_{0,1} \Delta T_k = 13.5, 27$  and  $40.5$  °C, respectively.

The design acting load  $N_{E,d}$  is generally caused by the action of both mechanical and thermal loads. The design resisting load  $N_{R,d}$  corresponds to the compression axial resisting load when no moments are applied, according to the strength domain of the analysed reinforced concrete cross-section.

The combined action of mechanical and heating thermal loads involves design variations in the axial load,  $N_{E,d}$ , that are, at worst, approximately 40% of the available design resisting load of the reinforced concrete cross-section,  $N_{R,d}$ . In other words, no structural ultimate limit states are involved in the combined action of mechanical and heating thermal loads in energy piles. The effect of thermal loads increases as the pile slenderness and diameter increase.

Increasing the concrete class for pile slenderness values that may be associated with applied design mechanical loads (i.e., coincident, at least theoretically, with the bearing capacity of the pile) greater than the axial resisting compressive load of cross-sections characterised by the minimum concrete class C25/30 predicted by the Eurocodes for an environmental exposition XC2 ensures greater safety against structural ultimate limit states.

Figure 2.9 shows the normalised axial load,  $N_{E,d}/N_{R,d}$ , experienced by the energy piles considered above for  $L/D = 50$  but characterised by the presence of a slab at their head of varying stiffness relative to the soil of  $K_{slab}D/G_{soil}(z = 0)$ . Considering a pile slenderness ratio  $L/D = 50$  allows commenting on results that are an upper bound for energy piles of any lower slenderness ratio because it represents the worst-case scenario for the thermally induced variation of an axial load.

The combined action of mechanical and heating thermal loads does not involve structural ultimate limit states in the energy piles, although a more burdensome effect of thermal loads is observed compared to situations where the energy piles are free to move at their head because of the presence of the slab (i.e.,  $N_{E,d}/N_{R,d} = 0.5$  instead of  $0.4$  at worst). The values of  $N_{E,d}/N_{R,d}$  for  $K_{slab}D/G_{soil}(z = 0) = 10^{-7}$  can be associated with an infinitely flexible slab and coincide with those presented in Figure 2.8 for the same  $L/D$ . The effect of the slab presence increases with the associated restraint for in-

creasing values of  $K_{slab}D/G_{soil}(z = 0)$  because of a pronounced variation of the effects of the applied thermal loads for relative stiffness values of approximately  $K_{slab}D/G_{soil}(z = 0) = 10$ . The effect of thermal loads also increases as the pile diameter increases.

### 2.6.2.2 Energy pile cooling

Figure 2.10 and Figure 2.11 present similar results to those shown in Figure 2.8 and Figure 2.9, respectively, but for load combinations involving design mechanical loads and cooling thermal loads applied to the energy piles. Only one load combination is considered in this case for the design cooling loads according to equation (2.44). In this combination, considering characteristic temperature variation values  $\Delta T_k = -5, -10$  and  $-15$  °C, the maximum foreseeable design temperature variation values  $\Delta T_d = \gamma_Q \Delta T_k = -7.5, -15$  and  $-22.5$  °C. The design acting load  $N_{E,d}^*$  is generally caused by the action of both mechanical and thermal loads. The design resisting load  $N_{R,d}^*$  corresponds to the traction axial resisting load represented by the distance between the actual design acting load caused by the thermal load, applied subsequently to the mechanical load, and the traction resisting load characterising the analysed reinforced concrete cross-section when no moments are applied.

The combined action of mechanical and cooling thermal loads involves design variations of the axial load,  $N_{E,d}^*$ , that can exceed the available design resisting load of the reinforced concrete cross-section,  $N_{R,d}^*$ . This phenomenon occurs according to numerical simulations accounting for (i) uncracked cross-sections, (ii) linear stress-strain relationships and (iii) mean values of the modulus of elasticity of the reinforced concrete, as suggested by the Eurocodes (EN 1992, 2004).

The effect of the cooling thermal loads is much more pronounced on the variation of the axial load in the reinforced concrete cross-sections of energy piles compared to the effect of heating thermal loads. This effect increases as the pile slenderness and pile diameter increase and, for the case of extremely rigid slabs, can involve normalised axial loads of up to  $N_{E,d}^*/N_{R,d}^* = 2$ .

## 2.5.3 Energy pile response for varying applied mechanical load and constant pile length

### 2.6.3.1 Energy pile heating

Figure 2.12 presents the normalised axial load,  $N_{E,d}/N_{R,d}$ , experienced in the most stressed section along the length of energy piles characterised by varying design mechanical loads,  $P_d/Q_{u,d}$ , and different pile diameters of  $D = 0.5, 0.75$  and  $1$  m. In all situations, fixed pile slenderness ratios  $L/D = 20$  and  $50$  are considered. The two load combinations considered thus far for mechanical loading and heating thermal loading are accounted for.

In all cases, no structural ultimate limit states are caused by the combined action of mechanical and heating thermal loads. Lower design mechanical loads ensure greater safety against the occurrence of a structural ultimate limit state potentially caused by thermal loads. However, lower design mechanical loads involve a greater impact of design thermal loads on the variation of the axial load along energy piles according to previously proposed arguments related to the state of restraint and reversibility of the pile-soil system.

Figure 2.13 and Figure 2.14 show the response of the same energy piles with slenderness ratios  $L/D = 20$  and  $50$  previously considered, respectively, except the piles are now characterised by a slab at their head of varying stiffness relative to the soil. Values of  $P_d/Q_{u,d} = 80$  and  $20$  are considered. The combined action of mechanical and heating thermal loads does not involve structural ultimate limit states in the energy piles.

In accordance with the aforementioned comments, the lower the design mechanical load, the greater the effect of subsequently applied thermal loads, e.g., an increase in the effect as the pile slenderness ratio and diameter increase.

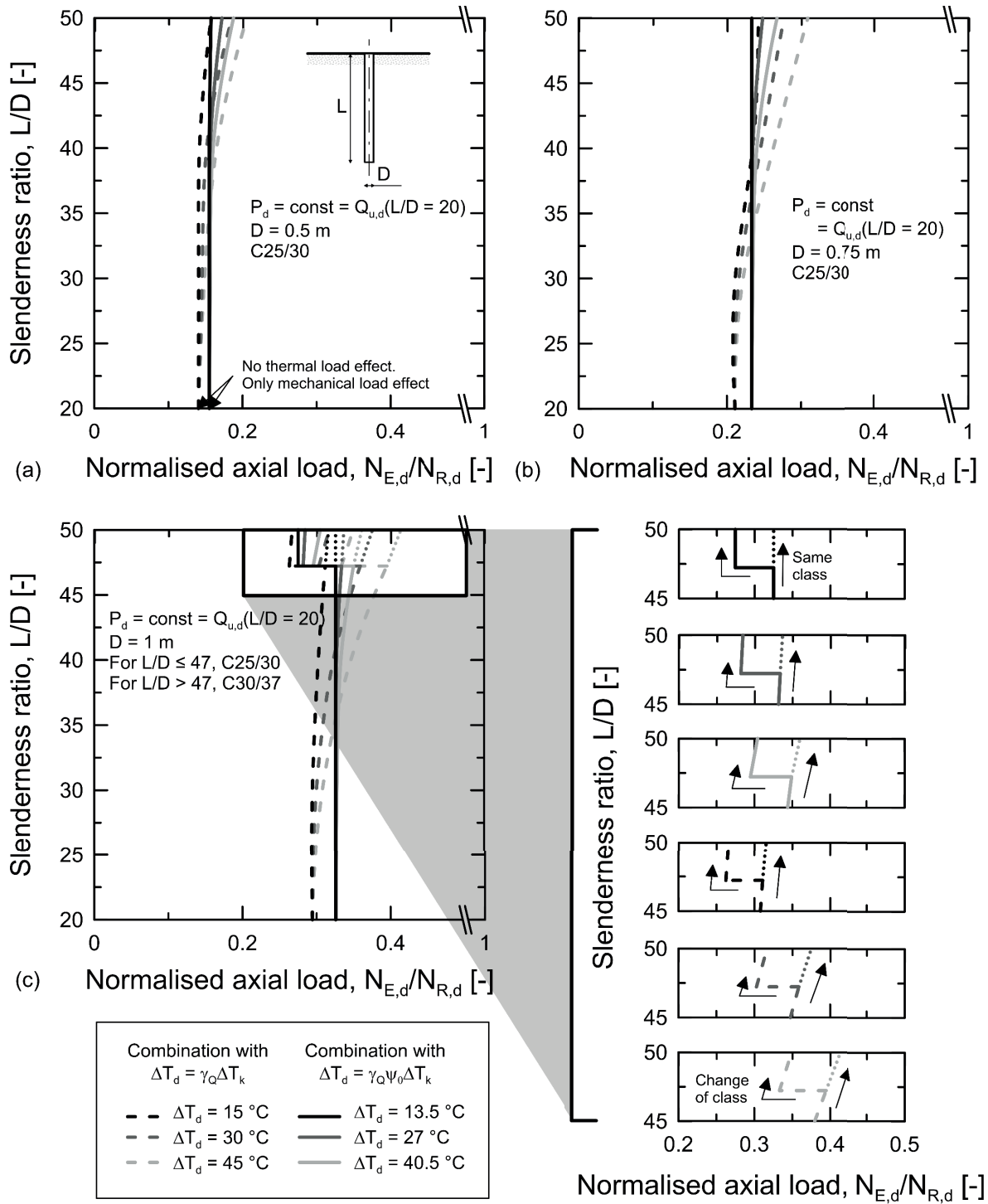
### 2.6.3.2 Energy pile cooling

Figure 2.15 as well as Figure 2.16 and Figure 2.17 present similar results to those shown in Figure 2.12, Figure 2.13 and Figure 2.14, respectively, but for load combinations involving design mechanical loads and cooling thermal loads applied to the energy piles. The unique load combination considered thus far for mechanical loading and cooling thermal loading is accounted for.

The combined action of mechanical and cooling thermal loads involves design variations in the axial load,  $N_{E,d}^*$ , that can exceed the available design resisting load of the reinforced concrete cross-section,  $N_{R,d}^*$ . This action is more pronounced for energy piles of varying applied mechanical loads and constant pile length compared to energy piles of constant applied mechanical load and varying pile length.

The lower the applied mechanical load, the larger the load range for which the soil response remains reversible (and stiffer compared to situations in which it becomes irreversible) for further thermal loading, and the more burdensome the effect of such loading on the variation of the axial load in the concrete cross-section. This phenomenon increases with the stiffness relative to the soil of a slab present at the head of the energy piles.

The effect of mechanical and cooling thermal loads can involve normalised axial loads of up to  $N_{E,d}^*/N_{R,d}^* = 2.3$ .





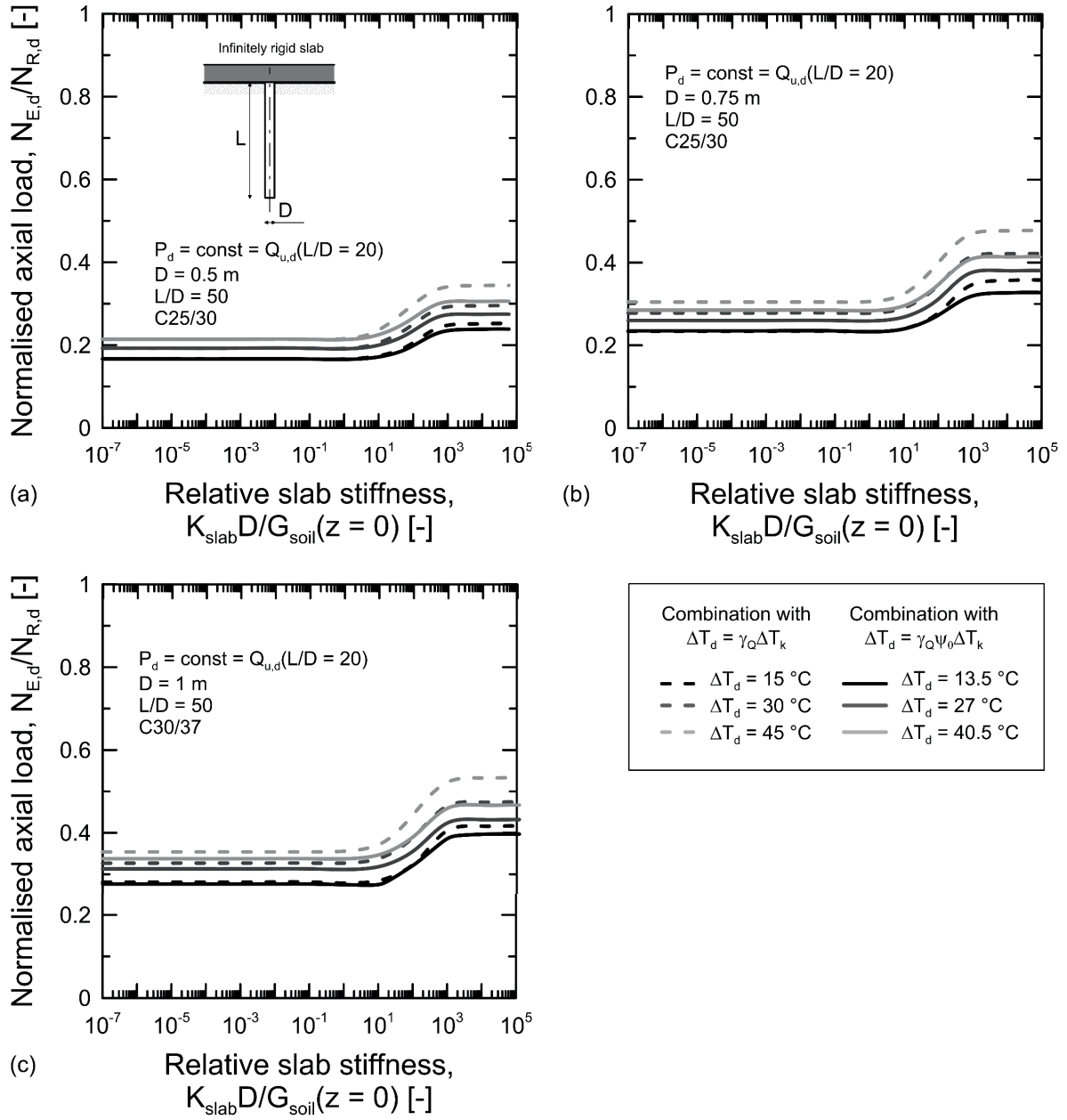


Figure 2.9: Normalised axial loads for energy piles restrained at their head and subjected to heating – constant applied mechanical load and varying pile length.

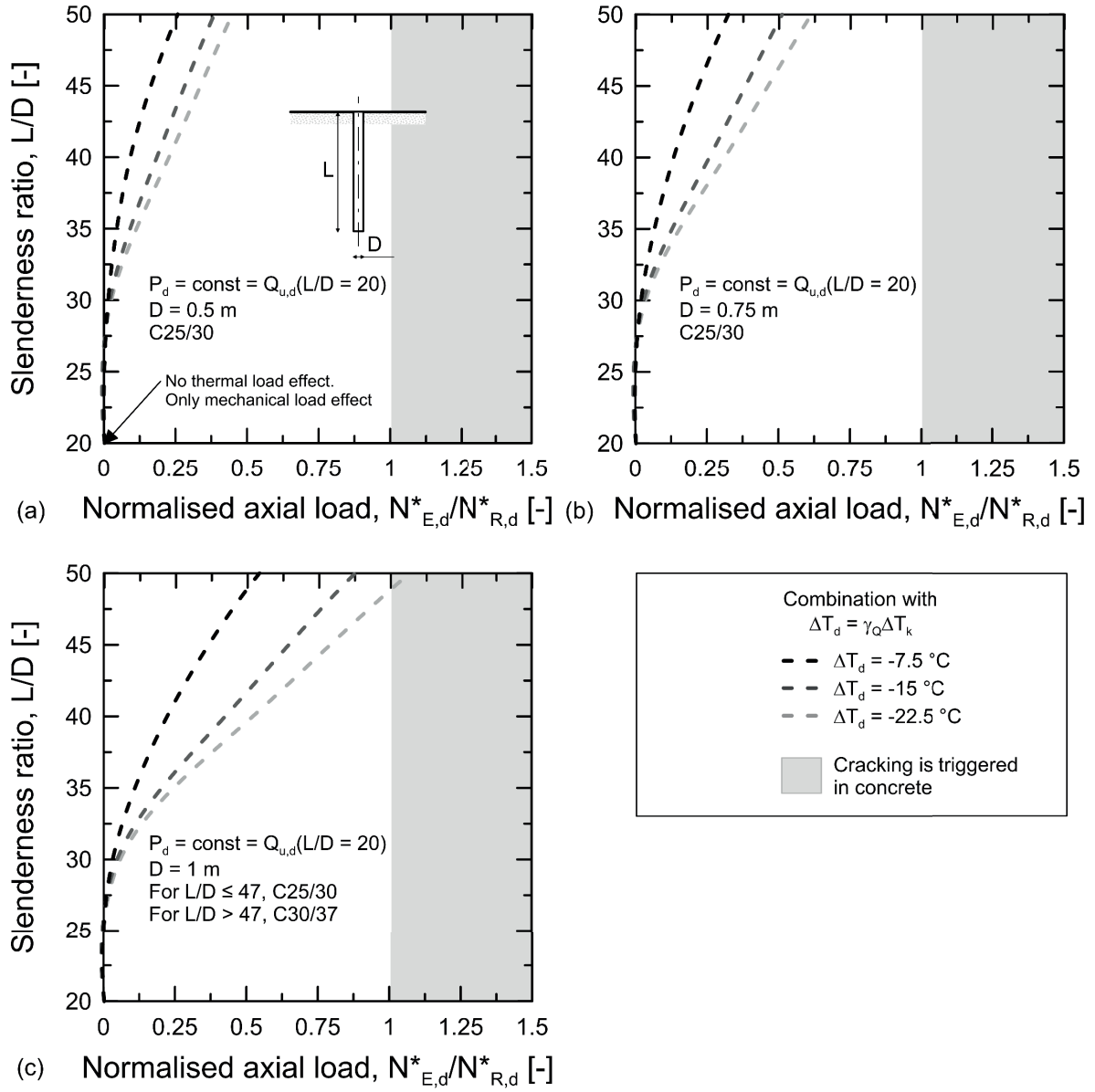


Figure 2.10: Normalised axial loads for energy piles that are free at their head and subjected to cooling – constant applied mechanical load and varying pile length.

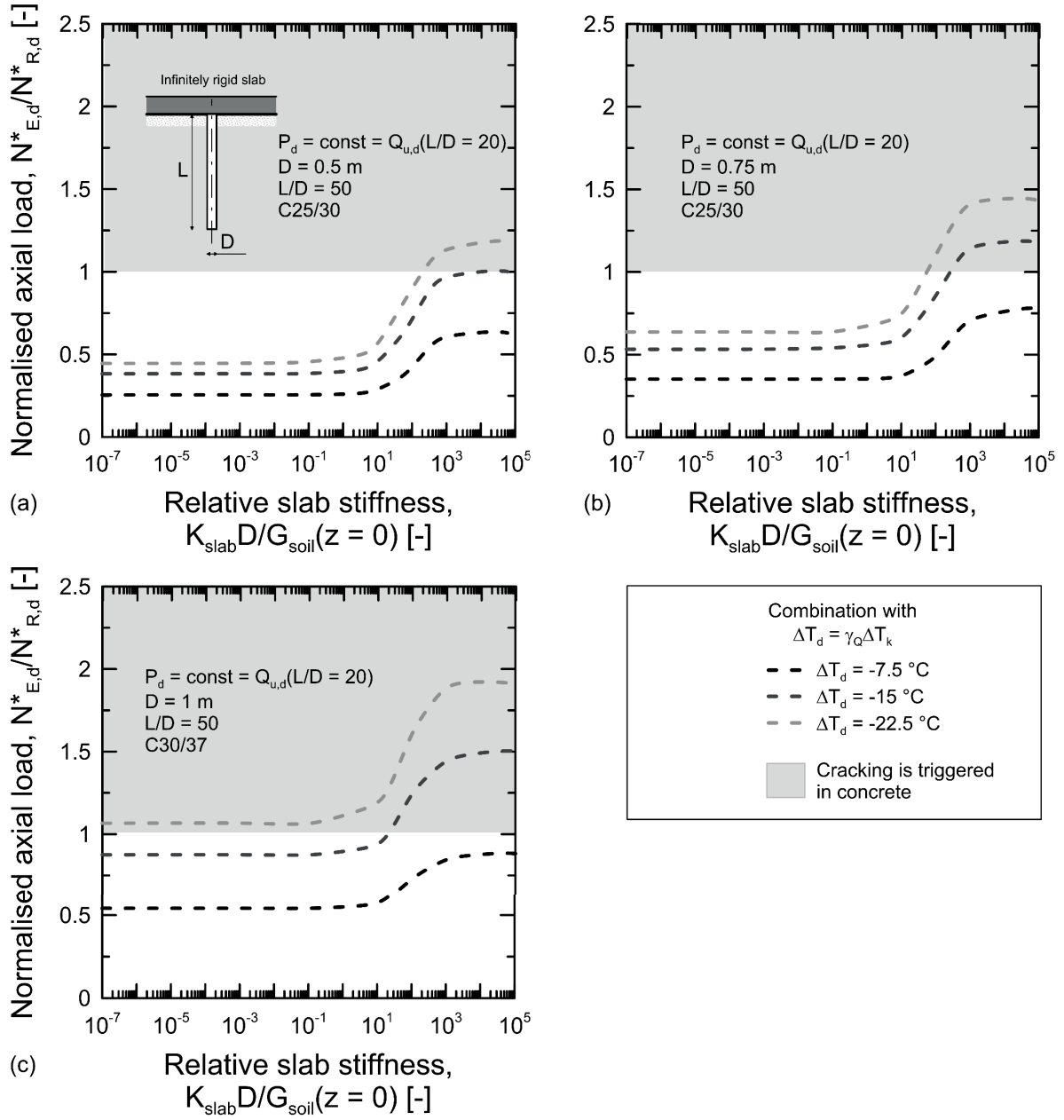


Figure 2.11: Normalised axial loads for energy piles restrained at their head and subjected to cooling – constant applied mechanical load and varying pile length.

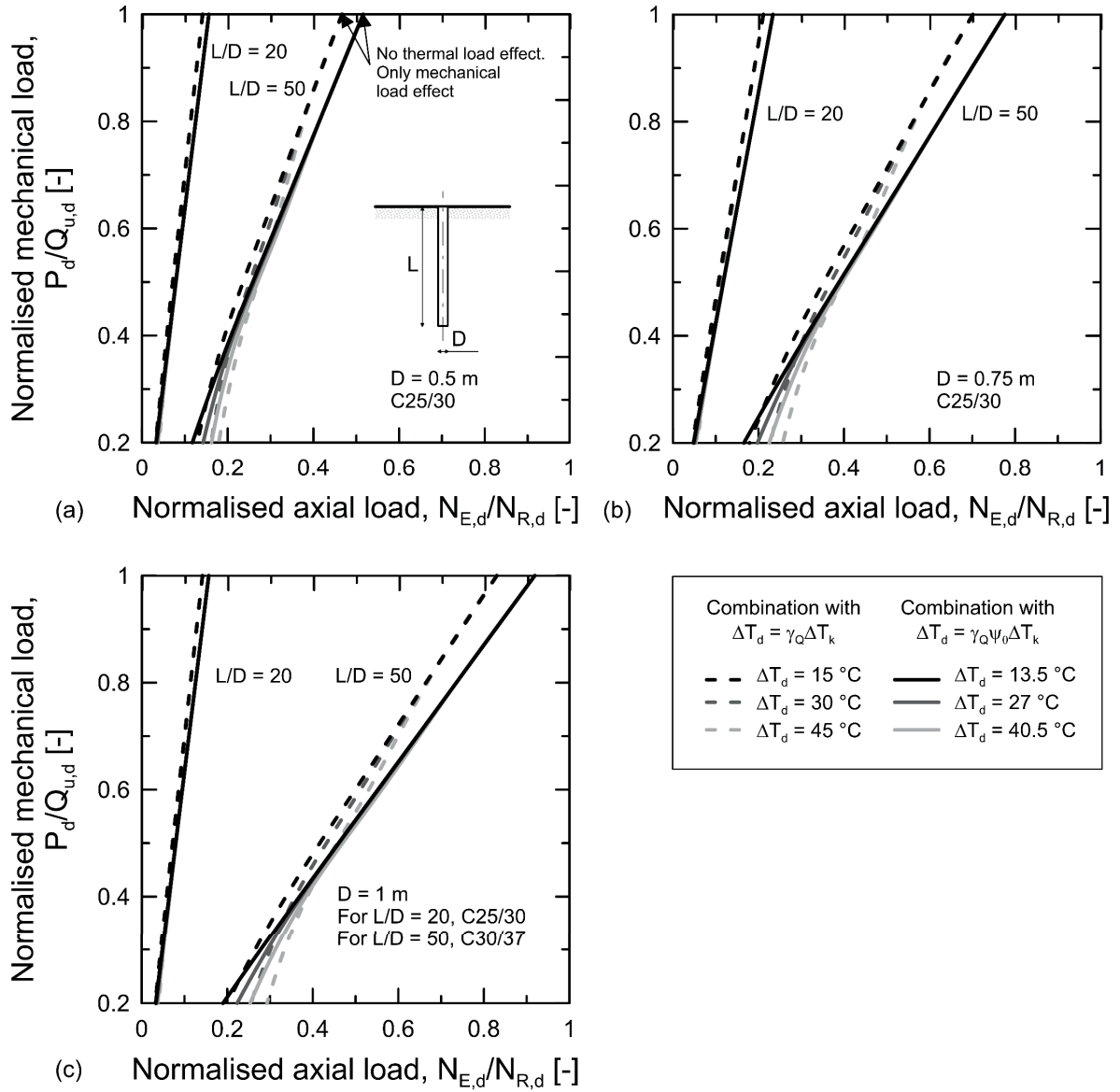


Figure 2.12: Normalised axial loads for energy piles that are free at their head and subjected to heating – varying applied mechanical load and constant pile length.

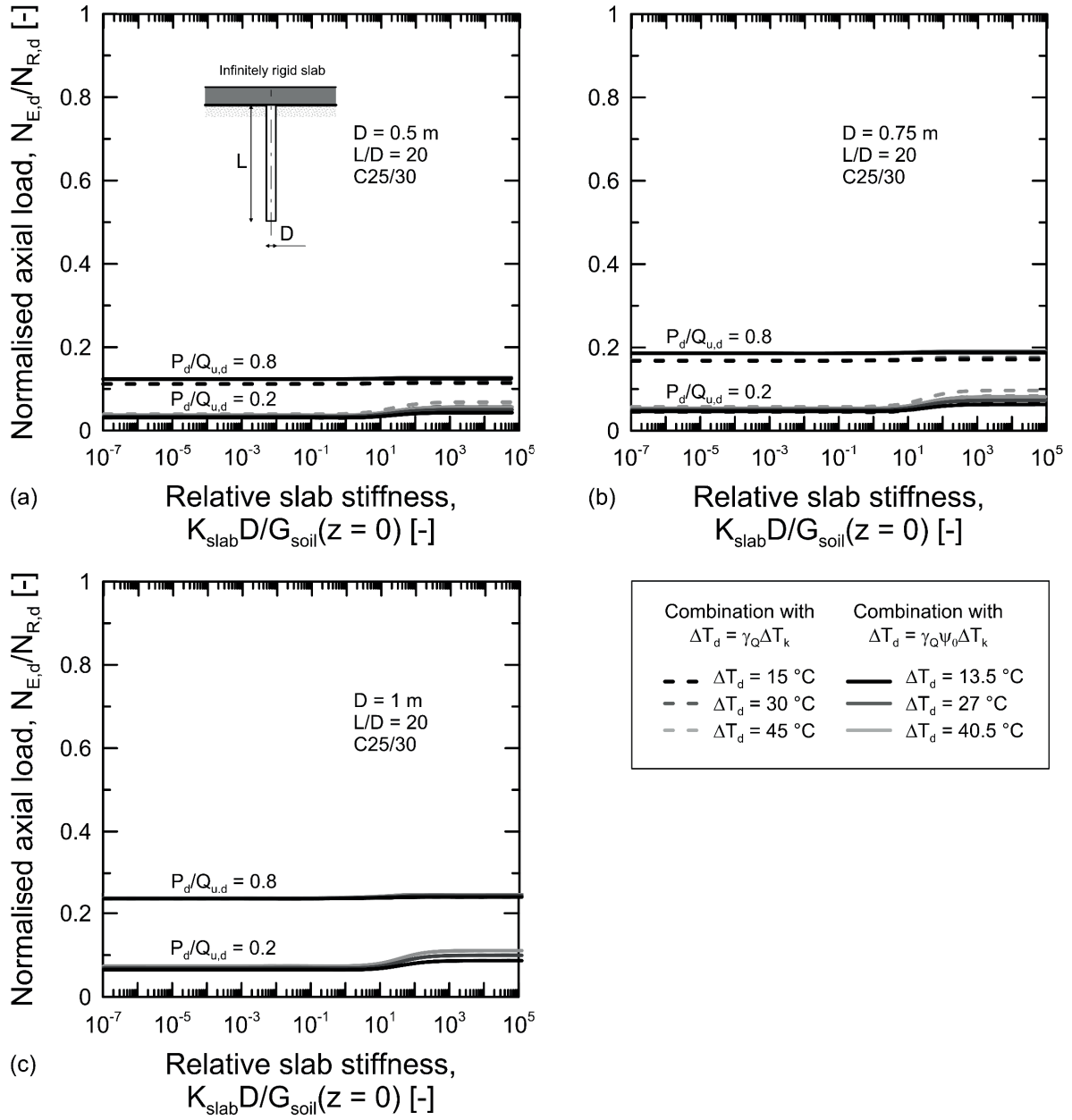


Figure 2.13: Normalised axial loads for energy piles of  $L/D = 20$  that are restrained at their head and subjected to heating – varying applied mechanical load and constant pile length.

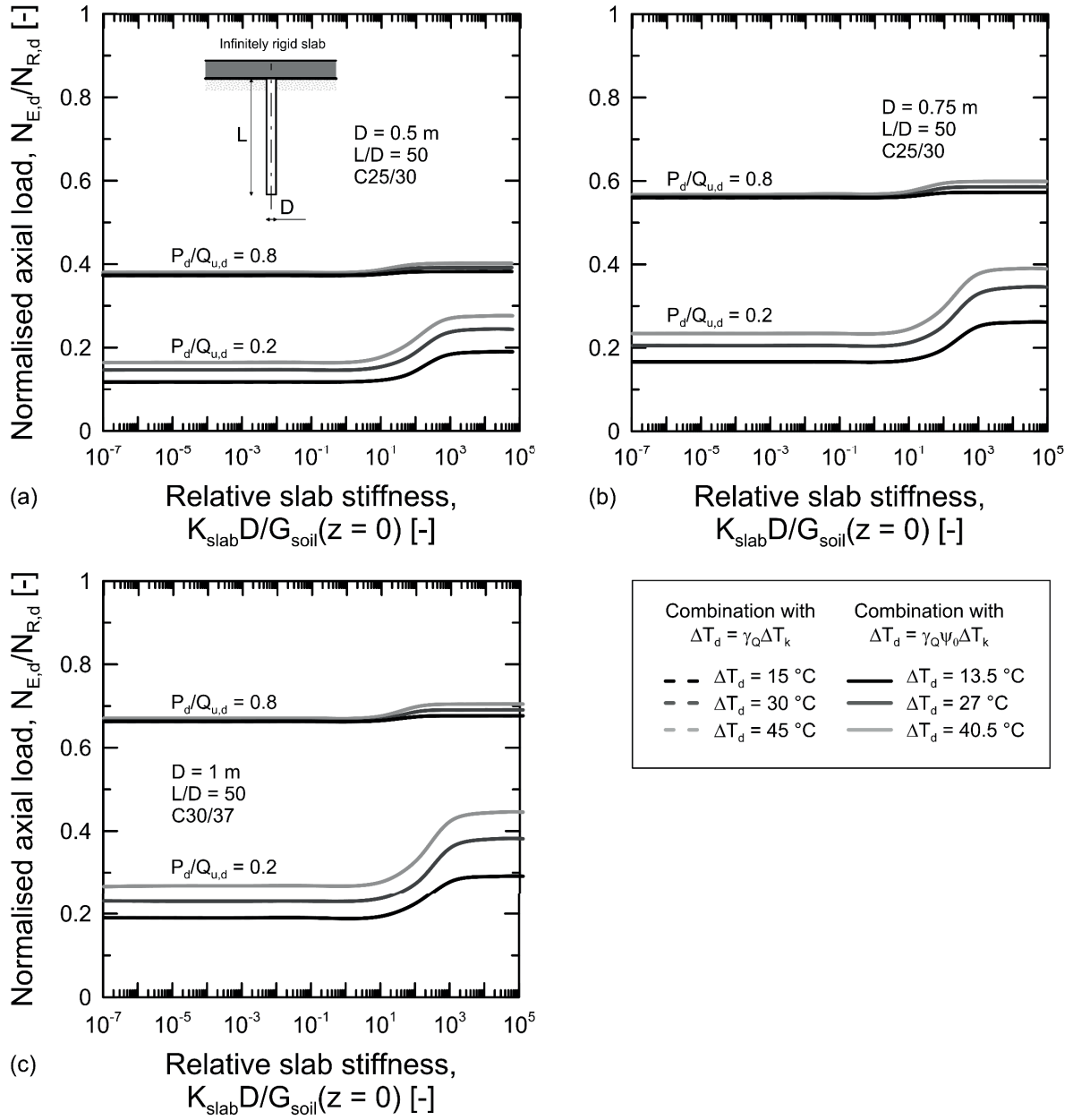


Figure 2.14: Normalised axial loads for energy piles of  $L/D = 50$  that are restrained at their head and subjected to heating – varying applied mechanical load and constant pile length.

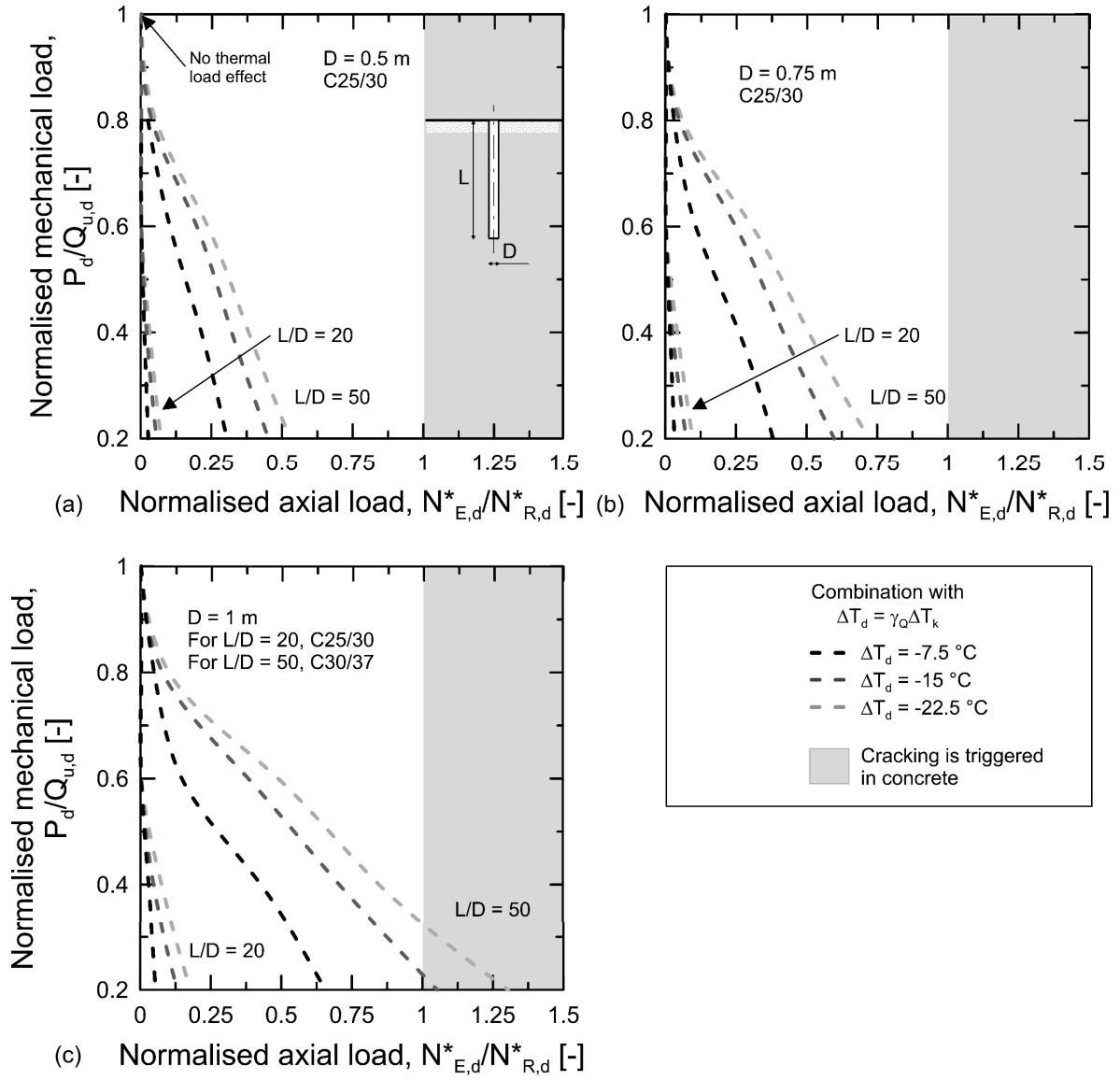


Figure 2.15: Normalised axial loads for energy piles that are free at their head and subjected to cooling – varying applied mechanical load and constant pile length.

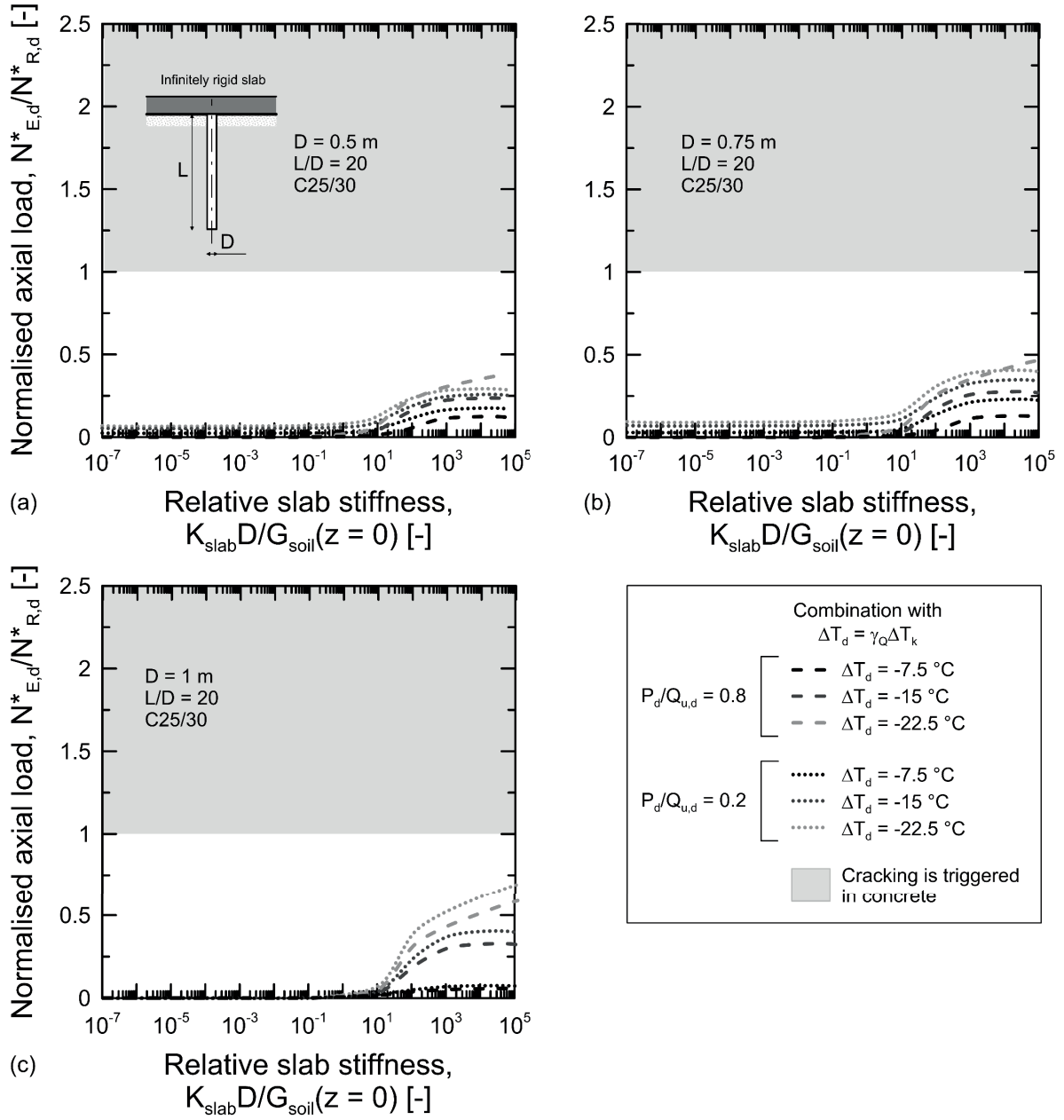


Figure 2.16: Normalised axial loads for energy piles of  $L/D = 20$  that are restrained at their head and subjected to cooling – varying applied mechanical load and constant pile length.



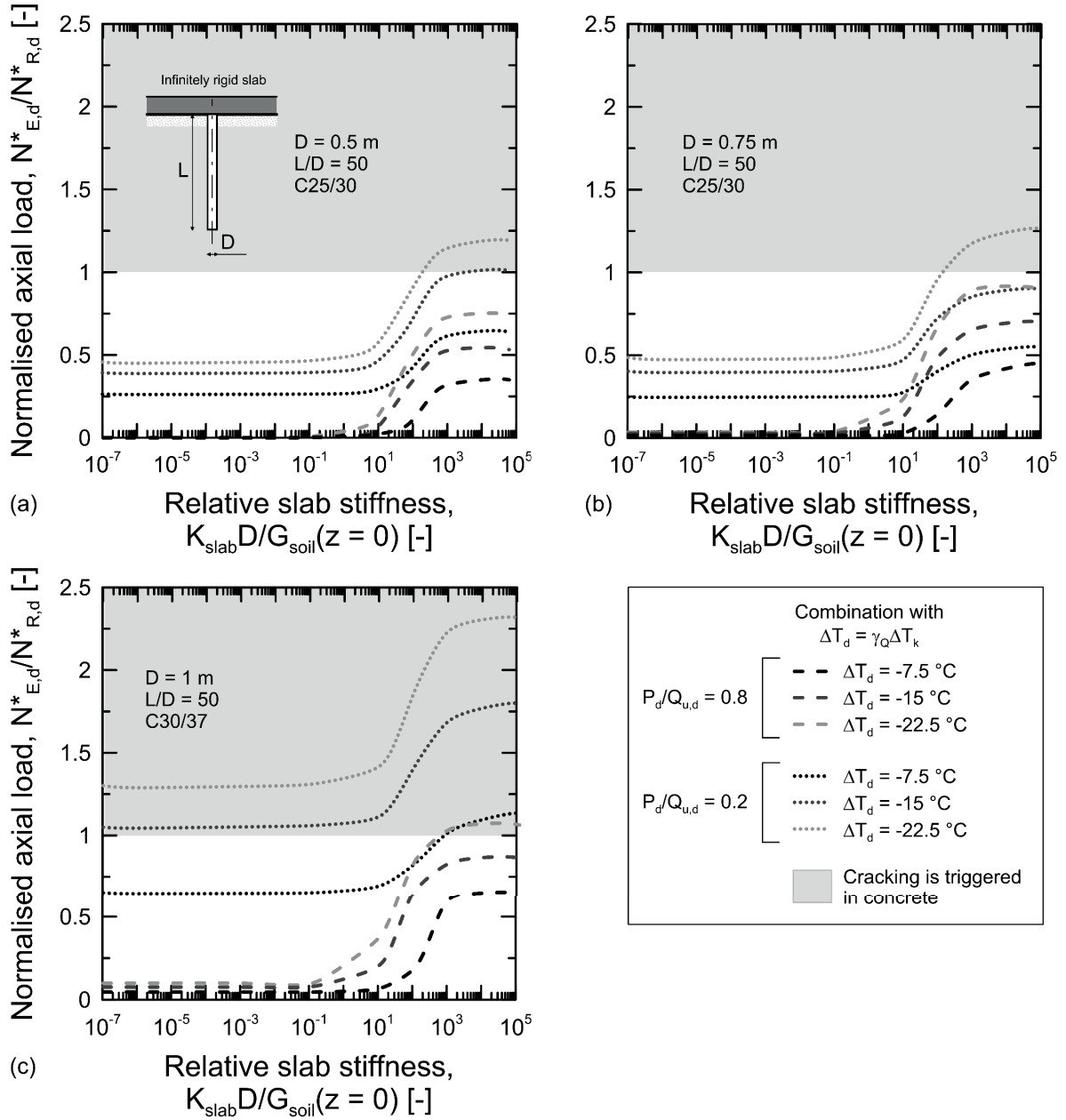


Figure 2.17: Normalised axial loads for energy piles of  $L/D = 50$  that are restrained at their head and subjected to cooling – varying applied mechanical load and constant pile length.

#### 2.5.4 Actual response of reinforced concrete members

Based on the results presented in Sections 2.5.2 and 2.5.3, the required structural performance of reinforced concrete sections constituting energy piles subjected to mechanical and heating thermal loads may be considered satisfied and does not involve ultimate limit states. Analysis results not presented here for energy piles embedded in stiffer soils show that the impact of heating thermal loads may further increase depending on the analysed situation. However, the design approach proposed in this work, with respect to the compressive strength of the reinforced concrete section and the pile

bearing capacity, prevents the involvement of ultimate limit states from a structural perspective against the action of mechanical and heating thermal loads. In this case, buckling may also be avoided because of the presence of the surrounding soil.

In contrast, based on the results presented in Sections 2.5.2 and 2.5.3, the required structural performance of reinforced concrete sections constituting energy piles subjected to mechanical and cooling thermal loads may not be considered satisfied according to the verifications included, e.g., in the Eurocodes. Analyses not presented here show that this evidence may further increase for energy piles embedded in stiffer soils.

The Eurocodes (EN 1992, 2004) currently highlight the following: “thermal effects should be considered for ultimate limit states only where they are significant (e.g., fatigue conditions, [...] second order effects [...]). In other cases, they need not be considered, provided that the ductility and rotation capacity of the elements are sufficient.” The reason for this is because, as far as a sufficient ductility capacity is ensured, imposed deformations, such as those caused by thermal loads, can be neglected because they are absorbed by the structure.

The above implies that thermal loads applied to energy piles do not involve, e.g., fatigue conditions and second order effects. It also involves that the occurrence of unsatisfied verifications related to the effects of thermal loads at ultimate limit states, such as those encountered previously, could actually be neglected.

To ensure adequate ductility capacity of reinforced concrete members, (i) the resisting axial force of the reinforced concrete cross-sections needs to be greater than or equal to the axial force needed to crack them in view of potential strain localisation effects, (ii) the reinforcement has to be characterised by a large deformation capacity and (iii) the ratio  $f_t/f_y$  has to respect a lower bound (where  $f_t$  is the tensile strength of the reinforcement steel).

In general, condition (i) implies that

$$N_R \geq N_{cr} \quad (2.46)$$

Equivalently,

$$f_y \rho_r A_{EP} \geq f_{ct} A_{EP} [1 + \rho_r (n_r - 1)] \approx f_{ct} A_{EP} \quad (2.47)$$

By simplifying equation (2.47), a minimum reinforcement ratio can be expressed as

$$\rho_r = \rho_{r,min} \geq \frac{f_{ct}}{f_y} \quad (2.48)$$

where  $f_{ct}$  and  $f_y$  are in this case appropriate values of the tensile strength of concrete and steel yield strength. A conservative value of  $f_{ct}$  that can be considered for condition (i) is the mean value of axial tensile strength of concrete,  $f_{ctm}$ . This value can be calculated according to the Eurocodes (for relevant concrete classes used in energy pile applications lower than or equal to C50/60) as  $f_{ctm} = 0.3f_{ck}^{2/3}$ , where  $f_{ck}$  is the characteristic compressive cylinder strength of concrete. Condition (ii) is related to the magnitude of the action effects. Condition (iii) is generally met because standards prescribe minimum values of the ratio  $f_t/f_y$ .

The current predictions of the Eurocodes for the minimum reinforcement areas of, e.g., bored piles, do not always satisfy inequality (2.48). Therefore, the quoted predictions for calculating the minimum reinforcement should be avoided but the proposed design approach related to the fulfilment of ductility may be employed for energy piles.

Figure 2.18 shows the actual relationship between the design traction axial load,  $N_d$ , and the normalised axial displacement,  $\Delta w/L$ , of a reinforced concrete member constituting an energy pile designed with reference to the proposed ductility-oriented approach. This relationship is compared with that of the same member characterised by the simultaneous occurrence of cracks (i.e., coinciding with the response of a single mean cross-section) as well as with the relationship of the reinforcement steel alone. Values of blocked normalised vertical displacement are plotted with reference to the worst-case scenario of fully restrained deformation conditions for the energy pile subjected to only the design cooling thermal loads considered thus far of  $\Delta T_d = -7.5, -15$  and  $-22.5$  °C. The effective reinforcement ratio of  $\rho_{r,eff} = 0.72\%$ , the pile diameter of  $D = 1$  m, the concrete class C30/37 and the B500B reinforcement steel are considered.

Although cracking may occur in concrete, sufficient ductility capacity is ensured by the proposed design approach and structural ultimate limit states involving a collapse mechanism, i.e., the energy pile being divided into different portions, cannot occur because of the action of the cooling thermal load. The above is considered to be further valid in other (more realistic) design conditions in which both compressive mechanical and cooling thermal loads are applied to energy piles and the deformation of these elements is not fully restrained. Concrete cracking should not be considered as an issue but as an ordinary property of concrete that needs to be controlled.

*From the foregoing considerations, it can be concluded not only that thermal loads (e.g., heating and cooling loads) may not be considered in the performance-based design process of energy piles at ultimate limit states, but also that the geotechnical and structural design process of such foundations at the considered limit states reduces to a conventional pile design process against the actions of only mechanical loads.* Thermal loads, together with the associated effects, may indeed be considered in the performance-based design process of energy piles at serviceability limit states, thus involving a modified version of the conventional design of piles subjected to mechanical loads only. The effects of thermal loads, in conjunction with those of mechanical loads, may be considered at serviceability limit states from the following aspects:

- Single and group vertical displacement (e.g., differential and average) limitation, considering group effects.

- Deflections and angular distortions control.
- Compressive stress limitation.
- Tensile stress limitation.
- Crack control.

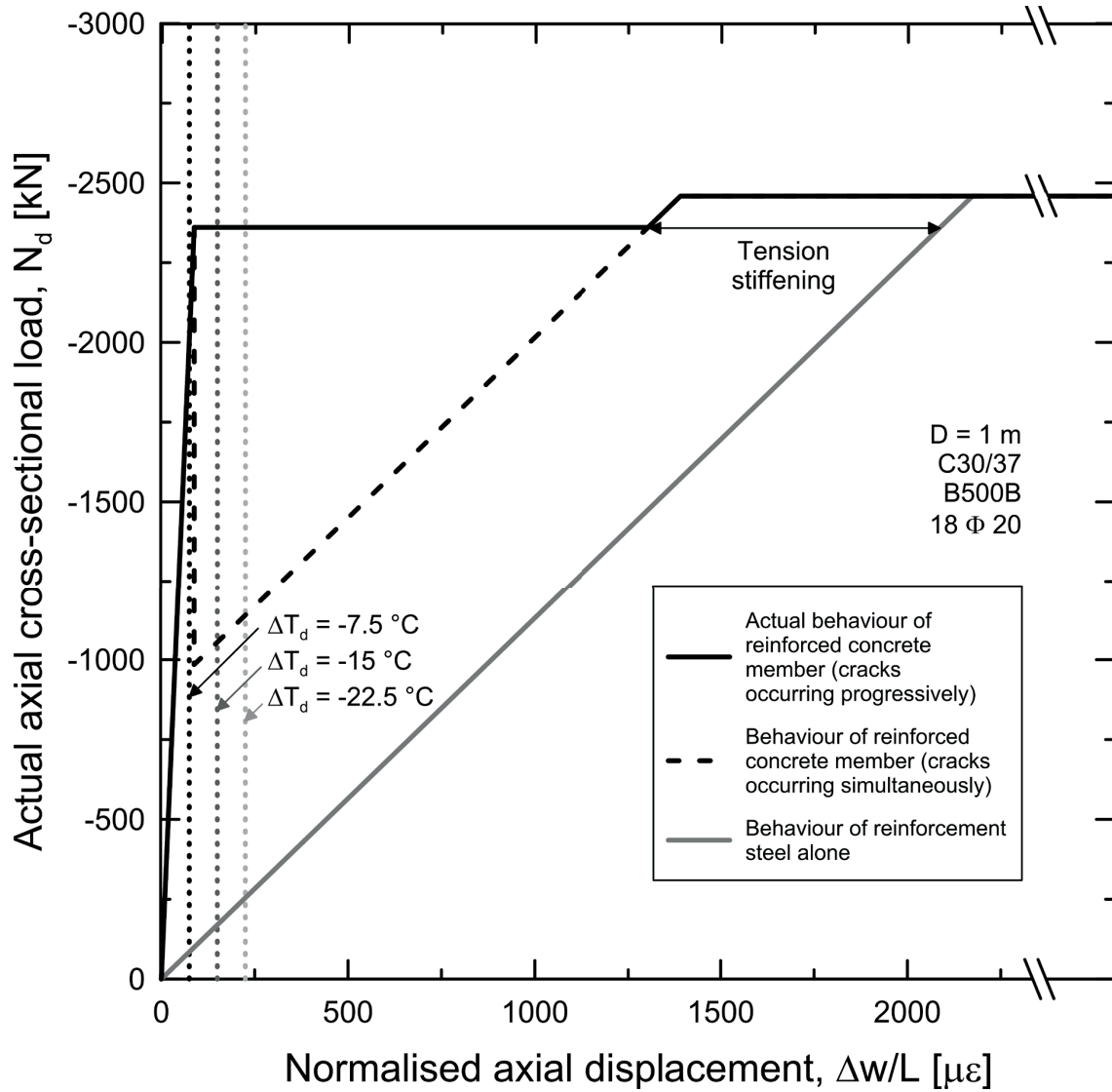


Figure 2.18: Relationships between axial cross-sectional load and normalised axial displacement for energy piles made of reinforced concrete.

## 2.6 Concluding remarks

To provide a basis for a novel performance-based design framework of energy piles subjected to mechanical and thermal loads, e.g., in the context of the limit state design of the so-called Eurocodes,

this study investigated, via a theoretical analysis and practical design examples, the role of thermal loads in the geotechnical and structural performance of energy piles (Rotta Loria et al., 2017a).

The following main conclusions can be drawn:

- Thermal loads involve effects that can be neglected in the performance-based design of energy piles at ultimate limit states, both from a geotechnical and a structural perspective, and that can only be considered relevant at serviceability limit states.
- The above conclusion holds when (i) a design compressive strength of the reinforced concrete section constituting the pile at least equal to the pile design bearing capacity and (ii) a minimum longitudinal reinforcement for the pile concrete cross-sectional area that can ensure sufficient ductility capacity are employed.
- The proposed design approach reduces the design and verification of energy piles at ultimate limit states as a conventional process against the action of mechanical loads only.
- The effects of thermal loads may indeed be considered in the performance-based design process of energy piles at serviceability limit states, thus necessitating a modified version of the conventional design of piles subjected to mechanical loads only.
- The effects of thermal loads, in conjunction with those of mechanical loads, may be considered at serviceability limit states from the following aspects: (i) single and group vertical displacement (e.g., differential and average) limitation, considering group effects; (ii) deflection and angular distortion control; (iii) compressive stress limitation; (iv) tensile stress limitation; and (v) crack control.
- When attempts are made to achieve a trouble-free performance using energy piles that are longer than needed, drawbacks occur related to the mechanical performance of such geostuctures against the effects of thermal loads. This occurrence is in contrast with the conventional justified belief that longer piles provide greater safety against the effects of mechanical loads.



## Chapter 3

# Thermally induced group effects among energy piles

The behaviour of conventional pile groups (e.g., closely spaced) that are subjected to mechanical loads has been shown to be different than the behaviour of single isolated piles. The so-called *group effects* are responsible for this behaviour and must be considered for an optimal design of pile foundations. In recent years, energy piles have shown potential to work as both structural supports and geothermal heat exchangers and thus are subjected to both mechanical and thermal loads. An increasing amount of research has investigated the previously unexplored impact of thermal loads on the thermo-mechanical behaviour of energy piles. However, no field data over typical time-scales of practical geothermal applications have been available to analyse the development and impact of thermally induced group effects between energy piles (e.g., closely spaced) on their thermo-mechanical behaviour. To investigate this problem, two full-scale *in situ* tests of a group of energy piles and coupled three-dimensional thermo-mechanical finite element analyses were performed and are presented in this work. This study demonstrates that significant thermally induced group effects characterise closely spaced energy piles. Attention must be devoted to these effects throughout the design process (e.g., geotechnical, structural and energy) of energy piles because they play an important role in the serviceability performance of these foundations.

### 3.1 Introduction

Pile groups can be divided into two classes: widely and closely spaced. In widely spaced pile groups, the piles are located far enough from each other that their individual responses can be considered independent and comparable to the case of an isolated pile. In closely spaced pile groups, the piles are close enough to each other that their individual responses are influenced by the presence of and loadings on the neighbouring piles and differ from that of an isolated pile. In the latter case, the influences between the individual pile responses of the group represent interactions (e.g., mechanical). These interactions occur between the piles, the connecting slab and the surrounding soil. They

have been shown to manifest through so-called *group effects* and to control the response of pile groups to loading. Extensive amounts of research (e.g., Poulos and Davis, 1980; Fleming et al., 2008) have been devoted to the analysis and classification of group effects among conventional piles because of their importance for suitable designs of such foundations. Prior to this study, the analysis and classification of group effects of energy piles was preliminary and thus was considered in this work.

Over the last decade, an increasing amount of research has investigated the impact of thermal loads on the thermo-mechanical behaviour of energy piles considered as single isolated elements. Various experimental tests, including a series of full-scale *in situ* tests (cf., Table 3.1), centrifuge tests (cf., Table 3.2) and model-scale tests (cf., Table 3.3) have been performed, as well as numerical analyses (Laloui et al., 2006; Suryatriyastuti et al., 2012; Olgun et al., 2014; Mimouni and Laloui, 2014; Saggu and Chakraborty, 2015; Batini et al., 2015; Rotta Loria et al., 2015b; Gawecka et al., 2016). Several *in situ* tests (Mimouni and Laloui, 2015) and numerical analyses (Salciarini et al., 2015; Jeong et al., 2014; Di Donna and Laloui, 2014; Suryatriyastuti et al., 2015; Di Donna et al., 2016; Salciarini et al., 2017; Saggu and Chakraborty, 2016) have recently investigated this problem for energy pile groups. To date, however, knowledge of the development and impact of thermally induced group effects among closely spaced energy piles on their thermo-mechanical behaviour has been limited due to the lack of field data about the exploitation of energy piles that either partially or entirely operate as geothermal heat exchangers for time-scales that are typical of practical applications.

To address this challenge, two full-scale *in situ* tests of a group of closely spaced energy piles that operate as geothermal heat exchangers were carried out over a time-scale that is typical of practical applications, and coupled three-dimensional (3-D) thermo-mechanical finite element analyses were performed (Rotta Loria and Laloui, 2017d; Rotta Loria and Laloui, 2017c). The analyses and results of this experimental and numerical investigation are presented in this study.

This work first describes the experimental and numerical methods. The experimental and numerical results are then compared and discussed. Finally, concluding remarks that can be drawn from this study are presented.

## **3.2 Experimental testing**

This section presents (i) the features of the experimental site, (ii) the main characteristics of the testing equipment and (iii) the details of the full-scale *in situ* tests. Detailed information about the testing equipment has been reported by Mimouni and Laloui (2015) and is presented in Appendix A.

### **3.2.1 The pile foundation and site**

The pile foundation that was considered for the experimental test is located under the recently built Swiss Tech Convention Centre, Lausanne, Switzerland (cf., Figure 3.1 (a)). The foundation supports a  $9 \times 25 \text{ m}^2$  water retention tank and comprises a group of four predominantly end-bearing energy piles (labelled EP1, EP2, EP3 and EP4 in Figure 3.1 (a)) and sixteen predominantly floating conventional piles (labelled P1-16 in Figure 3.1 (a)) below a heavily reinforced 0.9 m-thick slab. Mimouni and Laloui (2015) indicated a thickness of the slab of 0.5 m based on the smallest value of height of the



cross-section characterising the central zone of this element in plan view. The thickness considered in this work (which corresponds to that proposed by Di Donna et al. (2016) and is supposed to be constant over the breadth and length of the slab in the numerical model) is the dimension of the height of the cross-section of the slab at the joint zones with the piles. Because this latter value of height is considered to predominantly characterise the response of the piles over the breadth and length of the slab, it is accounted for in the following analyses. In plan view, the energy piles form a triangle within a 4.21 m square in which the central pile, EP1, is located 3 m from the others, EP2, 3 and 4. The energy piles are 28 m long and 0.9 m in diameter, and the conventional piles are 16 m long and 0.6 m in diameter. All of the piles were bored, cast onsite and are made of reinforced concrete. Vertical loads of 0, 800, 2200 and 2100 kN are applied to energy piles EP1, 2, 3 and 4, respectively. Vertical loads of 300 kN are applied to each of the conventional piles. The values of vertical loads are characteristic values that were calculated by the company involved in the geotechnical and structural designs of the foundation. Throughout the design process, these loads were considered as imposed on the uppermost surface of the slab in correspondence with the area delimited by the cross-sectional surface of the underlying piles. This loading situation is considered in this work (as in that presented by Di Donna et al. (2016)). The energy piles were equipped with four 24-m-long high-density polyethylene U-loops that are connected in series. The inlets and outlets of the absorber pipes were thermally insulated to a depth of 4 m below the pile heads to limit the influence of the climatic conditions on the heat exchange process.

All of the energy piles were instrumented with vibrating wire strain gauges and thermocouples along their lengths (model EM-5 from Roctest), optical fibres (SOFO system from Roctest) as well as with pressure cells (model TPC from Roctest) at their toes. Piezometers (model PWS with stainless steel filters from Roctest) and thermistors (model TH-T from Roctest) (labelled P+T1 and P+T2 in Figure 3.1 (b)) were also installed in two boreholes in the soil. These instruments (cf., Figure 3.1 (b)) allow the thermo-hydro-mechanical response of the northwestern corner of the foundation to be monitored during the simulation of potentially different operations of the energy piles via the use of a dedicated heating module.

The soil stratigraphy of the site (cf., Figure 3.1 (c)) was extrapolated based on information that was obtained during the construction of the foundation and data from Laloui et al. (2003; 2006) for another experimental site that is located 200 m away, at the Swiss Federal Institute of Technology in Lausanne (EPFL). During the construction of the piles, the groundwater table was located at the top of the deposit, which is estimated to be in an overconsolidated condition. Layers of alluvial soil and sandy-gravelly moraine were encountered at shallow depths. The upper soil profile of the alluvial soil was inferred to reach a depth from the uppermost surface of the successively built slab of  $z = 8.6$  m. The lower sandy-gravelly moraine layer was located between depths of  $z = 8.6$  and 16.6 m (Laloui et al., 2003; Laloui et al., 2006). A thin layer of bottom moraine was present below the sandy-gravelly moraine layer between depths of  $z = 16.6$  and 20.1 m and laid on a molasse layer. The energy piles were socketed 8.8 m into this bottom molasse layer from a depth of  $z = 20.1$  m to a depth of  $z = 28.9$  m.

Table 3.1: Available experimental tests on single full-scale energy piles.

Reference	Test label	Soil type	Pile type	Pile material	Pile length, $L$ [m]	Pile slenderness ratio, $L/D$ [-]	Head restraint condition	Loading type	Loading sequence	Loading magnitude ( $\Delta T$ [°C] and $P$ [kN]) in sequence (*)
Laloui et al. (2003) (7 tests performed on 1 pile)	Test 1	Stratified overconsolidated clayey and sandy soil resting on sandstone	Predominantly end-bearing	Reinforced concrete	25.8	29.3	Free	Thermal	Cyclic one-way thermal loading (1 cycle)	$P = 0$ kN; $\Delta T = +22$ °C
	Test 2						Blocked	Mechanical and thermal	Monotonic mechanical and cyclic one-way thermal loading (1 cycle)	$P = 1300$ kN and $\Delta T = +15$ °C
Bourne-Webb et al. (2009) (3 tests performed on 1 pile)	-	Overconsolidated clayey soil (London Clay)	Predominantly floating	Reinforced concrete	23	38.3	Free	Mechanical and thermal	Monotonic mechanical load and cyclic two-way thermal loading (2 cycles), followed by maximal mechanical loading	$P = 1200$ kN and $\Delta T = -6$ °C; $\Delta T = +40$ °C; $\Delta T = -6$ °C; $P_{max} = 3600$ kN
McCartney and Murphy (2012) (1 test performed on 2 piles)	Foundation A	Medium dense clayey soil with gravel resting on hard sandy claystone	Predominantly bearing	Reinforced concrete	14.8	13.5	Blocked	Mechanical and thermal	Monotonic mechanical and cyclic two-way thermal loading (1 cycle)	$P = 3840$ kN and $\Delta T = -5$ °C; $\Delta T = +3$ °C
	Foundation B				13.4	12.2				$P = 3650$ kN and $\Delta T = -5$ °C; $\Delta T = +3$ °C

Reference	Test label	Soil type	Pile type	Pile material	Pile length, $L$ [m]	Pile slenderness ratio, $L/D$ [-]	Head restraint condition	Loading type	Loading sequence	Loading magnitude ( $\Delta T$ [°C] and $P$ [kN]) in sequence (*)
Murphy et al. (2015) (7 tests performed on 8 piles)	Foundation 4	Silty sandstone	Predominantly end-bearing	Reinforced concrete	15.2	24.9	Blocked	Mechanical and thermal	Monotonic mechanical and cyclic one-way thermal loading (1 cycle)	$P$ = building load and $\Delta T$ = +19 °C;
Murphy and McCartney (2015) (1 test performed on 2 piles)	Foundation A	Medium dense clayey soil with gravel resting on hard sandy claystone	Predominantly end-bearing	Reinforced concrete	14.8	13.5	Blocked	Mechanical and thermal	Monotonic mechanical and cyclic two-way thermal loading (2 cycles)	$P$ = 3840 kN and $\Delta T$ = -5 °C; $\Delta T$ = +14 °C
	Foundation B				13.4	12.2				$P$ = 3650 kN and $\Delta T$ = -5 °C; $\Delta T$ = +14 °C
Wang et al. (2014) (5 tests performed on 1 pile)	-	Very dense sandy soil	Predominantly floating	Reinforced concrete	16.1	26.8	Free	Mechanical and thermal	Alternate one-way thermal (2 cycles) and mechanical loading	$\Delta T$ = 0 °C; $P$ = 1650 kN; $\Delta T$ = +20 °C; $P$ = 1885 kN; $\Delta T$ = 0 °C; $P$ = 1700 kN; $\Delta T$ = +27 °C; $P$ = 1885 kN; $\Delta T$ = 0 °C; $P$ = 1750 kN

Reference	Test label	Soil type	Pile type	Pile material	Pile length, $L$ [m]	Pile slenderness ratio, $L/D$ [-]	Head restraint condition	Loading type	Loading sequence	Loading magnitude ( $\Delta T$ [°C] and $P$ [kN]) in sequence (*)
Akrouh et al. (2014) (5 tests performed on 1 pile)	-	Very stiff high plasticity clay	Predominantly floating	Reinforced concrete	5.5	30.6	Free	Mechanical and thermal	One-way thermal loading (1 cycle) under different values of mechanical loading	$P = 40$ kN and $\Delta T = +10$ -15 °C; $P = 100$ kN and $\Delta T = +10$ -15 °C; $P = 150$ kN and $\Delta T = +10$ -15 °C; $P = 200$ kN and $\Delta T = +10$ -15 °C; $P = 256$ kN and $\Delta T = +10$ -15 °C;
Sutman et al. (2015) (3 tests performed on 3 piles)	TP1	Stratified stiff clayey soils resting on very dense sandy soil	Predominantly end-bearing	Reinforced concrete	15.24	33.3	Free	Thermal	Cyclic two-way thermal loading (5 cycles)	$\Delta T = +21$ °C; $\Delta T = -35$ °C;
You et al. (2016) (5 tests performed on 4 piles)	N. 1	Layered soft silty clay, sandy silt soil	Predominantly floating	Reinforced concrete	18	42.9	Free	Thermal	Constant one-way thermal loading (2 cycles)	$\Delta T = +9.5$ °C $P = 0$ kN
	N. 3							Mechanical	Monotonic maximal mechanical loading	$P_{max} = 1089$ kN;
	N. 1							Mechanical and thermal	Monotonic maximal mechanical loading and one-	$\Delta T = +9$ °C and $P_{max} = 1089$ kN;

Reference	Test label	Soil type	Pile type	Pile material	Pile length, $L$ [m]	Pile slenderness ratio, $L/D$ [-]	Head restraint condition	Loading type	Loading sequence	Loading magnitude ( $\Delta T$ [°C] and $P$ [kN]) in sequence (*)
									way cyclic thermal loading (1 cycle)	
	N. 5								Monotonic maximal mechanical loading and one-way cyclic thermal loading (1 cycle)	$\Delta T = -7$ °C and $P_{max} = 1089$ kN;
	N. 6								Monotonic mechanical loading and two-way cyclic thermal loading (1 cycle)	$P = 400$ kN and $\Delta T = +9$ °C; $\Delta T = -7$ °C
Sutman et al. (2017) (3 tests performed on 3 piles)	TP3	Stratified stiff clayey soils resting on very dense sandy soil	Predominantly end-bearing	Reinforced concrete	15.24	33.3	Free	Mechanical and thermal	Monotonic mechanical loading and two-way cyclic thermal loading (1 cycle)	$P =$ design load with security factor of 2, and $\Delta T = +22$ °C; $\Delta T = -37$ °C;
Luo et al. (2017) (3 tests performed on 2 piles)	Plie N.12	Sandy clayey soils resting on sandstones	Predominantly floating	Reinforced concrete	18.5	30.8	Free	Thermal	Thermal one-way cyclic thermal loading (1 cycle)	$\Delta T = +13$ °C;
Chen et al. (2017)	-	Silty clayey soil and silty clayey soil with sand	Predominantly floating	Pre-stressed reinforced concrete	23	60	Free	Thermal	Thermal one-way cyclic thermal loading (2 cycles)	$\Delta T = +30$ °C; $\Delta T = -6$ °C;

Reference	Test label	Soil type	Pile type	Pile material	Pile length, $L$ [m]	Pile slenderness ratio, $L/D$ [-]	Head restraint condition	Loading type	Loading sequence	Loading magnitude ( $\Delta T$ [°C] and $P$ [kN]) in sequence (*)
(2 tests performed on 1 pile)										
Allani et al. (2017) (5 tests performed on 5 piles)	Screw pile	Alternate soft clayey soil and dense sandy soil	Predominantly floating	Reinforced concrete	11.5	25	Free	Mechanical and thermal	Monotonic mechanical loading under two-way cyclic thermal loading (1 cycle)	$P = 400$ kN and $\Delta T = +40$ °C; $\Delta T = -5$ °C;
McCartney and Murphy (2017)	Foundation A	Medium dense clayey soil with gravel resting on hard sandy claystone	Predominantly end-bearing	Reinforced concrete	14.8	13.5	Blocked	Mechanical and thermal	Monotonic mechanical and cyclic two-way thermal loading (5 cycles)	$P = 3840$ kN and $\Delta T = -5$ °C; $\Delta T = +14$ °C
	Foundation B				13.4	12.2				$P = 3650$ kN and $\Delta T = -5$ °C; $\Delta T = +14$ °C
(*) For the temperature changes $\Delta T$ , “+” and “-” involve positive and negative values of imposed temperature to the energy piles compared to their initial temperature. The symbol “,” means that a load is retrieved after its application before the application of another load. The word “and” means that an additional load is applied.										

Table 3.2: Available centrifuge tests on single energy piles.

Reference	Test label	Soil type	Pile type	Pile material	Pile length, $L$ [m]	Pile slenderness ratio, $L/D$ [-]	Head restraint condition	Loading type	Loading sequence	Loading magnitude ( $\Delta T$ [°C] and $P$ [kN]) in sequence (*)
Stewart and McCartney (2014) (1 test performed on 1 pile)	-	Unsaturated inorganic low plasticity silt layer (Bonny silt)	Predominantly end-bearing	Reinforced concrete	0.533 (model scale) 12.8 (prototype scale, 24-g)	10.5	Free	Mechanical and thermal	Monotonic mechanical loading under cyclic two-way thermal loading (4 cycles)	$P = 443$ kN and $\Delta T = +19$ °C (initial heating) $\Delta T = -10$ °C; $\Delta T = +10$ °C; (normal heating)
	EP 1	Lightly over-consolidated clayey soil (Kaolin clay)	Predominantly floating	Aluminium	0.42 (model scale) 16.8 (prototype scale, 40-g)	19.1	Free	Mechanical and thermal	Constant mechanical loading under cyclic two-way thermal loading (5 cycles)	$P = 96$ kN and $\Delta T = +16$ °C (initial heating) $\Delta T = -20$ °C; $\Delta T = +20$ °C; (normal heating)
Ng et al. (2014) (2 tests performed on 2 piles)	EP 2	Heavily over-consolidated clayey soil (Kaolin clay)								$P = 192$ kN and $\Delta T = +16$ °C (initial heating) $\Delta T = -20$ °C; $\Delta T = +20$ °C; (normal heating)

Reference	Test label	Soil type	Pile type	Pile material	Pile length, $L$ [m]	Pile slenderness ratio, $L/D$ [-]	Head restraint condition	Loading type	Loading sequence	Loading magnitude ( $\Delta T$ [°C] and $P$ [kN]) in sequence (*)
Goode and McCartney (2015) (10 tests performed on 9 piles)	Test 1	Dry dense sand (Nevada sand)	Pre-dominantly floating	Reinforced concrete	0.343 (model scale) 8.2 (prototype scale, 24- $g$ )	5.4	Free	Mechanical and thermal	Constant thermal one-way cyclic loading (1 cycle) under different values mechanical loading	$P = 360$ kN and $\Delta T = 0$ °C; $P = 2400$ kN
	Test 2									$P = 360$ kN and $\Delta T = +7$ °C; $P = 2400$ kN
	Test 3									$P = 360$ kN and $\Delta T = +12$ °C; $P = 2400$ kN
	Test 4									$P = 360$ kN and $\Delta T = +18$ °C; $P = 2400$ kN
	Test 5	Compacted unsaturated silty soil (Bonny silt)	End-bearing		8.16	Different thermal one-way cyclic loading (1 cycle) under cyclic mechanical loads (4 cycles)				$P = 360$ kN and $\Delta T = 0$ °C; $P = 2400$ kN
	Test 6									$P = 360$ kN and $\Delta T = +10$ °C; $P = 2400$ kN
	Test 7									$P = 360$ kN and $\Delta T = +18$ °C; $P = 2400$ kN
	Test 8	Dry dense Nevada sand								$P = 1260$ kN and $\Delta T = +11.1$ °C; $P = 1500$ kN and $\Delta T = +11.8$ °C;
	Test 9									$\Delta T = 0$ °C and $P = 2400$ kN; $\Delta T = +7$ °C and $P = 2400$ kN; $\Delta T = +12$ °C and $P = 2400$ kN; $\Delta T = +18$ °C and $P = 2400$ kN;
	Test 10	Compacted unsaturated silty soil (Bonny silt)								



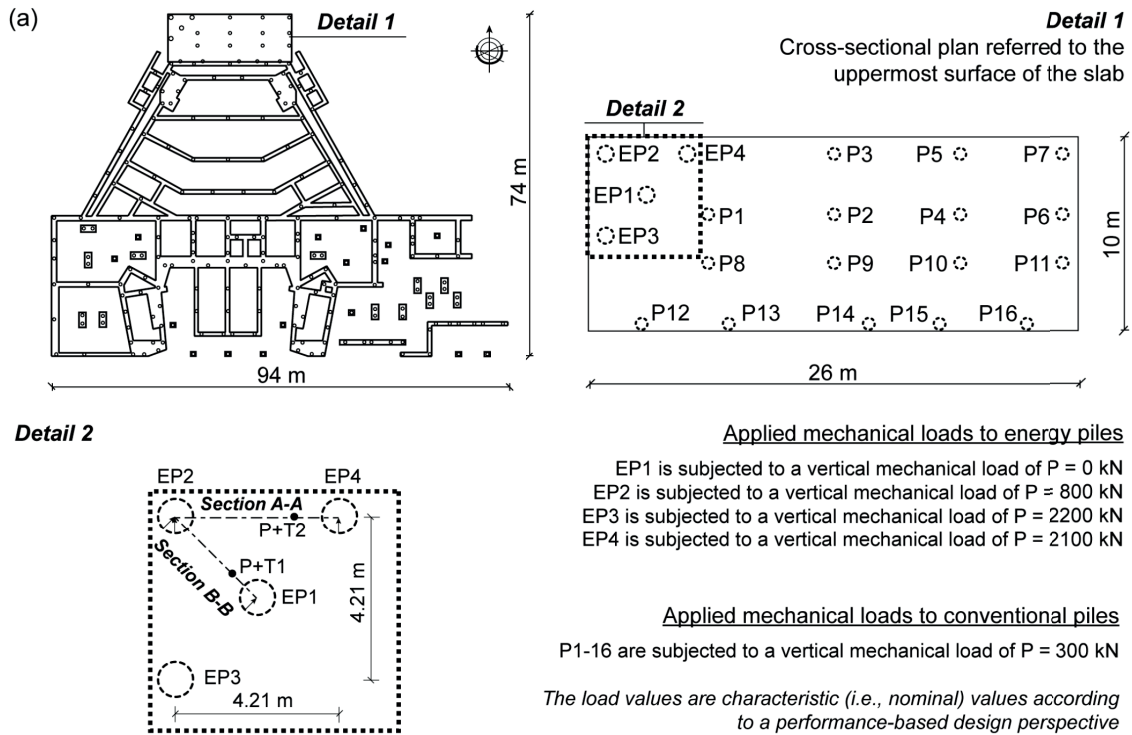
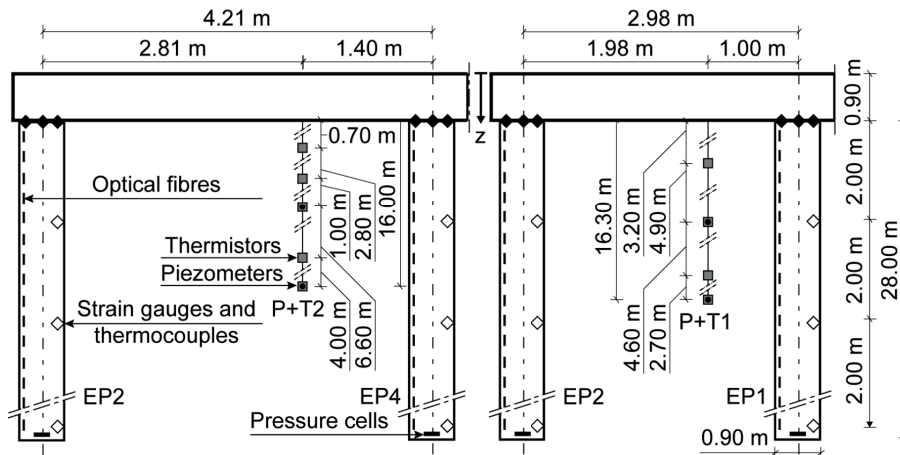
Reference	Test label	Soil type	Pile type	Pile material	Pile length, $L$ [m]	Pile slenderness ratio, $L/D$ [-]	Head restraint condition	Loading type	Loading sequence	Loading magnitude ( $\Delta T$ [°C] and $P$ [kN]) in sequence (*)
Ng et al. (2015) (3 tests performed on 3 piles)	EP 1	Medium dense saturated sand (Toyoura sand)	Pre-dominantly floating	Aluminium	0.6 (model scale) 24 (prototype scale, 40- $g$ )	27.3	Free	Mechanical and thermal	Increasing mechanical loading under cyclic one-way thermal loading (1 cycle)	$\Delta T = +15$ °C and $P_{max} = 1890$ kN;
	EP 2								Increasing mechanical loading under cyclic one-way thermal loading (1 cycle)	$\Delta T = +30$ °C and $P_{max} = 2160$ kN;
	EP 3								Mechanical loading, followed by cyclic one-way thermal loading (1 cycle) and increasing mechanical loading	$P = 835$ kN and $\Delta T = +30$ °C; $P_{max} > 3000$ kN;
Ng et al. (2016b) (2 tests performed on 2 piles)	EP-R	Saturated sand (Toyoura sand)	Pre-dominantly floating	Aluminium	0.6 (model scale) 24 (prototype scale, 40- $g$ )	27.3	Free	Mechanical and thermal	Incremental mechanical load until $P$ , and two-way cyclic thermal loading (5 cycles)	$P = 500$ N (800 kN in prototype scale) and $\Delta T = +15$ °C; $\Delta T = -15$ °C;
	EP-D								Constant mechanical load under two-way cyclic thermal loading (5 cycles)	
(*) For the temperature changes $\Delta T$ , “+” and “-” involve positive and negative values of imposed temperature to the energy piles compared to their initial temperature. The symbol “,” means that a load is retrieved after its application before the application of another load. The word “and” means that an additional load is applied.										

Table 3.3: Available laboratory tests on single energy piles.

Reference	Test label	Soil type	Pile type	Pile material	Pile length, $L$ [m]	Pile slenderness ratio, $L/D$ [-]	Head restraint condition	Loading type	Loading sequence	Loading magnitude $\Delta T$ [°C] and $P$ [kN] in sequence (*)
Kalandidou et al. (2012) (4 tests performed)	-	Dry compacted sand (Fontainebleau sand)	Predominantly floating	Aluminum	0.8	40	Free	Mechanical and thermal	Mechanical monotonic loading under two-way thermal cyclic loading (2 cycles)	$P = 0$ kN; $\Delta T = +25$ °C; $-25$ °C; $P = 200$ kN; $\Delta T = +25$ °C; $-25$ °C; $P = 400$ kN; $\Delta T = +25$ °C; $-25$ °C; $P = 525$ kN; $\Delta T = +25$ °C; $-25$ °C;
Yavari et al. (2014) (7 tests performed)	-	Dry sand compacted (Fontainebleau sand)	Predominantly floating	Aluminum	0.8	40	Free	Mechanical and thermal	Mechanical monotonic loading under two-way thermal cyclic loading (2 cycles)	$P = 0$ kN and $\Delta T = +30$ °C; $-30$ °C; $P = 100$ kN $= 0.3P_{max}$ and $\Delta T = +30$ °C; $-30$ °C; $P = 150$ kN $= 0.4P_{max}$ and $\Delta T = +30$ °C; $-30$ °C; $P = 200$ kN $= 0.5P_{max}$ and $\Delta T = +30$ °C; $-30$ °C; $P = 250$ kN $= 0.6P_{max}$ and $\Delta T = +30$ °C; $-30$ °C; $P = 300$ kN $= 0.7P_{max}$ and $\Delta T = +30$ °C; $-30$ °C;

Reference	Test label	Soil type	Pile type	Pile material	Pile length, $L$ [m]	Pile slenderness ratio, $L/D$ [-]	Head restraint condition	Loading type	Loading sequence	Loading magnitude $\Delta T$ [°C] and $P$ [kN] in sequence (*)
Kramer and Basu (2014) (3 tests performed)	-	Fine silica sand (Ottawa sand)	Predominantly floating	Precast concrete	1.22	12.2	Free	Mechanical and thermal	Mechanical loading before and after one-way cyclic thermal loading (1 cycle)	$\Delta T = 0$ °C and $P = 3.2$ kN; $\Delta T = 21$ °C and $P = 3.2$ kN;
Marto et al. (2015) (6 tests performed)	-	Soft compacted cohesive clayey soil (Kaolin clay)	Predominantly floating	Aluminium	0.15	10	Free	Mechanical and thermal	Increasing mechanical loading under thermal one-way cyclic loading (1 cycle)	$\Delta T = +8$ °C and $P = 100$ kN; $P = 200$ kN $\Delta T = +5$ °C and $P = 100$ kN; $P = 200$ kN
Yavari et al. (2016) (7 tests performed)	F3-7	Saturated clay	Predominantly floating	Aluminium	0.8	40	Free	Mechanical and thermal	Two-way cyclic thermal loading under various constant mechanical loading	$P = 100$ kN and $\Delta T = +5$ °C; $-5$ °C; $-5$ °C; $+5$ °C; $P = 150$ kN and $\Delta T = +5$ °C; $-5$ °C; $-5$ °C; $+5$ °C; $P = 200$ kN and $\Delta T = +5$ °C; $-5$ °C; $-5$ °C; $+5$ °C; $P = 250$ kN and $\Delta T = +5$ °C; $-5$ °C; $-5$ °C; $+5$ °C; $P = 300$ kN and $\Delta T = +5$ °C; $-5$ °C; $-5$ °C; $+5$ °C;

Reference	Test label	Soil type	Pile type	Pile material	Pile length, $L$ [m]	Pile slenderness ratio, $L/D$ [-]	Head restraint condition	Loading type	Loading sequence	Loading magnitude $\Delta T$ [°C] and $P$ [kN] in sequence (*)
Nguyen et al. (2017) (3 tests performed)	T3	Dry sand compacted (Fontainebleau sand)	Predominantly floating	Aluminium	0.8	40	Free	Mechanical and thermal	Mechanical various monotonic loading under two-way thermal cycle (30 cycles)	$P = 0$ kN and $\Delta T = +3$ °C; $-3$ °C; $P = 100$ kN $= 0.2 P_{max}$ and $\Delta T = +3$ °C; $-3$ °C; $P = 200$ kN $= 0.4 P_{max}$ and $\Delta T = +3$ °C; $-3$ °C; $P = 300$ kN $= 0.6 P_{max}$ and $\Delta T = +3$ °C; $-3$ °C;
(*) For the temperature changes $\Delta T$ , “+” and “-” involve positive and negative values of imposed temperature to the energy piles compared to their initial temperature. The symbol “,” means that a load is retrieved after its application before the application of another load. The word “and” means that an additional load is applied.										

(b) **Section A-A** (left) and **Section B-B** (right)**Strain gauges and thermocouples**

First row of 3 strain gauges at the head of the energy piles:  
 ◆  $z = 0.9$  m

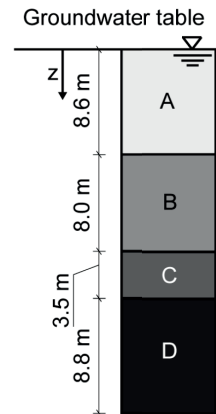
Subsequent 14 strain gauges:  
 ◇  $z = 2.9, 4.9, 6.9, 8.9, 10.9, 12.9, 14.9, 16.9, 18.9, 20.9, 22.9, 24.9, 26.9, 28.9$  m (inter-axis of 2 m)

**Piezometers and thermistors**

P+T1  
 •  $z = 9.0, 16.3$  m  
 ■  $z = 4.1, 9.0, 13.6, 16.3$  m

P+T2  
 •  $z = 5.4, 16.0$  m  
 ■  $z = 1.6, 4.4, 5.4, 12.0, 16.0$  m

(c)



- A** Alluvial soil - A  
 $z = [0; 8.6]$  m
- B** Sandy-gravelly moraine - B  
 $z = [8.6; 16.6]$  m
- C** Bottom moraine - C  
 $z = [16.6; 20.1]$  m
- D** Molasse - D  
 $z = [20.1; 28.9]$  m

Figure 3.1: (a) Plan view of the EPFL Swiss Tech Convention Centre foundation; (b) vertical cross-sections depicting the monitoring instrumentation that was installed in the energy piles and soil; (c) schematic diagram of the soil stratigraphy. Views not to scale.

### 3.2.2 Features of the experimental tests

Two experimental tests were performed. The first test, which was presented by Rotta Loria and Laloui (2017d), involved the application of a heating-passive cooling cycle to energy pile EP1 (hereafter, this test is referred to as Test 20EP1), which was the only energy pile in the group that operated as a geothermal heat exchanger (cf., Figure 3.1 (a)). The second test, which was presented by Rotta Loria and Laloui (2017c), involved the application of a heating-cooling cycle to all of the energy piles (i.e., EP1, 2, 3 and 4; hereafter, this test is referred to as Test 20EPall) (cf., Figure 3.1 (a)).

A dedicated heating module (Mattsson et al., 2008) was used to apply the heating-passive cooling cycle to the operating energy pile(s). A unique module was used in Test 20EP1. Four modules were employed in Test 20EPall (parallel configuration). For both tests, the experiment consisted of three phases:

1. In the first phase, the heat carrier fluid was circulated in the pipes of the operating energy pile(s) for 1 day with the heater turned off to determine the average ground temperature at the site and to homogenise the temperature field within the energy piles.
2. In the second phase, a constant thermal power of 3 kW was applied to *each* operating energy pile to achieve the heating of such foundation elements. This thermal power was applied to EP1 for approximately 5 months (156 days) in Test 20EP1 and to EP1, 2, 3 and 4 for approximately 2 months (60 days) in Test 20EPall.
3. In the third and final phase, the passive cooling of the foundation was implemented by switching the heater off and allowing the heat carrier fluid to circulate in the pipes of the previously operating energy pile(s). This phase lasted approximately 10 months: 300 days in both Test 20EP1 and Test 20EPall.

Both tests were performed after the building was constructed. Hence, constant superstructure mechanical loads were applied to the foundation. Because of the aforementioned features, the experiments are representative of one-season cooling or thermal energy storage applications for energy piles. Throughout the tests, a constant flow rate of 21 l/min was applied to the circulating fluid in the pipes of the operating energy pile(s). The inlet temperature and velocity of the fluid were continuously recorded, and the strain, temperature and stress variations in all of the energy piles were monitored over time. The variations in the pore water pressure and temperature in the two soil profiles (P+T1 and P+T2) were also measured.

### 3.3 Numerical modelling

This section presents (i) the features of the finite element model that was constructed to simulate the experimental tests and obtain complementary information about the problem that may have been difficult if not impossible to collect otherwise, (ii) the assumptions and main characteristics of the mathematical formulation that was used for the numerical analyses, and (iii) the boundary conditions and

material properties that were used for the numerical simulations. Detailed information about the mathematical formulation employed in the finite element analyses has been proposed by Batini et al. (2015) and is presented in Appendix B.

### 3.3.1 Finite element model

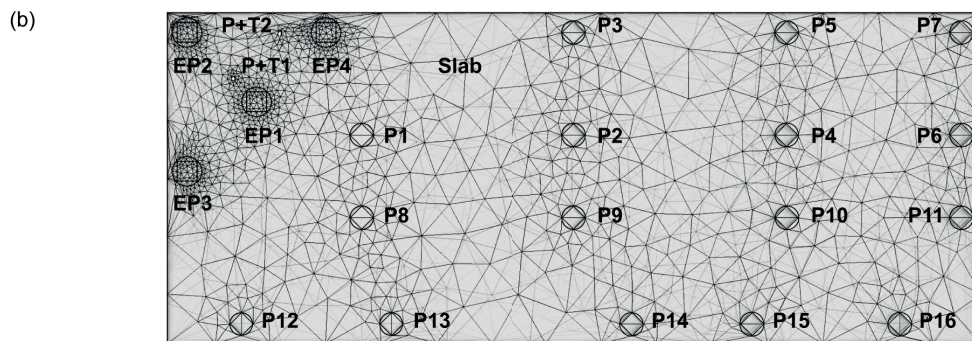
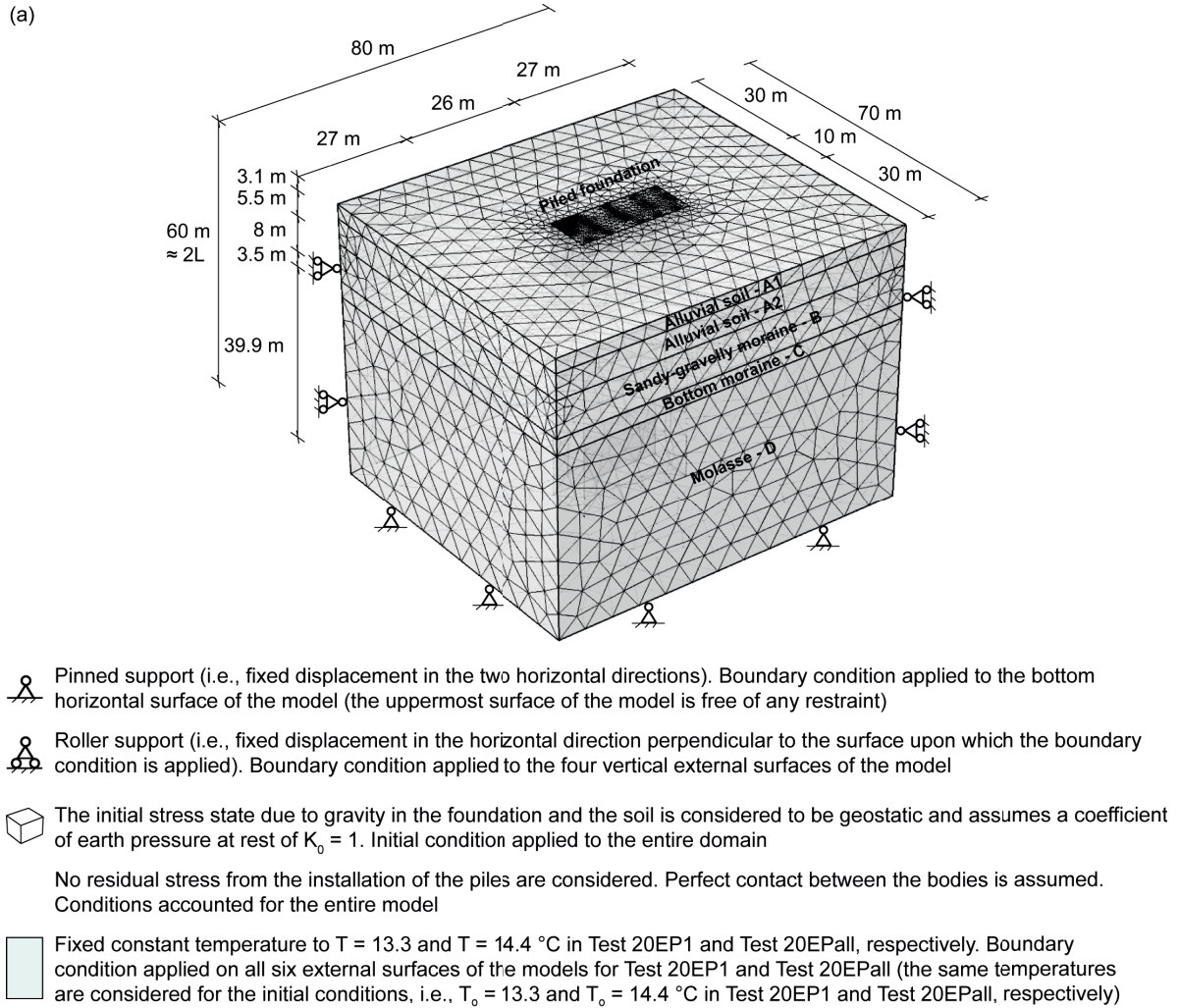
A 3-D finite element model of the site was developed using the software COMSOL Multiphysics (COMSOL, 2014) (cf., Figure 3.2). The  $80 \times 70 \times 60 \text{ m}^3$  model is composed of 438,443 tetrahedral, prismatic, triangular, quadrilateral, linear and vertex elements. The model reproduces the entire foundation supporting the water retention tank. It also accounts for the presence of the pipes in the energy piles through linear entities in which a heat carrier fluid is assumed to flow, which allows the problem of the heat exchange that occurs in the pipes-pile-soil system to be considered. This finite element model was used by Rotta Loria and Laloui (2017d) to run thermo-mechanical finite element predictions of Test 20EP1 and was employed for the same purpose by Rotta Loria and Laloui (2017c) to predict Test 20EPall.

### 3.3.2 Modelling choices

The numerical analysis of the response of the reinforced concrete foundation in the soil under mechanical and thermal loads is based on the following assumptions: (i) the displacements and deformations of all of the materials can be representatively described through a linear kinematic approach under quasi-static conditions (i.e., negligible inertial effects); (ii) the materials that constitute the pile foundation are considered to be isotropic with pores that are fully filled by air and are assumed to be purely conductive domains with equivalent thermo-physical properties that are given by the fluid and the solid phases; (iii) the materials that make up the soil layers are assumed to be isotropic, fully saturated by water and purely conductive domains with equivalent thermo-physical properties that are given by the fluid and the solid phases; (iv) the loads that are associated with this problem have a negligible impact on the variation of the hydraulic field in the soil; and (v) all the materials are considered to be representatively described by linear thermo-elastic behaviours. Under these conditions, a thermo-mechanical mathematical formulation is employed.

Water may be potentially present in some of the pores characterising the buried concrete in the real case, especially in the regions of this material directly adjacent to the soil. This fact may lead to a greater thermal conductivity of the concrete compared to that assumed in the present numerical analyses. While this phenomenon cannot be verified with reference to the tested foundation, the adherence between the results of the numerical analyses and the experimental test presented in Sections 3.4 and 3.5 supports the hypothesis made.





EP1-4 Energy piles (length,  $L = 28$  m; diameter,  $D = 0.9$  m). EP1 is subjected to a vertical mechanical load of  $P = 0$  kN. EP2 is subjected to  $P = 800$  kN. EP3 is subjected to  $P = 2200$  kN. EP4 is subjected to  $P = 2100$  kN

P1-16 Conventional piles (length,  $L = 16$  m; diameter,  $D = 0.6$  m). Each of the piles is subjected to a vertical mechanical load of  $P = 300$  kN

P+T1/2 Piezometers + Thermistors

Figure 3.2: (a) Geometry, initial and boundary conditions of the finite element model and (b) plan view of the foundation listing the piles and other relevant features. Views not to scale.



### 3.3.3 Boundary and initial conditions

Restrictions are applied to both the vertical and horizontal displacements on the base of the model (i.e., pinned boundary) and to the horizontal displacements on the sides (i.e., roller boundaries).

The initial stress state due to gravity in the foundation and the soil is considered to be geostatic and assumes a coefficient of Earth pressure at rest of  $K_0 = 1$ . This value of  $K_0$  approximately characterises the *in situ* stress state based on the values of the coefficients of Earth pressure at rest of the different soil layers that may be calculated according to the formula proposed by Schmidt (1966) through the values of angle of shear strength proposed by Di Donna et al. (2016) and assuming a constant value of overconsolidation ratio  $OCR = 4$  with depth. The considered value of  $OCR$  is based on experimental evidence (Laloui et al., 1999) for the moraine layers surrounding the foundation tested by Laloui et al. (2003) that were also identified in this study. The same  $OCR$  was assumed to characterise the other soil layers surrounding the foundation tested in this study for hypothesis.

No residual stresses from the installation of the piles are considered in these elements and in the adjacent region of soil. This hypothesis may not be completely representative of reality but can be applied successfully in almost all methods of pile groups deformation analysis by choosing appropriate values of the soil moduli (Poulos and Davis, 1980).

Perfect contact between the piles and the soil is considered, i.e., the pile-soil interfaces are not modelled. The piles are modelled as perfectly jointed members (full moment connection) with the slab, such an element being characterised by a perfect contact with the surrounding soil. The pipes in the energy piles are considered to have a perfect contact with the surrounding reinforced concrete.

The initial temperature of the finite element model is fixed to  $T_0 = 13.3$  °C in Test 20EP1 and to  $T_0 = 14.4$  °C in Test 20EPall. These temperatures refer to the mean temperature recorded at the beginning of the tests, which corresponds to the portions of the energy piles where the pipes were not thermally insulated (i.e., between depths of  $z = 4.9$  and  $28.9$  m). These temperature values are also fixed on all the six external boundaries of the finite element model. The temperatures differed between the two tests because of the natural seasonal fluctuation of the temperature field in the shallow subsurface in the Lausanne area (i.e., between  $T = 13$  and  $15$  °C).

The fluid that circulates inside the pipes is water. The inner diameter of the pipes is  $d_{p,in} = 26.2$  mm (the outer diameter is 32 mm and the wall thickness is 2.9 mm). A thermal conductivity of  $\lambda_p = 0$  W/(m °C) is imposed in the shallowest 4 meters of the inlet and outlet of the pipes to simulate the thermal insulation near the ground surface.

Figure 3.3 presents the trends of the inlet temperature and velocity of the heat carrier fluid circulating in the pipes of the energy pile EP1 that were experimentally recorded throughout Test 20EP1. Figure 3.4 shows the average trends of the same variables for energy piles EP1, 2, 3 and 4 referring to Test 20EPall.

Average values of the fluid inlet temperature and velocity were considered in the simulation of Test 20EPall to verify the potential of such a simplified approach in capturing the overall behaviour of energy pile groups. This choice, which is validated in the following based on the limited discrepancy

between the numerical and experimental results, was justified by the low average population standard deviation over time characterising the inflow temperatures and velocities of the fluid circulating in the pipes of energy piles EP1, 2, 3 and 4 throughout Test 20EPall, i.e.,  $\bar{\sigma}_d = 0.73$  °C and 0.02 m/s, respectively. The same rationale is considered hereafter in the analysis of the results by plotting average variables for Test 20EPall. This approach, together with the choice of using average input variables, may be unsuitable for the analysis of large energy pile groups in which notable variations in temperature, stress, strain and displacement field may arise among piles.

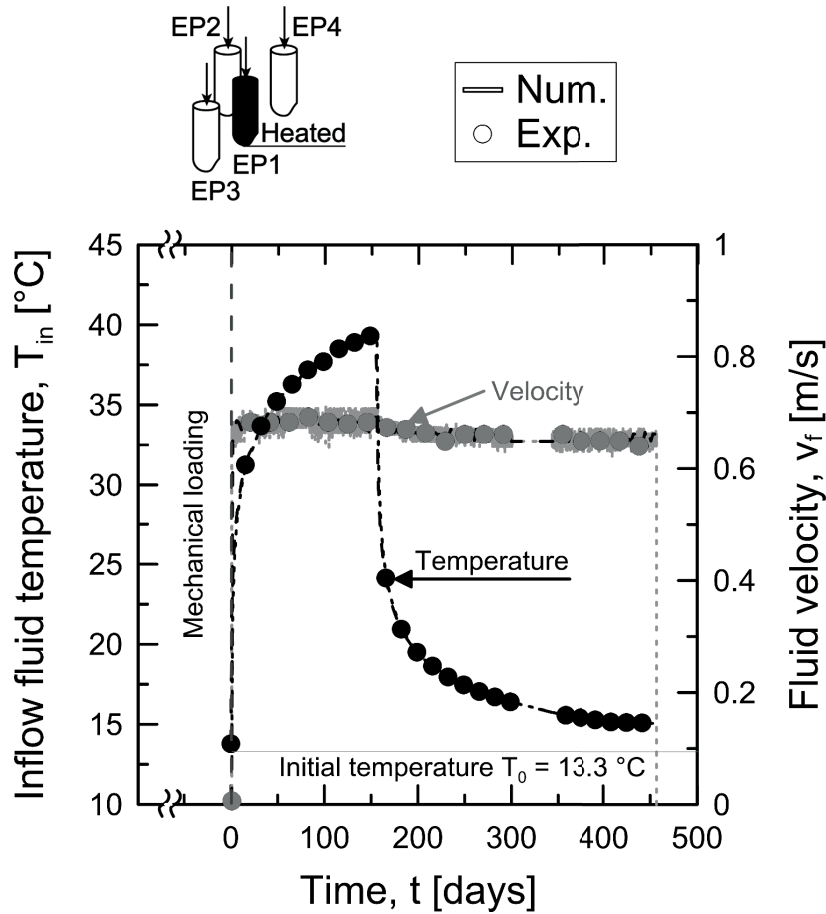


Figure 3.3: Experimentally and numerically imposed inflow temperatures and velocities of the fluid circulating in the pipes of the operating energy pile EP1 with time (Test 20EP1).

### 3.3.4 Classification of the numerical simulations and material properties

Two types of numerical simulations were performed to simulate Test 20EP1: Class B1 and Class C1 predictions (Lambe, 1973). A unique Class C1 prediction was carried out to simulate Test 20EPall, by employing the material parameters used for the Class C1 prediction of Test 20EP1. Table 3.4 summarises the material properties considered for the numerical simulations (in brackets are the values of the material properties that were initially used for the Class B1 prediction).

A Class B1 prediction was carried out while the modelled *in situ* Test 20EP1 was performed and with the associated results available. This prediction employed the material properties proposed by Di Donna et al. (2016) for the characterisation of the site.

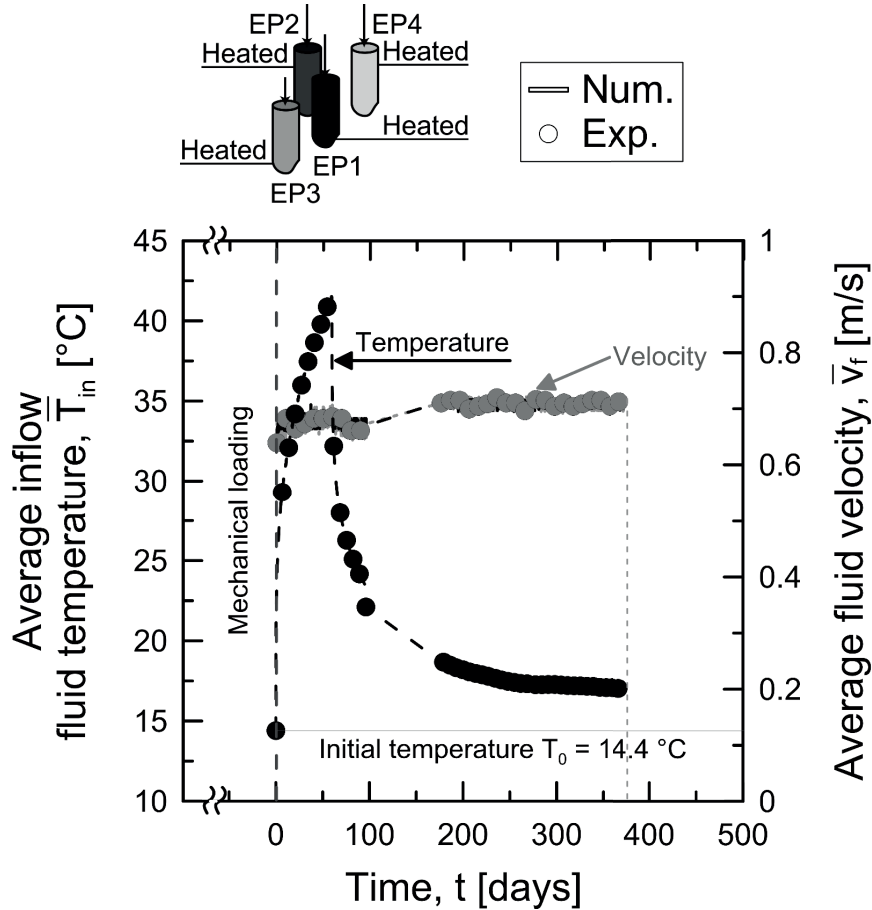


Figure 3.4: Experimentally and numerically imposed average inflow temperatures and velocities of the fluid circulating in the pipes of the operating energy piles EP1, 2, 3 and 4 with time (Test 20EPall).

Different Class C1 predictions were carried out after the modelled *in situ* Test 20EP1 was performed and with the associated results available. The final Class C1 prediction employed the material properties proposed by Di Donna et al. (2016) with two main changes. These changes included the linear thermal expansion coefficient of the soil layers B, C and D as well as the thermal conductivity of the solid particles of all of the soil layers. The variation of the former parameter was based on the ranges of variability that typically characterise the thermal expansion coefficient of moraine and molasse deposits in the geographical area of Lausanne. This variation was necessary to reproduce the thermally induced mechanical behaviour of the foundation at successive stages of the heating phase of EP1. Furthermore, this variation suggests an inhomogeneity of such material property for the considered layers based on the difference with the values presented by Laloui et al. (2006) for another experimental site at the EPFL campus that were considered by Di Donna et al. (2016). The variation of the latter parameter was based on the determination (without accounting for capacitive effects) of an

effective thermal conductivity for the soil deposit of  $\lambda_{eff} = 2.78 \text{ W/(m } ^\circ\text{C)}$ . This average value of effective thermal conductivity was determined experimentally with reference to the soil around the thermally active portion of the operating energy pile EP1 and is slightly lower than the value of  $\lambda_{eff} = 3.1 \text{ W/(m } ^\circ\text{C)}$  suggested by Mimouni and Laloui (2015) that was considered by Di Donna et al. (2016). Knowledge of  $\lambda_{eff}$ , together with the porosity values of all of the soil layers, allowed calculating the thermal conductivity of solid particles of the various layers that were subsequently modified based on a comparison with the experimental results for best capturing the thermal behaviour of the foundation.

### 3.4 Comparison between experimental and numerical results – Test 20EP1

This section compares the experimental data that were collected during the development of the full-scale *in situ* Test 20EP1 and the numerical results that were obtained through the final Class C1 prediction. A discussion on the results obtained throughout the numerical prediction process (Class B1 and C1 predictions) is presented in Section 3.6.

The experimental and numerical data include *variations* of the parameters from the beginning of the test over time. Therefore, they reflect the impact of the geothermal operation of the energy piles on the thermo-mechanical behaviour of the foundation. The stress states generated from body loads in the different media (i.e., *in situ* conditions) and from the application of the mechanical loads of the superstructure to the piles are not included in the stress and strain curves.

A problem arose when comparing the readings of the strain gauges and thermocouples that were installed along the piles with the numerical results of Test 20EP1 because even though these instruments were fixed along the reinforcing cages, their precise positions were not known. The approach that was used to overcome this issue was to find the location in the numerical model along a 0.76-m-diameter circle (corresponding to the diameter of the reinforcing cages placed in the energy piles in the reality) that was centred on the pile axes where the temperature profiles matched best and then compare the strain profiles at the same location. A similar problem occurred when comparing the readings of the pressure cells because the recorded data referred to an area of a 0.23-m-diameter circle that was centred at the pile toes (corresponding to the region occupied by the pressure cells placed in the energy piles in the reality), whereas the numerical results referred to point graphs. In this case, the location in the region of interest where the temperature data matched best was identified, and the stress data were then compared. The choice of these “temperature-driven” approaches was based on the important role that changes of temperature play in the variation of the mechanical behaviour of energy piles. It was also needed due to the inhomogeneity of the temperature, strain, stress and displacement fields that were observed within the cross-sections of the piles with depth. Average variations of these fields up to 20% were observed in this study along the tested piles over their cross-sectional area. The inhomogeneity of these fields has also been highlighted by Caulk et al. (2016) and Abdelaziz and Ozudogru (2016a).

Table 3.4: Material properties used for the Class C1 and B1 (in brackets) numerical predictions.

Soil layers							
	Young's modulus, $E$ [MPa]	Poisson's ratio, $\nu$ [-]	Porosity, $n$ [-]	Density of solid particles, $\rho_s$ [kg/m <sup>3</sup> ]	Specific heat of solid particles, $c_{p,s}$ [J/(kg°C)]	Thermal conductivity of solid particles, $\lambda_s$ [W/(m °C)]	Linear thermal expansion coefficient, $\alpha$ [1/°C]
A	190	0.22	0.1	2769	880	1.49 (3.38)	$3.3 \cdot 10^{-6}$
B	84	0.4	0.35	2735	890	3.68 (4.45)	$3.3 \cdot 10^{-6}$ ( $3.3 \cdot 10^{-5}$ )
C	90	0.4	0.3	2740	890	3.46 (4.17)	$3.3 \cdot 10^{-6}$ ( $3.3 \cdot 10^{-5}$ )
D	3000	0.3	0.1	2167	923	3.82 (3.38)	$2.3 \cdot 10^{-5}$ ( $3.3 \cdot 10^{-7}$ )
Reinforced concrete piles and slab							
Piles	28000	0.25	0.1	2722	837	1.628	$1 \cdot 10^{-5}$
Slab	35000	0.25	0.1	2722	837	1.628	$1 \cdot 10^{-5}$
High-density polyethylene pipes							
						Thermal conductivity of the pipe, $\lambda_p$ [W/(m °C)]	
Pipes	-	-	-	-	-	0.42	-

### 3.4.1 Temperature variations along the energy piles

Figure 3.5 presents the temperature variations that were determined experimentally through the readings of the thermocouples and numerically through the finite element model along the lengths of the operating energy pile EP1 and of the non-operating energy piles EP2, 3 and 4.

The geothermal operation of energy pile EP1 involved average temperature changes along its uninsulated portion of  $\overline{\Delta T}_{EP1} = 5, 10, 15$  and  $20$  °C after  $t = 2, 8, 35$ , and  $156$  days, respectively. These changes were observed in both the experimental and numerical results (cf., Figure 3.5 (a)).

After  $t = 2$  and  $8$  days (i.e., during the early stages of the heating phase of energy pile EP1), the corresponding portions of the non-operating energy piles EP2, 3 and 4 were characterised by no changes in temperature. However, temperature changes were observed over time because heat diffused through the soil from EP1 and indirectly heated them. After  $t = 35$  and  $156$  days (i.e., during the successive stages of the heating phase of EP1), heat diffusion resulted in average experimental temperature variations of  $\overline{\Delta T} = 1.6, 0.7$  and  $1.1$  °C and  $\overline{\Delta T} = 5.3, 3.6$  and  $4.5$  °C, respectively. The

numerical results showed slightly higher average temperature changes than the experimental results (cf., Figure 3.5 (b-d)). This discrepancy was attributed to differences between the actual and modelled heat diffusion processes in the foundation, which were inferred to be caused by (i) potential inhomogeneity (spatial and of material properties) of the soil layers of the site that were not accounted for in the numerical model and (ii) different positions of the pipes inside EP1 than those that were considered in the simulation.

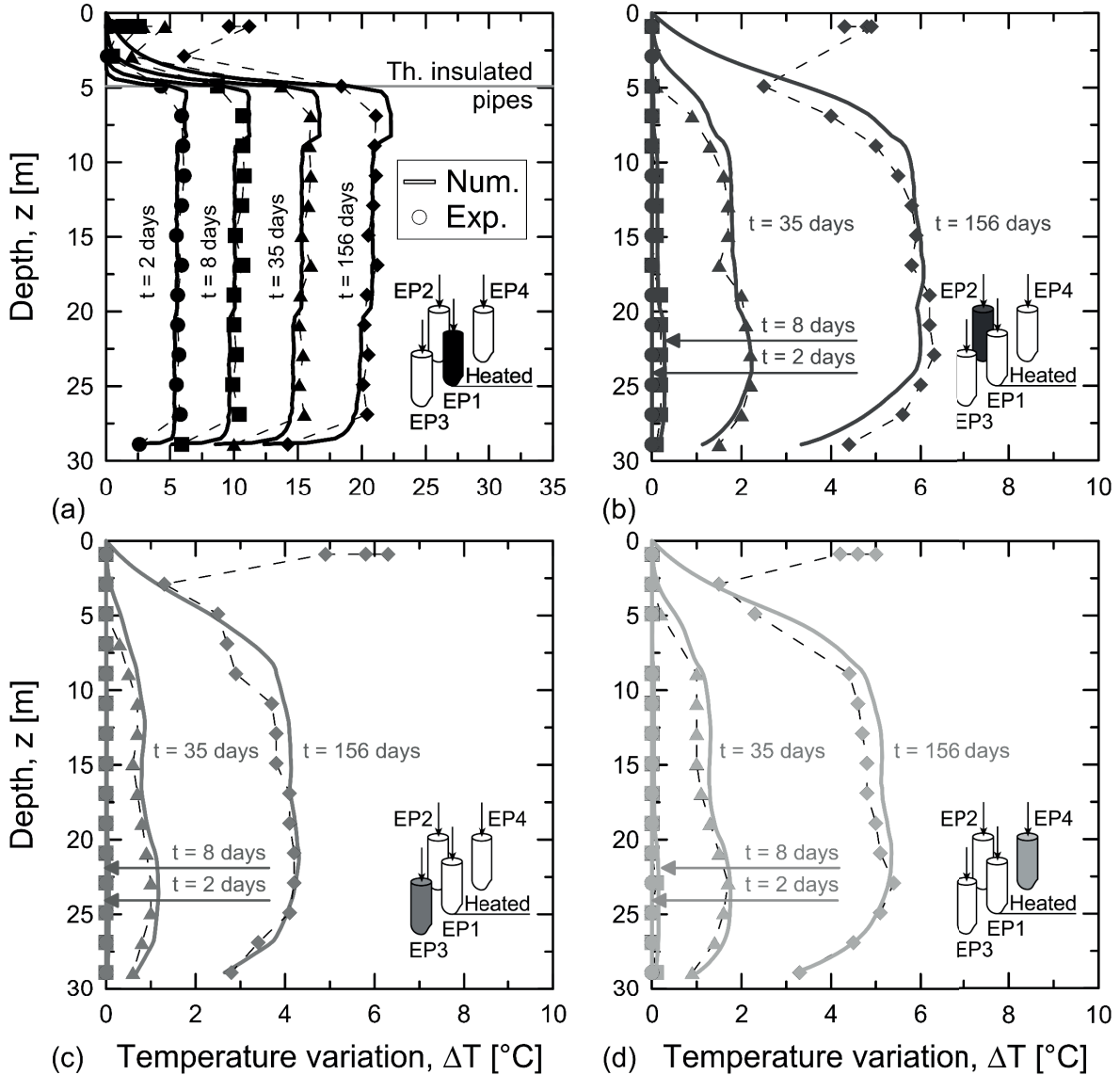


Figure 3.5: Comparison between the experimental and numerical temperature variations observed along (a) the operating energy pile EP1 and (b-d) the non-operating energy piles EP2, 3, and 4, after  $t = 2, 8, 35$  and 156 days of testing.

In addition to the observed temperature changes with time that corresponded to the uninsulated portion of energy pile EP1, temperature variations also occurred in the shallowest 4 m of EP1, 2, 3 and 4 even though the pipes of EP1 were thermally insulated at these depths. This behaviour was observed

in both the experimental and numerical results and was attributed to the impact of the heat exchange operation of energy pile EP1 on the thermal field characterising the shallower portion of the foundation. The experimental results indicated changes in temperature also approximately at the surface of the foundation. In particular, at the depth of  $z = 0.9$  m (where three temperature sensors were placed at different locations within the cross-section of the energy piles), temperature changes were observed and were not characterised by the same magnitude even within the same energy piles. This phenomenon remarked a combined effect played by the variation of the surface thermal conditions during the experimental test and by the inhomogeneity of the temperature field within the cross-section of the piles.

The numerical results showed slightly smaller temperature variations in the shallowest 4 m of all of the piles than the experimental results. They also indicated that no changes in temperature occurred at the surface of the foundation. These results were consistent with the fixed temperature boundary condition that was imposed on the top surface of the numerical model. As illustrated by the results presented below, although not thoroughly representative of the real case, this boundary condition did not compromise the accuracy of the numerical analysis in representing the thermally induced mechanical behaviour of the foundation. Furthermore, this boundary condition did allow the overall thermal behaviour of the foundation to be captured in view of the close comparison between the trends of the outflow fluid temperature from the pipes of EP1 determined experimentally and numerically (cf., Figure 3.6).

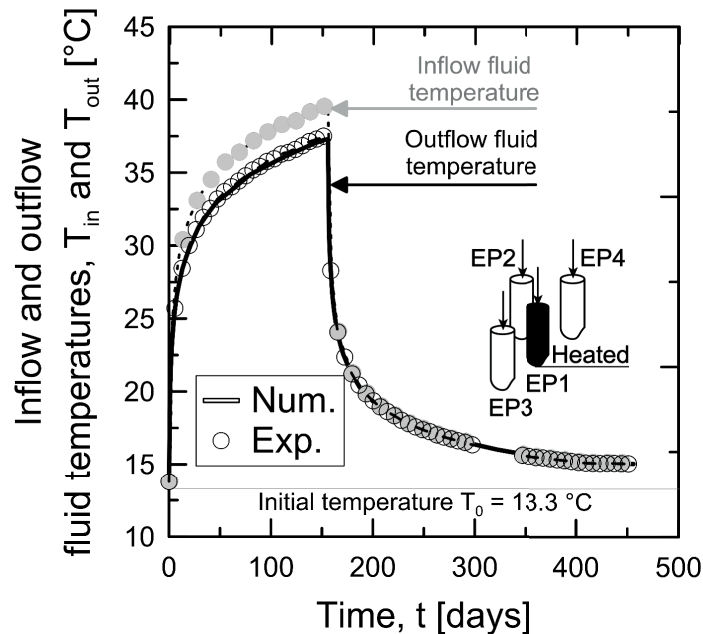


Figure 3.6: Comparison between the experimental and numerical trends of fluid temperature flowing from the pipes of the operating energy pile EP1.



### 3.4.2 Temperature trends at the energy pile toes

Figure 3.7 presents the temperature variations that were determined experimentally through the readings of the pressure cells and numerically through the finite element model at the energy pile toes.

The results show progressive changes in temperature at the toes of energy piles EP1, 2, 3 and 4. The geothermal operation of energy pile EP1 induced a progressively increase in temperature at its toe up to the experimentally observed value of  $\overline{\Delta T} = 13.4$  °C after  $t = 156$  days. Temperature variations were not observed in the non-operating energy piles EP2, 3 and 4 within  $t = 10$  days of testing. However, after approximately  $t = 10$  days, the temperatures at these elements increased with time due to the diffusion of heat through the soil from EP1. An average temperature variation of  $\overline{\Delta T} = 3.5$  °C was observed in the experiment at the toe of these elements after  $t = 156$  days. The temperature rises numerically determined at the toes of EP2, 3 and 4 at the early and successive stages of the heating phase of EP1 were slightly faster and slower than those observed experimentally, respectively. A residual temperature variation was numerically determined at the toe of the operating energy pile EP1 toward the end of the test differently than the negligible temperature variation that was observed experimentally. Both the experimental and numerical results agreed well in indicating a residual average temperature variation at the toes of the non-operating energy piles EP2, 3 and 4 toward the end of the test. The differences between the numerical and experimental results were addressed to (i) differences between the materials description and the geometry of the pipes in EP1 in the numerical model and those characterising the real case, and (ii) different sensitivities to a temperature variation of the nodes of the finite element model (that were used to determine the temperature variations at the pile toes) and of the pressure cells. The impact of all of these aspects was more notable at the late stages of the test (e.g., passive cooling phase of EP1) because capacity effects governed the heat exchange process characterising the foundation. The considered differences may be associated to localised variations between the modelled and actual mechanical behaviours of the foundation addressed in the following.

### 3.4.3 Temperature variations in the soil

Figure 3.8 shows the temperature variations in the soil that were determined experimentally through the readings of the thermistors and numerically through the finite element model. The variations in temperature along the lengths of profiles P+T1 (cf., Figure 3.8 (a)) and P+T2 (cf., Figure 3.8 (b)) show the stages of the test during which the operating energy pile EP1 was subjected to average temperature variations of  $\overline{\Delta T}_{EP1} = 5, 10, 15$  and  $20$  °C (i.e., at  $t = 2, 8, 35$  and  $156$  days of testing, respectively). The trends of temperature variations (cf., Figure 3.8 (c)) refer to selected points along the profiles.

The heating of energy pile EP1 had a notable impact on the temperature field of the surrounding soil. The experimental results show that after  $t = 156$  days, the profile at a radial distance of 1 m from the axis of the EP1 (i.e., P+T1) was subjected to an average temperature variation of  $\overline{\Delta T} = 12$  °C (cf., Figure 3.8 (a)). At the same time, a lower average temperature variation of  $\overline{\Delta T} = 5$  °C was observed along the profile at a radial distance of 2.2 m (i.e., P+T2; cf., Figure 3.8 (b)). Comparable temperature variations were observed along the lengths of the profiles with time in the numerical results (cf.,



Figure 3.8 (c)), although larger changes than those that were measured experimentally were generally observed in the top portion of the foundation. This difference was again attributed to differences between the modelled and actual heat exchange processes characterising this portion of the foundation.

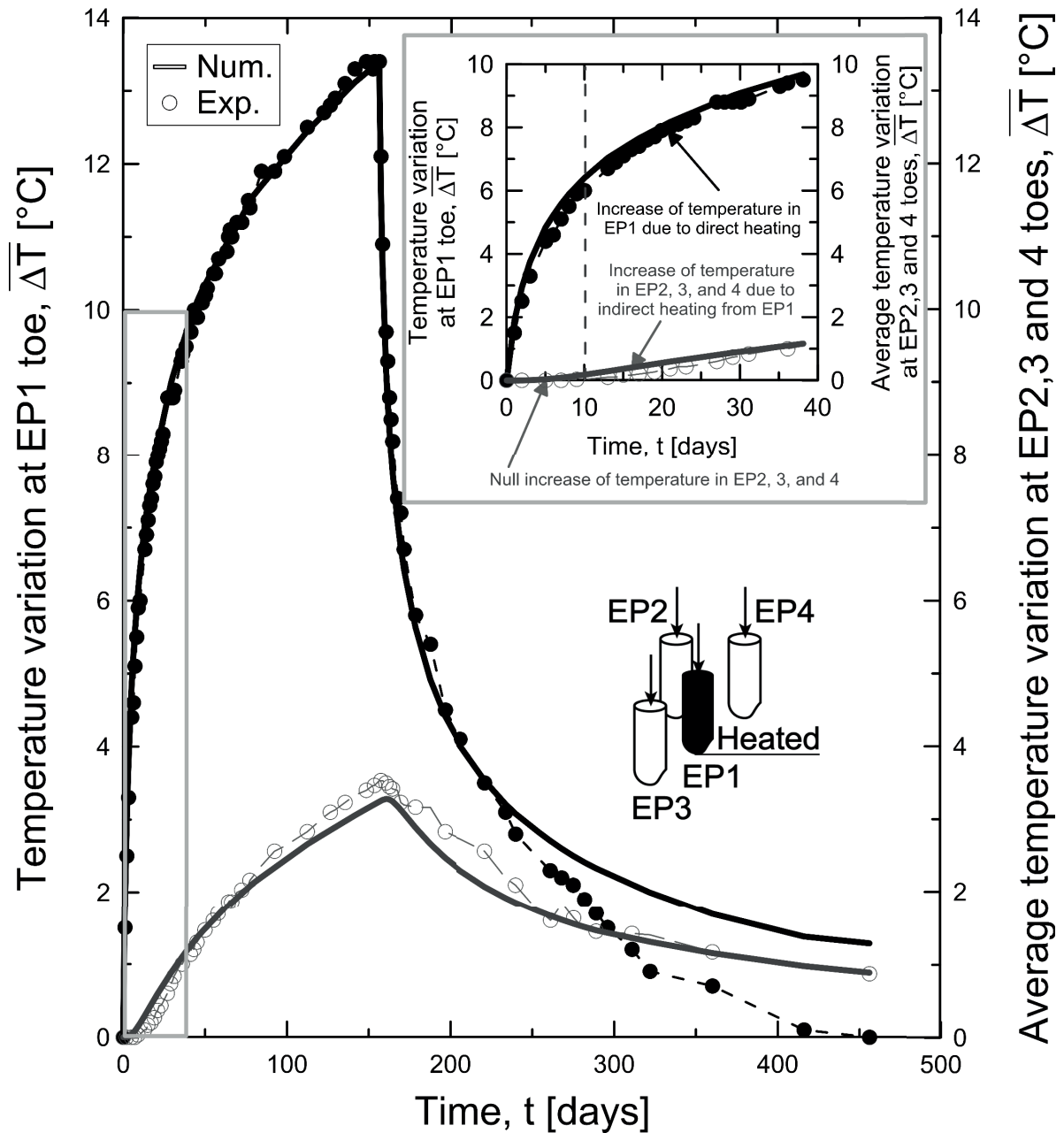


Figure 3.7: Comparison between the experimental and numerical temperature variations observed at the energy pile toes with time.

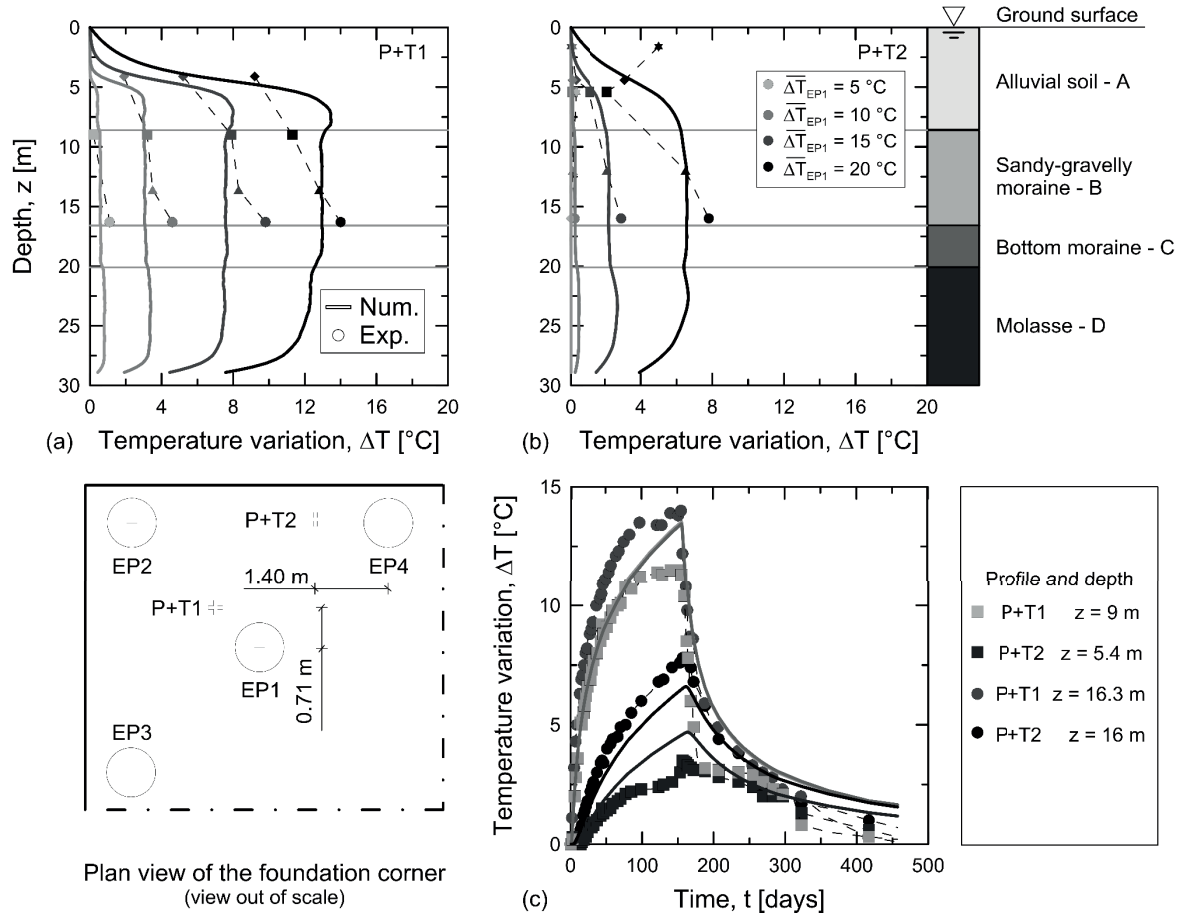


Figure 3.8: Comparison between the experimental and numerical temperature variations along profiles (a) P+T1 and (b) P+T2 in the soil at the time steps at which the operating energy pile EP1 was subjected to average temperature variations of  $\overline{\Delta T}_{EP1} = 5, 10, 15$  and  $20^\circ\text{C}$  ( $t = 2, 8, 35$  and  $156$  days of testing, respectively). (c) Trends of temperature variations at selected points along the profiles.

Inhomogeneity of the sandy-gravelly moraine was suggested by the different variations in temperature that were observed at the top and bottom of this layer (trends for points at  $z = 9$  m and  $z = 16.3$  m in P+T1; cf., Figure 3.8 (c)). Because the finite element model did not account for material inhomogeneity, this aspect of the problem was not represented by the numerical analysis. The residual temperature variation previously remarked for the toes of the non-operating energy piles EP2, 3 and 4 toward the end of the test was similarly observed along the length of P+T1 and P+T2 during the same period of the test in both the experimental and numerical results. All of these temperature variations reflected the impact of the residual temperature variation that characterised the heat carrier fluid circulating inside the pipes of EP1 with reference to the initial condition (cf., Figure 3.5) on the thermal field of the foundation. These temperature variations caused in zones of the pile group residual strain and stress variations addressed experimentally and numerically in the following.

The comparisons between the temperature variations observed experimentally and numerically along the lengths of soil profiles P+T1 and P+T2 indicated greater differences than those observed along the non-operating energy piles EP2, 3 and 4. This is a consequence of the temperature driven approach

that was used to select the potential positions of the thermocouples installed along the piles for comparing the experimental and numerical results. Different actual positions of the thermocouples in the piles, which may more closely reflect the greater differences in the temperature variations characterising the soil in correspondence with the known locations of the thermistors, cannot be discounted.

#### 3.4.4 Vertical strain variations along the energy piles

Figure 3.9 shows the variations in vertical strain that were determined experimentally through the readings of the thermocouples and the vibrating wire strain gauges along energy piles EP1, 2, 3 and 4, and numerically through the finite element model.

The heating due to the geothermal operation of energy pile EP1 during the first phase of the test resulted in an expansion of the portion of EP1 in which the pipes were not thermally insulated and a contraction of the thermally insulated portion because of the entrapment with the slab (cf., Figure 3.9 (a)). The contraction of the shallower portion of EP1 would not have occurred if the pipes were not thermally insulated in that region and the thermal field was more uniform along the pile length. Maximum expansive (negative) vertical strains of  $\Delta\varepsilon_z = -22, -56, -109$  and  $-167 \mu\epsilon$  were recorded along the uninsulated portion of energy pile EP1 during the experiment when it was subjected to temperature variations of  $\overline{\Delta T}_{EP1} = 5, 10, 15$  and  $20^\circ\text{C}$ , respectively (i.e., after  $t = 2, 8, 35$ , and  $156$  days, respectively). Maximum contractive (positive) vertical strains variations of  $\Delta\varepsilon_z = 31, 56, 68$  and  $79 \mu\epsilon$  were recorded along the insulated portion during the same stages of the test. Marked expansive vertical strains were observed with time in the bottom portion of this pile. Similar results were obtained by the numerical analysis.

The heating of the operating energy pile EP1 also induced an expansion of the surrounding non-operating energy piles EP2, 3 and 4 (cf., Figure 3.9 (b-d)). After  $t = 2$  and  $8$  days (i.e., during the early stages of the heating phase of EP1), the expansions of EP2, 3 and 4 were caused by (i) the expansion of pile EP1 as a result of its direct heating and (ii) the associated upward deformation of the slab. This deformation was thus purely mechanical (as described above, the temperature variations were zero or very small along the non-operating energy piles EP2, 3 and 4 during these stages of the test). The evolution of deformation along the piles (decreasing from top to bottom) indicates that the deformation was comparable to that caused by an upward force applied at their heads. After  $t = 35$  and  $156$  days (i.e., during the successive stages of the heating phase of EP1), the expansions of piles EP2, 3 and 4 were caused by (i) the expansion of EP1 as a result of its direct heating, (ii) the associated upward deformation of the slab, (iii) the expansions of these elements as a result of their indirect heating and (iv) the expansion of the soil as a result of its heating. In contrast to the deformation of the non-operating energy piles EP2, 3 and 4 during the early stages of the geothermal operation of energy pile EP1, this deformation was characterised by both mechanical and thermal contributions. Marked expansions of up to  $\Delta\varepsilon_z = -106 \mu\epsilon$  were observed during these stages in the lower portions of EP2, 3 and 4 in both the experimental and numerical results. These expansions were significantly greater than those that developed in the top portions of these elements (i.e., between  $\Delta\varepsilon_z = -10$  and  $-30 \mu\epsilon$ ). They were also greater than the strain under free thermal expansion conditions,  $\Delta\varepsilon_f^{th}$  (cf., Figure 3.10 for energy pile EP2 after  $t = 156$  days, in which  $\alpha_{EP}$  is the linear thermal expansion coefficient of the energy piles).

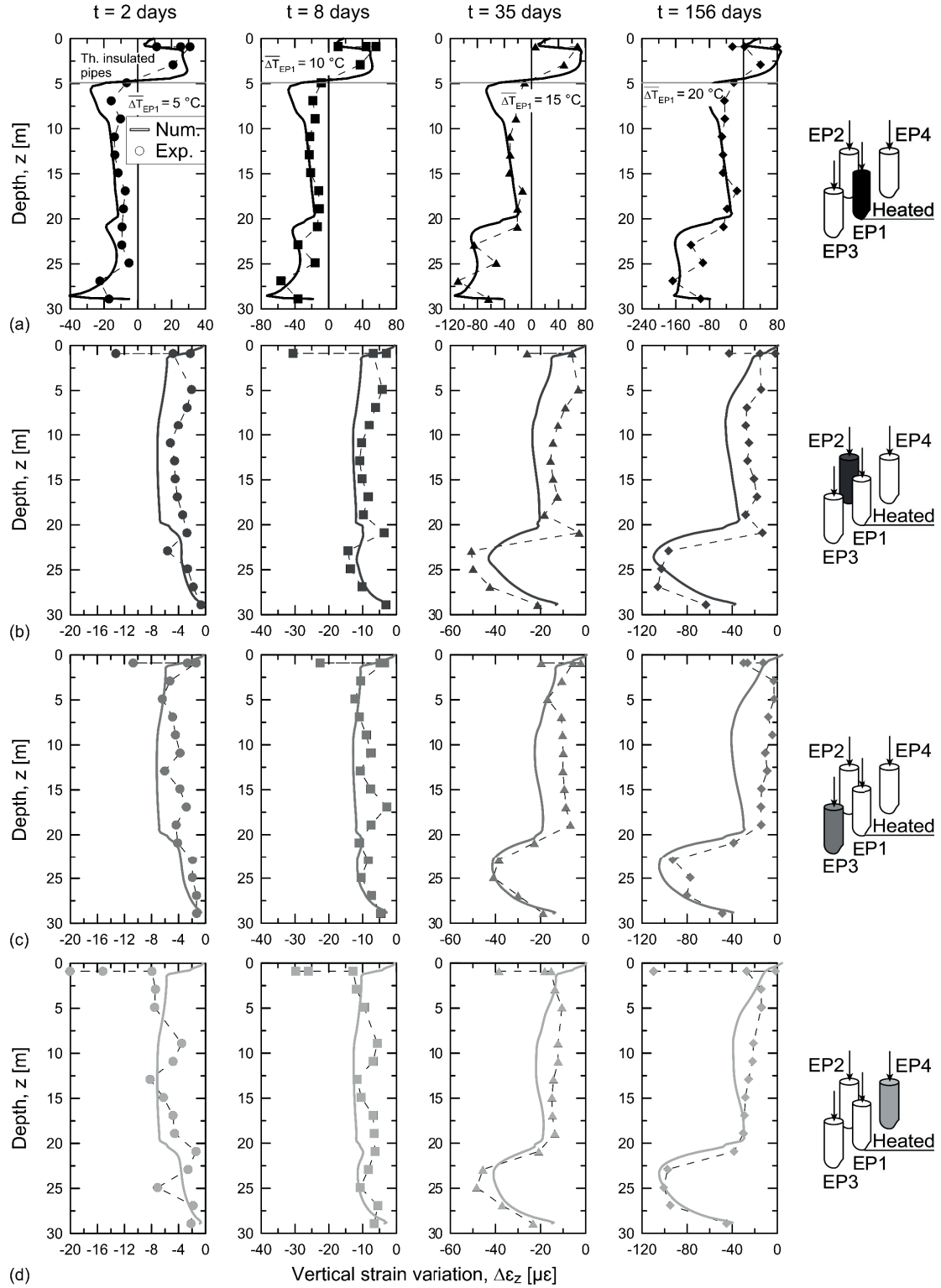


Figure 3.9: Comparison between the experimental and numerical variations in vertical strain observed along (a) the operating energy pile EP1 and (b-d) the non-operating energy piles EP2, 3, and 4, after  $t = 2, 8, 35$  and 156 days of testing.

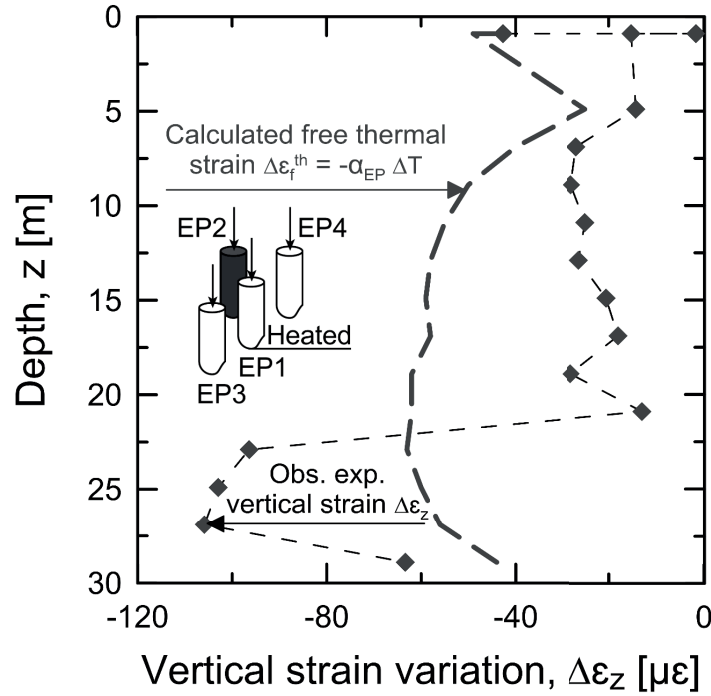


Figure 3.10: Comparison between the experimentally observed variations in vertical strain in the non-operating energy pile EP2 after  $t = 156$  days of testing and calculated with reference to free thermal expansion conditions.

The marked expansive vertical strains that were observed in the bottom portions of all of the piles during the successive stages of the heating phase of EP1 occurred because as heat diffused through the system, the mechanical response of the foundation was governed by the thermally induced deformation of the molasse layer. These strain variations were caused not only by the interplay between the thermally induced deformations (direct and indirect) of the piles and the slab but also and primarily by the thermally induced deformation of the soil mass (e.g., molasse layer) surrounding the piles. The value of the thermal expansion coefficient of the molasse layer, which was found to be greater than that of the piles based on the results of the numerical analysis, was the key factor of this phenomenon. Heating the very stiff molasse layer over time caused a marked expansion of this layer. This field was superimposed on the expansion field of the bottom portions of the piles. Remarkably high expansive vertical strains therefore developed in these settings.

### 3.4.5 Vertical stress variations along the energy piles

Figure 3.11 shows the experimental and numerical variations in vertical stress along energy piles EP1, 2, 3 and 4. The experimental vertical stress variations were calculated based on the experimentally observed vertical strain variations using a one-dimensional scheme, i.e.,  $\Delta\sigma_z = \Delta\sigma_o^{th} = E_{EP}\Delta\varepsilon_b^{th} = E_{EP}(\Delta\varepsilon_o^{th} - \Delta\varepsilon_f^{th}) = E_{EP}(\Delta\varepsilon_z + \alpha_{EP}\Delta T)$  (where  $\Delta\sigma_o^{th}$  is the thermally induced vertical stress,  $E_{EP}$  is the Young's modulus of the pile,  $\Delta\varepsilon_b^{th}$  is the blocked thermally induced strain and  $\Delta\varepsilon_o^{th}$  is the observed thermally induced strain). It is worth mentioning that the strains that are associated

with free thermal expansion conditions were null for the non-operating energy piles EP2, 3 and 4 during the early stages of the geothermal operation of energy pile EP1 because no variations in temperature were observed in these elements. The numerical vertical stress variations were determined through the finite element model.

The heating that was associated with the geothermal operation of EP1 during the first phase of the test resulted in an increasing compressive (positive) vertical stress along its length (cf., Figure 3.11 (a)). The maximum compressive vertical stress variation of  $\Delta\sigma_z = 5500$  kPa was observed after  $t = 156$  days. This phenomenon occurred because the expansive strain potential that is associated with the temperature variation in the pile was restrained by the presence of the soil and slab and caused an increase of the compressive stress in this element. The order of magnitude of the observed vertical stress variation was comparable to other experimental data from the literature (e.g., Murphy et al., 2015) that involved significant energy exploitations through the use of energy piles. Lower compressive vertical stress variations were observed in the bottom portion of EP1. Consistent results were obtained by the numerical analysis.

The heating of the operating energy pile EP1 also induced vertical stress variations in the surrounding non-operating energy piles EP2, 3 and 4 (cf., Figure 3.11 (b-d)). After  $t = 2$  and 8 days (i.e., during the early stages of the heating phase of EP1), energy piles EP2, 3 and 4 were subjected to tensile stress variations of up to the maximum experimental negative value of approximately  $\Delta\sigma_z = -250$  kPa at their heads. Decreases in the tensile stress variations from the top to the bottom of these elements were observed during this stage of the test in both the experimental and numerical results. These vertical stress variations were associated with the corresponding deformation field that was described previously. After  $t = 35$  and 156 days (i.e., during the successive stages of the heating phase of energy pile EP1), maximum compressive vertical stress variations of up to  $\Delta\sigma_z = 1370$  kPa and tensile vertical stress variations of up to  $\Delta\sigma_z = -1419$  kPa were measured in EP2, 3 and 4.

The previously observed tensile vertical stress variations along the lengths of these elements decreased to compressive values in their top portions but increased toward higher tensile values in their bottom portions. Similar results were obtained by the numerical analysis.

The effect of the more pronounced thermally induced deformation of the molasse layer than the deformation in the bottom portions of the piles was again evident during the successive stages of the heating phase of energy pile EP1. The deformation of this layer pulled both the operating energy pile EP1 and the non-operating energy piles EP2, 3 and 4 and caused the reductions of the compressive thermally induced stress fields that were measured along the bottom portions of all of the piles. Because EP1 was directly heated and the compressive thermally induced stress variation in this element was more pronounced than the tensile stress variation that was exerted by the molasse, a compressive stress field governed this pile. Because EP2, 3 and 4 were indirectly heated and the compressive thermally induced stress variations in these elements were smaller than the tensile stress variations that were exerted by the molasse, a tensile stress field governed the bottom portions of these piles.

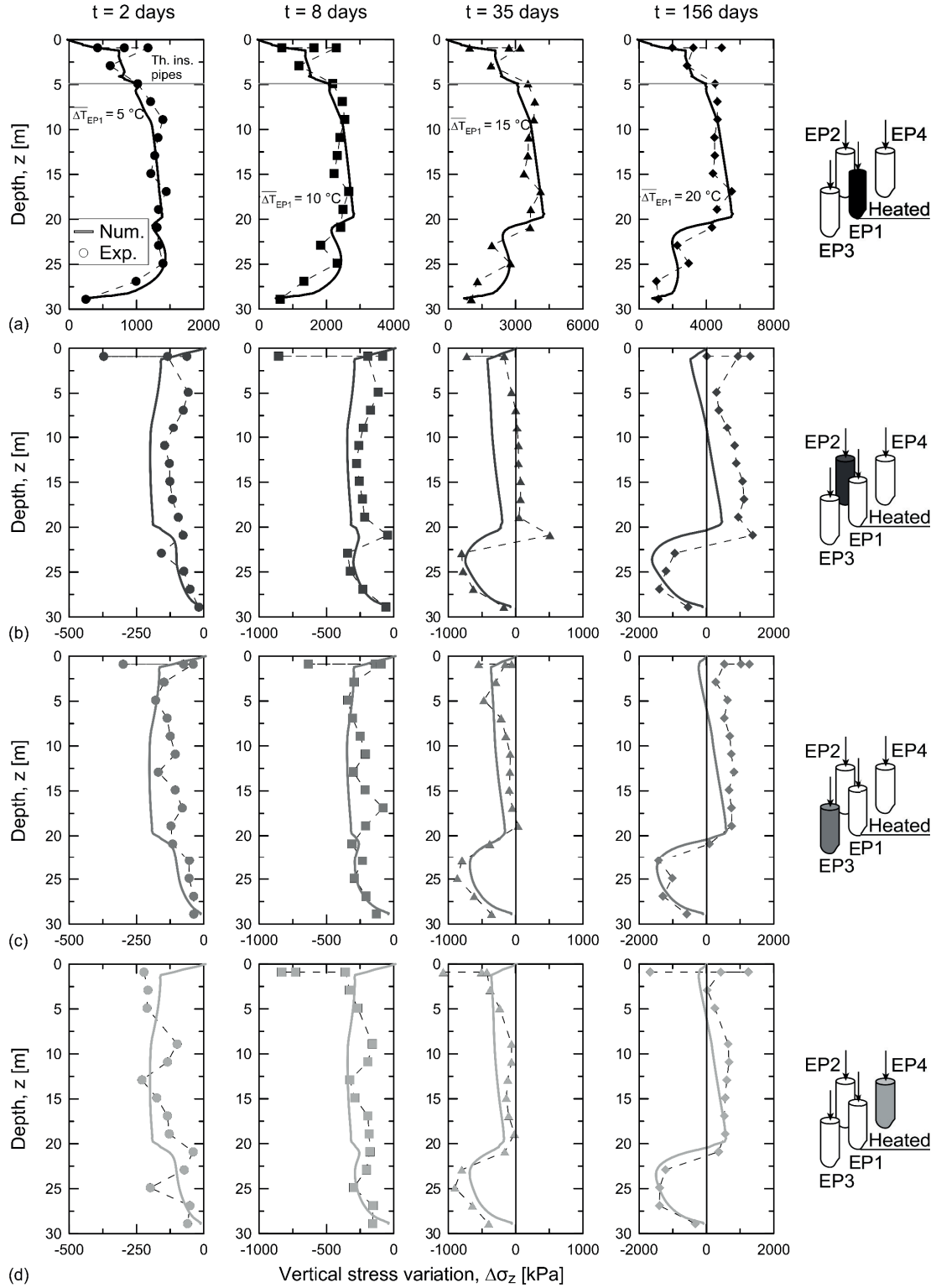


Figure 3.11: Comparison between the experimental and numerical vertical stress variations observed along (a) the operating energy pile EP1 and (b-d) the non-operating energy piles EP2, 3, and 4, after  $t = 2, 8, 35$  and  $156$  days of testing.



Together with the aforementioned phenomena, the presence of the slab played a crucial role in the variation of the stress fields in all the piles. The reason is because the deformation of the slab, which was caused by the thermally induced deformation of EP1 and the soil, resulted in an imposed deformation on EP2, 3 and 4 that caused stress variations in these elements. This phenomenon occurred as a consequence of (i) the continuity and compatibility of the displacements characterising the piles, the soil and the slab as perfectly jointed solids, and (ii) the role of the slab as a constant stiffness boundary condition for the pile-soil system (which differently to a constant load boundary condition involves a load variation – and thus a stress variation – for a displacement variation in deformation-related problems). The bending rigidity per unit area of the slab is  $D_b = (E_{slab} t_{slab}^3) / [12(1 - \nu_{slab}^2) B_{slab} L_{slab}] = 10080 \text{ kN/m}$  where  $E_{slab}$  and  $\nu_{slab}$  are the Young's modulus and Poisson's ratio of the slab, respectively, and  $B_{slab}$ ,  $L_{slab}$  and  $t_{slab}$  are the breadth, length and thickness of the slab, respectively.

#### 3.4.6 Vertical stress variations at the toe of the operating energy pile

Figure 3.12 shows the vertical stress variations that were determined experimentally through the readings of the pressure cell at the toe of the operating energy pile EP1 and numerically through the finite element model.

A remarkable increase of the compressive stress was observed at the toe of EP1 within the first month of geothermal operation in both the experimental and numerical results. The vertical stress increased along with the observed increase of temperature due to the restrained thermal expansion of the pile. Less pronounced increases of the vertical stress were observed experimentally and numerically at the toe of the operating energy pile EP1 over time during its heating phase to the asymptotic value of approximately  $\overline{\Delta\sigma_z} = 1000 \text{ kPa}$ . This phenomenon was attributed to (i) the progressively approaching steady state thermal conditions in the system that involved a smaller development (and restraint) of thermally induced deformation of the pile and (ii) the pulling (i.e., relieving) thermally induced action that was exerted by the molasse around the bottom portion of the pile. At the end of the test, the toe of the operating energy pile EP1 was unloaded by the increase of the compressive stress that was described above. This phenomenon was observed in both the experimental and numerical results.

#### 3.4.7 Variations of radial strain in the operating energy pile

Figure 3.13 shows the variations in radial strain that were determined experimentally through the readings of an optical fibre that was mounted along the reinforcing cage of the operating energy pile EP1 at a depth of  $z = 9 \text{ m}$  and numerically through the finite element model. The trend of radial strain under free thermal expansion conditions that was calculated based on the point value of temperature variation recorded by a thermocouple at  $z = 8.9 \text{ m}$  is also plotted for reference. The numerical results refer to an average of the strain variations of 10 points that were selected in the numerical model along the circumference representing the reinforcing cage placed in EP1 in the real case.



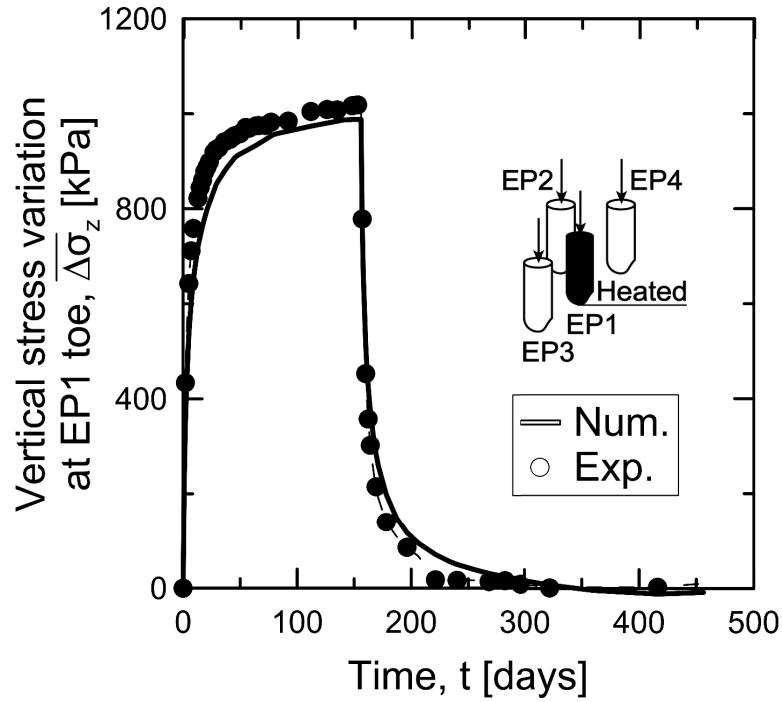


Figure 3.12: Comparison between the experimental and numerical vertical stress variations observed at the toe of the operating energy pile EP1 with time.

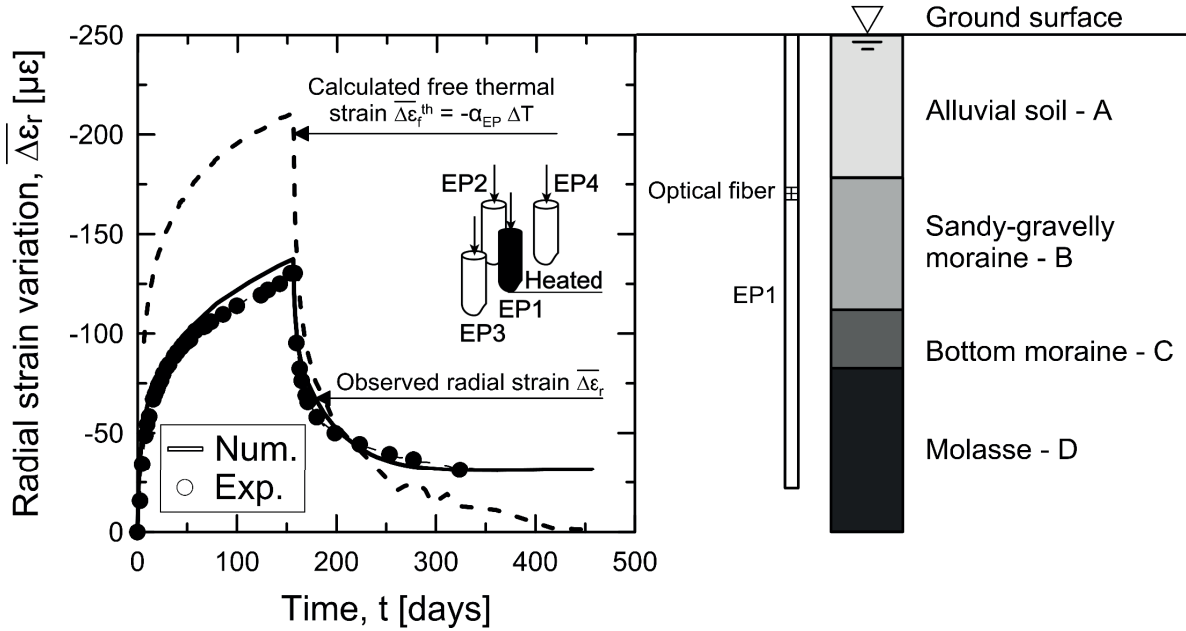


Figure 3.13: Comparison between the experimental and numerical radial strain variations observed at a depth of  $z = 9$  m in the operating energy pile EP1 with time.

A progressive increase in the variation of the expansive strain was observed with time during the heating phase of energy pile EP1 because of the positive temperature variation observed in the considered element. A maximum variation in the expansive radial strain of  $\Delta\epsilon_r = -130 \mu\epsilon$  was observed

after  $t = 156$  days in both the experimental and numerical results. The variation of the expansive strain that was observed experimentally and numerically throughout the heating phase of energy pile EP1 was smaller than that calculated under free thermal expansion conditions. This condition did not hold toward the end of the passive cooling phase of EP1. Such a phenomenon can be addressed to the different average temperature variation characterising the cross-section of EP1 at a depth of  $z = 9$  m compared to the punctual value of temperature variation recorded at  $z = 8.9$  m by the thermocouple.

### 3.5 Comparison between experimental and numerical results – Test 20EPall

This section compares the experimental data that were collected during the development of the full-scale *in situ* Test 20EPall and the numerical results that were obtained through the Class C1 prediction. The same locations that were used to interpret the numerical results referring to Test 20EP1 were used for Test 20EPall.

As before, the experimental and numerical data include *variations* of the parameters from the beginning of the test over time. Therefore, they reflect the impact of the geothermal operation of the energy piles on the thermo-mechanical behaviour of the foundation. The stress states generated from body loads in the different media (i.e., *in situ* conditions) and from the application of the mechanical loads of the superstructure to the piles are not included in the stress and strain curves.

#### 3.5.1 Impact of number of operating energy piles on vertical deformation

Figure 3.14 presents the variations in vertical strain determined experimentally and numerically along the length of energy pile EP1 when this pile was the only pile in the group operating as a geothermal heat exchanger (in Test 20EP1) and along (on average) the lengths of energy piles EP1, 2, 3 and 4 when all of these piles operated as geothermal heat exchangers (in Test 20EPall). The strain variations,  $\Delta\varepsilon_z$ , correspond to the average temperature variations along the uninsulated portion of EP1 of  $\overline{\Delta T}_{EP1} = 5, 10, 15$  and  $20$  °C after  $t = 2, 8, 35$  and  $156$  days of testing, respectively, during the heating phase of Test 20EP1. The strain variations,  $\overline{\Delta\varepsilon_z}$ , correspond to the mean value of the average temperature variations along the uninsulated portions of EP1, 2, 3 and 4 of  $\overline{\Delta T}_{EPall} = 5, 10, 15$  and  $20$  °C after  $t = 2, 9, 28$  and  $60$  days of testing, respectively, during the heating phase of Test 20EPall.

When the number of operating energy piles in the group increased, the thermally induced vertical strain variation increased with depth for the same average temperature variation applied to the piles because of group effects. In the operation of multiple energy piles, this average temperature was achieved at a faster rate because of thermal interactions between the energy piles at successive stages of the test. The abovementioned finding was highlighted by both the experimental and numerical results. Notable differences can be identified between the experimental and numerical results pertaining to Test 20EPall during the initial stages of the geothermal operation of the energy piles (cf., Figure 3.14 (a) and (b)). These differences were related to the interplay between the “average” modelling of the group and the discrepancies between the variation of the temperature field from the initial conditions on site (non-uniform, based on recorded temperature data in the piles and in the soil) and in the numerical model (uniform and constant). This phenomenon became less pronounced at successive

stages of the geothermal operation of the energy piles and yielded thermally induced vertical strain values closer to those measured experimentally.

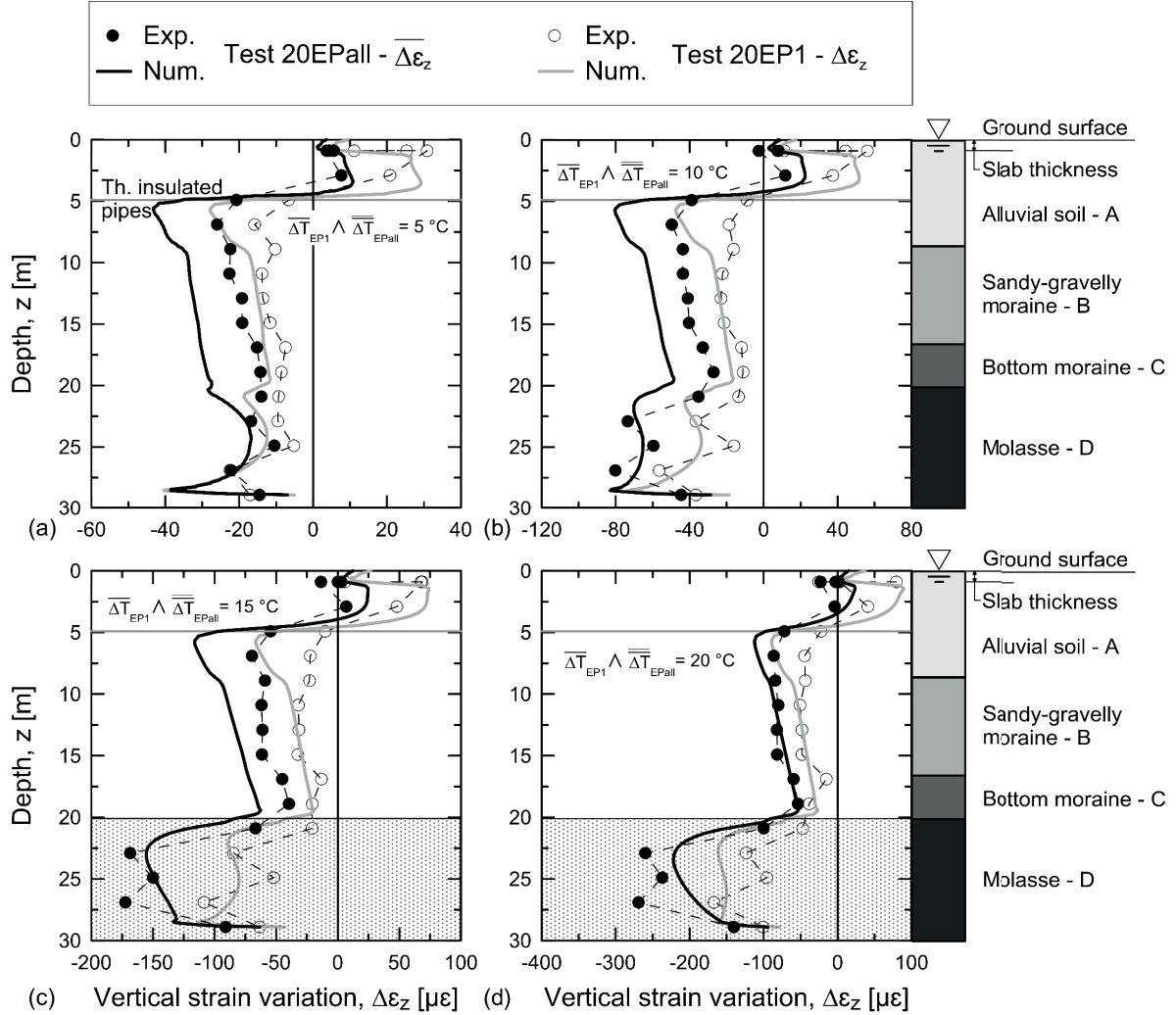


Figure 3.14: Comparison between the experimentally and numerically observed vertical strain variations. The strain variations,  $\Delta\epsilon_z$ , correspond to the average temperature variations along the uninsulated portion of EP1 of  $\overline{\Delta T}_{EP1} = 5, 10, 15$  and  $20$  °C (panels (a), (b), (c) and (d), respectively) after  $t = 2, 8, 35$  and  $156$  days of testing, respectively, during the heating phase of Test 20EP1. The strain variations,  $\overline{\Delta\epsilon_z}$ , correspond to the mean value of the average temperature variations along the uninsulated portions of EP1, 2, 3 and 4 of  $\overline{\Delta T}_{EPall} = 5, 10, 15$  and  $20$  °C (panels (a), (b), (c) and (d), respectively) after  $t = 2, 9, 28$  and  $60$  days of testing, respectively, during the heating phase of Test 20EPall.

The presence of thermally induced group effects governs the higher development of vertical strain when more energy piles operate as geothermal heat exchangers in a closely spaced pile group than when only one energy pile serves this purpose. This phenomenon corroborates the motivation for and the results of recently developed analytical methods for capturing this aspect of the behaviour of energy pile groups (Rotta Loria and Laloui, 2016b; Rotta Loria and Laloui, 2017a; Rotta Loria and Laloui, 2017b; Rotta Loria et al., 2017c).

In Test 20EP1, the *non-operating* energy piles EP2, 3, and 4 were characterised by greater thermally induced vertical strain than may be associated with free expansion conditions. These findings were based on the linear thermal expansion coefficient of the piles,  $\alpha_{EP}$ , and the applied temperature variation,  $\Delta T$  (i.e.,  $\Delta \varepsilon_f^{th} = -\alpha_{EP} \Delta T$ ).

The same phenomenon was observed in Test 20EPall during successive stages of the geothermal operation of energy piles EP1, 2, 3 and 4 (cf., Figure 3.14 (c) and (d)). The crucial difference was that the *operating* energy piles were characterised by greater average thermally induced vertical strain than that under free expansion. According to previous arguments, this phenomenon could be attributed to the significant impact of the thermally induced deformation of the molasse on the deformation of the energy piles due to the greater linear thermal expansion coefficient of the former relative to the latter (cf., Figure 3.15 after  $t = 60$  days).

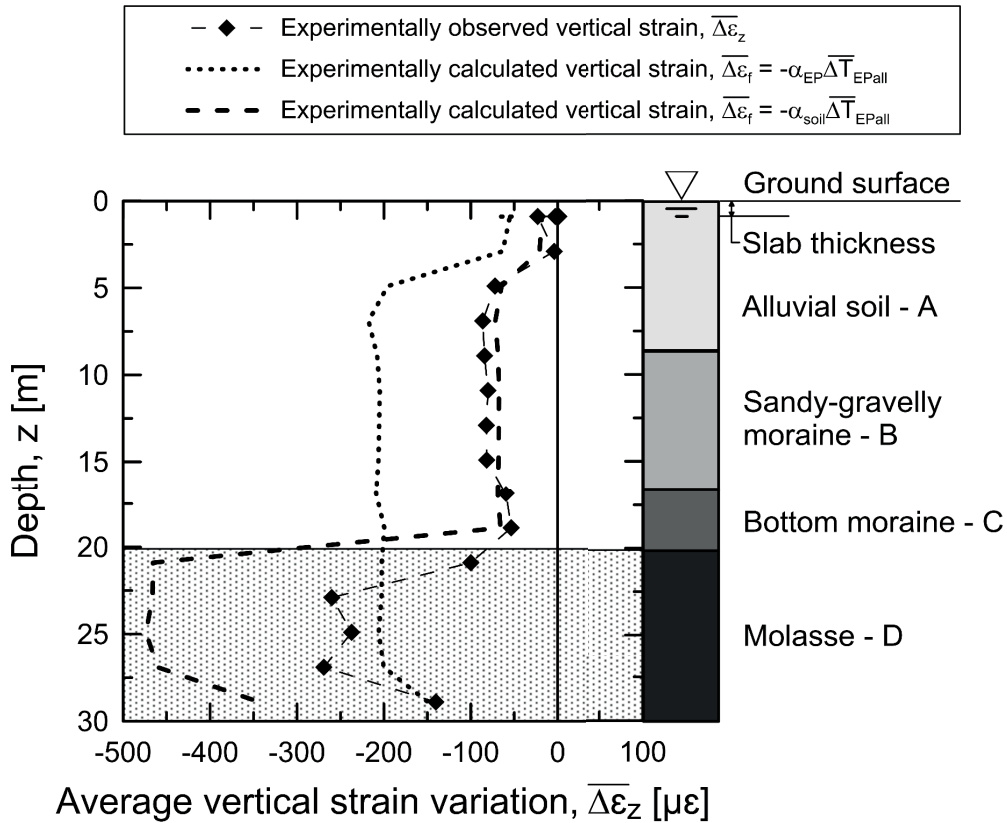


Figure 3.15: Impact of the energy piles and soil thermal expansion potential on the vertical deformation of the piles during successive stages of the geothermal operation based on experimental results (Test 20EPall).

### 3.5.2 Impact of number of operating energy piles on vertical stress

Figure 3.16 presents the variations in vertical stress determined experimentally and numerically along the length of energy pile EP1 when this pile was the only one operating as a geothermal heat exchanger (in Test 20EP1) and along (on average) the lengths of energy piles EP1, 2, 3 and 4 when all of these piles operated as geothermal heat exchangers (in Test 20EPall). The same time intervals

accounted for thus far are considered for the vertical stress,  $\Delta\sigma_z$ , along the operating energy pile EP1 in Test 20EP1 and the average vertical stress,  $\overline{\Delta\sigma_z}$ , along the operating energy piles EP1, 2, 3 and 4 in Test 20EPall.

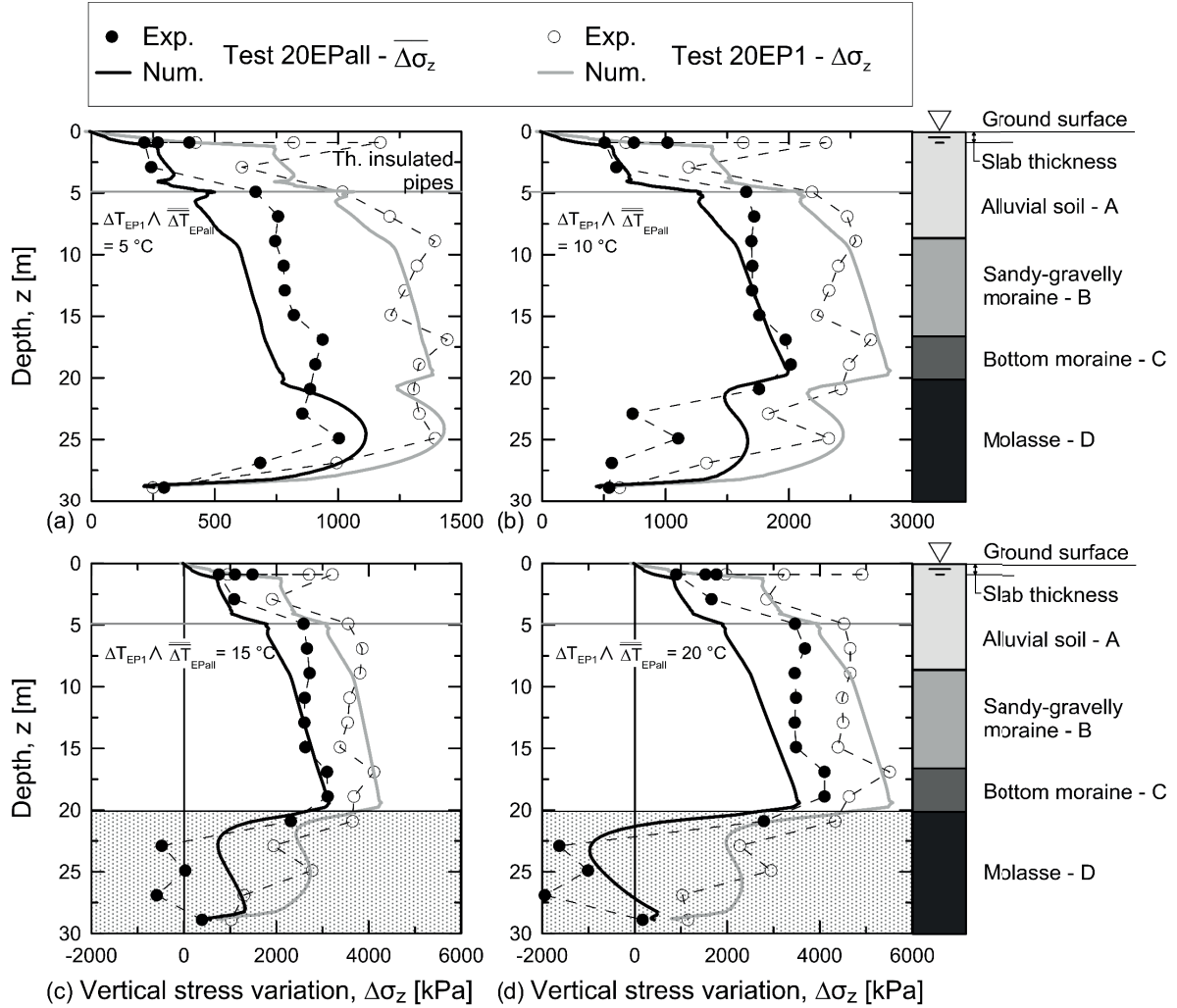


Figure 3.16: Comparison of the experimentally and numerically observed vertical stress variations. The stress variations,  $\Delta\sigma_z$ , correspond to the average temperature variations along the uninsulated portion of EP1 of  $\overline{\Delta T}_{EP1} = 5, 10, 15$  and  $20^\circ\text{C}$  (panels (a), (b), (c) and (d), respectively) after  $t = 2, 8, 35$  and  $156$  days of testing, respectively, during the heating phase of Test 20EP1. The stress variations,  $\overline{\Delta\sigma_z}$ , correspond to the mean value of the average temperature variations along the uninsulated portions of EP1, 2, 3 and 4 of  $\overline{\Delta T}_{EPall} = 5, 10, 15$  and  $20^\circ\text{C}$  (panels (a), (b), (c) and (d), respectively) after  $t = 2, 9, 28$  and  $60$  days of testing, respectively, during the heating phase of Test 20EPall.

When the number of operating energy piles in the group was increased, the thermally induced vertical stress variation decreased with depth for the same temperature variation applied to the piles. This result was highlighted by both the experimental and numerical results, which had discrepancies comparable to those reported above for the vertical strain. This result also corroborates the motivation for and outcomes of recently developed numerical studies investigating the thermo-mechanical behaviour of energy pile groups (Salciarini et al., 2015; Jeong et al., 2014; Di Donna and Laloui, 2014;

Suryatriyastuti et al., 2015; Di Donna et al., 2016; Saggu and Chakraborty, 2016; Salciarini et al., 2017).

A notable phenomenon occurred at successive stages of the geothermal operation of the energy piles in Test 20EPall (cf., Figure 3.16 (c) and (d)). According to previous arguments about Test 20EP1, the presence of a soil layer with a greater linear thermal expansion coefficient than the piles (e.g., the molasse layer) resulted in a less pronounced increase in the vertical stress in energy pile EP1 as the temperature increased in successive stages of geothermal operation. This phenomenon was caused by the thermally induced expansion of the soil, which resulted in a pulling action of the piles that reduced their vertical stress. Because only one operating energy pile was present in Test 20EP1, the variations in vertical stress remained compressive at successive stages of the geothermal operation, consistent with the soil layer characterised by a greater thermal expansion coefficient. That is, the compressive stress variation induced in energy pile EP1 by its restrained expansion was more pronounced than the tensile stress variation exerted by the surrounding soil layer (expanding more than the piles) under the applied heating thermal load. However, because more energy piles were operating as geothermal heat exchangers in Test 20EPall and because a more significant and widespread temperature variation was experienced by the soil, the variations in the vertical stress affected tensile stresses in the parts of the piles located in the soil layer with a thermal expansion coefficient greater than that of the piles. That is, the compressive stress variation induced in energy piles EP1, 2, 3 and 4 by their restrained expansion was less pronounced than the tensile stress variation exerted by the surrounding soil layer under the heating load. Therefore, tensile stress can arise in energy piles when they are heated. This phenomenon experimentally confirms for the first time the evidence presented by Bourne-Webb et al. (2016a). More generally, for more prolonged operation of various energy piles, when the soil has a greater thermal expansion coefficient than the pile, stress variations that are the opposite of the variations expected based on the type of applied thermal load (i.e., heating or cooling load) can develop in the piles.

Group effects and interactions imply increased deformation of the piles. That is, when the same average temperature variation is applied to the energy piles, the proportion of the observed thermally induced vertical strain,  $\varepsilon_o^{th}$ , increases with the number of (e.g., thermally) loaded piles. Consequently, under the same temperature variation, lower magnitudes of thermally induced blocked strain,  $\varepsilon_b^{th} = \varepsilon_o^{th} - \varepsilon_f^{th}$ , and observed vertical stress,  $\sigma_o^{th} = E_{EP}\varepsilon_b^{th}$  develop in various operating energy piles than in a single operating energy pile. This phenomenon becomes more pronounced as the number of energy piles operating as geothermal heat exchangers increases, as highlighted in Figure 3.17 using the experimental results for Test 20EP1 and Test 20EPall. In this figure, the average vertical stress  $\overline{\Delta\sigma_z}$  (in the operating energy pile EP1) is plotted against the average temperature variation  $\overline{\Delta T}_{EP1}$  for Test 20EP1, and the average vertical stress  $\overline{\Delta\sigma_z}$  (in operating energy piles EP1, 2, 3 and 4) is plotted against the average temperature variation  $\overline{\Delta T}_{EPall}$  for Test 20EPall. The vertical stress is normalised by the thermally induced vertical stress for an energy pile under completely blocked conditions  $\sigma_b^{th} = E_{EP}\varepsilon_b^{th} = E_{EP}\alpha_{EP}\Delta T$ . Under the same temperature variation, a group of four operating energy piles shows a 36% average decrease in the thermally induced vertical stress relative to one operating energy pile.



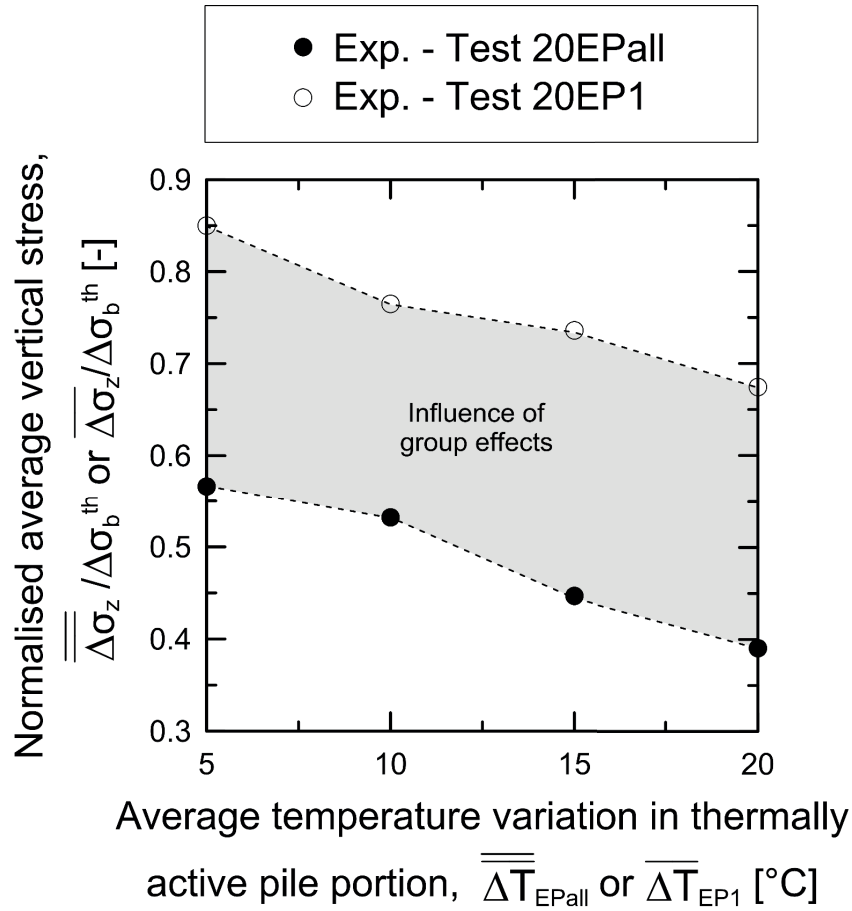


Figure 3.17: Impact of the number of operating energy piles on the group vertical stress variation according to the experimental results.

### 3.6 Discussion

#### 3.6.1 Comparison between the Class B1 and C1 prediction results – Test 20EP1

Figure 3.18 shows the comparison between the variations in vertical strain that were determined through the Class B1 and final Class C1 numerical predictions along the lengths of energy piles EP1 and 2. The experimental results are plotted for reference. The role of the different values of thermal expansion coefficient used for characterising the layers B, C and D in the Class B1 and C1 predictions on the thermally induced mechanical behaviour of the foundation is shown.

At the early stages of the heating phase of energy pile EP1, a small difference between the variations in vertical strain that were determined through the numerical analyses was observed and the results agreed well with the experimental observations. At these stages, a limited volume of soil was subjected to a temperature variation. Thus, despite the different values of thermal expansion coefficient used in the Class B1 and C1 predictions, the thermally induced deformation of the soil was limited and a small impact of the deformation of this material on that of both the operating and non-operating energy piles was observed.

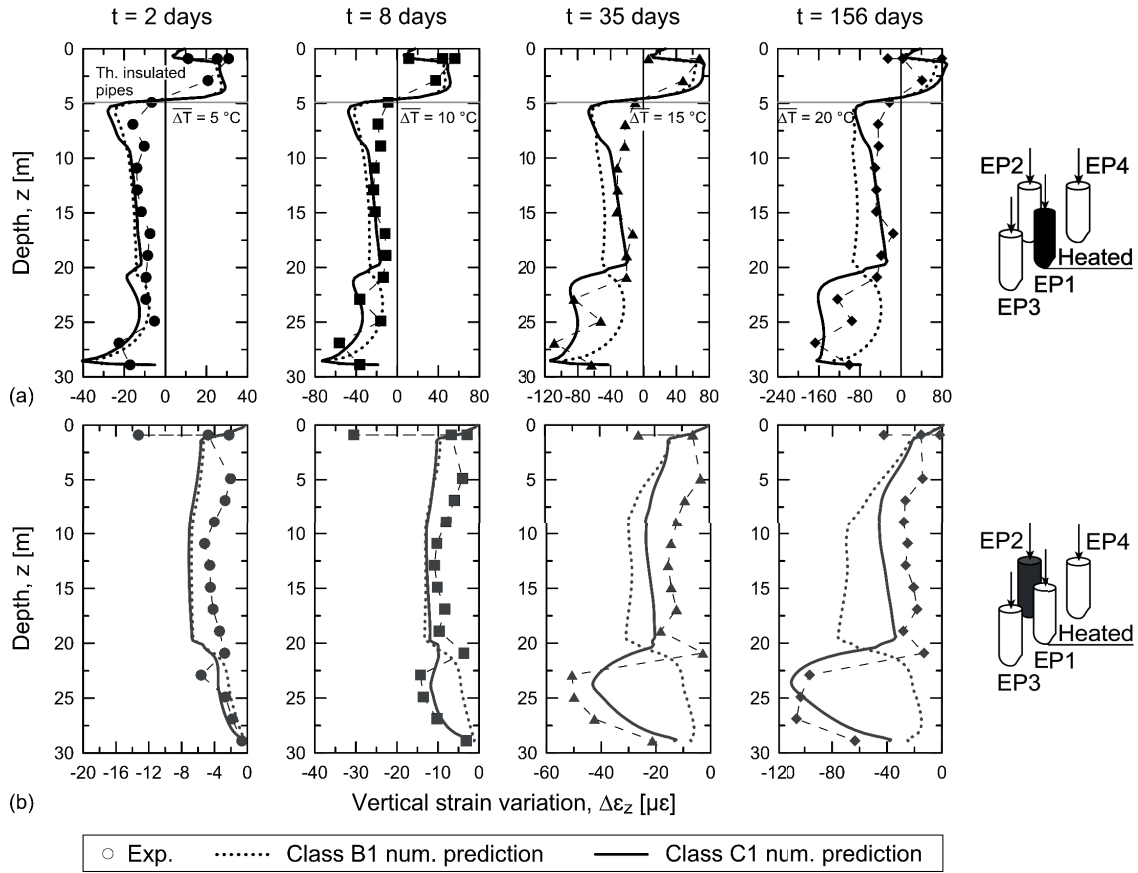


Figure 3.18: Comparison between the variations in vertical strain observed through the Class B1 and C1 numerical predictions and the experimental test along (a) the operating energy pile EP1 and (b) the non-operating energy pile EP2, after  $t = 2, 8, 35$  and  $156$  days of testing.

At the successive stages of the heating phase of energy pile EP1, an increasing difference between the variations in vertical strain that were estimated through the numerical analyses was noted. The results of the Class B1 prediction indicated an opposite evolution in vertical strain along the lengths of the energy piles compared to the experimental observations and, at a later stage, of the Class C1 prediction results. In general, greater variations in vertical strain were observed in the layers characterised by the greater thermal expansion coefficients. Greater strain variations were determined in the shallower portions of the energy piles by the Class B1 prediction compared to the smaller variations determined experimentally and by the Class C1 prediction. Smaller strain variations were determined in the deeper portions of the energy piles by the Class B1 prediction compared to the greater variations determined experimentally and by the Class C1 prediction. Marked differences between the variations in vertical stress along the lengths of all of the energy piles resulted as a consequence of this occurrence. The reason for the observed difference between the Class B1 prediction results and the experimental and Class C1 prediction results is because at the successive stages of the heating phase of energy pile EP1, a noteworthy volume of soil was subjected to a temperature variation. This phenomenon involved a thermally induced deformation of the soil with a marked impact on the variation of the deformation of both the operating and non-operating energy piles. Thus, the use in the Class B1



prediction of unsuitable values of thermal expansion coefficient for characterising layers B, C and D resulted in the differences described above. This fact highlights the essential role of a thorough estimation of the thermal expansion coefficient of the materials involved in energy pile-related problems for obtaining representative results of reality through any type of prediction performed (e.g., Class A predictions).

### 3.6.2 Key aspects governing the behaviour of energy pile groups

The results that were described in the previous sections demonstrate that the behaviour of groups of closely spaced energy piles that operate partially or entirely as geothermal heat exchangers over time-scales that are typical of practical applications is characterised by significant *thermally induced group effects*. These group effects are evidenced through thermal and thermally induced mechanical interactions between the operating and non-operating energy piles, the soil and the slab.

*Thermal interactions* appear during successive stages of geothermal operations. For the same geometrical features of the pile group (e.g., the length of the piles and the centre-to-centre spacing between the piles) and a given thermal load applied to the operating energy piles, the magnitude and development of these interactions are governed by (i) the energy design solutions characterising the operating energy piles (e.g., the pipe configuration, the mass flow rate of the fluid circulating in the pipes and the fluid mixture composition), and (ii) the thermal and hydraulic properties of the foundation. These interactions were not observed by Mimouni and Laloui (2015) because of the short duration of their tests but are considered to be important for the analysis and design (e.g., geotechnical, structural and energy) of these foundations.

*Thermally induced mechanical interactions* are always present throughout the geothermal operations. For the same geometrical features of the pile group (e.g., the length of the piles and the centre-to-centre spacing between the piles) and a given thermal load applied to the operating energy piles, the magnitude and development of these interactions are governed by (i) the relative amount of thermally induced deformation of soil to pile per unit temperature variation, (ii) the relative stiffness of slab to soil and (iii) the relative stiffness of pile to soil. These characteristics of energy pile groups can be classified through three dimensionless ratios, i.e. (Rotta Loria and Laloui, 2017d):

- The *soil-pile thermal expansion coefficient ratio*

$$X = \frac{\alpha_{soil}}{\alpha_{EP}} \quad (3.1)$$

where  $\alpha_{soil}$  is the linear thermal expansion coefficient of the soil. The soil-pile thermal expansion coefficient ratio allows envisaging the roles of the thermally induced deformations of the soil and the piles in the deformation of the energy pile group at *successive stages* of geothermal operations. Values of  $X > 1$  correspond to a deformation of the energy pile group governed by the thermally induced deformation of the soil surrounding the piles, whereas

values of  $X \leq 1$  to a deformation of the energy pile group governed by the thermally induced deformation of the piles. Practical ranges of  $X$  are between 0.1 and 4. According to the findings provided by Bourne-Webb et al. (2016a) for single isolated energy piles, the spatial extent of the field that involves temperature variations in the soil around the energy piles governs the effect of  $X$  on the thermally induced deformation of the energy pile group. The greater the volume of soil subjected to a temperature variation is, the more pronounced the relative deformation between the energy piles and the soil is.

- The *slab-soil stiffness ratio*

$$K_{ss} = \frac{4 E_{slab} B_{slab} t_{slab}^3 (1 - \nu_{soil}^2)}{3 \pi E_{soil} L_{slab}^4 (1 - \nu_{slab}^2)} \quad (3.2)$$

where  $E_{soil}$  and  $\nu_{soil}$  are the Young's modulus and the Poisson's ratio of the soil, respectively. The definition of this ratio is based on the work of Brown (1975) for the analysis of strip footings. It was formulated and exploited by Clancy and Randolph (1996) for the analysis of slabs connecting conventional piles and is extended herein to the analysis of slabs connecting energy piles. The slab-soil stiffness ratio allows estimating the impact of the presence of the slab on the load and displacement redistributions in the energy pile group. Values of  $K_{ss} \approx 0.001$  correspond to a flexible slab whereas values of  $K_{ss} \approx 0.1$  correspond to an almost rigid slab (Brown, 1975). Practical ranges of  $K_{ss}$  are between 0.001 and 10 (Clancy and Randolph, 1996).

- The *pile-soil stiffness ratio*

$$\Lambda = \frac{E_{EP}}{G_{soil}} \quad (3.3)$$

where  $G_{soil}$  is the shear modulus of the soil. The definition of this ratio is based on the work of Randolph and Wroth (1978) for the analysis of conventional piles subjected to solely mechanical loads and is extended herein to the analysis of energy pile groups subjected to both mechanical and thermal loads. It considers the shear modulus of the soil (which is preferred to the Young's modulus) because in pile-related problems the soil deforms primarily in shear and because the shear modulus is usually assumed to be unaffected by whether the loading is drained or undrained. The pile-soil stiffness ratio characterises the load-displacement relationship between each of the single piles in the group and the surrounding soil. Values of  $\Lambda \approx 10$  correspond to a compressible pile whereas values of  $\Lambda \approx 10000$  to an almost rigid pile (Poulos and Davis, 1980). Practical ranges of  $\Lambda$  are between 100 and 10000 (Randolph and Clancy, 1993).

Significant attention must be paid to the thermally induced mechanical interactions because they are important in the analysis and design (i.e., geotechnical and structural) of energy pile groups.

*Thermally induced mechanical interactions* can also be classified depending on two criteria, i.e., (i) the time of heat exchange characterising the energy foundation (Rotta Loria and Laloui, 2016a) and (ii) the objects of interaction (Rotta Loria and Laloui, 2017c). The former classification includes the latter. Both classifications may be applied to characterise thermal interactions with similar arguments.

The classification of thermally induced mechanical interactions based on time includes two types of interactions:

1. *First-kind interactions*: this type of interactions develops during early stages of geothermal operations of energy piles and is primarily caused by the direct heating and associated thermally induced deformation of the operating energy piles.
2. *Second-kind interactions*: this type of interactions develops during successive stages of geothermal operations of energy piles and is caused by (i) the direct heating and related thermally induced deformation of the operating energy piles and (ii) the indirect heating and related thermally induced deformation of the soil surrounding the operating energy piles as well as of the non-operating energy piles. The magnitude and development of these interactions are governed by the interplay between the thermally induced responses of the operating and non-operating energy piles and soil to temperature variations. The presence of the slab represents a key contribution for the development of all of the aforementioned interactions.

The classification of thermally induced mechanical interactions based on the objects of interaction includes three types of interactions:

1. *Pile-soil-pile interaction*: This type of interaction is governed by the relative influence between the deformation of the (i.e., operating) energy piles and the surrounding soil. This influence is primarily characterised by the deformation of the energy piles under the applied temperature variations during early stages of geothermal operations. However, it can be more strongly characterised by the deformation of the soil at successive stages of geothermal operations, especially where the thermal expansion coefficient of the soil may exceed that of the energy piles.
2. *Pile-slab-pile interaction*: This type of interaction is governed by the relative influence between the deformation of the energy piles and the connecting slab. This influence increases as the slab stiffness increases. Moreover, this interaction is less affected by the relative thermal expansion potential of the piles and the slab than the interaction between the piles and the soil. Indeed, in practice, the concrete mix design used for the piles and the slab will be generally the same, and as a result, (at least theoretically) these members will have the same thermal expansion coefficient.

3. *Slab-soil interaction*: This type of interaction is governed by the relative influence between the deformation of the slab and the soil. Similar to the pile-slab-pile interaction, the slab-soil interaction predominantly depends on the relative stiffness of the bodies in contact rather than on their relative thermal expansion coefficients. In practice, although different thermal expansion coefficients may characterise the soil and the slab connecting the energy piles, the shallower depths where the slab is located will not be significantly affected by the geothermal operation of the piles due to the typical thermal insulation of the pipes. Nothing more unusual than the surface conditions may be expected to affect the interplay between the deformation of the slab and the underlying shallow soil. This phenomenon minimally contributes to the overall deformation of the system because, as in most applications, thermal insulation may be assumed between the slab floor and the upper environment. In any case, the influence of surface conditions may be considered negligible when compared to the effect of the geothermal operation of the energy piles on the deformation of the slab and soil.

### 3.6.3 Design considerations for energy pile groups

Significant increases in compressive stress compared to the variation that is induced by the superstructure's mechanical loads were observed in the operating energy pile in Test 20EP1. These vertical stress variations (up to  $\Delta\sigma_z = 5500$  kPa) are greater than those that were numerically estimated to be induced by the applied superstructure mechanical loads in both the operating and non-operating energy piles (cf., Figure 3.19). Based on the characteristic compressive strength of the concrete that was used in this study - a higher-than-typical class of compressive strength of concrete was conservatively used for the energy piles based on the experiments foreseen - (e.g.,  $f_{ck} = 45$  MPa), the observed compressive vertical stress variations are not considered to be an issue for the structural integrity of the pile. Although the temperature variation that was induced in the operating energy pile in this study is significant and the features of the foundation are favourable for the development of large compressive vertical stress variations (e.g., compared to a floating pile foundation), worse conditions cannot be discounted (stiffer bearing soil layers and slab). Thus, the vertical stress variations that are induced by temperature variations in operating energy piles should be considered throughout the structural design of energy pile groups that partially and entirely operate as geothermal heat exchangers (with reference, e.g., to the serviceability limit state).

Notable decreases in compressive stress compared to the variation that is induced by the superstructure's mechanical loads were observed in the non-operating energy piles because of the thermally induced group effects in Test 20EP1. Notable negative stress variations were also observed at successive stages of the geothermal operation of the operating energy piles in their bottom portions in Test 20EPall. The absolute values of these vertical stress variations (up to  $\Delta\sigma_z = -1419$  kPa) are comparable to those that were numerically estimated to be induced by the superstructure's mechanical loads in these elements (cf., Figure 3.19). These results indicate that tensile stresses do not develop, and such stress variations are not considered to be an issue for the structural integrity of the piles in this study. However, cases that utilise greater numbers of operating energy piles than in this study are common and may be a concern especially with reference to non-operating energy piles characterised by low or null values of applied mechanical loads. Thus, the vertical stress variations in non-operating

energy piles as a result of the thermally induced deformation of operating energy piles should be considered throughout the structural design of groups of such foundations (with reference, e.g., to the serviceability limit state).

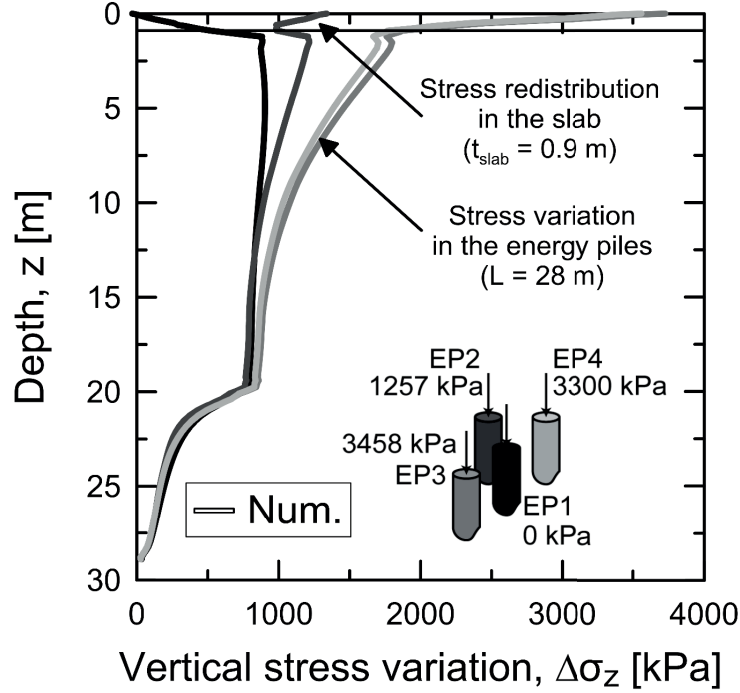


Figure 3.19: Numerical vertical stress variations induced by the superstructure's mechanical loads along energy piles EP1, 2, 3 and 4 (the stress distributions that are associated with the *in situ* conditions have been subtracted).

Significant vertical displacement variations were observed in both the operating and non-operating energy piles in Test 20EP1. As shown in Figure 3.20, these variations in vertical displacement, which were determined from the numerical analysis, are greater than those that were induced by the superstructure's mechanical loads. The superstructure's mechanical loads were initially found to induce pile settlements of up to  $\Delta w = 0.98$  mm. At the end of the heating phase of energy pile EP1, the temperature variations in the foundation were found to induce pile heaves of up to  $\Delta w = -1.10$  mm. The thermally induced displacements were thus up to double those that were induced by the superstructure's mechanical loads. Even more significant vertical displacement variations were observed with the increasing number of operating energy piles under the same temperature variation, by means of the numerical analysis. An evidence of this phenomenon, which was again caused by group effects, is given in Figure 3.21 using the numerical results for Test 20EP1 and Test 20EPall. In this figure, the average vertical displacement  $\overline{\Delta w}$  (at the uppermost level of the slab, which corresponds to operating energy pile EP1) is plotted against the average temperature variation  $\overline{\Delta T}_{EP1}$  for Test 20EP1, and the average vertical displacement  $\overline{\Delta w}$  (at the uppermost level of the slab, which corresponds to operating energy piles EP1, 2, 3 and 4) is plotted against the average temperature variation  $\overline{\Delta T}_{EPall}$  for Test 20EPall. The vertical displacement is normalised by the energy pile diameter. Under the same temperature variation, a group of four operating energy piles shows an average increase of 158% in

the thermally induced vertical displacement relative to one operating energy pile. That is, when the same average temperature variation is applied to energy piles, the thermally induced vertical displacement increases with the number of (e.g., thermally) loaded piles. This phenomenon becomes more pronounced as the number of energy piles operating as geothermal heat exchangers increases. The observed displacement variations are not critical under current European design standards (EN 1997, 2004) for serviceability conditions. They may, however, represent a concern for a greater number of operating energy piles. This consideration appears to be particularly relevant for piles characterised by a prevalent end-bearing character, surrounded by soft soil deposits and connected to remarkably flexible slabs. For this reason, the vertical displacements that are induced by temperature variations in operating and non-operating energy piles should be considered throughout the structural and geotechnical designs of energy pile groups (with reference, e.g., to the serviceability limit state).

Based on the above, two main phenomena are highlighted:

- i. When the number of operating energy piles increases, greater thermally induced vertical strain and lower thermally induced vertical stress develop in the piles under the same average temperature variation along the piles.
- ii. For more prolonged operation of multiple energy piles, when the soil has a greater thermal expansion coefficient than that of the piles, stress variations that are the opposite of the variations expected based on the type of applied thermal load can develop in the piles. This phenomenon can be mathematically expressed as follows. When the soil-pile thermal expansion coefficient ratio  $X = \alpha_{soil}/\alpha_{EP} > 1$ , in successive stages of geothermal operations, unlike in the usual framework (Laloui et al., 2003; Bourne-Webb et al., 2011)

$$\varepsilon_o^{th} > \varepsilon_f^{th} = -\alpha_{EP}\Delta T \quad (3.4)$$

The reason for this response is that the thermally induced deformation of the energy pile is governed by the soil deformation. Therefore, for energy piles subjected to heating thermal loads, the thermally induced stress can be negative (i.e., tensile stress):

$$\sigma_o^{th} = E_{EP}\varepsilon_b^{th} = E_{EP}(\varepsilon_o^{th} - \varepsilon_f^{th}) = E_{EP}(\varepsilon_o^{th} + \alpha_{EP}\Delta T) < 0 \quad (3.5)$$

The opposite is true for cooling thermal loads applied to energy piles.

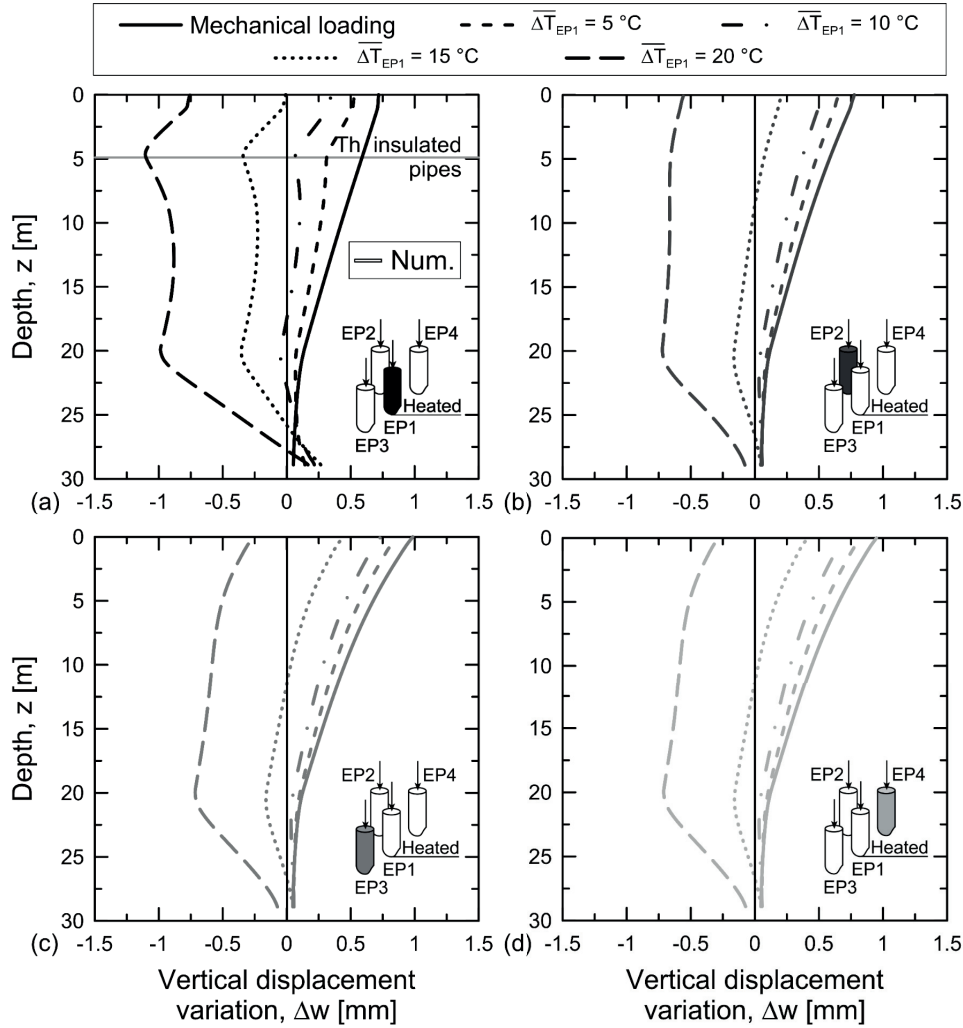


Figure 3.20: Numerical vertical displacement variations induced by the superstructure's mechanical loads and temperature variations along energy piles EP1, 2, 3 and 4 (the displacement distributions that are associated with the in situ conditions have been subtracted).

These phenomena have three main consequences for the geotechnical and structural design of energy piles:

- Because a greater thermally induced vertical strain arises for the same average temperature variation along the piles as the number of operating energy piles increases, deformation analyses of single energy piles are not exhaustive and cannot represent the actual behaviour for energy piles operating in a group. Therefore, these analyses are potentially misleading in design. As a result, no energy pile analysis or design can be considered complete without accounting for the (mechanically and thermally) induced group effects among energy piles.
- Because the thermally induced vertical stress decreases under the same average temperature variation along the piles as the number of operating energy piles increases, analyses of a single



energy pile are not exhaustive and cannot represent the actual behaviour for energy piles operating in a group. However, these analyses are considered useful in the preliminary design stages. Provided that similar head restraint conditions are accounted for a given energy pile in a soil deposit, considering the vertical stress of an isolated energy pile will always be conservative with regards to the thermally induced vertical stress of operating energy piles in a group.

- c. Because during the more prolonged operation of various energy piles stress variations opposite those that may be expected based on the type of applied thermal load can develop in energy piles where the soil has a thermal expansion coefficient higher than that of the piles, attention must be paid to the geotechnical characterisation of sites. The use of unsuitable values of thermal expansion coefficients to characterise the energy piles and surrounding soil may generate analytical results for design and research applications with marked pitfalls.

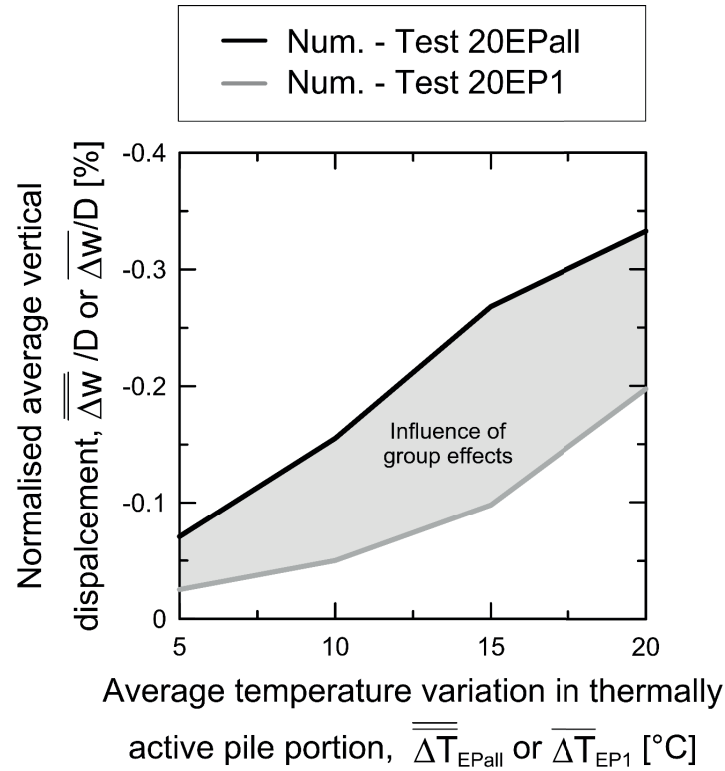


Figure 3.21: Impact of the number of operating energy piles on the average vertical pile group displacement. The average vertical displacement  $\Delta w$  (at the uppermost level of the slab, which corresponds to operating energy pile EP1) is plotted against the average temperature variation  $\Delta T_{EP1}$  for Test 20EP1, and the average vertical displacement  $\Delta w$  (at the uppermost level of the slab, which corresponds to operating energy piles EP1, 2, 3 and 4) is plotted against the average temperature variation  $\Delta T_{EPall}$  for Test 20EPall. The vertical displacement is normalised by the energy pile diameter,  $D$ .



#### 3.6.4 Suitability and limitations of using thermo-elasticity for simulating energy pile groups

Analyses that are based on linear elasticity theory have been shown to successfully reproduce the mechanical behaviour of an extensive number of conventional pile-groups subjected to mechanical loads of limited magnitude (e.g., Poulos and Davis, 1980; Fleming et al., 2008). Similarly, analyses that are based on linear thermo-elasticity theory appear to be suitable for reproducing the thermo-mechanical behaviour of energy pile groups subjected to mechanical and thermal loads of limited magnitude. With the term “limited”, reference is made to magnitudes of mechanical and thermal loads which combined action involves effects that are far from inducing the geotechnical and/or structural failure (ultimate limit state) of the pile(s), and are characteristic of the serviceability limit state. In other words, reference is made to loads which induced effects are reversible (i.e., elastic). Under these conditions, this statement appears to be valid for both monotonic and cyclic thermal loads that are applied to the energy piles.

The capability of linear thermo-elasticity theory to describe the behaviour of energy piles such as the end-bearing group that was analysed in this study is corroborated by the reversible response that was found experimentally to characterise the operating energy pile EP1 throughout, e.g., Test 20EP1. This is shown in Figure 3.22 (a), which depicts the experimental and numerical distribution of vertical strain along the operating energy pile EP1 for an average temperature variation of  $\Delta T = 5\text{ }^{\circ}\text{C}$  that was observed along the uninsulated portion of this pile during the heating and passive cooling phases of the test. Figure 3.22 (b) presents the evolution of this temperature variation along the length of EP1. The differences between the strain curves (especially in the molasse layer) are attributed to the different thermal field that was observed experimentally and numerically to characterise the soil, the non-operating energy piles EP2, 3 and 4, and the operating energy pile EP1 when this latter pile was subjected to the same average temperature variation during the heating and passive cooling phases of the test. Residual temperature variations were observed during the late stages of the passive cooling of EP1 in a number of regions of the pile group. These temperature variations involved thermally induced expansions of the materials that caused a residual deformation of the energy pile group (and thus, of EP1) with reference to the initial condition. The differences between the experimental and numerical curves referred to the same phase of the test (especially in the molasse layer) are caused by differences in the temperature fields characterising the energy pile group in the real case and in the numerical model.

The suitability of linear thermo-elasticity for the analysis of end-bearing energy piles such as the group that was analysed in this study is extended to other testing conditions and sites based on the experimental observations of Murphy et al. (2015), Mimouni and Laloui (2015), and Wang et al. (2014) as well as the numerical results of Di Donna et al. (2016). Linear thermo-elasticity appears to be suitable also for the analysis of groups of friction energy piles.

When dealing with situations in which significant magnitudes of mechanical and thermal loads are applied to energy pile groups, careful judgement on the suitability of a linear thermo-elastic approach of analysis has to be considered. The inappropriate use of thermo-elasticity theory may involve marked pitfalls in the analysis and/or design of energy pile groups because of differences between the actual and modelled mechanical behaviours of the piles and surrounding soil. This comment appears to be particularly relevant for groups of friction energy piles. The reason is because for the same applied load, friction energy piles mobilise a greater proportion of shear stress at the pile-soil interface

compared to end-bearing energy piles. This distribution of shear stress may be associated to plastic strain at the pile-soil interface. Notable variations in the behaviour of friction energy piles may consequently arise because of the marked sensitivity of these foundations to the response of the pile-soil interface (Rotta Loria et al., 2015b). These variations may increase for cyclic thermal loads applied to the piles with time (Yavari et al., 2014; Ng et al., 2014; Di Donna and Laloui, 2014; Suryatriyastuti et al., 2015; Saggi and Chakraborty, 2015; Vieira and Maranh, 2016; Ng et al., 2016a), such a consideration suggesting the unsuitability of an elastic approach of analysis in those situations. Thermo-elastic analyses can be considered unsuitable also for situations that involve phenomena inducing plastic strain in the soil surrounding the piles irrespective of the magnitude of the applied loads. Situations that involve energy piles socketed in normally consolidated clayey soils are a key example because the responses of these soils to heating have been shown to be inelastic (Campanella and Mitchell, 1968; Plum and Esrig, 1969; Demars and Charles, 1981; Baldi et al., 1988; Hueckel and Baldi, 1990; Burghignoli et al., 2000; Cekerevac and Laloui, 2004; Vega and McCartney, 2014; Di Donna and Laloui, 2015).

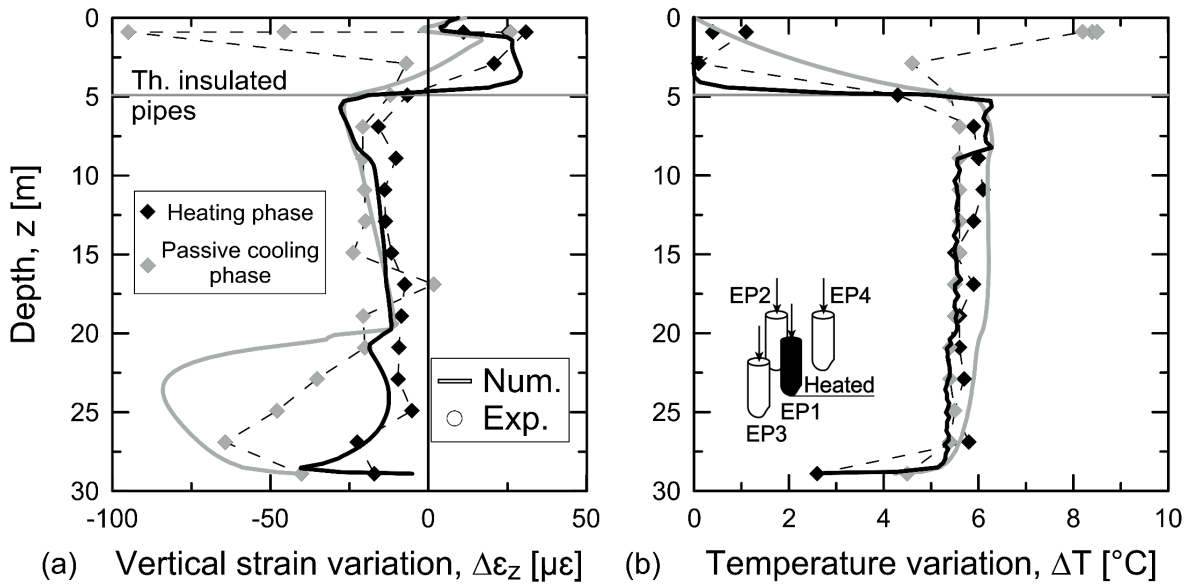


Figure 3.22: Experimentally and numerically observed (a) vertical strain variations along the operating energy pile EP1 for (b) approximately the same average temperature variation that was recorded with depth during the heating and passive cooling phases of the test.

### 3.6.5 Suitability and limitations of using thermo-mechanical analyses for simulating energy pile groups

The use of thermo-mechanical analyses to reproduce the thermo-mechanical behaviour of energy pile groups that are subjected to mechanical and thermal loads in saturated soil deposits without intrinsic groundwater flow appears to be suitable in most applications.

This consideration is corroborated with reference to the analysed tests by the negligible variation of the hydraulic field experimentally determined through the readings of the piezometers and of the thermistors in the soil. This phenomenon can be noted referring to Figure 3.23 and Figure 3.24, which

show the maximum pore water pressures that were observed throughout Test 20EP1 along soil profiles P+T1 and P+T2, and the trends of pore water pressure variations at selected points along soil profiles P+T1 and P+T2, respectively. Negligible pore water pressure variations were also observed to characterise the considered site by Mimouni and Laloui (2015) and Di Donna et al. (2016) based on experimental and numerical results, respectively. Di Donna et al. (2016) further noted a negligible variation of the hydraulic field in soil layers of low intrinsic permeability and coefficient of compressibility of the solid particles forming the skeleton that were subjected to even higher magnitudes and rates of temperature variations than those in this study. Yet, Di Donna et al. (2016) observed that the magnitude of the pore water pressure variations characterising P+T1 and P+T2 was comparable to that numerically estimated in the region of soil adjacent to the operating energy pile(s) (i.e., the pile-soil interface(s)). Based on this consideration and the results presented in Figure 3.23 and Figure 3.24, it appears justified to suppose negligible pore water pressure variations at the pile-soil interface(s) in the considered experiment; i.e., drained conditions are preserved upon heating.

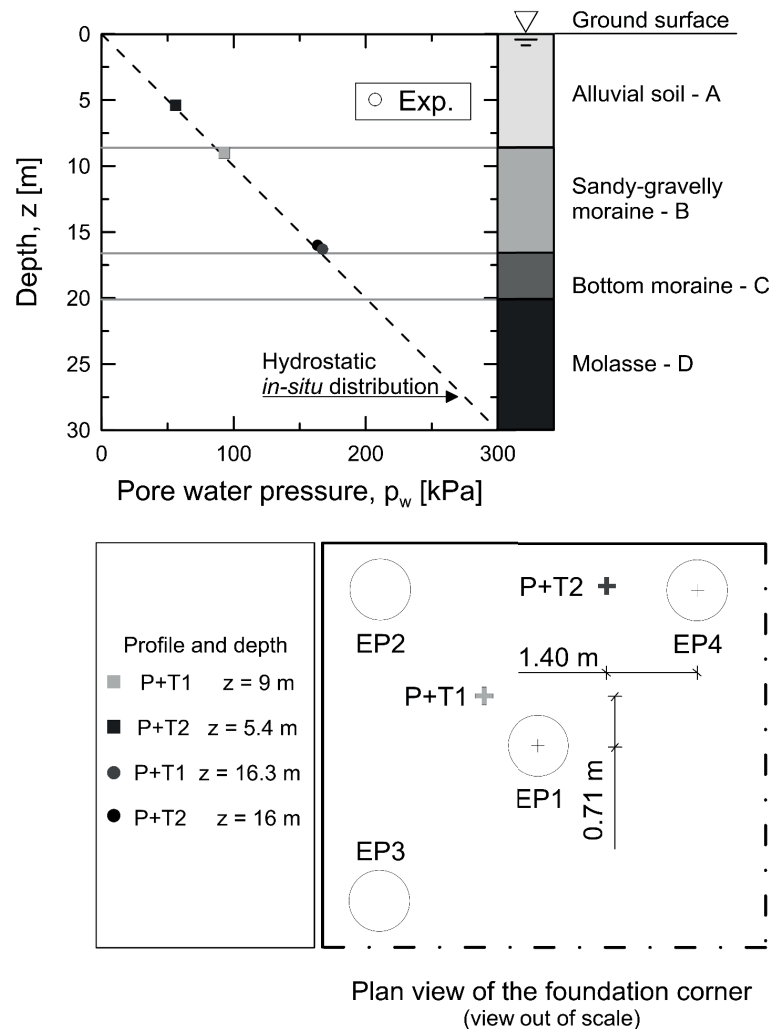


Figure 3.23: Maximum experimental pore water pressure variations along profiles P+T1 and P+T2 in the soil.

The use of thermo-hydro-mechanical analyses can be considered essential for situations that involve energy pile groups that are subjected to mechanical and thermal loads in saturated soil deposits with intrinsic groundwater flow or characterised by remarkably low intrinsic permeability and coefficient of compressibility (e.g., values of intrinsic permeability lower than  $1 \cdot 10^{-17} \text{ m}^2$  and coefficient of compressibility of the solid particles forming the skeleton lower than  $2.5 \cdot 10^{-10} \text{ 1/Pa}$  based on the results of numerical analyses). In the former case, differences between the actual and modelled thermal behaviour of the operating energy piles may arise irrespective of the magnitude of the applied loads because of the preponderant convective character of the heat exchange process. In the latter case, differences between the actual and modelled mechanical behaviour of both the operating and non-operating energy piles may arise as a consequence of the application of high magnitudes of mechanical and thermal loads because of the induced variation in the hydraulic field (effective stress concept).

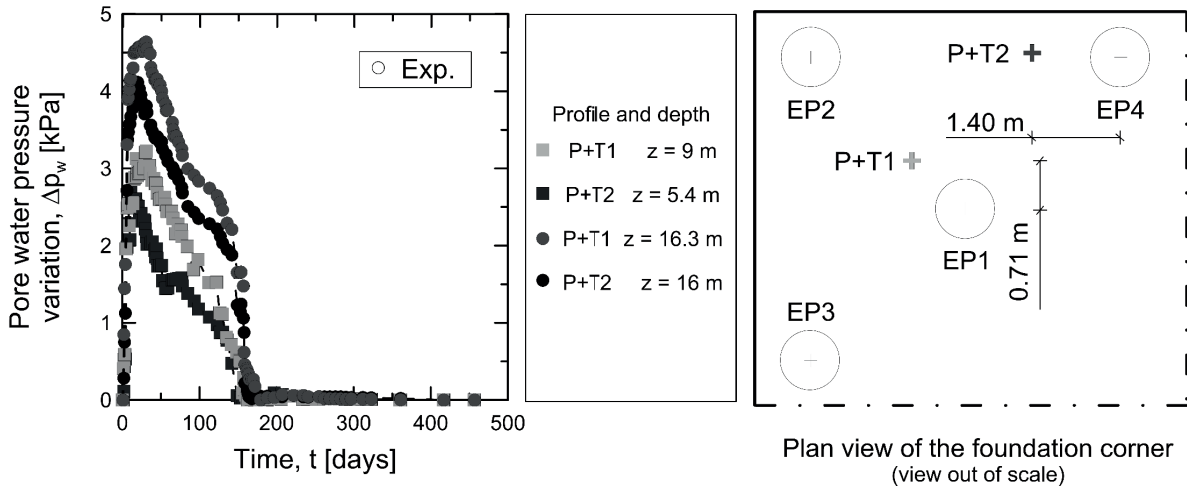


Figure 3.24: Experimentally observed pore water pressure variations at selected points along profiles P+T1 and P+T2 with time.

### 3.7 Concluding remarks

This study experimentally and numerically investigated the *thermally induced group effects* of closely spaced energy piles that operate as geothermal heat exchangers over a time-scale that is typical of practical applications. Some of the main conclusions that can be drawn from this work are (Rotta Loria and Laloui, 2017d; Rotta Loria and Laloui, 2017c):

- Thermal interactions between operating and non-operating energy piles occur during successive stages of geothermal operations. For the same geometrical features of the pile group (e.g., the length of the piles and the centre-to-centre spacing between the piles) and a given thermal load applied to the operating energy piles, these interactions are governed by (i) the energy design solutions characterising the operating energy piles (e.g., the pipe configuration, the

mass flow rate of the fluid circulating in the pipes and the fluid mixture composition) and (ii) the thermal and hydraulic properties of the foundation.

- Thermally induced mechanical interactions are always present throughout geothermal operations. For the same geometrical features of the pile group (e.g., the length of the piles and the centre-to-centre spacing between the piles) and a given thermal load applied to the operating energy piles, these interactions are governed by (i) the relative amount of thermally induced deformation of soil to pile per unit temperature variation (i.e., the soil-pile thermal expansion coefficient ratio), (ii) the relative stiffness of slab to soil (i.e., the slab-soil stiffness ratio), and (iii) the relative stiffness of pile to soil (i.e., the pile-soil stiffness ratio). The thermal field characterising the foundation governs the magnitude and impact of aspect (i) on the development of thermally induced mechanical interactions.
- Thermal and thermally induced mechanical interactions are considered to be important for the analysis and design (e.g., geotechnical, structural and energy) of energy pile groups.
- Significant stress, strain and displacement variations are induced in both the operating and non-operating energy piles by all of these interactions. These vertical stress, strain and displacement variations are not critical for the serviceability performance of the piles tested in this study. However, attention must be devoted to these phenomena throughout the design process (e.g., geotechnical and structural) of energy pile groups at the serviceability limit state. Their magnitudes can be comparable and even higher than those of the superstructure mechanical loads.
- Greater thermally induced vertical strain arises for the same average temperature variation along the piles as the number of operating energy piles increases. Therefore, analyses of the deformation of single energy piles are not exhaustive and cannot represent the actual behaviour of energy piles operating in a group. Thus, these analyses cannot be used for the complete design of energy piles.
- Lower thermally induced vertical stress arises for the same average temperature variation along the piles as the number of operating energy piles increases. Therefore, analyses of single energy piles are considered useful, especially in preliminary design stages. Indeed, provided that similar head restraint conditions are considered for a given energy pile in a soil deposit, these analyses will always give a conservative estimate of the thermally induced vertical stress along operating energy piles in a group.
- Stress variations opposite those that may be expected based on the type of applied thermal load can develop in piles where the soil has a greater thermal expansion coefficient than the piles during more prolonged operation of various energy piles. Hence, attention must be paid to the geotechnical characterisation of sites. Using unsuitable thermal expansion coefficients to characterise energy foundations may lead to marked pitfalls in analysis and design.
- Linear thermo-elasticity theory appears to be an expedient and sufficiently accurate tool to describe the geotechnical and structural behaviour of a wide number of energy pile groups for both research and engineering purposes.

- Thermo-mechanical numerical analyses appear to be suitable tools for modelling the geotechnical, structural and energy behaviour of most energy pile groups surrounded by saturated soil deposits without intrinsic groundwater flow. Consideration of the pipes-pile-soil system appears to be important to modelling the energy behaviour of energy pile groups because it allows the thermo-mechanical response of the energy piles with a phase shift to be reproduced for a variety of boundary conditions.

## **Chapter 4**

# **The interaction factor method for energy pile groups based on design charts**

Prior to this study, no simplified yet rational methods were available for estimating the vertical displacements of energy pile groups subjected to thermal loads. Observing such a challenge, the goal of this study has been threefold: (i) to extend the interaction factor concept from the framework of conventional pile groups to that of energy pile groups considering both predominantly floating and end-bearing piles, (ii) to present charts for the analysis of the displacement interaction between two identical energy piles over a broad range of design conditions, and (iii) to propose, apply and validate the interaction factor method for the displacement analysis of energy pile groups.

### **4.1 Introduction**

Over the last century, a substantial amount of research has been devoted to the analysis and design of conventional pile foundations because of their extensive application in the support of many structures and infrastructures. Classically, pile foundations have been applied to exploit adequate bearing capacities from soils of favourable strength and deformability characteristics, as well as to limit the use of surface area in densely built zones. In recent years, pile foundations have been increasingly used in an innovative form of energy piles to couple the aforementioned advantages associated with the structural support role of conventional deep foundations with the advantages associated with the role of the geothermal heat exchanger for satisfying the energy needs of building environments (Laloui and Di Donna, 2013). When addressing energy piles, a new challenge arises for civil engineers: the consideration of the mechanisms and phenomena induced by the application of thermal loads, in conjunction with those associated with the conventionally applied superstructure mechanical loads, on the mechanical behaviour of such foundations.



In the framework of the analysis and design of pile groups in which the piles are located sufficiently close to each other that their individual responses differ from that of an isolated pile because of the so-called “group effects” (i.e., closely spaced pile groups), two main aspects need to be considered (with reference to, e.g., the serviceability performance): (i) the vertical displacement – differential and average – of the piles in the group and (ii) the load redistribution among the piles in the group. The former aspect represents the subject matter of this work.

To address the vertical displacement estimation of conventional pile groups subjected to mechanical loads, various numerical and analytical methods have been proposed. These methods include the finite element method (e.g., Ottaviani, 1975; Pressley and Poulos, 1986), the boundary element method (e.g., Butterfield and Banerjee, 1971; Banerjee and Davies, 1978), the finite difference method (e.g., Poulos, 1994), the interaction factor method (e.g., Poulos, 1968; Randolph and Wroth, 1979b; Mylonakis and Gazetas, 1998; O'Neill et al., 1977; Chow, 1986), the equivalent pier and raft methods (e.g., Poulos and Davis, 1980; Poulos, 1993; Randolph, 1994), and the settlement ratio method (e.g., Poulos, 1989). The finite element method, while providing the most rigorous and exhaustive representation of the pile group-related problem, is generally computationally expensive and considered mainly a research tool rather than a design tool. Conversely, the versatility of simplified (approximate) methods, such as the interaction factor approach that allows capturing the (e.g., vertical) displacements of any general pile group by the analysis of the displacement interaction between two identical piles and by the use of the elastic principle of superposition of effects, makes them attractive as design tools because they allow for the use of expedient parametric studies under various design conditions.

In contrast to the various approaches that have been used to estimate the vertical displacements of conventional pile groups subjected to mechanical loads, to date, only the finite element method (e.g., Di Donna et al., 2016; Rotta Loria and Laloui, 2017d) has been applied for the same purpose for energy pile groups subjected to thermal loads and no detailed studies have been available on the analysis of the displacement behaviour of such foundations. This is because no simplified yet rational methods were available prior to this study for the vertical displacement estimation of energy pile groups subjected to thermal loads.

To address these challenges, the goal of this research has been threefold (Rotta Loria and Laloui, 2016b; Rotta Loria and Laloui, 2017a): (i) to extend the interaction factor concept from the framework of conventional pile groups to that of energy pile groups, (ii) to present charts for the analysis of the displacement interaction between two identical energy piles under a broad range of design conditions, and (iii) to propose and apply the interaction factor method for the analysis of the vertical displacement of energy pile groups subjected to thermal loads.

In addressing aspect (i), the key contributions concerning the displacement interaction between two identical predominantly floating and end-bearing energy piles (i.e., the simplest system representing a pile group) subjected to a temperature variation are described. In contrast to the description of the displacement interaction originally proposed by Poulos (1968) and Poulos and Mattes (1974) for conventional piles subjected to mechanical loads, which was based on boundary element analyses, the description of the displacement interaction for energy piles subjected to thermal loads presented in this study is based on thermo-mechanical finite element analyses.

In addressing aspect (ii), the effects of many variables, including the pile spacing, the pile slenderness ratio, the pile-soil stiffness ratio, the Poisson's ratio of the soil, the depth of a finite layer, the non-



uniform soil modulus, the soil-pile thermal expansion coefficient ratio and the base-to-shaft soil Young's modulus ratio, are investigated. According to the approach described by Poulos (1977), although it is not possible to present theoretical solutions that cover all possible cases, those presented in this study are considered to be sufficient to enable an approximation of the vertical displacement of energy pile groups to be made for most cases likely to be encountered in practice.

In addressing aspect (iii), the interaction factor concept defined for a group of two energy piles is first applied to the displacement analysis of symmetrical energy pile groups by exploiting the elastic principle of superposition of effects. This concept is next validated based on a comparison with results of three-dimensional (3-D) thermo-mechanical finite element analyses. Then, a simplified (approximate) method for the displacement analysis of general energy pile groups with any configuration of piles in the group is formulated, although the solutions proposed in this work refer to square groups of energy piles containing up to twenty-five piles. Finally, the interaction factor method is validated based on the comparison with results of 3-D thermo-mechanical finite element analyses on general energy pile groups subjected to thermal loads surrounded by soils with different thermal expansion coefficients.

## **4.2 The interaction factor concept**

### **4.2.1 The problem: a group of two energy piles**

The simplest system representing an energy pile group can be considered as consisting of two energy piles in a deep soil deposit. The energy piles may be considered predominantly floating and embedded in a uniform soil layer. They may also be considered predominantly end-bearing, to be surrounded by a shallow uniform soil layer and to rest on a deep uniform soil stratum.

In the considered problem, the energy piles are (i) subjected to a thermal load, (ii) free of superstructure mechanical loads, and (iii) free to move vertically at their head.

The thermal load (i.e., aspect (i)) applied to the energy piles is a result of the geothermal operation of these elements. Cooling and/or thermal energy storage operations of energy piles can be associated to positive temperature variations applied to these elements. Heating operations of energy piles can be associated to negative temperature variations applied to these elements. Reference to a situation in which no superstructure mechanical load is applied to the energy piles (i.e., aspect (ii)) allows focusing on the impact of the thermal load on the response of these elements. The consideration of piles free to move at their head (i.e., aspect (iii)) has been generally accounted for in the analysis of conventional pile groups subjected to mechanical loads for estimates of the vertical displacement on the safety side. This approach appears to also be valuable for displacement analysis of energy pile groups and is considered in the following.

### **4.2.2 Idealisation**

The previously described system is idealised considering the following assumptions. The energy piles are two identical isotropic, homogeneous and uniform cylindrical solids. The soil is assumed to be a

semi-infinite, isotropic, homogeneous and uniform mass where predominantly floating energy piles are considered. The soil is a semi-infinite mass characterised by a layer surrounding the shaft of the energy piles and a layer located below the toe of the energy piles where predominantly end-bearing energy piles are considered. The same uniform temperature variation is applied along the length of each of the energy piles. No mechanical load is applied to the energy piles. No head restraint is present (i.e., perfectly flexible slab). The energy piles are characterised by a linear thermo-elastic behaviour, whereas the soil is characterised by a linear elastic behaviour (i.e., the soil is an infinite heat reservoir that remains at a fixed constant temperature). No slip or yielding occurs between each of the energy piles and the adjacent soil (perfect contact between the pile and soil is assumed), and thus, reference is made to loading situations in which elastic (i.e., reversible) conditions prevail. Although not valid in situations where mechanical and thermal loads of significant magnitudes are applied to energy piles (especially if predominantly floating) (Rotta Loria et al., 2015b), these conditions have been demonstrated to characterise normal working situations based on the results of full-scale experimental tests (Murphy et al., 2015; Mimouni and Laloui, 2015; Wang et al., 2014) and numerical analyses (Di Donna et al., 2016; Rotta Loria and Laloui, 2017d).

The application of the temperature variation to the energy piles involves a thermally induced deformation of these elements. An expansion of the energy piles is observed for cooling and/or thermal energy storage operations of these elements (positive temperature variations applied to the energy piles) whereas a contraction of the energy piles is observed for heating operations of these elements (negative temperature variations applied). In the former case, the upper portion of each energy pile displaces upwards, whereas the lower portion displaces downwards around a setting characterised by zero thermally induced displacements (defined as the null point referring to one-dimensional conditions (Laloui et al., 2003)). In the latter case, the upper portion of each energy pile displaces downwards, whereas the lower portion displaces upwards<sup>1</sup>. The considered elastic assumption involves that the null point does not move depending on whether positive or negative temperature variations are applied to the energy piles. Hence, the displacement variation along the length of these elements for a unitary temperature variation associated to their heating or cooling is the same in absolute value. The displacement field generated in each of the energy piles is transmitted in the adjacent soil. Interaction of the displacement fields generated by the thermally induced deformation of the energy piles thus occurs.

Assuming that the resulting deformation field of a group of two energy piles subjected to a temperature difference can be representatively decomposed through the elastic principle of superposition of effects, two (e.g., symmetrical) individual systems can be considered to describe the analysed problem. Figure 4.1 provides an example of this decomposition for a situation in which a positive temperature variation is applied to predominantly floating and end-bearing energy piles. This decomposition approach has been proved to be suitable for describing the displacement interaction between conventional piles subjected to mechanical loads (Poulos and Davis, 1980; Fleming et al., 2008).

---

<sup>1</sup> The phenomena characterising energy pile-related problems involve a remarkably different behaviour of the piles compared to that characterising most conventional pile-related problems in which a superstructure mechanical load (e.g., downward) is applied at the head of the piles inducing their overall settlement.

The elementary unit (cf., Figure 4.2) composing the problem described above involves a source pile  $i$  subjected to a temperature variation  $\Delta T$  (i.e., thermally loaded) and a receiver pile  $j$  located at a certain spacing (i.e., centre-to-centre distance between the piles)  $s$  in the soil layer. As previously specified, the energy piles have the same length  $L$  and shaft diameter  $D$ .

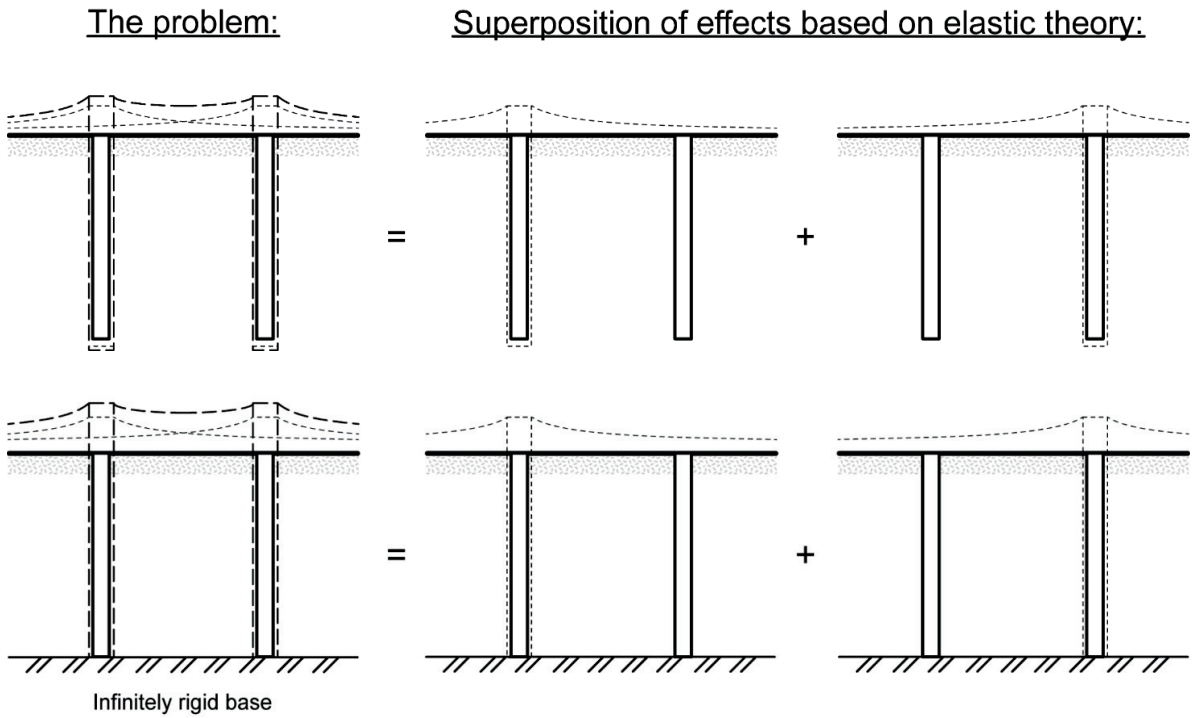


Figure 4.1: The modelling approach.

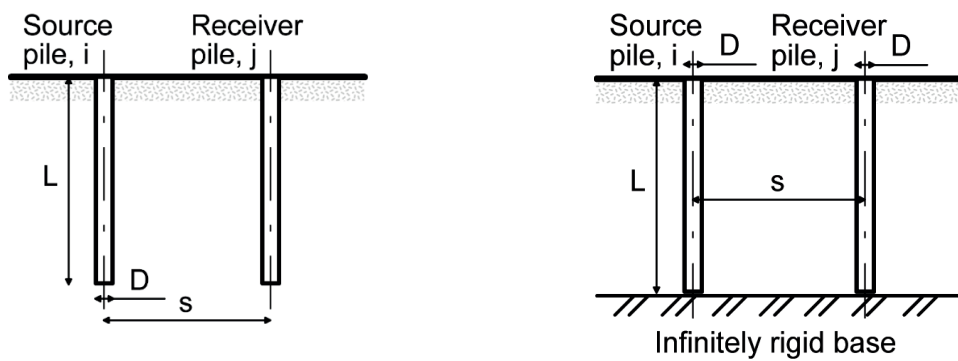


Figure 4.2: The elementary unit.

### 4.2.3 Finite element analysis

#### 4.2.3.1 Numerical models

Finite element modelling with the software COMSOL Multiphysics (COMSOL, 2014) is used in this study as an analysis and validation tool. 3-D and axisymmetric finite element simulations are used as the analysis tool (i) to propose a description of the displacement field characterising the elementary unit described above and a single isolated energy pile, respectively; (ii) to present the interaction factor concept for energy pile groups; and (iii) to introduce design charts for the analysis of the displacement interaction between two identical energy piles. 3-D finite element simulations are used as a validation tool to compare the results obtained in the displacement analysis of symmetrical and general energy pile groups through the simplified method presented in this study with a more rigorous approach.

In the analyses, unless otherwise specified, the idealised soil mass is approximated to a model of depth of  $h_l = 25L$ . This mass is considered to be composed of a unique uniform soil layer where predominantly floating energy piles are considered, whereas it is assumed to be composed of two different soil layers with a depth of  $h_{l1} = L$  from the ground surface to the pile toe and of depth of  $h_{l2} = 24L$  below the pile toe where predominantly end-bearing energy piles are considered. This model has a width of  $x = 500D$  in the axisymmetric simulations, whereas a width of  $x = 1000D + (\tilde{n}_{EP} - 1)s$  and a breadth of  $y = 1000D + (\tilde{n}_{EP} - 1)s$  are used in the 3-D simulations, where  $\tilde{n}_{EP}$  is the number of energy piles along a row or a column of the group in plan view in the considered direction. Extremely fine tetrahedral meshes are used to describe the energy pile and soil domains.

#### 4.2.3.2 Mathematical formulation

Two types of thermo-mechanical finite element analyses are performed: stationary and time-dependent analyses (cf., equations (B1-3) in Appendix B). The stationary analyses refer to idealised problems, such as those presented in Section 4.2.2, in which the energy pile and soil domains exhibit linear thermo-elastic and elastic behaviours, respectively (i.e., the soil is an infinite heat reservoir that remains at a fixed constant temperature). The time-dependent analyses refer to problems closer to reality in which both the energy pile and soil domains follow linear thermo-elastic behaviours (i.e., the soil is a mass that can be subjected to temperature variations and thermally induced volumetric variations).

#### 4.2.3.3 Boundary and initial conditions

Restrictions are applied to both the vertical and horizontal displacements on the bases of the models (i.e., pinned boundary) and to the horizontal displacements on the sides (i.e., roller boundaries).

No residual stresses from the installation of the piles are considered in these elements and in the adjacent region of soil. This hypothesis may not be completely representative of reality but can be applied successfully in methods of pile group deformation analysis by choosing appropriate values of the soil moduli (Poulos and Davis, 1980).

In the steady-state analyses, the initial temperature of all the nodes of the energy pile(s) is set to  $T = 15\text{ }^{\circ}\text{C}$ . Throughout these simulations, a temperature variation of  $\Delta T = 10\text{ }^{\circ}\text{C}$  is applied to these nodes. The soil domain is treated as an infinite heat reservoir.

In the time-dependent analyses, the initial temperature of all the nodes of the energy pile(s) and soil domains is set to  $T = 15\text{ }^{\circ}\text{C}$ . Throughout these simulations, a temperature variation of  $\Delta T = 10\text{ }^{\circ}\text{C}$  is applied to all the nodes of the energy pile(s) for a time of  $t = 6$  months. The temperature of the external vertical and horizontal (bottom) boundaries of the model is fixed to  $T = 15\text{ }^{\circ}\text{C}$ . The horizontal (top) boundary described by the soil surface is treated as adiabatic.

The impact of the elastic assumption on the location of the null point highlighted in Section 4.2.2 involves that, in all of the modelled pile(s)-soil systems, a temperature variation of  $\Delta T = -10\text{ }^{\circ}\text{C}$  induces a symmetrical (equal in absolute value) response of the pile(s) and soil to that observed for a temperature variation of  $\Delta T = 10\text{ }^{\circ}\text{C}$ .

#### 4.2.3.4 Material properties and parameters

The material properties considered in the analyses are reported in Table 4.1. The properties of the energy pile(s) are typical of reinforced concrete. The soil properties have been successfully employed by Rotta Loria et al. (2015a) to model the behaviour of energy piles in dry Nevada sand with reference to physical observations (Goode and McCartney, 2015). Table 4.2 reports parameters that are considered of interest for the analysis of energy pile groups. Table 4.3 lists groups of dimensionless parameters that are considered useful for the same purpose, their typical ranges of variation and the values that are used for the purposes of this study. Table 4.4 presents the values of linear thermal expansion coefficient of the soil used to address the response of energy pile groups resting on stiff soil strata using 3-D thermo-mechanical finite element analyses. In this study, reference to a pile diameter  $D = 1\text{ m}$  is made.

Table 4.1: Material properties used for the numerical analysis.

Reinforced concrete pile parameters	Value (thermo-elastic description)	Soil parameters	Value (elastic description)	Value (thermo-elastic description)
$E_{EP}$ : [MPa]	30000	$G_{soil}$ : [MPa]		30 (*)
$\nu_{EP}$ : [-]	0.25	$\nu_{soil}$ : [-]		0.30 (*)
$\rho_{EP}$ : [kg/m <sup>3</sup> ]	2450	$\rho_{soil}$ : [kg/m <sup>3</sup> ]		1537
$\alpha_{EP}$ : [1/ $^{\circ}\text{C}$ ]	$1 \cdot 10^{-5}$	$\alpha_{soil}$ : [1/ $^{\circ}\text{C}$ ]	-	$1 \cdot 10^{-5}$ (*)
$\lambda_{EP}$ : [W/(m $^{\circ}\text{C}$ )]	1.47	$\lambda_{soil}$ : [W/(m $^{\circ}\text{C}$ )]	-	0.25
$c_{p,EP}$ : [J/(kg $^{\circ}\text{C}$ )]	854	$c_{p,soil}$ : [J/(kg $^{\circ}\text{C}$ )]	-	961

(\*) Parameter varied throughout the simulations (cf., Table 4.3)

Table 4.2: Parameters of interest for the analysis of energy pile groups.

Pile	Notation	Soil	Notation
Length	$L$	Depth of layer	$h$
Diameter	$D$	Shear modulus	$G_{soil}^{(**)}$
Spacing	$s$	Poisson's ratio	$\nu_{soil}^{(**)}$
Young's modulus	$E_{EP}$	Linear thermal expansion coefficient	$\alpha_{soil}^{(**)}$
Linear thermal expansion coefficient	$\alpha_{EP}$		

(\*\*)When labelled with the subscripts  $s$  or  $b$ , the soil parameters refer to the soil portion located in correspondence of the shaft or base of energy piles.

Table 4.3: Dimensionless groups of parameters of interest for analysis of energy pile groups, typical values and values used in this study.

Dimensionless group	Notation	Practical range	Considered values
Pile spacing ratio	$s/D$	3 – 10	1.05, 1.25, 1.5, 2, 2.5, 3, 5, 10, 20
Pile breadth ratio	$D/s$	0.33 – 0.1	0.95, 0.8, 0.67, 0.5, 0.4, 0.33, 0.2, 0.1, 0.05
Pile slenderness ratio	$L/D$	10 – 50	10, 25, 50
Pile-soil stiffness ratio (piles surrounded by uniform soil deposit or resting on infinitely rigid base)	$\Lambda = E_{EP}/G_{soil}$	100 – 10000	10, 100, 500, 1000, 2000, 10000
Pile-soil stiffness ratio (piles resting on finitely rigid base)	$\Lambda = E_{EP}/G_{soil,s}$	100 – 10000	100, 500, 1000, 2000
Poisson's ratio of soil	$\nu_{soil}$	0.1 – 0.5	0.1, 0.15, 0.2, 0.3, 0.4, 0.5
Soil-pile thermal expansion coefficient ratio	$X = \alpha_{soil}/\alpha_{EP}$	0.25 – 4	0, 0.5, 1, 2
Depth of layer	$h_l/L$	-	1, 1.05, 1.1, 1.25, 2.5, $\rightarrow \infty$
Base-to-shaft soil Young's modulus ratio	$E_{soil,b}/E_{soil,s}$	1 – 10000	1, 2, 5, 10, 100, 1000, 10000

Table 4.4: Values of linear thermal expansion coefficient used for addressing non-uniform soil deposits.

Condition	Sub-condition	Parametric value
$\alpha_{soil,b} = \alpha_{soil,s}$	-	0
		$0.5\alpha_{EP}$
		$\alpha_{EP}$
		$2\alpha_{EP}$
$\alpha_{soil,b} > \alpha_{soil,s}$	$\alpha_{soil,s} = \alpha_{EP}$	$\alpha_{soil,b} = 2\alpha_{EP}$
	$\alpha_{soil,s} > \alpha_{EP}$	$\alpha_{soil,b} = 2\alpha_{EP}; \alpha_{soil,s} = 1.5\alpha_{EP}$
	$\alpha_{soil,s} < \alpha_{EP}$	$\alpha_{soil,b} = 0.5\alpha_{EP}; \alpha_{soil,s} = 0$
		$\alpha_{soil,b} = \alpha_{EP}; \alpha_{soil,s} = 0$
$\alpha_{soil,b} < \alpha_{soil,s}$	$\alpha_{soil,s} = \alpha_{EP}$	$\alpha_{soil,b} = 0.5\alpha_{EP}$
		$\alpha_{soil,b} = 0.5\alpha_{EP}; \alpha_{soil,s} = 2\alpha_{EP}$
	$\alpha_{soil,s} > \alpha_{EP}$	$\alpha_{soil,b} = \alpha_{EP}; \alpha_{soil,s} = 2\alpha_{EP}$
	$\alpha_{soil,s} < \alpha_{EP}$	$\alpha_{soil,b} = 1.5\alpha_{EP}; \alpha_{soil,s} = 2\alpha_{EP}$
		$\alpha_{soil,b} = 0; \alpha_{soil,s} = 0.5\alpha_{EP}$

#### 4.2.4 The interaction factor

The displacement field and the interaction factor characterising energy piles are analysed in the following. The case of predominantly floating energy piles in a deep, uniform and compressible soil layer is considered with reference to the case of geometrically identical predominantly end-bearing energy piles in a deep soil deposit consisting of a (shallower) uniform and compressible soil layer and a (deeper) uniform and infinitely rigid soil stratum. The stiffness of the soil layer characterising the case of the predominantly floating energy piles is considered to be the same as that of the soil layer surrounding the shaft of the predominantly end-bearing energy piles.

The elementary units characterising both cases, together with the corresponding situations in which a single isolated pile is subjected to the same temperature variation that is applied to the source pile in the elementary units, are analysed to this aim. The solutions were obtained using stationary finite element analyses (cf., Section 4.2.3).

Figure 4.3 presents the evolution of the normalised vertical head displacement of the piles of the elementary units with a normalised centre-to-centre distance between the piles. The normalised vertical head displacement of the single isolated piles and the evolution of the normalised vertical displacement of the adjacent soil at the ground surface as a function of horizontal distance are also plotted. The vertical displacement is normalised with respect to the head displacement of the single pile under free thermal expansion conditions,  $w_f^{th} = -\alpha_{EP}\Delta TL/2$ .

The essence of the displacement interaction between a source pile subjected to a temperature variation and a neighbouring receiver pile is shown.



#### *4.2.4.1 Displacement of the source pile*

As highlighted in Section 4.2.2, the application of the thermal load to the source pile induces a thermally induced deformation of this element that involves a modification of the displacement field along its length. This displacement is lower for smaller centre-to-centre distances to the receiver pile, whereas this displacement increases and tends to the displacement of a single isolated pile subjected to the same temperature variation for centre-to-centre distances that approach infinity (cf., Figure 4.3 (a)). This result is caused by the effect of the stiffness of the receiver pile on the deformation of the source pile.

The effect of the stiffness of the receiver pile on the deformation of the source pile is less pronounced for predominantly floating piles surrounded by uniform soil deposits compared to predominantly end-bearing piles resting on infinitely rigid soil strata. The pile vertical head displacement is lower for predominantly floating piles surrounded by uniform soil deposits compared to that for predominantly end-bearing piles resting on infinitely rigid soil strata subjected to the same temperature variation. This phenomenon occurs because of the partial and complete upward pile deformation under the application of the temperature variation characterising the former and latter case, respectively, as a consequence of the different null point positioning (above the pile toe in the former and at the toe in the latter).

#### *4.2.4.2 Displacement of the receiver pile*

The thermally induced deformation of the source pile is transmitted to the surrounding soil and influences the displacement field of the receiver pile (cf., Figure 4.3 (b)). This displacement is equal to that of the source pile for zero spacing between the two (i.e., one pile superimposed on the other, corresponding to the case of a single isolated pile subjected to a temperature variation), whereas this displacement decreases and tends to zero for centre-to-centre distances that approach infinity. Yet, this displacement is always smaller than the displacement characterising the soil at the ground surface around a single isolated pile subjected to the same temperature variation applied to the source pile in the elementary unit. This result is caused by the higher stiffness of the receiver pile compared to the stiffness of the soil.

The impact of the difference in stiffness between the receiver pile and the soil on the displacement of the receiver pile becomes more pronounced with increasing pile spacing for predominantly end-bearing piles resting on infinitely rigid soil strata compared to predominantly floating piles surrounded by uniform soil deposits.

#### *4.2.4.3 The displacement interaction factor*

The displacement interaction between piles implies that, when subjected to loading in a group, they present greater displacements compared to the case in which they are isolated and characterised by the same loading.



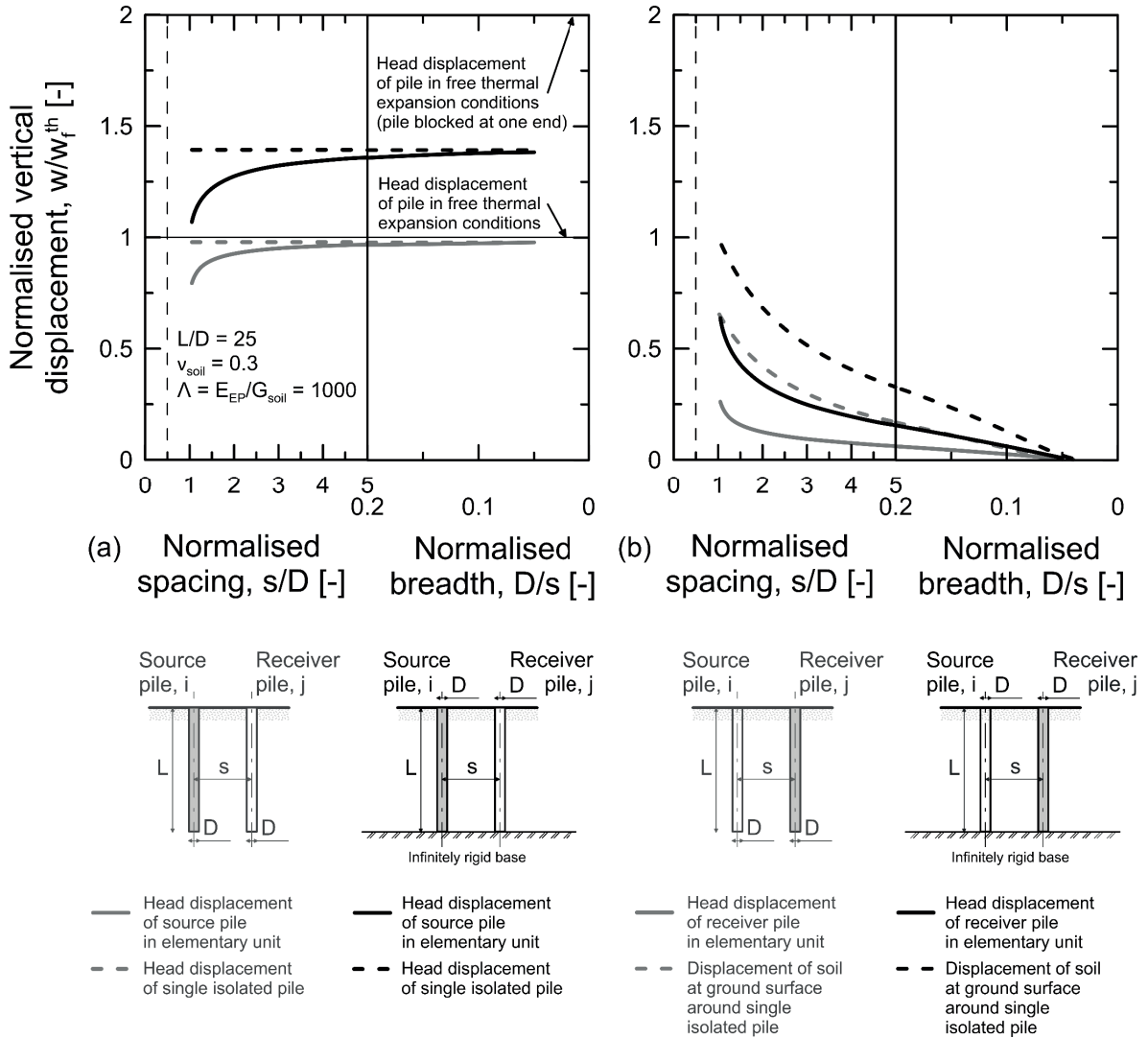


Figure 4.3: Vertical head displacement characterising a source and receiver pile in the elementary units, as well as corresponding single isolated piles subjected to the same temperature variation applied to the source piles.

The additional displacement of a pile due to the loading (e.g., thermal) of an adjacent pile is expressed in this study in terms of an interaction factor  $\Omega$ , where

$$\Omega = \frac{\text{additional displacement due to adjacent pile}}{\text{displacement of single isolated pile}} = \frac{w_j}{w_i} \quad (4.1)$$

In defining the interaction factor,  $w_j$  is the vertical head displacement of a receiver pile in a pair, whereas  $w_i$  is the vertical head displacement of a single isolated pile subjected to the same load applied to the source pile in the elementary unit. This definition of the interaction factor relates the effect of loading a source pile on a receiver pile in a pair with the response of the source pile in an isolated case.

Figure 4.4 presents the typical evolution of the interaction factor with a normalised centre-to-centre distance between two predominantly floating piles in the case of thermal and mechanical loading. The interaction decreases with increasing centre-to-centre distance between the piles. Mechanical loading causes a more pronounced displacement interaction between the piles compared to thermal loading.

Figure 4.5 presents the typical evolution of the interaction factor with a normalised centre-to-centre distance between the piles in the elementary units previously considered. The interaction factor for predominantly end-bearing energy piles resting on infinitely rigid soil strata is greater than that for predominantly floating energy piles embedded in uniform soil deposits (on average 43% higher). This phenomenon is generally observed for any pile spacing and pile slenderness ratio.

The above indicates that the interaction factor for energy piles resting on finitely rigid soil strata generally lies between the interaction factor for energy piles resting on infinitely rigid soil strata and the interaction factor for energy piles surrounded by deep uniform soil deposits. Drawing from the investigations of Poulos and Mattes (1974), the corrected interaction factor for energy piles resting on finitely rigid soil strata may consequently be expressed as

$$\Omega(\text{corrected}) = \Omega(\text{floating}) + F_b(\Omega(\text{end-bearing}) - \Omega(\text{floating})) \quad (4.2)$$

where  $\Omega(\text{floating})$  is the interaction factor for predominantly floating energy piles,  $F_b$  is a correction factor indicating the effect of the bearing stratum and  $\Omega(\text{end-bearing})$  is the interaction factor for predominantly end-bearing energy piles resting on infinitely rigid soil strata.

The term  $F_b$  is a function of (i) the base-to-shaft soil Young's modulus ratio,  $E_{soil,b}/E_{soil,s}$ , (for which  $E_{soil,b}$  is the Young's modulus of the soil stratum below the pile toe and  $E_{soil,s}$  is the Young's modulus of the soil layer around the pile shaft), (ii) the pile slenderness ratio,  $L/D$ , (iii) the normalised pile spacing,  $s/D$ , and (iv) the ratio of base-to-shaft soil Poisson's ratio,  $\nu_{soil,b}/\nu_{soil,s}$  (for which  $\nu_{soil,b}$  is the Poisson's ratio of the soil stratum below the pile toe and  $\nu_{soil,s}$  is the Poisson's ratio of the soil layer around the pile shaft). The characteristics governing the variation of  $F_b$  are aspects (i) and (ii). Aspect (iii) causes a notable variation of  $F_b$  for the impractical centre-to-centre distances between energy piles of approximately  $s \leq 3D$ , whereas a negligible variation of  $F_b$  for the most practical distances of  $s > 3D$  and certainly of  $s \geq 5D$ . Aspect (iv) has a negligible influence on the variation of  $F_b$ . Based on the above, aspects (i) and (ii) are considered in the following analyses whereas aspect (iv) is neglected. Aspect (iii) is accounted for by referring to the commonly utilised centre-to-centre distance between energy piles of  $s = 5D$ .

The limiting values for  $F_b$  are  $F_b = 0$  for predominantly floating piles socketed in a deep uniform soil deposit, i.e.,  $E_{soil,b}/E_{soil,s} = 1$ , and  $F_b = 1$  for predominantly end-bearing energy piles resting on an infinitely rigid soil stratum, i.e.,  $E_{soil,b}/E_{soil,s} = \infty$ .

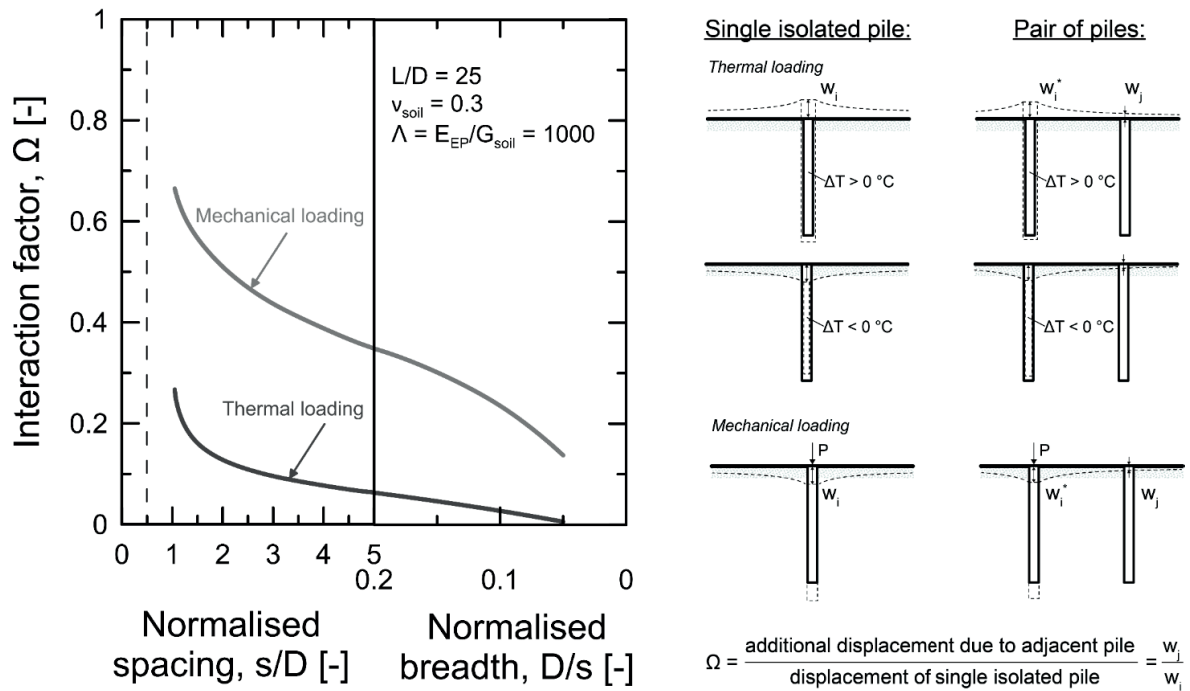


Figure 4.4: Displacement interaction between two piles in a deep soil layer.

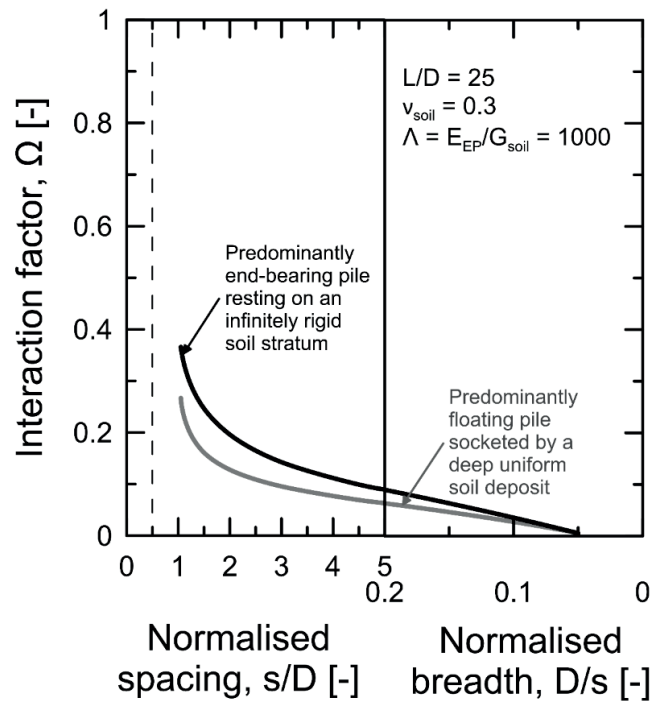


Figure 4.5: Interaction factor for predominantly floating and end-bearing energy piles resting on infinitely rigid soil strata and socketed in uniform soil deposits, respectively, under the application of a thermal load.

### 4.3 Design charts

The evolution of the interaction factor for varying design features characterising a group of two energy piles, including the pile spacing, the pile slenderness ratio, the pile-soil stiffness ratio, the Poisson's ratio of the soil, the depth of a finite layer, non-uniform soil moduli, the soil-pile thermal expansion coefficient ratio and the base-to-shaft soil Young's modulus ratio, is presented in the following. Unless otherwise specified, the solutions have been obtained through stationary finite element analyses (cf., Section 4.2.3) and are valid for both positive and negative temperature variations applied to the energy piles.

#### 4.3.1 Effect of pile spacing, pile slenderness ratio and pile-soil stiffness ratio - piles embedded in uniform soil mass

Figure 4.6, Figure 4.7 and Figure 4.8 present the evolution of the interaction factor for a group of two predominantly floating energy piles embedded in a uniform mass as a function of the normalised centre-to-centre distance between the piles for various slenderness ratios  $L/D$  and pile-soil stiffness ratios  $\Lambda = E_{EP}/G_{soil}$ . The decreasing interaction with increasing centre-to-centre distance is shown according to the aforementioned comments. The interaction increases as  $L/D$  increases and  $\Lambda$  decreases, i.e., as the piles become slender or less stiff. The latter result indicates an opposite role of the stiffness compared to that found by Poulos (1968) for conventional piles subjected to mechanical loads, i.e., increasing interaction as  $\Lambda$  increases and thus as the piles become stiffer.

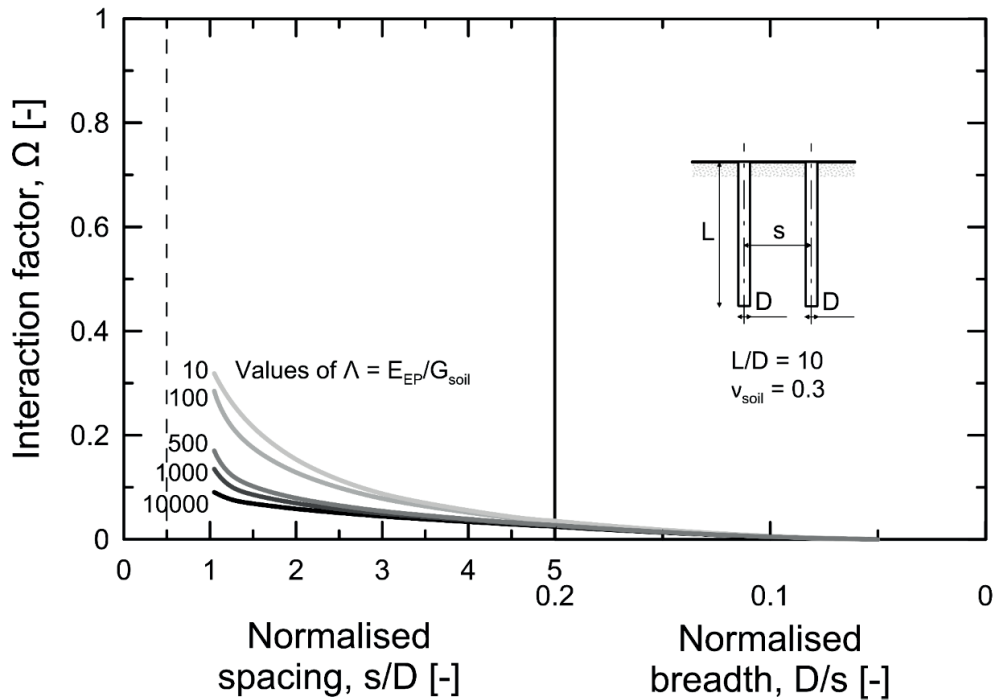


Figure 4.6: Interaction factors for predominantly floating energy piles of  $L/D = 10$ .

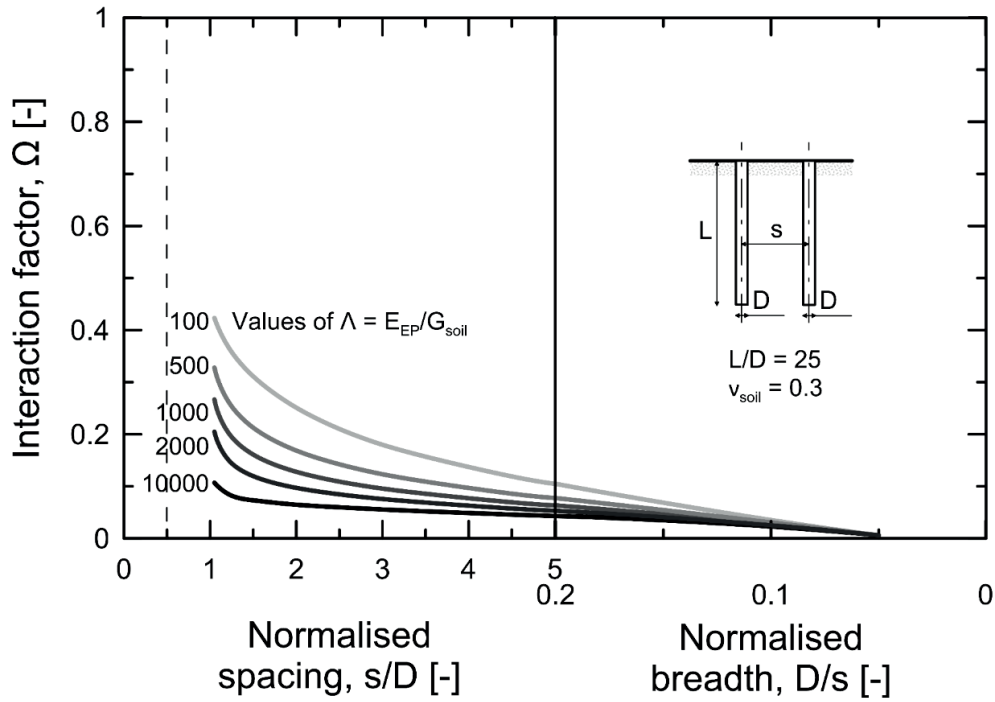


Figure 4.7: Interaction factors for predominantly floating energy piles of  $L/D = 25$ .

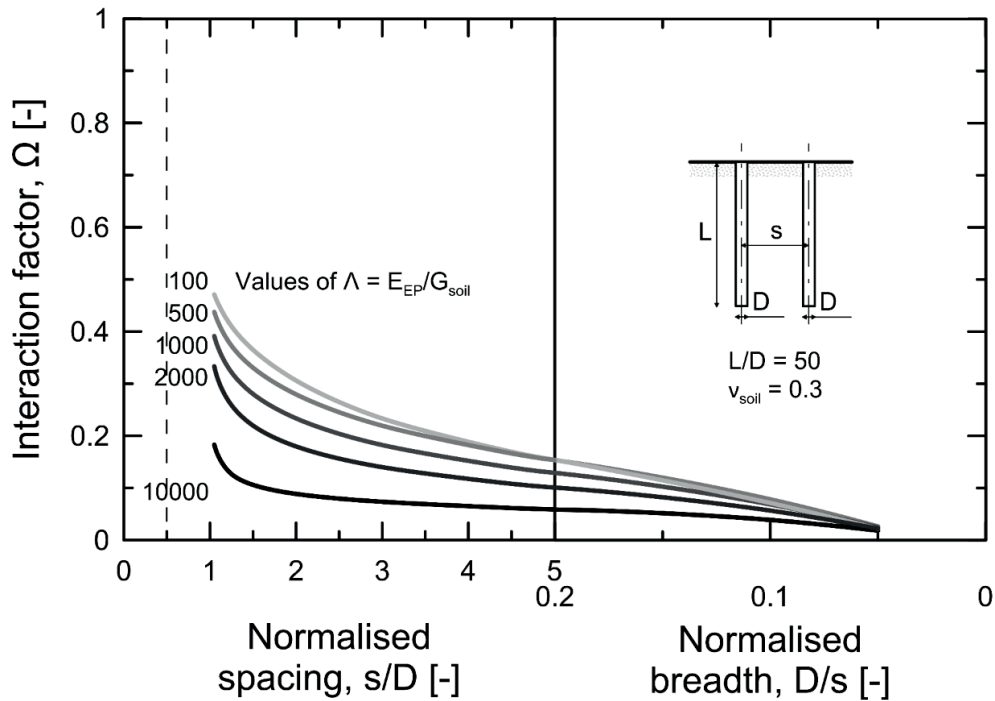


Figure 4.8: Interaction factors for predominantly floating energy piles of  $L/D = 50$ .

#### 4.3.2 Effect of pile spacing, pile slenderness ratio and pile-soil stiffness ratio - piles resting on infinitely rigid soil strata

Figure 4.9, Figure 4.10 and Figure 4.11 present the evolution of the interaction factor for a group of two predominantly end-bearing energy piles resting on infinitely rigid soil strata as a function of the normalised centre-to-centre distance between the piles for various slenderness ratios  $L/D$  and pile-soil stiffness ratios  $\Lambda = E_{EP}/G_{soil}$ . The interaction decreases with increasing centre-to-centre distance. The interaction increases as  $L/D$  increases and  $\Lambda$  decreases, i.e., as the piles become slender or less stiff. The latter result indicates (i) the same role of the stiffness compared to that found for predominantly floating energy piles subjected to thermal loads; (ii) the same role of the stiffness compared to that found by Poulos and Mattes (1974) for predominantly end-bearing conventional piles subjected to mechanical loads; and (iii) the opposite role of the stiffness compared to that found by Poulos (1968) for predominantly floating conventional piles subjected to mechanical loads, i.e., increasing interaction as  $\Lambda$  increases and thus as the piles become stiffer.

#### 4.3.3 Effect of pile slenderness ratio, pile-soil stiffness ratio and base-to-shaft modulus ratio - piles resting on finitely rigid soil strata

Figure 4.12 and Figure 4.13 present the evolution of the correction factor for a group of two predominantly end-bearing energy piles resting on finitely rigid soil strata as a function of the base-to-shaft soil Young's modulus ratio  $E_{soil,b}/E_{soil,s}$  for various slenderness ratios  $L/D$  and pile-soil stiffness ratios  $\Lambda = E_{EP}/G_{soil,s}$  ( $G_{soil,s}$  is the shear modulus of the soil layer around the pile shaft). The correction factor generally increases with increasing  $\Lambda$  and  $E_{soil,b}/E_{soil,s}$ . This result indicates the opposite role of  $\Lambda$  compared to that found by Poulos and Mattes (1974) for predominantly end-bearing conventional piles subjected to mechanical loads, i.e., increasing  $F_b$  as  $\Lambda$  decreases and thus as the piles become less stiff. The smaller the value of  $L/D$  or the greater the value of  $\Lambda$ , the smaller the value of  $E_{soil,b}/E_{soil,s}$  for which  $F_b$  tends to 1, i.e., the corrected interaction factor tends to the interaction factor for predominantly end-bearing energy piles resting on infinitely rigid soil strata. Although the values of  $F_b$  shown are exact only for a normalised pile spacing of  $s/D = 5$ , they apply to other centre-to-centre distances between the piles sufficiently accurately for practical purposes. Note that for values of  $E_{soil,b}/E_{soil,s}$  greater than 1000 the value of  $F_b$  remains approximately unchanged, i.e., the effect of the rigidity of the bearing soil layer involves a pile response comparable to that for the case of an infinitely rigid base.

#### 4.3.4 Effect of Poisson's ratio of soil

Figure 4.14 presents the effect of the Poisson's ratio of the soil  $\nu_{soil}$ , where a correction factor  $N_\nu$  is plotted for  $L/D = 25$  and  $\Lambda = 1000$ . The interaction factor for any value of  $\nu_{soil}$  is given by

$$\Omega = N_\nu \Omega_{\nu_{soil}=0.3} \quad (4.3)$$

where  $\Omega_{\nu_{soil}=0.3}$  is the interaction factor for  $\nu_{soil} = 0.3$ . The interaction increases as the value of  $\nu_{soil}$  decreases. This effect becomes more notable as the centre-to-centre distance between the piles increases.

#### 4.3.5 Effect of finite layer depth

Figure 4.15 presents the effect of the finite layer depth  $h_l/L$ , where a correction factor  $N_{h_l}$  is plotted for  $L/D = 25$  and  $\Lambda = 1000$ . The interaction factor for any value of  $h_l/L$  is given by

$$\Omega = N_{h_l} \Omega_{h_l/L \rightarrow \infty} \quad (4.4)$$

where  $\Omega_{h_l/L \rightarrow \infty}$  is the interaction factor for the deep soil layer ( $h_l/L \rightarrow \infty$ ). The interaction increases as the value of  $h_l/L$  decreases. This effect becomes more notable as  $L/D$  increases and  $\Lambda$  decreases. Although presented for specific values of  $L/D$  and  $\Lambda$ , the values of the factor  $N_{h_l}$  presented in Figure 4.15 can be approximately applied for other values of  $L/D$  and  $\Lambda$ . The results demonstrate an opposite role of the depth of the soil layer compared to that found by Poulos (1968) for conventional piles subjected to mechanical loads, i.e., decreasing interaction as  $h_l/L$  decreases.

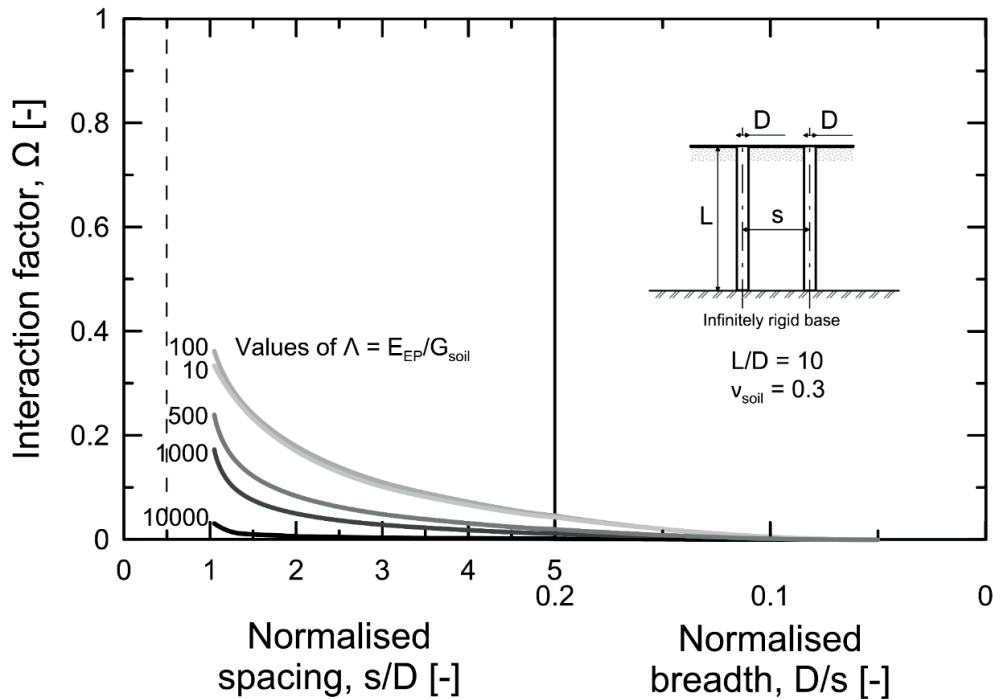


Figure 4.9: Interaction factors for predominantly end-bearing energy piles of  $L/D = 10$ .

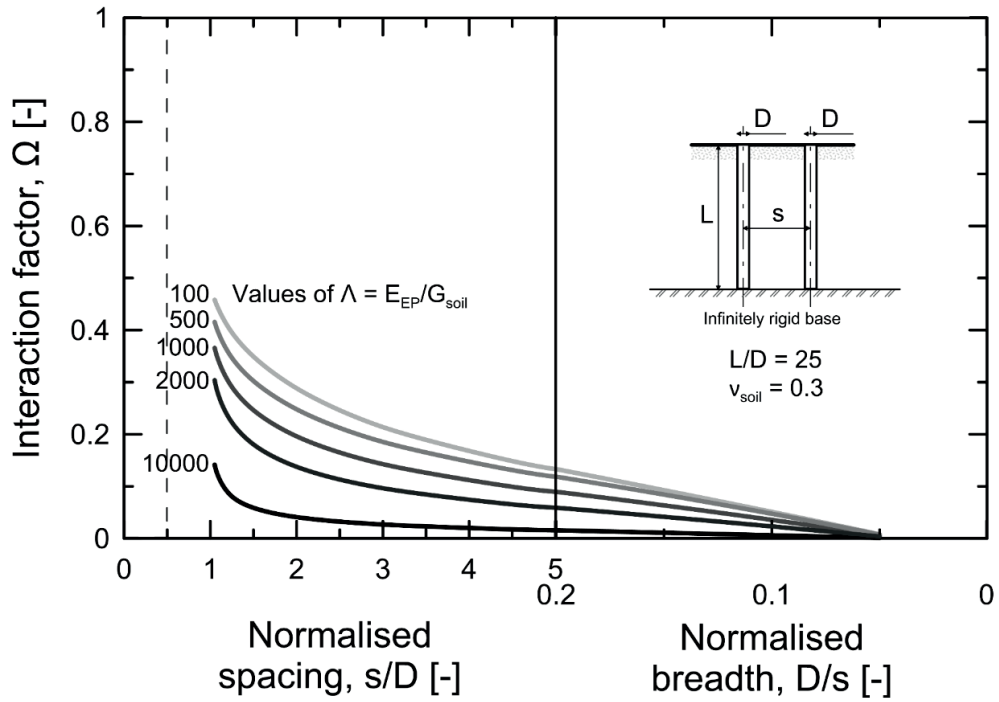


Figure 4.10: Interaction factors for predominantly end-bearing energy piles of  $L/D = 25$ .

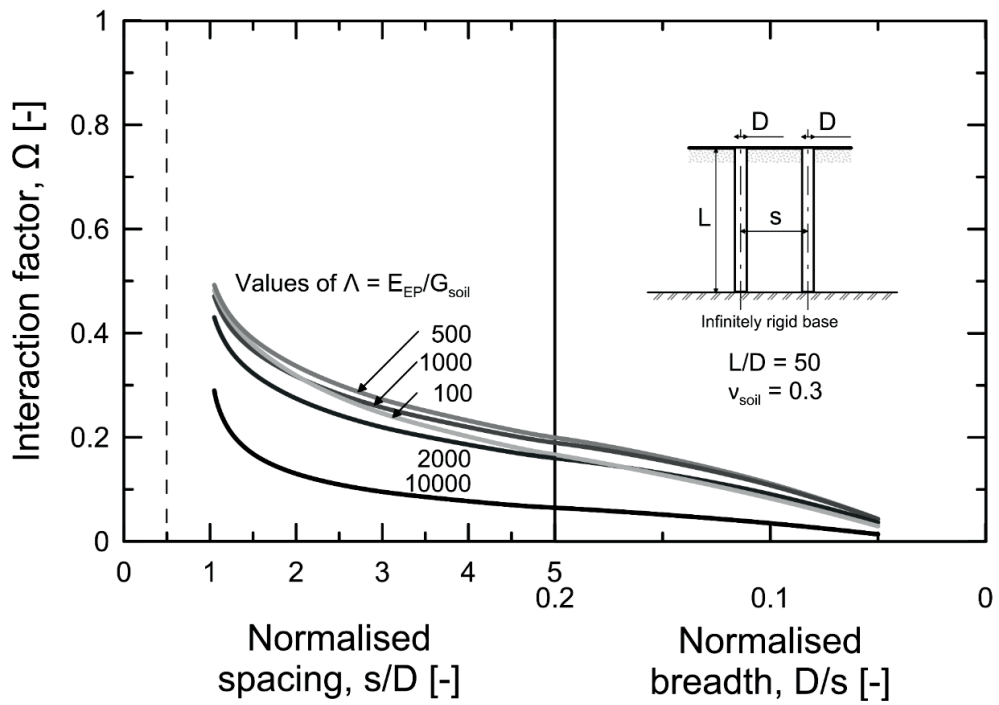


Figure 4.11: Interaction factors for predominantly end-bearing energy piles of  $L/D = 50$ .



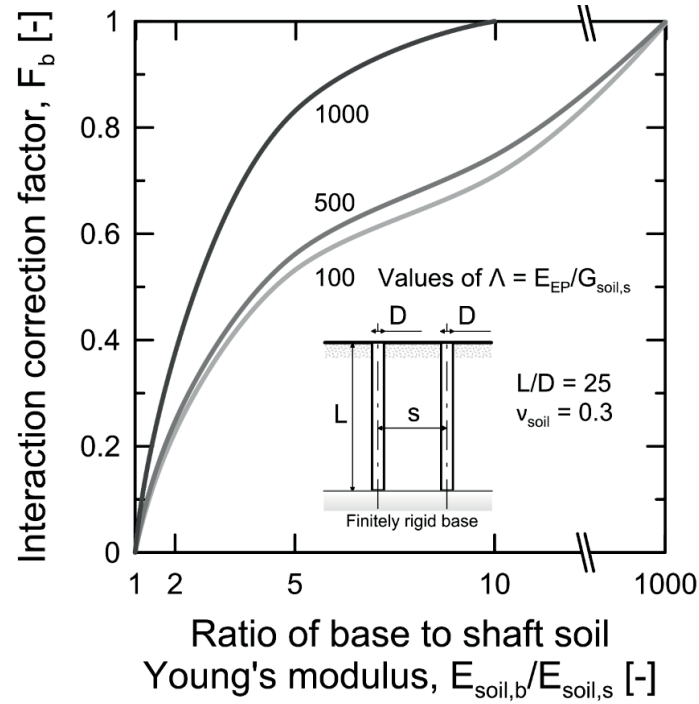


Figure 4.12: Correction factor  $F_b$  to account for the effect of a finitely rigid bearing stratum for  $L/D = 25$ .

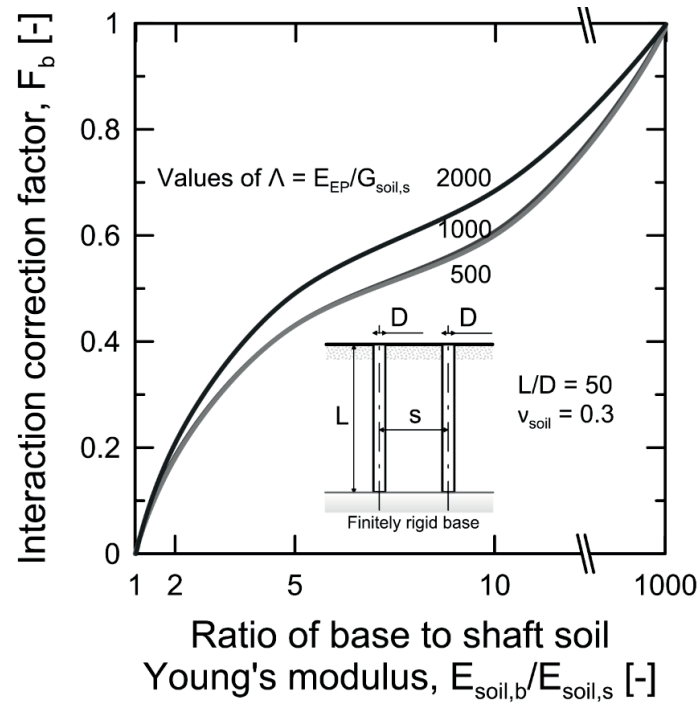
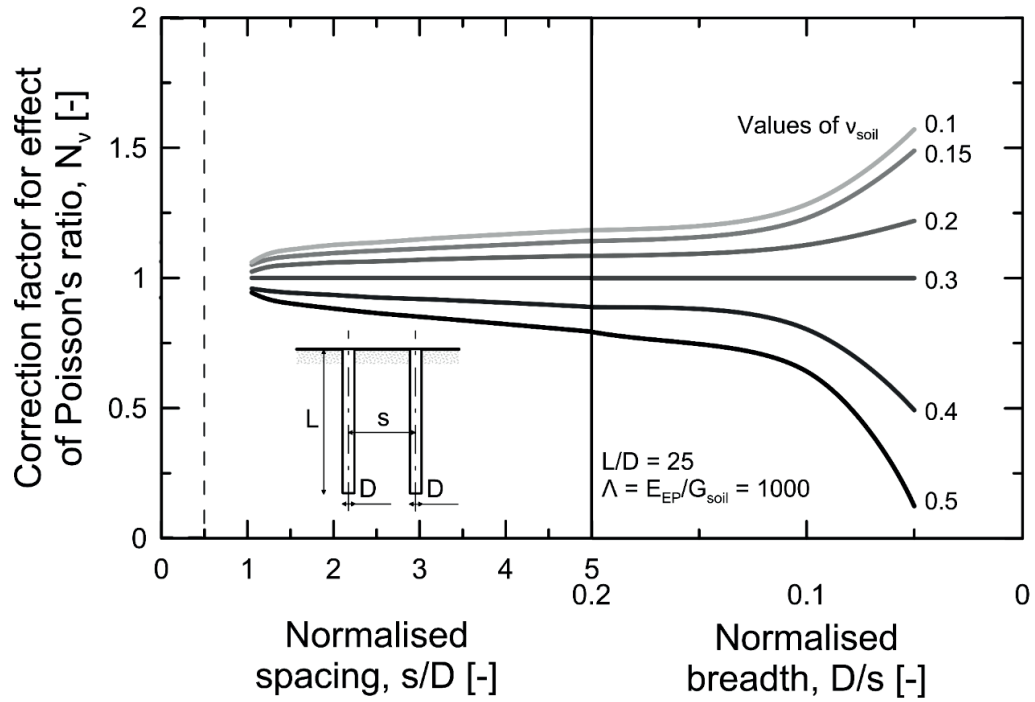
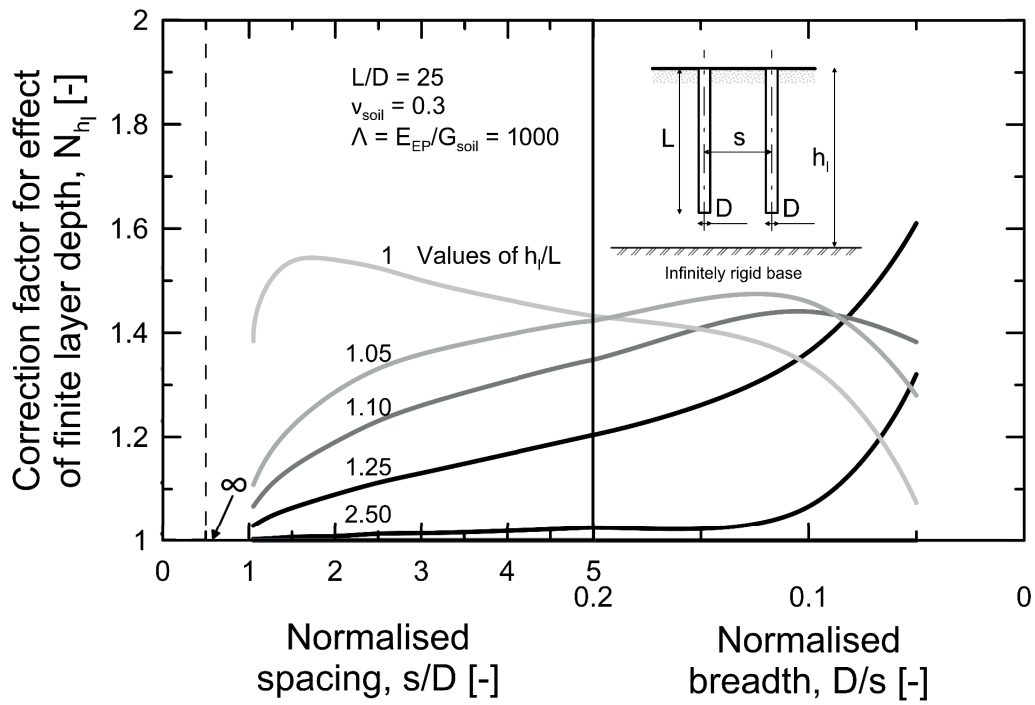


Figure 4.13: Correction factor  $F_b$  to account for the effect of a finitely rigid bearing stratum for  $L/D = 50$ .

Figure 4.14: Correction factor  $N_v$  for effect of Poisson's ratio of soil.Figure 4.15: Correction factor  $N_{h_l}$  for effect of finite layer depth.

#### 4.3.6 Effect of non-uniform soil modulus

The solutions presented above for the interaction factor all assume a uniform soil modulus along the pile shaft. In some cases, a closer approximation to reality is to consider the soil modulus as increasing linearly with depth (Gibson's soil) (Poulos, 1968).

Figure 4.16 shows the effect of a non-uniform soil modulus along the pile shaft on the interaction factor. A comparison between the interaction factor evolutions with normalised centre-to-centre distance between the piles for a constant and a linearly increasing soil modulus with depth (the latter being equal, on average, to the constant distribution along the pile length) is presented. The evolution law for the soil modulus is as follows

$$E_{soil}(z) = 0.5E_{soil} + \frac{z}{L}E_{soil} \quad (4.5)$$

The value of  $\Omega$  for the piles in the non-homogeneous soil is up to 2% smaller than for the homogeneous soil at any considered centre-to-centre distance. Thus, the use of interaction factors for the case of piles in a homogeneous soil gives conservative estimates of the interaction for cases in which the modulus increases with depth. The effect of non-uniform soil moduli on the displacement interaction between piles subjected to thermal loads is less marked compared to that characterising piles subjected to mechanical loads, for which the difference with the uniform case was from 20 to 25% (Poulos, 1968).

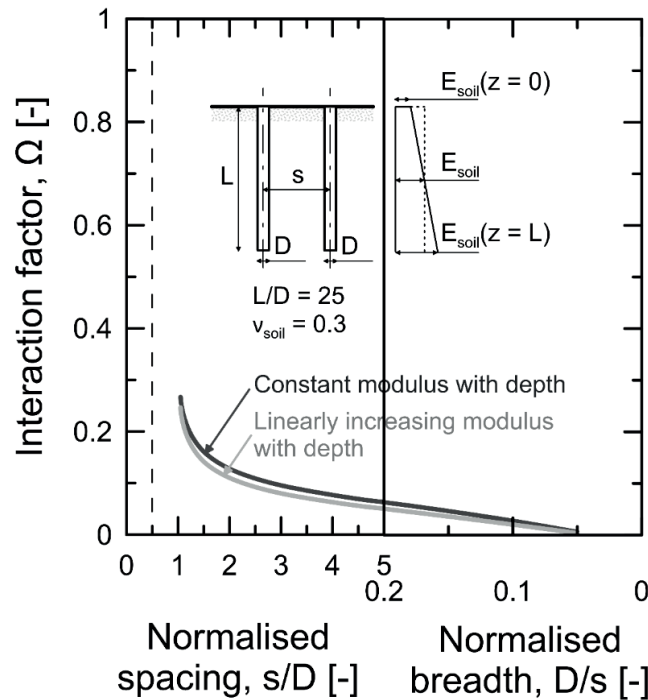


Figure 4.16: Effect of non-uniform soil modulus on interaction factor.

### 4.3.7 Effect of soil-pile thermal expansion coefficient ratio

The solutions presented above for the interaction factor all assume an isothermal soil (infinite heat reservoir) that is characterised by an elastic behaviour. The effect of the ratio between the thermal expansion coefficient of soil and that of the pile (e.g., linear), namely,  $X = \alpha_{soil}/\alpha_{EP}$ , on the interaction factor is investigated herein. The solutions have been obtained through time-dependent finite element analyses (cf., Section 4.2.3). In these analyses, the thermal expansion coefficient of the receiver pile is set to zero to highlight only the effect of thermally induced volumetric variations in the soil on the interaction previously defined with reference to the elastic soil.

Figure 4.17 presents the effect of the soil-pile thermal expansion coefficient ratio on the interaction factor. The interaction increases with increasing thermal expansion coefficient of the soil. Values of  $X = 0.5$  and 1 have a similar impact on the interaction factor compared to  $\nu_{soil} = 0.15$ , i.e., they induce a relative average increase of 12% compared to the increase of 15% from the reference value of  $\Omega$ . Values of the thermal expansion coefficient of soil greater than that of the pile (e.g.,  $X = \alpha_{soil}/\alpha_{EP} = 2$ ) have a considerably stronger effect on the interaction, i.e., up to an average increase compared to the reference value of  $\Omega$  of 200%. The time (and thus the spatial extent) of heat diffusion in the soil crucially characterises the effect of the soil-pile thermal expansion coefficient ratio on the interaction because it involves varying amounts of mobilised thermal expansion coefficient of soil.

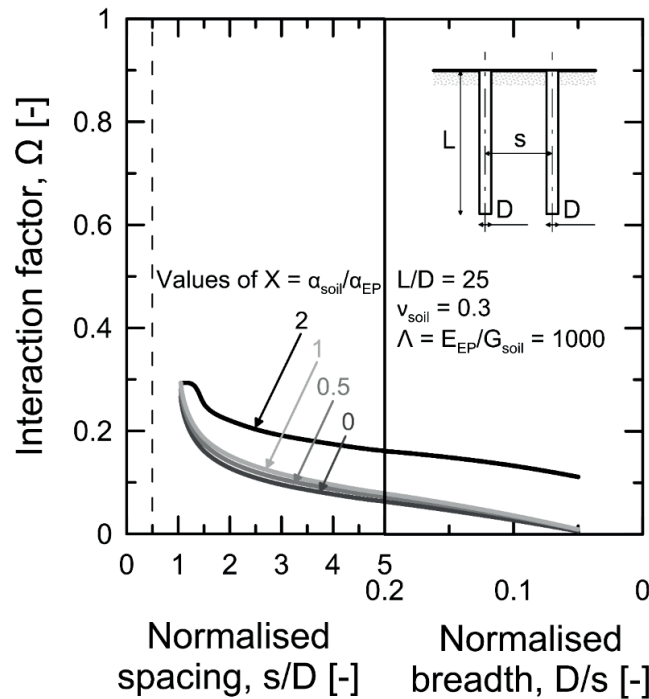


Figure 4.17: Effect of soil thermal expansion coefficient on interaction factor.

## 4.4 Application and validation of the interaction factor concept

### 4.4.1 Analysis of symmetrical energy pile groups

In considering the displacement interaction between conventional piles subjected to mechanical loading, Poulos (1968) remarked that the analysis of the interaction between two piles can be extended to any number of piles, provided that the arrangement of the piles in the group is such that they all behave identically. Such pile groups are defined as symmetrical pile groups. In a symmetrical pile group, all the piles are equally spaced around the circumference of a circle, and each pile displaces equally while carrying the same amount of load.

The approach described above, which is based on the elastic principle of superposition of effects, is also adopted here for applying the interaction factor concept to the analysis of symmetrical energy pile groups. Groups of 2, 3 and 4 predominantly floating energy piles subjected to the same temperature variation in an elastic soil are considered.

### 4.4.2 Application of the interaction factor concept

In analysing the displacement characterising energy pile groups, knowledge of a parameter defined in this work as the displacement ratio  $D_r$  appears convenient. The definition of the displacement ratio has been extended from that of the settlement ratio  $R_s$  proposed by Poulos (1968) for conventional piles subjected to mechanical loads. The displacement ratio is

$$D_r = \frac{\text{average displacement of group}}{\text{displacement of single pile subjected to same average load}} \quad (4.6)$$

Reference is made to the pile head vertical displacement. It is worth noting that the general definition of “displacement of single pile subjected to same average load” allows  $D_r$  to be determined in two ways.

The first way is to determine the displacement ratio with reference to the displacement of a single isolated energy pile subjected to a temperature variation, that is,  $w_i$ , by determining analytically the increase in displacement of the group in which all the piles are subjected to the same temperature variation through superposition with the use of the interaction factor  $\Omega$ . In this case, the displacement ratio is

$$D_r = \frac{w_i(1+\Omega_{s/D})}{w_i} = 1 + \Omega_{s/D} \text{ for a 2-pile group,}$$

$$D_r = \frac{w_i(1+2\Omega_{s/D})}{w_i} = 1 + 2\Omega_{s/D} \text{ for a 3-pile group, and}$$

$$D_r = \frac{w_i(1+2\Omega_{s/D}+\Omega_{s\sqrt{2}/D})}{w_i} = 1 + 2\Omega_{s/D} + \Omega_{s\sqrt{2}/D} \text{ for a 4-pile group,}$$

where  $\Omega_{s/D}$  is the interaction factor between two piles at any normalised centre-to-centre distance and  $\Omega_{s\sqrt{2}/D}$  is the interaction factor between two piles in the 4-pile group along the diagonal of the square, whose side has a normalised length of  $s/D$ .

The second way is to determine the displacement ratio based on the results of a more rigorous approach, such as the finite element method, by calculating (through two different analyses) the displacement of a single source pile in the group subjected to a temperature variation, that is,  $w^*$ , and the average displacement of the group in which all the piles are subjected to the same temperature variation, that is,  $\bar{w}$  (for symmetrical pile groups, corresponding to the displacement of any single pile in the group). In this case, for any normalised centre-to-centre distance between the energy piles, the displacement ratio is

$$D_r = \frac{2w_l/2}{w_l^*} = \frac{\bar{w}}{w_l^*} \text{ for a 2-pile group,}$$

$$D_r = \frac{3w_m/3}{w_m^*} = \frac{\bar{w}}{w_m^*} \text{ for a 3-pile group, and}$$

$$D_r = \frac{4w_n/4}{w_n^*} = \frac{\bar{w}}{w_n^*} \text{ for a 4-pile group,}$$

where  $w_l$ ,  $w_m$  and  $w_n$  are the displacements of the piles composing the 2-, 3- and 4-pile groups when all the piles are subjected to the same temperature variation, whereas  $w_l^*$ ,  $w_m^*$  and  $w_n^*$  are the displacements of the single source pile subjected to the same average temperature variation in the 2-, 3- and 4-pile groups. It is worth noting that  $w_n > w_m > w_l$  because of the more pronounced interactions in pile groups with higher numbers of piles. It is also worth noting that  $w_n^* < w_m^* < w_l^*$  because of the greater effect of the stiffness of the receiver piles on the deformation of the source pile in pile groups with higher numbers of piles.

#### 4.4.3 Validation of the interaction factor concept

Figure 4.18 presents the evolution of the displacement ratio as a function of the normalised centre-to-centre distance between the piles constituting the 2-, 3- and 4-energy-pile groups subjected to the same temperature variation. The figure shows the case for piles with a slenderness ratio of  $L/D = 25$ , pile-soil stiffness ratio of  $\Lambda = E_{EP}/G_{soil} = 1000$  and Poisson's ratio of soil (considered as an infinite heat reservoir at a fixed constant temperature) of  $\nu_{soil} = 0.3$ . The displacement ratio has been calculated according to the two approaches proposed in Section 4.4.2, i.e., analytical application of the interaction factor concept and finite element analysis.

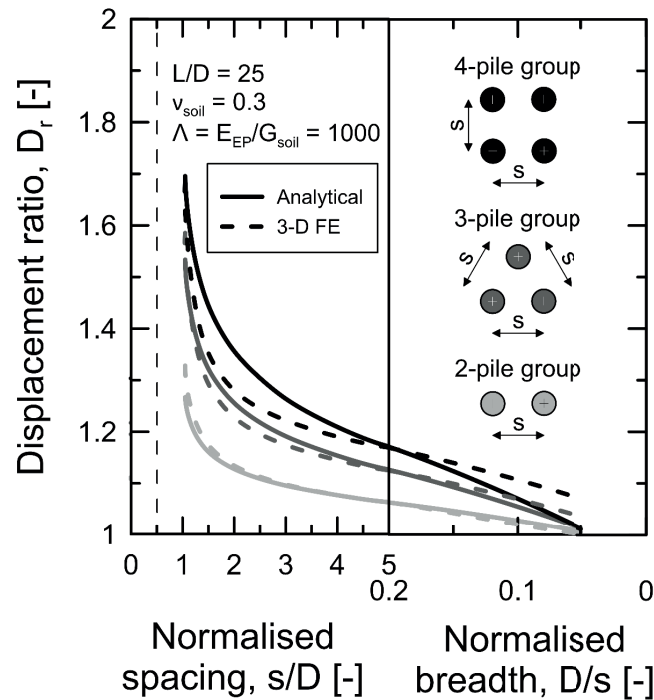


Figure 4.18: Displacement ratio for symmetrical energy pile groups.

The displacement ratio increases with increasing number of piles and decreases with increasing centre-to-centre distance between the piles because of the less pronounced interaction. Each of the symmetrical pile groups is characterised by a higher average displacement compared to that of a single pile subjected to the same average temperature variation. For example, the displacement ratio of the 3-pile group for  $s/D = 5$  is  $D_r = 1.13$ , i.e., the average vertical head displacement of the group is 13% higher than the vertical head displacement of a single pile subjected to the same average temperature variation. For a limited number of piles in the group (e.g., up to 4 piles), the influence of the interactions between the piles (group effects) on the displacement behaviour of the group may be considered small and negligible for practical purposes. This consideration appears to be valid for groups of predominantly piles. It is not necessarily valid for groups of predominantly end-bearing piles because interactions have been proved to be on average 43% higher than those characteristics of the previous situations for a wide range of pile spacing.

The evolutions of the displacement ratio defined through the analytical and finite element approaches are well comparable in all cases, despite the accuracy of the analytical method decreasing with increasing number of piles in the group. The decrease in accuracy of the analytical method with increasing number of piles is caused by the variation in the stress field characterising the lengths of these elements compared to that of the 2-pile group. This variation in the stress field involves a different displacement field and associated location of the null point along the length of the piles in groups of more than 2 piles. Such an effect is not considered by the application of the interaction factor concept through the elastic principle of superposition of effects because reference is made to the displacement interaction between two piles.

A result of the different distribution of stress along the length of a single isolated energy pile compared to that characterising each of the energy piles in the 2-pile group as well as in the 3- and 4-pile groups for to the same positive temperature variation applied to these elements is presented in Figure 4.19. Figure 4.19 (a) presents the evolution of the normalised base resistance<sup>2</sup> with the normalised centre-to-centre distance between the energy piles in the group compared to the case of a single isolated energy pile. The interaction causes a decrease in the stress transmitted to the base of each energy pile in the group compared with the case of a single isolated energy pile, with such a mechanism becoming increasingly marked as the number of piles in the group increases. The aforementioned mechanism is opposite to that characterising conventional piles subjected to mechanical loads, in which interaction causes an increase in the stress transmitted to the base of each pile in the group compared with the case of a single isolated pile (Poulos, 1968). Figure 4.19 (b) depicts the distribution of the normalised shaft friction<sup>3</sup> along the normalised depth compared to the case of a single isolated energy pile for  $s/D = 3$ . As the number of piles in the group increases, a redistribution of shear stress occurs at the shaft to ensure equilibrium as a consequence of the different amounts of stress transmitted to the base. The distribution of shear stress becomes sharper along the major part of the length of the pile compared to that characterising a single isolated energy pile, and a more pronounced increase in shear stress occurs at the pile ends.

The applicability of the elastic principle of superposition of effects in approximately describing the displacement interaction in groups of 3 and 4 energy piles suggests that the head displacement of any symmetrical energy pile group may be estimated through analytical calculations by applying the interaction factor concept without having to resort to more rigorous albeit time-consuming approaches. Further, it appears reasonable to extend the use of the elastic principle of superposition of effects and the application of the interaction factor to the analysis of the displacement behaviour of general energy pile groups.

---

<sup>2</sup> The ultimate base resistance of the single isolated energy pile is calculated based on a “rigid approach” as  $q_b = \sigma_{vb}$  (where  $\sigma_{vb}$  is the total vertical stress at the base of the pile) to account for a limited contribution in base capacity provided by the considered soil. The considered value of base capacity is much smaller than the values that may be estimated through usual analytical formulae based on bearing capacity factors for deep foundations. This limited contribution in base capacity has been found to characterise piles of similar length than that considered in this study based on available data. The tested pile may thus be considered as an almost fully floating pile.

<sup>3</sup> The shear stress mobilised at the pile shaft is normalised by the average shaft resistance of the single isolated energy pile that is calculated as  $q_s = (\sigma_b K_o \tan \delta)/2 + c$  (where  $\delta$  is the pile-soil interface angle of shear strength and  $c$  is the soil cohesion).



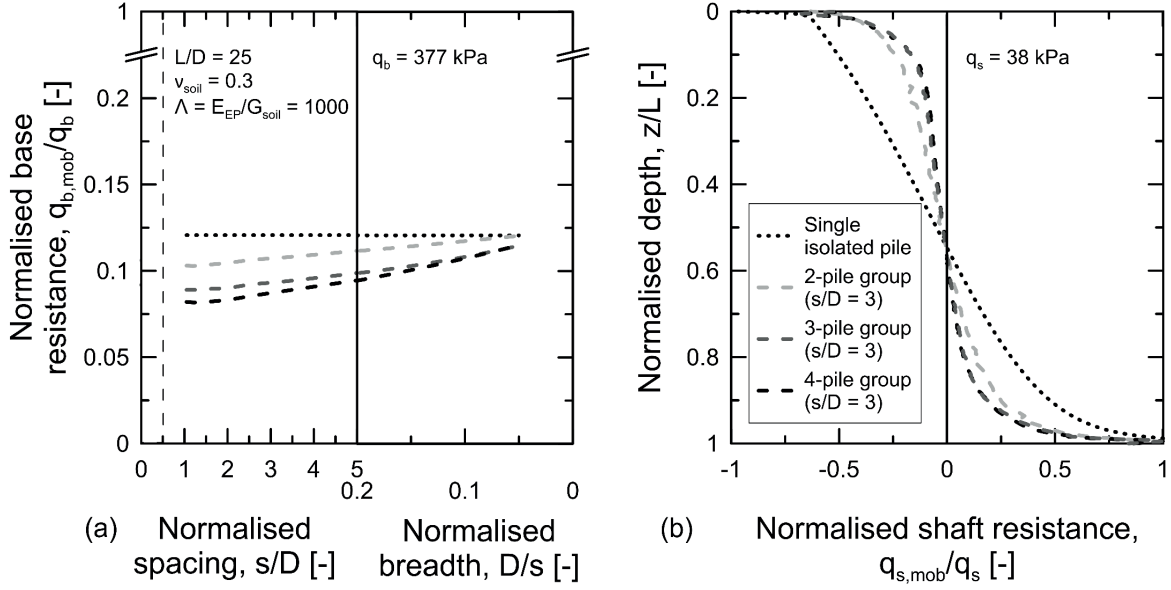


Figure 4.19: (a) Effect of interaction on mobilised base resistance,  $q_{b,mob}$ . (b) Effect of interaction on distribution of mobilised shaft friction,  $q_{s,mob}$ .

## 4.5 The interaction factor method

### 4.5.1 Analysis of general energy pile groups

Supposing that the elastic principle of superposition of effects holds for the analysis of a general group of total number of piles  $n_{EP}$ , the vertical head displacement of any pile  $k$  in the group can be estimated as (Rotta Loria and Laloui, 2016b)

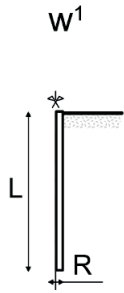
$$w_k = w^1 \sum_{i=1}^{i=n_{EP}} \Delta T_i \Omega_{ik} \quad (4.7)$$

where  $w^1$  is the unitary vertical head displacement of a single isolated pile,  $\Delta T_i$  is the applied temperature variation to pile  $i$ , and  $\Omega_{ik}$  is the interaction factor for two piles corresponding to the centre-to-centre distance between pile  $i$  and pile  $k$ . The displacement analysis of any general pile group in which some or all piles are subjected to a temperature variation may therefore be performed based on the knowledge of the unitary head displacement of a single isolated pile  $w^1$  and on the relationship between the interaction factor  $\Omega$  and the centre-to-centre distance between the piles  $s/D$  for a group of two piles. This represents the essence of the interaction factor method.

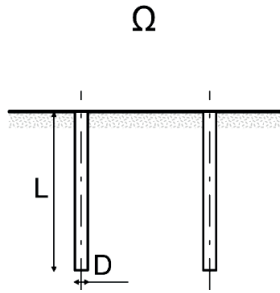
The procedure used to apply the interaction factor method for the displacement analysis of general energy pile groups consists of three key steps (cf., Figure 4.20):

1. The analysis of a single isolated pile subjected to a temperature variation to define  $w^1$ . This analysis can be carried out by referring to the charts presented from Figure 4.21 to Figure 4.26, in which absolute values of  $w^1$  for the design situations considered thus far are depicted. Otherwise, it may be performed with any numerical method available for such purpose.
2. The definition of  $\Omega$  for a pair of two piles at any given centre-to-centre distance. This step can be accomplished by referring to the design charts proposed in this work.
3. The analytical analysis of the displacement behaviour of the pile group. This analysis can be developed by applying equation (4.7).

1. Analysis of single isolated pile



2. Definition of interaction factor for a pair of piles



3. Analytical analysis of general pile groups

$$w_k = w^1 \sum_{i=1}^{i=n_{EP}} \Delta T_i \Omega_{ik}$$

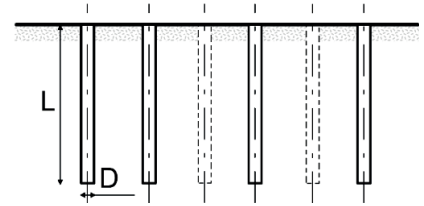


Figure 4.20: Key steps for the application of the interaction factor method.

The proposed approach for the displacement analysis of energy pile groups, as well as all present approaches based on the interaction factor concept for the estimation of the displacements of conventional pile groups subjected to mechanical loads (Poulos, 1968; Randolph and Wroth, 1979b; Mylonakis and Gazetas, 1998; O'Neill et al., 1977; Chow, 1986), is indeed a simplified method because it involves approximations to obtain an answer even for the idealised situation. Because it is based on the analysis of the displacement interaction between two piles in a pair, in considering general pile groups, the method suffers from the drawbacks of not accounting for the following: (i) the redistribution of forces among the piles, which involves a variation in the displacement field compared to that characterising a group of two piles (cf., Section 4.4.3); (ii) the presence of piles between the pile at which the displacement is calculated and the pile whose influence is considered, which involves a reinforcing effect of the soil that tends to vary the influence of a pile on another pile compared to that characterising a group of two piles (Poulos, 1968); and (iii) the effect of the stiffness of the receiver piles on the deformation of the source pile(s) in the group, which involves an approximation of the unitary displacement of these elements, especially for greater numbers of piles and shorter centre-to-centre distances between the piles.

Some inaccuracy may result from the approximations made in the formulation of the proposed method. According to Poulos (1968), these approximations appear however to be justified because their consideration would result in an increase in complexity of the solution not commensurate with any increase in accuracy that might be obtained. The proposed approach thus represents a simplified

yet rational method for the displacement analysis of energy pile groups. Further justification of the method of analysis is provided later based on a comparison between estimates of the vertical head displacement of general energy pile groups obtained through the considered approach and the more rigorous finite element method.

A notable feature of the proposed method is that it allows performing the displacement analysis of general energy pile groups also in situations in which some of the piles may be subjected to significant temperature variations that may induce non-linear phenomena (e.g., plastic strains) in the narrow region of soil adjacent to or in the vicinity of such elements, i.e., the pile-soil interface. The reason is because displacement interactions among piles are essentially elastic (Chow, 1986). Reference to situations in which the soil surrounding the piles may be approximated to behave according to an elastic-perfectly plastic constitutive law allows considering that only the elastic component of deformation is transmitted from source piles (e.g., subjected to significant loads) to receiver piles (e.g., potentially subjected to less pronounced loads). Yet, in situations in which the soil region adjacent to receiver piles is in a (perfectly) plastic state no deformation is transmitted from source piles to receiver piles. The reason for these phenomena is that when the shear strength of the pile-soil interface is fully mobilised, full slippage between the soil and the pile can be considered to occur. This fact includes the formation of a displacement discontinuity at the pile-soil interface. Therefore, while the displacement resulting from an elastic component of deformation that may be associated to a plastic state at the pile-soil interface of a source pile is transmitted in the surrounding bulk of the soil, the displacement induced by an elastic component of deformation from a source pile is no more transmitted to the receiver pile if its interface is in a plastic state. The elastic character of displacement interactions involves that a non-linear response of piles subjected to significant loads can be co-present to a linear response of piles subjected to less remarkable loads in the same group (Caputo and Viggiani, 1984). In these situations, the estimation of the displacement of the piles in the group may be performed by calculating through a suitable analysis the displacement of these elements with reference to a single isolated case and by applying the interaction factors only up to the limit corresponding to the elastic component of this displacement as well as only to the piles whose interface is not in a plastic state.

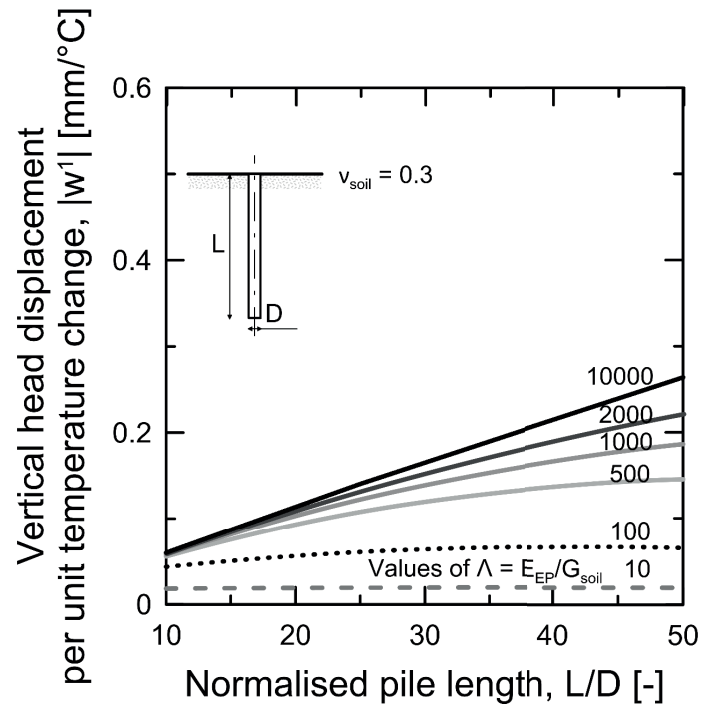


Figure 4.21: Vertical head displacement per unit temperature variation for different  $L/D$  – predominantly floating energy pile embedded in uniform mass.

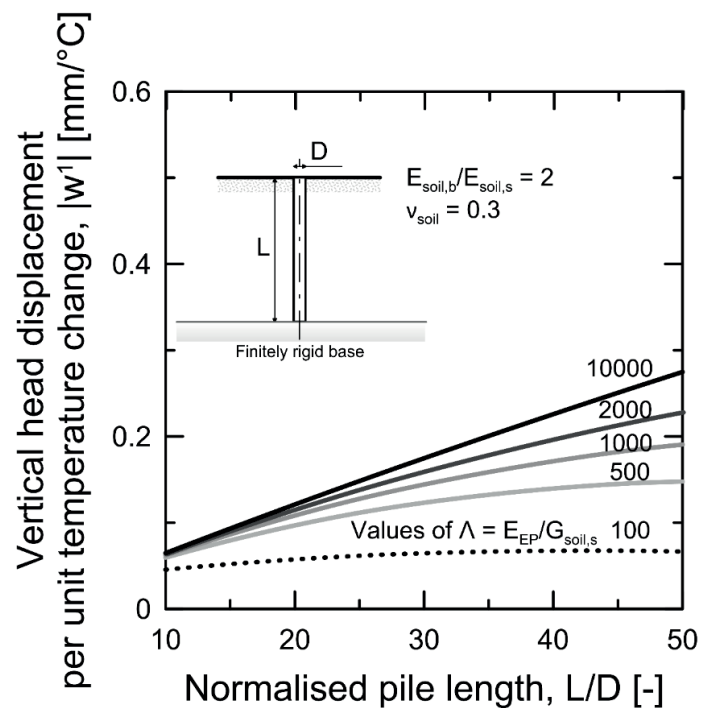


Figure 4.22: Vertical head displacement per unit temperature variation for different  $L/D$  – predominantly end-bearing pile resting on finitely rigid soil strata ( $E_{soil,b}/E_{soil,s} = 2$ ).

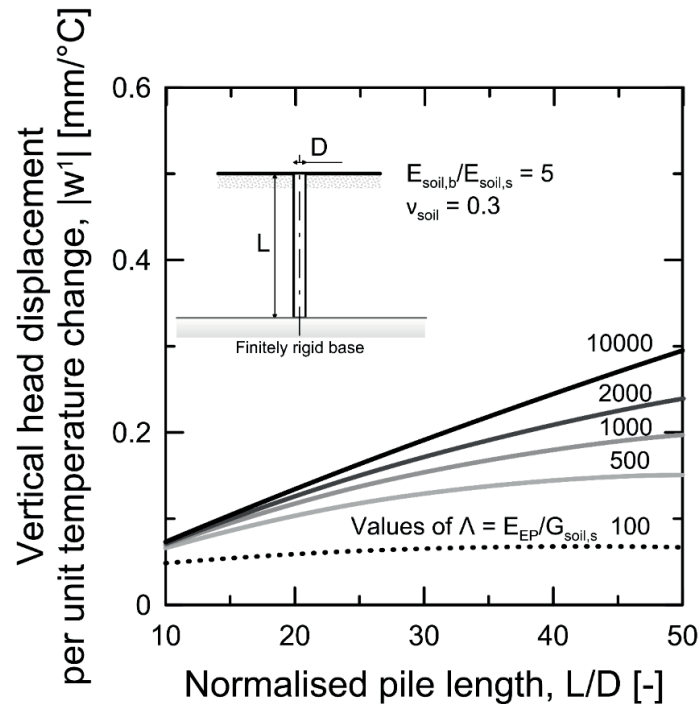


Figure 4.23: Vertical head displacement per unit temperature variation for different  $L/D$  – predominantly end-bearing pile resting on finitely rigid soil strata ( $E_{soil,b}/E_{soil,s} = 5$ ).

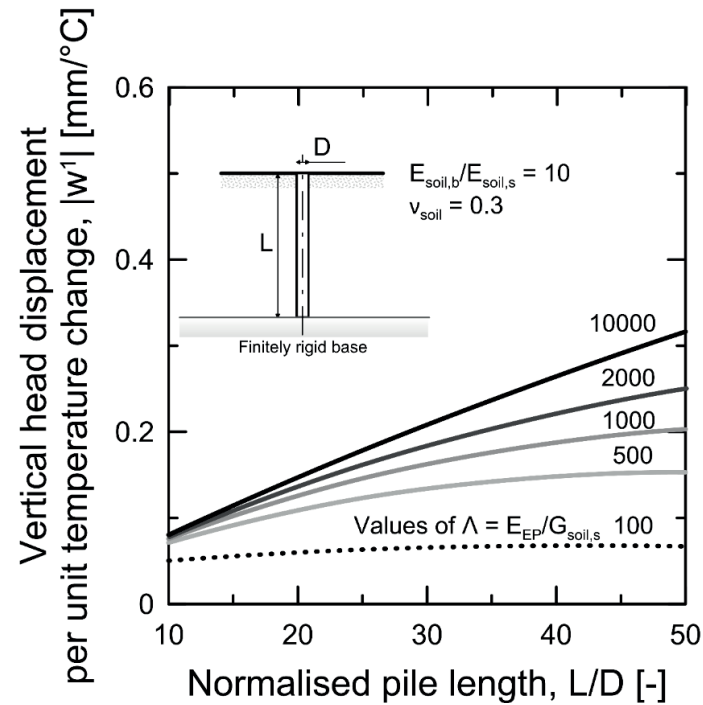
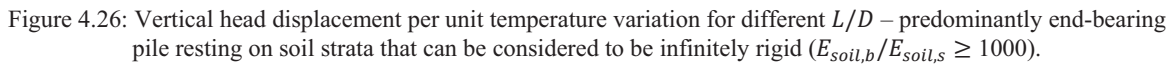
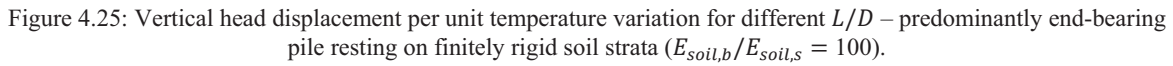


Figure 4.24: Vertical head displacement per unit temperature variation for different  $L/D$  – predominantly end-bearing pile resting on finitely rigid soil strata ( $E_{soil,b}/E_{soil,s} = 10$ ).



#### 4.5.2 Application of the interaction factor method

Solutions for the displacement behaviour of general predominantly floating energy pile groups obtained through the analytical application of the proposed interaction factor method are presented in the following. Reference is made to a situation in which all the piles are subjected to the same temperature variation and are surrounded by an elastic soil. In obtaining these solutions, variables that crucially characterise the behaviour of pile groups are considered, including the number of piles in the group, the centre-to-centre distance between the piles in the group, the slenderness ratio of the piles in the group, the Poisson's ratio of the soil and the relative depth of the soil layer. Attention is devoted to square groups of 4, 9, 16 and 25 energy piles, which are referred to in the following as 2×2, 3×3, 4×4 and 5×5 pile groups, respectively.

##### 4.5.2.1 Maximum average vertical head displacement

Figure 4.27 presents the evolution of the displacement ratio with the normalised centre-to-centre distance between the piles. Groups of 3×3, 4×4 and 5×5 energy piles of slenderness ratio of  $L/D = 25$  and pile-soil stiffness ratio of  $\Lambda = E_{EP}/G_{soil} = 1000$  are considered. The displacement ratio increases with increasing number of piles in the group, with such a mechanism becoming less pronounced for increased centre-to-centre distances between the piles in the group because of the weaker interactions. The displacement ratio for the same group of energy piles in a soil mass with a greater Poisson's ratio decreases because of the weaker interactions among the piles. These results are in accordance with the analyses presented above.

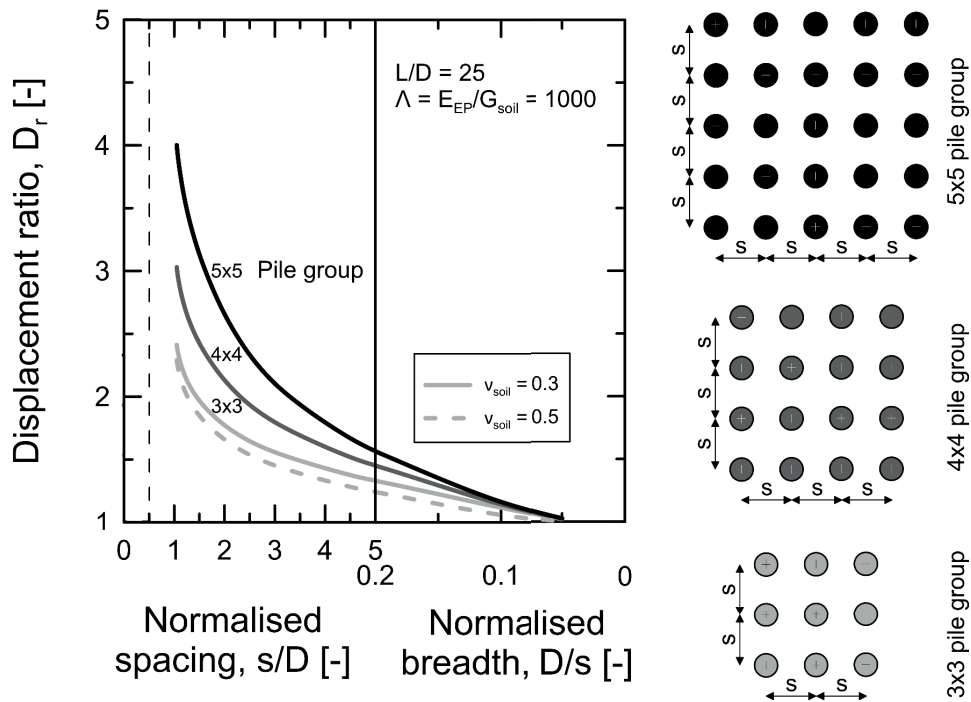


Figure 4.27: Effect of Poisson's ratio of soil on the displacement ratio.

#### 4.5.2.2 Maximum vertical head displacement

Figure 4.28 presents the evolution of the normalised vertical head displacement for the centre, side and corner energy piles in a 3×3 group of piles with normalised centre-to-centre distance between the piles. Energy piles characterised by a  $\Lambda = 1000$  and a soil of  $\nu_{soil} = 0.3$  are considered. For a general square group of energy piles in which all the piles are subjected to the same temperature variation, the maximum vertical head displacement occurs at the centre pile(s), whereas the minimum displacement occurs at the corner piles. The vertical head displacement of the side piles is intermediate. This result is also found in groups of conventional piles subjected to mechanical loads because of the more pronounced interaction among the piles in the centre zone of the group. The vertical displacement of piles, whose arrangement in two corresponding groups is the same, increases with increasing slenderness ratio of the piles. This phenomenon is in accordance with the analyses presented above.

#### 4.5.2.3 Maximum differential vertical head displacement

Figure 4.29 shows the evolution of the maximum differential displacement normalised by the maximum displacement as a function of the normalised centre-to-centre distance between the piles. Groups of 3×3, 4×4 and 5×5 energy piles of  $L/D = 25$  and  $\Lambda = 1000$  are considered. The normalised maximum differential displacement increases as the number of piles in the group increases, although increasingly less markedly for greater numbers of piles in the group. The normalised differential displacement increases with decreasing depth of the soil layer. This result is in accordance to the results presented thus far.

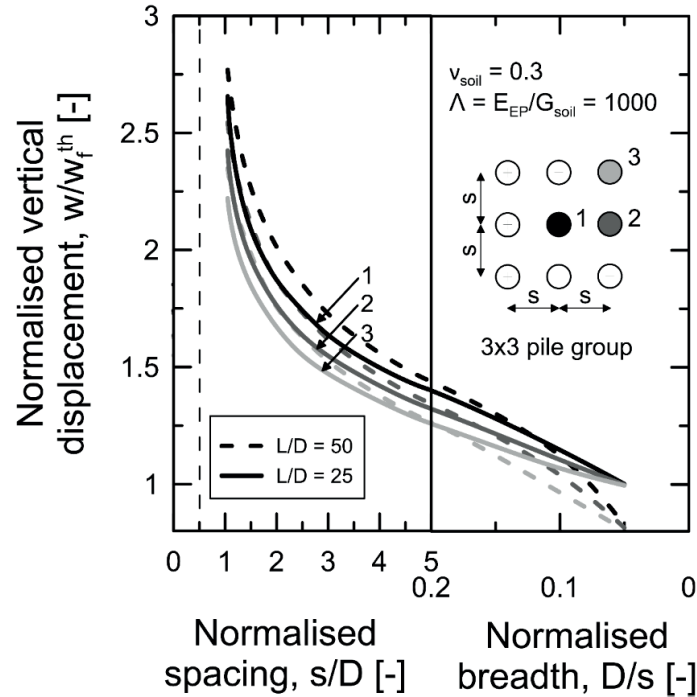


Figure 4.28: Effect of position on the vertical displacement of the piles.



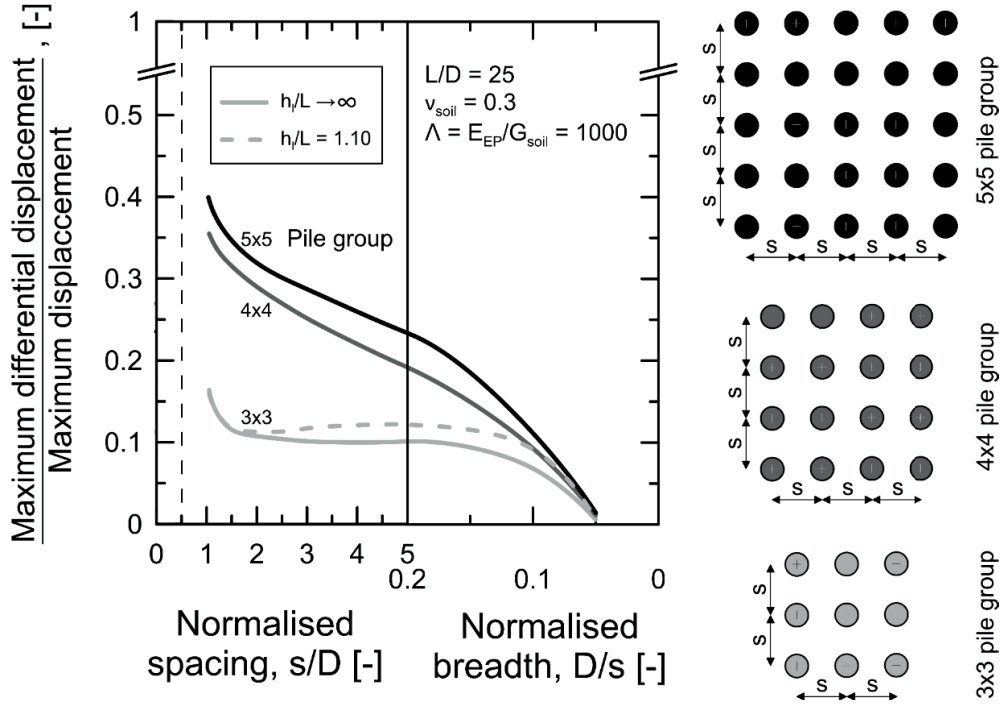


Figure 4.29: Effect of finite layer depth on the differential displacement of the piles.

#### 4.5.2.4 Illustrative example

This section presents an introduction to the types of predictions possible through the application of the proposed interaction factor method. The square group of four predominantly floating energy piles represented in Figure 4.30 with the material properties specified in Table 4.1 is considered. The energy piles are all (i) subjected to the same temperature variation of  $\Delta T = 10^\circ\text{C}$ , (ii) free of superstructure mechanical load and (iii) without any head restraint.

The objective of the analysis is to estimate the maximum average vertical head displacement of the group that may reasonably occur in a corresponding real case. While the analysis of this problem may be considered of limited practical importance because of the weak displacement interactions expected among the piles, its purpose is to highlight the features of the proposed method in an effective way. In the analytical estimation of the displacement, reference is made to an idealised group of energy piles surrounded by an elastic soil that behaves as an infinite heat reservoir at a fixed constant temperature. A comparison between the obtained displacement value and those derived from more rigorous 3-D thermo-mechanical finite element analyses is also made. Stationary analyses are performed to consider the problem wherein the soil behaves as an infinite heat reservoir at a fixed constant temperature and is characterised by a zero linear thermal expansion coefficient. Time-dependent analyses are performed to consider the problem wherein the soil can be subjected to thermally induced volumetric variations according to linear thermal expansion coefficients of  $\alpha_{soil} = 0.5, 1$  and  $2 \cdot 10^{-5} 1/^\circ\text{C}$ .

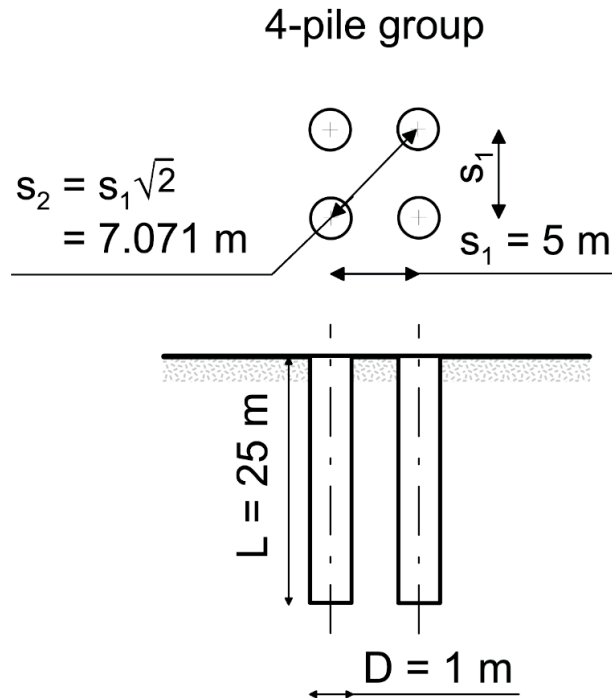


Figure 4.30: Configuration of the practical example.

Following the procedure described in Section 4.5.1, the average displacement of the pile group can be determined as follows:

1. An axisymmetric stationary finite element analysis of a single pile subjected to the considered temperature variation in an elastic soil gives

$$w^1 = -0.122 \text{ mm/}^\circ\text{C}$$

i.e., a vertical head displacement of the energy pile of  $w_i = -1.22 \text{ mm}$ .

2. The charts presented in this work enable the definition of the interaction factors for the two characteristic centre-to-centre distances between the piles

$$\Omega_{s_1} = 0.063$$

$$\Omega_{s_2} = 0.045$$

3. By applying the elastic principle of superposition of effects, the average vertical head displacement of the group is determined analytically as

$$w_k = \bar{w} = w^1 \sum_{i=1}^{i=n_{EP}} \Delta T_i \Omega_{ik} = w_i + 2(w^1 \Delta T \Omega_{s_1}) + w^1 \Delta T \Omega_{s_2} = -1.43 \text{ mm}$$

Table 4.5 presents a comparison between the average vertical head displacement of the group estimated through the interaction factor method and that determined through the more rigorous finite element method. The percentage error obtained when applying the proposed simplified method and the finite element approach is also presented. For the analysed pile group, the consideration of a displacement of unity, obtained through an axisymmetric finite element analysis in which the soil is characterised by an elastic behaviour (as in the idealisation of the pile group when applying the interaction factor concept), enables an estimate of the average vertical head displacement of the group that can be considered on the side of safety for most practical cases in which the soil thermal expansion coefficient is lower or equal than that of the piles. This does not appear to be the case for soil-pile thermal expansion coefficient ratios of greater than unity. This result is highlighted for example in the case of  $X = \alpha_{soil}/\alpha_{EP} = 2$ , for which an underestimation of the displacement of 11.40% made by the analytical prediction occurs.

Table 4.5: Comparison of predicted results for a 2×2 group of energy piles.

	Reference prediction analysis	Interaction factor method – Analytical (use of $w_i, \alpha_{soil}/\alpha_{EP}=0$ )	Interaction factor method – Analytical (use of $w_i, \alpha_{soil}/\alpha_{EP}=2$ )
	Estimated average head displacement [mm]	-1.43	-1.56
Type of alternative analysis	Calculated average head displacement [mm]	Prediction error (*) [%]	Prediction error (*) [%]
3-D FE – Elastic isothermal soil – $\alpha_{soil}/\alpha_{EP} = 0$	-1.37	4.38	12.29
3-D FE – Thermo-elastic soil – $\alpha_{soil}/\alpha_{EP} = 0.5$	-1.43	0.43	8.67
3-D FE – Thermo-elastic soil – $\alpha_{soil}/\alpha_{EP} = 1$	-1.48	-3.51	5.05
3-D FE – Thermo-elastic soil – $\alpha_{soil}/\alpha_{EP} = 2$	-1.60	-11.40	-2.18

(\*) Positive sign indicates a prediction on the side of safety.

An approach that appears suitable for overcoming this issue is the consideration of a unitary displacement obtained through an axisymmetric finite element analysis (or any other available approach suitable for such purpose) in which the soil, as the energy pile, is characterised by a thermo-elastic behaviour (in contrast to the idealisation of the pile group when applying the interaction factor concept).

In such a case, the resulting analysis of the pile-soil interaction for the single isolated pile better approaches reality. The use of this displacement value in applying the interaction factor concept allows one to obtain an estimate of the average vertical head displacement of the group that can be considered on the side of safety for most practical cases, including those in which the soil thermal expansion coefficient is higher than that of the piles. This result is corroborated by the data proposed in the last column of Table 4.5 and the results presented later.

#### 4.6 Validation of the interaction factor method

Figure 4.31 presents a comparison between the results obtained through the application of the proposed interaction factor method and more rigorous 3-D thermo-mechanical finite element analyses devoted to investigating the displacement behaviour of square groups of 4, 9, 16 and 25 predominantly floating energy piles subjected to the same positive temperature variation considered thus far. The evolution of the normalised average vertical head displacement with practical values of the normalised centre-to-centre distance between the piles is presented. The finite element analyses consider the aforementioned pile groups in soil deposits with different thermal expansion coefficients. They are considered to represent with accuracy real situations where the temperature sensitivity of the soil involves thermally induced volume variations of this medium that influence the actual displacement field of the energy pile groups.

The estimates of average vertical head displacement of the considered pile groups are always greater than the vertical head displacement characterising a single isolated pile subjected to the same temperature variation. In particular, variations of the average displacement of the pile groups comparable and even greater than those that characterise a single isolated pile can occur for increasing number of piles, such an effect becoming more pronounced for situations in which the soil-pile thermal expansion coefficient ratio exceeds unity. This phenomenon is in accordance with the considerations presented above.

According to the approximations of the proposed method, the inaccuracy between the displacement values estimated through the interaction factor method and the finite element method is greater at closer spacing between the energy piles, with such an effect becoming more pronounced as the number of piles in the group increases. A more accurate description of the problem is observed for centre-to-centre distances between the piles greater than or equal to  $s/D = 5$ , for which the application of the considered method is suggested. It is worth noting that normalised spacing comprised between  $s/D = 3$  and 5 (in correspondence of which the more pronounced lack of accuracy of the proposed method is observed) are rarely considered for practical applications of geothermal heat exchangers such as energy piles. This design choice often allows limiting thermal interactions between the energy piles and ensuring their optimal energy performance. The lack of accuracy of the proposed method for centre-to-centre distances between the piles smaller than  $s/D = 5$  appears thus to be acceptable for most of the practical analyses of energy piles. Although the suggested application of the method for normalised spacing between the piles greater than or equal to  $s/D = 5$  is associated to a weaker increase in displacement of the energy piles compared to smaller spacing because of the weaker interaction effects among these elements, this application is considered important in the analysis and design of energy pile groups. The estimates of the increase in displacement that correspond to the

application of the proposed method in the considered situations appear paramount for a thorough analysis of the displacement behaviour of energy pile groups. This statement seems to be particularly valid for energy pile groups comprising a notable number of piles and of further importance when such groups may rest on stiff soil strata or may be embedded in soil layers involving a soil-pile thermal expansion coefficient ratio greater than unity.

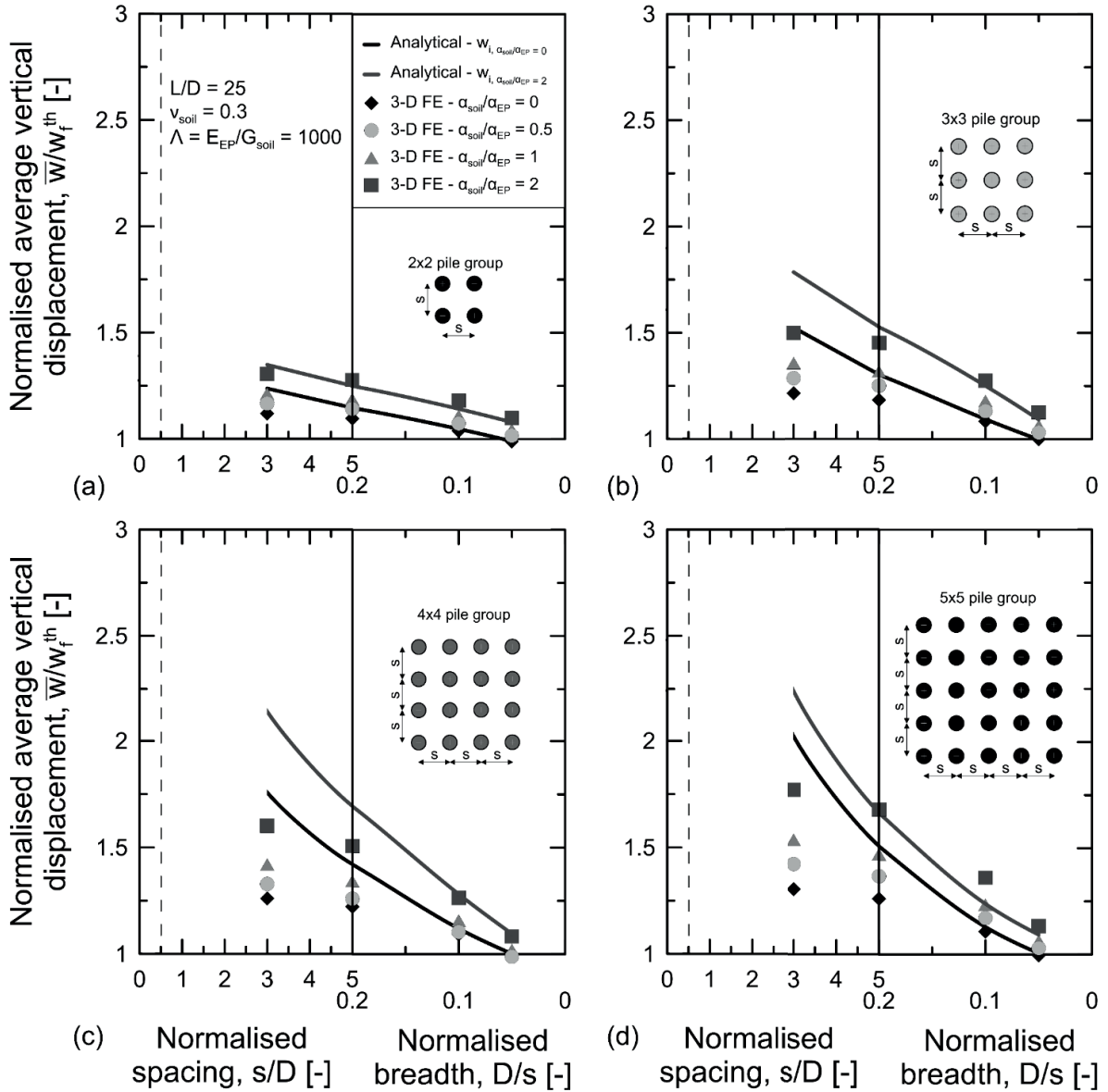


Figure 4.31: Comparison between the results obtained through the proposed analytical approach and those obtained through more rigorous 3-D thermo-mechanical finite element analyses.

The use of the two approaches referring to a unitary displacement of a single isolated energy pile in an elastic or thermo-elastic soil mass for estimating the displacement behaviour of the group, is con-

sidered to be validated based on the obtained results. The estimates of the average vertical head displacement appear to be on the side of safety in most of the considered cases. Where an underestimation is noted, the difference is small compared to the values obtained through the more rigorous finite element solutions. In particular, the estimates of the average vertical head displacement are considered sufficiently accurate for practical purposes.

Figure 4.32 presents a comparison between the results obtained by applying the interaction factor method and more rigorous 3-D thermo-mechanical finite element analyses devoted to investigating the displacement behaviour of square groups of 9 predominantly end-bearing energy piles (3×3 pile groups) subjected to the same positive temperature variation considered thus far. The normalised centre-to-centre distance between the piles of  $s/D = 6$  and the pile slenderness ratio of  $L/D = 25$  are considered. The evolution of the normalised average vertical head displacement with the base-to-shaft soil Young's modulus ratio is presented for the different values of the pile-soil stiffness ratio of  $\Lambda = E_{EP}/G_{soil,s} = 100$  and 1000 and the soil Poisson's ratio of  $\nu_{soil} = 0.3$ .

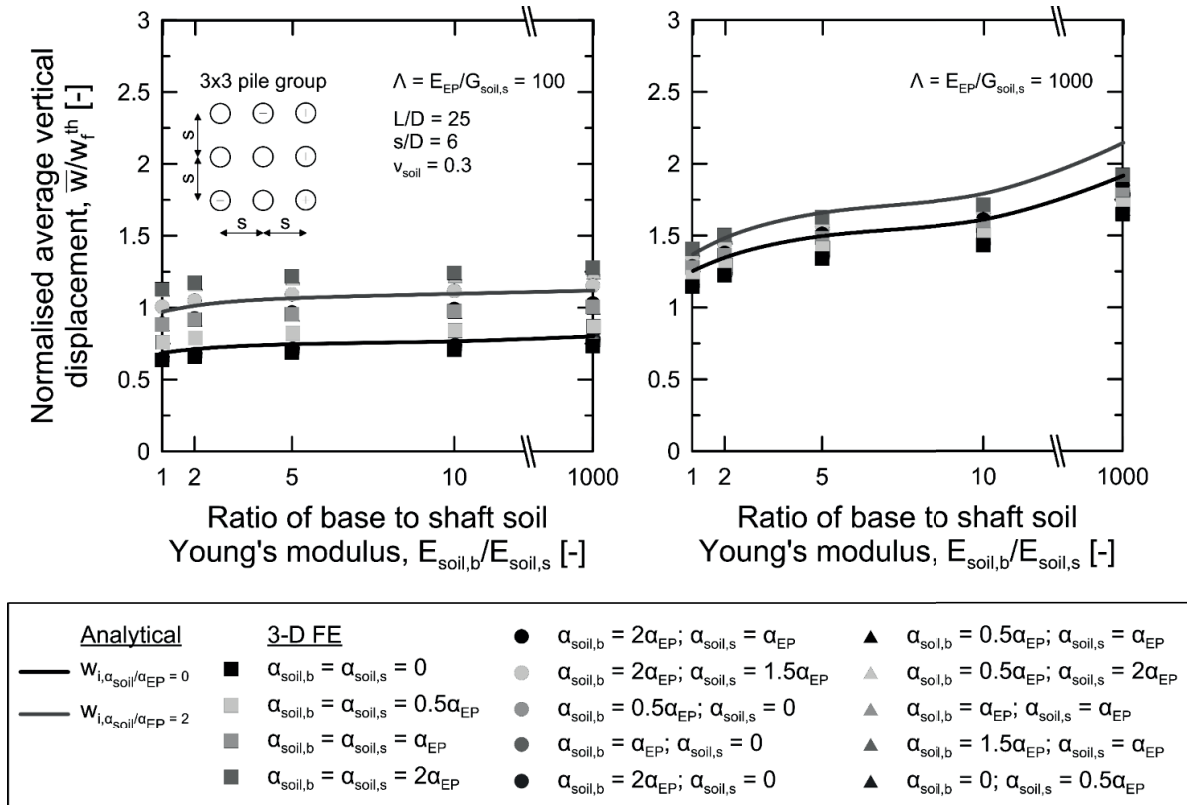


Figure 4.32: Comparison between the results obtained using the proposed analytical approach and those obtained using more rigorous 3-D thermo-mechanical finite element analyses.

Again, the average vertical head displacement of the considered pile groups is always greater than the vertical head displacement characterising a single isolated pile subjected to the same temperature variation. This phenomenon occurs because of the group effects and interactions among the piles. A greater increase of the average vertical head displacement of the group is observed for a greater pile-

soil stiffness ratio and any given base-to-shaft modulus ratio. This evidence can be attributed to the increase of the thermally induced pile displacement with increasing pile-soil stiffness ratio, irrespective of the presence of interactions among the piles.

The impact of  $\Lambda$  and  $E_{soil,b}/E_{soil,s}$  on the vertical displacement confirms the evidence highlighted in this work, for which the interaction among pile groups subjected to thermal loads increases with decreasing pile-soil stiffness ratio as well as with the presence (and increasing rigidity) of a bearing soil stratum below the pile toe.

The impact of  $\alpha_{soil,b}$  and  $\alpha_{soil,s}$  on the vertical displacement confirms the evidence presented by Rotta Loria and Laloui (2017d) (cf., Chapter 3), for which the thermally induced deformation of energy pile groups is markedly characterised by that of the surrounding soil in situations where the linear thermal expansion coefficient of the soil is higher than that of the piles. Increasing values of average vertical head displacement are generally observed for situations where  $\alpha_{soil,b} \vee \alpha_{soil,s} > \alpha_{EP}$ , the highest value of displacement characterising the situation where  $\alpha_{soil,b} = \alpha_{soil,s} = 2\alpha_{EP}$ . The reason for this is that, in these situations, the thermally induced volume variations of the soil associated with the temperature sensitivity of this medium are so noteworthy that they crucially contribute to the overall displacement field of the energy piles. The considered situations markedly differ from usual situations where  $\alpha_{soil,b} \wedge \alpha_{soil,s} \leq \alpha_{EP}$ , for which the thermally induced deformation of energy pile groups predominantly depends on that of the energy piles rather than on the thermally induced deformation of the soil. The reason for this is that, in these situations, the thermally induced volume variations of the soil that are associated with the temperature sensitivity of this medium are so small that they negligibly contribute to the overall displacement field of the energy pile groups. The usual occurrence of situations where  $\alpha_{soil,b} \wedge \alpha_{soil,s} \leq \alpha_{EP}$  and the associated negligible impact of the thermally induced soil deformation on the pile group deformation corroborate the formulation of interaction factors using an isothermal soil as reference. Such a formulation also allows determining design charts that are independent of the time that characterises the heat exchange process occurring in the energy pile groups, being thus valid for a large number of design situations irrespective of the considered stage of geothermal operation of the energy piles. The impact of  $\alpha_{soil,b}$  and  $\alpha_{soil,s}$  on the variation of the average vertical head displacement decreases with increasing values of  $\Lambda$ .

The estimates of the average vertical head displacement appear to be conservative and sufficiently accurate for practical purposes in most considered cases. In some of the cases in which an underestimation is noted, the difference is small compared to the values obtained using the more rigorous finite element simulations. However, there are cases in which the estimates of the average vertical head displacement may be considered inadequate due to the non-conservative predictions of the finite element solutions. This occurrence, which arises for the higher values of the thermal expansion coefficient of the soil layers socketing the energy pile groups and is more pronounced for the lower pile-soil stiffness ratios, is a consequence of the hypothesis of the interaction factor method to neglect the sensitivity to temperature variations for the soil surrounding the piles, but which is conversely accounted for in the finite element analyses. The use of the two approaches referring to a unitary displacement of a single isolated energy pile in an elastic or thermo-elastic soil mass for estimating the displacement behaviour of the group, is again considered to be validated based on the obtained results where  $\alpha_{soil,b} \vee \alpha_{soil,s} > \alpha_{EP}$ .



The above validates the use of the proposed design charts using the interaction factor method for estimating the average vertical head displacement of predominantly end-bearing energy pile groups resting on different stiff soil strata characterised by varying thermal expansion coefficients.

From the foregoing considerations, it may generally be concluded that the theoretical approach described in this work is capable of predicting the magnitude of vertical head displacements within the group with reasonable accuracy for most practical values of spacing between the energy piles.

According to the remarks made by Poulos (1968) when describing the usefulness of the interaction factor method in addressing conventional pile groups, it must be borne in mind that the presented theory does not consider various aspects that may influence the behaviour of pile groups such as the order of the driving of the piles, the residual stresses at the pile shaft, the layering of the soil and potential construction imperfections. This theory also does not consider cyclic aspects related to the exploitation of the energy piles as geothermal heat exchangers and the pile-slab-soil interaction. At present, the consideration of the energy piles with no head restraint appears however to include any such action in the displacement analysis of these foundations through an approach on the side of safety that may be exploited for the preliminary design of such foundations.

#### **4.7 Concluding remarks**

The method of analysis presented in this work allows the displacement behaviour of any general configuration of pile groups subjected to thermal loads to be estimated by considering only the effects of interactions between two piles and superimposing the individual effects of adjacent piles in the group. This method can be coupled to currently available classical interaction factor approaches based on design charts to estimate the displacement behaviour of pile groups subjected to mechanical loads (e.g., Poulos, 1968; Poulos and Mattes, 1974) for performing a complete analysis of the impact that both thermal and mechanical loads have on the behaviour of such foundations. This appears a notable advance in the analysis and design of energy pile groups, for which no simplified yet rational methods for investigating the group displacement behaviour were available prior to this research (Rotta Loria and Laloui, 2016b; Rotta Loria and Laloui, 2017a).

Design charts have been proposed for the analysis of the displacement interaction between semi-floating energy piles in a broad range of conditions. These charts address the displacement interaction between energy piles subjected to positive and negative temperature variations that may be associated to cooling and/or thermal energy storage operations and heating operations of these elements, respectively. The impact of many variables on this interaction, including the pile spacing, the pile slenderness ratio, the pile-soil stiffness ratio, the Poisson's ratio of soil, the depth of a finite layer, the base-to-shaft soil Young's modulus ratio, non-uniform soil moduli and the soil-pile thermal expansion coefficient ratio, has been investigated. The influence of the number of piles in the group, the spacing between the piles in the group, the slenderness ratio of the piles in the group, the Poisson's ratio of the soil and the relative depth of the soil layer on the behaviour of symmetrical and general energy pile groups has also been analysed.

Some of the main conclusions that can be drawn from this work are as follows (Rotta Loria and Laloui, 2016b; Rotta Loria and Laloui, 2017a):



- The displacement interaction factor is greater for predominantly end-bearing piles resting on infinitely rigid soil strata compared to that for predominantly floating piles surrounded by uniform soil deposits and subjected to a temperature variation.
- The interaction factor for energy piles resting on finitely rigid, i.e., compressible, soil strata generally lies between the interaction factor for energy piles resting on infinitely rigid soil strata (i.e., predominantly end-bearing energy piles) and the interaction factor for energy piles surrounded by deep uniform soil deposits (e.g., predominantly floating energy piles).
- For a group of two piles subjected to a temperature variation, the displacement interaction between the piles at a given centre-to-centre distance increases for (i) higher slenderness ratios of the piles  $L/D$ , (ii) lower pile-soil stiffness ratios  $\Lambda = E_{EP}/G_{soil}$ , (iii) lower values of the Poisson's ratio of the soil  $\nu_{soil}$ , (iv) lower layer depths  $h_l/L$ , (v) higher base-to-shaft ratios of the Young's modulus of the soil,  $E_{soil,b}/E_{soil,s}$ , (vi) higher uniformity of the soil modulus  $E_{soil}$ , and (vii) higher soil-pile thermal expansion coefficient ratio  $X = \alpha_{soil}/\alpha_{EP}$ . Interaction decreases with increasing centre-to-centre distance between the piles. Interaction is strongly characterised by the slenderness ratio of the piles.
- The effects of the aforementioned variables on the displacement interaction between two piles have a proportional influence on the displacement behaviour of any general pile group. Larger displacements are generally caused by stronger interactions among the piles in the group.
- For any given spacing between the piles, the displacement behaviour of a general pile group is markedly influenced by the number of piles. The displacement ratio  $D_r$ , which has been proposed in this work as a parameter suitable for representing the increase in displacement in a pile group in which all the piles are subjected to the same temperature variation compared to the displacement of a single pile subjected to the same average temperature variation, increases with increasing number of piles. For a limited number of piles in the group (e.g., up to 4 piles), the influence of the interactions between the piles (group effects) on the displacement behaviour of the group may be considered small and negligible for practical purposes. This consideration appears to be valid for groups of floating and semi-floating piles. It is not necessarily valid for groups of end-bearing piles because interactions have been proved to be on average 43% higher than those characteristics of the previous situations for a wide range of pile spacing. The influence of the interactions between the piles on the displacement behaviour of the group is generally considered to be significant as the number of piles increases, especially for situations in which the soil-pile thermal expansion coefficient ratio exceeds unity. Comparable and even greater variations of the average displacement of any pile group subjected to a given average temperature variation than the displacement of a single isolated pile of the same geometry and material properties of the piles of the group, and subjected to the same temperature variation, can occur.
- For a general group of energy piles in which all the piles are subjected to the same temperature variation, the maximum vertical displacement occurs at the centre pile(s), whereas the minimum displacement occurs at the corner piles. The vertical displacement of the side piles is intermediate. This phenomenon occurs because of the more pronounced interaction among

the piles in the centre zone of the group. Such a result is a consequence of the greater number of surrounding piles (and stronger associated interaction) characterising a given pile in the centre zone of the group compared to an external pile.

- The normalised maximum differential displacement increases as the number of piles in the group increases, although increasing less markedly for greater numbers of piles in the group.
- The proposed interaction factor method for the displacement analysis of general energy pile groups consists of three key steps:
  - The analysis of a single isolated pile subjected to a temperature variation to define its displacement per unit temperature variation, that is,  $w_1$ . This analysis can be carried out by referring to a chart proposed in this work that depicts absolute values of  $w_1$  for the considered design situations. Otherwise, it may be performed with any analytical or numerical method currently available for such purpose.
  - The definition of the interaction factor  $\Omega$  for a pair of two piles at any given centre-to-centre distance. This step can be accomplished by referring to the design charts proposed in this work.
  - The analytical analysis of the displacement behaviour of the pile group. This analysis can be performed by employing the elastic principle of superposition of effects with reference to the displacement interaction for a group of two piles and by applying the equation proposed in this work.
- Attention has to be paid in the geotechnical characterisation of sites to the presence and rigidity of bearing soil strata because these characteristics have a marked effect on the vertical displacement of pile groups subjected to thermal loads. The group effects among piles subjected to thermal loads may be markedly underestimated if reference may be made to predominantly floating rather than end-bearing pile groups.
- Comparisons with results of 3-D thermo-mechanical finite element analyses allow concluding that the theoretical method described in this work is capable of predicting the magnitude of vertical head displacements within energy pile groups with comparable accuracy to that obtained by applying more rigorous approaches such as the finite element method. This statement appears to be valid for most of the problems encountered in practice, although experimental evidence is needed for its further validation.

## **Chapter 5**

# **The interaction factor method for energy pile groups based on analytical models**

Over the last fifty years, the interaction factor method has been widely used to address the vertical displacement and the increased deformation of conventional pile groups subjected to mechanical loads when group effects and interactions occur among the piles. Design charts and analytical models have been proposed to serve the considered analysis method. In recent years, the interaction factor method has been extended to address energy pile groups subjected to thermal loads. Design charts have been proposed. However, prior to this study, no analytical models capable of analysing the vertical displacement and the increased deformation of energy piles subjected to thermal loads in a more comprehensive and flexible way than through design charts have been available. To address this challenge, this study presents two analytical performance models for analysing the vertical displacement of energy pile groups subjected to thermal loads, based on the analysis of a single isolated energy pile. Comparisons with three-dimensional finite element analyses outline that the models can accurately capture the displacement of energy piles without the expense of a full rigorous analysis. This evidence makes the present performance models useful tools for the analysis and design of energy piles under serviceability conditions.

### **5.1 Introduction**

Over the last fifty years, the interaction factor method proposed by Poulos (1968) has been widely used for the analysis of the vertical displacement and increased deformation of pile groups caused by mechanical loads when group effects and interactions are present. This method assumes that the vertical displacement of any pile group, e.g., under serviceability conditions, may be estimated through elastic theory and superposition of effects by knowing (i) the displacement interaction relationship –

quantified by an interaction factor – among two piles of the group considered in an isolated pair, (ii) the vertical displacement of one reference pile in the group that is the source of interaction for the receiver pile in the pair and (iii) the loads applied to the piles. The expediency and capability of this method to model the problem previously described, which, although being an approximation of reality, is often considered for design purposes, have played a major role for its diffusion.

Originally, design charts for floating and end-bearing conventional piles have been proposed by Poulos (1968) and Poulos and Mattes (1974), respectively, to serve the aforementioned method in estimating the interaction factor. Afterward, analytical models have been proposed for floating and end-bearing conventional piles by Randolph and Wroth (1979b) and Randolph and Wroth (1979a), respectively. An alternative formulation of these models by Chow (1986) and an improvement related to the definition of the interaction factor by Mylonakis and Gazetas (1998) have been later presented. The analytical models have been developed due to their capability of estimating the interaction factor in a broader range of conditions and performing more comprehensively and flexibly than the charts in the analysis of pile groups. In these models, differently from the original method proposed by Poulos (1968), the interaction factor has been defined with reference to the vertical displacement of a source pile assumed to be isolated. The main reason for this choice has been the possibility to estimate the vertical displacement caused by mechanical loads through closed form solutions.

In recent years, the interaction factor method has been extended and proven to be a suitable means for estimating the vertical displacement of energy piles subjected to thermal loads (Rotta Loria and Laloui, 2016b).

Design charts have been proposed for floating and end-bearing energy piles by Rotta Loria and Laloui (2016b) and Rotta Loria and Laloui (2017a), respectively (cf., Chapter 4). The design charts and interaction factor method for energy piles have been developed with reference to the vertical displacement of an isolated energy pile. The main reason for this choice has been that the vertical displacement of piles subjected to thermal loads cannot be determined through closed form solutions, i.e., running a numerical analysis is required. Therefore, considering the source pile as isolated allows for the use of a simpler analysis (e.g., axisymmetric) than that required for a pile in a pair (e.g., three-dimensional), and preserves the expediency of a simplified procedure such as the interaction factor method that would vanish otherwise.

Despite the aforementioned developments, prior to this study no analytical models capable of estimating the vertical displacement of energy pile groups subjected to thermal loads and accounting for group effects and interactions have been available.

Observing such a challenge, the present study (Rotta Loria et al., 2017b) addresses the development of two analytical performance models, i.e., a *layer model* and a *continuous model*, capable of the following: (i) estimating the vertical displacement with depth of a thermally loaded source pile and receiver pile in a pair starting from the analysis of a single isolated pile; (ii) defining the interaction factor with depth between these piles regardless of the design situation; and (iii) analysing the vertical displacement with depth of any energy pile groups using the interaction factor method.

## 5.2 Problem definition and solution approach

### 5.2.1 The problem

In the problem addressed by the interaction factor method (see for further details, e.g., Randolph and Wroth, 1979b; Mylonakis and Gazetas, 1998; Rotta Loria and Laloui, 2016b), the piles are identical cylindrical solids characterised by a length,  $L$ , and a diameter,  $D$ . When considered in a pair, the piles are located at a centre-to-centre distance (i.e., spacing),  $s$ , apart from each other.

When accounting for the effects caused by thermal loads, the source pile is assumed to be subjected to a (positive or negative) temperature variation,  $\Delta T$ . The influence of vertical mechanical loads may be considered as well by assuming that the source pile is subjected to a vertical mechanical load applied at its head,  $P$ . The piles are assumed to be free to move vertically at their head.

The loading of the source pile results in a deformation of this element that modifies the displacement field along its length, influences the surrounding soil and changes the displacement field of the receiver pile. Thermal loads involve a proportion of the pile (and surroundings) that moves upwards while another one moves downwards around the so-called null point of the vertical displacement (Laloui et al., 2003). Mechanical loads involve a movement of the pile (and surroundings) in the same direction of the applied load along the entire pile length.

In principle, a complete description of the problem described above would require three-dimensional (3-D) time-dependent numerical analyses because of its three-dimensional and time-dependent character. For example, the vertical displacement field is generally not homogeneous in the three-dimensional space because of the stiffness and presence of the piles. Bending moments occur in the piles and in the soil due to the compatibility and continuity of the displacement field. The heat exchange involves temperature variations with time that cause thermally induced deformations of the soil and potentially of the receiver pile.

In practice, an approximate yet realistic analytical description of the considered problem can be performed based on a number of simplifying hypotheses and considerations presented below.

### 5.2.2 Idealisation, hypotheses and considerations

In the following, the idealisation of the problem described above and a number of hypotheses and considerations that have been widely used in developments of the interaction factor method for piles subjected to mechanical loads (Poulos and Davis, 1980; Fleming et al., 2008) are extended to piles subjected to thermal loads based on previous studies (Rotta Loria and Laloui, 2016b; Rotta Loria and Laloui, 2017a) (cf., Chapter 4).

The piles are identical, isotropic, homogeneous and uniform cylindrical solids. The soil is a semi-infinite isotropic mass assumed to be composed of a unique homogeneous layer or different horizontal layers. The aforementioned assumptions represent typical approximations of reality employed in engineering theory. When applied with judgement, however, they can adequately represent real problems (Poulos and Davis, 1980).

A uniform temperature variation is applied to the source pile. A vertical mechanical load may be applied at the pile head as well. The temperature variations observed within energy piles are not uniform (Abdelaziz and Ozudogru, 2016a; Rotta Loria and Laloui, 2017d) but can be considered uniform by choosing representative values of the temperature field within the cross-section and along the length of the pile (Abdelaziz and Ozudogru, 2016b; Loveridge and Powrie, 2016). The consideration of a constant mechanical load applied at the pile head follows the widely used assumption of a negligible contribution of the uppermost slabs or other shallow foundations in the bearing capacity of piles for preliminary analyses and designs on the safety side (Poulos and Davis, 1980; Bowles, 1988; Fleming et al., 2008).

No head restraint is present (i.e., infinitely flexible slab). This assumption conservatively analyses the vertical displacement of piles according to the widely used assumption of a negligible contribution of the uppermost slabs or other shallow foundations in the deformation of piles, at least for preliminary analyses and designs (Poulos and Davis, 1980; Bowles, 1988; Fleming et al., 2008).

No slip or yielding occurs between the piles and the adjacent soil (i.e., perfect contact between the pile and soil is assumed). Although not valid in situations where mechanical and thermal loads of significant magnitudes may be applied to energy piles (especially if predominantly floating) (Rotta Loria et al., 2015b), these conditions have been shown through full-scale experimental tests and numerical analyses (Rotta Loria and Laloui, 2017d) to characterise serviceability conditions targeted by the interaction factor method.

The piles are characterised by a linear thermo-elastic behaviour. The soil is characterised by a linear elastic behaviour. Loading situations in which reversible conditions prevail are thus assumed, according to the previous hypothesis of no slip or yielding between the piles and the adjacent soil. The present hypothesis involves that the effect of thermal and mechanical loads can be superimposed at any time, based on the principle of superposition of effects, via separate analyses addressing thermal and mechanical loads.

Considering the soil to be characterised by an elastic behaviour involves assuming it is an infinite heat reservoir that remains at a constant fixed temperature. Hence, no influence caused by any temperature sensitivity of the soil or thermal interaction between the source pile and the receiver pile is considered. Although approximate, this approach has been proven to be valuable (Rotta Loria and Laloui, 2016b; Rotta Loria and Laloui, 2017a) because (i) it develops solutions of the interaction factor that are independent of the actual heat exchange occurring in the pile group and (ii) it takes advantage of the negligible role of the thermally induced soil deformation on the interaction between piles characterising all usual situations where the thermal expansion coefficient of the soil is (significantly) lower than or (at least theoretically) equal to that of the piles (Rotta Loria and Laloui, 2017d; Rotta Loria and Laloui, 2016b). Only in situations where the thermal expansion coefficient of the soil is higher than that of the piles does the thermally induced soil deformation have a marked effect on the pile interaction, especially at successive stages of geothermal operations of the piles (Rotta Loria and Laloui, 2017d). In these situations, a simplified yet valuable approach for capturing the group displacement via the design charts has been proven to result from interaction factors still referring to pile pairs in isothermal soil (Rotta Loria and Laloui, 2016b; Rotta Loria and Laloui, 2017a). As it is shown later in this work, the referenced approach is not needed for capturing the group displacement via the analytical performance models presented. The reason for this is because these models give the



lower and upper boundaries of the displacement that may be expected for energy pile groups embedded in soils characterised by all of thermal expansion coefficient values likely to be found in practice.

The displacement field characterising the thermally loaded source pile in the pair is assumed to be equal to that in the single isolated case. This assumption disregards the effect of the stiffness of the receiver pile on the deformation of the source pile, which appears to be justified in view of the impractical spacing between the piles for which this effect is observed and is significant (Rotta Loria and Laloui, 2016b).

The displacement field characterising the receiver pile is considered to be lower than that of the soil around the source pile. This assumption accounts for the greater stiffness of piles than that of the surrounding soil.

The displacement field in the soil around a single isolated pile is assumed to be homogeneous, whereas that around a pair of piles is considered to be non-homogeneous. This approach captures the actual deformation behaviour of the source and receiver piles in a pair with accuracy.

The displacement field within the piles is assumed to be homogeneous. This hypothesis is justified in view of the notable stiffness that usually characterises energy piles compared to that of the soil.

The effect of bending moments on the displacement field of the piles and the soil is neglected. This consideration is justified in view of the small impact of bending moments on the vertical displacement of the piles in the considered problem.

### 5.2.3 The solution approach

The main consequence arising from the considerations specified above is that the analysis of the vertical displacement of a loaded source pile and a receiver pile in a pair may be performed based on the analysis of a single *isolated* pile subjected to the same load through the interaction factor method. In this framework, two alternative analytical performance models devoted to the considered purpose, with reference to the influence of thermal loads (e.g., with depth), are presented. To date, this analysis may have been performed only by referring to the head of piles through design charts (Rotta Loria and Laloui, 2016b; Rotta Loria and Laloui, 2017a) (cf., Chapter 4). This (semi-analytical) analysis may be similarly applied to pile groups subjected to vertical mechanical loads. It consists of five key steps (cf., Figure 5.1):

1. The analysis of a single isolated source pile subjected to a temperature variation to define the vertical displacement,  $w_i(z)$ , and the shear stress,  $\tau_i(z)$ , along the pile shaft. This analysis can be performed with any of the numerical methods currently available for this purpose, although preferably with the finite element method.
2. The determination of the vertical displacement field of the soil,  $w(r, z)$ , at any given radial distance,  $r$ , from the axis of the previously analysed single isolated pile subjected to a temperature variation, and along the vertical coordinate,  $z$ . This step can be performed using the performance models presented in this work and determines the approximate pile-soil interaction factor as

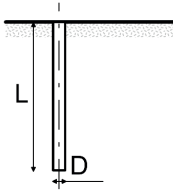
$$\tilde{\Omega}(r, z) = \frac{w(r, z)}{w_i(z)} \quad (5.1)$$

3. The analysis of the vertical displacement,  $w_j(s, z)$ , of a receiver pile located at a spacing  $s = r + R$  (where  $R = 0.5D$  is the pile radius) from the source pile that was previously considered to be isolated. This step can also be performed with the performance models presented in this work.
4. The determination of the corrected pile-soil-pile interaction factor as (Randolph and Wroth, 1979b; Mylonakis and Gazetas, 1998; Rotta Loria and Laloui, 2016b)

$$\Omega(s, z) = \frac{w_j(s, z)}{w_i(z)} \quad (5.2)$$

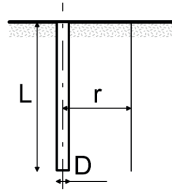
1. Analysis of single isolated pile

$w_i(z), \tau(z)$



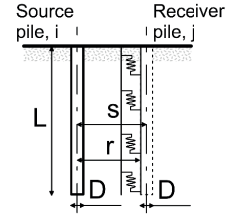
2. Definition of vertical displacement of soil and approximate interaction factor

$$w(r, z) \quad \tilde{\Omega}(r, z) = \frac{w(r, z)}{w_i(z)}$$



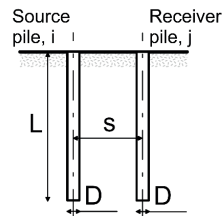
3. Analysis of vertical displacement of receiver pile

$w_j(s, z)$



4. Definition of corrected interaction factor

$$\Omega(s, z) = \frac{w_j(s, z)}{w_i(z)}$$



5. Analytical analysis of general pile groups

$$w_j(z) = w^1(z) \sum_{i=1}^{i=n_{EP}} \Delta T_i \Omega_{ij}(s, z)$$

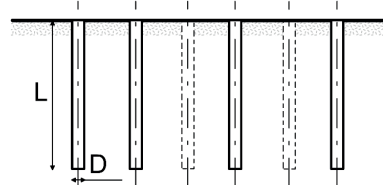


Figure 5.1: The solution approach for analysing the vertical displacement of general energy pile groups.



5. The analysis of the vertical displacement of any pile,  $j$ , composing a general group with a total number of piles,  $n_{EP}$ , in which some or all of the piles may be subjected to a temperature variation as (Rotta Loria and Laloui, 2016b)

$$w_j(z) = w^1(z) \sum_{i=1}^{i=n_{EP}} \Delta T_i \Omega_{ij}(s, z) \quad (5.3)$$

where  $w^1(z)$  is the vertical displacement along the length of a single isolated pile per unit temperature variation,  $\Delta T_i$  is the applied temperature variation to pile  $i$ , and  $\Omega_{ij}$  is the interaction factor for two piles in a pair corresponding to the spacing between pile  $i$  and pile  $j$ .

Throughout the following development of the performance models that constitute the core of steps 2 and 3,  $w_i(z)$  and  $\tau_i(z)$  are assumed to be known.

### 5.3 Layer model

#### 5.3.1 Soil vertical displacement and approximate pile-soil interaction factor

The present model assumes that the soil around the shaft of piles subjected to loads that induce vertical deformation may be idealised as consisting of concentric cylindrical elements, with shear stresses distributed on the surface of each element (cf., Figure 5.2 (a)). For vertical equilibrium, the magnitude of the shear stress on each cylindrical element must decrease inversely with the vertical surface area of the element (Cooke et al., 1981).

The equilibrium equation along  $z$  written for an element with regards to a reference cylindrical coordinate system  $(r, \theta, z)$  in which the effects of volume forces due to body loads are neglected is

$$\frac{\partial \tau_{rz}}{\partial r} + \frac{\tau_{rz}}{r} + \frac{\partial \sigma_{zz}}{\partial z} = 0 \quad (5.4)$$

where  $\tau_{rz} = \tau$  is the shear stress increment and  $\sigma_{zz} = \sigma_z$  is the vertical stress increment. The application of thermal loads in the framework of energy piles assumes that  $\partial \tau / \partial r \gg \partial \sigma / \partial z$ . This phenomenon, which has been verified through finite element analyses, characterises regions of soil in the vicinity of the pile shaft. It was also observed for the application of mechanical loads in the framework of conventional piles (Frank, 1975; Baguelin and Frank, 1979). From this consideration, it follows that equation (5.4) may be simplified as shown by Frank (1975) and integrated to yield the general solution for the shear stress in the soil as

$$\tau(r, z) = \frac{\tau_i(z)R}{r} \quad (5.5)$$

The shear stress may be considered to be constant with depth in conventional applications of piles subjected to mechanical loads. The reason for this is because the vertical deformation of piles subjected to mechanical loads can be considered in a plane state of strain, i.e., independent of the depth. The application of a mechanical load at the head of piles involves an approximately constant distribution of the vertical displacement with depth. This consideration is particularly applicable to the analysis of rigid piles with a predominantly friction character but is also acceptable for most piles.

The shear stress varies significantly with depth in innovative applications of piles subjected to thermal loads, i.e., energy piles. The reason for this is because the vertical deformation of piles subjected to thermal loads is crucially dependent on the depth and thus not associated with a plane state of strain. The application of a thermal load along the length of piles involves at best a linear distribution of the vertical displacement with depth and at worst a notably non-linear distribution of the vertical displacement (becoming more pronounced with increasing pile compressibility and slenderness). This consideration is applicable to the analysis of both rigid and deformable piles whether they have a predominantly frictional or end-bearing character.

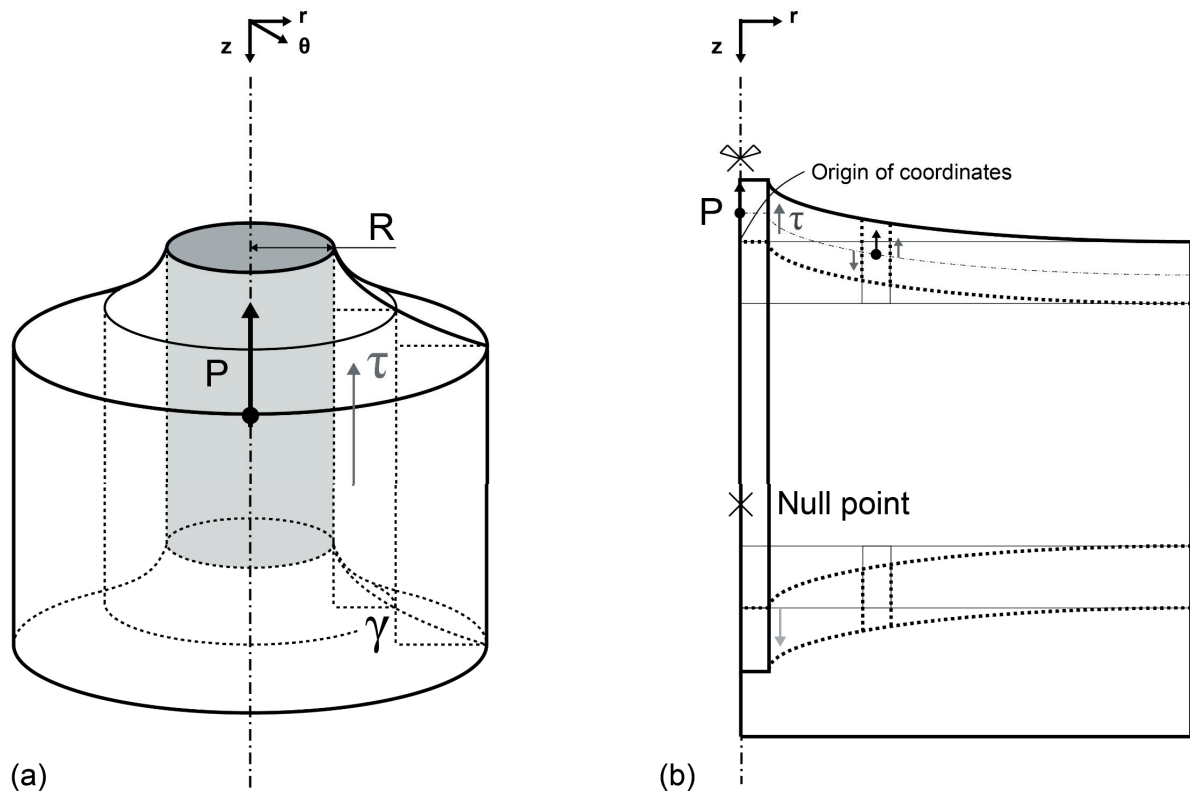


Figure 5.2: The layer model concept: (a) the mode of deformation of a layer of cylindrical elements characterising any pile-soil system and (b) the effect of this mode of deformation.

The shear strain associated with the aforementioned shear stress can be computed according to the elastic theory as

$$\gamma = \frac{\partial w}{\partial r} + \frac{\partial u}{\partial z} = -\frac{\tau}{G_{soil}} \quad (5.6)$$

where  $u$  is the radial displacement and  $G_{soil}$  is the shear modulus of the soil. In the present problem, both  $u$  and  $w$  depend only on  $r$  and  $z$ , respectively, and not on the angular coordinate,  $\theta$ . This aspect arises because there is an invariance of the displacement field around the latter axis. Moreover, because no twist characterises the pile, there is no orthoradial component,  $v$ , in the displacement field.

The application of thermal loads in the framework of energy piles assumes that  $\partial w / \partial r \gg \partial u / \partial z$ . This phenomenon, which has been verified through finite element analyses, characterises regions of soil in the vicinity of the pile shaft. Together with the assumption of a negligible variation of  $\partial \sigma / \partial z$ , it physically represents a negligible interaction between different soil layers with depth (cf., Figure 5.2 (b)).

From the above consideration and the combination of equations (5.5) and (5.6), the first-order partial differential equation is found

$$\frac{\partial w}{\partial r} = -\frac{\tau_i(z)R}{rG_{soil}} \quad (5.7)$$

Integration of equation (5.7) yields the general solution for the vertical displacement of the soil as (Randolph and Wroth, 1978)

$$w(r, z) = w_i(z) - \frac{\tau_i(z)R}{G_{soil}} \ln\left(\frac{r}{R}\right) \quad (5.8)$$

The general solution for  $w(r, z)$  expressed in equation (5.8) can be normalised with respect to  $w_i(z)$  to give the approximate pile-soil interaction factor as

$$\tilde{\Omega}(r, z) = 1 - \frac{\tau_i(z)R}{w_i(z)G_{soil}} \ln\left(\frac{r}{R}\right) \quad (5.9)$$

The parameter  $\tilde{\Omega}(r, z)$  expresses the effect of loading a single isolated source pile on the surrounding soil in terms of a displacement variation.

Randolph and Wroth (1978) solved equation (5.7) for determining the displacement of the pile at its shaft,  $w_i$ , by introducing a “magical radius”,  $r_m$ , at which the shear stresses (and thus the vertical displacements) in the soil become vanishingly small. Randolph and Wroth (1979b) also obtained a

general expression for the vertical displacement of the soil expressed in equation (5.8) that is effectively independent of  $w_i$  and heavily dependent on  $r_m$ . In the framework of conventional piles subjected to mechanical loads, the magical distance  $r_m$  has been found (Randolph and Wroth, 1978) to be (i) almost constant with depth as a consequence of the aforementioned plane state of strain and (ii) greater than the length of the pile, i.e.,  $r_m = 2.5L(1 - \nu_{soil})$  for predominantly friction piles. In the framework of energy piles subjected to thermal loads, this magical distance has been found to be (i) not constant with depth and (ii) generally smaller than the length of the pile, e.g.,  $r_m = 0.5L(1 - \nu_{soil})$  at the ends of predominantly friction piles. Based on these considerations, the application of relationships such as those proposed by Randolph and Wroth (Randolph and Wroth, 1979b; Randolph and Wroth, 1978) for describing conventional piles subjected to mechanical loads appears to be unsuitable for describing piles subjected to thermal loads. The above relationships would be valid only for certain regions of piles subjected to thermal loads because of the variable character of  $r_m$  with depth. A proof of the notable variability of  $r_m$  for piles subjected to thermal loads is given in Section 5.5. The lower magnitude of  $r_m$  for piles subjected to thermal loads compared to that for piles subjected to mechanical loads may be considered to be representative of the interaction effects on pile group behaviour.

The dependence on the depth of the layer model expressed in equations (5.7) and (5.8), together with the assumption of no interaction between the elements and associated layers in the surrounding soil, make this model easily applicable to analysing the vertical displacement of stratified (non-uniform) soil deposits. Application examples to these design situations are given in Section 5.5.6.

### 5.3.2 Receiver pile vertical displacement and corrected pile-soil-pile interaction factor

The presence of a receiver pile usually decreases the displacement of the soil (Mylonakis and Gazetas, 1998). This effect becomes larger with increasing relative stiffness of the receiver pile compared to that of the soil.

To account in a simple yet realistic way for the interplay between a receiver pile and the soil, the receiver pile is modelled as a beam supported with springs of a given stiffness characteristic of the surrounding soil medium,  $K_s$ . A possible formulation for  $K_s$  reads (Mylonakis, 2001)

$$K_s \approx \frac{1.3G_{soil}}{\pi D} \left( \frac{E_{EP}}{E_{soil}} \right)^{-\frac{1}{40}} \left( 1 + 7 \left( \frac{L}{D} \right)^{-0.6} \right) \quad (5.10)$$

where  $E_{EP}$  is the Young's modulus of the pile and  $E_{soil}$  is the Young's modulus of the soil.

Considering the vertical equilibrium of an element of a receiver pile whose axis is located at a spacing  $s$  from that of a corresponding element of the thermally loaded source pile gives the following equation (cf., Figure 5.3)

$$\left( \sigma_z \left( z - \frac{dz}{2} \right) - \sigma_z \left( z + \frac{dz}{2} \right) \right) A_{EP} + \iint K_s (w(\tilde{r}, \tilde{z}) - w_j(s, \tilde{z})) dS = 0 \quad (5.11)$$

where  $dz$  is the infinitesimal height of the element,  $A_{EP}$  is its cross-sectional area,  $s - R \leq \tilde{r} \leq s + R$ ,  $z - \frac{dz}{2} \leq \tilde{z} \leq z + \frac{dz}{2}$  and  $dS$  is an infinitesimal increment of the vertical external surface of the considered element. A rigorous solution of equation (5.11) would require integration of  $(w(\tilde{r}, \tilde{z}) - w_j(s, \tilde{z}))$  over  $dS$  because of its non-homogeneity along the perimeter of the cross-section and the height of the element. An approximate yet realistic approach for solving this equation relies on considering a value of displacement  $w(\tilde{r}, \tilde{z}) = w(r, z)$ , where  $r = s - R$ . Three main advantages arise from this choice: (i) the greater average shear stress that is mobilised over the vertical external surface of the elements of a receiver pile compared to the shear stress mobilised in the soil at a distance  $s$  from a single isolated pile is implicitly accounted for through a conservative approach; (ii) the non-homogeneity of the displacement that is mobilised over the vertical external surface of the elements of a receiver pile is implicitly considered; and (iii) integrating the displacement  $(w(\tilde{r}, \tilde{z}) - w_j(s, \tilde{z}))$  over  $dS$  can be avoided with a simpler and expedient resolution of equation (5.11). Based on these considerations, equation (5.11) becomes

$$\frac{d\sigma_z}{dz} A_{EP} dz - \pi D K_s (w(r, z) - w_j(s, z)) dz = 0 \quad (5.12)$$

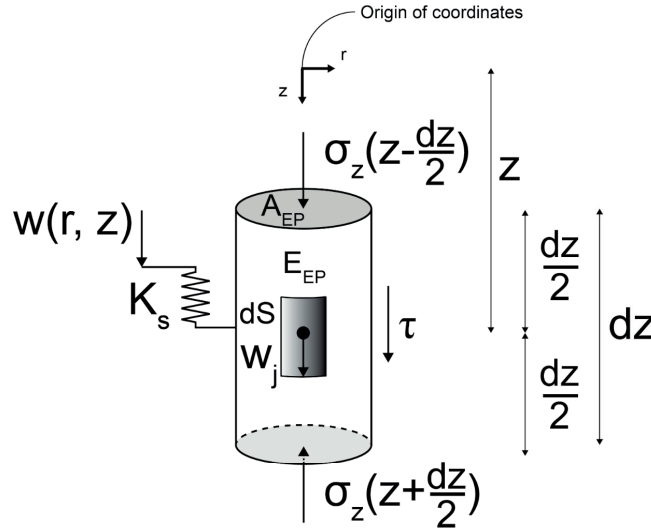


Figure 5.3: Vertical equilibrium of an element of a receiver pile.

Using the constitutive equations, equation (5.12) can be rewritten in the form of the second-order differential equation governing the equilibrium of *each element* of the receiver pile (Mylonakis and Gazetas, 1998)

$$\frac{\partial^2 w_j}{\partial z^2} - \lambda_{lt}^2 (w(r, z) - w_j(s, z)) = 0 \quad (5.13)$$

where  $\lambda_{lt}$  is a load-transfer coefficient given by

$$\lambda_{lt} = \sqrt{\frac{\pi D K_s}{A_{EP} E_{EP}}} \quad (5.14)$$

In principle, the presence of the relative displacement ( $w(r, z) - w_j(s, z)$ ) in equation (5.13) is not in accordance with the no slip hypothesis presented in Section 5.2.2. However, in practice, it can be associated with the non-homogeneous distribution of the shear stress around a receiver pile in a pair and more generally around any piles in a group.

Equation (5.13) needs two boundary conditions to be solved. The first boundary condition is chosen based on the consideration that because the pile is free to displace vertically at its head no vertical stress will be present in this setting. This condition can be mathematically expressed through the constitutive equations as (Mylonakis and Gazetas, 1998)

$$\left. \frac{\partial w_j}{\partial z} \right|_{z=0} = 0 \quad (5.15)$$

The second boundary condition is chosen from the assumption that where the shear stress is equal to zero along the soil profile adjacent to a receiver pile, the displacement of this pile is the same as that of the soil (i.e.,  $w(r, z) - w_j(s, z) = 0$ ). Because the present layer model accounts for no interaction between the different layers of elements, it may be considered that the location where zero thermally induced shear stress occurs coincides with the location where zero thermally induced vertical displacement occurs. This phenomenon arises because, for compatibility, upward, downward and zero vertical displacements will be caused if and only if upward, downward and zero shear stresses are applied *at the corresponding element* in the *adjacent soil*. Knowledge of the location where the vertical displacement of the soil is  $w(r, z) = w_j(s, z) = 0$  is thus of interest to define the second boundary condition. This location can be determined from the analysis of a single isolated pile according to equation (5.8). The discussed boundary condition can be mathematically expressed as

$$w_j(s, z = z|_{w=0}) = w(r, z = z|_{w=0}) = 0 \quad (5.16)$$

Equation (5.13), together with the boundary conditions expressed in equations (5.15) and (5.16), can calculate the values of  $w_j(s, z)$ . These values finally determine the values of the corrected pile-soil-pile interaction factor,  $\Omega(s, z)$ .

## 5.4 Continuous model

### 5.4.1 Soil vertical displacement and approximate pile-soil interaction factor

The present model assumes that the continuous distribution of the shear stresses at the pile shaft can be approximated as a distribution of point loads acting at the centre of the elements composing these piles as if they were linear entities generated by nodes (cf., Figure 5.4 (a)). At some distance, the effects of such stresses and point loads are indistinguishable (Chow, 1986).

The assumption highlighted above involves the equations of Mindlin (1936) for a vertical point load acting in a semi-infinite, homogeneous and isotropic elastic half-space being exploited to determine through the elastic principle of superposition of effects the vertical displacement caused by a distribution of point loads acting on a single isolated (thermally loaded) source pile at any location in the surrounding soil.

The vertical displacement of the soil can be defined as (Mindlin, 1936)

$$\begin{aligned}
 w(r, z) &= \sum_{l=1}^m w_{kl} \\
 &= \sum_{l=1}^m \frac{P_l}{16\pi G_{soil}(1 - \nu_{soil})} \left( \frac{3 - 4\nu_{soil}}{R_1} + \frac{8(1 - \nu_{soil})^2 - (3 - 4\nu_{soil})}{R_2} \right. \\
 &\quad \left. + \frac{(z_l - z_k)^2}{R_1^3} + \frac{(3 - 4\nu_{soil})(z_l + z_k)^2 - 2z_l z_k}{R_2^3} + \frac{6z_l z_k (z_l + z_k)^2}{R_2^5} \right) \quad (5.17)
 \end{aligned}$$

where  $w_{kl}$  is the vertical displacement of any soil node,  $k$ , caused by a point load,  $P_l = 2\pi R L_{seg} \tau_l$ , applied to the node,  $l$ , of a source pile (for which  $L_{seg}$  is the length of the element and  $\tau_l$  is the shear stress acting along it);  $m$  are the elements of the source pile from which the effects of the point loads are calculated;  $R_1 = \sqrt{r_k^2 + (z_k - z_l)^2}$  (for which  $r_k$  is the horizontal distance between node  $l$  at which the load is applied and node  $k$  at which the influence is considered,  $z_k$  is the depth of node  $k$ , and  $z_l$  is the depth of node  $l$ ); and  $R_2 = \sqrt{r_k^2 + (z_k + z_l)^2}$ .

Point loads acting on the nodes of a pile that is effectively considered to be a line avoids the need for integrating (analytically and numerically) the equations of Mindlin (1936) along and around the circumference of the elements constituting the pile. This fact, which has been verified through finite element analyses, results in a notable expediency and comparable accuracy of the analysis.

The equations of Mindlin (1936) involve that the present continuous model allows the vertical displacement of stratified (non-homogeneous) soil deposits to be estimated only approximately. However, an effective and accurate procedure has been shown in this context to consider a mean value of the shear modulus of the soil layer where the displacement is calculated at any soil node,  $k$ , and the shear modulus of the soil layer where the point load is applied at any pile node,  $l$  (Poulos and Davis,

1980). Application examples to the considered design situations that employ the aforementioned approach are given in Section 5.5.6.

Equation (5.17) highlights that the present continuous model considers the effects of the shear stress acting on any element of a source pile on all of the elements of the surrounding soil in a “continuous” way, regardless of the layer (cf., Figure 5.4 (b)).

The general solution for the vertical displacement of the soil expressed in equation (5.17) can be normalised with respect to the vertical displacement at the pile shaft to give the approximate pile-soil interaction factor, as suggested by equation (5.1).

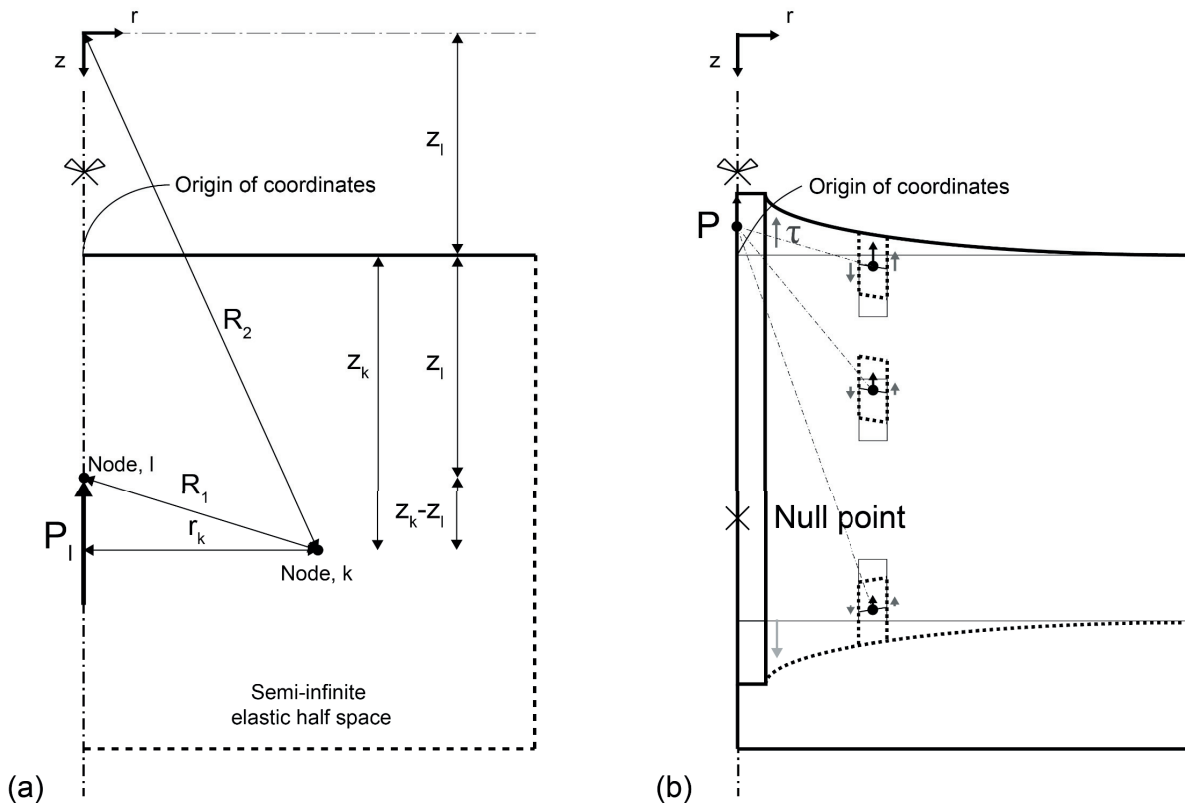


Figure 5.4: The continuous model concept: (a) the reference situation for Mindlin's problem (Mindlin, 1936) and (b) the transposition of this problem to that of a single isolated pile subjected to thermal loading.

#### 5.4.2 Receiver pile vertical displacement and corrected pile-soil-pile interaction factor

In contrast to the approach that was previously considered to define the second boundary condition for solving equation (5.13) (cf., Section 5.3.2), a different approach is employed in the present context to properly address the hypotheses and considerations characterising the continuous model.

Unlike the layer model, the continuous model accounts for interaction between the different layers of elements. According to this hypothesis and to continuum mechanics theory, it may be considered that the location where zero thermally induced shear stress occurs does not coincide with the location where zero thermally induced vertical displacement occurs. Knowledge of the location where the



vertical displacement of the soil is  $w(r, z) = w_j(s, z) \neq 0$  is thus of interest to define the second boundary condition. To overcome the issue that the specific value of  $w(r, z) \neq 0$  and the associated location where  $\tau(r, z) = 0$  is not known a priori, the equations of Mindlin (1936) can be exploited to determine through the elastic principle of superposition of effects the shear stress caused by a distribution of point loads acting on a single isolated source pile at any location in the surrounding soil. This approach, which accounts for the continuous character of the present performance model, allows for the direct determination of the location in the soil where  $\tau(r, z) = 0$  and thus where  $w(r, z) = w_j(s, z) \neq 0$  from the analysis of a single isolated pile. The shear stress in the soil can be defined as (Mindlin, 1936)

$$\begin{aligned} \tau(r, z) &= \sum_{l=1}^m \tau_{kl} \\ &= \sum_{l=1}^m \frac{P_l r_k}{8\pi(1 - \nu_{soil})} \left( -\frac{1 - 2\nu_{soil}}{R_1^3} + \frac{1 - 2\nu_{soil}}{R_2^3} - \frac{3(z_k - z_l)^2}{R_1^5} \right. \\ &\quad \left. - \frac{3(3 - 4\nu_{soil})z_k(z_k + z_l) - 3z_l(3z_k + z_l)}{R_2^5} - \frac{30z_k z_l (z_k + z_l)^2}{R_2^7} \right) \end{aligned} \quad (5.18)$$

where  $\tau_{kl}$  is the shear stress acting on any soil node,  $k$ , caused by a point load,  $P_l$ , applied to the node,  $l$ , of a source pile. The discussed boundary condition can be mathematically expressed as

$$w_j(s, z = z|_{\tau=0}) = w(r, z = z|_{\tau=0}) \quad (5.19)$$

Equation (5.13), together with equations (5.15) and (5.19), can calculate the values of  $w_j(s, z)$ . As before, these values can determine the values of  $\Omega(s, z)$ .

The shear stress distribution that is found through equation (5.18) is an approximation of the actual shear stress distribution along the shaft of a receiver pile in a pair. The actual shear stress distribution caused by loading a source pile on a receiver pile in a pair may be determined rigorously as shown by Poulos and Davis (1980). However, the null point position of the shear stress distribution in the soil that is estimated through equation (5.18) has been verified through finite element analyses to be generally close to that along a receiver pile in a pair, e.g., within the distance of half a pile diameter. This fact, together with the consideration of the vertical displacement of the soil at the same distance  $r$  from the axis of the source pile, makes equation (5.18) suitable to solve equation (5.13) for estimating the vertical displacement of a receiver pile whose axis is located at a distance  $s$ . Furthermore, it is in accordance with the interaction factor analysis procedure based on the analysis of a single *isolated* pile. The close adherence between results obtained through the continuous model and more rigorous finite element analyses that will be shown in the following strengthen the aforementioned approach.

In principle, an alternative second boundary condition that addresses the relationship highlighted by Randolph and Wroth (1978) between the load applied at the toe of piles and the related displacement may be used to solve equation (5.13) with reference to the receiver pile. This condition was employed by Mylonakis and Gazetas (1998) to model piles subjected to mechanical loads. In practice, because of the incapability of explicitly considering the presence of the null point, this boundary condition has been verified to lead to an overestimate of the vertical displacement of receiver piles when source piles in a pair are subjected to thermal loads (Rotta Loria et al., 2017c). Therefore, it is considered unsuitable to model piles subjected to thermal loads but only piles subjected to mechanical loads.

## 5.5 Application and validation of the performance models

### 5.5.1 General information about analyses performed

In this work, thermo-mechanical finite element modelling is performed with the software COMSOL Multiphysics (COMSOL, 2014) and serves as an analysis and validation tool. Thermo-mechanical axisymmetric and 3-D finite element analyses are carried out. The former simulations address the behaviour of single isolated source piles. They provide the evolutions of  $w_i(z)$  and  $\tau_i(z)$  that are needed in the application of the performance models and results for comparison (e.g., displacement field around the source piles and approximate interaction factor). The latter simulations address the behaviour of energy pile groups and provide additional results for comparison (e.g., corrected interaction factor and vertical displacement of energy pile groups).

While considering the general assumptions presented in Section 5.2.2 and accounting for a temperature variation of  $\Delta T = 10^\circ\text{C}$  applied to the energy piles, in all cases except in Section 5.6 the finite element analyses are stationary and neglect the temperature sensitivity of the soil (i.e., they refer to soils characterised by a soil-pile thermal expansion coefficient ratio of  $X = \alpha_{\text{soil}}/\alpha_{\text{EP}} = 0$ , for which  $\alpha_{\text{soil}}$  and  $\alpha_{\text{EP}}$  are the linear thermal expansion coefficients of the soil and energy pile, respectively). The above is true for the 3-D finite element analyses as well, except in Section 5.5.6, in which the 3-D finite element analyses are time-dependent, consider the applied temperature variation to be constant for  $t = 6$  months and account for the temperature sensitivity of the soil (when  $X \neq 0$ ).

Unless stated otherwise, energy piles with a slenderness ratio of  $L/D = 25$ , with  $D = 1$  m, are considered to be embedded in uniform soil. Piles with  $L/D = 50$  and non-uniform soil are also investigated.

The material parameters employed in the analysis for the reference case study are summarised in Table 5.1. Reference is made to Rotta Loria and Laloui (2016b) and Rotta Loria and Laloui (2017a) for information about the mathematical formulation employed in the numerical analysis (cf., equations (B1-3) in Appendix B) and the features of the numerical models (cf., Chapter 4).

### 5.5.2 Analysis of vertical displacement of a single isolated pile

Figure 5.5 presents the evolution of the vertical displacement against the shear stress along the shaft of a single isolated pile. The vertical displacement along the pile length,  $w$ , is normalised with respect

to the absolute value of the head displacement of a single pile under free thermal expansion conditions,  $|w_f^{th}| = |-\alpha_{EP} \Delta T L/2|$ . The shear stress mobilised along the pile length,  $\tau$ , is normalised by the soil shear modulus.

Boundary effects characterise the results of the finite element analysis, involving a non-linear variation of the  $\tau - w$  curve (especially at the pile ends) that is asymmetric with respect to the mid-length of the piles and representing the reason why in equation (5.9), for example, the ratio  $\tau_i(z)/w_i(z)$  included in the multiplying coefficient of the logarithm is not expressed through the constant  $K_s$ . The location of the null point of the shear stress differs from that of the vertical displacement, involving a  $\tau - w$  relationship that does not cross the origin of the axes. This phenomenon is caused by the capability of the finite element analysis to capture the effects of the shear stress acting on any element of a source pile on all of the elements of the pile in a continuous way.

Table 5.1: Material properties used for the numerical analyses (Rotta Loria and Laloui, 2016b).

Reinforced concrete pile parameters	Value (thermo-elastic description)	Soil parameters	Value (elastic description)	Value (thermo-elastic description)
$E_{EP}$ : [MPa]	30000	$G_{soil}$ : [MPa]		30 (*)
$\nu_{EP}$ : [-]	0.25	$\nu_{soil}$ : [-]		0.30
$\rho_{EP}$ : [kg/m <sup>3</sup> ]	2450	$\rho_{soil}$ : [kg/m <sup>3</sup> ]		1537
$\alpha_{EP}$ : [1/°C]	$1 \cdot 10^{-5}$	$\alpha_{soil}$ : [1/°C]	-	$1 \cdot 10^{-5}$ (*)
$\lambda_{EP}$ : [W/(m °C)]	1.47	$\lambda_{soil}$ : [W/(m °C)]	-	0.25
$c_{p,EP}$ : [J/(kg °C)]	854	$c_{p,soil}$ : [J/(kg °C)]	-	961

(\*) Parameter varied throughout the simulations.

### 5.5.3 Analysis of soil vertical displacement and approximate interaction factor

Figure 5.6 presents the evolutions of the normalised vertical displacement of the soil and the approximate interaction factor with the normalised depth for normalised radial distances from the axis of the single isolated pile of  $r/D = 2.5$  and  $4.5$ . The depth,  $z$ , is normalised by the pile length,  $L$ .

A close adherence between the results obtained with the layer and continuous models and the finite element analysis is observed. A difference between the predictions of the layer and continuous models is noted in the soil at depths corresponding to the pile ends. The layer model considers the effects of the shear stress at every element of the pile shaft to affect each corresponding layer of elements in the soil alone, while the continuous model considers for the shear stress to affect all of the elements in the soil. Therefore, the boundary effects observed for the  $\tau - w$  relationship at the pile ends in the source axisymmetric finite element analysis have a notable influence on the estimate of the vertical displacement of the soil provided by the layer model in these settings but a negligible influence for the continuous model.

The results of the finite element analysis indicate that the null point of the vertical displacement does not correspond to that of the shear stress and moves downward for increasing radial distances in the soil. This phenomenon is caused by the capability of finite element analyses to capture the effects of

the shear stress acting on any element of a source pile on all of the elements of the surrounding soil in a continuous way. The downward movement of the null point of the vertical displacement is captured by both the continuous and layer models due to the “continuous” nature of the source data.

The downward movement of the null point of the vertical displacement with increasing radial distance involves notable variations of the approximate pile-soil interaction factor at locations that are close to the null point of the vertical displacement (at these locations, the source pile displacement is divided by a value of soil displacement close to zero and non-necessarily of the same sign). These variations involve values of the pile-soil interaction factor (as well as of the pile-soil-pile interaction factor, cf., Section 5.5.4) that may be lower than 0 and greater than 1 (These values have not been included in the present figures for clarity). This is a crucial difference compared to the values of the interaction factor that characterise conventional piles subjected to mechanical loads (Randolph and Wroth, 1979b; Poulos, 1968), i.e., varying between 0 and 1.

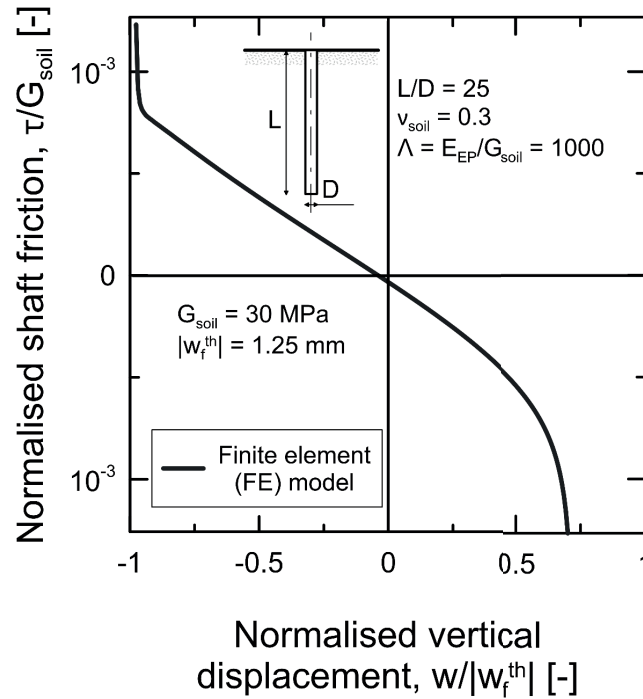


Figure 5.5: Vertical displacement-shear stress relationship estimated through an axisymmetric finite element analysis.

#### 5.5.4 Analysis of receiver pile vertical displacement and corrected interaction factor

Figure 5.7 presents the evolutions of the corrected interaction factor with the normalised depth for normalised spacing from the axis of the source pile of  $s/D = 3$  and 5.

In general, the evolution of the corrected pile-soil-pile interaction factor with depth is thoroughly captured by the performance models. The evolution of the corrected interaction factor suggested by the layer model may be on average considered to be representative of the displacement behaviour of a receiver pile. Hence, it is considered acceptable for practical analyses of the vertical displacement of piles subjected to thermal loads.

Figure 5.8 presents the evolution of the corrected and approximate interaction factors for the heads of the pair of piles with the normalised horizontal distance.

Correcting the interaction factor to account for the effect of the stiffness of a receiver pile on its effective deformation compared to the deformation that would characterise the soil in the same location if this pile was not present appears fundamental. The difference between the approximate pile-soil interaction factor and the corrected pile-soil-pile interaction factor is significant, with the latter being considerably smaller than the former. This difference increases with increasing relative stiffness of the piles compared to that of the soil.

### 5.5.5 Corrected interaction factor for a range of design situations

Figure 5.9 and Figure 5.10 compare the evolution of the corrected interaction factor with the normalised horizontal distance for the head of pile pairs of  $L/D = 25$  and  $50$ . The piles are considered to be embedded in uniform soils with pile-soil stiffness ratios of  $\Lambda = E_{EP}/G_{soil} = 100, 1000$  and  $10000$  and a Poisson's ratio of  $\nu_{soil} = 0.3$ .

The displacement interaction factor curves described by the performance models accurately reproduce the curves obtained using more rigorous finite element analyses (Rotta Loria and Laloui, 2016b) despite some differences. A greater difference between the results obtained from the application of the performance models and the development of the finite element analyses is generally observed for the lower pile slenderness ratios. The layer model tends to underestimate the corrected pile-soil-pile interaction factor compared to the values estimated by the continuous model and the finite element analyses, especially for decreasing values of the pile-soil stiffness ratio. However, in reality, the non-linear nature of soil deformation leads to less interaction than that predicted from a linear elastic analysis because the deformation is more confined to the immediate vicinity of the pile (Randolph and Wroth, 1979b; Poulos, 1988; Rotta Loria et al., 2017c). Based on this consideration, the layer model may provide more realistic predictions of pile interaction than those given by the continuous model or by finite element analyses. Both models are still considered of paramount importance for a comprehensive displacement analysis of piles subjected to thermal loads because they provide lower and upper boundaries of the pile interaction that may be encountered in practice.

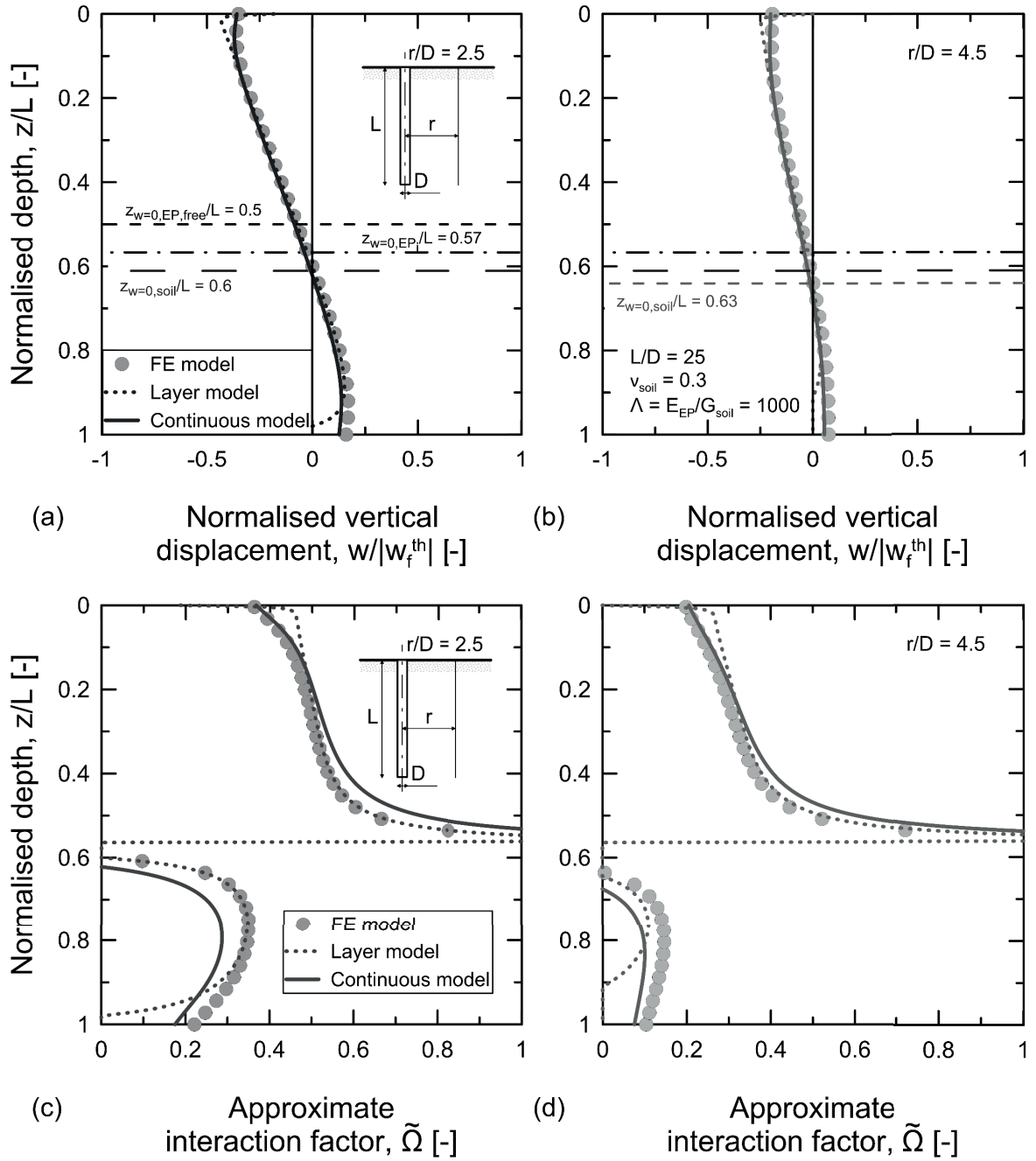


Figure 5.6: Evolution of the normalised vertical displacement of the soil with the normalised depth for normalised radial distances of (a)  $r/D = 2.5$  and (b)  $r/D = 4.5$ ; evolution of the associated approximate interaction factor with the normalised depth for normalised radial distances of (c)  $r/D = 2.5$  and (d)  $r/D = 4.5$ .

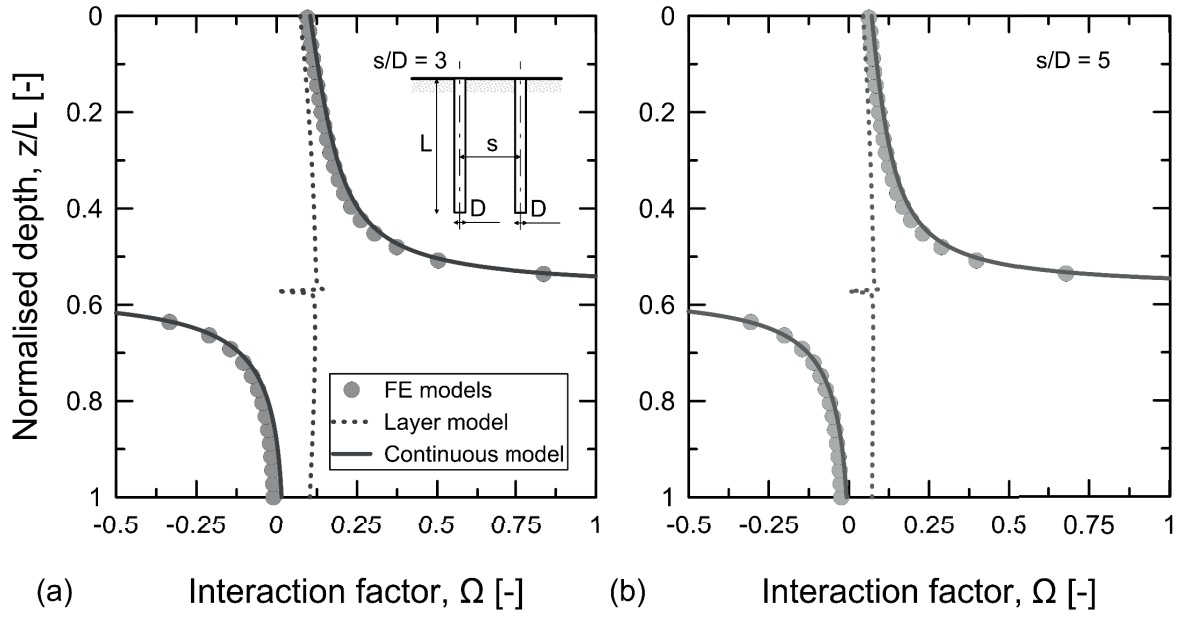


Figure 5.7: Evolution of the corrected interaction factor with the normalised depth for a normalised spacing of (a)  $s/D = 3$  and (b)  $s/D = 5$ .

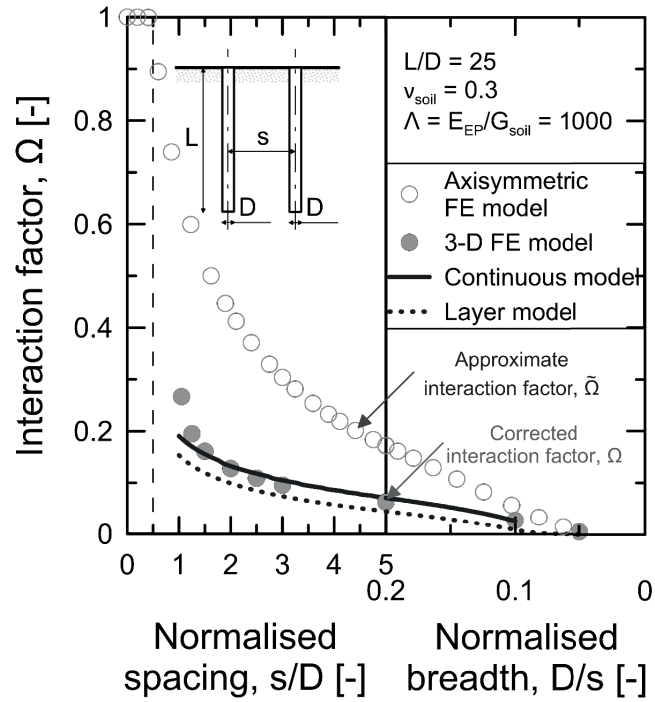
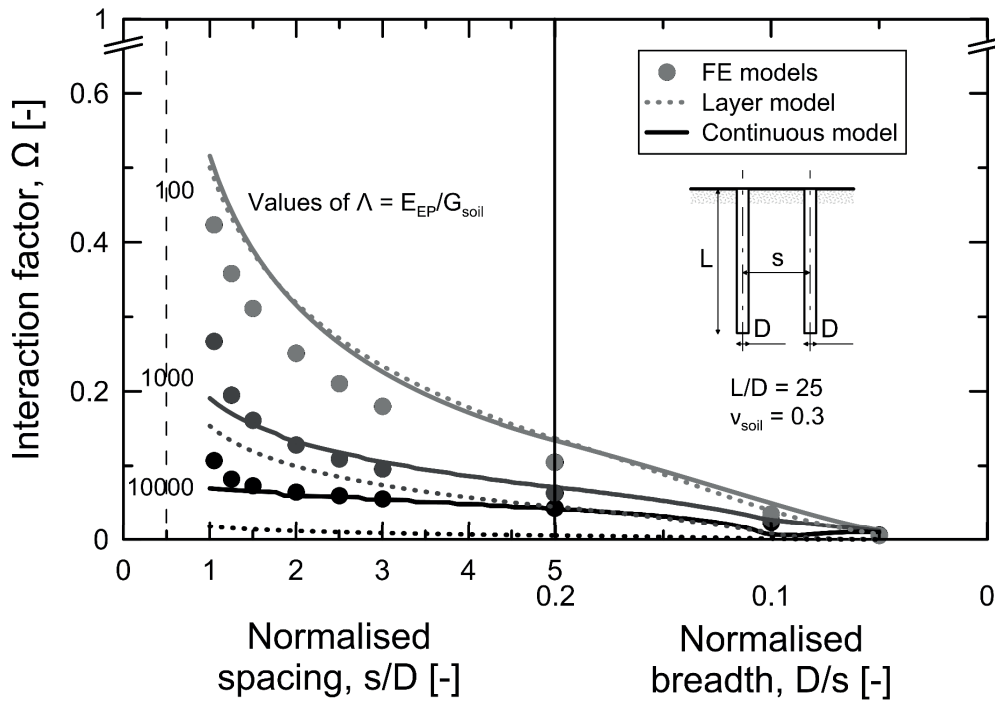
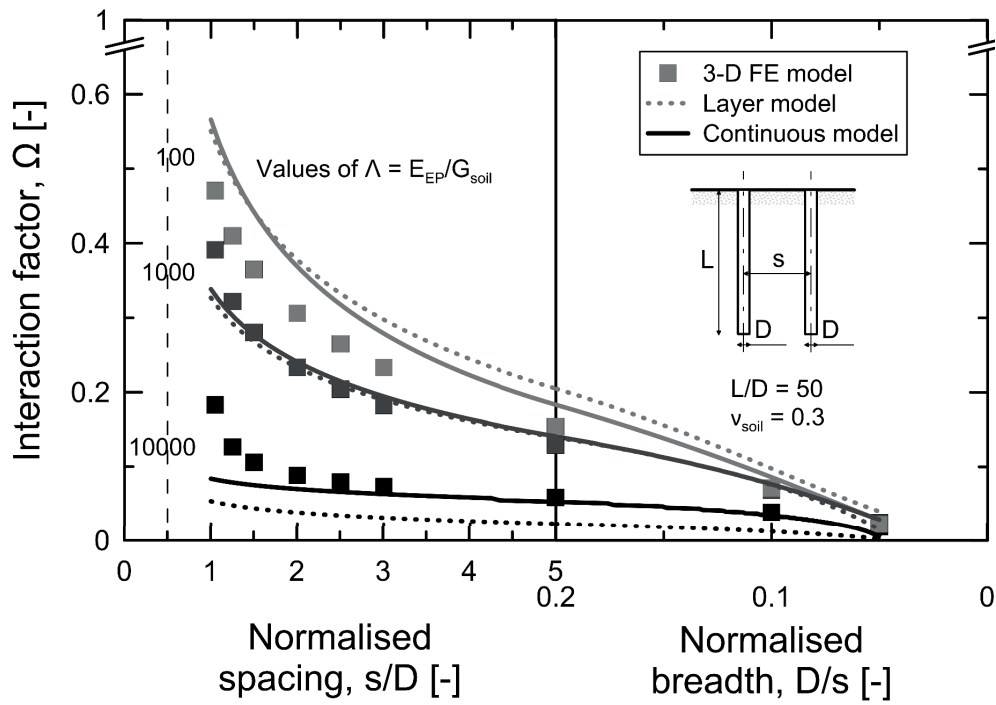


Figure 5.8: Evolution of the corrected and approximate interaction factors with the normalised horizontal distance.

Figure 5.9: Corrected interaction factors referred to the pile head for  $L/D = 25$  in various design conditions.Figure 5.10: Corrected interaction factors referred to the pile head for  $L/D = 50$  in various design conditions.



### 5.5.6 Analysis of $5 \times 5$ square energy pile groups

This section presents evidence for a further validation of the analytical performance models presented in this work as well as the interaction factor method for piles subjected to thermal loads (following previous studies (Rotta Loria and Laloui, 2016b; Rotta Loria and Laloui, 2017a)).

Two different design situations for energy pile groups composed of 25 energy piles ( $5 \times 5$  group, cf., Figure 5.11) are modelled: (i) predominantly floating energy piles embedded in uniform soil and (ii) predominantly end-bearing energy piles embedded in non-uniform soil constituted by two layers. Piles with a typical slenderness ratio of  $L/D = 25$  are analysed for values of normalised centre-to-centre spacing of  $s/D = 3, 5$  and  $10$ , and pile-soil stiffness ratios of  $\Lambda = E_{EP}/G_{soil} = 1000$  and  $10000$ . The non-uniform soil is characterised by a deeper soil layer with the same material properties of the shallower layer, except for a double shear modulus. Soil deposits characterised by soil-pile thermal expansion coefficient ratios of  $X = \alpha_{soil}/\alpha_{EP} = 0, 1$  and  $2$  are considered.

The interaction factor method based on the presented analytical models neglects the temperature sensitivity of the soil and the related effects on the thermo-mechanical behaviour of the piles. The 3-D finite element analyses rigorously account for these phenomena where  $X \neq 0$ . In principle, the above involves that the results obtained via the analytical performance models are only comparable with the 3-D finite element analyses for soil deposits characterised by  $X = 0$ . However, as shown hereafter, the predictions of the performance models give the lower and upper boundaries of pile group vertical displacement that may be expected for any practical value of  $X$ .

The average vertical head displacement of the modelled pile groups can be estimated according to the five steps that constitute the analysis approach based on the layer and continuous models presented in this study (cf., Section 5.2.3) as follows.

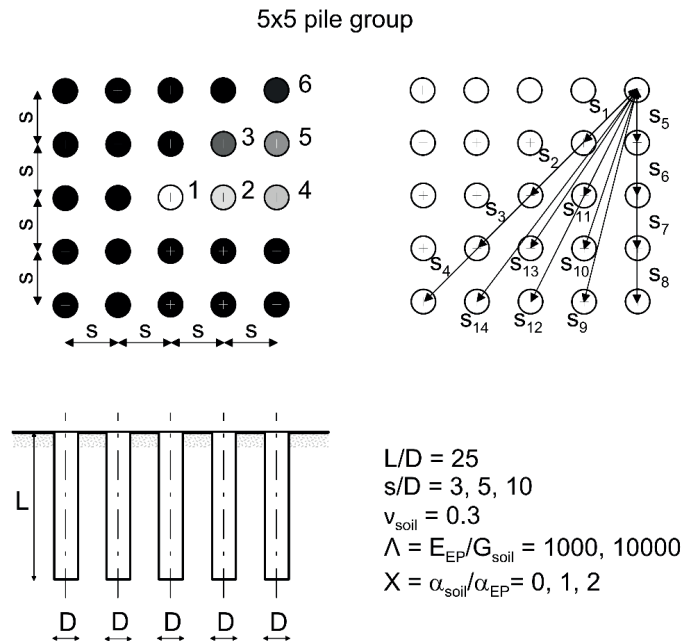


Figure 5.11: Configuration of the practical example.

*Step 1:* The vertical displacement,  $w_i(z)$ , and the shear stress,  $\tau_i(z)$ , along the shaft of a single isolated pile that is representative of those in the group are determined.

*Step 2-4:* The approximate pile-soil interaction factors,  $\tilde{\Omega}(r, z)$ , and corrected pile-soil-pile interaction factors,  $\Omega(s, z)$ , are calculated for the characteristic centre-to-centre distances that describe all of the singular pile pairs constituting the energy pile group. Because in this example the vertical displacements of interest are those of the pile heads, the relevant interaction factors are  $\tilde{\Omega}(r = r_1, r_2, \dots, r_{14}, z = 0)$  and  $\Omega(s = s_1, s_2, \dots, s_{14}, z = 0)$ , where  $s_1, s_2, \dots, s_{14}$  are the fourteen characteristic centre-to-centre distances between the pile pairs that describe the considered energy pile groups (cf., Figure 5.11). For the design situation involving piles in non-uniform soil, the layer model directly accounts for the different properties of the soil layers with depth while the continuous model implicitly considers the different properties of the soil layers according to the procedure proposed by Poulos and Davis (1980) (cf., Section 5.4.1).

*Step 5:* The vertical head displacement of each of the characteristic energy piles of the groups is determined. In this example, six characteristic energy piles, 1, 2, ..., 6 (cf., Figure 5.11), describe the pile group. The associated vertical head displacements that need to be determined for calculating the average vertical head displacement of the group are  $w_1, w_2, \dots, w_6$  (i.e.,  $w_1(z = 0), w_2(z = 0), \dots, w_6(z = 0)$ ). A calculation example of the vertical head displacement is given below for the centre pile 1 and the corner pile 6, considering in equation (3)  $w_j(z) = w_j(z = 0) = w_j$ ,  $w^1(z) = w^1(z = 0) = w^1$ ,  $\Delta T_i = \Delta T$ ,  $w^1 \Delta T = w_i$ , and  $\Omega_{ij}(s, z) = \Omega(s = s_1, s_2, \dots, s_{14}, z = 0) = \Omega_{s_1, s_2, \dots, s_{14}}$ .

$$w_1 = w_i [1 + 4\Omega_{s_1} + 4\Omega_{s_2} + 4\Omega_{s_5} + 4\Omega_{s_6} + 8\Omega_{s_{11}}]$$

$$w_6 = w_i \left[ \frac{1 + \Omega_{s_1} + \Omega_{s_2} + \Omega_{s_3} + \Omega_{s_4}}{+2\Omega_{s_5} + 2\Omega_{s_6} + 2\Omega_{s_7} + 2\Omega_{s_8} + 2\Omega_{s_9} + 2\Omega_{s_{10}} + 2\Omega_{s_{11}} + 2\Omega_{s_{12}} + 2\Omega_{s_{13}} + 2\Omega_{s_{14}}} \right]$$

Once the vertical head displacement of all of the characteristic energy piles is known, the average vertical head displacement of the group, which is below normalised by the head displacement of a single pile under free thermal expansion conditions, can be calculated as

$$\frac{\bar{w}}{D} = \frac{w_1 + 4w_2 + 4w_3 + 4w_4 + 8w_5 + 4w_6}{25D}$$

Figure 5.12 compares absolute values of the normalised average vertical head displacement of the considered energy pile groups given by the analyses performed. Agreement between the displacement

values obtained via the analytical performance models and the 3-D finite element analyses is observed, with discrepancies that can be considered acceptable for practical analysis and design of energy piles. In almost cases, the results of the layer and continuous model bound those of the 3-D finite element analyses for any values of  $X$ . The above can be considered to be valid not only for varying pile-soil stiffness ratios, but also for different types of energy piles. In particular, the interaction factor method based on the layer and continuous models is considered to capture the vertical displacement of both predominantly floating and end-bearing energy piles in uniform and non-uniform soil deposits.

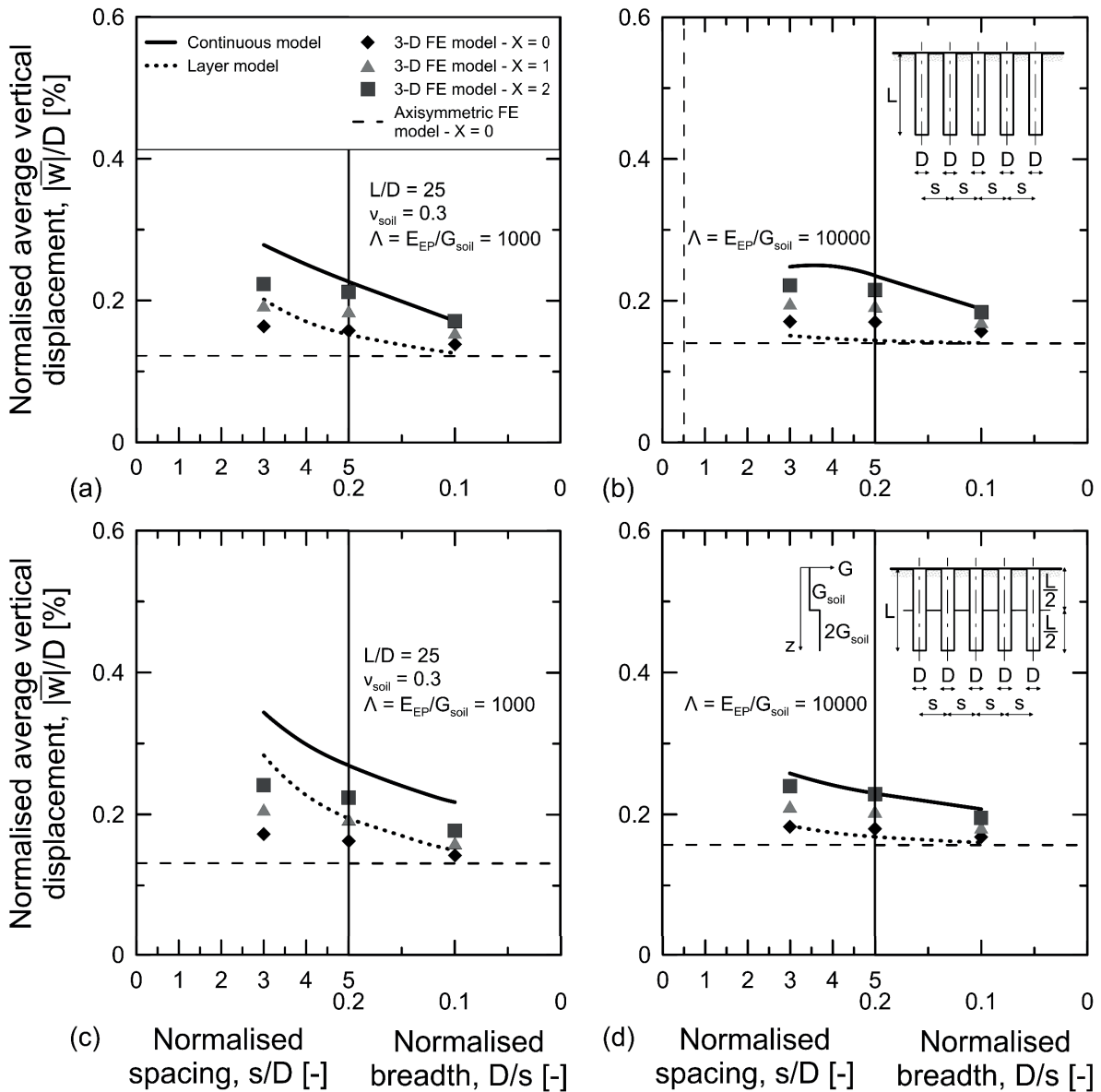


Figure 5.12: Analysis of 5x5 energy pile groups of  $L/D = 25$  in various design conditions: (a-b) uniform soil mass and (c-d) non-uniform soil mass.

The differences observed between the predictions of the performance models and the finite element analyses result from the diverse capabilities of these models in capturing the displacement interaction among piles. Greater values of pile group displacements are observed for decreasing values of  $s/D$ , increasing values of  $\Lambda$  and  $X$ , and because of the presence of a bearing stratum. The higher values of group displacement observed for increasing values of  $\Lambda$ , in contrast to the lower displacement interaction among the piles for greater values of the considered parameter, is caused by the higher displacement of each of the piles in the group due to the lower restraint provided by the soil to the pile deformation. In all cases, the vertical displacement of the pile groups is greater than the displacement of a single isolated pile representative of those in the corresponding group because of the occurrence of pile-soil-pile interaction. The above confirms previous evidence shown by Rotta Loria and Laloui (2016b; 2017a).

## 5.6 Concluding remarks

This work presented two analytical performance models, i.e., a *layer model* and a *continuous model*, to address through the interaction factor method the displacement analysis of general configurations of energy pile groups subjected to thermal (and mechanical) loads, based on the analysis of a single isolated pile. The proposed analytical performance models unify, modify and extend most of the analytical models that have been developed over the last fifty years for conventional piles groups subjected to only mechanical loads.

The main conclusions that can be drawn from this work are as follows (Rotta Loria et al., 2017b):

- A comparison of the results obtained from the performance models with those of more rigorous axisymmetric and 3-D thermo-mechanical finite element analyses of pile groups subjected to thermal loads shows close agreement. This agreement is observed for both predominantly floating and end-bearing piles embedded in soil deposits characterised by varying pile-soil stiffness ratios, pile slenderness ratios, soil-pile thermal expansion coefficient ratios and (when applicable) normalised centre-to-centre spacing between the piles.
- Both the layer and continuous models can be used to analyse the displacement of pile groups embedded in uniform and non-uniform (stratified) soil deposits. This feature gives these models a broad capability to analyse practical energy pile-related problems.
- The layer and continuous models can be considered to give the lower and upper boundaries of the pile interaction expected to be encountered in practice, respectively, for any values of the soil-pile thermal expansion coefficient ratio.
- Both the layer and continuous models, similar to all the simplified models that have been proposed in the framework of conventional piles for capturing the vertical deformation of such foundations, are characterised by limitations. However, these models are versatile for analyses and designs of energy pile groups subjected to thermal (and mechanical) loads. They are particularly useful to understand the most influential parameters on energy pile group response and analysing the resulting effects.

- The described performance models have been applied based on the results of an axisymmetric thermo-mechanical finite element analysis of a single isolated source pile. The performance models have been applied in the same way based on source data of a finite difference analysis using the load-transfer method. However, because of some different underlying hypotheses, the load-transfer method appears less suitable than the finite element method in serving interaction factor analyses of energy pile groups.



## Chapter 6

# Non-linear soil deformation and energy pile interaction

This study investigates the effect of non-linear soil deformation on the displacement interaction among energy piles. The work is based on interaction factor analyses of full-scale pile group tests, whose results are compared with experimental evidence. The results presented highlight the tendency of interaction factor analyses that ignore non-linear soil deformation to overestimate the interaction and the displacement of energy pile groups. This outcome, in accordance with previous studies for conventional pile groups subjected to mechanical loads, may be considered in the analysis and design of energy pile groups subjected to thermal (and mechanical) loads through the interaction factor method.

### 6.1 Introduction

Over the last thirty years, a number of experimental (Caputo and Viggiani, 1984) and theoretical (O'Neill et al., 1981; Chow, 1986; Jardine et al., 1986; Poulos, 1988; Randolph, 1994; Mandolini and Viggiani, 1997; Poulos, 2006; Leung et al., 2010) investigations based on interaction factor analysis have been performed to address the effect of non-linear soil deformation on the vertical displacement of and interaction between conventional piles subjected to mechanical loads. There are multiple reasons for these investigations. Soil deformation can often be non-linear and may involve reversible (i.e., elastic) or irreversible (i.e., plastic) stress-strain behaviour. As a consequence of this non-linearity, different deformation modulus values can be associated with the varying shear strain levels that characterise the soil surrounding piles (e.g., as a result of loading or construction effects). Consideration of these deformation modulus values has been proven to be essential to analyse and design pile groups (O'Neill et al., 1981; Poulos, 1988; Randolph, 1994).

The soil region adjacent to or in the vicinity of the shaft of single piles subjected to mechanical loads undergoes high shear strains on the order of 0.005 to 0.015% (Randolph, 1994). These strain levels are associated with lower soil modulus values and generally correspond to either reversible or irreversible soil behaviour that remains localised close to the pile (Caputo and Viggiani, 1984; Jardine et al., 1986; Chow, 1986).

The bulk of the soil between piles experiences low shear strains that may be orders of magnitude smaller than those near the piles and typically less than approximately 0.001% (Randolph, 1994). These strain levels are associated with higher soil modulus values and generally correspond to a soil behaviour that may be considered to be reversible, as are the interactions between the piles (Caputo and Viggiani, 1984; Chow, 1986).

The aforementioned considerations justify a specific approach for the interaction factor analysis of pile groups (O'Neill et al., 1981; Jardine et al., 1986; Poulos, 1988; Mandolini and Viggiani, 1997; Randolph, 1994). Soil modulus values that are associated with high strain levels can be used to characterise the vertical displacement behaviour of the single piles composing any group. On the other hand, soil modulus values that are associated with low strain levels can be used to estimate the interaction between the piles. With this approach, interaction factor analysis based on appropriate soil modulus values can be used to capture the vertical displacement of conventional pile groups subjected to mechanical loads almost irrespective of the mathematical formulation employed for describing the soil behaviour and the related pile response (Leung et al., 2010; Mandolini and Viggiani, 1997). The above is justified by the close adherence to reality of results of interaction factor analysis of conventional pile groups that exploit either different (Poulos, 1988; Poulos, 2006) or varying (Chow, 1986; Randolph, 1994; Leung et al., 2010; Zhang et al., 2010; Wang et al., 2012) soil modulus values, and linear elastic (Poulos, 1988; Poulos, 2006), non-linear elastic (Randolph, 1994; Leung et al., 2010) or non-linear elasto-plastic (Chow, 1986; Zhang et al., 2010; Wang et al., 2012) stress-strain relationships.

Thermal loads applied to energy piles induce a pattern of the deformation field that differs from that induced by mechanical loads. However, these loads are associated with a comparable evolution of the strain levels in the soil that can be related to different deformation modulus values. The results of full-scale *in situ* tests of single (Laloui et al., 2003; Bourne-Webb et al., 2009; Wang et al., 2014; Akrouh et al., 2014; You et al., 2016; Sutman et al., 2014) and groups (McCartney and Murphy, 2012; Mimouni and Laloui, 2015; Rotta Loria and Laloui, 2017d; Murphy et al., 2015) of energy piles further highlight that the effects caused by thermal loads on the piles and the soil, although often smaller for geothermal exploitations under serviceability conditions, can be comparable and even greater than those induced by mechanical loads. This fact involves different magnitudes and combinations of mechanical and thermal loads applied to energy piles causing either a reversible or irreversible soil and pile response, similarly to what can occur when (only) mechanical loads are applied to conventional piles. The above appears to be relevant especially for predominantly floating energy piles (Rotta Loria et al., 2015b). The reason behind this is that, for the same applied load, floating piles mobilise a greater proportion of shear strain and shear stress at the pile-soil interface compared to end-bearing piles.

Currently, interaction factor analysis methods aimed at estimating the vertical displacement of and interaction between energy piles subjected to thermal loads ignore non-linear soil deformation. This is caused by the fact that these methods consider a unique soil modulus value to characterise both the single pile response and the interactions among the piles (Rotta Loria and Laloui, 2016b; Rotta Loria and Laloui, 2017a) (cf., Chapter 4). In particular, prior to this study, no simplified yet rational methods have been formulated and applied to expediently address the effect of non-linear soil deformation on the interaction among energy piles subjected to thermal loads.



To address this challenge, this work (Rotta Loria et al., 2017c) (i) modifies and extends the procedure for determining the interaction factors proposed by Poulos (1988) for conventional pile groups subjected to (only) mechanical loads in non-linearly deforming soils to energy pile groups subjected to thermal (and mechanical) loads, and (ii) investigates the effect of non-linear soil deformation on the vertical displacement of and interaction between energy piles.

The use of linear elastic theory, constant material properties and linear mathematical formulations are the fundamental assumptions underlying the procedure presented here to describe non-linear soil deformation and the related vertical displacement of piles and interaction between them. Although this procedure is approximate in principle, it has in practice been capable of accurately and expediently reproducing the vertical displacement behaviour of conventional pile groups. In this work, it demonstrates the same capability for energy pile groups.

The effects of the potential irreversible behaviour of soil regions adjacent to or in the vicinity of piles are not analysed in this study because reference is made to serviceability conditions in which reversible conditions prevail. However, these effects are considered to be comparable to those that will be analysed in this work because they may be tackled similarly (although more approximately) during loading by considering different soil modulus values as performed in this study.

In the following, the considered procedure is first applied and validated against the experimental evidence reported by O'Neill et al. (1981) involving full-scale *in situ* tests of conventional pile groups subjected to mechanical loads in overconsolidated clay where non-linear soil deformation was observed. To address energy piles, these pile group tests are then modelled by considering the piles to be subjected to thermal loads. Finally, the effect of non-linear soil deformation on the vertical displacement of energy piles subjected to thermal loads and interaction between them is analysed and discussed, and concluding remarks are summarised.

## **6.2 Interaction factor analysis of energy pile groups**

### **6.2.1 Classical interaction factor analysis approach**

Currently, both design charts (Poulos, 1968; Poulos and Mattes, 1974; Rotta Loria and Laloui, 2016b; Rotta Loria and Laloui, 2017a) and performance models (Randolph and Wroth, 1979b; Mylonakis and Gazetas, 1998; Chow, 1986) are available to address the displacement interaction factor relationship between any two conventional or energy piles. This relationship allows the interaction factor analysis of any pile group to be performed.

In this study, the approach to determine the displacement interaction factor between a pair of energy piles proposed by Rotta Loria et al. (2017b) (cf., Chapter 5) is considered and the influence of both thermal and mechanical loads is addressed.

The interaction factor analysis of any pile group subjected to thermal and/or mechanical loads consists of five key steps:

1. The analysis of a single isolated source pile subjected to thermal or mechanical loading to define the vertical displacement,  $w_i(z)$ , and the shear stress,  $\tau_i(z)$ , along the pile shaft ( $z$  is the vertical coordinate). This analysis is developed in the present work using finite element analysis.
2. The determination of the vertical displacement of the soil,  $w(r, z)$ , at any given radial distance,  $r$ , from the axis of the previously analysed single isolated pile subjected to loading, and along the vertical coordinate,  $z$ . This step can be performed by using the continuous performance model presented by (Rotta Loria et al., 2017b) (cf., Chapter 5) for energy piles subjected to thermal loads based on the work of Chow (1986) for conventional piles subjected to mechanical loads. According to this model, the vertical displacement of the soil caused by a distribution of point loads associated with the effects of the thermal or mechanical load applied to the source pile may be calculated through the equations of Mindlin (1936) and the elastic principle of superposition of effects (cf., equation (5.17)).
3. The correction of the vertical displacement of the soil,  $w(r, z)$ , to address the actual vertical displacement of a receiver pile,  $w_j(s, z)$ , located at a centre-to-centre spacing,  $s$ , from the source pile that was previously considered to be isolated, and generally characterised by a greater stiffness than that of the soil. This step can be performed by solving the second-order differential equation (5.13) governing the equilibrium of each node of the receiver pile

It is recalled that equation (5.13) needs two boundary conditions to be solved. The first boundary condition is chosen with reference to the state of restraint that characterises the head of the receiver pile. Because the pile is free to displace vertically at its head no vertical stress will be present in this setting. This condition can be mathematically expressed through equation (5.15).

The second boundary condition needs to be preferably chosen by considering whether the source pile is subjected to thermal or mechanical loading. The application of this boundary condition must also refer to the shear stress induced by either thermal loading or mechanical loading separately. In the case of thermal loading, the second boundary condition is chosen with reference to the so-called “null point” of the shear stress of the receiver pile through equation (5.19). In the case of mechanical loading, the second boundary condition is chosen with reference to the base of the receiver pile. Because the pile base acts as a rigid punch on the lower layer of soil (Randolph and Wroth, 1979b), there is a specific relation between the point load applied at the pile base,  $P_b = A_{EP} \sigma_z(z = L)$ , (where  $\sigma_z(z = L)$  is the normal stress acting on  $A_{EP}$  at the pile base) and the displacement of the rigid circular disc,  $w_j(z = L)$  (Timoshenko and Goodier, 1970) (cf., Figure 6.1). This relation can be mathematically expressed through the constitutive equations (Mylonakis and Gazetas, 1998) to become the second boundary condition for the case of mechanical loading as

$$E_{EP} A_{EP} \left. \frac{\partial w_j}{\partial z} \right|_{z=L} + K_b w_j(z = L) = 0 \quad (6.1)$$

where (Boussinesq, 1878)

$$K_b = \frac{2DG_{soil}}{1-\nu_{soil}} \quad (6.2)$$

4. The determination of the corrected pile-soil-pile interaction factor defined as in equation (5.2).
5. The analysis of the vertical displacement  $w_j(z)$  of any pile,  $j$ , composing a general group with a total number of piles,  $n_{EP}$ , in which some or all of the piles may be subjected to loading through the interaction factor method.

In the case of piles subjected to thermal loads, this analysis can be performed as (Rotta Loria and Laloui, 2016b)

$$w_j(z) = w^{1,th}(z) \sum_{i=1}^{i=n_{EP}} \Delta T_i \Omega_{ij}^{th}(s, z) \quad (6.3)$$

where  $w^{1,th}(z)$  is the vertical displacement along the length of a single isolated pile per unit temperature variation,  $\Delta T_i$  is the applied temperature variation to pile  $i$ , and  $\Omega_{ij}^{th}$  is the interaction factor for two piles subjected to thermal loading in a pair corresponding to the centre-to-centre distance between pile  $i$  and pile  $j$ .

In the case of piles subjected to mechanical loads, this analysis can be performed as (Poulos, 1968)

$$w_j(z) = w^{1,m}(z) \sum_{i=1}^{i=n_{EP}} P_i \Omega_{ij}^m(s, z) \quad (6.4)$$

where  $w^{1,m}(z)$  is the vertical displacement along the length of a single isolated pile per unit mechanical load,  $P_i$  is the applied mechanical load to the head of pile  $i$ , and  $\Omega_{ij}^m$  is the interaction factor for two piles subjected to mechanical loading in a pair corresponding to the centre-to-centre distance between pile  $i$  and pile  $j$ .

It is worth noting that the described interaction analysis can consider pile groups in both uniform and non-uniform (e.g., stratified) soil deposits. The response of any single isolated pile in non-uniform soil deposits can be considered with accuracy by developing the finite element analysis highlighted in step 1. The definition of the vertical displacement of the soil surrounding the source pile and that of the receiver pile addressed in steps 2 and 3, respectively, can approximately be performed by considering a mean value of the shear modulus of the soil layer where the displacement is calculated at any soil node,  $k$ , and the shear modulus of the soil layer where the point load is applied at any pile node,  $l$ , through step 2. The resulting definition of the interaction factor addressed in step 4 and the

subsequent interaction factor analysis targeted in step 5 can finally refer to situations involving pile groups in both uniform and non-uniform soil deposits.

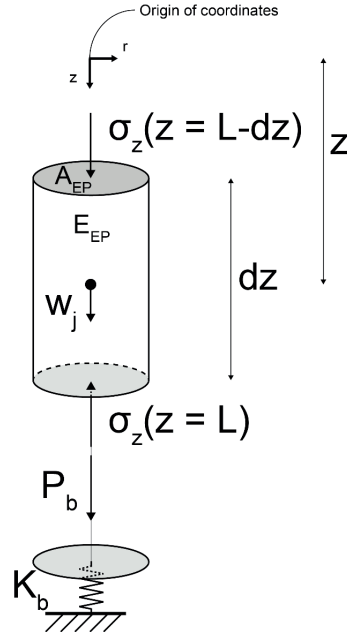


Figure 6.1: Vertical equilibrium of a base element of a receiver pile.

### 6.2.2 Modified interaction factor analysis approach

Currently, both  $w_i(z)$  (step 1 of the analysis approach presented in Section 6.2.1) and  $w_j(s, z)$  (steps 2 and 3) are computed using the same value of soil Young's modulus adjacent to the pile, i.e., the "near-pile" soil modulus  $E_{soil}$ . The resulting interaction factor analysis is linear elastic and does not account for non-linear soil deformation.

In the following, a modified procedure for addressing non-linear soil deformation is proposed for energy piles. This procedure has been extended and modified from that of Poulos (1988) based on the different definitions of the interaction factor used in this work and in the referenced one, and the related mathematical needs to rigorously describe the deformation problem of pairs of piles.

In this procedure, the vertical displacement of the single isolated source pile,  $w_i(z)$ , is calculated (step 1) using the near-pile soil modulus,  $E_{soil}$ , whereas the vertical displacement of the receiver pile in the pair,  $w_j(s, z)$ , is calculated (steps 2 and 3) using an average soil modulus,  $\bar{E}_{soil}$ , which accounts for the smaller strain levels between the piles. The resulting modified interaction factor analysis is linear elastic and accounts for non-linear soil deformation.

The average soil modulus is given by the following expressions (cf., Figure 6.2)

$$\bar{E}_{soil}(s) = E_{soil} \left( 1 + \frac{(\mu_E - 1)(s - D)}{2s_t} \right) \quad \text{for } s < s_t + D \quad (a) \quad (6.5)$$

$$\bar{E}_{soil}(s) = E_{soil} \left( \mu_E + \frac{(1-\mu_E)s_t}{2(s-D)} \right) \quad \text{for } s \geq s_t + D \quad (b)$$

where  $\mu_E = E_{soil,m}/E_{soil}$  (for which  $E_{soil,m}$  is the soil “mass” modulus between the piles) is likely to lie within the range of 3 and 10 and  $s_t$  is a transition distance likely to be between  $3D$  and  $6D$  (Poulos, 1988).

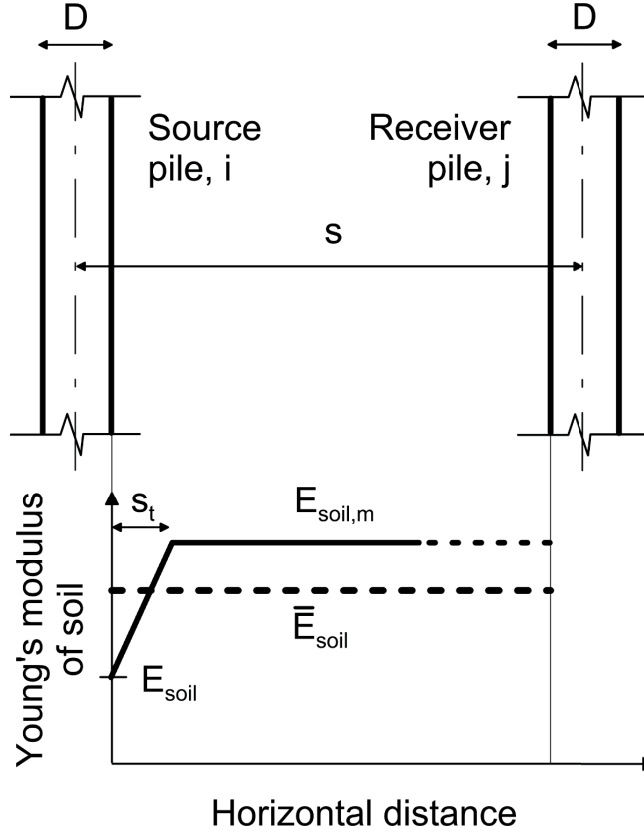


Figure 6.2: Assumed distribution of soil modulus between two piles.  $E_{soil}$  = near-pile soil modulus (characteristic of high strain levels);  $E_{soil,m} = \mu_E E_{soil}$  (with  $\mu_E \geq 1$ ) = soil mass modulus (characteristic of low strain levels);  $\bar{E}_{soil}$  = average soil modulus for computing interactions;  $s_t$  = transition distance.

The described distribution of soil modulus to determine  $\bar{E}_{soil}$  for calculating  $w_j(s, z)$  is indeed simplified for a number of reasons. First, because the non-linear soil deformation is considered through a linear distribution of soil modulus between the piles. Next, because the ratio of the soil mass to the near-pile soil modulus needed to define this linear distribution may be somewhat arbitrarily defined (Leung et al., 2010). Then, because the problem of non-linear soil deformation is solved by considering a constant and unique value of average soil modulus between the piles, and linear elastic soil behaviour. Finally, because the interaction factor calculated with reference to two different distributions of soil modulus characterising the single pile and the pair of piles will generally differ from the

interaction factor calculated with reference to a unique distribution of soil modulus that merges the previous ones and characterises both the single pile and pair of piles. In principle, extensive experimental evidence may be of help for formulating a procedure more adherent to reality. In practice, (i) the lack of such evidence, (ii) the resulting increase in complexity of the procedure that would not commensurably improve the results of the analysis and (iii) the success of the analogous procedure proposed by Poulos (1988) corroborate the use of the considered approach.

## **6.3 Modelling of pile group tests**

### **6.3.1 Experimental tests reported by O'Neill et al. (1981)**

#### *6.3.1.1 Site and pile group characterisation*

The results of a comprehensive programme of full-scale *in situ* tests performed on eleven conventional piles subjected to vertical mechanical loading were reported by O'Neill et al. (1981). The piles were socketed in an overconsolidated clayey soil deposit and consisted in closed-end tubular steel pipes of an external diameter of  $D = 273$  mm, a wall thickness of  $t_w = 9.27$  mm, and an embedded length of  $L = 13.11$  m (cf., Figure 6.3). Two piles were driven as isolated reference piles. Nine other piles were driven in a square  $3 \times 3$  arrangement. The two reference piles were located at a spacing of  $s = 10.4D$  from the centre of the pile group. The piles in the group were located at spacing of  $s = 3D$  apart from each other (cf., Figure 6.3). A rigid slab made of reinforced concrete connected the piles in the group with the possibility to be detached from any pile to form subgroups. A geotechnical characterisation of the site was performed through standard penetration tests, cone penetration tests, pressuremeter tests, unconsolidated undrained triaxial tests, laboratory consolidation tests and cross-hole seismic tests. Further information is given by O'Neill et al. (1981).

#### *6.3.1.2 Pile group tests*

Different tests were performed in the aforementioned campaign (O'Neill et al., 1981). Those included (cf., Figure 6.4) the vertical mechanical loading of the two reference piles (reference pile tests 1), of the 9-pile group (9-pile group test 1), of a 5-pile subgroup (5-pile subgroup test) and of a 4-pile subgroup (4-pile subgroup test). Measurements of the vertical displacement of the piles and of the soil as well as of the load redistribution in the pile groups were made and are detailed by O'Neill et al. (1981).

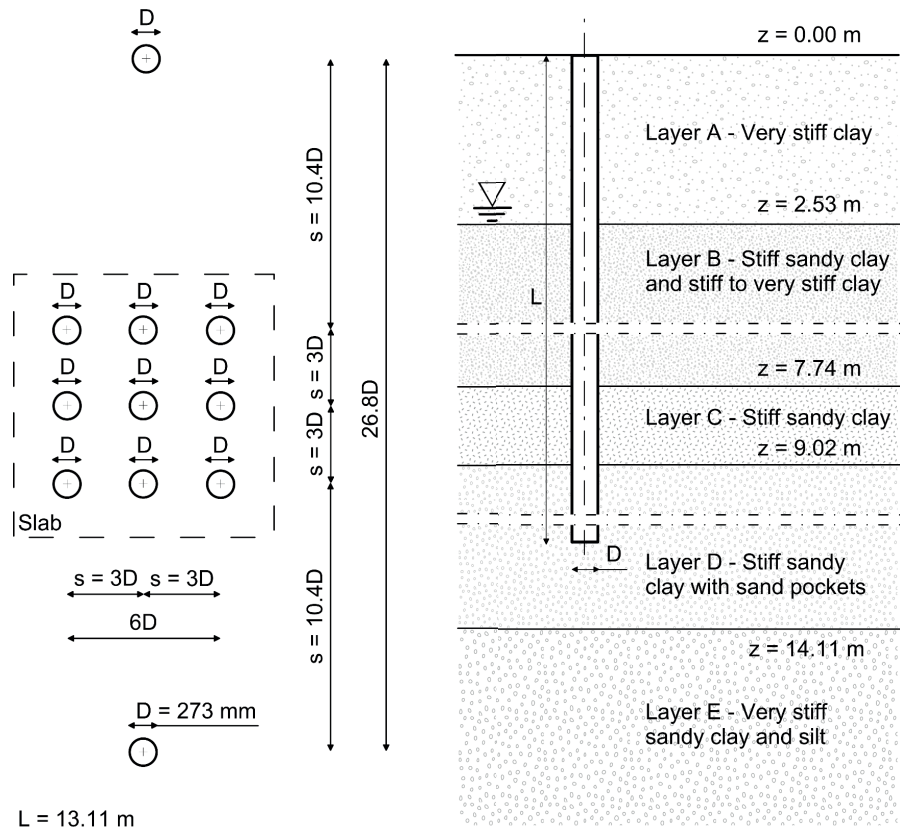


Figure 6.3: The features of the considered site, based on the information reported by O'Neill et al. (1981).

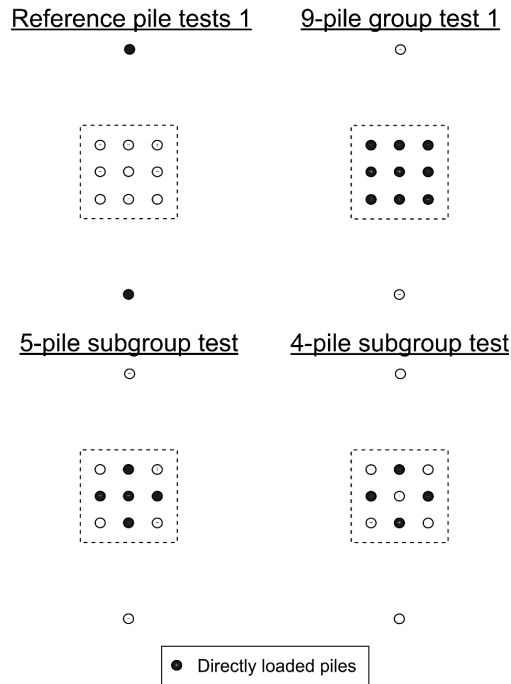


Figure 6.4: Geometrical configuration of the piles tested by O'Neill et al. (1981) for mechanical loading, further considered in this work for thermal loading.

### 6.3.2 Models

#### 6.3.2.1 Modelling choices

Two stationary thermo-mechanical finite element analyses characterised by the mathematical formulation reported by Rotta Loria and Laloui (2016b) (cf., equations (B1-3) in Appendix B) are performed using the software COMSOL Multiphysics (COMSOL, 2014). The first analysis simulates the response of the single isolated piles tested by O'Neill et al. (1981) under mechanical loading. Because the considered numerical analysis was performed after the occurrence of the modelled event and with the associated results available, it is classified as a Class C1 prediction (Lambe, 1973). The second analysis simulates the response of the same single isolated piles under thermal loading.

Two series of analytical analyses carried out using the classical and modified interaction factor approaches are also performed. The first series of analyses (i) applies the classical and modified interaction factor approaches for simulating the real case study tested by O'Neill et al. (1981) involving pile groups subjected to mechanical loads where non-linear soil deformation was observed, (ii) validates the proposed analysis approach by comparing the experimental and modelling results, and (iii) addresses the effects of non-linear soil deformation on the vertical displacement of pile groups subjected to mechanical loads following the analyses of Poulos (1988). The second series of analyses (i) applies the classical and modified interaction factor approaches for investigating pile groups subjected to thermal loads and (ii) expands on the effect of non-linear soil deformation on the vertical displacement of and interaction among energy pile groups subjected to thermal loads.

In all of the analyses: (i) the piles are assumed to be isotropic, homogeneous and uniform cylindrical solids that are considered to be representatively described by linear thermo-elastic behaviour; (ii) the soil layer is assumed to be an isotropic, homogeneous and uniform mass that can be considered to be semi-infinite and representatively described by linear elastic behaviour (i.e., the soil is an infinite heat reservoir that remains at a fixed constant temperature); and (iii) the same loads that are applied to the piles in the single isolated case are also considered to be applied uniformly to the piles in the groups.

#### 6.3.2.2 Finite element model

An axisymmetric finite element model characterised by a depth of  $h_l = 25L$  and a width of  $x = 500D$  is made to simulate the response of the single isolated piles (cf., Figure 6.5). In this model, extremely fine tetrahedral meshes are used to describe the pile and soil domains.

#### 6.3.2.3 Boundary and initial conditions

In the analyses, restrictions are applied to both the vertical and horizontal displacements on the bottom horizontal boundary that may be considered to characterise the deep soil domain surrounding the piles (i.e., pinned boundary), and to the horizontal displacements on the vertical boundary (i.e., roller boundary). No restrictions are applied to the displacements on the top boundary of the pile and soil surfaces.



No residual stresses from the installation of the piles are considered in these elements and in the adjacent soil region. This hypothesis may not be completely representative of reality but can be applied successfully in methods of pile deformation analysis by choosing appropriate soil modulus values (Poulos and Davis, 1980).

When addressing the response of the piles subjected to mechanical loads, the experimentally observed vertical mechanical load of  $Q_u = 678$  kN for which the single isolated pile failure was observed (O'Neill et al., 1981) is considered to be applied at the pile heads. However, the results presented in the following generally refer to the reference mechanical load  $P_{ref} = 356$  kN.

When addressing the response of the piles subjected to thermal loads, the temperature variation of  $\Delta T = 10$  °C is considered to be applied to these elements. The soil domain is treated as an infinite heat reservoir. The initial temperature of the piles is assumed to be  $T_0 = 15$  °C.

Figure 6.5 summarises the boundary conditions considered in the analyses, with reference to the axisymmetric finite element model.

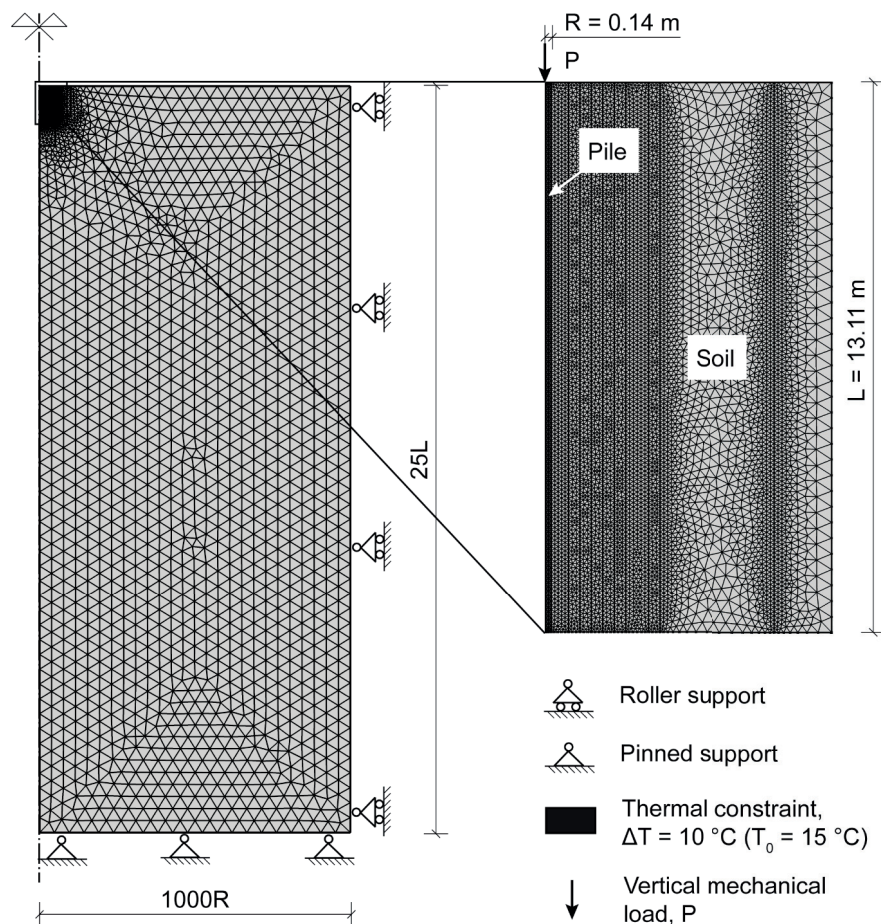


Figure 6.5: The finite element model of the single isolated pile.

### 6.3.2.4 Material parameters

Table 6.1 presents the material parameters that were reported by O'Neill et al. (1981) for the site, based on experimental test results. Table 6.2 reports the material parameters used in this study. The same value of Poisson's ratio of the soil reported by O'Neill et al. (1981) was considered in the analyses, by referring to undrained conditions. Lower values of this parameter, which may have been more appropriate to describe the actual soil behaviour under thermal loading, were also used in preliminary analyses ( $0.3 \leq \nu_{soil} \leq 0.5$ ). However, a variation of these values within the considered range was found to involve a limited influence on the results. Hence, the value of  $\nu_{soil} = 0.5$  was eventually used for preserving agreement with the indications of O'Neill et al. (1981). Differently to the experimental observation, the piles are characterised by a uniform and homogeneous cross-section made of steel, and the soil is characterised by constant values with depth of the near-pile modulus (steps 1-3 in the classical interaction factor approach and step 1 in the modified interaction factor approach) and average modulus (steps 2-3 in the modified interaction factor approach). The near-pile soil modulus was determined according to the pressuremeter test data and the considerations of O'Neill et al. (1981). The soil mass modulus used to calculate the average soil modulus was determined according to the crosshole seismic test data and the considerations of Poulos (1988). Figure 6.6 presents the evolution of the normalised soil Young's modulus with the normalised pile depth presented by O'Neill et al. (1981) and assumed for this study. A transition distance of  $s_t = 3D$ , as suggested by Poulos (1988), is considered in the modified interaction factor analysis approach.

Table 6.1: Material parameters reported by O'Neill et al. (1981) characterising the considered problem.

Experiment	
Soil parameters	
Near-pile Young's modulus, $E_{soil}(z = 0)$ : [MPa]	17.2
Near-pile Young's modulus, $E_{soil}(z = L)$ : [MPa]	79.2
Mass Young's modulus, $E_{soil,m}(z = 0)$ : [MPa]	92.0
Mass Young's modulus, $E_{soil,m}(z = L)$ : [MPa]	453.3
Poisson's ratio, $\nu_{soil}$ : [-]	0.5

Table 6.2: Material parameters used to model the considered problem.

Model			
Soil parameters		Pile parameters	
Near-pile Young's modulus, $E_{soil}$ : [MPa]	49	Young's modulus, $E_{EP}$ : [MPa]	210000
Mass Young's modulus, $E_{soil,m}$ : [MPa]	272.6	Poisson's ratio, $\nu_{EP}$ : [-]	0.3
Poisson's ratio, $\nu_{soil}$ : [-]	0.5	Normalised transition distance, $s_t/D$ : [-]	3
Linear thermal expansion coefficient, $\alpha_{soil}$ : [1/°C]	-	Linear thermal expansion coefficient, $\alpha_{EP}$ : [1/°C]	$1.2 \cdot 10^{-5}$

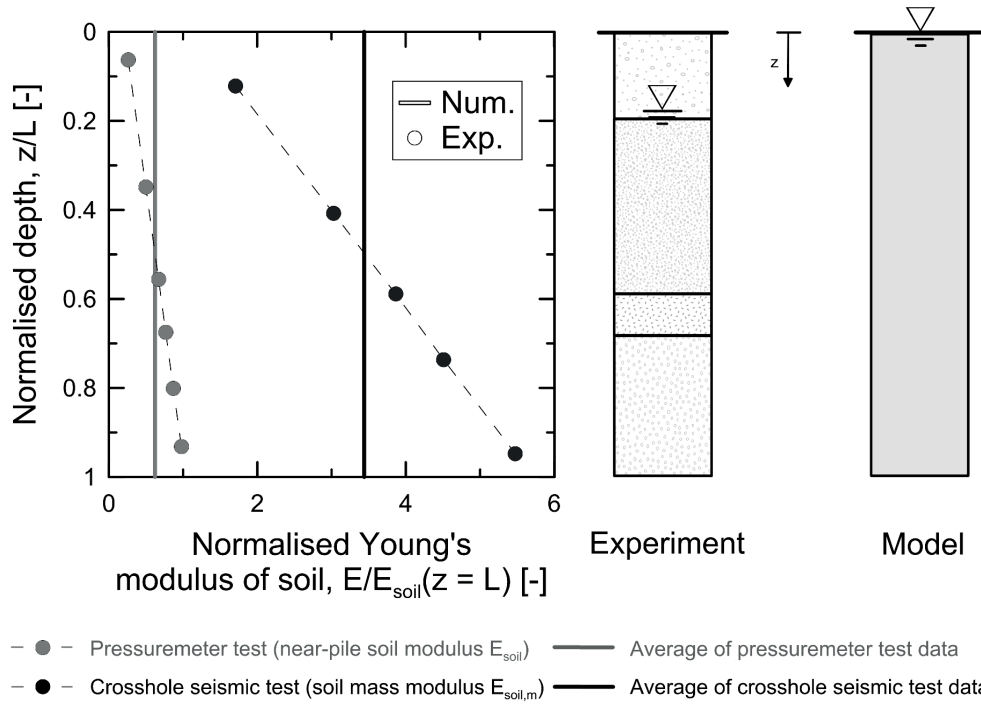


Figure 6.6: Evolution of the normalised soil Young's modulus with the normalised pile depth presented by O'Neill et al. (1981) and assumed for this study.

## 6.4 Results

### 6.4.1 Validation of the numerical model against experimental results

Figure 6.7 (a) presents a comparison between the numerically modelled and experimentally observed load-displacement curves for the single isolated pile. The vertical head displacement of the pile is normalised by the pile diameter. The applied vertical load is normalised by the value of mechanical load corresponding to failure. The numerical results are in close agreement with the experimental observations, although the former fail in capturing the latter when plastic strains occur in the soil surrounding the pile for a normalised vertical load approximately greater than  $P/Q_u = 0.6$ . This result is in accordance with the linear elastic soil behaviour considered in the numerical analysis and the associated incapability of the analysis of capturing plastic strains. The agreement between the results for a normalised vertical load of approximately up to  $P/Q_u = 0.6$ , i.e., within the elastic branch of the load-settlement curve, justifies the hypothesis of using a constant value of soil Young's modulus for characterising the elastic response of the single isolated pile in the numerical model.

Figure 6.7 (b) presents a comparison between the numerically modelled and experimentally observed evolution of the normalised vertical load in the pile with the normalised pile depth. The normalised reference mechanical load applied at the pile head of  $P_{ref}/Q_u = 0.52$  is considered. The numerical results are highly comparable to the experimental data and together with the results presented in Figure 6.7 (a) prove the capability of the axisymmetric analysis of capturing the response of the single isolated pile under the serviceability conditions that are of interest for this study.

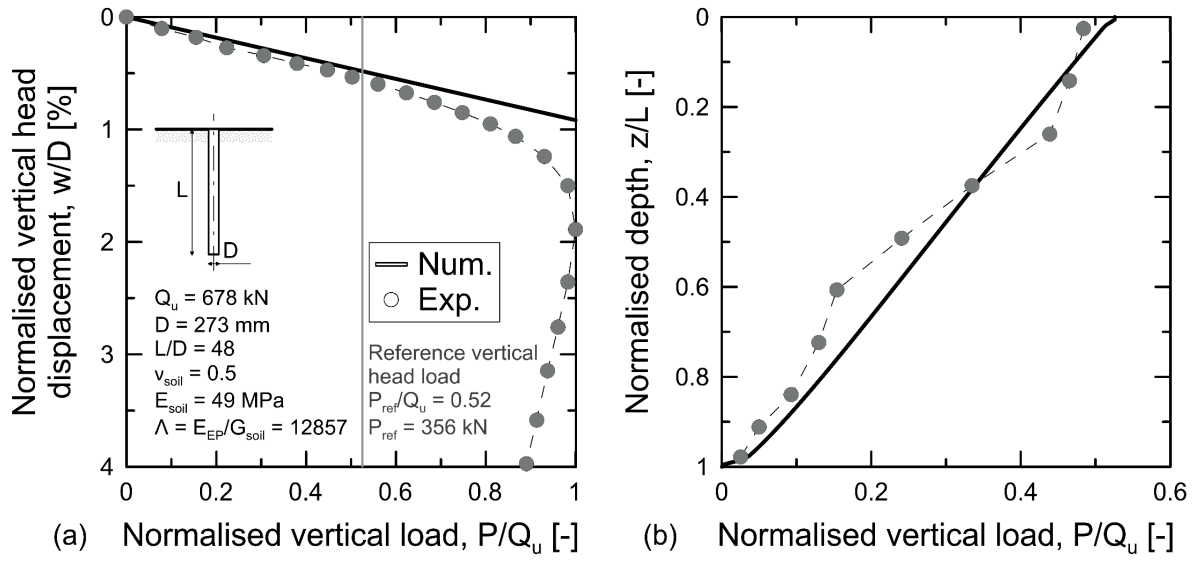


Figure 6.7: Comparison between the numerically modelled and experimentally observed (a) load-displacement curves for the single isolated pile and (b) evolution of the normalised vertical load with the normalised depth in the pile.

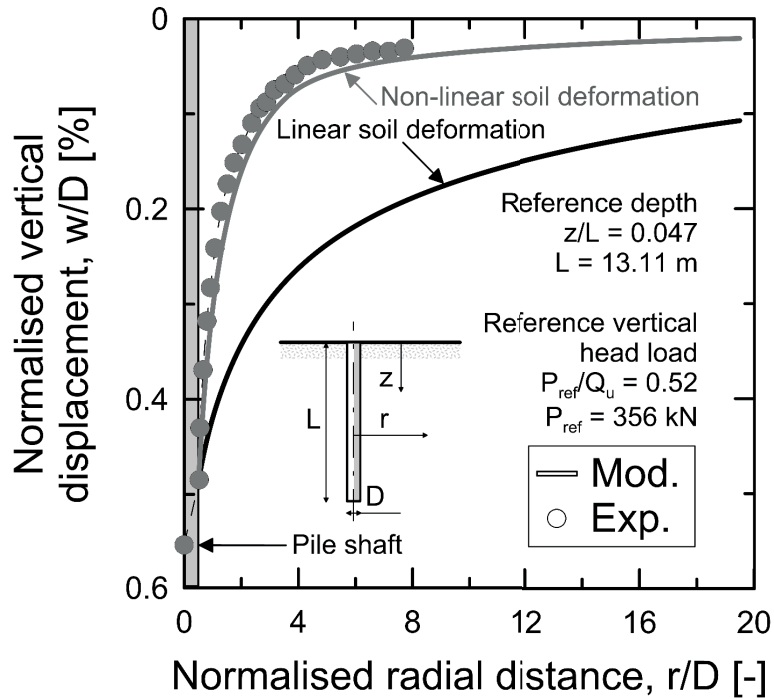


Figure 6.8: Comparison between the modelled and experimentally observed evolutions of the normalised vertical displacement with the normalised radial distance from the pile axis.

Figure 6.8 presents a comparison between the modelled and experimentally observed evolutions of the normalised vertical displacement with the normalised radial distance from the pile axis. Reference is made to a normalised depth of  $z/L = 0.047$ . The results of two different analyses are presented:

- An analysis that addresses linear soil deformation based on steps 1 and 2 of the classical interaction factor approach. In this analysis, the soil displacement,  $w(r, z)$ , is calculated analytically (step 2) based on the vertical displacement,  $w_i(z)$ , and shear stress,  $\tau_i(z)$ , distributions characterising the single isolated source pile using the same value of near-pile soil modulus,  $E_{soil}$ , that is used in the numerical analysis to define  $w_i(z)$  and  $\tau_i(z)$  (step 1).
- An analysis that addresses non-linear soil deformation based on steps 1 and 2 of the modified interaction factor approach. In this analysis, the soil displacement,  $w(r, z)$ , is calculated analytically (step 2) based on the vertical displacement,  $w_i(z)$ , and shear stress,  $\tau_i(z)$ , distributions characterising the single isolated source pile using a different value of soil modulus,  $\bar{E}_{soil}$ , compared to the near-pile soil modulus,  $E_{soil}$ , that is used in the numerical analysis to define  $w_i(z)$  and  $\tau_i(z)$  (step 1).

The close comparison between the modelling results addressing the non-linear soil deformation and the experimental results proves the occurrence of the considered phenomenon. This phenomenon was originally remarked by O'Neill et al. (1981). The agreement between the obtained results validates also the choice of the transition distance of  $s_t = 3D$  suggested by Poulos (1988) for the considered site.

The above validates the numerical model against the results of the full-scale *in situ* reference pile tests 1.

#### 6.4.2 Pile group vertical displacement induced by mechanical loading

Figure 6.9 presents a comparison between the modelled and experimentally observed evolutions of the normalised average vertical head displacement of the piles,  $\bar{w}$ , with the number of directly (mechanically) loaded piles,  $n_{LP}$ , for the reference pile tests 1, the 9-pile group test 1, the 5-pile subgroup test and the 4-pile subgroup test. The normalised reference mechanical load applied at the pile heads of  $P_{ref}/Q_u = 0.52$  is considered. The results of two different modelling analyses addressing linear soil deformation based on the classical interaction factor approach and non-linear soil deformation based on the modified interaction factor approach are presented. The results of the modified interaction factor analysis approach considering non-linear soil deformation are in close agreement with the experimental observations for the pile groups considered, differently from the results obtained through the classical interaction factor analysis approach. This evidence underscores the tendency of the classical interaction factor analysis approach to overestimate group effects and displacement interactions among the piles, and thus, the average vertical displacement of pile groups subjected to mechanical loads. This result also highlights the capability of the modified interaction factor analysis approach of capturing the vertical displacement of pile groups in non-linearly deforming soils.

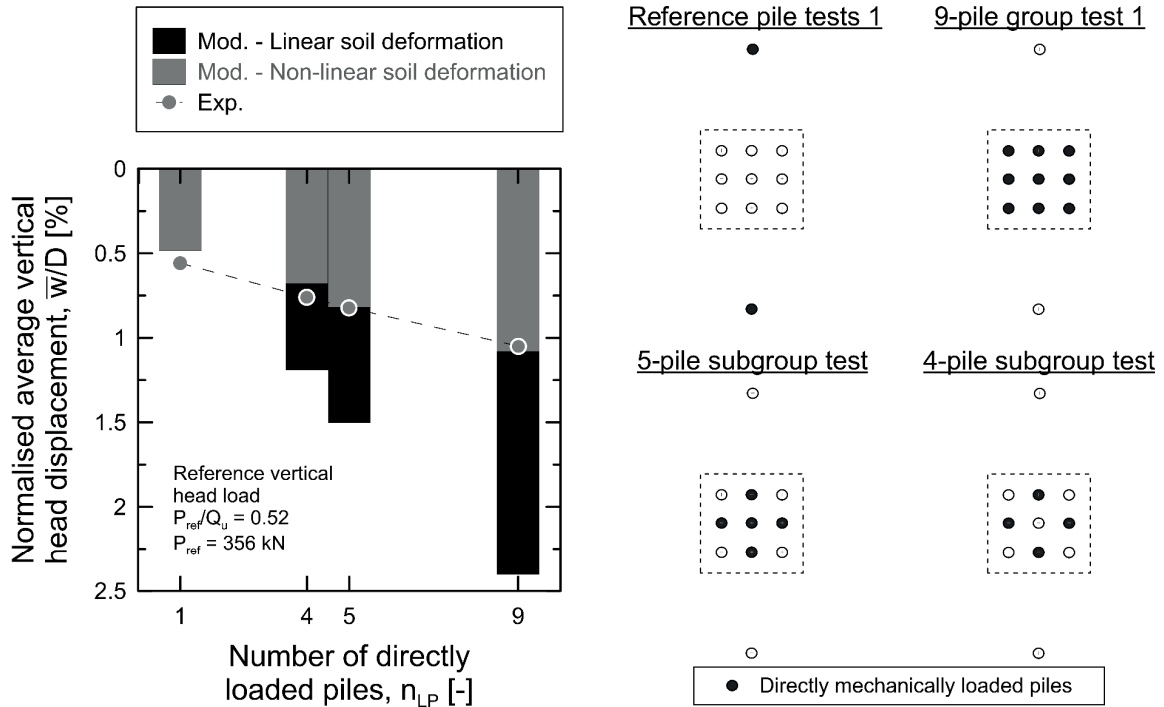


Figure 6.9: Comparison between the modelled and experimentally observed evolutions of the normalised average vertical head displacement of the piles with the number of directly mechanically loaded piles for the different pile tests considered.

Figure 6.10 presents the values of the normalised average soil Young's modulus corresponding to the centre-to-centre spacing between different pairs of piles that are used in the modified interaction factor analysis approach to define the interaction factor and the vertical displacement for different numbers and locations of piles subjected to loading. The average Young's modulus of soil is normalised by the near-pile Young's modulus. Although for any given distance between two piles a constant soil mass modulus value is used, the normalised average soil Young's modulus varies non-linearly for different pile spacing according to equation (6.5). This fact highlights the capability of the modified interaction factor analysis approach to consider non-linear soil deformation (through a linear elastic behaviour of the soil surrounding the piles) depending on the geometrical configuration of the piles in any group, in addition to the material properties characterising the group.

#### 6.4.3 Pile group vertical displacement induced by thermal loading

Figure 6.11 (a) presents a comparison between the modelled evolutions of the normalised average vertical head displacement of the piles with the number of directly (thermally) loaded piles for the reference pile tests 1, the 9-pile group test 1, the 5-pile subgroup test and the 4-pile subgroup test. The temperature variation applied to the piles of  $\Delta T = 10^\circ \text{C}$  is considered. The results of two different modelling analyses addressing linear soil deformation based on the classical interaction factor approach and non-linear soil deformation based on the modified interaction factor approach are presented. In both of these analyses, the corrected vertical displacement of the piles in the groups is determined by referring to the boundary condition referred to the position of the null point of the



shear stress. As previously observed for the case in which the piles are mechanically loaded, the classical interaction factor analysis approach determines a greater average vertical head displacement of the pile groups compared to the modified interaction factor analysis approach. The overestimation of the group displacement associated with the application of the classical interaction factor analysis approach compared to the estimate achieved through the application of the modified interaction factor analysis approach increases with the number of thermally loaded piles in the group.

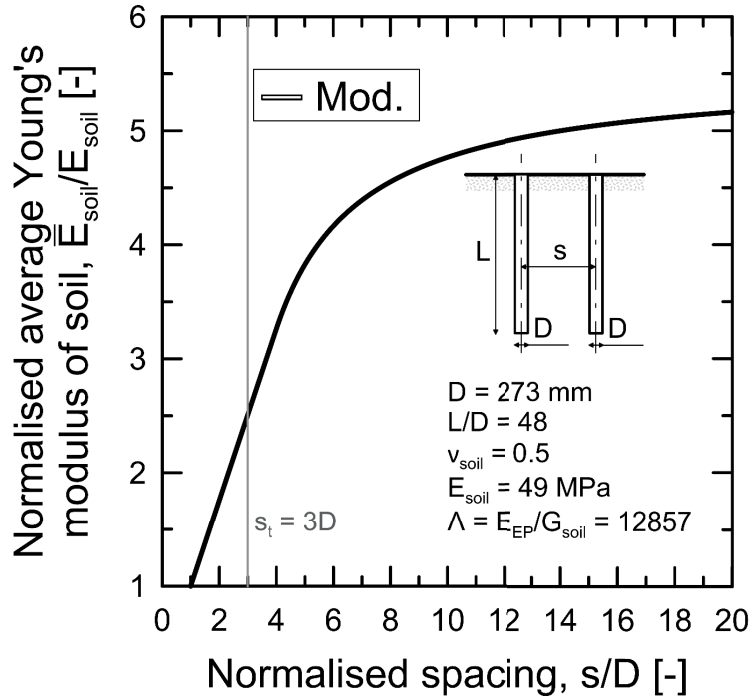


Figure 6.10: Values of the normalised average soil Young's modulus corresponding to the centre-to-centre spacing between different pairs of piles that are used in the modified interaction factor analysis approach.

Figure 6.11 (b) presents the results of equivalent analyses compared to those used for obtaining the results summarised in Figure 6.11 (a), except for the use of the boundary condition referring to the pile base, instead of the boundary condition referring to the null point of the shear stress. The considered modelling approach effectively coincides with that proposed by Mylonakis and Gazetas (1998) for the vertical deformation of piles subjected to mechanical loads. This modelling approach does not account for the key distinguishing feature characterising the vertical deformation of piles subjected to thermal loads compared to that of piles subjected to mechanical loads, i.e., the presence of the null point. Therefore, this modelling approach yields a less accurate though valid analysis of the vertical deformation of piles subjected to thermal loads. This result confirms the preferable use of the boundary condition expressed in equation (5.15) for solving the equilibrium equation (5.13) that was proposed for piles subjected to thermal loads. The reason for this is that the approach based on the use of equation (5.15) estimates a group displacement that is considered to be more adherent to reality and lower than the vertical displacement that may be estimated through the approach based on the use of equation (6.1).

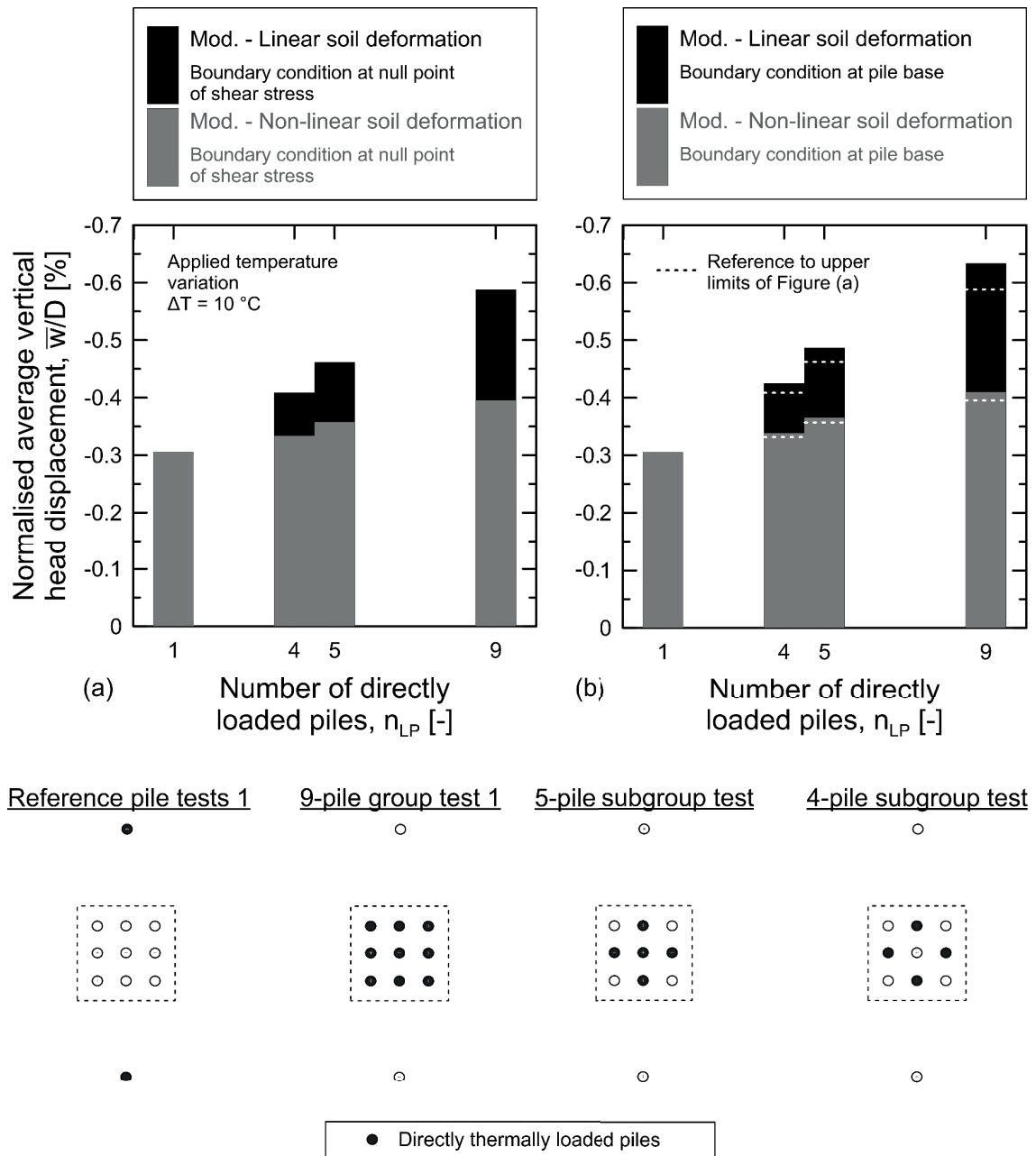


Figure 6.11: The modelled evolutions of the normalised average vertical head displacement of the piles with the number of directly thermally loaded piles for the different pile tests considered.

#### 6.4.4 Interaction factor for energy piles in non-linearly deforming soil

Figure 6.12 shows the fundamental reason why the modified interaction factor analysis approach addressing non-linear soil deformation estimates a smaller group displacement compared to the classical interaction factor analysis approach addressing linear soil deformation.



The evolution of the interaction factor with the centre-to-centre spacing between a pair of piles characterised by the features considered thus far is shown for interaction factor analyses considering and neglecting non-linear soil deformation, respectively. It is evident that considering non-linear soil deformation through the modified interaction factor analysis approach involves a smaller estimate of the interaction factor among the piles compared to that obtained when neglecting such a phenomenon through the classical interaction factor analysis approach.

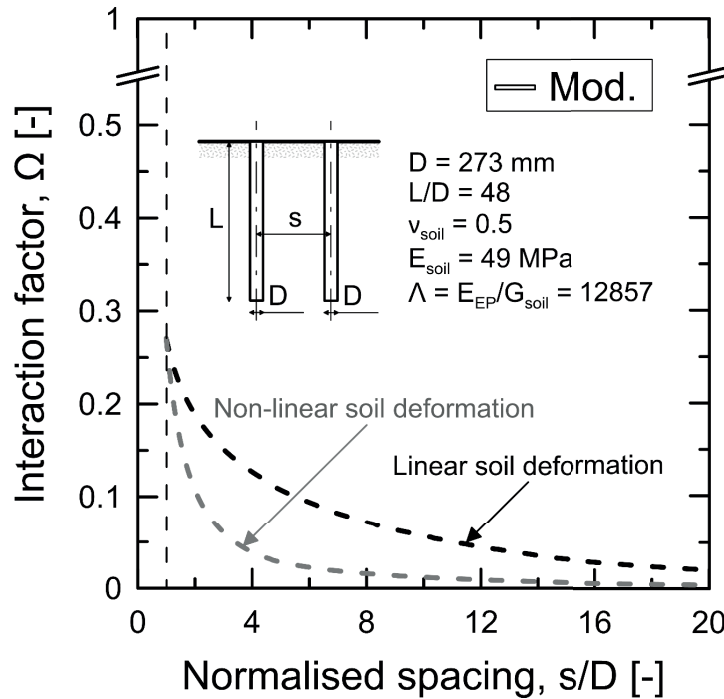


Figure 6.12: Evolution of the interaction factor with the centre-to-centre spacing between a pair of piles characterised by linear or non-linear soil deformation.

The relative reduction in the interaction factor described by the modified analysis approach compared to that estimated by the classical approach decreases with the increasing pile spacing. This result is caused by the smaller impact of non-linear soil deformation on pile-soil-pile interaction with increasing distance between the piles as a consequence of the localisation of non-linear soil deformation in the close vicinity of the piles. In the interaction factor analysis approach, higher estimates of the interaction factor result in greater computed group displacements for the same displacement of the single isolated reference pile. Therefore, the classical interaction factor analysis approach is considered to be remarkably conservative for design situations in which soil deformation may be non-linear compared to the modified interaction factor analysis approach. The decrease in the interaction factor relationship characterising situations where non-linear soil deformation is observed may suggest negligible displacement interactions among piles. This may be the case for design situations characterised by very few short and stiff piles located in a group. However, displacement interactions among piles are generally considered to deserve attention in the analysis and design of pile groups, especially when many long and compressible piles may be subjected to thermal and/or mechanical loads.

## 6.5 Concluding remarks

This work presented an analysis of the effect of non-linear soil deformation on the displacement interaction among energy pile groups. The work is based on a modified interaction factor analysis approach that (i) has been validated against experimental evidence involving full-scale pile group tests available in the literature and (ii) may be expediently used to estimate the vertical displacement of general configurations of pile groups subjected to thermal and/or mechanical loads in situations where non-linear soil deformation is noteworthy.

The main conclusions that can be drawn from this study are as follows (Rotta Loria et al., 2017c):

- The displacement interaction among piles subjected to thermal loads decreases in situations where soil deformation is non-linear compared to situations in which soil deformation is linear.
- This result is in accordance with evidence for pile groups subjected to mechanical loads that has been expanded in this work.
- For given material properties and shapes of the piles composing any group, the extent of the decrease of the displacement interaction depends on (i) the ratio between the soil modulus characterising the bulk between the piles (i.e., the soil mass modulus) and the regions close to the piles (i.e., the near-pile soil modulus); (ii) the number of piles; and (iii) the centre-to-centre spacing between the piles.
- The classical interaction factor analysis approach tends to overestimate the vertical displacement of pile groups subjected to thermal and/or mechanical loads in situations where soil deformation is non-linear.
- Although the classical interaction factor analysis approach may be remarkably conservative in situations where soil deformation is non-linear, it is considered to be easier to apply than the modified interaction factor analysis approach and thus still valuable for practical analysis and design of pile groups subjected to thermal and/or mechanical loads.
- Although non-linear soil deformation involves lower displacement interactions among piles subjected to loading compared to the case in which soil deformation may be linear, interaction factor analyses are considered of paramount importance for a comprehensive design of pile groups. This consideration appears to be particularly valuable for groups of numerous long and compressible piles (e.g., subjected to thermal loads).

## Chapter 7

# The equivalent pier method for energy pile groups

This study presents a method for estimating the average vertical displacement of energy pile groups subjected to thermal loads. The method consists of replacing any regular energy pile group with a single equivalent pier of the same length and an equivalent diameter. This equivalent pier is described by material properties that are a homogenisation of those of the piles and the surrounding soil and by a load-displacement relationship of a characteristic energy pile in the group. The load-displacement relationship of the equivalent pier differs from that of a single isolated energy pile because it is modified to account for group effects. These effects include a greater vertical displacement of the piles subjected to loading in the group compared to the case in which they are isolated, thus involving a more pronounced average group displacement. Comparisons with results obtained through the interaction factor and finite element methods prove that the proposed approach can accurately estimate the average vertical displacement of energy pile groups. This novel formulation of the equivalent pier method may be used at both preliminary and successive stages of the analysis and design of energy pile groups to expediently assess the thermally induced displacement response of such foundations.

### 7.1 Introduction

The analysis and assessment of the displacement of pile groups subjected to loading are key steps for the design of such foundations. The reason for this is that the displacement of piles subjected to a load in a group is generally greater than the displacement that may be estimated for each of the piles in the group when dimensioned as a single isolated element for supporting the same load. This phenomenon arises because when the piles are located sufficiently close to each other, group effects induced by interactions between the displacement fields of the piles occur, and a different behaviour from that of a single isolated pile is involved. Group effects have been widely evidenced in conventional applications of piles subjected to mechanical loads when serving as structural supports for on- and off-shore constructions (e.g., Whitaker, 1957; Sowers et al., 1961; Poulos, 1968; O'Neill, 1983). They have also been recently observed in innovative applications of energy piles subjected to both

mechanical and thermal loads when serving as structural supports and geothermal heat exchangers for civil structures and infrastructures (e.g., Di Donna et al., 2016; Rotta Loria and Laloui, 2017d).

To address the displacement response of conventional pile groups subjected to mechanical loads, consideration of a solid block composed of piles and the soil contained between them is a widely used approach in geotechnical engineering. The roots of this approach date back to over forty years ago, when studies (Poulos, 1968; Poulos and Davis, 1980; Butterfield and Douglas, 1981) highlighted the effectiveness and suitability of replacing any pile group by a single equivalent pier that displaces an equal amount. Two types of approximations have generally been considered for this purpose: (i) a single pier of the same circumscribed plan area as the group with an equivalent length (Poulos, 1968) and (ii) a single equivalent pier of the same length as the piles with an equivalent diameter (Poulos, 1993). This analysis approach, often termed the *equivalent pier method*, has been applied in various forms, including early formulations based on an elastic description of the pier-soil interaction that were applied through the boundary element method (Poulos and Davis, 1980; Poulos, 1993) and successive formulations based on an elasto-plastic description of the pier-soil interaction that were applied through the load-transfer method (Randolph and Clancy, 1993; Randolph, 1994; Clancy and Randolph, 1996; Horikoshi and Randolph, 1998; Castelli and Maugeri, 2002; Castelli and Motta, 2003; McCabe and Lehane, 2006; Sheil and McCabe, 2014). The equivalent pier method is useful for a number of purposes, including the estimation of (i) the average vertical displacement of any relatively small pile group and (ii) the average and differential vertical displacement of any large foundation comprising a number of pile groups with the aid of other methods (e.g., the interaction factor method) to consider intergroup interaction. This method has been proven to provide results adherent to reality when applied to the analysis of closely spaced pile groups (Castelli and Maugeri, 2002; Castelli and Motta, 2003; McCabe and Lehane, 2006; Sheil and McCabe, 2014). Applying the equivalent pier method is generally suggested when the response of pile groups is predominantly elastic because the effects of the interactions among the piles that the method aims to capture are elastic. The method may still be applied for analysing the load-displacement behaviour of pile groups where non-linear soil response occurs around each pile. Based on these facts, European Standards (EN 1997, 2004) currently propose to analyse and design pile groups subjected to axial mechanical loads at both ultimate (collapse-related) and serviceability (deformation-related) limit states with this method.

Although characterised by different mechanisms and additional governing material parameters, the behaviour of energy pile groups subjected to thermal loads is considered to be characterised by a number of common physical factors related to the behaviour of conventional pile groups subjected to mechanical loads. These include the dependence of the capacity behaviour of any single energy pile in the group on the conditions at the pile-soil interface (e.g., floating piles) and pile base (e.g., end-bearing piles) (Rotta Loria et al., 2015b) and the dependence of the deformation behaviour of the group on the conditions in the soil away (i.e., far field) from the single energy piles composing it (Rotta Loria and Laloui, 2017d). To address the displacement response of closely spaced energy pile groups subjected to thermal loads, considering the behaviour of a solid block constituted by the energy piles and the soil surrounding them may thus be suitable. This assessment appears attractive in view of the expedient capabilities of the equivalent pier approach for capturing the displacement response of conventional pile groups and the availability of only a simplified method for considering that of energy pile groups (Rotta Loria and Laloui, 2016b).

Based on the above considerations, the goal of this study (Rotta Loria and Laloui, 2017b) is to propose for the first time a formulation of the equivalent pier method for estimating the average vertical displacement of energy pile groups subjected to thermal loads by considering the mechanisms and variables governing the behaviour of such foundations.

In the following, the hypotheses and the mathematical formulation constituting the proposed method are first presented. The method is then applied to simulate the behaviour of groups of  $2 \times 2$ ,  $3 \times 3$ ,  $4 \times 4$  and  $5 \times 5$  energy piles and is validated based on a comparison with results obtained through the interaction factor and finite element methods (Rotta Loria and Laloui, 2016b). Finally, concluding remarks that can be drawn from this work are proposed.

## 7.2 The equivalent pier method for energy pile groups

### 7.2.1 Hypotheses and considerations

Reference is made in this study to energy piles and equivalent piers that are (i) free to move vertically at their heads (i.e., no head restraint), (ii) characterised by an infinitely flexible slab and (iii) free of superstructure mechanical loads. Aspect (i) allows a safety side analysis against the effects of both monotonic and cyclic thermal loads (involving potentially irreversible effects at the pile-soil interface) to be made. Aspects (ii) and (iii) allow focusing for the purpose of the present study on the effects of the thermal loads applied to the energy piles rather than on those of the mechanical loads. Considering the presence of a slab connecting the energy piles and characterising the equivalent piers may indeed be feasible. In those cases, an effective approach may consist in assuming the slab as infinitely rigid. Poulos and Davis (1974) and Selvadurai (1979) propose formulae for calculating the stiffness of slabs assumed as infinitely rigid elements. Poulos and Davis (1980) remark, however, that the average vertical displacement of a pile group characterised by an infinitely flexible slab is approximately equal to that of the same group with an infinitely rigid slab.

The energy piles are approximated as solid cylindrical prisms and form a regular geometry in plan view (e.g., square groups of energy piles). The equivalent piers are also considered to be solid cylindrical prisms. The proposed approach can also consider other cross-sectional shapes of the energy piles and the equivalent piers as well as other energy piles arrangements.

The materials constituting the energy pile, the equivalent pier and the soil domains are assumed to be isotropic, homogeneous and uniform. The material properties are considered to be insensitive to the considered temperature variations. The pipes inside the energy piles and the equivalent piers are not modelled. This choice involves considering the temperature field in these domains as that of the heat carrier fluid circulating inside the pipes in the reality. The materials constituting the energy piles and the equivalent piers follow a linear thermo-elastic behaviour. The soil follows an elasto-plastic behaviour, although the impact of the temperature variations observed in reality in this material on the response of the pile group is implicitly considered in the analyses.

The energy piles are considered to be embedded in a deep soil layer at the same initial temperature  $T_0$  and are subjected to a temperature variation,  $\Delta T = T - T_0$ , where  $T$  is an actual temperature value. This temperature variation is assumed to be (i) applied instantaneously and uniformly along the length

of all of the piles in the group, (ii) constant with time, and (iii) equal for all the piles. The same temperature variation is assumed to be applied to the equivalent piers. Considering situations in which different temperature variations or (equal or different) thermal powers would be applied to the energy piles may indeed be feasible.

The dominant mode of heat transfer in the soil is considered to be conduction. Moisture migration is negligible. The impact of ground water advection is considered to be negligible. Thermal contact resistance between the energy piles and the soil is discounted. The variation of the thermal field at the ground surface as a consequence of a potential variation in the environmental conditions is assumed to be negligible. The aforementioned assumptions allow an expedient although simplified analytical resolution of the thermal problem characterising the single energy piles that may be needed when defining the homogenised material properties of the equivalent piers (cf., Section 7.2.3). The temperature at the far fields from the pile group, i.e., the (bottom) horizontal and vertical boundaries that may be considered to characterise the deep soil domain surrounding the piles, is assumed to remain constant with time and equal to  $T_{\infty} = T_0$ . The horizontal (top) boundary described by the soil surface is treated as adiabatic. Differences in the thermal field around the energy piles are expected for scenarios where the soil surface may be assumed to be adiabatic or characterised by a fixed constant temperature, with a consequent impact on the mechanical behaviour of these ground structures (Bodas Freitas et al., 2013). However, because the former condition appears to more closely characterise real energy pile applications than the latter (especially for piles located far from the external boundaries of large thermally insulated buildings), it is considered in this work.

The load-displacement behaviour of the equivalent piers is modelled using the one-dimensional load-transfer method proposed by Coyle and Reese (1966). Only the axial displacements of the equivalent piers are considered. The radial displacements are neglected according to the considered one-dimensional approach. This choice appears to be justified based on the small values of radial displacements characterising single energy piles (Olgun et al., 2014) and the consequent limited impact of these displacements on the vertical displacement behaviour of the group. Horizontal stress decrease may occur at the shaft of single energy piles due to the application of cyclic thermo-mechanical loads involving non-linear soil response in this setting (Ng et al., 2016a). However, while a decrease of the displacement interaction among the piles may be expected because of this phenomenon, this effect would be counterbalanced by the increase in vertical displacement of the piles, resulting in an average group displacement almost unaffected. The self-weight of the material constituting the equivalent piers is neglected. The load-displacement relationship characterising the equivalent piers relies on a modification to account for the group effects of the relationships proposed by Knellwolf et al. (2011) and by Frank and Zhao (1982). This modified load-transfer relationship has been implemented in software called Thermo-Pile for the analysis and design of energy piles. The load-displacement relationships used for characterising the single isolated energy piles and the equivalent piers are considered to be unaffected by any potential temperature effects. Although these effects were remarked for single energy piles in some situations (McCartney and Rosenberg, 2011; Wang et al., 2011; Ng et al., 2015) they were not identified in others (Regueiro et al., 2012; Goode et al., 2014; Kramer and Basu, 2014). These effects are considered to be negligible in the examples presented in this work because they belong to the latter situations. Their consideration may improve the adherence of analyses to situations where the load-displacement relationship of single energy piles may be sensitive to temperature effects. Consideration of methods and relationships other than those used in this work to



characterise the load-displacement behaviour of the energy piles and the equivalent piers may be possible.

In the following, compressive stresses, contractive strains and downward displacements (i.e., settlements) are considered to be positive.

### 7.2.2 Geometry of the equivalent pier

The key concept of the equivalent pier approach is that any regular pile group can be modelled as a single equivalent pier by considering the soil region in which the piles are embedded as a homogenised continuum (cf., Figure 7.1). Such an equivalent pier is characterised by a length coincident with the average length of the piles and by an equivalent diameter that can be calculated as (Poulos, 1993)

$$\begin{aligned} D_{eq} &\approx 1.27\sqrt{A_g} && \text{for predominantly floating piles} && (a) \\ D_{eq} &= \frac{2}{\sqrt{\pi}}\sqrt{A_g} \approx 1.13\sqrt{A_g} && \text{for predominantly end-bearing piles} && (b) \end{aligned} \quad (7.1)$$

where  $A_g$  is the plan area of the group. For any general configuration of piles,  $A_g$  can be determined as

$$A_g = A_{t,EP} + A_{soil} \quad (7.2)$$

where  $A_{t,EP}$  is the total cross-sectional area of the piles composing the group ( $A_{t,EP} = n_{EP}A_{EP}$  where  $n_{EP}$  is the number of piles in the group and  $A_{EP}$  is the cross-sectional area of a single pile) and  $A_{soil}$  is the plan area of soil surrounding the piles delimited by the simplest polygon that better reproduces the shape of the pile group. For a square geometry of piles,  $A_g$  can be calculated as

$$A_g = [(\sqrt{n_{EP}} - 1)s + D]^2 \quad (7.3)$$

where  $s$  is the centre-to-centre spacing between the piles and  $D$  is the pile diameter.

Numerical analyses performed suggest that the choice of using equations (7.1) to determine  $D_{eq}$  leads to differences of up to 5% between the estimated values of average vertical displacement. This result holds for both low and high magnitudes of thermal loads and mechanical loads imposed prior to the temperature variations to equivalent piers for common pile and soil strata stiffness and pile spacing.

Considering an equivalent pier of the same (average) length of the piles in the group and of an equivalent diameter appears to be preferable to considering an equivalent pier of the same circumscribed plan area as the group and an equivalent length. Reference to the same length of the piles allows

considering the properties (e.g., thermal and mechanical) of the soil layers that may surround the pile group and govern its deformation and capacity behaviours.

Based on the considered approach, any pile group with a total cross-sectional area of piles

$$A_{t,EP} = \pi \frac{D^2}{4} n_{EP} \quad (7.4)$$

is replaced by a single equivalent pier of cross-sectional area

$$A_{eq} = \pi \frac{D_{eq}^2}{4} \quad (7.5)$$

The shape of the pile group can be categorised by the “aspect ratio”, which can be determined for a square geometry of piles in plan view as (Randolph and Clancy, 1993)

$$AR = \sqrt{\frac{n_{EPS}}{L}} \quad (7.6)$$

where  $L$  is the (average) length of the piles. The equivalent pier approach has been proven to provide a representative description of the behaviour (e.g., deformation and capacity) of conventional pile groups subjected to mechanical loads for values of  $AR$  smaller than 4 and certainly less than 2 (Randolph, 1994). This approach has also been suggested to provide sufficiently accurate results for practical purposes (characterised by a 20% variation with those obtained with more rigorous approaches) for pile groups with a centre-to-centre pile spacing of up to 5 diameters (Poulos et al., 2002). The reason for this is that for larger aspect ratios ( $AR > 3 \div 4$ ) and wider pile spacing ( $s > 5D$ ), the pile group resembles a “shallow” foundation more than a “deep” foundation, so the hypothesis of a block-behaviour of the group is no longer valid. Numerical analyses performed over a broad range of design conditions suggest that the considerations summarised above for conventional pile groups subjected to axial mechanical loads are also valid for energy pile groups subjected to thermal loads.



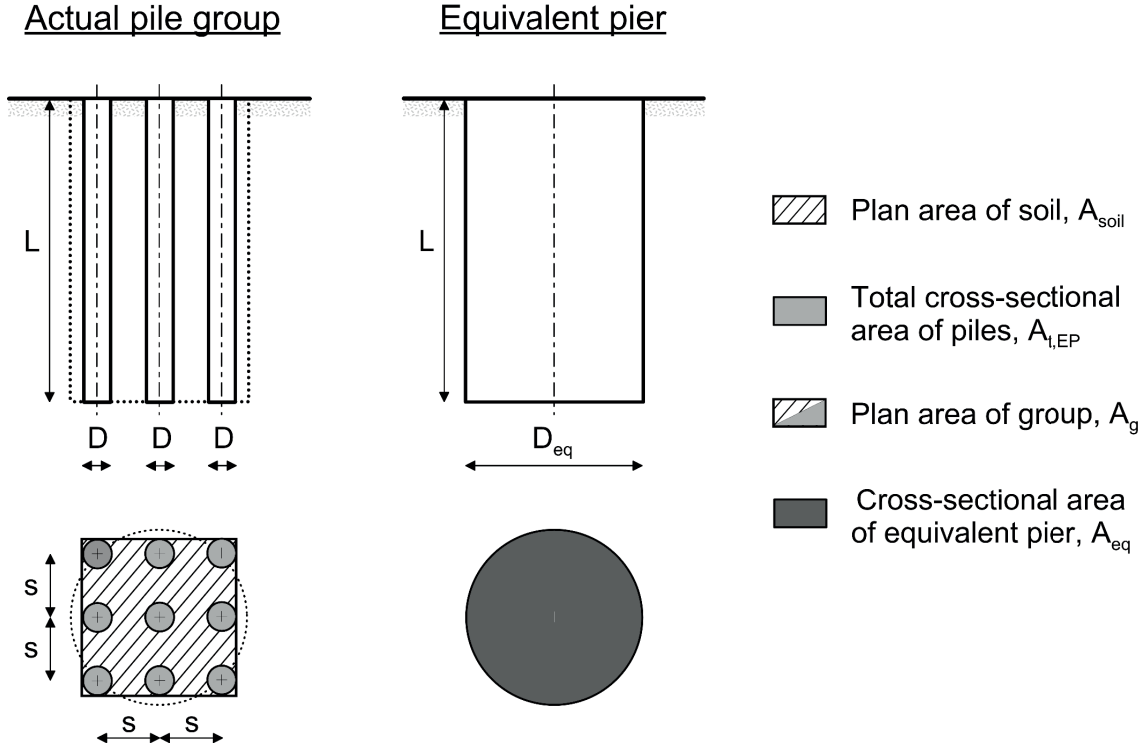


Figure 7.1: The modelling approach.

### 7.2.3 Homogenised material properties of the equivalent pier

There are two crucial dimensionless parameters that characterise the response of energy pile groups subjected to thermal and mechanical loads, assuming that the loads and all other material properties of the groups are the same (Rotta Loria and Laloui, 2017d; Rotta Loria and Laloui, 2016b): the pile-soil stiffness ratio,  $\Lambda = E_{EP}/G_{soil}$ , where  $E_{EP}$  is the Young's modulus of the piles composing the group and  $G_{soil}$  is the shear modulus of the soil ( $G_{soil} = E_{soil}/(2(1 + \nu_{soil}))$ ), in which  $E_{soil}$  is the Young's modulus of the soil and  $\nu_{soil}$  is the Poisson's ratio of the soil), and the soil-pile thermal expansion coefficient ratio,  $X = \alpha_{soil}/\alpha_{EP}$ , where  $\alpha_{soil}$  is the linear thermal expansion coefficient of the soil and  $\alpha_{EP}$  is the linear thermal expansion coefficient of the piles. The material properties involved in defining these two dimensionless ratios are considered for determining two key material properties in the characterisation of the response of the equivalent pier to thermal (and mechanical) loads: the equivalent Young's modulus,  $E_{eq}$ , and the equivalent linear thermal expansion coefficient,  $\alpha_{eq}$ .

The equivalent pier can be characterised by an equivalent Young's modulus effectively homogenising that of the piles and of the soil embedded between them that can be calculated as the weighted average of the Young's modulus of these bodies as (Poulos, 1993)

$$E_{eq} = \frac{A_{t,EP}E_{EP} + A_{soil}E_{soil}}{A_{t,EP} + A_{soil}} = E_{EP} \frac{A_{t,EP}}{A_g} + E_{soil} \left(1 - \frac{A_{t,EP}}{A_g}\right) \quad (7.7)$$

This definition of the equivalent pier modulus accounts for the effect that the excess stiffness of the piles compared to that of the soil has on the deformability problem by considering superposition of the representative areas involved (cf., Figure 7.2).

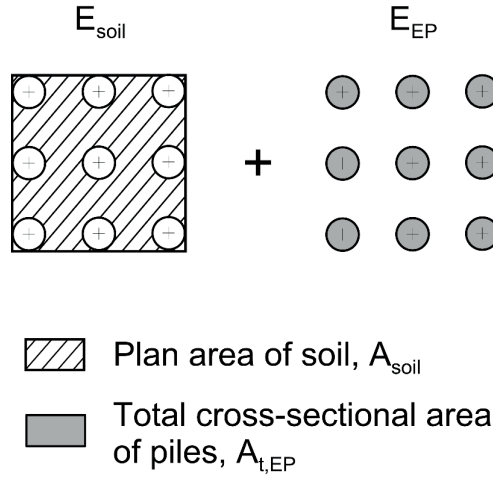


Figure 7.2: Schematic for the calculation of the Young's modulus of the equivalent pier.

The equivalent pier can then be characterised by an equivalent linear thermal expansion coefficient that can be calculated as (Rotta Loria and Laloui, 2017b)

$$\begin{aligned} \alpha_{eq} &= \alpha_{EP} & \text{for } X = \alpha_{soil}/\alpha_{EP} \leq 1 & \quad (a) \\ \alpha_{eq} &= \frac{A_{EP}\alpha_{EP} + A_{exc}\alpha_{soil}Y}{A_{EP} + A_{exc}} = \alpha_{EP} \frac{A_{EP} + A_{exc}XY}{A_{EP} + A_{exc}} & \text{for } X = \alpha_{soil}/\alpha_{EP} > 1 & \quad (b) \end{aligned} \quad (7.8)$$

where  $Y$  is a coefficient that relates the average temperature variation in the soil to that in the energy piles within the plan area  $A_{exc}$  in which the thermal strain potential of the soil is in excess compared to the thermal strain potential of the energy piles (cf., Figure 7.3). The formulation (b) of equation (7.8), together with the associated assumptions and governing parameters, is presented below.

Equations (7.8) represent the key novelty that allows applying the classical equivalent pier concept originally proposed for the displacement analysis of conventional pile groups subjected to only mechanical loads to energy pile groups that are also subjected to thermal loads. Formulation (a) of equation (7.8) expresses that when  $X = \alpha_{soil}/\alpha_{EP} \leq 1$ , the deformation of the energy pile group may be interpreted and described by considering only the thermal expansion coefficient of the piles and the related thermally induced deformation because it governs that of the group. Formulation (b) of equation (7.8) highlights that when  $X = \alpha_{soil}/\alpha_{EP} > 1$ , the deformation of the energy pile group may be interpreted and described by considering also the thermal expansion coefficient of the soil surrounding the piles and the related thermally induced deformation because it profoundly characterises that of the group. In particular, the definition of formulation (b) of equation (7.8) is based on a similar

concept to that characterising equation (7.7). Formulation (b) of equation (7.8) accounts for the impact of a linear thermal expansion coefficient of the soil in excess compared to that of the piles on the deformability problem by considering superposition of the representative areas involved. The phenomena described by equations (7.8) have been recently observed to characterise the deformation behaviour of energy pile groups subjected to thermal loads (Rotta Loria and Laloui, 2017d; Rotta Loria and Laloui, 2016b) (cf., Chapter 3).

The fundamental assumption that allows obtaining the simple formulation of the equivalent linear thermal expansion coefficient expressed in formulation (b) of equation (7.8) is that thermal interactions between the energy piles in any considered group are negligible.

This choice may represent an approximation of the real temperature field around the energy piles for long-term durations of applied thermal loads, especially in situations characterised by (i) soil deposits with high values of effective thermal conductivity, (ii) small centre-to-centre spacing among the piles in the group, and (iii) soil deposits presenting groundwater flow (all of these aspects may facilitate the development of thermal interactions), and may rarely characterise reality.

However, this choice is valuable because it involves determining the temperature field around the energy piles as if they were isolated heat sources, with a consequent effective determination of the parameters  $Y$  and  $A_{exc}$  needed in formulation (b) of equation (7.8).

The theoretical development of formulation (b) of equation (7.8) is as follows.

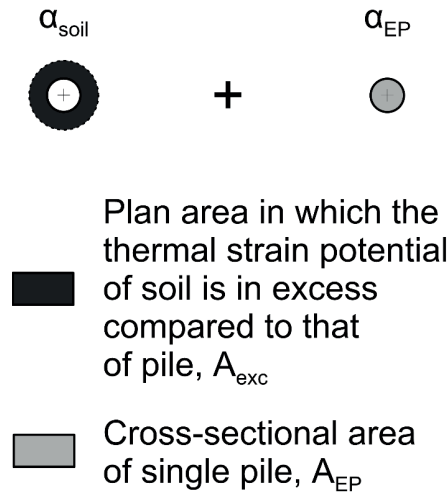


Figure 7.3: Schematic for the calculation of the linear thermal expansion coefficient of the equivalent pier.

### Context

In situations characterised by  $X = \alpha_{soil}/\alpha_{EP} > 1$ , interest lies in determining the extent of the plan area of soil  $A_{exc}$  in which the thermal strain potential of this body is in excess compared to the thermal strain potential of the energy piles. There is a radial distance,  $R_{exc}$ , in the soil for which this condition is satisfied and coincides with a temperature variation,  $\Delta T_{soil}$ , that can be expressed with reference to free thermal expansion conditions as

$$|\varepsilon_{f,soil}^{th}| > |\varepsilon_{f,EP}^{th}| \rightarrow |-\alpha_{soil}\Delta T_{soil}| > |-\alpha_{EP}\Delta T_{EP}| \rightarrow |\Delta T_{soil}| > \frac{\alpha_{EP}}{\alpha_{soil}} |\Delta T_{EP}| \Rightarrow \Delta T_{soil} = \frac{\Delta T_{EP}}{X}$$

where  $\varepsilon_{f,soil}^{th}$  and  $\varepsilon_{f,EP}^{th}$  are the thermal strains of the soil and the energy piles under free thermal expansion conditions and  $\Delta T_{EP}$  is the temperature variation characterising (e.g., applied to) the energy piles. In normalised form, this temperature variation is

$$\frac{\Delta T_{soil}}{\Delta T_{EP}} = \frac{1}{X} \quad (7.9)$$

#### *Determination of $A_{exc}$*

Knowledge of the evolution in space and with time of the temperature field around a single isolated energy pile enables  $R_{exc}$  to be determined with reference to the normalised temperature variation expressed in equation (7.9). The availability of  $R_{exc}$  allows calculating the plan area of interest as

$$A_{exc} = \pi \frac{D_{exc}^2 - D^2}{4} \quad (7.10)$$

where  $D_{exc} = 2R_{exc}$ .

The hypothesis of no thermal interactions allows the temperature field around a single isolated energy pile to be expediently assessed through a number of analytical and semi-analytical solutions. In this work, the energy piles are considered to be a single isolated infinite heat source with a spherical gap subjected to a constant temperature variation according to the conditions described in Section 7.2.1. Consideration of the heat source as a continuous infinite spherical body eliminates the need for the two boundary conditions related to the top and bottom boundaries of the soil domain described in Section 7.2.1. The evolution of the temperature field for radial distances,  $r$ , greater than the energy pile radius,  $R$ , with time,  $t$ , can consequently be determined semi-analytically as (Bergman et al., 2011)

$$T(r, t) = T_{\infty} + (T_R - T_{\infty}) \frac{R}{r} \operatorname{erfc} \left( \frac{r - R}{\sqrt{4t\alpha_d}} \right) \quad (7.11)$$

where  $T_R$  is the temperature at the energy pile radius (constant and uniform in the pile domain),  $\operatorname{erfc}$  is the complementary Gaussian error function and  $\alpha_d = \lambda/(\rho c_p)$  is the soil thermal diffusivity (where  $\lambda$  is the thermal conductivity,  $\rho$  is the bulk density and  $c_p$  is the specific heat). The parameter

$\alpha_d$  may be calculated as an average value from the thermal diffusivity of different soil layers surrounding the pile length. This fact makes the present equivalent pier approach capable of approximately considering the thermal (and mechanical) behaviour of energy pile groups in layered soils.

#### Determination of $Y$

The plan area of soil  $A_{exc}$  is characterised by an average temperature variation,  $\overline{\Delta T}_{soil}$ , that can be determined analytically based on the results of equation (7.11). This average temperature variation in the soil is related to the temperature variation in the energy piles through a factor

$$Y = \frac{\overline{\Delta T}_{soil}}{\Delta T_{EP}} \quad \text{with } \frac{1}{X} < Y \leq 1 \quad (7.12)$$

#### Definition of $\alpha_{eq}$ (formulation (b) of equation (7.8))

The average thermal strain potential of the soil under free thermal expansion conditions that is associated to  $\overline{\Delta T}_{soil}$  in  $A_{exc}$  is

$$\bar{\varepsilon}_{f,soil}^{th} = -\alpha_{soil} \overline{\Delta T}_{soil} = -\alpha_{soil} \Delta T_{EP} Y$$

Therefore, the thermal strain potential under free thermal expansion conditions of any equivalent pier, considered as a system of  $n_{EP}$  energy piles of cross-sectional area  $A_{EP}$  and  $n_{EP}$  soil areas  $A_{exc}$ , is

$$\varepsilon_{f,eq}^{th} = \frac{n_{EP} A_{EP} \varepsilon_{f,EP}^{th} + n_{EP} A_{exc} \bar{\varepsilon}_{f,soil}^{th}}{n_{EP} A_{EP} + n_{EP} A_{exc}} = \frac{A_{EP} \varepsilon_{f,EP}^{th} + A_{exc} \bar{\varepsilon}_{f,soil}^{th}}{A_{EP} + A_{exc}}$$

Because the temperature variation applied to the equivalent pier,  $\Delta T_{eq}$ , is assumed to be the same as that applied to the energy piles, from the above it is found the formulation of the equivalent linear thermal expansion coefficient of the pier expressed in formulation (b) of equation (7.8).

$$-\alpha_{eq} \Delta T_{eq} = -\alpha_{eq} \Delta T_{EP} = -\frac{A_{EP} \alpha_{EP} \Delta T_{EP} + A_{exc} \alpha_{soil} \Delta T_{EP} Y}{A_{EP} + A_{exc}} \Rightarrow \alpha_{eq} = \frac{A_{EP} \alpha_{EP} + A_{exc} \alpha_{soil} Y}{A_{EP} + A_{exc}}$$

Neglecting the thermal interactions among the energy piles involves disregarding the effect of the spacing among and position of the energy piles on the definition of  $A_{exc}$  and  $Y$ . A dependence of the thermal expansion coefficient of the equivalent pier on these features may be present in reality.

### Validation of semi-analytical solution (equation (11))

Figure 7.4 presents a comparison between the results obtained through the semi-analytical solution presented in equation (7.11) and a more rigorous thermal finite element analysis performed with the software COMSOL Multiphysics (COMSOL, 2014). The evolution of normalised temperature variation with radial distance from the axis of a single isolated energy pile subjected to a temperature variation of  $\Delta T = 10\text{ }^{\circ}\text{C}$  for  $t = 6$  months (for the reference material properties referred in Section 7.3.2) is presented. The radial distance  $R_{exc}$  that can be used for calculating  $A_{exc}$  is highlighted for the case in which  $X = \alpha_{soil}/\alpha_{EP} = 2$ . Based on the comparison between the obtained results, it appears that the semi-analytical solution expressed in equation (7.11), among others, accurately captures the evolution of temperature variation around a single isolated energy pile that can be obtained through more rigorous approaches of analysis such as the finite element method. Therefore, equation (7.11) is suitable for calculating the parameters  $A_{exc}$  and  $Y$  needed in formulation (b) of equation (7.8).

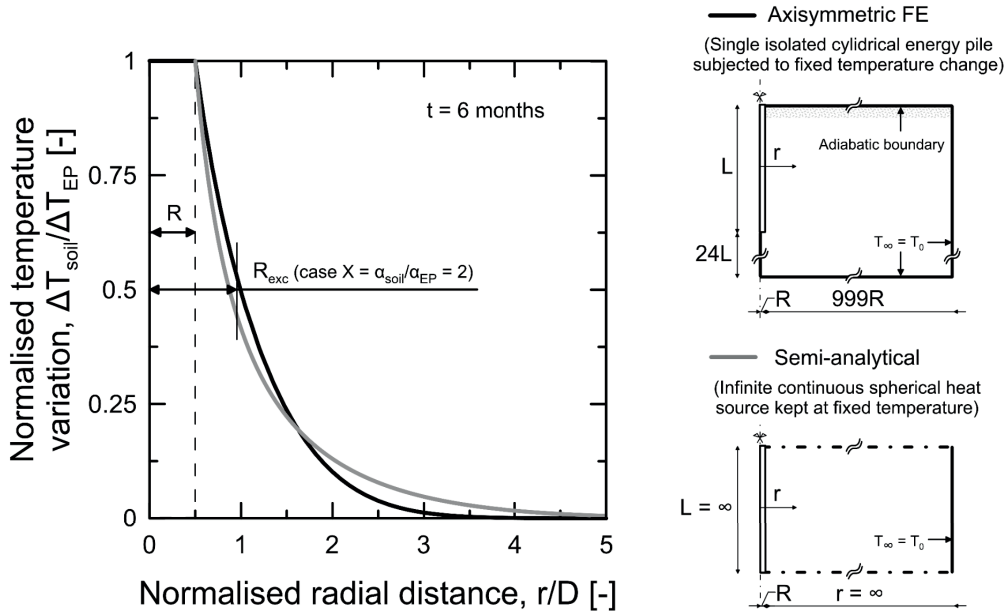


Figure 7.4: Comparison between the evolutions of the normalised temperature variation with radial distance obtained using the semi-analytical solution and the finite element (FE) method.

### 7.2.4 Load-displacement description of the equivalent pier

An advantageous feature of the equivalent pier method is that the analysis of the displacement behaviour of the equivalent pier under loading can be based on solutions or methods proposed for the analysis of single isolated piles. However, these solutions must be modified for considering the group effects caused by the displacement interactions among the piles on the load-displacement response of the pile group. Such group effects involve a more pronounced average group displacement and thus a greater displacement of the equivalent pier.

To characterise the load-displacement relationship of the equivalent pier, reference is made in this study to a characteristic energy pile in the group that is subjected to the displacement interactions highlighted above. This characteristic energy pile can be considered to be representative of the displacement behaviour of most of the piles in the group. The characteristic energy pile may be considered as a side pile for small pile groups, whereas for large pile groups as a pile located at an intermediate position between the centre and corner regions of the group. The reason for this definition is that centre and corner energy piles are characterised by the highest and lowest interactions, respectively, and are thus not representative of the behaviour of most of the piles in the group.

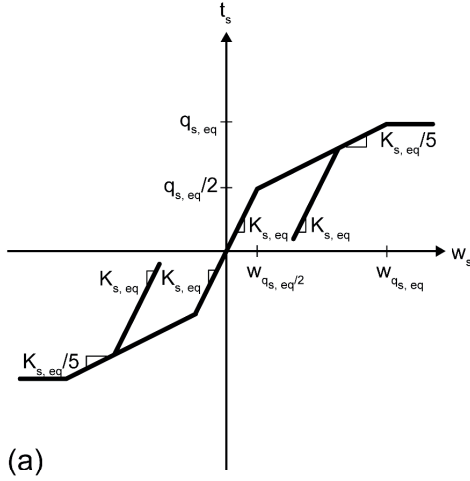
The load-transfer method considered in this work (Coyle and Reese, 1966) for analysing the load-displacement behaviour of the equivalent pier relies on modelling this body as being composed of several rigid elements that are connected by springs representing the elastic pier stiffness. Each of these rigid elements is characterised at its side (i.e., a proportion of the shaft) by an elasto-plastic interaction with the soil. The element at the toe of the pier is characterised at its base by an elasto-plastic interaction with the soil. The element at the head of the pier is characterised at its top by a spring representing the elastic pier-structure interaction (the stiffness of this spring is considered to be null in the current application, following the assumptions made in Section 7.2.1).

The elasto-plastic load-displacement relationships characterised by the features depicted in Figure 7.5 (a) and (b) are considered in this work to govern the shaft and base resistance mobilisation for shaft and base displacement of the equivalent pier, respectively. The schematics of those relationships have been extended to energy pile groups from those that were proposed by Knellwolf et al. (2011) (cf., Figure 7.5 (c) and (d)) for single isolated energy piles based on the ones presented by Frank and Zhao (1982) for single isolated conventional piles. The shape of these functions is characterised by (i) a first loading/unloading linear branch that describes the elastic response of the shaft/base of the equivalent pier/energy pile, (ii) a next loading linear branch that refers to the inelastic response of the shaft/base of the equivalent pier/energy pile, (iii) an unloading linear branch that describes the elastic response of the shaft/base when unloading occurs from a stress state along the inelastic branch, and (iv) a final plateau that can be associated with the perfectly plastic response of the shaft/base of the equivalent pier/energy pile when the ultimate shaft/base resistance value is attained.

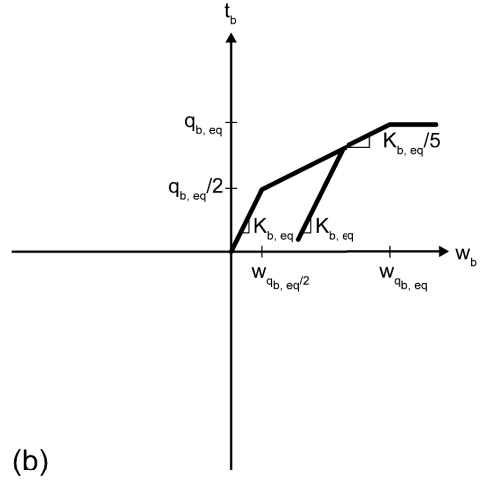
The first linear parts of the shaft and the base load-displacement (or load-transfer) functions of the equivalent pier cover shaft and base displacements of  $w_{q_{s,eq}/2}$  and  $w_{q_{b,eq}/2}$  until shaft and base resistances of  $q_{s,eq}/2$  and  $q_{b,eq}/2$  are mobilised, respectively. These values of shaft and base resistances are half of the ultimate shaft and base resistances of  $q_{s,eq}$  and  $q_{b,eq}$  of the equivalent pier, respectively. The same condition was considered by Frank and Zhao (1982) for single isolated piles, with reference to shaft and base displacements of  $w_{q_s/2}$  and  $w_{q_b/2}$ , intermediate shaft and base resistances of  $q_s/2$  and  $q_b/2$ , and ultimate shaft and base resistances of  $q_s$  and  $q_b$ , respectively. The slopes  $K_{s,eq}$  and  $K_{b,eq}$  of the loading/unloading elastic branches of the load-displacement functions of the equivalent pier represent the stiffness of the shaft and base springs that govern the elastic pier-soil interaction, respectively. The same physical meaning was considered by Frank and Zhao (1982) for single isolated piles, with reference to the shaft and base stiffness  $K_s$  and  $K_b$ , respectively. The slopes of the loading/unloading elastic branches of the shaft and base load-displacement functions of the equivalent pier are determined in this work (Rotta Loria and Laloui, 2017b) based on an extrapolation from the

definitions presented by Frank et al. (1991) for single isolated piles and a correction through a novel parameter to account for the group effects as

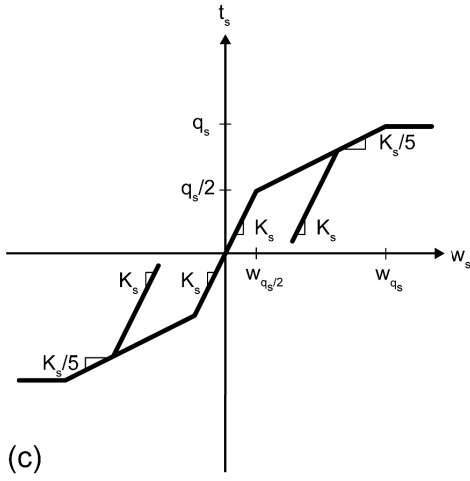
Load-transfer relationship for shaft of equivalent pier



Load-transfer relationship for base of equivalent pier



Load-transfer relationship for shaft of single isolated pile



Load-transfer relationship for base of single isolated pile

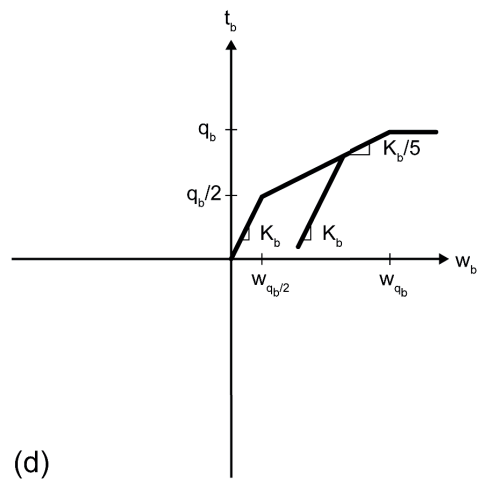


Figure 7.5: Load-displacement relationships for the shaft and base of equivalent piers ((a) and (b)) and single isolated energy piles ((c) and (d)).

$$\begin{aligned}
 K_{s,eq} &= 0.8 \frac{E_M}{D} \zeta & \text{for coarse-grained soils} & \quad (a) \\
 K_{b,eq} &= 4.8 \frac{E_M}{D} \zeta & & \quad (b)
 \end{aligned} \tag{7.13}$$

$$\begin{aligned}
 K_{s,eq} &= 2 \frac{E_M}{D} \zeta & \text{for fine-grained soils} & \quad (a) \\
 K_{b,eq} &= 11 \frac{E_M}{D} \zeta & & \quad (b)
 \end{aligned} \tag{7.14}$$



where  $E_M$  is the Menard pressuremeter modulus and  $\zeta$  is a stiffness reduction factor. The Menard pressuremeter modulus can be related to the Young's modulus of the soil according to different methods available in the literature (Clarke, 1994; Frank, 2009).

The stiffness reduction factor,  $\zeta$ , represents the key parameter to account for the group effects caused by the displacement interactions among the energy piles on the displacement response of the equivalent pier with reference to the behaviour of the characteristic energy pile. The definition of this parameter is based on a statement proposed by Randolph and Clancy (1993) for which the interaction between the piles in any group can be broadly quantified through the ratio between the length of the piles and their centre-to-centre spacing, i.e.,  $L/s$ . This statement is corroborated by considerable evidence available in the literature for both conventional and energy pile groups (e.g., Poulos, 1968; Randolph and Wroth, 1979b; Rotta Loria and Laloui, 2016b), which highlights that the interaction in any group increases with increasing pile length and decreases with increasing spacing between the piles. It thus appears rational to define a reduction factor for the stiffness of a single characteristic energy pile in any considered pile group that accounts for the interaction effects on the increase in displacement as (Rotta Loria and Laloui, 2017b)

$$\zeta = \frac{s}{L} \quad (7.15)$$

The factor  $\zeta$  varies between 0.04 and 0.5 in the practical pile applications for which the use of the equivalent pier method is suggested (cf., Section 7.2.2). It physically represents a softening of the shaft and base load-transfer curves of single isolated piles for characterising those of the equivalent pier and addresses the difference in the displacement behaviour between single isolated energy piles and groups of energy piles under the same conditions. When this stiffness reduction factor attains the theoretical upper value of  $\zeta = 1$ , equations (7.13) and (7.14) become the original relations proposed by Frank et al. (1991) for describing  $K_s$  and  $K_b$ .

Various analyses were performed to define other appropriate formulations of  $\zeta$ . These analyses considered various combinations and/or selections of the parameters that may theoretically influence the deformation of pile groups (including, e.g.,  $D$  and  $D_{eq}$ ), in linear and non-linear forms. However, the best results were found by using the proposed formulation. Although the definition of  $\zeta$  does not include the pile diameter, this parameter is taken into account in the formulations of the shaft and base stiffness  $K_s$  and  $K_b$  proposed by Frank and Zhao (1982) that are multiplied by  $\zeta$  to obtain the shaft and base stiffness of the equivalent pier  $K_{s,eq}$  and  $K_{b,eq}$ . The definitions of the shaft and based stiffness of the equivalent pier thus account for three of the characteristics that are generally recognised to most influence the behaviour of pile groups, i.e., the pile diameter,  $D$ , the pile spacing,  $s$ , and the pile length,  $L$ . Consideration of these characteristics in a linear form appears to be suitable for and in accordance with the linear nature of the load-displacement relationship employed to characterise the equivalent pier and single pile behaviours. Other formulations of the stiffness of the equivalent pier may indeed be considered and those presented in this work may alternatively be calibrated with available experimental measurements.

The loading inelastic branches of the shaft and base load-displacement functions of the equivalent pier cover shaft and base displacements greater than  $w_{q_{s,eq}/2}$  and  $w_{q_{b,eq}/2}$  until the ultimate shaft and base resistances of  $q_{s,eq}$  and  $q_{b,eq}$  are mobilised, respectively. The slopes of the inelastic branches of the equivalent pier related to the shaft and base are equal to  $K_{s,eq}/5$  and  $K_{b,eq}/5$ , respectively. The same condition was considered by Frank and Zhao (1982) for single isolated piles with reference to  $K_s/5$  and  $K_b/5$ .

The ultimate shaft and base resistances of the equivalent pier  $q_{s,eq}$  and  $q_{b,eq}$ , respectively, may be determined considering (i) the type of soil surrounding the piles, (ii) the method and order of installing the piles, and (iii) the shaft and base resistances of the single piles composing the group  $q_s$  and  $q_b$ , respectively. An extensive summary of methods that can be considered for this purpose are presented by Poulos and Davis (1980), and Bowles (1988), among others.

## 7.3 Application and validation of the method

### 7.3.1 Analysed problems

The reference problems analysed in this work comprise square groups of  $2 \times 2$ ,  $3 \times 3$ ,  $4 \times 4$  and  $5 \times 5$  semi-floating energy piles subjected to a temperature variation of  $\Delta T = 10^\circ\text{C}$  in soil deposits with different thermal expansion coefficients. An initial temperature in the energy pile and soil domains of  $T_0 = 15^\circ\text{C}$  is considered. The temperature variation applied to the energy piles is imposed instantaneously and kept constant for  $t = 6$  months. Energy piles with a length of  $L = 25$  m and a diameter of  $D = 1$  m are analysed. Normalised centre-to-centre spacing between the energy piles of  $s/D = 2, 2.5, 3$  and  $5$ , which represent the aspect ratios reported in Table 7.1 for the different energy pile groups analysed, are considered. Reference is made to Section 7.2.1 for hypotheses and modelling considerations that may have been omitted.

The displacement behaviour of the energy pile groups described in this section was recently modelled by Rotta Loria and Laloui (2016b) using the interaction factor method and more rigorous 3-D thermo-mechanical finite element analyses. The results of these analyses are considered the references for comparison with the results obtained using the equivalent pier method proposed in this work and the related validation. Detailed information on the analyses performed through the interaction factor and finite element methods is presented in Chapter 4.

Table 7.1: Values of the aspect ratio,  $AR$ , for the analysed energy pile groups.

Values of $AR$ : [-]				
$s/D$ : [-]	$2 \times 2$ energy pile group	$3 \times 3$ energy pile group	$4 \times 4$ energy pile group	$5 \times 5$ energy pile group
2	0.57	0.85	1.13	1.41
2.5	0.63	0.95	1.26	1.58
3	0.69	1.04	1.39	1.73
5	0.89	1.34	1.79	2.24

### 7.3.2 Material parameters

Relevant parameters characterising the single energy piles composing the different groups and the surrounding soil are reported in Table 7.2. The properties of the energy piles are typical of reinforced concrete. The soil properties, for the nominal value of linear thermal expansion coefficient indicated, are characteristic of dry Nevada sand. These properties have been successfully employed by Rotta Loria et al. (2015a) to model the behaviour of energy piles in the considered soil with reference to physical observations (e.g., centrifuge tests of non-displacement energy piles performed by Goode et al. (2014)). Useful equivalent pier-soil interaction parameters are summarised in Table 7.3. Relevant parameters characterising the equivalent piers reproducing the different energy pile groups analysed are reported from Table 7.4 to Table 7.7.

The ultimate shaft and base resistances of the equivalent piers are calculated by distributing the total shaft and base capacities of each group (calculated as the shaft and base capacities of the single isolated energy piles multiplied by the number of piles in the group for hypothesis) on the shaft and base area of the equivalent piers, respectively. This implies that

$$q_{s,eq} = q_s \frac{D}{D_{eq}} n_{EP} \quad (7.16)$$

and

$$q_{b,eq} = q_b \frac{D^2}{D_{eq}^2} n_{EP} \quad (7.17)$$

When possible, the estimation of  $q_{s,eq}$  and  $q_{b,eq}$  should be based on representative experimental evidence.

Table 7.2: Material parameters for the energy piles and the soil.

Energy pile parameters		Soil parameters			
$E_{EP}$ : [MPa]	30000	$G_{soil}$ : [MPa]	30	$K_s$ : [MPa/m]	28
$\nu_{EP}$ : [-]	0.25	$\nu_{soil}$ : [-]	0.30	$K_b$ : [MPa/m]	168
$\rho_{EP}$ : [kg/m <sup>3</sup> ]	2450	$\rho_{soil}$ : [kg/m <sup>3</sup> ]	1537		
$\alpha_{EP}$ : [1/°C]	1·10 <sup>-5</sup>	$\alpha_{soil}$ : [1/°C]	0, 0.5·10 <sup>-5</sup> , 1·10 <sup>-5</sup> (*), 2·10 <sup>-5</sup>		
$\lambda_{EP}$ : [W/(m °C)]	1.47	$\lambda_{soil}$ : [W/(m °C)]	0.25	$q_s$ : [kPa]	38
$c_{p,EP}$ : [J/(kg °C)]	854	$c_{p,soil}$ : [J/(kg °C)]	961	$q_b$ : [kPa]	377

(\*) Value of linear thermal expansion coefficient characterising dry Nevada sand (Rotta Loria et al., 2015a).

Table 7.3: Equivalent pier-soil interaction parameters.

$s/D$ : [-]	$\zeta$ : [-]	$K_{s,eq}$ : [MPa/m]	$K_{b,eq}$ : [MPa/m]
2	0.08	2.24	13.44
2.5	0.10	2.80	16.80
3	0.12	3.36	20.16
5	0.20	5.60	33.60

Table 7.4: Parameters for the 2×2 energy pile groups.

2×2 energy pile groups					
$s/D$ : [-]	$A_g$ : [m <sup>2</sup> ]	$D_{eq}$ : [m]	$E_{eq}$ : [MPa]	$q_{s,eq}$ : [kPa]	$q_{b,eq}$ : [kPa]
2	9	3.81	10523	40	104
2.5	12.3	4.45	7752	34	76
3	16	5.08	5953	30	58
5	36	7.62	2689	20	26

Table 7.5: Parameters for the 3×3 energy pile groups.

3×3 energy pile groups					
$s/D$ : [-]	$A_g$ : [m <sup>2</sup> ]	$D_{eq}$ : [m]	$E_{eq}$ : [MPa]	$q_{s,eq}$ : [kPa]	$q_{b,eq}$ : [kPa]
2	25	6.35	8538	54	84
2.5	36	7.62	5953	45	58
3	49	8.89	4394	38	43
5	121	13.97	1826	24	17

Table 7.6: Parameters for the 4×4 energy pile groups.

4×4 energy pile groups					
$s/D$ : [-]	$A_g$ : [m <sup>2</sup> ]	$D_{eq}$ : [m]	$E_{eq}$ : [MPa]	$q_{s,eq}$ : [kPa]	$q_{b,eq}$ : [kPa]
2	49	8.89	7752	68	76
2.5	72.3	10.80	5282	56	52
3	100	12.70	3838	48	37
5	256	20.32	1547	30	15

Table 7.7: Parameters for the 5×5 energy pile groups.

5×5 energy pile groups					
$s/D$ : [-]	$A_g$ : [m <sup>2</sup> ]	$D_{eq}$ : [m]	$E_{eq}$ : [MPa]	$q_{s,eq}$ : [kPa]	$q_{b,eq}$ : [kPa]
2	81	11.43	7331	83	72
2.5	121	13.97	4934	68	48
3	169	16.51	3554	57	35
5	441	26.67	1410	36	13

### 7.3.3 Results

Figure 7.6 presents a comparison between the results obtained through the application of the proposed equivalent pier method and the results obtained by Rotta Loria and Laloui (2016b) using the interaction factor method and more rigorous 3-D thermo-mechanical finite element analyses to investigate the displacement behaviour of square groups of 2×2, 3×3, 4×4 and 5×5 energy piles. The evolution of the normalised average vertical head displacement with close values of the normalised centre-to-centre distance between energy piles that may be encountered in practice is presented. The vertical displacement is normalised with respect to the head displacement of a single energy pile under free thermal expansion conditions,  $w_f^{th} = -\alpha_{EP} \Delta T L/2$ . The equivalent pier and interaction factor methods consider the evolution of the normalised average vertical head displacement of the energy pile groups in soil deposits characterised by soil-pile thermal expansion coefficient ratios of  $X = \alpha_{soil}/\alpha_{EP} = 0$  and 2. The curves predicted by the equivalent pier and interaction factor methods for  $\alpha_{soil}/\alpha_{EP} = 2$  are considered to be representative of the behaviour of energy pile groups for situations in which their deformation is governed by the thermally induced deformation of the soil (i.e., likely in all situations in which  $\alpha_{soil}/\alpha_{EP} > 1$ ). The curves predicted by these methods for  $\alpha_{soil}/\alpha_{EP} = 0$  are considered to be representative of the behaviour of energy pile groups for all of the other situations in which their deformation is governed by the thermally induced deformation of the piles (i.e., situations in which  $\alpha_{soil}/\alpha_{EP} \leq 1$ ).

The results suggest a greater average vertical head displacement of the energy pile groups than the vertical head displacement characterising a single isolated energy pile subjected to the same temperature variation under identical conditions. The displacement of the energy pile groups is also greater than that characterising a single energy pile under free thermal expansion conditions. This phenomenon arises because of the group effects and the related thermally induced interactions among the energy piles, and highlights the difference in the displacement behaviour of energy pile groups compared to single isolated energy piles.

The evolution of the displacement curves described by the results of both the finite element and equivalent pier analyses is not monotonic, differently from that suggested by the interaction factor analysis. This phenomenon arises because the smaller the spacing between the piles is, the more damped are the individual deformations of the piles by the presence and the stiffness of these elements. Therefore, the average group displacement is not generally greater at closer pile spacing than at wider pile spacing and does not follow the approximately logarithmic evolution (decreasing with

increasing pile spacing) that may be expected as a consequence of the displacement interaction relationship among piles. The evolution of the displacement curves described by the results of the interaction factor analysis is monotonic because of the limitations involved with this approach for describing the displacement behaviour of pile groups based on the displacement interaction between two piles in a pair and the displacement behaviour of a single isolated pile (Rotta Loria and Laloui, 2016b).

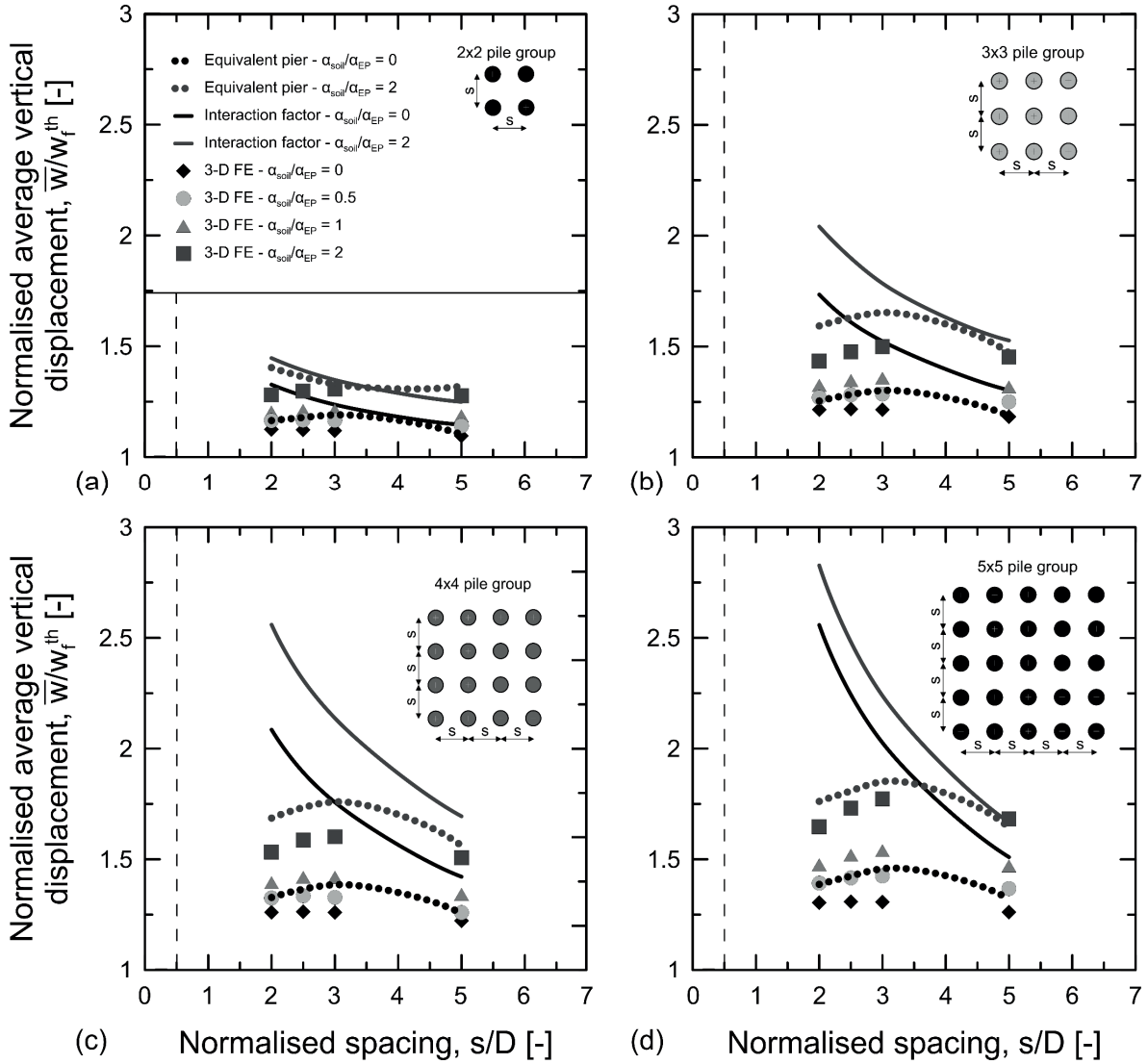


Figure 7.6: Comparison between the results obtained using the proposed equivalent pier method, the interaction factor method and 3-D thermo-mechanical finite element analyses.

The use of the equivalent pier method through the approaches described in Section 7.2.3 captures the behaviour of energy pile groups. The estimates of the average vertical head displacement appear to be on the conservative side in most of the considered cases, if reference is made to the more rigorous finite element solutions. In cases in which an underestimation is noted, the difference is (i) small compared to the values obtained through the finite element solutions, (ii) justified by the different

features of the analyses and (iii) considered to be acceptable for practical applications of the equivalent pier method. The percentage variation between the average vertical head displacement of the energy pile groups obtained through the equivalent pier analyses and the 3-D finite element analyses is in absolute value of up to 11%. This percentage variation is of the same order of magnitude than that of 8% characterising the vertical head displacement of the single energy pile composing the analysed groups based on the results of one-dimensional load-transfer analyses and axisymmetric finite element analyses. The above proves the comparable capability of the equivalent pier method of capturing the vertical head displacement of energy pile groups to that of the 3-D finite element method. The equivalent pier method is able to predict both the evolution and magnitude of normalised vertical head displacement with much greater accuracy compared to the interaction factor method for close spacing between the energy piles of up to 5 diameters. In particular, while the latter method has been suggested for spacing between the piles greater than 5 diameters (Rotta Loria and Laloui, 2016b), the method proposed in this work is suggested for the analysis of particularly closely spaced energy pile groups with pile spacing of up to 5 diameters. Despite being characterised by simplifying hypotheses and related shortcomings similar to most approximate methods, the equivalent pier and interaction factor methods are considered to be complementary approaches for investigating the behaviour of energy pile groups in a wide range of conditions. In particular, the equivalent pier and interaction factor methods are considered to be economically viable solutions for the analysis and design of energy pile groups. These methods may be preferred especially in early design stages to the more time consuming, albeit more rigorous, finite element method.

## 7.4 Concluding remarks

The simplified yet rational method of analysis presented in this work (Rotta Loria and Laloui, 2017b) allows the average displacement behaviour of regular configurations of energy pile groups subjected to thermal loads to be estimated by considering the behaviour of a single equivalent pier.

The equivalent pier is a cylindrical solid with the same (average) length,  $L$ , of the energy piles composing any considered pile group and with an equivalent diameter,  $D_{eq}$ . It is characterised by an equivalent Young's modulus,  $E_{eq}$ , and by an equivalent linear thermal expansion coefficient,  $\alpha_{eq}$ , that effectively homogenise those properties of the energy piles and soil. The definition through a dedicated approach presented in this work of the equivalent linear thermal expansion coefficient of the pier represents the key novelty of the proposed equivalent pier method compared to classical equivalent pier formulations devoted to describing the behaviour of conventional pile groups subjected to (only) mechanical loads. The reason for this is that it allows the response of energy pile groups (also) subjected to thermal loads to be suitably considered depending on whether the behaviour of these groups is governed by the thermally induced deformation of the piles or of the surrounding soil. The displacement behaviour of the equivalent pier is modelled using the load-transfer method. Its load-displacement relationship is based on classical relationships proposed for the analysis of single isolated conventional and energy piles that are extrapolated and extended in this work to energy pile groups through the application of a stiffness reduction factor,  $\zeta$ . The factor  $\zeta$  has been defined in this work as a parameter that can be broadly considered to characterise displacement interactions in pile groups, i.e., the ratio  $s/L$  of the centre-to-centre spacing between the piles to their



length. Application of this factor to the load-displacement functions defined for the shaft and base of single isolated piles accounts for the increase in the pile displacement in any pile group due to the group effects. The modified load-displacement relationships resulting from this approach, which are used to characterise the equivalent pier, may be associated with those of a characteristic pile in any considered pile group as it is representative of the displacement behaviour of most of the piles in the group. Although the approach presented in this work for modifying the considered load-displacement relationships of single isolated piles appears to be rational and leads to satisfying results, experimental evidence is needed for its further validation.

Based on the results presented in this study, the main conclusions that can be drawn from this work are as follows:

- Comparisons with results obtained through the simplified yet rational interaction factor method and the more rigorous 3-D finite element method prove that the theoretical approach described in this work not only enables various trends in energy pile group behaviour to be studied but is also capable of accurately predicting the magnitude of the average vertical head displacement of energy pile groups.
- Despite being characterised by simplifying hypotheses and related shortcomings similar to most approximate methods, the proposed equivalent pier method is considered to be an economically viable and expedient solution for the analysis and design of energy pile groups. Its capabilities to (i) consider the material parameters governing the deformation (e.g., mechanically and/or thermally induced) and capacity of the energy piles and of any surrounding soil deposit, (ii) capture the potential non-linear behaviour of the soil surrounding energy pile groups and (iii) account for various soil layers surrounding the energy piles with properties that vary with depth make this method attractive compared to the more time consuming, albeit more rigorous, finite element method, especially in early stages of design.
- Application of this method is suggested for the analysis of energy pile groups characterised by an aspect ratio  $AR$  less than 4 and normalised pile spacing of  $s/D$  less than 5; for greater values of the considered parameters, the block-behaviour hypothesis of the pile group becomes less valid and the application of the method has a lower accuracy.



## Chapter 8

# Conclusions and perspectives

### 8.1 Summary

This doctoral thesis focussed on the thermo-mechanical behaviour and performance of an innovative, multifunctional technology that can be used for energy transfer applications as well as for providing structural support to any type of built environment, i.e., energy piles. Energy piles are geostructures generally applied in groups that operate as structural supports and geothermal heat exchangers. As a consequence of their twofold operation, these geostructures are subjected to the unprecedented coupled action of mechanical and thermal loads. This action involves innovative challenges for engineers, particularly from analysis and design viewpoints. The reason is that it causes variations in the temperature, stress, deformation and displacement field in the subsurface. These phenomena profoundly influence the energy, geotechnical and structural behaviour and performance of the energy piles, with a consequential impact on the behaviour and performance of the superstructures they support and supply with energy.

Prior to this work, a substantial amount of research had been made available to address the thermo-mechanical performance of single energy piles. Design guidance has also been proposed to advise in the geotechnical and structural design of energy piles. However, in contrast to the currently available knowledge for conventional piles subjected to only mechanical loads,

1. Limited knowledge, if available, was present to address the thermo-mechanical behaviour and performance of energy pile groups subjected to thermal and mechanical loads.
2. No simplified models and methods were accessible to perform the analysis and design of energy pile groups against the action of thermal (and mechanical) loads.
3. No comprehensive framework for the effect of thermal (and mechanical) loads on the performance and the related design of both single and groups of energy piles was available.

To address the aforementioned challenges, this doctoral thesis took the following steps:

1. Investigated the thermo-mechanical behaviour and performance of energy pile groups over typical time-scales of practical applications.
2. Provided the only simplified (approximate) models and methods for predicting the vertical deformation of energy pile groups subjected to thermal (and mechanical) loads.
3. Proposed an extensive framework for the effect of thermal (and mechanical) loads on the performance and related performance-based design (e.g., geotechnical and structural) of both single and groups of energy piles.

The methods employed in this doctoral research comprised (i) full-scale *in situ* testing, (ii) numerical modelling and (iii) analytical modelling. In these contexts:

- i) The first two worldwide available field tests of a group of energy piles operating as geothermal heat exchangers for the typical time-scales of practical applications were carried out. This activity was aimed at presenting experimental evidence on the potential presence and impact of group effects caused by thermal loads on the thermo-mechanical behaviour and performance of such foundations.
- ii) Extensive multidimensional, thermo-mechanical finite element analyses of single and groups of energy piles were performed. This activity was aimed at providing a fundamental characterisation of the response of energy piles to thermal and mechanical loads, which may have been difficult or impossible to achieve otherwise.
- iii) For the first time, an extensive number of parametric solutions summarised in design charts and the only two analytical models for energy pile groups were developed and validated. This activity was aimed at addressing the vertical deformation of energy pile groups subjected to thermal (and mechanical) loads.

Idealisations were made in various instances throughout this thesis, especially for the mathematical modelling of the response of energy piles to mechanical and thermal loads. The major hypothesis may resort to elastic soil behaviour (under isothermal or non-isothermal conditions). This material behaviour is characteristic of limited deformation levels caused by the loading processes and is reversible upon unloading. Currently, advanced computer techniques, software and mathematical formulations (e.g., constitutive models) have become available for the analysis of complex multiphysical engineering problems and the behaviour and performance of materials. At first glance, these capabilities may render the considered idealisation overly simplified. However, this approach appears tremendously useful. In fact, in most cases, anything more complicated than analyses based on elasticity still (a) remains extremely challenging to calibrate; (b) lacks useful generality; (c) and is daunting or even inaccessible for engineering purposes. The above appears to be particularly applicable to early stages of scientific developments, such as those that characterised the field of energy pile groups prior

to this research. Elastic theory has been employed for over fifty years to address the response of conventional pile foundations subjected to mechanical loads. When used with engineering judgement and in adequate conditions, this theory has been proven to be a powerful tool in predicting the response (e.g., vertical deformation) of both single and groups of piles subjected to mechanical loads. By considering that mechanical and thermal loads generally involve limited deformation levels, this theory was employed and proven to be suitable to address the response (e.g., vertical deformation) of energy piles to mechanical and thermal loads with two main advantages: (i) it served as a tool for the identification of the parameters that involve a significant influence on the thermo-mechanical behaviour and performance of energy piles, and (ii) it facilitated understanding of the interaction between two or more piles and the relation that only one energy pile has with the surrounding soil.

## 8.2 General conclusions

The results presented in this doctoral research work allow drawing, without being limited to, the following conclusions:

- When energy piles are located sufficiently close to each other, group effects and interactions caused by the presence and loading of the neighbouring piles occur. These group effects and interactions are not only caused by the action of the conventionally applied mechanical loads, but also by the action of the unprecedentedly applied thermal loads. The group effects caused by mechanical and thermal loads influence in conjunction the behaviour of energy piles.
- Group effects and interactions involve a complex multiphysical interplay between the energy piles, the slab and the surrounding soil. This interplay depends on various features of energy pile groups, such as (i) the pile spacing, (ii) the pile slenderness, (iii) the energy design solutions for the energy piles, (iv) the thermal and hydraulic properties and features of the foundation, (v) the relative amount of thermally induced deformation of soil to pile per unit temperature variation, (vi) the relative stiffness of pile to soil, (vii) the presence and relative stiffness of slab to soil, and (viii) the presence and stiffness of a bearing layer.
- The group effects and interactions among energy piles cause a different behaviour of these geostructures compared to that expected if they were single isolated elements. The influence of group effects and interactions caused by thermal loads on the thermo-mechanical behaviour of energy piles is different compared to that caused by mechanical loads.
- The group effects and interactions caused by thermal loads profoundly characterise the thermo-mechanical behaviour and performance of energy pile groups as well as the energy, geotechnical and structural response of such geostructures.
- The group effects and interactions caused by mechanical loads markedly characterise the mechanical behaviour and performance of energy pile groups as well as the geotechnical and structural response of such geostructures.
- Group effects and interactions involve an increased vertical pile deformation for the same average applied load (e.g., thermal or mechanical). Therefore, analyses of the deformation of

single energy piles are not exhaustive and cannot represent the actual behaviour of energy piles operating in a group. Thus, these analyses cannot be used for the complete design of energy piles.

- Group effects and interactions involve a lower vertical stress for the same average applied load (e.g., thermal or mechanical). Therefore, analyses of single energy piles are considered useful, especially in preliminary design stages. Provided that similar head restraint conditions are considered for a given energy pile in a soil deposit, these analyses will always give a conservative estimate of the vertical stress along operating energy piles in a group caused by thermal and mechanical loads.
- During more prolonged operation of various energy piles, stress variations that are opposite those that may be expected based on the type of applied thermal load (i.e., heating or cooling load) can develop in the piles when the soil has a greater thermal expansion coefficient than the piles. Hence, attention must be paid to the geotechnical characterisation of sites. Using unsuitable thermal expansion coefficients to characterise energy foundations may lead to marked pitfalls in analysis and design.
- Thermal loads involve effects that can be neglected in the performance and related performance-based design of energy piles at ultimate limit states, both from a geotechnical and a structural perspective, provided that the design approach proposed in this work is employed. The influence of thermal loads can only be considered relevant at serviceability limit states. This consideration reduces the design and verification of energy piles at ultimate limit states as a conventional process against the action of mechanical loads only.
- The effects of thermal loads may indeed be considered in the performance-based design process of energy piles at serviceability limit states, in conjunction with the effects caused by mechanical loads, thus necessitating a modified version of the conventional design of piles subjected to mechanical loads only. However, nothing new or different than what currently foreseen in the so-called Eurocodes, for example, should be considered in the design process at serviceability limit states against the action of mechanical and thermal loads applied to energy piles.
- The effects of thermal loads, in conjunction with those of mechanical loads, may be considered at serviceability limit states from the following aspects: (i) single and group vertical displacement (e.g., differential and average) limitation, considering group effects; (ii) deflection and angular distortion control; (iii) compressive stress limitation; (iv) tensile stress limitation; and (v) crack control.
- To address the single and group vertical displacement (i.e., aforementioned aspect (i)), the interaction factor method and the equivalent pier method proposed in this work can be employed to obtain results of comparable accuracy to more rigorous, three-dimensional, thermo-mechanical finite element analyses. This capability makes the models constituting the interaction factor and equivalent pier methods accurate and versatile for practical analyses and designs of energy pile groups subjected to thermal (and mechanical) loads.

- When attempts are made to achieve a trouble-free performance using energy piles that are longer than needed, drawbacks occur related to the mechanical performance of such geostructures against the effects of thermal loads. This occurrence is in contrast with the conventional justified belief that longer piles provide greater safety against the effects of mechanical loads. If the aim is to limit the vertical displacement and vertical stress of energy piles caused by thermal loads, longer pile lengths should be avoided, while greater pile diameters should be employed.
- Linear thermo-elasticity theory appears to be an expedient and sufficiently accurate tool for describing the geotechnical and structural behaviour of a wide number of energy pile groups for both research and engineering purposes.
- Thermo-mechanical numerical analyses appear to be suitable tools for modelling the geotechnical, structural and energy behaviour of most energy pile groups surrounded by saturated soil deposits without intrinsic groundwater flow.

### 8.3 Perspectives

This doctoral thesis aimed at providing a sound characterisation of the thermo-mechanical behaviour and performance of energy pile groups via a theoretical and experimental approach, based on the belief that only coupling theory with empiricism can result in a full understanding of any problem.

The considered research served as the groundwork for the multiphysical characterisation of energy pile groups. Broad perspectives and opportunities for development are still present. These perspectives and opportunities can be considered with regards to both fundamental and applied problems characterising the investigated scope.

From a fundamental perspective, the (e.g., multiphysical) behaviour of structures and soils is certainly far from being fully understood. This consideration appears to be particularly applicable to the long-term behaviour of energy pile groups, for which very limited knowledge remains available to date. The consideration of the mechanical behaviour of reinforced concrete with regards to long-term phenomena caused by temperature variations such as creep may provide novel insights for fully understanding the response of single and groups of energy piles to thermal (and mechanical) loads, e.g., at the serviceability limit state. Accounting for the actual non-linear behaviour of reinforced concrete may also contribute to the currently available knowledge on energy pile performance. The response of soils and soil-concrete interfaces to extensive applied thermal cycles still remains a major challenge and may contribute to the development of reliable, long-term predictions of the behaviour and performance of energy pile groups.

From a practical perspective, the current interest in the energy geostructure technology poses notable pressure on the scientific community. The development of simplified (approximate) yet reliable analysis and design tools for the energy geostructure technology is necessary. At the present time, there are many situations in practice in which imperfect analyses and designs of energy geostructures are performed by construction companies. Simplified models that account for more advanced aspects of soil behaviour compared to a thermo-elastic response and consider more realistic end-restraint conditions (e.g., presence of superstructure elements) may definitely contribute to a better understanding

of the behaviour and performance of energy pile groups. It is a challenge for the scientific community to serve practitioners with adequate tools to overcome the abovementioned limitations. In the context of innovative technologies such as energy geostructures, the considered involvement will undoubtedly contribute to the improvement of human progress goals in an environmentally friendly way and, from a broader perspective, for a better world.

# Bibliography

- Abdelaziz, S. & Ozudogru, T. Y. (2016a) Non-uniform thermal strains and stresses in energy piles. *Environmental Geotechnics* **3**(4):237-252.
- Abdelaziz, S. L. & Ozudogru, T. Y. (2016b) Selection of the design temperature change for energy piles. *Applied Thermal Engineering* **107**:1036-1045.
- Akrouch, G. A., Sánchez, M. & Briaud, J.-L. (2014) Thermo-mechanical behavior of energy piles in high plasticity clays. *Acta Geotechnica* **9**(3):399-412.
- Allani, M., Van Lysebetten, G. & Huybrechts, N. (2017) Experimental and numerical study of the thermo-mechanical behaviour of energy piles for Belgian practice. In *Advances in Laboratory Testing and Modelling of Soils and Shales*. Springer, pp. 405-412.
- Amatya, B. L., Soga, K., Bourne-Webb, P. J., Amis, T. & Laloui, L. (2012) Thermo-mechanical behaviour of energy piles. *Géotechnique* **62**(6):503-519.
- Armstead, H. C. H. (1973) *Geothermal energy. Review of research and development*. Chambéry, France, UNESCO.
- Baguelin, F. & Frank, R. (1979) Theoretical studies of piles using the finite element method. In *Numerical Methods in Offshore Piling*, vol. 1, pp. 83-91.
- Baldi, G., Hueckel, T. & Pellegrini, R. (1988) Thermal volume changes of the mineral water-system in low-porosity clay soils. *Canadian Geotechnical Journal* **25**(4):807-825.
- Banerjee, P. & Davies, T. (1978) The behaviour of axially and laterally loaded single piles embedded in nonhomogeneous soils. *Géotechnique* **28**(3):309-326.
- Barbier, E. (2002) Geothermal energy technology and current status: an overview. *Renewable and Sustainable Energy Reviews* **6**(1):3-65.
- Batini, N., Rotta Loria, A. F., Conti, P., Testi, D., Grassi, W. & Laloui, L. (2015) Energy and geotechnical behaviour of energy piles for different design solutions. *Applied Thermal Engineering* **86**(1):199-213.
- Bergman, T., Incropera, F., Lavine, A. & DeWitt, D. (2011) *Fundamentals of Heat and Mass Transfer*. Wiley.
- Bodas Freitas, T., Cruz Silva, F. & Bourne-Webb, P. (2013) The response of energy foundations under thermo-mechanical loading In *Proceedings of 18th International Conference on Soil Mechanics and Geotechnical Engineering*. Comité Français de Mécanique des Sols et de Géotechnique vol. 4, pp. 3347-3350.
- Boehler, R. (1996) Melting temperature of the Earth's mantle and core: Earth's thermal structure. *Annual Review of Earth and Planetary Sciences* **24**(1):15-40.
- Boënnec, O. (2008) Shallow ground energy systems. *Proceedings of the ICE-Energy* **161**(2):57-61.
- Bourne-Webb, P., Bodas Freitas, T. & Freitas Assunção, R. (2016a) Soil-pile thermal interactions in energy foundations. *Géotechnique* **66**(2):167-171.
- Bourne-Webb, P., Burlon, S., Javed, S., Kürten, S. & Loveridge, F. (2016b) Analysis and design methods for energy geostructures. *Renewable and Sustainable Energy Reviews* **65**:402-419.
- Bourne-Webb, P. J., Amatya, B. & Soga, K. (2011) A framework for understanding energy pile behaviour. *Proceedings of the ICE-Geotechnical Engineering* **166**(2):170-177.



- Bourne-Webb, P. J., Amatya, B. L., Soga, K., Amis, T., Davidson, C. & Payne, P. (2009) Energy pile test at Lambeth College, London: geotechnical and thermodynamic aspects of pile response to heat cycles. *Géotechnique* **59**(3):237-248.
- Boussinesq, J. (1878) Équilibre d'élasticité d'un sol isotrope sans pesanteur, supportant différents poids. *Comptes Rendus de l'Académie des Sciences* **86**:1260-1263.
- Bowles, J. E. (1988) *Foundation analysis and design*. McGraw-Hill.
- Brandl, H. (2006) Energy foundations and other thermo-active ground structures. *Géotechnique* **56**(2):81-122.
- Brown, P. (1975) Strip footing with concentrated loads on deep elastic foundations. *Journal of Geotechnical Engineering* **6**(1):1-13.
- Burghignoli, A., Desideri, A. & Miliziano, S. (2000) A laboratory study on the thermomechanical behaviour of clayey soils. *Canadian Geotechnical Journal* **37**(4):764-780.
- Burland, J. B. (1973) Shaft friction of piles in clay - a simple fundamental approach. *Ground Engineering* **6**(3):30-42.
- Burlon, S., Habert, J., Szymkiewicz, F., Suryatriyastuti, M. & Mroueh, H. (2013) Towards a design approach of bearing capacity of thermo-active piles. In *European Geothermal Congress*. pp. 1-6.
- Butterfield, R. & Banerjee, P. (1971) The elastic analysis of compressible piles and pile groups. *Géotechnique* **21**(1):43-60.
- Butterfield, R. & Douglas, R. (1981) *Flexibility coefficients for the design of piles and pile groups*. Report 086017171X, pp. 81.
- Campanella, R. G. & Mitchell, J. K. (1968) Influence of the temperature variations on soil behaviour. *Journal of the Soil Mechanics and Foundation Engineering Division ASCE* **94**(SM3):709-734.
- Caputo, V. & Viggiani, C. (1984) Pile foundation analysis: a simple approach to nonlinearity effects. *Rivista Italiana di Geotecnica* **18**(2):32-51.
- Castelli, F. & Maugeri, M. (2002) Simplified nonlinear analysis for settlement prediction of pile groups. *Journal of Geotechnical and Geoenvironmental Engineering* **128**(1):76-84.
- Castelli, F. & Motta, E. (2003) Settlement prevision of piles under vertical load. *Proceedings of the Institution of Civil Engineers-Geotechnical Engineering* **156**(4):183-191.
- Cataldi, R. (1999) *The year zero of geothermics*. Association, G. R. C. I. G., Sacramento, California, United States of America, pp. 7-17.
- Caulk, R., Ghazanfari, E. & McCartney, J. S. (2016) Parameterization of a calibrated geothermal energy pile model. *Geomechanics for Energy and the Environment* **5**:1-15.
- Cekerevac, C. & Laloui, L. (2004) Experimental study of thermal effects on the mechanical behaviour of a clay. *International Journal for Numerical and Analytical Methods in Geomechanics* **28**(3):209-228.
- CFMS-SYNTEC-SOFFONS-FNTP (2017) *Recommandations pour la conception, le dimensionnement et la mise en œuvre des géostructures thermiques*. pp. 120.
- Chen, Y., Xu, J., Li, H., Chen, L., Ng, C. W. & Liu, H. (2017) Performance of a prestressed concrete pipe energy pile during heating and cooling. *Journal of Performance of Constructed Facilities* **31**(3):06017001.
- Chow, Y. (1986) Analysis of vertically loaded pile groups. *International Journal for Numerical and Analytical Methods in Geomechanics* **10**(1):59-72.
- Clancy, P. & Randolph, M. (1996) Simple design tools for piled raft foundations. *Géotechnique* **46**(2):313-328.
- Clarke, B. G. (1994) *Pressuremeters in geotechnical design*. CRC Press.
- COMSOL (2014) *COMSOL Multiphysics version 4.4: user's guide and reference manual*. Burlington, Massachusetts, United States of America.



- Cooke, R., Sillett, D., Smith, D. & Gooch, M. (1981) Some observations of the foundation loading and settlement of a multi-storey building on a piled raft foundation in London clay. In *ICE Proceedings*. Thomas Telford, vol. 70, pp. 433-460.
- Coulomb, C. (1773) *Essai sur une application des règles de maximis et minimis à quelques problèmes de statique, relatifs à l'architecture*. Paris, France.
- Coyle, H. M. & Reese, L. C. (1966) Load transfer for axially loaded piles in clay. *Journal of Soil Mechanics & Foundations Div* **92**(SM2, **Proc Paper 4702**).
- Dalley, S. (2002) *Mari and Karana: two old Babylonian cities*. Gorgias Press LLC.
- Demars, K. R. & Charles, R. D. (1981) Soil volume changes induced by temperature cycling. *Canadian Geotechnical Journal* **19**(2):188-194.
- Di Donna, A., Ferrari, A. & Laloui, L. (2015) Experimental investigations of the soil-concrete interface: physical mechanisms, cyclic mobilisation and behaviour at different temperatures. *Canadian Geotechnical Journal* **53**(4):659-672.
- Di Donna, A. & Laloui, L. (2014) Numerical analysis of the geotechnical behaviour of energy piles. *International Journal for Numerical and Analytical Methods in Geomechanics* **39**(8):861-888.
- Di Donna, A. & Laloui, L. (2015) Response of soil subjected to thermal cyclic loading: experimental and constitutive study. *Engineering Geology* **190**(1):65-76.
- Di Donna, A., Rotta Loria, A. F. & Laloui, L. (2016) Numerical study on the response of a group of energy piles under different combinations of thermo-mechanical loads. *Computers and Geotechnics* **72**(1):126-142.
- EN 1990 (2002) *Eurocode: Basis of structural design*. London, United Kingdom, pp. 90.
- EN 1991 (2003) *Eurocode 1: Actions on structures - Part 1-5: General actions - Thermal actions*. London, United Kingdom, pp. 46.
- EN 1992 (2004) *Design of concrete structures - Part 1-1: General rules and rules for buildings*. London, United Kingdom, pp. 225.
- EN 1997 (2004) *Eurocode 7: Geotechnical design*. London, United Kingdom, pp. 171.
- Energy Performance of Buildings Directive, E. P. B. D. (2002) Directive 2002/91/EC of the European Parliament and of the Council of 16 December 2002 on the Energy Performance of Buildings. *Official Journal of the European Union* **1**:65-71.
- Energy Performance of Buildings Directive, E. P. B. D. r. (2010) Directive 2010/31/EU of the European Parliament and of the Council of 19 May 2010 on the energy performance of buildings (recast). *Official Journal of the European Union* **153**:13-35.
- Eslami, H., Rosin-Paumier, S., Abdallah, A. & Masrouri, F. (2017) Pressuremeter test parameters of a compacted illitic soil under thermal cycling. *Acta Geotechnica*:1-14.
- Eurostat (2017) Europe in figures - Eurostat yearbook. Office for Official Publications.
- Fleming, K., Weltman, A., Randolph, M. & Elson, K. (2008) *Piling engineering*. CRC press.
- Frank, R. (1975) Etude théorique du comportement des pieux sous charge verticale: Introduction de la dilatance. Laboratoires des Ponts et Chaussées, Ph.D. Thesis, pp. 243.
- Frank, R. (2009) Design of foundations in France with the use of Menard pressuremeter tests (MPM). *Soil Mechanics and Foundation Engineering* **46**(6):219-231.
- Frank, R., Kalteziotis, N., Bustamante, M., Christoulas, S. & Zervogiannis, H. (1991) Evaluation of performance of two piles using pressuremeter method. *Journal of Geotechnical Engineering* **117**(5):695-713.
- Frank, R. & Zhao, S. (1982) Estimation par les paramètres pressiométriques de l'enfoncement sous charge axiale de pieux forés dans des sols fins. *Bull. Liaison Labo. P. et Ch.* **(119)**:17-24.
- Gao, J., Zhang, X., Liu, J., Li, K. S. & Yang, J. (2008) Thermal performance and ground temperature of vertical pile-foundation heat exchangers: A case study. *Applied Thermal Engineering* **28**(17-18):2295-2304.

- Gawecka, K. A., Taborda, D. M., Potts, D. M., Cui, W., Zdravković, L. & Haji Kasri, M. S. (2016) Numerical modelling of thermo-active piles in London Clay. *Proceedings of the Institution of Civil Engineers-Geotechnical Engineering*:1-19.
- Gnielinski, V. (1976) New equations for heat and mass transfer in turbulent pipe and channel flow. *International Chemical Engineering* **16(1)**:359-368.
- Goode, J., III & McCartney, J. S. (2015) Centrifuge modeling of boundary restraint effects in energy foundations. *Journal of Geotechnical and Geoenvironmental Engineering* **141(8)**:04015034.
- Goode, J., III, Zhang, M. & McCartney, J. S. (2014) Centrifuge modeling of energy foundations in sand In *Proceedings of 8th International Conference on Physical Modelling in Geotechnics (ICPMG2014)*. Taylor and Francis, London, United Kingdom, pp. 729-736.
- Ground Source Heat Pump Association, N. E. C. (2012) Thermal pile design, installation & materials standards. Davy Avenue, Knowlhill, Milton Keynes, pp. 86.
- Haaland, S. (1983) Simple and Explicit Formulas for the Friction Factor in Turbulent flow. *Journal of Fluids Engineering – Transactions of the ASME* **103(1)**:89-90.
- Hansen, J. B. (1970) A revised and extended formula for bearing capacity. *Danish Geotechnical Institute Bulletin* **28**:5-11.
- Herle, I. & Gudehus, G. (1999) Determination of parameters of a hypoplastic constitutive model from properties of grain assemblies. *Mechanics of Cohesive - frictional Materials* **4(5)**:461-486.
- Horikoshi, K. & Randolph, M. (1998) A contribution to optimum design of piled rafts. *Géotechnique* **48(3)**:301-317.
- Hueckel, T. & Baldi, G. (1990) Thermoplasticity of saturated clays - experimental constitutive study. *Journal of Geotechnical Engineering* **116(12)**:1778-1796.
- Ingersoll, L. R., Zabel, O. J. & Ingersoll, A. C. (1954) *Heat conduction with engineering, geological, and other applications*. Mc-Graw Hill.
- International Energy Agency, I. E. A. (2015) *Energy and climate change*.
- International Energy Agency, I. E. A. (2016a) *CO2 emissions from fuel combustion*.
- International Energy Agency, I. E. A. (2016b) *Energy and air pollution*.
- International Energy Agency, I. E. A. (2016c) *Key world energy statistics*.
- IPCC (2013) *Climate Change 2013: The Physical Science Basis. Contribution of Working Group I to the Fifth Assessment Report of the Intergovernmental Panel on Climate Change*. Cambridge, Cambridge University Press.
- Jardine, R., Fourie, A., Potts, D. & Burland, J. (1986) Studies of the influence of non-linear stress-strain characteristics in soil-structure interaction. *Géotechnique* **36(3)**:377-396.
- Jeong, S., Min, H. & Lee, J. K. (2014) Thermally induced mechanical response of energy piles in axially loaded pile groups. *Applied Thermal Engineering* **71(1)**:608–615.
- Kalantidou, A., Tang, A. M., Pereira, J. & Hassen, G. (2012) Preliminary study on the mechanical behaviour of heat exchanger pile in physical model. *Géotechnique* **62(11)**:1047-1051.
- Kemmler, A., Piégsa, A., Ley, A., Keller, M., Jakob, M. & Catenazzi, G. (2013) *Analysis of the Swiss energy consumption according to the end use*. Bern, Switzerland.
- Knellwolf, C., Peron, H. & Laloui, L. (2011) Geotechnical analysis of heat exchanger piles. *Journal of Geotechnical and Geoenvironmental Engineering* **137(10)**:890-902.
- Kramer, C. A. & Basu, P. (2014) Performance of a model geothermal pile in sand In *Proceedings of 8th International Conference on Physical Modelling in Geotechnics* (Balkema (ed)). CRC Press, pp. 771-777.
- Laloui, L. & Di Donna, A. (2011) Understanding the behaviour of energy geo-structures. *Proceedings of the Institution of Civil Engineers - Civil Engineering* **164(4)**:184-191.
- Laloui, L. & Di Donna, A. (2013) *Energy geostructures: innovation in underground engineering*. Wiley-ISTE.

- Laloui, L., Moreni, M., Steinmann, G., Fromentin, A. & Pahud, D. (1999) *Test en conditions réelles du comportement statique d'un pieu soumis à des sollicitations thermomécaniques*. Lausanne, Switzerland.
- Laloui, L., Moreni, M. & Vulliet, L. (2003) Comportement d'un pieu bi-fonction, fondation et échangeur de chaleur. *Canadian Geotechnical Journal* **40**(2):388-402.
- Laloui, L., Nuth, M. & Vulliet, L. (2006) Experimental and numerical investigations of the behaviour of a heat exchanger pile. *International Journal for Numerical and Analytical Methods in Geomechanics* **30**(8):763-781.
- Lambe, T. (1973) Predictions in soil engineering. *Géotechnique* **23**(2):151-202.
- Lazzari, S., Priarone, A. & Zanchini, E. (2010) Long-term performance of BHE (borehole heat exchanger) fields with negligible groundwater movement. *Energy* **35**(12):4966-4974.
- Lee, S., Speight, J. G. & Loyalka, S. K. (2007) *Handbook of alternative fuel technologies*. CRC Press.
- Leung, Y., Soga, K., Lehane, B. & Klar, A. (2010) Role of linear elasticity in pile group analysis and load test interpretation. *Journal of Geotechnical and Geoenvironmental Engineering* **136**(12):1686-1694.
- Loveridge, F., Powrie, W., Amis, T., Wischy, M. & Kiauk, J. (2016) Long term monitoring of CFA energy pile schemes in the UK. In *Energy Geotechnics*. CRC Press, pp. 585-592.
- Loveridge, F. A. & Powrie, W. (2016) The average temperature of energy piles. In *Geo-Chicago 2016*, pp. 166-175.
- Lund, J. W. (2009) Utilisation of geothermal resources. *Proceedings of the ICE-Energy* **162**(1):3-12.
- Lungonelli, M. (2003) *Piero Ginori Conti: scienza, cultura e innovazione industriale nella Toscana del Novecento*. Laterza.
- Luo, J., Zhao, H., Gui, S., Xiang, W. & Rohn, J. (2017) Study of thermal migration and induced mechanical effects in double U-tube energy piles. *Computers and Geotechnics* **91**:1-11.
- Maehr, M. & Herle, I. (2004) Volume loss and soil dilatancy. *Rivista Italiana di Geotecnica* **38**(4).
- Magee, L., Scerri, A., James, P., Thom, J. A., Padgham, L., Hickmott, S., Deng, H. & Cahill, F. (2013) Reframing social sustainability reporting: towards an engaged approach. *Environment, Development and Sustainability* **15**(1):225-243.
- Mandolini, A. & Viggiani, C. (1997) Settlement of piled foundations. *Géotechnique* **47**(4):791-816.
- Marto, A., Amaludin, A. & Hatta Bin Satar, M. (2015) Experiments on shallow geothermal energy model piles embedded in soft soil. *Electronic Journal of Geotechnical Engineering* **20**:12687-12698.
- Mattsson, N., Steinmann, G. & Laloui, L. (2008) Advanced compact device for the in-situ determination of geothermal characteristics of soils. *Energy and Buildings* **40**(7):1344-1352.
- McCabe, B. & Lehane, B. (2006) Behavior of axially loaded pile groups driven in clayey silt. *Journal of Geotechnical and Geoenvironmental Engineering* **132**(3):401-410.
- McCartney, J. S. & Murphy, K. D. (2012) Strain distributions in full-scale energy foundations. *DFI Journal* **6**(2):26-38.
- McCartney, J. S. & Murphy, K. D. (2017) Investigation of potential dragdown/uplift effects on energy piles. *Geomechanics for Energy and the Environment* **10**:21-28.
- McCartney, J. S. & Rosenberg, J. E. (2011) Impact of heat exchange on side shear in thermo-active foundations In *Proceedings of Geo-Frontiers: Advances in Geotechnical Engineering*. ASCE, pp. 488-498.
- Mimouni, T. & Laloui, L. (2014) Towards a secure basis for the design of geothermal piles. *Acta Geotechnica* **9**(3):355-366.
- Mimouni, T. & Laloui, L. (2015) Behaviour of a group of energy piles. *Canadian Geotechnical Journal* **52**(12):1913-1929.
- Mindlin, R. D. (1936) Force at a point in the interior of a semi-infinite solid. *Journal of Applied Physics* **7**(5):195-202.

- Murphy, K. & McCartney, J. S. (2015) Seasonal response of energy foundations during building operation. *Geotechnical and Geological Engineering* **33**(2):343-356.
- Murphy, K. D., McCartney, J. S. & Henry, K. S. (2015) Evaluation of thermo-mechanical and thermal behavior of full-scale energy foundations. *Acta Geotechnica* **10**(2):1-17.
- Mylonakis, G. (2001) Winkler modulus for axially loaded piles. *Géotechnique* **51**(5):455-462.
- Mylonakis, G. & Gazetas, G. (1998) Settlement and additional internal forces of grouped piles in layered soil. *Géotechnique* **48**(1):55-72.
- Narsilio, G. A., Bidarmaghaz, A. & Colls, S. (2014) Geothermal energy: introducing an emerging technology In *Proceedings of International Conference on Advances in Civil Engineering for Sustainable Development*, pp. 141-154.
- Ng, C. W. W., Ma, Q. J. & Gunawan, A. (2016a) Horizontal stress change of energy piles subjected to thermal cycles in sand. *Computers and Geotechnics* **78**:54-61.
- Ng, C. W. W., Shi, C., Gunawan, A. & Laloui, L. (2014) Centrifuge modelling of energy piles subjected to heating and cooling cycles in clay. *Géotechnique Letters* **4**(October–December):310-316.
- Ng, C. W. W., Shi, C., Gunawan, A., Laloui, L. & Liu, H. L. (2015) Centrifuge modelling of heating effects on energy pile performance in saturated sand. *Canadian Geotechnical Journal* **52**(8):1045-1057.
- Ng, C. W. W., Wang, S. H. & Zhou, C. (2016b) Volume change behaviour of saturated sand under thermal cycles. *Géotechnique Letters* **6**(2):124-131.
- Nguyen, V. T., Tang, A. M. & Pereira, J.-M. (2017) Long-term thermo-mechanical behavior of energy pile in dry sand. *Acta Geotechnica*:1-9.
- O'Neill, M. W. (1983) Group action in offshore piles In *Proceedings of Geotechnical Practice in Offshore Engineering*. ASCE, pp. 25-64.
- O'Neill, M. W., Ghazzaly, O. I. & Ha, H. B. (1977) Analysis of three-dimensional pile groups with nonlinear soil response and pile-soil-pile interaction. In *9th Annual Offshore Technology Conference*. Houston, Texas, United States of America, pp. 245-256.
- O'Neill, M. W., Hawkins, R. A. & Mahar, L. J. (1981) *Field study of pile group action*. pp. 195.
- Ohde, J. (1939) *Zur theorie der druckverteilung im baugrund*.
- Olgun, C. G., Ozudogru, T. Y. & Arson, C. (2014) Thermo-mechanical radial expansion of heat exchanger piles and possible effects on contact pressures at pile–soil interface. *Géotechnique Letters* **4**(July–September):170-178.
- Ottaviani, M. (1975) Three-dimensional finite element analysis of vertically loaded pile groups. *Géotechnique* **25**(2):159-174.
- Pahud, D. (2002) *Geothermal energy and heat storage*. pp. 133.
- Pahud, D. & Hubbuch, M. (2007) Measured thermal performances of the energy pile system of the dock midfield at Zürich Airport In *Proceedings of European Geothermal Congress*. Bundesverband Geothermie.
- Plum, R. L. & Esrig, M. I. (1969) Some temperature effects on soil compressibility and pore water pressure. In *Highway Research Board Special Report*, vol. 103.
- Poulos, H. G. (1968) Analysis of the settlement of pile groups. *Géotechnique* **18**(4):449-471.
- Poulos, H. G. (1977) Estimation of pile group settlements. *Ground Engineering* **10**(2):40-50.
- Poulos, H. G. (1988) Modified calculation of pile-group settlement interaction. *Journal of Geotechnical Engineering* **114**(6):697-706.
- Poulos, H. G. (1989) Pile behaviour—theory and application. *Géotechnique* **39**(3):365-415.
- Poulos, H. G. (1993) Settlement prediction for bored pile groups In *Proceedings of Deep Foundations on Bored and Auger Piles*. Balkema, Rotterdam, pp. 103-117.
- Poulos, H. G. (1994) An approximate numerical analysis of pile–raft interaction. *International Journal for Numerical and Analytical Methods in Geomechanics* **18**(2):73-92.



- Poulos, H. G. (2006) Pile group settlement estimation: Research to practice. In *GeoShanghai International Conference 2006*. ASCE Geotechnical Special Publication, Shanghai, China, vol. 153, pp. 1-22.
- Poulos, H. G., Carter, J. P. & Small, J. C. (2002) Foundations and retaining structures-Research and practice. In *International Conference on Soil Mechanics and Geotechnical Engineering*. Balkema, vol. 4, pp. 2527-2606.
- Poulos, H. G. & Davis, E. H. (1974) *Elastic solutions for soil and rock mechanics*. Wiley.
- Poulos, H. G. & Davis, E. H. (1980) *Pile foundation analysis and design*. Wiley.
- Poulos, H. G. & Mattes, N. S. (1974) Settlement of pile groups bearing on stiffer strata. *Journal of Geotechnical and Geoenvironmental Engineering* **100**(GT2):185-190.
- Powrie, W. (2013) *Soil mechanics: concepts and applications*. CRC Press.
- Pressley, J. S. & Poulos, H. G. (1986) Finite element analysis of mechanisms of pile group behaviour. *International Journal for Numerical and Analytical Methods in Geomechanics* **10**(2):213-221.
- Randolph, M. (1994) Design methods for pile groups and piled rafts In *Proceedings of Thirteenth International Conference on Soil Mechanics and Foundation Engineering*, pp. 61-82.
- Randolph, M. & Clancy, P. (1993) Efficient design of piled rafts. In *Deep Foundations on Bored and Auger Piles*. Balkema, Rotterdam, Ghent, pp. 119-130.
- Randolph, M. & Wroth, C. (1979a) A simple approach to pile design and the evaluation of pile tests. In *Behavior of Deep Foundations*. ASTM International.
- Randolph, M. F. & Wroth, C. (1979b) An analysis of the vertical deformation of pile groups. *Géotechnique* **29**(4):423-439.
- Randolph, M. F. & Wroth, C. P. (1978) Analysis of deformation of vertically loaded piles. *Journal of the Geotechnical Engineering Division* **104**(12):1465-1488.
- Regueiro, R. A., Wang, W., Stewart, M. A. & McCartney, J. S. (2012) Coupled thermo-poro-mechanical finite element analysis of an energy foundation centrifuge experiment in saturated silt In *Proceedings of GeoCongress*. ASCE, pp. 4406-4415.
- Rotta Loria, A. F., Bocco, M., Garbellini, C., Muttoni, A. & Laloui, L. (2017a) The role of thermal loads in the geotechnical and structural performance-based design of energy piles. *Géotechnique*:Under review.
- Rotta Loria, A. F., Di Donna, A. & Laloui, L. (2015a) Numerical study on the suitability of centrifuge testing the thermal-induced mechanical behavior of energy piles. *Journal of Geotechnical and Geoenvironmental Engineering* **141**(10):04015042.
- Rotta Loria, A. F., Gunawan, A., Shi, C., Laloui, L. & Ng, C. W. (2015b) Numerical modelling of energy piles in saturated sand subjected to thermo-mechanical loads. *Geomechanics for Energy and the Environment* **1**(1):1-15.
- Rotta Loria, A. F. & Laloui, L. (2016a) Analysis of thermally induced mechanical interactions in energy pile groups In *Proceedings of First International Conference on Energy Geotechnics, ICEGT 2016*. CRC Press vol. 1, pp. 171-178.
- Rotta Loria, A. F. & Laloui, L. (2016b) The interaction factor method for energy pile groups. *Computers and Geotechnics* **80**:121-137.
- Rotta Loria, A. F. & Laloui, L. (2017a) Displacement interaction among energy piles bearing on stiff soil strata. *Computers and Geotechnics* **90**:144-154.
- Rotta Loria, A. F. & Laloui, L. (2017b) The equivalent pier method for energy pile groups. *Géotechnique* **67**(8):691-702.
- Rotta Loria, A. F. & Laloui, L. (2017c) Group action caused by various operating energy piles. *Géotechnique*: 10.1680/jgeot.17.P.213.
- Rotta Loria, A. F. & Laloui, L. (2017d) Thermally induced group effects among energy piles. *Géotechnique* **67**(5):374-393.

- Rotta Loria, A. F., Vadrot, A. & Laloui, L. (2017b) Analysis of the vertical displacement of energy pile groups. *Geomechanics for Energy and the Environment*: Under review.
- Rotta Loria, A. F., Vadrot, A. & Laloui, L. (2017c) Effect of non-linear soil deformation on the interaction among energy piles. *Computers and Geotechnics* **86**:9-20.
- Saggu, R. & Chakraborty, T. (2015) Cyclic thermo-mechanical analysis of energy piles in sand. *Geotechnical and Geological Engineering* **33**(1):1-22.
- Saggu, R. & Chakraborty, T. (2016) Thermomechanical response of geothermal energy pile groups in sand. *International Journal of Geomechanics* **16**(4):04015100.
- Salciarini, D., Ronchi, F., Cattoni, E. & Tamagnini, C. (2015) Thermomechanical effects induced by energy piles operation in a small piled raft. *International Journal of Geomechanics* **15**(2):04014042.
- Salciarini, D., Ronchi, F. & Tamagnini, C. (2017) Thermo-hydro-mechanical response of a large piled raft equipped with energy piles: a parametric study. *Acta Geotechnica*:10.1007/s1144:1-26.
- Schmidt, B. (1966) Earth pressures at rest related to stress history. *Canadian Geotechnical Journal* **3**(4):239-242.
- Selvadurai, A. P. (1979) *Elastic analysis of soil-foundation interaction*. Elsevier.
- Sheil, B. B. & McCabe, B. A. (2014) A finite element-based approach for predictions of rigid pile group stiffness efficiency in clays. *Acta Geotechnica* **9**(3):469-484.
- SIA-D0190 (2005) *Utilisation de la Chaleur du Sol par des Ouvrages de Fondation et de Soutènement en Béton. Guide pour la Conception, la Realisation et la Maintenance*. Zurich, Switzerland.
- Sims, R. E. H., Schock, R. N., Adegbululge, A., Fenhann, J., Konstantinaviciute, I., Moomaw, W., Nimir, H. B., Schlamadinger, B., Torres-Martínez, J., Turner, C., Uchiyama, Y., Vuori, S. J. V., Wamukonya, N. & Zhang, X. (2007) Energy supply. In *Climate Change 2007: Mitigation. Contribution of Working Group III to the Fourth Assessment Report of the Intergovernmental Panel on Climate Change*. (Metz, B., Davidson, O. R., Bosch, P. R., Dave, R., and Meyer, L. A. (eds)) Cambridge University Press, Cambridge, United Kingdom and United States of America.
- Sowers, G. F., Martin, C., Wilson, L. L. & Fausold, M. (1961) The bearing capacity of friction pile groups in homogeneous clay from model studies. In *Fifth International Conference on Soil Mechanics and Foundation Engineering*, pp. 155-159.
- Stewart, M. A. & McCartney, J. S. (2014) Centrifuge modeling of soil-structure interaction in energy foundations. *Journal of Geotechnical and Geoenvironmental Engineering* **140**(4):04013044.
- Suryatriyastuti, M., Burlon, S. & Mroueh, H. (2015) On the understanding of cyclic interaction mechanisms in an energy pile group. *International Journal for Numerical and Analytical Methods in Geomechanics*:10.1002/nag.2382.
- Suryatriyastuti, M., Mroueh, H. & Burlon, S. (2012) Understanding the temperature-induced mechanical behaviour of energy pile foundations. *Renewable and Sustainable Energy Reviews* **16**(5):3344-3354.
- Sutman, M., Brettmann, T. & Olgun, C. (2014) Thermo-mechanical behavior of energy piles: full-scale field test verification. In *DFI 39th Annual Conference on Deep Foundations*. Atlanta, United States of America, pp. 1-11.
- Sutman, M., Olgun, C. & Brettmann, T. (2015) Full-scale field testing of energy piles In *Proceedings of IFCEE 2015*. ASCE vol. 1, pp. 1638-1647.
- Sutman, M., Olgun, G., Laloui, L. & Brettmann, T. (2017) Effect of end-restraint conditions on energy pile behavior. In *Geotechnical Frontiers 2017*, pp. 165-174.
- Timoshenko, S. & Goodier, J. (1970) *Theory of elasticity*. McGraw-Hill.
- United Nations, U. N. (2017) World Population Prospects: The 2017 Revision. (Department of Economic and Social Affairs, P. D. (ed)) United Nations, New York.

- Vega, A. & McCartney, J. S. (2014) Cyclic heating effects on thermal volume change of silt. *Environmental Geotechnics* **2(5)**:257-268.
- Vieira, A. & Maranhã, J. R. (2016) Thermoplastic analysis of a thermoactive pile in a normally consolidated clay. *International Journal of Geomechanics* **17(1)**:04016030.
- Wang, B., Bouazza, A. & Haberfield, C. (2011) Preliminary observations from laboratory scale model geothermal pile subjected to thermal-mechanical loading In *Proceedings of Geo-Frontiers 2011: Advances in Geotechnical Engineering*. ASCE, pp. 430-439.
- Wang, B., Bouazza, A., Singh, R. M., Haberfield, C., Barry-Macaulay, D. & Baycan, S. (2014) Posttemperature effects on shaft capacity of a full-scale geothermal energy pile. *Journal of Geotechnical and Geoenvironmental Engineering* **141(4)**:04014125.
- Wang, Z., Xie, X. & Wang, J. (2012) A new nonlinear method for vertical settlement prediction of a single pile and pile groups in layered soils. *Computers and Geotechnics* **45**:118-126.
- Whitaker, T. (1957) Experiments with model piles in groups. *Géotechnique* **7(4)**:147-167.
- Xiao, J., Luo, Z., Martin, J. R., Gong, W. & Wang, L. (2016) Probabilistic geotechnical analysis of energy piles in granular soils. *Engineering Geology* **209**:119-127.
- Yavari, N., Tang, A. M., Pereira, J.-M. & Hassen, G. (2014) Experimental study on the mechanical behaviour of a heat exchanger pile using physical modelling. *Acta Geotechnica* **9(3)**:385-398.
- Yavari, N., Tang, A. M., Pereira, J.-M. & Hassen, G. (2016) Effect of temperature on the shear strength of soils and the soil–structure interface. *Canadian Geotechnical Journal* **53(999)**:1-9.
- You, S., Cheng, X., Guo, H. & Yao, Z. (2016) Experimental study on structural response of CFG energy piles. *Applied Thermal Engineering* **96(1)**:640-651.
- Yunus, A. C. & Michael, A. B. (2006) *Thermodynamics: an engineering approach*. McGraw-Hill.
- Zhang, Q.-Q., Zhang, Z.-M. & He, J.-Y. (2010) A simplified approach for settlement analysis of single pile and pile groups considering interaction between identical piles in multilayered soils. *Computers and Geotechnics* **37(7)**:969-976.





# Appendix A – *In situ* testing equipment

## A.1 Heating module

A module that was developed for testing the thermal response of soil (Mattsson et al., 2008) allows several energy piles to be heated. The module can be used to inject a heat rate of up to 9 kW at three different flow rates of up to 21 l/min. A modem and a data logger allow the temperatures inside and outside of the suitcase in which the module is placed, the inlet and outlet fluid temperatures in the pipes, the inlet and outlet fluid pressures, the flow rate, and the electrical consumption of the module to be observed and recorded during the test.

## A.2 Vibrating wire strain gauges

Vibrating wire strain gauges (model EM-5 from Roctest) allow the vertical deformation and temperature variations in the piles to be measured. These sensors are fixed at the connections between the vertical steel reinforcement bars and the 0.76-m-diameter reinforcing cages. Three strain gauges are installed at each pile head in different locations (relative depth from the slab extrados of  $z = 0.9$  m). One strain gauge is then mounted every 2 m on a line along the foundation depth. The vertical strain variations,  $\Delta\varepsilon_z$ , can be calculated based on the recorded values of the wire frequency and temperature as

$$\Delta\varepsilon_z = \frac{K_g}{1000} (F^2 - F_0^2) + \alpha_{wire}(T - T_0) \quad (\text{A.1})$$

where  $K_g$  is a gauge factor that is provided by the sensor supplier that depends on the wire characteristics,  $F$  and  $F_0$  are the wire resonant frequencies at the actual ( $t$ ) and reference ( $t_0$ ) times, respectively,  $\alpha_{wire}$  is the linear thermal expansion coefficient of the wire ( $11.5 \mu\text{ε}/^\circ\text{C}$ ), and  $T$  and  $T_0$  are the actual and reference wire temperatures, respectively.

## A.3 Optical fibres

Optical fibres (SOFO system from Roctest) allow additional measurements of the vertical strain variations in all of the piles as well as of the radial strain variations in the central pile. Only the radial optical fibre was used during the experimental test. This fibre is mounted along the reinforcing cage of the central pile at a depth of  $z = 9$  m. A dedicated reading unit with a pilot computer allows the lengthening of the optical fibre,  $\Delta l_{OF}$ , to be measured during the test. Assuming a homogeneous radial deformation field in the cross-section of the pile, the radial strain variations,  $\Delta\varepsilon_r$ , can be estimated as

$$\Delta \varepsilon_r = -\frac{\Delta l_{OF}}{l_{OF}} \quad (\text{A.2})$$

where  $l_{OF}$  is the initial length of the fibre.

#### A.4 Pressure cells

Pressure cells (model TPC from Roctest; 229 mm in diameter) with vibrating wire transducers allow variations in the vertical stress at the pile toes to be monitored. These cells are installed at the base of each pile and are attached to a welded cross-section. The vertical stress variations can be calculated as

$$\Delta \sigma_z = A^* \frac{K_g^2}{1000^2} (F^4 - F_0^4) + B^* \frac{K_g}{1000} (F^2 - F_0^2) - C^* (T - T_0) \quad (\text{A.3})$$

where  $A^*$ ,  $B^*$  and  $C^*$  are calibration factors that are provided by the sensor supplier.

#### A.5 Piezometers and thermistors

Piezometers (model PWS with stainless steel filters from Roctest) and 3 k $\Omega$  thermistors (model TH-T from Roctest) deployed in two boreholes allow temperature and pore water pressure variations in the soil to be measured. Two piezometers are installed in each borehole in the sandy-gravelly moraine layer. In borehole P+T1, the piezometers are located at depths of  $z = 9$  and 16.3 m; in borehole P+T2, they are located at depths of  $z = 5.4$  and 16 m. The piezometers are equipped with thermistors because they use vibrating wire transducers that require temperature corrections. The temperature profiles in the two boreholes are measured using a series of single thermistors that are installed at approximate depths of  $z = 4.1$  and 13.6 m in P+T1 and  $z = 1.6$ , 4.4 and 12 m in P+T2. The pore water pressure variations are calculated using equation (A.3) with the calibration factors of the sensors.

## Appendix B - Mathematical formulation employed in the finite element analyses

The equilibrium equation can be written as

$$\nabla \cdot \sigma_{ij} + \rho g_i = 0 \quad (\text{B.1})$$

where  $\nabla \cdot$  denotes the divergence,  $\sigma_{ij}$  denotes the total stress tensor,  $\rho = n\rho_f + (1 - n)\rho_s$  represents the bulk density of the porous material, which is calculated based on the density of the fluid  $\rho_f$  and the density of the solid particles  $\rho_s$  through the porosity  $n$ , and  $g_i$  is the gravity vector. The stress tensor can be expressed as

$$\sigma_{ij} = D_{ijkl}[\varepsilon_{kl} + \beta_{kl}(T - T_0)] \quad (\text{B.2})$$

where  $D_{ijkl}$  is the elastic stiffness tensor, which contains the material properties (e.g., Young's modulus  $E$  and Poisson's ratio  $\nu$ );  $\varepsilon_{kl}$  is the total strain tensor;  $\beta_{kl}$  is a vector that comprises the linear thermal expansion coefficient of the material; and  $T - T_0 = \Delta T$  is the temperature variation.

The energy conservation equation reads

$$\rho c_p \frac{\partial T}{\partial t} - \nabla \cdot (\lambda \nabla T) = 0 \quad (\text{B.3})$$

where  $c_p$  is the specific heat, which is calculated based on the specific heat of the fluid and solid components  $c_{p,f}$  and  $c_{p,s}$ , respectively,  $t$  is the time,  $\lambda$  is the thermal conductivity, which is calculated based on the thermal conductivity of the fluid and solid components  $\lambda_f$  and  $\lambda_s$ , respectively, and  $\nabla$  represents the gradient. The thermal properties of the foundation and surrounding soil are considered to be temperature independent.

The fluid flow inside the pipes and the associated convective heat transfer is simulated by an equivalent solid (Lazzari et al., 2010) that has the same heat capacity per unit volume (i.e., specific heat multiplied by bulk density) and thermal conductivity as the actual circulation fluid. The properties of this material are considered to be temperature dependent.

The energy conservation equation for the incompressible fluid in the pipes of the heat exchanger pile can be written as

$$\rho_f c_{p,f} A_p \frac{\partial T_f}{\partial t} + \rho_f c_{p,f} A_p v_i \cdot \nabla T_f = \nabla \cdot [A_p \lambda_f \nabla T_f] + \dot{q}_l \quad (\text{B.4})$$

where  $\rho_f$ ,  $c_{p,f}$ ,  $A_p$ ,  $T_f$ ,  $v_i$ ,  $\lambda_f$  are the density, specific heat, pipe cross-sectional area, bulk temperature, longitudinal velocity vector and thermal conductivity of the operative fluid, respectively, and  $\dot{q}_l$  represents the heat flux per unit length that is exchanged through the pipe wall, which is given by

$$\dot{q}_l = U P_p (T_{ext} - T_f) \quad (\text{B.5})$$

where  $U$  is the effective value of the pipe heat transfer coefficient,  $P_p = 2\pi r_{p,in}$  is the wetted perimeter of the cross-section and  $T_{ext}$  is the temperature at the outer pipe side. The overall heat transfer coefficient, including the internal film resistance and the wall resistance, can be obtained as

$$U = \frac{1}{\frac{1}{h_{in}} + \frac{r_{p,in}}{\lambda_p} \ln\left(\frac{r_{p,out}}{r_{p,in}}\right)} \quad (\text{B.6})$$

where  $h_{in} = Nu \lambda_f / d_p$  is the convective heat transfer coefficient inside the pipe,  $\lambda_p$  is the thermal conductivity of the pipe,  $r_{p,out}$  and  $r_{p,in}$  are the external and internal radii, respectively,  $d_p = 4A_p/P_p$  is the hydraulic diameter, and  $Nu$  is the Nusselt number. For a given geometry,  $Nu$  is a function of the Reynolds,  $Re$ , and Prandtl,  $Pr$ , numbers, with

$$Nu = \max(3.66; Nu_{turb}) \quad (\text{B.7})$$

$$Nu_{turb} = \frac{\left(\frac{f_M}{8}\right)^{(Re-1000)Pr}}{1 + 12.7 \sqrt{\frac{f_M}{8}} (Pr^{\frac{2}{3}} - 1)} \quad (\text{B.8})$$

$$f_M = \left[ -1.8 \log_{10} \left( \frac{6.9}{Re} \right) \right]^{-1} \quad (\text{B.9})$$

Where, for a fluid of dynamic viscosity  $\mu_f$ ,

$$Re = \frac{\rho_f v_f d_p}{\mu_f} \quad Pr = \frac{\mu_f c_{p,f}}{\lambda_f}$$

Equation (B.8) is the Gnielinski formula (Gnielinski, 1976) for turbulent flows; the friction factor,  $f_M$ , is evaluated using the Haaland equation (Haaland, 1983), which is valid for very low relative roughness values.

# Alessandro Francesco Rotta Loria

*Institutional address:* Swiss Federal Institute of Technology in Lausanne, EPFL

Station 18, Batiment GC, 1015 Lausanne, Switzerland

*E-mail & phone:* alessandro.rottaloria@epfl.ch, +41 76 3399362

## Professional experience and appointments

Jan. 2018 – date to be det.	<b>Post-Doctoral Researcher, Swiss Federal Institute of Technology in Lausanne</b> <i>Supervisor:</i> Prof. Lyesse Laloui
2017 – present	<b>Professional Engineering Consultant</b>
Nov. 2013 – Dec. 2017	<b>Ph.D. Student, Swiss Federal Institute of Technology in Lausanne</b> <i>Supervisor:</i> Prof. Lyesse Laloui
Nov. 2013 – Dec. 2013	<b>Visiting Ph.D. Student, Hong Kong University of Science and Technology</b> <i>Supervisors:</i> Prof. Charles W. W. Ng and Prof. Lyesse Laloui
Apr. 2013 – Nov. 2013	<b>Research Student, Swiss Federal Institute of Technology in Lausanne</b> <i>Supervisors:</i> Prof. Lyesse Laloui and Dr. Alice Di Donna <i>Scholarship:</i> EOS Holding and EPFL

## Higher education

Nov. 2013 – Dec. 2017	<b>Ph.D. in Mechanics, Swiss Federal Institute of Technology in Lausanne</b> <i>Dissertation:</i> “Thermo-mechanical performance of energy pile groups” <i>Supervisor:</i> Prof. Lyesse Laloui
Oct. 2011 – Jul. 2013	<b>M.Sc. in Building Engineering, Politecnico di Torino</b> <i>Dissertation:</i> “A theoretical and experimental approach to Permafrost mechanical behaviour” <i>Supervisors:</i> Prof. Bernardino M. Chiaia and Prof. Claudio Scavia <i>Co-supervisors:</i> Dr. Barbara Frigo and Dr. Silvia Duca <i>Final grade:</i> 110/110 <i>cum laude</i>
Oct. 2008 – Jul. 2011	<b>B.Sc. in Building Engineering, Politecnico di Torino</b> <i>Dissertation:</i> “The Golden Section in structures: an aesthetic canon and a possible structural property” <i>Supervisor:</i> Prof. Bernardino M. Chiaia <i>Final grade:</i> 110/110 (graduate track with 1 <sup>st</sup> year in English)

## Professional qualifications and affiliations

2017	<b>Professional Engineer Qualification</b> <i>Specification:</i> Qualification as Civil and Environmental Engineer, Italian Order of Engineers
2017	<b>Member of the Deep Foundation Institute</b> <i>Specification:</i> Membership to the Deep Foundation Institute, United States of America
2011	<b>Safety Coordinator for Construction Sites Qualification</b> <i>Specification:</i> Certification according to the Italian D.lgs. 81/2008

## Fields of interest

Geomechanics; Structural mechanics; Energy; Multiphysical phenomena; Environmental sustainability.

## Awards and honours

2017	<p><b>Earth Sciences and Engineering best paper award, EPFL</b>  <i>Reference:</i> Rotta Loria, A. F. and Laloui, L. (2017) “Thermally induced group effects among energy piles”. <i>Géotechnique</i> 67(5):374-393.</p> <p><b>Most cited article in the journal Geomechanics for Energy and the Environment</b>  <i>Reference:</i> Rotta Loria, A. F., Gunawan, A., Shi, C., Laloui, L. and Ng, C. W. W. (2015) “Numerical modelling of energy piles in saturated sand subjected to thermo-mechanical loads”. <i>Geomechanics for Energy and the Environment</i> 1(1):1-15.  <i>Period:</i> 2015 – 2016</p>
2016	<p><b>Excellence in scientific research award, EPFL</b></p> <p><b>Most downloaded article in the journal Computers and Geotechnics</b>  <i>Reference:</i> Rotta Loria, A. F. and Laloui, L. (2016) “The interaction factor method for energy pile groups”. <i>Computers and Geotechnics</i> 80:121-137.  <i>Period:</i> 2016 – 2017</p>
2015	<p><b>Most downloaded article in the journal Geomechanics for Energy and the Environment</b>  <i>Reference:</i> Rotta Loria, A. F., Gunawan, A., Shi, C., Laloui, L. and Ng, C. W. W. (2015) “Numerical modelling of energy piles in saturated sand subjected to thermo-mechanical loads”. <i>Geomechanics for Energy and the Environment</i> 1(1):1-15.  <i>Period:</i> 2015 – present</p> <p><b>Top 25 hottest article in the journal Computers and Geotechnics</b>  <i>Reference:</i> Rotta Loria, A. F., Orellana, F., Minardi, A., Furbringer, J.-M. and Laloui, L. (2015) “Predicting the axial capacity of piles in sand”. <i>Computers and Geotechnics</i> 69(1):485-495.  <i>Period:</i> 2015 – 2016</p>
2013	<p><b>Optime Award for excellence in M.Sc. studies</b></p> <p><b>Winter School in Accessibility with ThyssenKrupp Encasa Award</b>  <i>Object:</i> Best structural and architectural engineering project devoted to making the University of Pavia accessible to people with disabilities</p>
2011	<p><b>Ivrea Gas Agency award for excellence in B.Sc. studies</b></p>

## Scientific publications

**H-index:** 6 (Google Scholar)    **Refereed journal papers:** 14 (12 published, 2 under review)    **Media:** 1  
**Citations:** 122    **Refereed conference papers and abstracts:** 14

## Refereed journal papers

### Published

1. Rotta Loria, A. F., Gunawan, A., Shi, C., Laloui, L. and Ng, C. W. W. (2015) **Numerical modelling of energy piles in saturated sand subjected to thermo-mechanical loads**. *Geomechanics for Energy and the Environment* 1(1):1-15.
2. Rotta Loria, A. F., Di Donna, A. and Laloui, L. (2015) **Numerical study on the suitability of centrifuge testing for capturing the thermal-induced mechanical behavior of energy piles**. *Journal of Geotechnical and Geoenvironmental Engineering* 141(10):04015042.
3. Batini, N., Rotta Loria, A. F., Conti, P., Testi, D., Grassi, W. and Laloui, L. (2015) **Energy and geotechnical behaviour of energy piles for different design solutions**. *Applied Thermal Engineering* 86(1):199-213.

4. Rotta Loria, A. F., Orellana, F., Minardi, A., Furbringer, J.-M. and Laloui, L. (2015) **Predicting the axial capacity of piles in sand.** Computers and Geotechnics 69(1):485-495.
5. Di Donna, A., Rotta Loria, A. F. and Laloui, L. (2016) **Numerical study on the response of a group of energy piles under different combinations of thermo-mechanical loads.** Computers and Geotechnics 72(1):126-142.
6. Rotta Loria, A. F. and Laloui, L. (2016) **The interaction factor method for energy pile groups.** Computers and Geotechnics 80:121-137.
7. Rotta Loria, A. F. and Laloui, L. (2017) **Thermally induced group effects among energy piles.** Géotechnique 67(5):374-393.
8. Rotta Loria, A. F., Frigo, B. and Chiaia B. M. (2017) **A non-linear constitutive model for capturing the mechanical behaviour of frozen ground and permafrost.** Cold Regions Science and Technology 133:63-69.
9. Rotta Loria, A. F., Vadrot, A. and Laloui, L. (2017) **Effect of non-linear soil deformation on the interaction among energy piles.** Computers and Geotechnics 86:9-20.
10. Rotta Loria, A. F. and Laloui, L. (2017) **The equivalent pier method for energy pile groups.** Géotechnique 67(8):691-702.
11. Rotta Loria, A. F. and Laloui, L. (2017) **Displacement interaction among energy piles bearing on stiff soil strata.** Computers and Geotechnics 90:144-154.
12. Rotta Loria, A. F. and Laloui, L. (2017) **Group action effects caused by various operating energy piles.** Géotechnique. 10.1680/jgeot.17.p.213.

#### Under review

13. Rotta Loria, A. F., Bocco, M., Garbellini, C., Muttoni, A. and Laloui, L. (2017) **The role of thermal loads in the geotechnical and structural performance-based design of energy piles.** Géotechnique. Under review.
14. Rotta Loria, A. F., Vadrot, A. and Laloui, L. (2017) **Analysis of the vertical displacement of energy pile groups.** Geomechanics for Energy and the Environment. Under review.

### Refereed conference papers

#### Published

1. Rotta Loria, A. F., Frigo, B. and Chiaia, B. M. The Classical Theory of Plasticity applied to Permafrost problems. *XXI Congresso Nazionale dell'Associazione Italiana di Meccanica Teorica e Applicata, AIMETA*. Turin, Italy. 2013.
2. Rotta Loria, A. F., Di Donna, A. and Laloui, L. Thermo-mechanical analysis of energy piles through numerical and centrifuge tests. *XV Pan-American Conference on Soil Mechanics and Geotechnical Engineering, XV PCSMGE 2015*. Buenos Aires, Argentina. 2015.
3. Laloui, L. and Rotta Loria, A. F. Geotechnical analysis of energy piles. *4<sup>th</sup> International Conference on New Developments in Soil Mechanics and Geotechnical Engineering, 4ICNDSMGE*. Nicosia, Cyprus. 2016.
4. Rotta Loria, A. F. and Laloui, L. Analysis of thermally induced mechanical interactions in energy pile groups. *1<sup>st</sup> International Conference on Energy Geotechnics, ICEGT 2016*. Kiel, Germany. 2016.
5. Laloui, L. and Rotta Loria, A. F. Multiphysical phenomena and mechanisms involved with energy piles. *1<sup>st</sup> International Conference on Energy Geotechnics, ICEGT 2016*. Kiel, Germany. 2016.
6. Rotta Loria, A. F. and Laloui, L. The role of thermally induced soil deformation on the serviceability of energy piles. *17<sup>th</sup> French-Polish Colloquium of Soil and Rock Mechanics, 17FPC*. Lodz, Poland. 2016.
7. Rotta Loria, A. F. and Laloui, L. Impact of thermally induced soil deformation on the serviceability of energy pile groups. *International Workshop on Advances in Laboratory Testing and Modelling of Soils and Shales, ATMSS 2017*. Villars, Switzerland. 2017.
8. Rotta Loria, A. F. and Laloui, L. Serviceability assessment of energy pile groups through design charts. *7<sup>th</sup> Geotechnical Symposium with International Attendance, 7.G 2017*. Istanbul, Turkey. 2017.
9. Laloui, L. and Rotta Loria, A. F. Recent developments in the multiphysical analysis and design of energy piles. *7<sup>th</sup> Geotechnical Symposium with International Attendance, 7.G 2017*. Istanbul, Turkey. 2017.

## Extended abstracts

### Published

1. Rotta Loria, A. F. and Laloui, L. Numerical study on the thermo-mechanical interactions of a group of energy piles under cooling loads. *1<sup>st</sup> International Symposium on Energy Geotechnics, SEG 2015*. Barcelona, Spain. 2015.
2. Rotta Loria, A. F., Gunawan, A., Shi, C., Ng, C. W. W. and Laloui, L. The role of null point movements on the thermo-mechanical analysis of energy piles. *1<sup>st</sup> International Conference on Geoenergy and Geoenvironment, GeGe 2015*. Hong Kong, China. 2015.
3. Rotta Loria, A. F. and Laloui, L. Estimation of the vertical displacement of energy pile groups through interaction factor charts. *2<sup>nd</sup> International Conference on Geoenergy and Geoenvironment, GeGe 2017*. Hangzhou, China. 2017.

### Accepted

4. Rotta Loria, A. F. and Laloui, L. Interaction factor analysis of energy piles. *2<sup>nd</sup> International Symposium on Energy Geotechnics, SEG 2018*. Lausanne, Switzerland. 2018.
5. Rotta Loria, A. F. and Laloui, L. Equivalent pier analysis of energy piles. *2<sup>nd</sup> International Symposium on Energy Geotechnics, SEG 2018*. Lausanne, Switzerland. 2018.

## Media

### Published

1. Laloui, L. and Rotta Loria, A. F. (2017) Energy geostructures: a powerful technology for the establishment of a low carbon built environment (in Czechoslovakian). *Geotechnika*. 1:3-18.

## Research grants and contracts

2015	<b>European Cooperation in Science and Technology</b> <i>Contribution:</i> Co-writer with Prof. Lyesse Laloui of a successful research proposal entitled “Thermo-mechanical performance of energy pile groups,” which was awarded funds totalling 184 kCHF (36-month contract)
2014	<b>Swiss National Science Foundation</b> <i>Contribution:</i> Co-writer with Prof. Lyesse Laloui of a successful research proposal entitled “Thermo-mechanical performance of energy pile groups,” which was awarded funds totalling 166 kCHF (31-month contract)

## Teaching experience and student supervision

2018	<b>Co-director and lecturer for the short-course “Energy geostructures analysis and design”</b> 3-day course organised with Prof. Lyesse Laloui for professionals and scientists.
2011–present	<b>Teaching assistant</b> <i>Swiss Federal Institute of Technology in Lausanne</i> 2018 – Energy Geostructures (M.Sc. 2 <sup>nd</sup> year, Prof. Lyesse Laloui) 2017 – Energy Geostructures (M.Sc. 2 <sup>nd</sup> year, Prof. Lyesse Laloui) 2016 – Sustainable Construction (M.Sc. 1 <sup>st</sup> year, Prof. Edgard Gnansounou and Prof. Lyesse Laloui) 2015 – Geomechanics (M.Sc. 1 <sup>st</sup> year, Prof. Lyesse Laloui) Slope stability (M.Sc. 1 <sup>st</sup> year, Prof. Lyesse Laloui and Prof. Alessio Ferrari) Sustainable Construction (see above) 2014 – Soil Mechanics (B.Sc. 3 <sup>rd</sup> year, Prof. Lyesse Laloui and Prof. Laurent Vulliet)



	<p><i>Politecnico di Torino</i></p> <p>2012 – Advanced Structural Mechanics (M.Sc. 1<sup>st</sup> year, Prof. Bernardino M. Chiaia)</p> <p>2011 – Fundamentals of Geotechnics (B.Sc. 2<sup>nd</sup> year, Prof. Claudio Scavia)</p>
2013 – present	<p><b>M.Sc. and B.Sc. student research supervisor</b></p> <p><i>Contribution:</i> Co-supervision of 16 research projects at the M.Sc. and B.Sc. levels in Civil and Energy Engineering</p> <p><i>Institutions involved:</i> Swiss Federal Institute of Technology in Lausanne (EPFL), University of Cambridge (UNICA), Ecole Normale Supérieure de Cachan (ENS), University of Pisa (UNIPi), Technical University of Munich (TUM), and Hohai University (HU)</p> <p><i>Collaborators involved:</i> Prof. Lyesse Laloui (EPFL), Prof. Kenichi Soga and Dr. Loizos Pelecanos (UNICA), Dr. Clément Desodt (ENS), Prof. Walter Grassi, Prof. Daniele Testi and Dr. Paolo Conti (UNIPi), Prof. Roberto Cudmani (TUM), and Prof. Gangquiang Kong (HU)</p> <p>2017 – Stefano Cingari (M.Sc. project, EPFL)  <i>Project title:</i> “Etude de faisabilité de l’utilisation de la géothermie dans les gares”</p> <p>Benoit Cousin (M.Sc. project, EPFL)  <i>Project title:</i> “Geothermal equipment of a tunnel in Switzerland”</p> <p>Margaux Peltier (M.Sc. project, EPFL)  <i>Project title:</i> “Potential of large-scale energy geostructures in Switzerland”</p> <p>Aymen Achich (M.Sc. project, EPFL and HU)  <i>Project title:</i> “Numerical simulation of deck de-icing using energy pile systems”</p> <p>José Vicente Catalá Oltra (M.Sc. project, EPFL and TUM)  <i>Project title:</i> “The equivalent pier method for analysing energy pile groups”</p> <p>Thibaut Duparc (M.Sc. project, EPFL)  <i>Project title:</i> “Geotechnical analysis of a metro station with energy geostructures”</p> <p>2016 – Etienne Dominguez (M.Sc. project, EPFL)  <i>Project title:</i> “Geotechnical, structural and energy design of energy piles”</p> <p>Thibaut Duparc (M.Sc. 1<sup>st</sup> year, EPFL)  <i>Project title:</i> “Performance of energy geostructures”</p> <p>Hani Taha (M.Sc. project, EPFL and UNICA)  <i>Project title:</i> “Thermo-mechanical behavior of heat-exchanger piles”</p> <p>Hani Taha (M.Sc. 1<sup>st</sup> year, EPFL)  <i>Project title:</i> “Thermo-mechanical performance of energy parking”</p> <p>Aurélien Vadrot (M.Sc. 1<sup>st</sup> year, EPFL and ENS)  <i>Project title:</i> “Analysis of the vertical displacement of energy pile groups”</p> <p>2015 – Benoit Cousin and Pia Hartmann (M.Sc. 1<sup>st</sup> year, EPFL)  <i>Project title:</i> “The equivalent pier method for energy pile groups”</p> <p>Lea Kaufmann and Hani Taha (M.Sc. 1<sup>st</sup> year, EPFL)  <i>Project title:</i> “The interaction factor method for energy pile groups”</p> <p>2014 – Niccoló Batini (M.Sc. project, EPFL and UNIPi)  <i>Project title:</i> “Energy and geotechnical performance of energy piles”</p> <p>Perrine Ratouis (M.Sc. 1<sup>st</sup> year, EPFL)  <i>Project title:</i> “Predicting the interactions of a group of energy piles”</p> <p>Samuel J. A. Kivell (B.Sc. 3<sup>rd</sup> year, EPFL)  <i>Project title:</i> “Centrifuge and numerical modelling for the design of energy piles”</p>
2016 – present	<p><b>Lecturer at “EPFL ENAC week”</b></p> <p><i>Contribution:</i> Lecturer, together with Prof. Lyesse Laloui, for a one-day course entitled “Energy geostructures engineering” at Prof. Arch. Dominique Perrault’s studio, Paris, France.</p> <p>2017 – Supervisor of more than ten EPFL student projects involving the engineering and architectural design of a building for the Olympic Village of Paris, France.</p>

2016 – Supervisor of more than ten EPFL student projects involving the engineering and architectural design of a building for the *Île de la Cité*, Paris, France.

## Management and administrative activities

Nov. 2017 – present	<b>Supervisor of software developer</b> <i>Contribution:</i> Supervisor of Mr. Fabrice Guibert in the development of a software for the numerical modelling and design of single and groups of energy piles for the Laboratory of Soil Mechanics of EPFL.
2013 – present	<b>Responsible of selling unit and customer care support – Thermo-Pile software</b> <i>Contribution:</i> Responsible of the considered services for the Laboratory of Soil Mechanics of EPFL, with more than ten software licenses sold to universities and engineering companies over four years.
May 2017 – July 2017	<b>Internship supervisor</b> <i>Contribution:</i> Supervisor of the internship of Ms. Louise Compigneaux, dedicated to develop sponsoring and commercial material for the Laboratory of Soil Mechanics of EPFL.
2013 – 2016	<b>Web-page designer of the Laboratory of Soil Mechanics of EPFL</b> <i>Contribution:</i> Responsible of the design and content of the web-page of the Laboratory of Soil Mechanics of EPFL about the research activities on energy geostructures.

## National and international research projects

2014-present	<b>GABI: European network for shallow geothermal energy applications in buildings and infrastructures (COST Action 1405)</b> <i>Institutions involved:</i> More than 33 European universities and engineering companies <i>Contribution:</i> Development of design codes for energy geostructures
2014 – present	<b>GOALI: Long-term thermo-mechanical performance and group effect considerations for design of energy piles</b> <i>Institutions involved:</i> Virginia Tech, Berkel & Company Contractors and Swiss Federal Institute of Technology in Lausanne <i>Contribution:</i> Development of numerical analyses
2013 – present	<b>Theoretical study and centrifuge modelling of energy piled foundations: geotechnical aspects</b> <i>Institutions involved:</i> Hong Kong University of Science and Technology and Swiss Federal Institute of Technology in Lausanne <i>Contribution:</i> Development of numerical analyses and centrifuge tests
2013	<b>From <i>in-situ</i> tests to numerical simulations: the response of an energy pile foundation</b> <i>Institutions involved:</i> EOS Holding and Swiss Federal Institute of Technology in Lausanne <i>Contribution:</i> Development of numerical analyses

## Expertise for external contractors

2017	<b>Quality control of energy foundation projects for the Line 2 of the Grand Paris</b> <i>Contribution:</i> Verification and validation, together with Prof. Lyesse Laloui, of two energy tunnel design projects for the Metro Line 2 of the Grand Paris, Paris, France.
	<b>Verification and validation of the energy foundation project for Testimonio II</b> <i>Contribution:</i> Verification and validation, together with Prof. Lyesse Laloui, of the Testimonio II design project, Principality of Monaco.

2014	<b>Thermo-mechanical analysis of soil characteristics from energy pile tests in Richmond, Texas, by Virginia Tech University</b> <i>Institutions involved:</i> Virginia Tech and Swiss Federal Institute of Technology in Lausanne <i>Contribution:</i> Development of experimental laboratory tests and co-authorship, together with Prof. Lyesse Laloui and Prof. Alessio Ferrari, of an expert report for Virginia Tech
2013	<b>Soil and concrete-soil response during thermal and mechanical cyclic loading</b> <i>Institutions involved:</i> ECOME Engineering and Swiss Federal Institute of Technology in Lausanne <i>Contribution:</i> Development and co-authorship, together with Prof. Lyesse Laloui, Dr. Alice Di Donna and Dr. Thomas Mimouni, of an expert report for ECOME Engineering

## Invited peer review activities

2017	<b>Energy; Journal of Geotechnical and Geoenvironmental Engineering; Geomechanics for Energy and the Environment; Géotechnique Letters</b>
------	--

## Languages and personal background

Languages	<b>Italian</b> (mother tongue), <b>English</b> (fluent), <b>French</b> (fluent), <b>German</b> (beginner)
Education	Gianni Rodari Primary School, Sandro Pertini Secondary School, Antonio Gramsci High School, all in the area of Turin (place of birth), Italy
Professional sport activities	2000 – 2008: athlete in the Ivrea Athletics Team; 2003 – 2005, 2007: participant in the Italian Athletics Championships (triple jump and long jump disciplines).

## International conferences and workshops

2017	<b>7<sup>th</sup> Geotechnical Symposium with International Attendance, Istanbul, Turkey</b> <i>Oral presentation:</i> “Serviceability assessment of energy pile groups through design charts” <i>Authors:</i> Alessandro F. Rotta Loria and Lyesse Laloui  <b>2<sup>nd</sup> International Conference on Geoenergy and Geoenvironment, Hangzhou, China</b> <i>Poster presentation:</i> “Estimation of the vertical displacement of energy pile groups through interaction factor charts” <i>Authors:</i> Alessandro F. Rotta Loria and Lyesse Laloui  <b>International Workshop on Advances in Laboratory Testing of Soils and Shales, Villars, Switzerland</b> <i>Oral presentation:</i> “Impact of thermally induced soil deformation on the serviceability of energy pile groups” <i>Authors:</i> Alessandro F. Rotta Loria and Lyesse Laloui
2016	<b>COST Action GABI interim meeting, Turin, Italy</b> <i>Oral presentation:</i> “Predicting the behaviour of energy piles for the GABI benchmark” <i>Authors:</i> Alessandro F. Rotta Loria and Lyesse Laloui  <b>17<sup>th</sup> French-Polish Colloquium of Soil and Rock Mechanics, Lodz, Poland</b> <i>Oral presentation:</i> “The role of thermally induced soil deformation on the serviceability of energy piles” <i>Authors:</i> Alessandro F. Rotta Loria and Lyesse Laloui  <b>1<sup>st</sup> International Conference on Energy Geotechnics, Kiel, Germany</b> <i>Oral presentation:</i> “Thermally induced group effects among energy piles” <i>Authors:</i> Alessandro F. Rotta Loria and Lyesse Laloui

	<p><b>COST Action GABI interim meeting, Cluj-Napoca, Romania</b>  <i>Invited oral presentation:</i> “Energy and geotechnical behaviour of energy piles for different design solutions”  <i>Authors:</i> Alessandro F. Rotta Loria and Lyesse Laloui</p>
2015	<p><b>1<sup>st</sup> International Conference on Geoenergy and Geoenvironment, Hong Kong, China</b>  <i>Oral presentation:</i> “The role of null point movements on the analysis of energy piles”  <i>Authors:</i> Alessandro F. Rotta Loria, Anthony Gunawan, Chao Shi, Charles W. W. Ng and Lyesse Laloui</p> <p><b>XV Pan-American Conference on Soil Mechanics and Geotechnical Engineering, Buenos Aires, Argentina</b>  <i>Oral presentation:</i> “Thermo-mechanical analysis of energy piles by numerical and centrifuge tests”  <i>Authors:</i> Alessandro F. Rotta Loria, Alice Di Donna and Lyesse Laloui</p> <p><b>COST Action GABI interim meeting, Brussels, Belgium</b>  <i>Oral presentation:</i> “Thermo-mechanical performance of energy pile groups”  <i>Authors:</i> Alessandro F. Rotta Loria, Alice Di Donna and Lyesse Laloui</p> <p><b>1<sup>st</sup> International Symposium on Energy Geotechnics, Barcelona, Spain</b>  <i>Oral presentation:</i> “Thermo-mechanical interactions of a group of energy piles subjected to heating loads”  <i>Authors:</i> Alessandro F. Rotta Loria, Alice Di Donna and Lyesse Laloui</p>
2014	<p><b>Journée Technique sur les Structures Géothermiques, Paris, France</b>  <i>Invited oral presentation:</i> “Thermo-Pile, un outil de dimensionnement des pieux thermo-actifs”  <i>Authors:</i> Lyesse Laloui and Alessandro F. Rotta Loria</p>
2013	<p><b>XXI Congresso Nazionale AIMETA, Turin, Italy</b>  <i>Oral presentation:</i> “A non-linear constitutive model for evolutionary permafrost”  <i>Authors:</i> Alessandro F. Rotta Loria, Barbara Frigo and Bernardino M. Chiaia</p>